Conceptual Study of a Micrometeoroid Deep Space Satellite

FINAL REPORT

Vol. II

Experimental Objectives and Systems

FACILITY FORM 602

N 66 35794 (ACCESSION NUMBER) (THRU)

316 (PAGES) 1 (CODE)

(NASA CR OR TMX OR AD NUMBER) (CATEGORY)

Distribution of this report is provided in the interest of information exchange. Responsibility for the contents resides in the author or organization that prepared it.

GPO PRICE $ _____

CSFTI PRICE(S) $ _____

Hard copy (HC) 7.00

Microfiche (MF) 1.75

ff 653 July 65

Conceptual Study of a Micrometeoroid Deep Space Satellite

FINAL REPORT

Vol. II

Experimental Objectives and Sensors Telecommunications

Edward C. Weissmann
Study Director

January 1965

ER 13700-II

Submitted to the NASA Langley Research Center
in compliance with Contract No. NAS 1-4162.

MARTIN
BALTIMORE DIVISION
BALTIMORE, MARYLAND 21203

CONTENTS

		Page
I.	Experimental Objectives and Sensors	I-1
	A. Conclusions and Recommendations	I-3
	B. Technical Discussion	I-8
	C. References	I-77
	Appendix I-1-1. Pressurized Sensor Analysis	I-1-1
II.	Telecommunication System	II-1
	A. Conclusions and Recommendations	II-5
	B. Technical Discussion	II-29
	C. References	II-139
	Appendix II-1. Link Calculations for VHF Telemetry and Command Links	II-1-1
	Appendix II-2. Tracking Link Calculations	II-2-1
	Appendix II-3. Modulation System Performance Comparisons	II-3-1
	Appendix II-4. Data Parity Check Error Probabilities	II-4-1
	Appendix II-5. Tradeoff Studies in Instrumentation	II-5-1
	Appendix II-6. Satellite Study Model for Tradeoff of Substorage and Fixed Word-Sequence Format Versus Variable Format	II-6-1
	Appendix II-7. Investigation of Memory Devices	II-7-1

I. EXPERIMENTAL OBJECTIVES AND SENSORS

Sidney L. Russak

I. EXPERIMENTAL OBJECTIVES AND SENSORS

Introduction

The meteoroid environment is of interest to astronomers, cosmologists, celestial mechanicists, astrobiologists, astrophysicists, and engineers designing spacecraft. The latter, however, are primarily--and perhaps solely-- interested in the penetrating and eroding properties, or even more specifically in the rate of penetration of or damage to spacecraft by meteoroids. The other groups are more interested in the incident properties of the meteoroids such as mass, velocity density and the temporal and spatial variations of these properties.

For this study we were asked to consider attaining four objectives, namely:

(1) Penetration rate variation with distance from the Earth.

(2) Impact rate variation.

(3) Mass distribution in the same environment.

(4) Velocity distribution in the same environment.

The first objective was to be assigned highest priority, the other three are shown in the approximate order of priority. Previous to the MDSS, no executed or planned program had all these objectives jointly.

During our earlier studies we had concluded that these objectives could all be attained using one spacecraft. In doing so we assumed that the chief region of interest in the primary objective was to obtain data on penetration of engineering (structural) thickness of material. It was presumed that ideally, the highest achievement of all objectives would result if the measurements of penetration, velocity, impact and mass were made at the same time and from the same sample, or, in other words, using one instrument. With such data an enormous improvement could be made--in one step--toward resolving both the uncertainties in the environmental model and in the interaction or penetration model. To no one's surprise, a sensor with such capabilities does not exist. Our earlier studies also indicated that sensors which could achieve all the objectives independently over a range of meteoroid masses capable of penetrating engineering (structural) thicknesses of material were also not in existence. Sensors were found which could satisfy all the objectives, some independently, but only on the basis of taking their samples from different mass regions of the micrometeoroid population.

The purpose of the present effort in this area was to survey and evaluate in greater detail the availability and state of the art of sensors required to achieve the objectives, to select the objectives considering their order of importance and requirements for implementation (mission time, measurement system size and reliability), and to select the best combination of sensors. The sensor selection was to be based on the state of the art, simplicity, reliability considerations, and environ - mental effects. Therefore, sensor and objective selections are not independent.

Summary

A survey of sensors to measure meteoroid incident and interaction parameters was made. The degree of detail that could be obtained varied. Sensors which could satisfy all the objectives were available and could be integrated within a spacecraft compatible with the capabilities of the launch vehicles.

Sizing of sensors for the primary objective was predicated upon the thickest gauge that could be used and still meet the guidelines for the number of sample points. The environmental model used for sensor sizing was conservative relative to other existing models, but was based upon the actual penetration frequency of Explorer XVI sensors. Sensors to achieve the secondary objectives over the same portion of the meteoroid population as the penetration sensors were not available. Available sensors had "sampling windows" equivalent to much smaller particles necessitating extrapolation over a number of decades of mass in order to correlate the data. On the other hand, such sensors were found to be relatively easy to accommodate physically . The largest requirement they imposed upon a spacecraft sized by penetration sensors was in data handling due to the increased sampling potential which extended over a number of decades of particle mass. A secondary requirement was for environmental measurements such as temperature and attitude needed for interpretation of their outputs.

The final sensor complement recommendation was for two thicknesses of capacitance penetration sensors. The mounting technique evolved for the capacitance sensors allowed the selection of a back-up penetration flash detector which is installed in the volume defined by two capacitance sensor panels and their frames.

Meteoroid sensors used on OGO and Mariner 1964 were also selected for measuring velocity, impact, and (derived) mass. Throughout this report, these two sensors are identified as the velocity gauge and the Mariner gauge, respectively.

Integration and data handling concepts were evolved to separate the primary sensor lines and allow for changes in the sensor outputs. The MDSS system conceived affords great flexibility and reliability. Sensors can be replaced by other existing sensors and/or sensors presently under development, or they can be eliminated altogether without unduly affecting the spacecraft. Also, by minimizing the possible effects of individual sensor failure, the conceived system has a high probability of achieving the primary objective.

A. CONCLUSIONS AND RECOMMENDATIONS

1. Satisfaction of Mission Objectives

All of the objectives of the MDSS mission can be satisfied by using--on a single spacecraft--a number of available state-of-the-art sensors that have similar or overlapping "sampling windows." However, that sampling window over which all of the objectives can be satisfied with state-of-the-art sensors occurs at particle sizes and masses which do not represent a hazard to space flight in terms of penetrating capability.

Even within the window no one sensor can work toward all the objectives, nor can the sampling of a single particle contribute to the satisfaction of all the objectives. The basic problem is the availability of sensors capable of determining the particle velocity and also the penetration and impact properties over the width of the window. The existing sensor most suitable must be considered at best only a threshold penetration detector although it can measure velocity and impact. Velocity is an incident property of the particle. The other two require that the particle's incident properties be drastically altered if not completely lost.

Within the current state of the art it is possible to satisfy all the objectives, some of them individually and some of them in combinations, during the sampling of one particle. If it is desired that all the objectives be satisfied within a common range of meteoroid parameters, that range could be very narrow and centered about 10^{-10} gm or about 0.1 mil. However, penetration data at 0.1 mil is of little engineering value and operating impact transducers or velocity sensors at 10^{-10} gm sacrifices at least two decades of sensitivity.

One solution would be to consider satisfying only the primary objective, i.e., penetration rate versus distance from the earth. In effect this solution was followed in sizing the spacecraft to obtain maximum penetration area, and in the design of the primary data handling and telemetry system. However, rather than neglect the remaining three objectives because of the different sampling windows of existing sensors,

it was decided to include sensors to satisfy all the objectives. This solution seemed reasonable because the associated sensors would be relatively easy to accommodate on the spacecraft. Each of the remaining objectives has intrinsic value. The velocity distribution of meteoroids smaller by two orders of magnitude than those meteoroids which penetrate the penetration sensors is a clue to the velocity distribution of the penetrating particles; same can be said for impact and mass data.

The proposed payload contains velocity and impact detectors with sensitivities to 10^{-13} gm and penetration detectors sized to give the required statistical sample corresponding to masses as high as 5×10^{-7} gm. An overlap can be provided by a 0.25-mil penetration gauge which would respond to particles of 6.6×10^{-10}, or well within the response of the sensors chosen to measure velocity and impact.

2. Definition of Sensor Complement

The suggested sensor complement is summarized in Table I-1.

Penetration measurements will be made using tension-mounted capacitance gages consisting of 1-mil aluminum (5052-H19) target plates and 2-mil target plates. These gages, and the corresponding areas, were based on the meteoroid models used during this study. Different models could result in different aluminum target plate thicknesses and areas, as discussed in detail in Section B1c. The initial calculations performed to determine the areas of capacitance sensor required were based on the mission objective of obtaining 80 penetrations in one year. During the early phases of this study, it was decided to design the spacecraft with sufficient sensor area to obtain the desired number of penetrations in 6 mo instead of 1 yr. Therefore, sensor area requirements became 50 sq ft for the 1-mil aluminum thickness and 530 sq ft for 2 mils. However, design restrictions in the present configuration (i.e., total gross panel area available, less structure, panel mounting doublers, air gaps, etc.) limit the net sensor areas to 39 sq ft and 503 sq ft, respectively, as shown in Chapter III, Volume III of this report. Therefore, using the same particle environment, it will require approximately 7.7 mo to obtain 80 penetrations in the 1-mil panel.

Several factors must be considered, however:

(1) The present configuration has an oversized structural area for the solar cell arrays. It is possible to reduce this area and thus add area to the 1-mil panels without further changes to the vehicle structure.

Instrument	Origin and Remarks	Size	Weight
Capacitance gages	LRC/Schjeldahl. 50 sq ft of 1-mil aluminum target plate gages plus 530 sq ft of 2-mil aluminum target plate. Sensor panels will form Z-configuration in each of four directions giving 12 wings. Each wing will be divided into 3 sensor bays. The 2 larger bays will have 2-mil panels on either side; the smaller bay will have 1-mil panels on either side. Penetrated sensor will be identified only as to one of six directions. IR sensor will identify bay so that penetrated sensor will be known to one of 3 or one of 5 segments.	1 mil, 10 x 35-1/2 2 mil, 49-1/2 x 35-1/2	0.59 psf 0.62 psf
Microphone capacitance gage plus thin film	GSFC/Mariner. Capacitor response will be pulse height analyzed for kinetic energy analog.	8 in. x 8 in.	0.5 lb each
Velocity tube	GSFC/OGO. Time of flight from 2-mc clock stopped by capacitor output. Capacitor output is also pulse height analyzed for energy response. Attitude needed but not necessarily measured at time of hit.	8-in. cube	4 lb
Light flash detector	Exotech, Inc. 2 sensors in each of the 36 bays. Each pair will be used in coincidence.	1 x 1 x 1/2 in. each	.05 lb each

*$8.3\ E\ -8 \equiv 8.3 \times 10^{-8}$
**n = 6
***per tube
****Alternate for level A and/or B

BLE I-1

ment--Six-Month Mission

Output Name	Response	Output Per Sensor (mass equivalent gm)*	Number of Hits per Zone per Orbit	Number of Sensors
Thickness 1, String 1	$(mv)^{1/3}$	8.3 x E-8	0.53	24 panels of 1-mil target plate, each subdivided electrically into 5 segments. 48 panels of 2-mil target plate, each subdivided electrically into 3 segments.
Thickness 1, String n**	$(mv)^{1/3}$	8.3 x E-8	0.53	
Thickness 2, String 1	$(mv)^{1/3}$	4.8 x E-7	0.53	
Thickness 2, String n**	$(mv)^{1/3}$	4.8 x E-7	0.53	
Mike, Level 1	Momentum	E-10	81.4	3 sensors = 6 surfaces; hit numbers are per sensor
Mike, Level 2	Momentum	5 x E-10	9.4	
Mike, Level 3	Momentum	E-9	3.7	
Mike, Level 4	Momentum	5 x E-9	0.43	
Cap, Level A	$(mv)^{x}$	E-12	39,040	
Cap, Level B	$(mv)^{x}$	E-11	1,783	
Cap, Level 1	$(mv)^{x}$	E-10	81.4	
Cap, Level 2	$(mv)^{x}$	5 x E-10	9.4	
Cap, Level 3	$(mv)^{x}$	E-9	3.7	
Cap, Level 4	$(mv)^{x}$	5 x E-9	0.43	
(Cap. Level 5)***	$(mv)^{x}$	(E-8)	(0.2)	
Velocity analog	Time of flight	$\geq$E-13	33.2	2 sensors = 8 tubes; hit numbers are per tube
Cap, Level 1	$(mv)^{x}$	E-13	33.2	
Cap, Level 2	$(mv)^{x}$	E-12	1.5	
Cap, Level 3	$(mv)^{x}$	5 x E-12	0.173	
Cap, Level 4	$(mv)^{x}$	E-11	0.07	
Mike, Level 1	Momentum	E-12	1.5	
Mike, Level 2	Momentum	5 x E-12	0.173	
Mike, Level 3	Momentum	E-11	0.07	
IR Level 1 (1-mil)	Penetration	>8.3 x E-8	0.53	72
IR Level 2 (2-mil)	Threshold only	>4.8 x E-7	0.53	

(2) While the capacitance sensor areas were sized for a 6-mo mission life, all other onboard sensors, as well as the flight plans, have been defined for a 1-yr lifetime.

(3) The capacitance sensor areas were based on a conservative estimate of the penetration equivalence of the mylar dielectric.

The anticipated capacitors will have thin film sputtered dielectric with vacuum deposited copper. However, throughout this report, the capacitors used are based on existing techniques, using mylar dielectric with vacuum deposited copper. A secondary penetration measurement will be made using infrared flash detectors mounted within the free volume defined by the capacitor sensors and the mounting frame. Extraneous light will be excluded by a flexible (conductive fabric) strip fastened to both the frame and the capacitor by a velcro fastener.

Velocity and impact as well as penetration kinetic energy will be measured by two GSFC Velocity Gages as used on the OGO satellite. Since the velocity section sensitivity exceeds the impact transducer sensitivity, velocity will be measured even though no coincident impact response occurs. (This is planned for the POGO version of the sensor).

Impact measurements will be extended to approximately 10^{-8} gm using three orthogonally mounted gages of the type developed by GSFC for Mariner 1964. These gages will be mounted on the ends of three spacecraft "wings." Output of the capacitance sensor will be analyzed for a kinetic energy response.

3. Alternate State-of-the-Art Sensors (See Table I-3)

Any one of the different capacitor sensors under development can be mounted within the spacecraft "wing" frames. This would include the double (coincidence) sensor as developed at Lewis Research Center or the thin film devices being developed. Multilayer capacitance gages could be mounted in the same manner. The most promising version under development would be the thin film sensor because of the relatively small thickness added to the target plate.

The gold grid type of penetration gage or the pressurized cylinder gage could also be mounted within the same frames. For the latter, a large weight penalty would exist due to the relatively large weight fraction of non-target material.

Since all of these penetration sensors are threshold sensors only, substitution would not affect the data handling system. Power differences should be of negligible effect. The last two sensors store the penetration record (by virtue of their destruction) so that they would not have to be monitored continuously.

Physical mounting of a ceramic beam sensor should present no problems. A housing may be required if mounted external to the systems module. However, internal mounting would probably be more desirable. The spacecraft background noise may be greater than in the Pioneer satellite (because of thermal flexing of the large sensor panels) and may be a factor limiting the sensitivity that could be attained.

4. Sensors Requiring Considerable Development

The modified version of the velocity tube, if available, can be physically substituted easily for the existing instrument. Because of the increased geometric factor, a much larger sample will be obtained and the sample can be extended to masses of 10^{-9} to 10^{-8} gm. The major new factor will however not be the total number of data sample per se but the sorting and storage of the 16 x 16 possible arrival directions in the velocity measurement. The increased resolution will also make it desirable to use an improved attitude sensing system. If the sensor were built with fewer matrix elements but the same sampling area, then the number of samples per resolvable arrival direction, would increase as the number of resolvable directions decreased. This would in effect increase the sample size at each momentum level and provide data up to larger mass particles. This exchange of velocity resolution for mass dynamic range would appear to be a worthwhile consideration for this reason as well as a means to decrease the data required to identify arrival direction. This would simplify the data handling with no loss of the sampling potential.

The basic improvement in the infrared flash sensor would be a reliable calibration of the flash intensity versus particle mass, velocity, penetration or related parameter and would not necessitate any modification over the present version insofar as the physical requirements of size and mounting. The outputs would be handled differently in that the signal from each sensor would be pulse-height analyzed, as opposed to most using the signal in coincidence from a set of two sensors as an event indicator.

Use of the ballistic pendulum and velocity sensor (which may be developed by NASA/MSC) should not present any mounting problems with respect to size and shape, but may be more sensitive to noise transmitted from the thermal flexing of the large sensor panels. The data rates and the output form should be easily accommodated.

B. TECHNICAL DISCUSSION

1. Experimental Objectives, Guidelines, and Design Models

a. Summation of objectives, guidelines, and models

The experimental objectives, in order of relative importance, to be considered for selection were:

(1) Penetration rate variation with distance from the earth.

(2) Impact rate variation with distance from the earth.

(3) Mass distribution in the same environment.

(4) Velocity distribution in the same environment.

The selections were to be made giving consideration to the:

(1) Probability of obtaining statistically significant results.

(2) Time required to achieve the objectives.

(3) Area required to achieve the objectives.

(4) Reliability of the systems required to achieve the objectives.

Statistically significant penetration and impact results would be obtained when the rate or rates obtained from these data have a 95% confidence interval in greater than $(0.50\,\overline{\psi},\ 1.50\,\overline{\psi})$ where $\overline{\psi}$ is the best present estimate of the mean penetration or impact rate. For velocity data the limits of the 95% confidence interval were no greater than $(0.75\ \overline{v},\ 1.25\ \overline{v})$ where $\overline{v}$ is the best present estimate of mean velocity. Using the test for the mean of the distribution given in RFP L-4313, 16 data points would be required to define a mean penetration or impact rate and 64 data points to define a mean velocity.

(1) Design models

Near earth meteoroid flux and penetration models. The design model of the near earth meteoroid environment was based upon a modification of the Whipple 1963 flux law (Ref. I-1). The penetration frequency determined from the 1-mil pressurized cylinders of Explorer XVI (Ref. I-31) was substituted into the flux equation to give the mass capable of penetrating 1 mil of beryllium copper. This mass was then substituted into a penetration equation of the form $P \alpha (mV)^{1/3}$ to obtain the constant of proportionality. The development is as follows:

(a) For flux mass curve use Whipple's equation with 1.34 slope compatible with a zero magnitude meteoroid of 2.5 gm.

Whipple's equation is $\log N = -1.34 \log m - 14.48$. To adjust from the 1-gm zero magnitude meteoroid, we subtract $-1.34 (\log 2.5/1) = -0.533$ to obtain $\log N = -1.34 \log m - 13.95$.

(b) From the flux corresponding to the puncture rate in the 1-mil cans of Explorer XVI find the mass of the penetrating meteoroid

$$0.031 \times \frac{4}{3} = 0.0413 \text{/sq ft/day (TM X-949)}$$

$$0.0413 \text{/sq ft/day} = 0.0413 \frac{10.76}{8.64 \times 10^4} = 0.0413 \times 1.245 \times 10^{-4}$$

$$= 5.14 \times 10^{-6} / m^2 / \text{sec}$$

$$\log (5.14 \times 10^{-6}) = -1.34 \log m - 13.95$$

$$-5.29 = -1.34 \log m - 13.95$$

$$1.34 \log m = 5.29 - 13.95$$

$$\log m = -8.66/1.34 = -6.463$$

$$m = \frac{1}{2.905 \times 10^6} = 0.344 \times 10^{-6} = 3.44 \times 10^{-7} \text{ gm}$$

(c) Adjust K values in penetration formula to agree with mass (V = 22 km/sec as agreed upon earlier)

$$P = K (mV)^{1/3}$$

$$0.001 = K (3.44 \times 10^{-7} \times 22)^{1/3}$$

$$= K (7.572 \times 10^{-6})^{1/3}$$

$$10^{-3} = K (1.965 \times 10^{-2})$$

$$K = \frac{10^{-3}}{1.965 \times 10^{-2}} = 0.509 \times 10^{-1}$$

$$= 0.0509 \text{ for BeCu and stainless steel}$$

$$K = 0.1018 \text{ for Al}$$

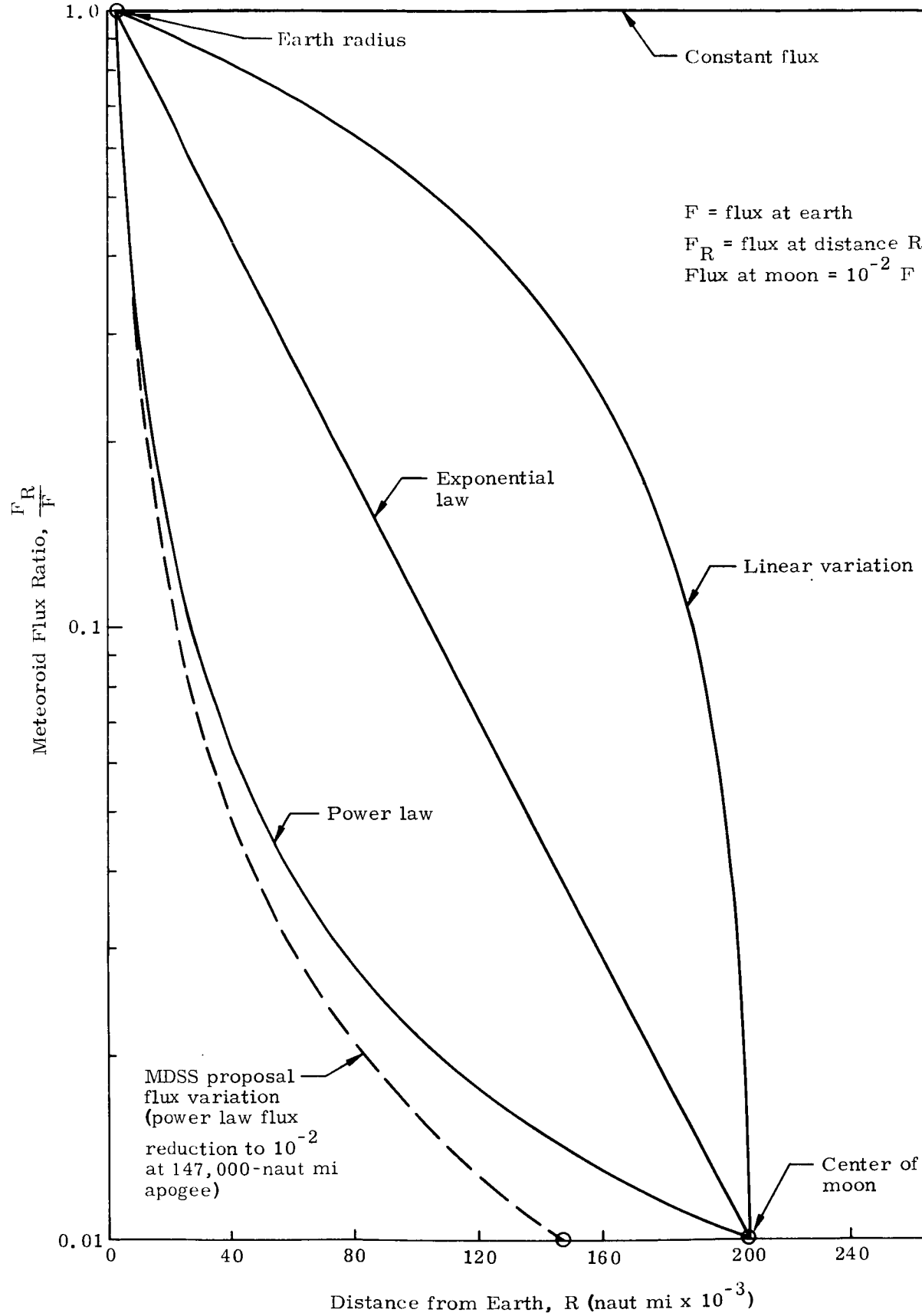


Fig. I-1. Variation of Meteoroid Flux with Distance from Earth

Combined model. The combined penetration and flux law for aluminum was then

$$N = \left(\frac{9.65 \times 10^{-5}}{P} \right)^{4.02}$$

where N is the number of particles per square meter per second which would penetrate P inches of aluminum.

Cislunar flux of meteoroids. For the purposes of sizing the sensor areas, and the data acquisition system and readout scheduling we considered a number of models of flux falloff by two orders of magnitude from earth to the moon. These were exponential, linear and power law functions of geocentric distance. Figure I-1 shows the flux ratio at different distances from earth along each of the flux falloff curves. It is apparent that sizing will be strongly dependent upon the perigee and apogee of the orbit as well as the flux falloff mode. An evaluation of the data acquisition schedule to be anticipated was made considering each of the three flux falloff laws. For a 144-hr orbit (apogee 147,000 naut mi, perigee 200 naut mi), the anticipated data acquisition schedules would be as shown on Fig. I-2. The curves have been normalized for 80 hits per year with the power law flux falloff factor. However, the relative positions of the curves would not change if another basis were chosen. Looking first at the number of hits expected, the ratios of the total data obtained in one-half an orbit are 0.66:2.8:9.1:19.4 or 1:4.24:13.8:29.4. Sizing the sensors on the basis of the power law falloff would result in about 30 times the data if in fact no falloff in flux existed and vice versa. The slope of the curves shows the relative data accumulation rate and it is apparent that the time of data rate variation is greatest along the power law falloff and decreases to zero with no falloff in flux. On the other hand, considering the altitude markers defining the limits of the 20 percentile data zones, it can be seen that the relative percentage of data obtained at large transmission distances is greatest if there is no falloff in flux with altitude (with 80% of the data received at altitudes in excess of 75,000 naut mi) and least with the power law falloff in flux (44% of the data received above 75,000 naut mi).

The design philosophy recommended was to size the sensors on the assumption that the power law falloff would be encountered. In the event that the falloff was less rapid (so that the sensor area would then be overdesigned), the capability for "count-only" data storage would be provided with a capacity up to 30 times in excess of that expected from the power law falloff. Storage capacity of high resolution data--which could include time of event, amplitude, attitude at event time, sensor identification and calibration--would be based upon the data rates expected with the power law falloff plus about 20% extra.

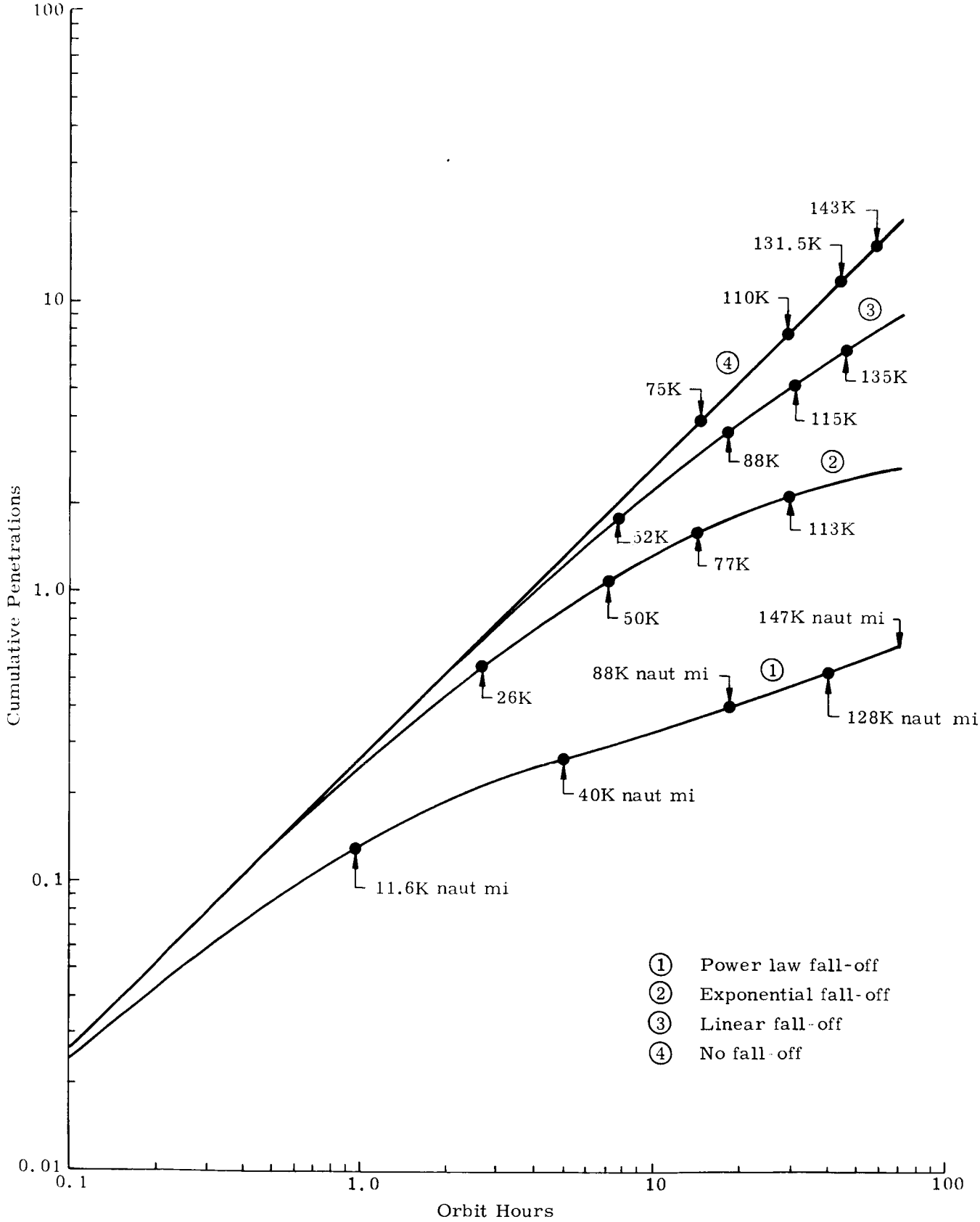


Fig. I-2. Data Accumulation Rate for Different Flux-Fall-off Factors to Give 35/yr for the Power Law Fall-off

b. Baseline sensor sizing and data acquisition

The 147,000-naut mi apogee orbit cited in the previous section was used as a baseline in order to arrive at an early quantitative "feel" for sensor sizing and data acquisition. This orbit would be stable and yet go far enough out for an evaluation of the variation of the meteoroid environment with distance from the earth. It was arbitrarily assumed that five statistically valid determinations of the measured parameters (penetration rate, impact rate, mass and velocity) would be made along the orbit. Therefore, sensor sizing should be for 16 x 5 or 80 data points for all except velocity sensors which would be 64 x 5 or 320 points. These points would then define five zones through each of which the mean value of the parameter would apply in the determination of its variation with distance from the earth. The sensor area required for a range of meteoroid masses is shown on Table I-2. The thickness of aluminum that can be penetrated by a meteoroid of each mass is also shown.

Early estimates of the sensor area that could be mounted within the fairings of the launch vehicles initially under consideration were about 600 sq ft for the Atlas combinations and at least 7000 sq ft (based on volume considerations only) for the two-stage Saturn. Penetration, impact and mass sensors on the Atlas launched spacecraft were area limited to measurements corresponding to masses of 6×10^{-7} gm or smaller. For the two-stage Saturn launched spacecraft the limiting mass was about 3×10^{-6} gm. For velocity measurements, the limiting mass would be about one-third of these values.

The baseline data acquisition schedule was shown on Fig. I-2 for the power law flux falloff curve for a one-year data collection period. For six months the ordinate would double. Count-only data acquisition would be at a rate up to twice that shown for curve No. 4 on Fig. I-2. A number of sensors under consideration were known to have dynamic ranges of at least three decades of meteoroid mass. Therefore, if the sensor areas were chosen to give 80 penetrations/6 months at the lowest sensitivity (largest mass), then approximately ten thousand more data points would be obtained at the highest sensitivity level. For wide dynamic range sensors it was therefore decided to consider scaling the high resolution data.

c. Variations about baseline considerations and their significance

It is obvious that if there were enough known about the meteoroid environment as is needed to properly design the spacecraft, there would be no need for the measurements planned for the spacecraft. It was therefore desirable to make a quantitative evaluation of the effects of uncertainties and variations of the factors which contributed to the baseline.

TABLE I-2

Required Sensor Areas

Log Meteoroid Mass (gm)	Aluminum Penetration (in.)	N (m^{-2} sec^{-1})	Area Required (m^2)				
			For One Impact/Day	Near Earth		Along Baseline Orbit	
				For 80/6 mo	For 320/6 mo	For 80/6 mo	For 320/6 mo
$\geq$ -12	2.9×10^{-5}	1.35×10^{2}	8.6×10^{-8}	3.8×10^{-8}	1.5×10^{-7}	1.1×10^{-6}	4.4×10^{-6}
$\geq$ -11	6.1×10^{-5}	6.2	1.9×10^{-6}	8.2×10^{-7}	3.3×10^{-6}	2.4×10^{-5}	9.7×10^{-5}
$\geq$ -10	1.3×10^{-4}	2.8×10^{-1}	4.1×10^{-5}	1.8×10^{-5}	7.2×10^{-5}	5.3×10^{-4}	2.1×10^{-3}
$\geq$ -9	2.9×10^{-4}	1.3×10^{-2}	9.0×10^{-4}	3.9×10^{-4}	1.6×10^{-3}	1.2×10^{-2}	4.6×10^{-2}
$\geq$ -8	6.1×10^{-4}	5.8×10^{-4}	2.0×10^{-2}	8.6×10^{-3}	3.5×10^{-2}	2.5×10^{-1}	1.0
$\geq$ -7	1.3×10^{-3}	2.6×10^{-5}	4.4×10^{-1}	1.9×10^{-1}	0.8	5.6	22.2
$\geq$ -6	2.9×10^{-3}	1.2×10^{-6}	9.5	4.1	16.6	121.7	487
$\geq$ -5	6.1×10^{-3}	5.5×10^{-8}	207	90.7	362.7	2.67×10^{3}	1.07×10^{4}

(1) Effects of design model uncertainties

Near earth flux. Sensor area required for a given number of meteoroid encounters in a given length of mission is governed solely by the flux equation, the orbit and flux falloff. This expressed simply as

$$\text{Area required} \propto 1/N \times CEF$$

where the near earth flux, $N = bm^{-a}$ and CEF is the Cumulative Exposure Factor which adjusts the near earth flux for the flux-altitude relation of the assumed flux falloff and the altitude-time history of the assumed orbit.

Values of "a" from terrestrial meteor observations (assuming the mass of meteoric material to be constant in each visual magnitude) range from 1 to 1.43. For particles of 10^{-5} gm and larger, sensor areas determined using "a" values of 1, 1.34 and 1.43 would be in the ratio of 0.35:1:50. For particles of 10^{-8} gm and larger the ratio would be 0.19:1:5.25. For 10^{-12} gm and larger particles, the sensor area ratio would be 12,000:1:0.016. The range of estimates of "b" (in terms of the daily rate over earth) based upon meteor observations imply a sensor area uncertainty of 28:1 possibly even greater considering the further uncertainty in the conversion from visual magnitude to mass. The zero visual magnitude meteor has been estimated at values ranging from 0.15 to 30 gm. The effect of uncertainties in the value of the visual magnitude to mass conversion can be quite large because sensor area would be proportioned to the "a" power of the ratio of two different estimates of the conversion factor. Considering the derivation of the design model from meteors in the magnitude range of 0 to 4--the Hawkins and Upton (Ref. I-2) original estimate was $m_0 = 30$ gm. Whipple (Ref. I-1) changed this to 1 gm. We have used 2.5 gm and now Hawkins (Ref. I-3) has revised it to 4.4 gm (and also separated the sporadic from the stream flux).

Flux laws derived from meteorite collections give "b" and "a" on a mass basis as 3.46 and -0.77 (Brown, Refs. I-4 and I-5). Hawkins (Ref. I-3) estimates 5.42 and -1 for stones in space and 2.64 and -0.7 for irons. Extension of these estimates to masses of 10^{-5} or less would greatly broaden the range of uncertainty.

Direct measurements of micrometeoroids as measured by McCracken and Alexander (Ref. I-6) indicate "b" and "a" on a mass basis as 2.65 and -1.7. For particles of 10^{-5} gm and larger, the ratio of sensor areas determined from the design model to those determined from the

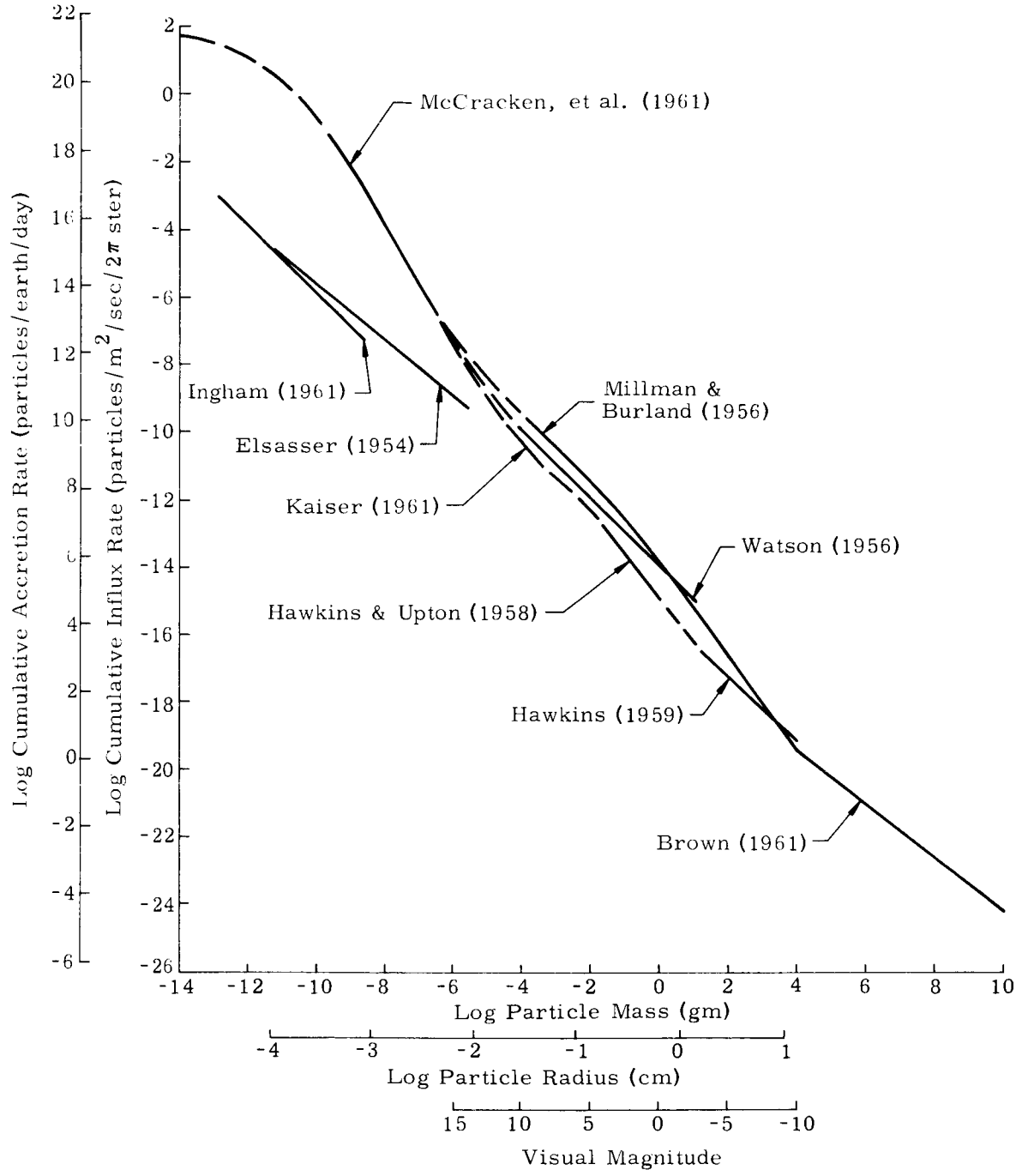


Fig. I-3. Flux Estimate Comparison

McCracken and Alexander data would be 1:35.5; at 10^{-8} gm and larger the ratio would be 1:2.8. At 10^{-12} the models have crossed and the ratio of sensor areas would be 1:0.11.

Distribution laws developed from observations of zodiacal light and the F-corona of the sun indicate that the different flux varies inversely as the 2.5 to the 5 power of the particle radius, or equivalent to a range of "a" values on a mass scale of 0.5 to 1.33. Estimates of "b" range over 10 decades with lower values (Van de Hulst, Ref. I-7) of "b" and "a" requiring sensor areas three or four orders of magnitude below that indicated by the meteor data. The most recent estimate (Ingham, Ref. I-8) using what is equivalent to an "a" of 1.0 (as compared to 0.53 for Van de Hulst) and a "b" value six decades higher than Van de Hulst gives a close agreement with the meteor data (Kaiser, Ref. I-9). However, it should be noted that both the meteor data and the new scattered light estimates are considerably below the flux estimates given by the measurements of McCracken and Alexander. The relative positions of the flux estimates can be seen from Fig. I-3. Kaiser recently has looked at much of the same data including particles recovered from deep sea sediments. In his plot representative data of each type or origin with the exception of the satellite data can be fitted by a simple curve on a log-log scale over a spread of less than two decades. He concludes that the satellite data refers to a cloud of particles in orbit around the earth, and that these particles have probably been captured from the zodiacal cloud.

Flux falloff. The effect upon sensor sizing of the flux falloff with distance from the earth was discussed somewhat in paragraph 1b, above. The estimate which gives the most rapidly decreasing flux was made by Whipple (Ref. I-10) in 1960 based upon rocket, satellite and deep space probe data. The flux ($\geq 10^{-9}$ gm) was shown to vary inversely with the 1.4 power of altitude above the earth's surface. Referenced to a base altitude of 100 km the flux would be 25 times lower at 1000 km, 630 times lower at 10,000 km, and 1660 times lower at 20,000 km. There has been some controversy regarding the validity of some of the data used and it may be significant to note that in his most recent paper (Ref. I-11) Professor Whipple says, "Similarly, it seems unlikely that in deep space the perforation rates will be much reduced if any over those observed near the Earth. Near the moon secondary meteoroids may increase the hazard."

Some other models of the cislunar meteoroid environment are summarized below.

(a) S. H. Dole, Rand (Ref. I-12)

Flux of particles near earth would be expected to vary with geocentric distance to the -1.66 power. The concentration should vary according to the -1.14 power of the distance. Mean geocentric particle speed is approximately equal to earth escape velocity.

(b) J. J. Volkoff, JPL (Ref. I-13)

Particle concentration varies with the -1.1 power of distance from earth. Mean particle velocity varies inversely with the square root of geocentric distance. (Mean particle flux would therefore be expected to vary with the -1.6 power of geocentric distance.) The intercepted flux is modified by the shielding effect of the earth. The planetary accretion effect is presumed to extend out to 41 earth radii (sun-planet equigravitational distance) but is then arbitrarily extended to 65 earth radii on the basis that planetary satellites will most likely increase the extent of the planetary effect.

(c) R. B. Southworth, SAO/HAO (Ref. I-14)

Southworth disputes Dole's analysis and derives the particle concentration as inversely proportional to the square root of geocentric distance. He goes on to show that his expression for the gravitational accretion mechanism proposed by Dole can produce no more than a twelvefold increase over the interplanetary concentration. However, only 1/2% of the particles are in trajectories amenable to Dole's mechanism. Therefore, the net effect of this mechanism is no more than 12 x 1/2 = 6%. That is, the gravitational process will increase the concentration near earth by 6% over the concentration in space.

(d) F. S. Singer, University of Maryland (University of Miami) (Ref. I-15)

Singer postulates a gravitational accretion model which gives as small an effect as only a few percent to perhaps fivefold increase in concentration depending upon the assumption of the particles geocentric velocity at infinity. The increase in concentration does not continue as the earth is approached but levels off due to the "shadow effect" of the planet producing a maximum at 2000 to 3000 km above the surface. On the other hand, Singer shows that the flux (impact rate) maximum occurs somewhat lower than the maximum concentration and may be anywhere from 4 to 200 times higher than the impact rate at infinity depending again upon the assumption of particle velocity infinity.

(e) D. B. Beard, Lockheed (University of California) (Ref. I-16)

In Beard's model the geocentric particle velocity is inversely proportional to the square root of distance from the earth and the concentration is inversely propostional to the 3/2 power of distance from the earth. The flux will therefore be inversely proportional to the square of the distance from the earth. Beard assumes that the accretion begins at some 100 earth radii so that the concentration near earth will be $100^{3/2}$ or 10^3 greater than the flux at 100 radii distance from earth.

(f) E. J. Öpik (University of Maryland) (Ref. I-17)

Öpik postulates that the most likely mechanisms for the increased flux of particles near the earth are

(1) Jacobi capture of particles in especially favorable orbits of the zodiacal cloud. The particles captured in retrograde orbits of small inclination and large eccentricity. This mechanism could be distinguished from the next mechanism and the deficiency of particles near the orbital plane of the moon. The deficiency would become less pronounced and perhaps even reverse near the moon. Unfortunately Opik gives no quantitative estimates for this or the next mechanism.

(2) Particles splashed off the moon and injected into geocentric closed orbits. This mechanism would result in a majority of the particles in direct motion and at small inclination.

(g) D. C. Bradford and R. D. Dycus, North American (Ref. I-18)

The gravitational convergence model results in a flux maximum at a geocentric distance of about seven earth radii. The effect is a symmetric being greatest on the antapex side of the earth. However, the maximum variation in flux due to this mechanism is less than 20% greater than the free space flux.

(h) Shelton, Stern and Hale, NASA/MSFC

The most detailed evaluation of the gravitational accretion effect of the earth has been made by Shelton, Stern and Hale (Ref. I-19) and by Hale and Wright (Ref. I-20). They have calculated the distribution of particle flux about an attractive center as a function of the velocity (at infinity) distance from the attractive body and angle. It is shown that a monoenergetic unidirectional particle stream will give a definite pattern of flux enhancement and shadow cone of zero flux about the attractive body. For the real geometry where the free space particle flux is neither monoenergetic nor unidirectional it appears reasonable to assume that the effect will be at least very complex if not completely

"washed out." For example, Bradford & Dycus have used a measured incident velocity distribution and found the net gravitational accretion and shadow effect to produce a 20% variation about the free space condition. Southworth has indicated only a maximum effect of 6% of the free space flux.

Of the various flux falloff models, Whipple's would have the most profound effect upon sensor sizing. For the baseline orbit, sizing the sensors to an expected flux law of $R^{-1.123}$ is equivalent to sizing them to an effective flux of 3.4% of that near earth. Sizing the sensors to the Whipple flux law would be equivalent to sizing them to an effective flux of about 10^{-2}% of that near earth or about 340 times bigger. However, for the reasons given before, we tend to discount the Whipple falloff model, and note that if such an extremely rapid falloff did exist it could most easily be measured by a near earth satellite with a slightly eccentric orbit such as Pegasus.

The next most rapid falloff was the $R^{-1.66}$ of Dole. This would give an effective flux over the baseline orbit of about 1% of the near earth flux so that the required sensor area should be 3.4 times greater than on the basis of the $R^{-1.123}$ falloff.

Penetration laws. The sizing of penetration sensors is subject not only to uncertainties in the flux but also in the penetration law adopted. In the model selected (as in many other penetration laws) the penetration depth is proportional to the particle size and therefore to the cube root of particle mass.

$$N = bm^{-1.34}, \quad \frac{1}{N} \quad \alpha \text{ sensor area required}$$

$$P = K(mV)^{1/3}$$

$$\text{Sensor area required } \alpha \frac{P^{4.02}}{b(KV^{1/3})} \quad 4.02$$

For a given thickness of material, the sensor area required for a given penetration rate is inversely proportional to the flux (which should include the flux falloff factor), inversely proportional to the fourth power of the penetration scaling terms, which in this equation is made up of a constant times the cube root of velocity.

Comparing first some of the aluminum penetration laws above, we may express the design model as $\frac{P}{(m)^{1/3}} = 0.285 \text{ in.}/\text{gm}^{1/3}$. Whipple

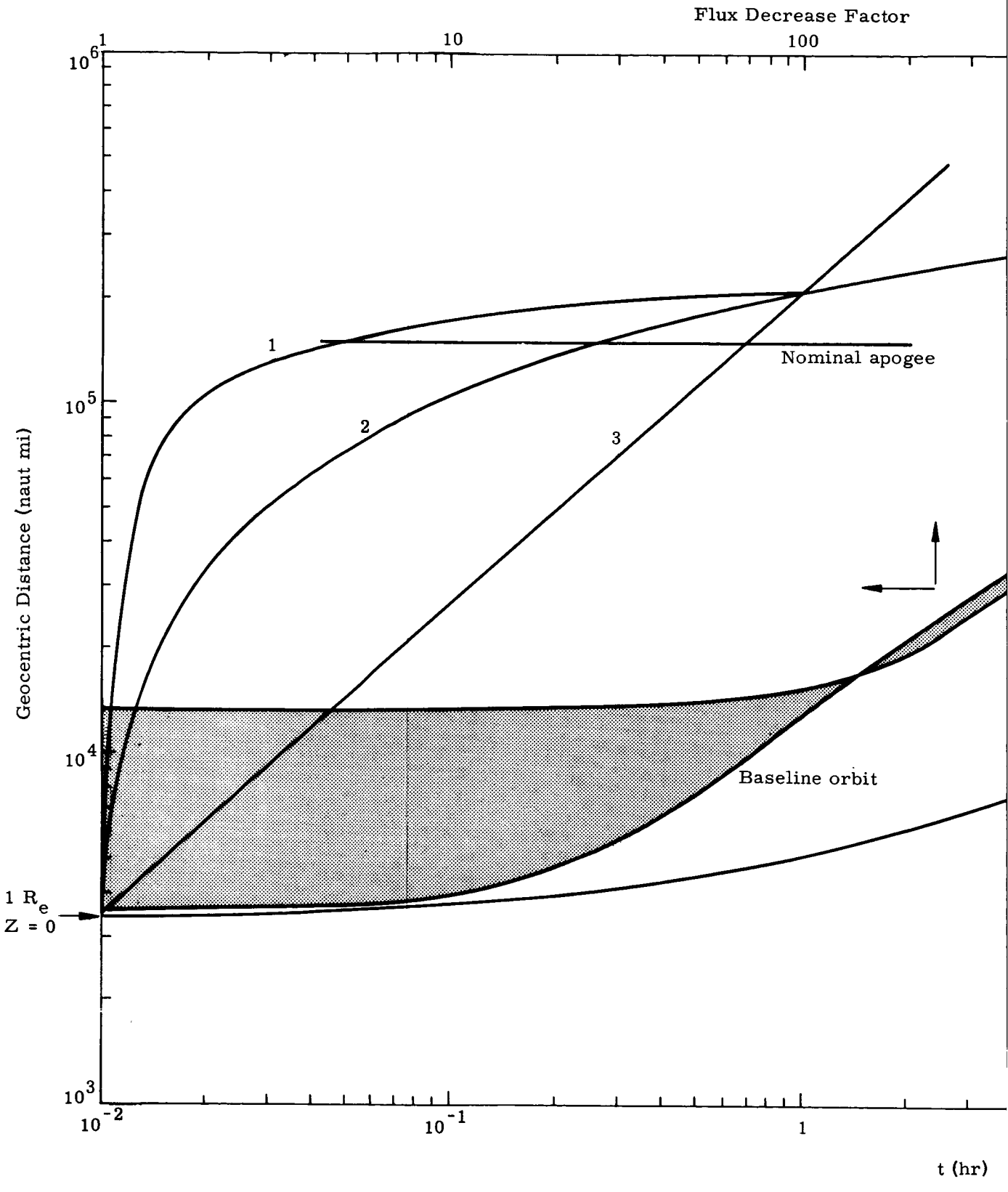
(Ref. I-11) gives a value for $P/m^{1/3}$ of 0.765 for the Herman Jones relationship, and 1.81 for the modified Bjork relationship both based upon a projectile density of 0.44 gm cm^{-3} and a velocity of 22 km sec^{-1}. The Summers penetration law with the same density and velocity would be about 1.74 in./$gm^{1/3}$. Therefore sensor areas sized to these three other penetration laws would be respectively $\left(\frac{0.765}{0.285}\right)$, $\left(\frac{1.81}{0.285}\right)$, $\left(\frac{1.74}{0.285}\right)$, or 52.7, 1660, and 1410 times smaller than areas based upon the design model. Whipple (Ref. I-11) has recently indicated 0.25 gm/cm^{-3} as a newer estimate of density. Adopting this value of density into the penetration laws would give sensor areas 13.2, 1190 and 670 times smaller than areas based upon the design model.

Generally the design model penetration law predicts less penetration than other laws. However the design model is based upon penetration data of 1-mil BeCu in the meteoroid environment, whereas the other empirical laws are based upon penetrations of semi-infinite targets with relatively massive particles, at generally much lower velocities than expected by meteoroidal particles. Applying these data to the meteoroid region implies extrapolations over at least a few orders of magnitude of mass. On that basis the Explorer XVI data must be given higher credence. The design model based upon the Explorer XVI puncture rate requires larger sensor areas than any of the other penetration laws (including a number not specifically mentioned). Therefore if this model is in error it should be expected to overestimate sensor area required and this results in more data than expected. On this basis, then, the design model is clearly conservative relative to other penetration laws.

Penetration data more nearly analogous to the meteoroid environment was obtained by Pollack, Winslow and Davison (Ref. I-21) during the test of capacitance sensors at NAA. Borosilicate glass particles ($m = 1.6 \times 10^{-7}$ gm, $\rho = 2.5$ gm/cm^{-3}) at 13.7 km/sec penetrated 2-mil stainless steel foils. Solving for K in the design model penetration law with the above values gives K = 0.154 for stainless steel or three times higher than that obtained. On the other hand, solving the Summers penetration equation for K using the above empirical data gives a value of 0.472 or 3.5 times smaller than the penetration predicted by the nominal K value of 1.67.

(2) Effects of orbit selection, injection uncertainties and orbital changes

Figure I-4 shows the envelope of perturbations that can occur around the baseline orbit. Also shown are the geocentric flux falloff curves for


Flux Decrease Factor
1
10
100
10^6
10^5
10^4
10^3
Geocentric Distance (naut mi)
1
2
3
Nominal apogee
Baseline orbit
1 R_e
Z = 0
10^{-2}
10^{-1}
1
t (hr)

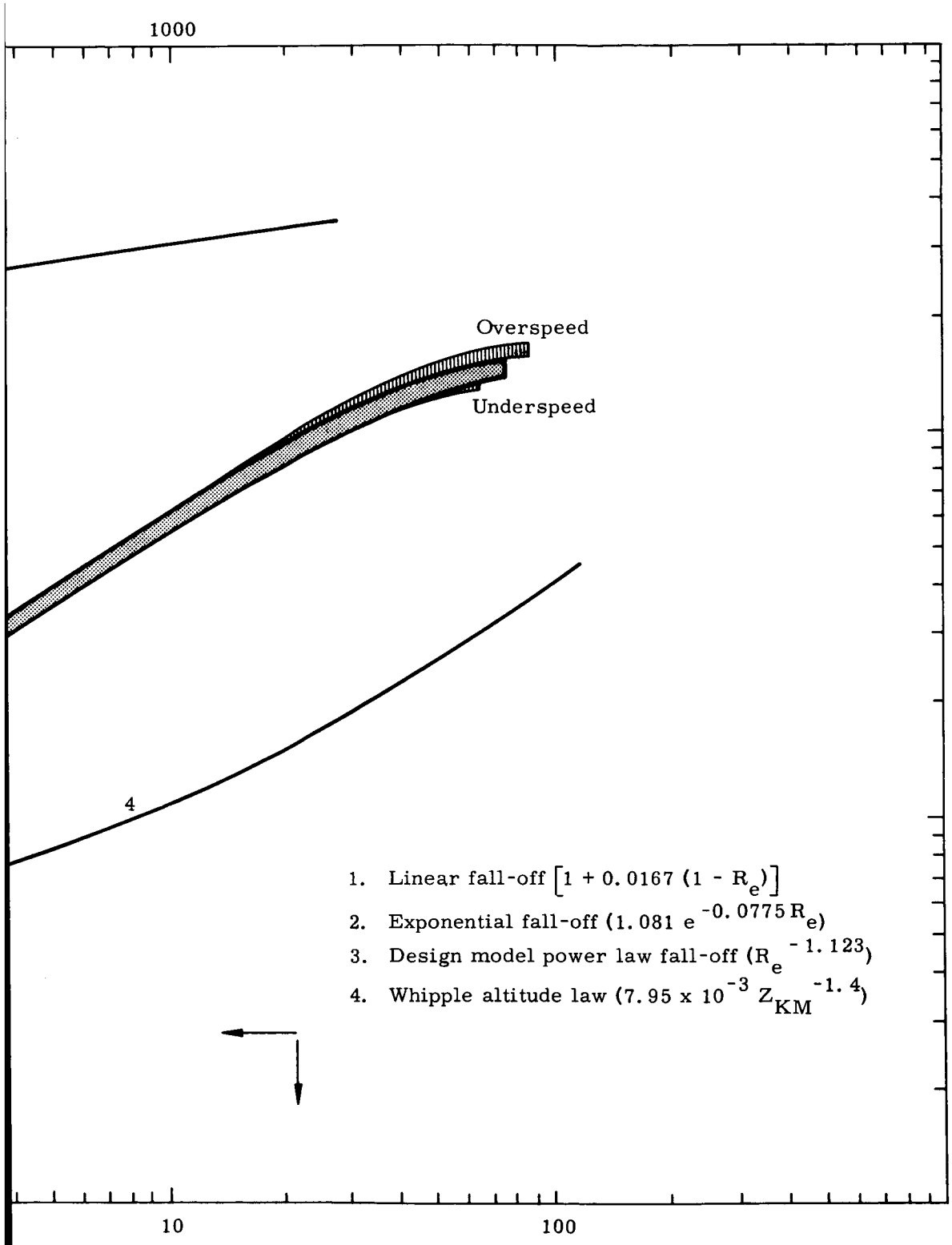


Fig. I-4. Perturbation Envelops of Baseline Orbit (nominal and ± 3 injection error) and Effect on Data Acquisition

the three cases considered and also the altitude flux falloff derived empirically by Whipple. Chapter II gives the details of the different perturbations comprising the envelope. The basic significance of the envelope is the indicated loss of data from the lowest zone. The envelope can be reduced by restricting the launch window or by decreasing apogee. The first is an operational limitation and would not affect the experiment objectives. Decreasing apogee on the other hand obviously curtails the objectives while enabling smaller sensor areas to be used because the average orbital flux will be increased. Figure I-4 of Vol. III may be used to give an indication of the range of perigee versus initial apogee. Considering only the secular effects it can be seen that apogee alittude must be reduced to about 100,000 naut mi in order to halve the perturbations on perigee altitude. This would not appear to be an efficient tradeoff.

The effect of injection inaccuracy is also shown on Fig. I-4. For the overspeed injection initial apogee will occur at an altitude of 165,000 naut mi (168,544 naut mi geocentric distance). Perigee will be perturbed (raised) within approximately the same envelope as for the baseline orbit. Apogee will perturb downward to 155,200 naut mi altitude (158,644 naut mi geocentric). The period will be approximately 180 hr.

For the underspeed injection the period will be about 128 hr. Initial perigee and perigee perturbations will be similar to the other two cases. Apogee altitude will be initially at 135,000 naut mi and decrease to 125,000 naut mi (138,444 and 128,644 naut mi geocentric).

Since the time history altitude envelope for both the over- and underspeed conditions is changed only at the lower and upper ends, it seems reasonable that only in those parts of the orbit will the sensors sized on the basis of the nominal orbit be incorrect.

Effectively, the perturbations can result in a loss of half the data in the lowest zone. The underspeed injection errors can add to this the loss of most of the data in the highest zone due to lower apogee and shorter period. The overspeed error increases the time spent in the upper two zones and increases the apogee so that although the exposure per orbit for the intermediary zones remains about the same, the different number of orbits in six months will increase the total data points in the middle zones for the underspeed condition and decrease them for the overspeed.

(3) Showers

A calendar time flux correction to account for showers has been developed (Ref. 32). Frost has eliminated the calendar considerations by means of a critical combination of sporadic and stream flux factors

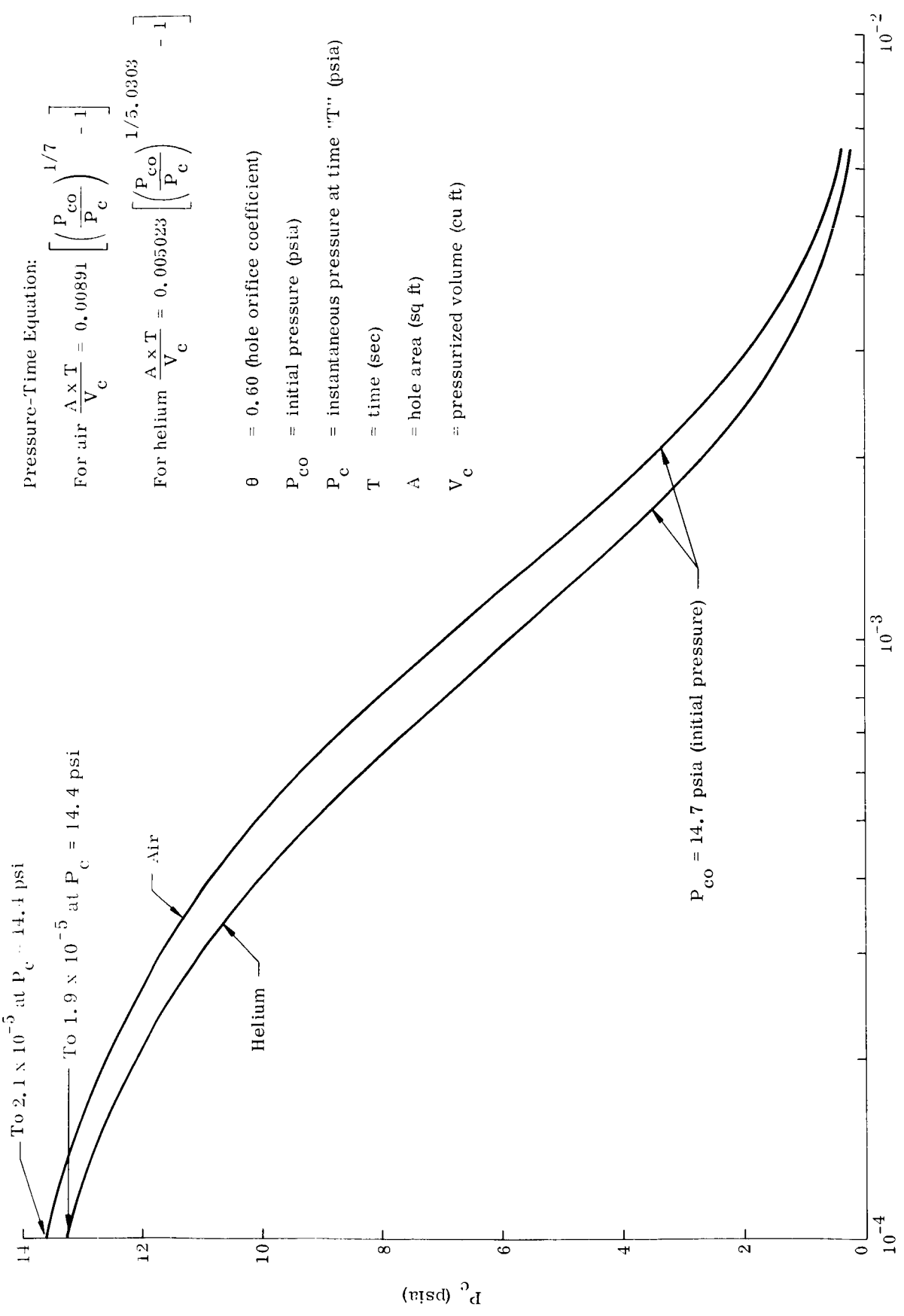


Fig. I-5. Pressure Loss Versus Time and Hole Size for Pressurized Container

(Ref. 33). The total flux at any time is a combination of the two fluxes. However the shower flux is unidirectional so only the projected area is used. For six months, the sporadic flux factor is 1.38 and the shower factor is 0.46. The total flux factor would be

$$1.38 + 0.46\left(\frac{A}{A_P}\right)$$

where A and A_P are the total and projected sensor areas. A reasonable estimate of $\frac{A}{A_P}$ is about 0.2 (0.25 for a sphere, 0.185 for the Z configuration). This gives a flux correction factor of 1.47. Increasing the anticipated flux by this factor would allow a decrease in sensor area by the same factor.

2. Sensors

The contractual work statement calls for a survey and evaluation of the availability and "state of the art" of sensors and data gathering techniques which are adequate to satisfy the objectives.

a. Sensor survey data

(1) Pressurized cell penetration detectors

Meteoroid penetration sensors using pressurized cells have been successfully used on the Explorer XVI and XXIII satellites. Consequently, this type of sensor was investigated during the study. Basic data on the operation of this type of sensor have not been included because they are well known. Qualified space-proven sensors are now within the state of the art. A qualitative comparison of this type of sensor with others is given in Table I-3. The main advantages of this sensor are its qualified status, simple verification of operating status, and retention of penetration condition. Conversely, the primary disadvantages are destruction after one penetration, high ratio of sensor elements to total sensor area, high fraction of unusable area and weight (due to curved surfaces and baroswitch assembly).

In order to more quantitatively evaluate these sensors, equations were developed for the pressure-time relationship for a pressurized cell puncture by a meteoroid. This relationship is important to the selection of sensor volume and the number of baroswitches required for a given exposed area of sensors.

Figure I-5 presents the pressure drop for air and helium as related to hole size, time, and volume of container. The initial pressure was

TABLE I-3

Sensors in Developmental or Qualified Status

Sensor	Status	Area: Weight (ft^2 lb^{-1})	Area: Volume (ft^{-1})	Favorable Features	Unfavorable Features	Response	Environmental Qualifications	Remarks and Suggestions for Modifications
Pressurized Cell Penetration Detectors								
Pressurized Semi-cylinder	Flown on Explorer XIII, XVI, XXIII	0.71	7.9	1 3b 4 5 6 8	1 3 5b, d, f 7	Unloaded pressure transducer opens microswitch.	Scout payload requirements also 12 sensors tested over 6600 cycles of pressure from 14 to 34 psi (Exp XIII). Ten sensors over 2000 cycles of temperature from 260° to -10° F (Exp XIII).	
Concept 1: End mounted full cylinders (Fig. I-7)	Conceptual	3.5	Same	Same + 7	Same - 7	Same		Increase sensor area and area-to-weight ratio by using pressure supported full cylinders.
Concept 2: Large interconnected cell pressurized honeycomb (Fig. I-9)	Conceptual	3.7	Increase	Same	Same	Same		Increase sensor area, area-to-weight and volume-to-weight ratios using pressurized honeycomb.
Concept 3: Use barometer instead of baroswitch	Conceptual	--	--	+3a -3b	+2 -3	Pressure time history		Relate penetration to hole size.
Capacitor Circuit Penetration Detectors	Stainless steel target gage segments flown on SI and Explorer XXIII							
Pegasus Foam Mounted (typical of capacitor sensors; foam mounting is, however, peculiar to Pegasus) aluminum target plate, 180 μin. glue, 1/4- to 1/2-mil Mylar, one to three ply, 30 μin. vapor deposited copper, 1/4-in. flexible foam, 1/2-in. rigid foam, 1/4-in. flexible foam, 30 μin. copper, etc.	Qualified for flight	3.28*	24*	2 4 7	2 3 5a 6b 8a, b	Discharge-recharge pulse of capacitor.	Saturn I payload requirements.	
Aluminized Mylar Multicapacitor. 5 layers of 1/2-mil Mylar plus 2500 Å aluminum plus glue	Flown on Rogallo kite last summer	54.2	--	2 3a, b 4 7	2 5e 6b 8a	Same	Paraglider and Aerobee payload requirements	
Lewis Research Center Double-Faced Capacitor (see Fig. I-10)	Laboratory proven; no work currently in progress	~3 x Pegasus	~24	2 4 7	2 3 5a** 6b	Same		

Thin Film Capacitors	Flown as part of OGO and Mariner meteoroid instruments	Increase	--	2 4	8a 2 3 6b			Nontarget materials greatly decreased in thickness; increase to large sensor sizes appears practical, spurious initiation of primary response by space radiation should be reduced.
Printed Circuit Penetration Detectors								
Stainless Steel over Gold Grid. 1-, 3- or 6-mil stainless steel, 1- to 1/4-mil Mylar with adhesive on both sides, 60 to 90 μin. gold foil, 2-mil lines and 2-mil spacing, 1/32-in. silicone rubber or 1/8-in. urethane foam backing.	Flown on Explorers XIII and XVI			1 3b 8	1 3 4a, b 5a, c 6a 7	Particle penetration breaks grid and opens circuit.	Scout payload requirements also. Thermal vacuum test of seven sensors. Two failed at 300° F and approximately 10^{-4} mm Hg. Flight packages exposed to 10^{-6} mm and temperature cycle of -50° to 150° F for 200 hours (50 cycles). Flight assemblies vibrated at 50 to 2000 cps, peak amplitude ≤ 10 g at 2 to 4 octaves/minute and lasting from 0.5 to 3 minutes.	Individual sensor areas may be increased to 1 ft^2. Thinner thermal coatings may be easily substituted.
Concept 1: Chemically milled interdigitated grid	Conceptual			2 6	2 3 5a	Particle penetration momentarily "makes" circuit.		Significance of categories 4, 7 and 8 features unknown.
Light Sensitive Penetration Detectors								
Cadmium Sulfide Cells	Flown on Explorers XIII, XVI, and XXIII	--	0.008 - 0.06	See remarks column. 3a 6 8	4a, b 5e 7 9	Cell resistance decreases with area of holes in opaque surface (photoresistive effect).	Scout payload requirements also. Cells tested to 100° C. Limiting temperature is indium melting point. No low temperature limits. Failure of one cell on Explorer XVI attributed to thermal cycling of telemeter.	Sensor is not destroyed and response is stored but available only when sun lines up with detector. Easily modified to use engineering material as target.
Infrared Detectors	Developmental	~200	~25	2 4 5	2 3, 4a 8a	Near infrared portion of penetration EMP.	Sensors qualified to Sidewinder requirements.	Proportionally responding (α to incident KE) sensor may be possible.

TABLE I-3 (continued)

Sensor	Status	Area: Weight (ft^2 lb^{-1})	Area: Volume (ft^{-1})	Favorable Features	Unfavorable Features	Response	Environmental Qualifications	Remarks and Suggestions for Modifications
Impact Transducer Momentum Detectors	Flown on Explorers V-2 and up							
Langley Microphone and Sounding Board	Flown on Explorers XIII and XVI	1.6***	--	2 3a 6	2 7 8a, b	Output of piezoelectric element.	Scout payload requirements.	Larger area sensors have been made.
Photomultipliers	Flown on various rockets	--	--	2 3a 6	5e 7 8a, b	EMP from penetration particle liberates photoelectrons, from cathode, which are multiplied and detected.		
Others and combinations								
Velocity Tube	Flown on OGO	5.5×10^{-3}	7.4×10^{-2}	2 3a 8 9a, b	2 4a, b 5e 6b 7 9	Pulse of ions from penetration of thin film starts timing, capacitor discharge downstream stops timing of time of flight. Penetration of capacitor gives proportional signal (α KE). Output of piezoelectric element gives proportional signal (α momentum).	OGO-1 payload requirements.	Feature 8 achieved partially by coincidence.
Mariner Gage	Flown on Mariner	1.80	--	2 3a 6 (mike) 8	2 5e 6b (capacitor)	Output of piezoelectric (barium titanate) element gives proportional (to momentum) response. Output of thin film capacitor discharge indicates which side of sounding board has been hit.	Mariner C requirements.	Feature 8 achieved partially by coincidence. Potential exists for favorable features 9a, b by analysis of capacitor output which may be proportional to KE. Therefore, particle mass may also be derived
Ceramic Beam plus Cadmium Sulfide	Qualified for PIQSY	0.07	1.5	1 (CdS) 2 3a 4 (spin) 6 8	2 4a, b (CdS) 5e 7	See impact momentum transducer and cadmium sulfide cell.	PIQSY requirements.	Ceramic beam uses dummy detector coincidence for noise rejection.

Ballistic Pendulum and Velocity Sensor	Developmental	--	--	9a, b? 2 3a 4 8 9a, b	9 2 6b	Time of flight measurement as in Velocity Tube plus measurement of x-y deflection of restrained pendulum mass via attached light source.	OSO-F requirements.	Spurious response partially rejected by coincidence.

NOTES:

*For 1-mil target; 55% of weight is in 1-in. foam.
**Particularly for configurations b and c of Fig. I-10.
***Depends upon sensitivity.

KEY TO NUMBERING OF FEATURES

Favorable Features	Unfavorable Features	Favorable Features	Unfavorable Features
1. Response is "stored" so that sensor need not be continuously monitored.	1. Sensor destroyed by particle.		8b. Nonsensor components may be significant in spurious response initiation.
2. Sensor not destroyed by particle but capable of repeated sensing.	2. Sensor must be active and monitored continuously as response is very short-lived.	9a. More than one property of particle measured within same instrument. 9b. Additional properties derivable.	9. Supporting measurements such as attitude, solar aspect, spacecraft velocity required for full interpretation of measurements.
3a. Sensor output is proportional to property of particle. 3b. Sensor outputs may be strung together into one primary output detector and read in steps.	3. Sensor output indicates only that threshold property has been reached or exceeded.		
4. Sensor response is independent of environmental effects.	4a. Sensor response must be corrected for environmental effects. 4b. These environmental effects require additional instrumentation or compensation.		
5. Penetration of target alone initiates response.	5a. Penetration of significant thickness of nontarget material required to provide response. 5b. Loading on target may give it different penetration properties than if unloaded. 5c. Thermal coatings may significantly alter penetration properties of target. 5d. Limitation on target materials that may be used. 5e. Nonengineering target material.		
6. Simple and repeatable nondestructive checkout of sensor primary response.	6a. Sensor primary response cannot be checkout out without destruction. 6b. Repeatable but difficult.		
7. Individual sensors larger than 1 sq ft.	7. Individual sensors smaller than 0.1 sq ft.		
8. No known spurious mechanism for initiation of primary response (excluding mechanical failure).	8a. Spurious initiation of primary response possible and discrimination or coincidence logic may be required.		

assumed as 14.7 psia. Similar curves for higher initial pressures can be readily developed from the equations.

Figure I-6 shows the pressure-time relation for meteoroid penetration of beryllium-copper and stainless steel targets. The relation is based on the hole size caused by a meteoroid that will just penetrate the specified target thickness. The length of time required for the pressure to be reduced to a value that activates the sensing device is most important if the spacecraft position and attitude are to be determined at the exact time of meteoroid penetration. It is apparent that for sensors of 1/2- to 2-mil BeCu, or 1- to 4-mil aluminum sensing delays of the order of 1000 sec must be expected.

It is to be noted that aluminum foil of thickness less than a few thousandths of an inch is not suitable for pressurized sensors since the material contains microscopic holes and therefore the initial pressure levels cannot be maintained.

Two different designs of pressurized sensors were considered. The first design consists of a long cylindrical tube mounted in a structural frame. Approximately 450 of these tubes of 1/2- and 1-mil BeCu or stainless steel mounted in panels would be needed to obtain the required number of data for the Atlas-Agena vehicle. A proposed design is shown in Fig. I-7. A preliminary stress analysis of pressurized tubes subjected to 15 g loading normal to the axis of the tube was made. It was found that the very thin wall tubes of beryllium-copper must be pressure-stabilized (in excess of atmosphere pressure) to prevent buckling due to bending under 15 g as indicated in Fig. I-8. The vibration frequency of 2-in. diameter tubes was also calculated.

Since it was desirable to maintain a 1-in. overall thickness for the sensor panels, the idea of using a pressurized sandwich sensor panel was conceived. The design is shown in Fig. I-9. The target faces of beryllium-copper are bonded to an aluminum core and the edge members to form a panel 12 in. by 36 in. The honeycomb cells have large holes in their walls to allow free flow of the pressurizing gas when a meteoroid penetrates the target. A pressurized sensing device would be located inside the panel to sense the pressure drop. A hundred of these panels would provide sufficient area to obtain the desired number of data at 1/2- and 1-mil of BeCu.

Of the two concepts, the pressurized sandwich panel appears to be better suited for the large area of sensor panels than the pressurized tube design.

See analysis of pressurized sensors in Appendix I-1.

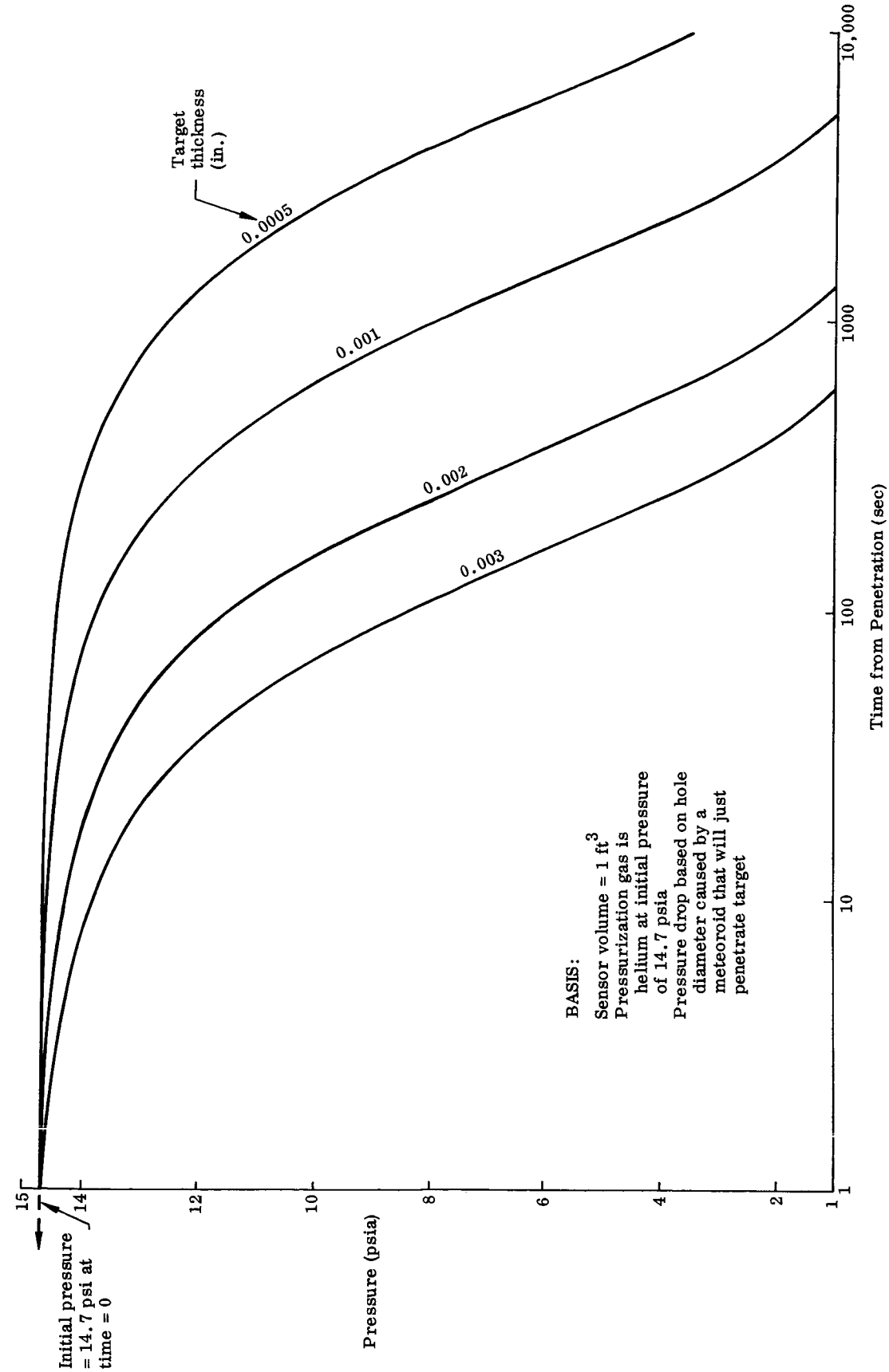


Fig. I-6. Pressure Decrease with Time from Penetration

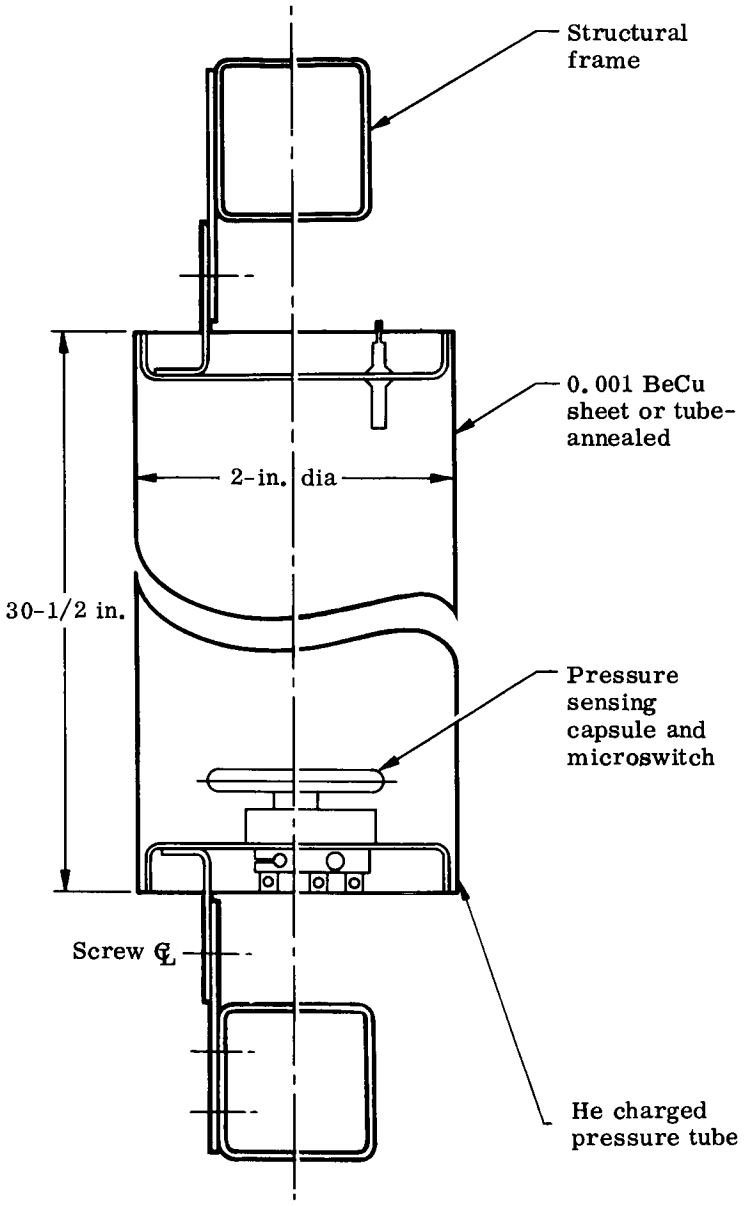


Fig. I-7. Pressurized Sensor--Cylindrical Tube Design

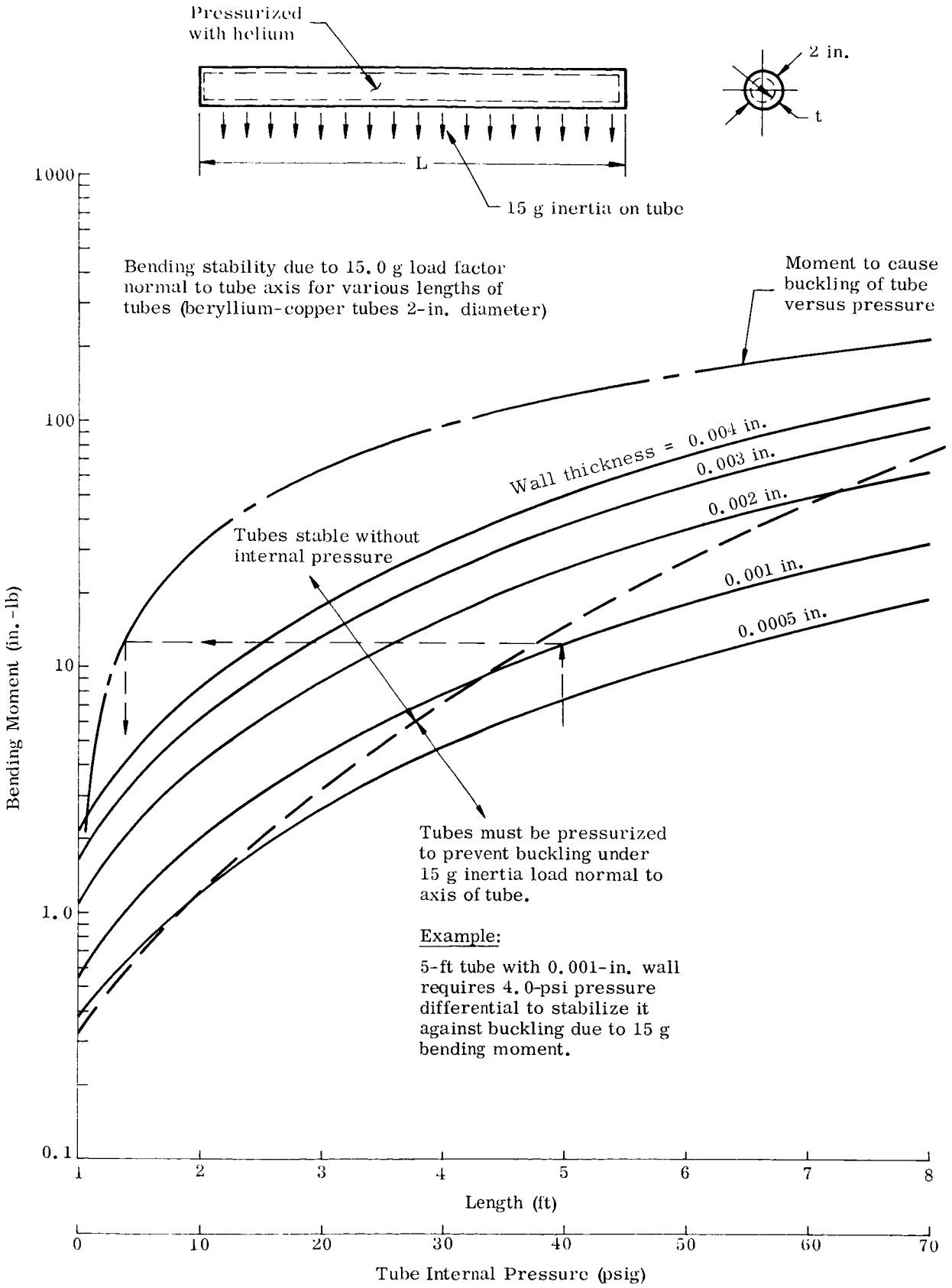


Fig. I-8. Pressurized Tube Sensors

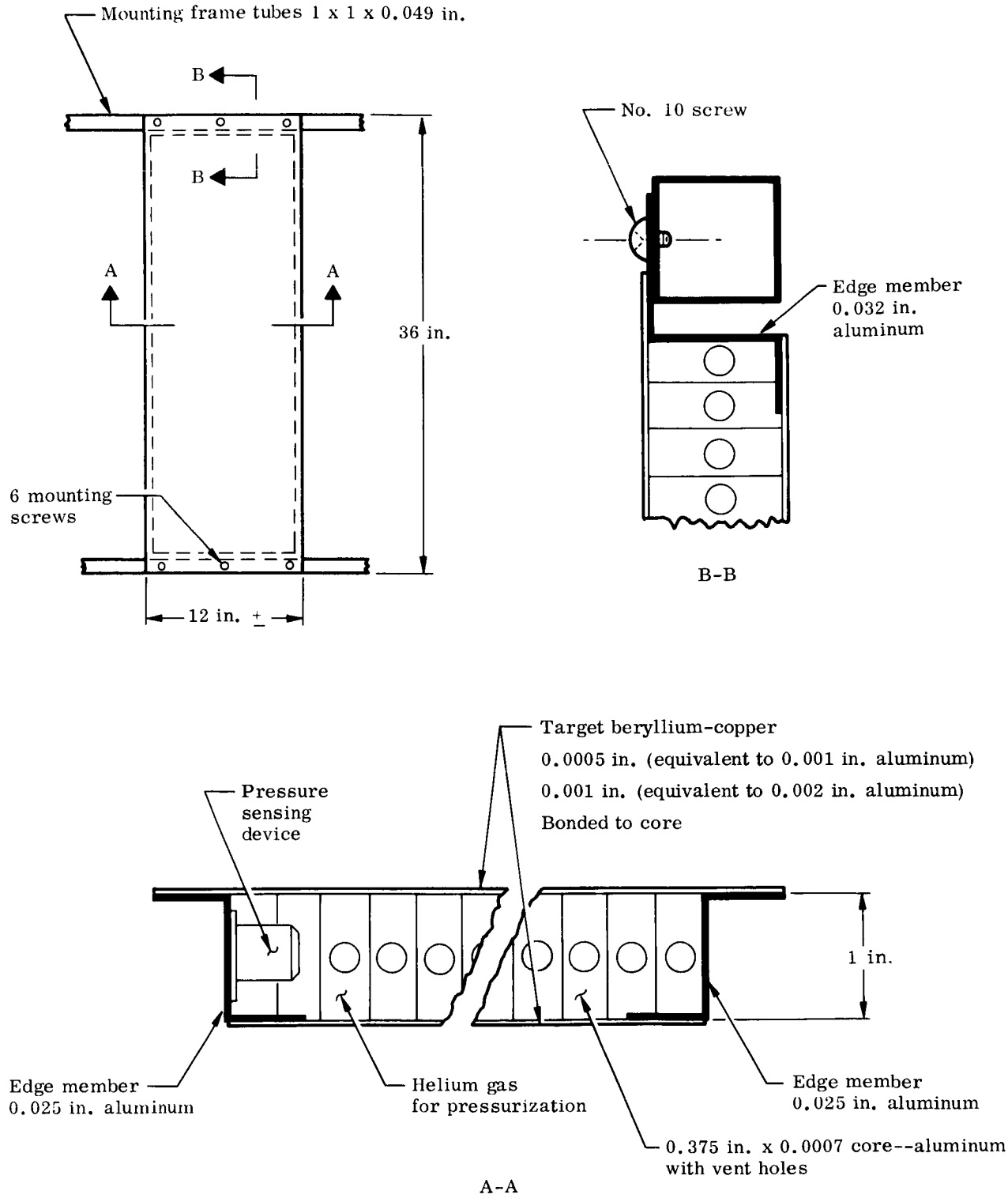


Fig. I-9. Pressurized Sandwich Sensor Panel Typical Panel

(2) Capacitor circuit penetration detectors

Types. A number of different sensor configurations are under development. The sensors to be flown on Pegasus consist of an aluminum target plate to which is bonded a three-ply Mylar sandwich as the dielectric. A vacuum deposition of copper to the exposed Mylar surface serves as the second plate of the capacitor. Previously, single sheet Mylar was used as the dielectric,and gold foil was used by the Fairchild Company early in the program as the second capacitor plate. A sensor of this basic concept has been flown mounted on the side of an early (nonorbiting) Saturn. Two sections of capacitor detectors with 1-mil stainless steel target plates were installed on the S55C, launched recently as Explorer XXIII. Currently, the Pegasus sensor configuration consists of a capacitor panel bonded to each side of a 1-in. foam core sandwich. The core prevents a micrometeoroid puncture of one panel from discharging the opposite panel. Core density was fixed at 4 lb/cu ft and core thickness at 1 in. A hard closed cell foam core was used initially. Heating one side of the unit to 250° F while keeping the other side at room temperature caused the unit to warp. The problem was eliminated by bonding a 5/16-in. sheet of soft open cell foam to each side of a 1/2-in. hard foam core. This core's average density is near 4 lb/cu ft.

Another capacitor sensor configuration is the multi-capacitor made up of a series of aluminized Mylar foils laminated together. Two hundred sq ft of this type of sensor attached to the top and bottom surfaces of the web (wing) of a Rogallo Kite as flown last summer as an Aerobee payload from WSPG. The experiment was to be launched during a meteor shower, spend about 5 min above 400,000 ft, and to be recovered.

A double faced capacitor sensor has been developed at Lewis Research Center in three different versions as shown in Fig. I-10. Although a fairly extensive developmental test program was undertaken, this configuration has not subsequently been used on any spacecraft and is not currently under development.

Another type of capacitor sensor configuration consists of sputtered or vapor deposited dielectric and conductors. Dielectrics of SiO_2 and MgO have been used. One variation has used anodic film formed upon aluminum as the dielectric. A few square inches of capacitor made up of glass sputtered between thin films of aluminum have been flown on OGO and Mariner '64, but not as penetration sensors.

State of the art. Capacitance penetration sensor state of the art was summarized in the final report dated 11/9/64 from the G.T. Schjeldahl Company to the Martin Company. The following is taken from Section IV of the G. T. Schjeldahl Company report.

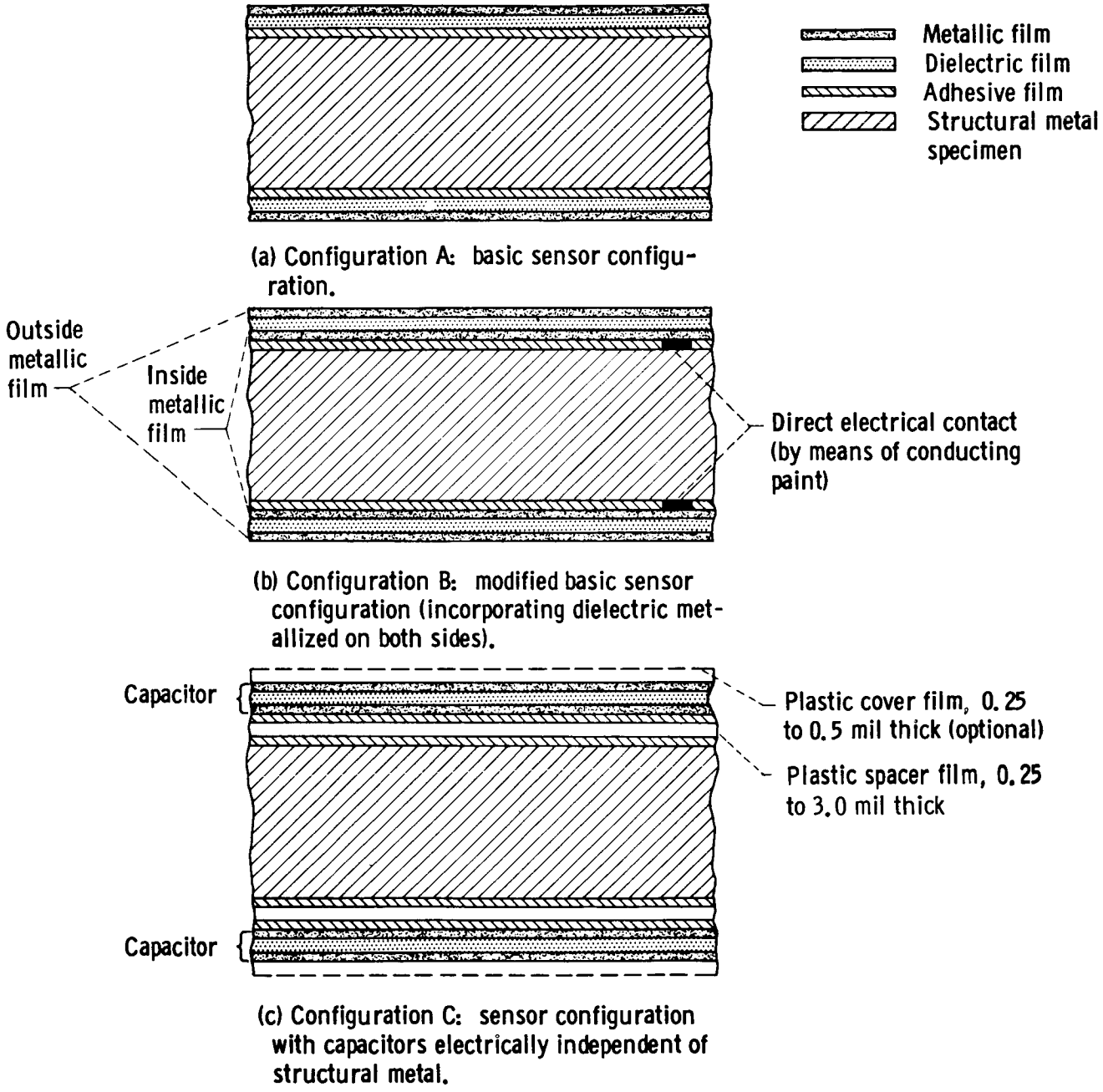


Fig. I-10. Various Configurations of Double Capacitor Coincidence Discharge Type Micrometeoroid Penetration Sensor Developed at Lewis Research Center

Early capacitance type micrometeoroid sensors were made of aluminized Mylar laminated to a target sheet. During lamination, stretching of the Mylar fractured the aluminizing, creating electrically isolated islands of aluminizing. It was also felt that pressure type electrical contacts to the aluminizing would be unreliable. The island problem was solved by first laminating plain Mylar to the target sheet, then vacuum depositing a conductor over the Mylar. The contact problem was solved by using vapor deposited copper rather than aluminum. It proved possible to solder electrical contacts to the copper without destroying the dielectric.

It was required that the copper be 25 ± 8 μin. thick and that it pass a scotch tape adhesion test. The thickness must be great enough to provide conductivity and thin enough to allow burnout on a "hit." Initially, it was thought that a capacitor with copper failing the tape test would delaminate easily from the core to which it was bonded. This has been shown to be untrue. Contact resistance is measured between the lead soldered to the copper and an aluminum foil electrode pressed against the copper in the neighborhood of the lead. The value measured is required to be less than 0.1 ohm. It is usually near 0.01 ohm. Sheet resistance of the copper across the length of the panel (40 in.) is found by subtracting the previous reading from that obtained when the aluminum foil electrode is set 40 in. from the contact. Sheet resistance is required to be less than 0.5 ohm. It is usually about 0.1 ohm. The state of oxidation of the copper surface appears to be of "cosmetic" importance only.

A capacitor having a 1/2-mil Mylar dielectric will be found to be electrically shorted right after fabrication. This shorting is associated with point defects in the Mylar. A low voltage (heavy current) applied across (through) the capacitor will heal the worst weak points. The mechanism of this healing process has not been identified. It may involve melting the Mylar at a weak point. As successively higher voltages are applied new shorts appear which, immediately after appearance, are healed by the short term--heavy current flow through the weak point. At the higher voltages, discharge of the capacitor through a weak point vaporizes the copper in the immediate vicinity of the weak point. The Mylar exposed apparently serves as an additional healing mechanism in that it physically isolates the copper conductor from the spot where the short occurred. The exposed Mylar is apparently uncharred.

Upon raising the voltage to a new level a sequence of healing bursts is heard, the time between individual bursts becoming greater, the longer one leaves the voltage on the capacitor. Capacitors presently being made will have 40 volts applied to them when deployed in space. When healing weak points on such capacitors, the maximum applied voltage is 250 volts. It is held at this value for 10 min. The clearing procedure is done in air at room temperature.

The insulation resistance, measured at 100 volts, of a cleared 1/2-mil single sheet Mylar dielectric capacitor is much less than that inferred from the literature values for bulk Mylar. It also decreases sharply with increasing temperature and, at a given temperature, varies erratically with time. Electrical requirements put on a 20-in. by 40-in. capacitor made with such a dielectric were that it exhibit greater than 1-megohm insulation resistance at 250° F in vacuum over a 30-min period. It was difficult to fill this requirement consistently with a single sheet Mylar dielectric. A trilaminate dielectric consisting of three layers of 0.15-mil Mylar laminated together was developed. It consistently meets the insulation resistance specification; it shows much less erratic variation of insulation resistance with time; it exhibits far fewer weak points during the clearing procedure. The capacitance of a 20- by 40-in. panel after thermal vacuum testing is about 1.0 microfarad.

An amorphous phosphate thermal balance layer is applied to that side of a capacitor target plate facing space. Requirements on this layer are that it exhibit an $E \geq 0.45$ and an $A/E \leq 1.05$ where A is the coating's solar absorptance and E its room temperature thermal emittance as measured by a Gier Dunkle mobile solar reflectometer and a Lion model 25-B emissometer, respectively. A calorimetric determination under vacuum yields a somewhat lower A/E. The latter is considered more nearly correct. Apparently a true $A/E \leq 1.0$ is required. A capacitor panel facing the sun for an extended period of time and backed by a perfect insulator would come to an equilibrium temperature of 247° F ($A/E = 1.0$). Satellite tumbling tends to reduce this temperature. No doubt the worst case considered above is the reason for measuring a capacitor's insulation resistance at 250° F.

The A/E of the amorphous phosphate apparently degrades somewhat at elevated temperatures ($\geq$ 250° F). For this reason, the coating is applied after the vacuum deposition. A layer of adhesive painted over the copper protects the copper during application of the thermal balance layer. A final check on a capacitor's A/E is made after it has undergone its last thermal vacuum test.

Reliability considerations. A procedure for healing electrical weak points in a capacitor's dielectric was described above. The procedure is carried out right after copper deposition. Basic to the procedure is the application of 250 volts across the capacitor for a 10-min period, the capacitor being at room temperature. Points which become weak enough in this 10-min period to discharge the capacitor are healed. Discharges have been seen throughout the 10-min period, but most occur almost immediately after application of the voltage. The fact that all weak points do not heal at the initial application of voltage means that there is a process going on which can convert a potential weak

point into an actual one. The final thermal vacuum test applies 100 volts across a capacitor heated to 250° F for an hour. Deployed capacitors will have 40 volts across them for up to a year. Not many micrometeoroid punctures are recorded in a year so that only a few weak points discharging can influence the data significantly. It is felt that after deployment the electronics should allow for increasing the voltage applied to a capacitor from 40 to 150 volts for several minutes a day to eliminate potential weak points. Discharges recorded during this period of high voltage are not counted as punctures.

In work for NASA Langley on 6- by 9-in. capacitors, the clearing procedure was carried out after soldering an electrical contact to the copper surface. The copper surface was charged via this contact. In no case was the contact damaged due to heavy current flow through the contact upon application of an initially low voltage to the shorted capacitor. Hence it also appears feasible to clear weak points which may have originated prior to and during deployment and which are of the type which can only be cleared by supplying a relatively high current to the capacitor at a relatively low voltage.

Radiation effects. Effort has been under way at a number of locations over the past 18 months to evaluate the transient space radiation effects upon capacitor sensors. Various configurations of sensors have been tested in the presence of high fluxes of electrons to determine the qualitative and quantitative characteristics of capacitor pulses that resulted from buildup and subsequent discharge of primary and secondary electrons.

Certain of the results have given qualitative guides to changing sensor configuration to minimize radiation induced pulse frequency and/or amplitude. Grounding of the target plate as opposed to grounding of the back plate of the capacitor reduced frequency and amplitude of pulses. The presence of a metal backing plate behind the rear capacitor plate (but electrically insulated) affected the pulse amplitude and frequency (Ref. I-22) with a pulse resulting about once per 5×10^{11} e cm^2 from incident electrons at 150 to 200 Kev. The target plate was only 1-mil so that none of the primary electrons were extinguished in the capacitor itself. In tests run at LTV (Ref. I-23) using Pegasus sensors and circuitry, 5000 radiation induced pulses (~0.1v) were measured. The discriminator (-10v) rejected these 100%. It would therefore appear that spurious signal pulses in the capacitor could be obviated by increasing the voltage across the plates and setting a sufficiently high bias setting for signal processing. Some general trends observed were that a flux approximately 2×10^{13} electrons cm^{-2} were required per pulse at room temperature. At -200° F, a pulse occurred for approximately every 2×10^{11} e cm^{-2}. At -200° F, the pulse rate varied over

a factor of three as incident energy was increased from 0.2 to 2.0 Mev. The pulse rate was relatively independent of the flux and only a function of the total number of particles. A size-to-pulse amplitude relationship was noted during tests of the gold foil (Fairchild) sensor configuration. The pulse rate of an 8- x 8-in. sensor was almost identical to that of an 8- x 4-in. sensor; however, in the sample of 200 pulses, the average pulse height for the 8- x 8-in. sensor was 4 volts compared to less than 2 volts for the smaller sensor area. The larger sensor had two pulses of 14 volts while the smaller sensor had a maximum amplitude pulse of 8 volts. Therefore a 10-volt discriminator would be inadequate. It is noted that for the actual Pegasus sensors (20 x 40 in.) the radiation pulses might therefore be quite large. It is also noted that added capacitance tends to decrease the radiation induced pulse height, so that, in particular, where sensors are parallel the amplitudes may be reduced. However, the experiments at Lewis Research Center have shown that increasing the capacitance also significantly decreases the pulse amplitude from a penetrating meteoroid (Ref. I-21).

Recent tests at LTV made on the latest configuration sensor (10- x 10-in., 8-mil Al target, Mylar dielectric with copper backing) resulted in a radiation induced pulse rate 10 times lower than observed previously. The improvement was subsequently attributed to the use of a 3-ply Mylar sandwich as the dielectric. Previous measurements had indicated two types of radiation induced discharges and led to an integrating discrimination technique to reject one type. That is most of the pulses were fast (of the order of μsec). Since particle discharge pulses were slower, discrimination could be based upon the pulse waveform plus the amplitude. However, some of the radiation induced pulses were "slow" (of the order of msec) and similar in waveform to penetrating particle pulses. These would be more difficult to reject.

The latest tests showed that from 1 to 10% of the radiation induced pulses were of the slow variety. However, none were larger than about four volts. Maximum "slow" pulse amplitude appeared to be only a function of electron beam diameter and not of detector size as indicated in the earlier tests.

It should be noted that any significance of space radiation effects is considerably smaller in a highly eccentric orbit because of the relatively short time spent in high flux regions. Maximum particle fluxes are about 10^{8} cm^{-2}/sec above 40 Kev, or about 10^{13} cm^{-2}/day. Since only about 2 to 3% (0.1 to 0.2 days) of an orbit is spent in the Van Allen regions, the incident flux should not exceed 2×10^{12} cm^{-2} and more likely would not exceed 2×10^{11} cm^{-2}. This would result in no more than about 0.1 slow pulses for each perigee pass.

Developmental capacitor sensors. Thin film capacitors have been developed which are attractive in that the dielectric thickness can be decreased to comprise a much smaller fraction of the target plate thickness. Thus penetration is more nearly representative of the target material alone. The thickness of the Mylar dielectric used has been, generally, about 0.1 to 0.45 mil. This plus the glue is a significant total relative to a 1.0- or 2.0-mil target plate. The thin film sensors also eliminate the glue and should have less tendency to delaminate upon penetration. The dielectrics used are nonorganic and may be less susceptible to charge accumulation from space radiation and subsequent discharge. Also being simpler molecules they will be less susceptible to actual radiation damage. They may also be better heat conductors so that the thermal gradient through the sensor will be less. Capacitors have been made up of aluminum vapor deposited on both sides of anodic film of aluminum oxide; vapor deposition of copper on an anodized surface of an aluminum target plate, and all-sputtered sensors of aluminum, glass and aluminum. The small capacitor sensors used by GSFC on the Mariner and OGO sensors are of this type as will be the sensor used with the NASA/MSC ballistic pendulum. These have not been used as penetration sensors per se. However, the Schjeldahl Company is developing a large area sputtered (MgO) dielectric sensor for use as a penetration gage.

Multilayer sensor analysis. One of the sensor concepts that was investigated during the study was a multilayer type as shown in Fig. I-11. Four layers of 0.0005-in. aluminum are separated by layers of 0.00025-in. Mylar and are electrically wired to measure meteoroid penetration into cork layers. There are two sets of the four layers in order to record impacts from either direction.

The concept of the multilayer sensor is that it would give penetration data through a range of thickness from 0.0005 in. to 4 x 0.005 = 0.002 in. while having about the same weight as single layer target of 0.002 in.

Since the first layer of 0.0005 in. is backed up by the other layers, it will act as a semi-infinite target to a meteoroid just capable of penetrating a thin sheet of 0.0005-in. aluminum. Thus, the analysis was based on treating the multilayer sensor as a semi-infinite target and using the corresponding penetration equation. This is not fully correct in that a meteoroid capable of penetrating a single layer target of 0.002 in. most likely could just as readily puncture four layers of 0.0005 in. Nevertheless, for the analysis, the semi-infinite penetration equation was used to give a consistent approach.

The penetration equation was based on that which was developed as the design model for thin targets which was multiplied by 1.5 to obtain penetrations into a semi-infinite target as given in the analysis in Table

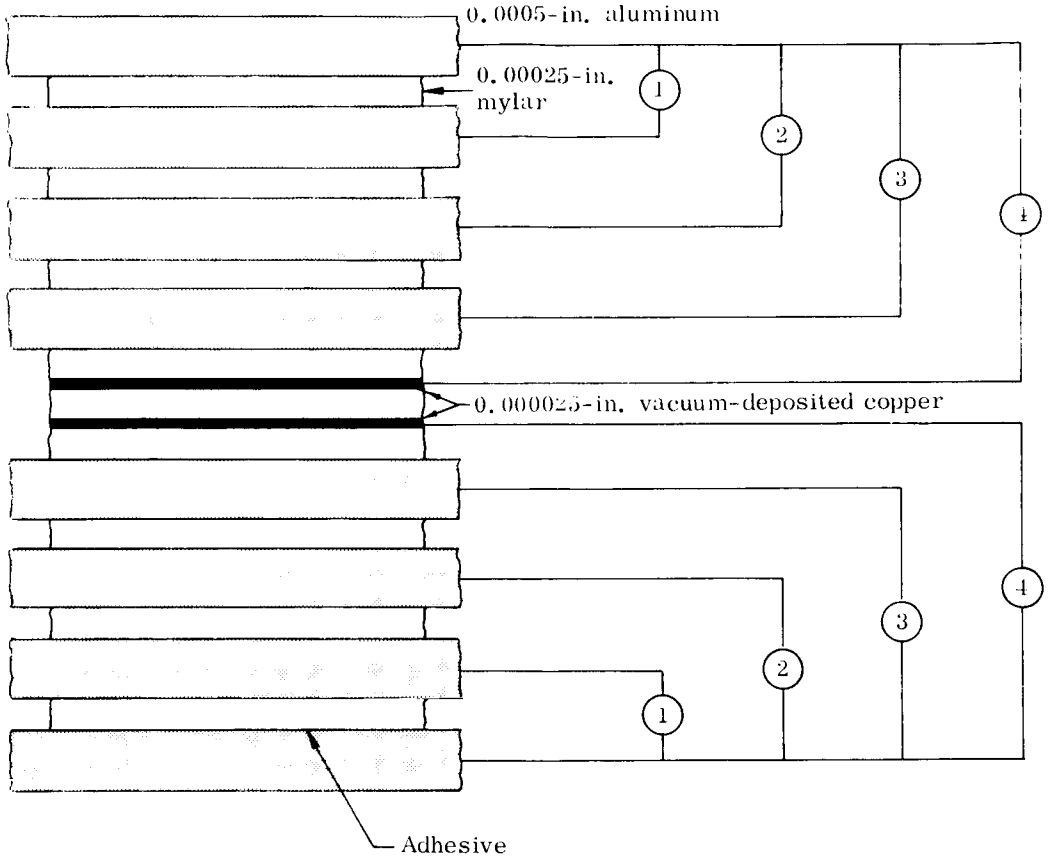


Fig. I-11. Penetration into Multilayer Sensors

I-4. The results in Table I-4 are plotted in Fig. I-12. By using the values of total penetrations in one year in Fig. I-13, it was possible to find the penetration depth of the multilayer sensor and the thin plate penetration and the corresponding penetrations to be expected in a square foot for cislunar trajectory. Table I-5 presents a summary of the expected penetration rates.

Results of this analysis indicate that a multilayer sensor (if feasible) would provide a means of detaining additional data from a given exposed surface. The sensor would be designed as a semi-infinite target with sufficient laminations to enable it to still act as a target for the deepest penetration anticipated. Table I-5 indicates the increased effective sheet thickness due to backup which must be considered in selecting laminate gages. Such a sensor would facilitate allowance for various meteoroid flux and penetration models and would be particularly applicable when the satellite was sensor-area critical. The depth of penetration might provide a means of obtaining data on the kinetic energy of the penetrating micrometeoroids. But, the behavior of the multilayer sensor under hypervelocity impact is not known and extensive experimental testing would be required to establish it. Comparative evaluation in space would also be necessary. Analysis of this concept was not carried any further but the idea of obtaining additional data from the same surface area is further explored in "Bumper-Type Sensors" which follows.

Bumper-type capacitor sensor. A bumper-type capacitor would yield additional data about meteoroid penetrations and bumper effectivity without increasing the sensor area. Four separated capacitors are mounted back-to-back in each panel with the thicker target outermost. The capacitor sensors consist of an aluminum target, Mylar dielectric and vacuum deposited copper. The meteoroids would impact on either of the outside sensors depending on their direction, giving penetration data in a single thin target. Penetration of the inner capacitor by a meteoroid would measure meteoroid penetration in spaced thin sheets with the first layer acting as a bumper for the second and breaking up.

One study version of the Atlas-Agena configuration provided 530 ft^2 of 0.002-in. aluminum target. This target area and thickness can be used to evaluate a bumper design. The 0.002-in. aluminum primary target would be penetrated about 265 times in a one-year period (based on a power-law flux falloff to 10^{-2} at the moon and a 147,000 naut mi apogee).

Penetration through both the 0.002-in. primary target and the 0.001-in. secondary target is dependent on the bumper effectivity of the primary target. Hypervelocity impact tests on spaced foils have shown that the bumper factor may be as high or higher than 2 or 3. The actual effectivity for meteoroid penetrations is unknown and is one of the questions which may be answered by data from a bumper-type sensor on a satellite.

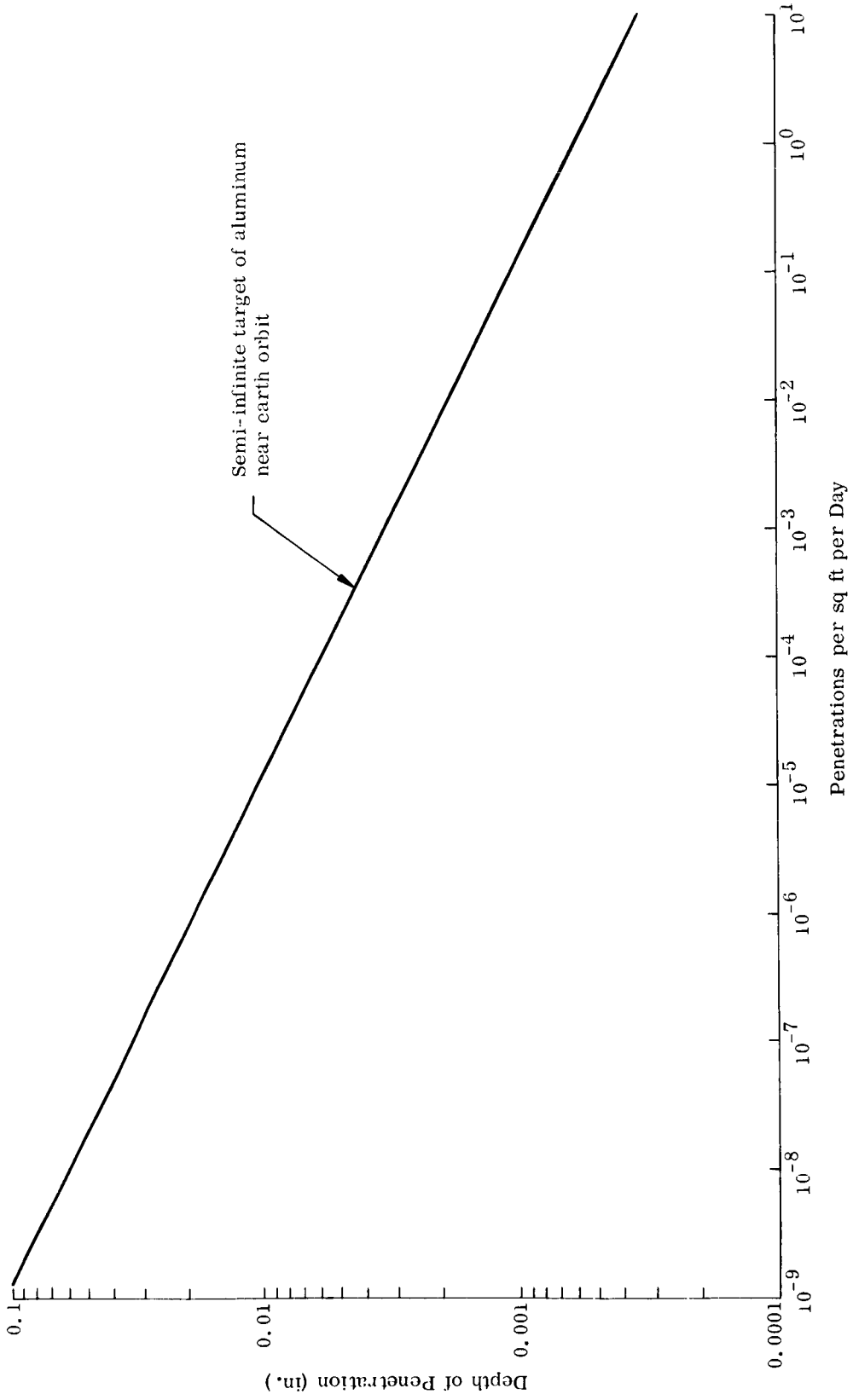


Fig. I-12. Penetration Depth Versus Penetration Rate

TABLE I-4

Penetration Rate Into Semi-Infinite Targets

Mass m (gm)	Flux N (No. /ft^2 per day)	Velocity V (km/sec)	mV	(mV)$^{1/3}$	Penetration Depth-Alum P (in.)
2.5	3.075×10^{-11}	22.	55.0	3.803	0.2586
10^{0}	9.01×10^{-11}	22.	22.0	2.802	0.1905
10^{-1}	1.971×10^{-9}	22.	2.2	1.301	0.0885
10^{-2}	4.313×10^{-8}	22.	0.22	0.6037	0.0411
10^{-3}	7.435×10^{-7}	22.	2.2×10^{-2}	0.2802	0.01905
10^{-4}	2.065×10^{-5}	22.	2.2×10^{-3}	0.1301	0.00885
10^{-5}	4.516×10^{-4}	22.	2.2×10^{-4}	0.0604	0.004107
10^{-6}	7.885×10^{-3}	22.	2.2×10^{-5}	0.02802	0.001905
10^{-7}	2.162×10^{-1}	22.	2.2×10^{-6}	0.01301	0.000885
10^{-8}	4.727×10^{0}	22.	2.2×10^{-7}	0.006037	0.000411
10^{-9}	1.035×10^{2}	22.	2.2×10^{-8}	0.002802	0.0001905
10^{-10}	2.255×10^{3}	22.	2.2×10^{-9}	0.001301	0.0000885
10^{-11}	4.951×10^{4}	22.	2.2×10^{-10}	0.000604	0.0000411
10^{-12}	1.082×10^{5}	22.	2.2×10^{-11}	0.0002802	0.0000191
	Near earth flux				For semi-infinite target

TABLE I-5

Penetration Rate in Multilayer Sensor

Penetration Depth (in.)	Penetration Rate-Near Earth Orbit (No. /ft^2/day)	No. of Penetrations per ft^2 for One Year in Cislunar Orbit (apogee = 147,000 naut mi)
① 0.000625	9×10^{-1}	10.90
② 0.001250	5.4×10^{-2}	0.619
③ 0.001875	1.0×10^{-2}	0.121
0.002	8.3×10^{-3}	0.1001
④ 0.00250	3.35×10^{-3}	0.0404
0.0005	1.05×10^{1}	1.33×10^{2}
0.002	4.15×10^{-2}	5.01×10^{-1}

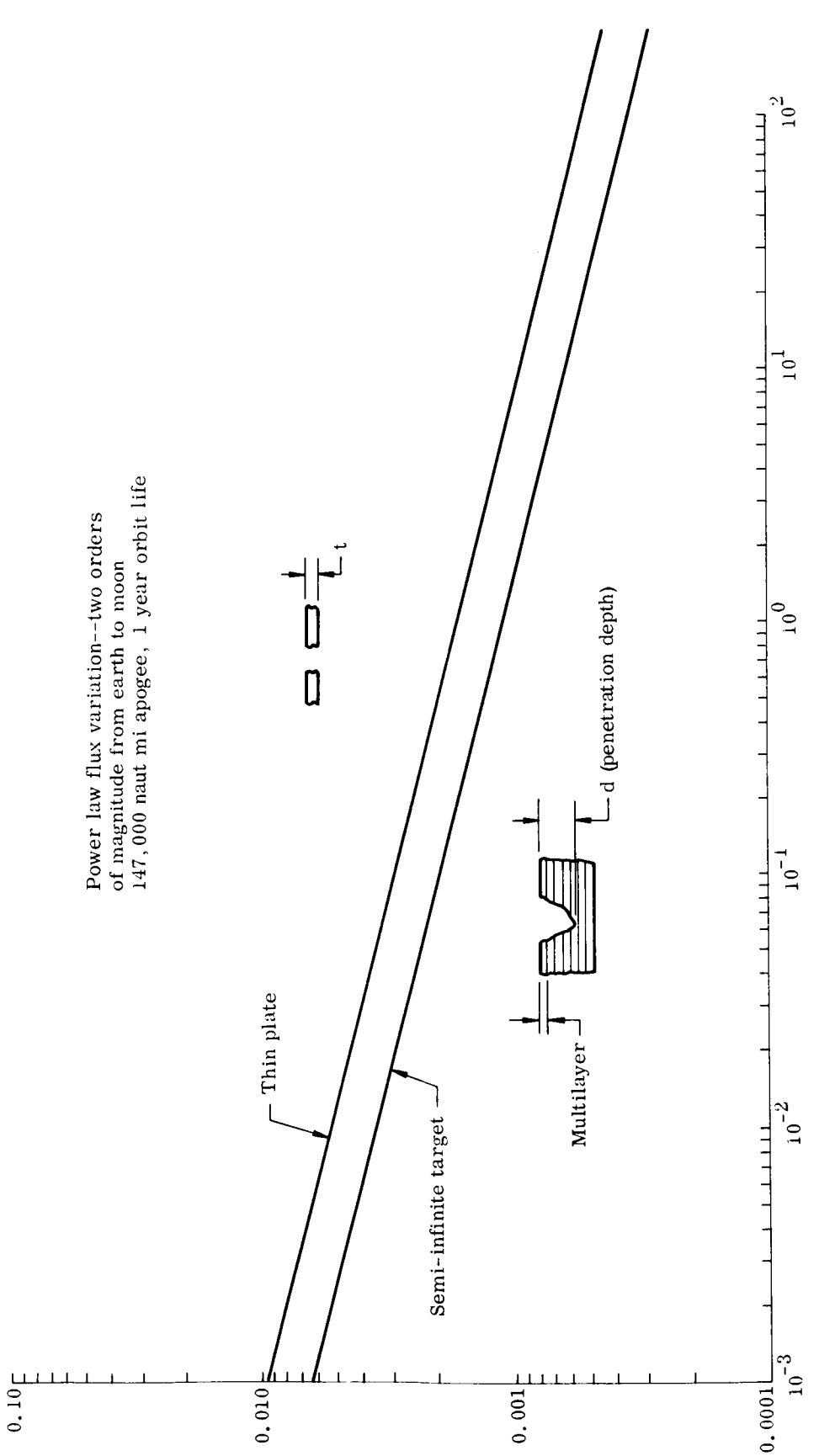


Fig. I-13. Penetrations Versus Sensor Thickness

Bumper-type capacitor sensor analysis. By assuming various values of the bumper effectivity and using the 4.02 power variation of penetrations with thickness, it is possible to determine the expected penetrations in a given time through both the primary and secondary targets as follows:

Primary Target Thickness (in.)	Secondary Target Thickness (in.)	Total Target Thickness t_T (in.)	Bumper Factor K	Equiv Single Target Thickness Kt_T (in.)	Expected Penetrations in One Year* on 530 ft^2	
0.002	0.001	0.003	1	0.003	51.8	
0.002	0.001	0.003	2	0.006	3.2	
0.002	0.001	0.003	3	0.009	0.621	**
0.002	0.001	0.003	4	0.012	0.197	
0.002	0.001	0.003	5	0.015	0.1179	
0.002	0	0.002	1	0.002	265	

*Power-law falloff.
**These rates do not take into account the dielectric thickness.

It is obvious from the last column of the above table that the data likely to be obtained on the penetration of both the primary and secondary targets will not meet a significant statistical criteria based on the power law falloff of the meteoroid flux. If the flux is greater than that given by the power-law, the use of the bumper-type sensor could yield usable data. Assuming that the flux is actually greater, the single layer sensor would only obtain data of more statistical significance on penetration of a single target thickness (i.e., more counts of penetration would be obtained). The bumper-type sensor would not only yield the data of the single layer sensor but could obtain data on the ability of meteoroids to penetrate spaced targets relative to single layer targets. Let us consider a configuration with an outside (primary) target of 0.002-in. aluminum and an inside (secondary) target of 0.001-in. aluminum.

Assume that in a given time, 100 penetrations of the 0.002-in. target are recorded. In the same time, assume that only two penetrations of the 0.001-in. secondary target are recorded. This would indicate that the layers of 0.002- and 0.001-in. together would have a penetration rate of $\frac{2}{100} = \frac{1}{50}$ or a single layer of 0.002-in. aluminum.

The relative penetration rate of 1:50 would be significant if the slope of the average penetration-rate material-thickness curve is known; for example, the 4.02 power function, if this is known, an estimated bumper factor can be calculated as follows:

0.002-in. target penetrations = 100

0.002-in. target + 0.001-in. target } 0.003-in. penetrations = 2

Therefore, the bumper factor = $\left(\frac{100}{2}\right)^{1/4.02} = 1.49$

However, the slope of the penetration curve is one of the things that the MDSS is to determine. The 4.02 power function is based on Whipple's 1963 estimate of the flux (Ref. I-1).

If the bumper factor is assumed to be known from hypervelocity impact tests, then this could be used to estimate the slope of the penetration rate curve as follows:

0.002-in. target penetrations = 100

0.002-in. target + 0.001-in. } 0.003-in. penetrations = 2

Therefore, the bumper factor = 3; this is equivalent to 0.003 x 3 = 0.009-in. single thickness

$$\left(\frac{0.002}{0.009}\right)^{K} = \frac{2}{100} \quad \text{from which } K = 2.6$$

Any value of "K" determined in this fashion would be questionable because of the assumption of a bumper factor based on hypervelocity impact data.

Conclusion. The following conclusions can be made:

(1) The single primary target will give significant penetration data in a single thickness (i.e., 16 hits/zone).

(2) The use of a bumper-type sensor (primary target with a secondary target) of the same area will not give significant statistical data for penetration through two separated sheets unless the meteoroid flux is greater than that calculated with a power-law falloff on which the sensor area is based.

(3) Any penetrations of both the primary and secondary target can be used to determine the bumper factor if the slope of the penetration rate-thickness is known from satellite data or it is assumed.

(4) A bumper-type sensor can give usable data of low confidence and its use should be considered, weight permitting.

(3) Printed circuit penetration detectors

Gages of this type have been flown on Explorers XIII and XVI. They are basically a stainless steel target plate to which is bonded a layer of Mylar backed with a continuous gold grid.

These gages were made for Lewis Research Center by Buckbee Mears Company of St. Paul, Minn. The process starts with a thin sheet of copper which is given a flash coating of nickel and then coated with a photo-sensitive material. A master pattern is used to form the grid pattern on the photo-sensitive material. The unexposed surface is washed away and gold is electrolytically deposited (90μ in.) on the clean nickel surface. The remaining photo-sensitive material is etched away leaving the gold grid on the nickel and copper substrate. Then, the grid and stainless steel test specimens are laminated to the dielectric Mylar layer (which has been precoated with a thermosetting adhesive) by feeding them into heated rollers. Finally, the copper and nickel are etched away.

Initial costs were about \$50 for a 9 in.^{2} sensor. The latest quote was \$20 for a 9 in.^{2} sensor.

Buckbee Mears was unsuccessful in attempts to simplify the process by flashing the gold directly on the Mylar by screening through a master. Attempts to start directly with gold foil and then etch the grid were likewise unsuccessful. Mr. Winslow of the Lewis Research Center (LRC) could give no details on the extent of the effort that went into these attempts.

Lewis Research Center suggested that 1 ft^2 might be about the maximum single grid that could be made. However, wiring gages together or wiring grids together on a large target plate should offer no problems. In Explorer XIII as many as 16 sensors were wired together in an 8 x 2 parallel-series pattern.

The gages on Explorer XIII and XVI, respectively, were glued to silicone rubber and to foam. They would have preferred a free mounting because of concern over thermal distortions in the aluminum ring

which served as their basic structure. It was feared these distortions would short some of the gold lines together. LRC said that edge mounting looked practical providing that little or no rippling type motion would occur. Lewis Research Center prepared a proposal to put 150 sq ft of this type of gage on an R&D Centaur in 1961.

LRC felt that aluminum could be used for the target plate instead of stainless steel. Approximately 600 1 ft^2 sensors would be needed to obtain penetration data (assuming 1- and 2-mil aluminum targets). In order to maintain a minimum change in input signal of at least 10% of full scale when one sensor is penetrated, no more than eight sensors per circuits were paralleled (Explorer XIII). This would require at least 75 circuits with a minimum resolution of 1/10 full scale.

Temperature sensitivity of the circuit is such that a 100° C temperature change in all 8 sensors of a parallel circuit were estimated to give no more than 4% of full scale change in the output to the telemetry circuit. A temperature cycle of at least 165° C is expected along the baseline orbit so that the temperature-induced changes in resistance should be proportionately larger. Thermistors were used on the Explorer sensors to monitor the performance of the thermal coatings and to provide data for a temperature correction to the sensor circuit output as the temperature cycle increased. Thermistors would therefore be very desirable if these sensors were used for the cislunar mission. The manufacturing process always left some places where gold bridged from one line to the other or where missing gold regions resulted in an open sensor. Each sensor was microscopically inspected and shorts and openings were repaired by hand. The work was time consuming and the repaired sections did not have the desired spacing and thickness of gold. The repairing or "healing" of the capacitance sensors does not require visual inspection or manual repair and leaves only point defects (i.e., dead spots in the sensor). A bridged gold line of the grid detector must be found and repaired manually or else it causes an effective loss of sensor area.

A variation of this type of sensor was suggested by Dr. D. Roiseland and Mr. S. Stenlund of the G. T. Schjeldahl Company. It consists of a chemically milled interdigitated grid of 2-mil grid lines and 2-mil spaces rather than the continuous gold grid. A penetrating particle makes a momentary connection between the adjacent positive and negative grid lines. The obvious advantage is continued operation of the sensor after repeated penetration. Breaking of one or more grid lines will not destroy the sensor since each of the positive segments is brought into a positive bus and similarly for the negative grid segments. An obvious disadvantage (common to all nondestructed sensors) is that the response is transient and the sensor must be activated and read out continually.

(4) Light sensitive penetration detectors

Cadmium sulfide cell. Cadmium sulfide light sensitive penetration detectors prepared by L. Secretan at GSFC have been used on Explorer VII and on each of the S-55 satellites (Explorers XIII, XVI and XXIII). The detection principle is the photo-resistive effect of the CdS for which an idealized response curve is shown in Fig. I-14. Sensor configuration has changed over this period. Areas are larger and volumes are lower. The sensor is now basically a flat disk of aluminized Mylar fastened across one face of the disk which prevents sunlight from reaching the cadmium sulfide surface on the inside of the opposite face of the disk. Meteoroid punctures of the Mylar allow sunlight to reach the light sensitive surface when the geometry is correct. A version of the sensor was made up in the form of an ellipsoidal (of revolution) flask mirrorized on the inside. The aluminized Mylar was stretched in one of the focal planes and the cadmium sulfide cell fastened in the other. For any given hole size, photoresistance will vary with the angle of incidence as the finite thickness of the Mylar cuts off some of the ray. A conservative estimate of hole diameter would be based upon the $\frac{P}{d}$ of the penetrating particle. A 3.4×10^{-7} gm particle with a density of 0.44 will be about 4.7 mil in diameter (5.4 mil if $\rho = 0.25$). This particle will penetrate 1-mil stainless steel. Five to one would therefore be a conservative estimate of the ratio of hole diameter to thickness in stainless steel. At this ratio, cutoff probably does not become important until the aspect falls below 45°. Use of a softer material such as aluminized Mylar will probably give a lower ratio so that solar aspect effect upon the interpretation of the cell response would become significant at better aspect. Therefore, an axial aspect cell is probably desirable for each cadmium sulfide detector. This would result in coincident aspect and detector readings and not necessitate an aspect extrapolation. Because of the thermal sensitivity of the cadmium sulfide cell, temperature measurements to within $\pm 1°$ are required.

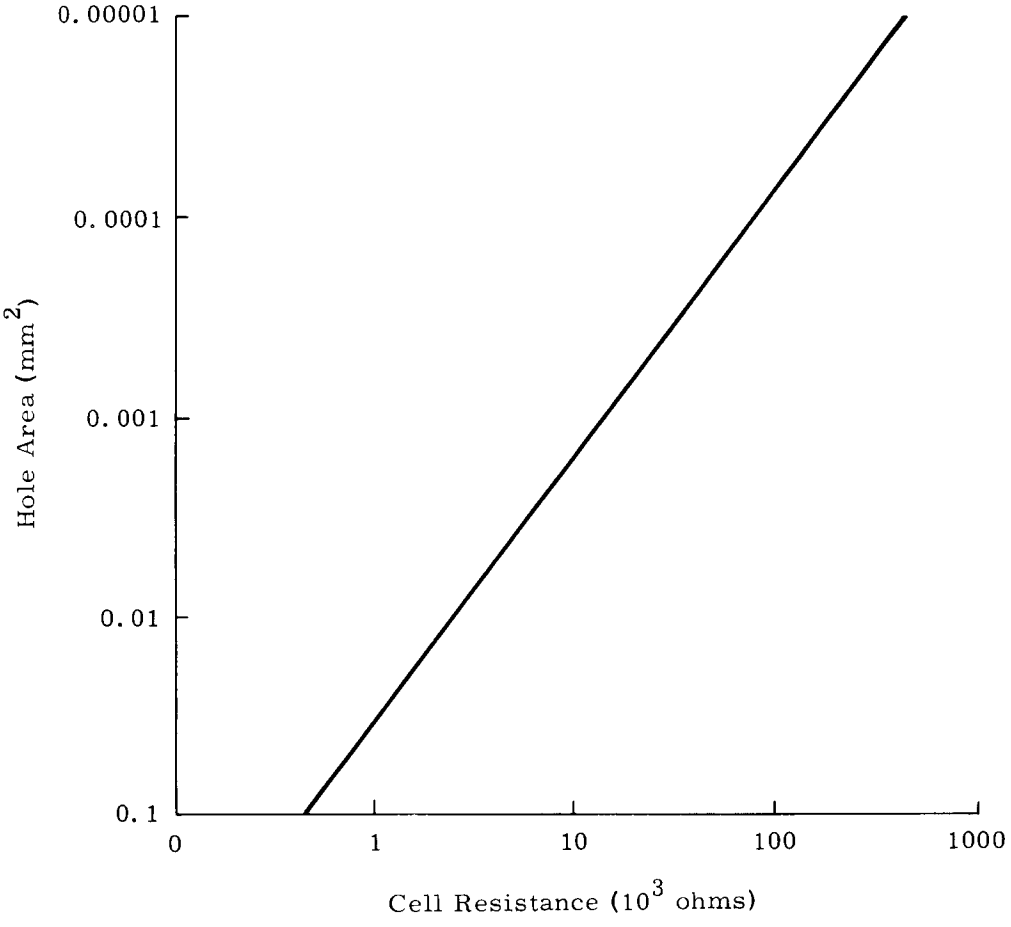


Fig. I-14. Idealized CdS Cell Sensitivity Curve

Exotech meteoroid puncture detector. The response mechanism of the sensor is to detect IR radiation associated with high velocity impact and/or penetration. The concept has been shown to be feasible and a laboratory system has been operated. Peak response to impact flash was shown to vary with the square of projectile diameter and with the cube of particle velocity for 380 to 1588-μ steel spheres impacting on aluminum for velocities in the range of 2.4 to 4.4 km/sec. Analysis suggests that the time integral of radiation from impact flash is proportional to kinetic energy of incident particle (Ref. I-24).

Response to penetration flash appears to vary less rapidly than the first power of kinetic energy. Signals were detected 36 ft away from 380-μ steel ball penetrating 406-μ thick aluminum with incident KE of 4×10^7 gm-cm^2/sec^2. Sensor response at 36 ft indicates that it should be capable of detecting the flash from the penetration of 1-mil aluminum up to at least 10 ft from the flash. Furthermore, there is an indication that the sensor response may provide a basis for determining the kinetic energy of penetrating particles beginning at some energy above that for which a minimum flash signal may be detected. This is indicated on Fig. I-15 where it can be seen that a proportional response occurs from particles that have an incident kinetic energy 2 to 3 times greater than the minimum penetrating particle.

(5) Impact transducer momentum detectors

Microphone sensors have been used since the V-2 flights for particle impact detection. The response is generally agreed to be proportional to a mass velocity impact parameter and less generally agreed to be proportional to impact momentum. Organizations that have concentrated on microphone development and application are GSFC, LRC, AFCRL, University of Oklahoma and Temple University. Threshold sensitivity is equivalent to particles as small as 10^{-12} to 10^{-13} gm, so that relatively small detector areas could receive large data samples. The most recent microphone sensor developed was launched during November 1964 as part of the Mariner spacecraft scientific payload. The sensor was developed at Goddard Space Flight Center and is shown schematically in Fig. I-16. Detailed information extracted from the JPL detector specification (Ref. I-25) is shown below:

The purpose of the Cosmic Dust Detector is to make direct measurements of the dust particle momentum and mass distribution in the near Earth-Moon system, interplanetary region, near Mars-Deimos-Phobos system, and the asteroid belt.

Figure I-17 shows the functional block diagram of the Cosmic Dust instrumentation for Mariner.

Punctures at 7500 fps through various thicknesses of stainless steel as indicated by number on points.

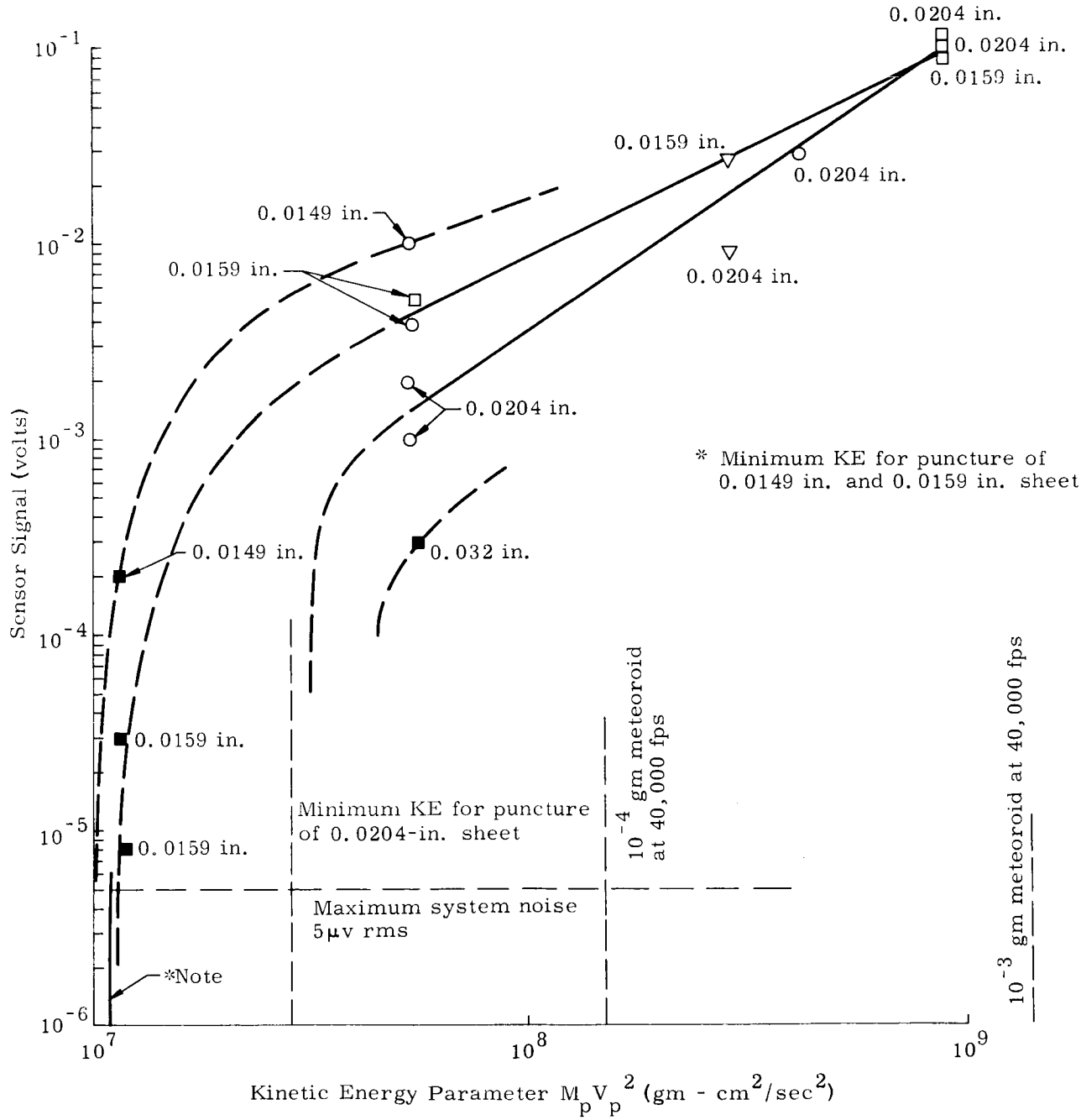


Fig. I-15. IR Signal at 36-ft Range Versus Kinetic Energy Parameter

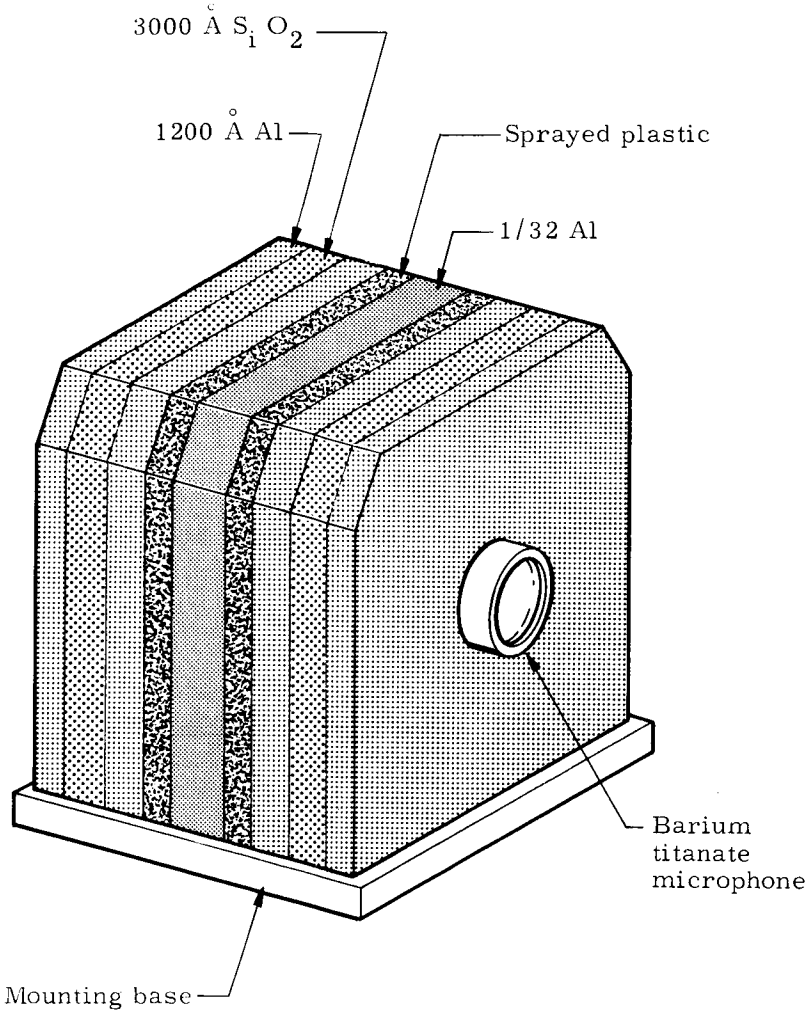


Fig. I-16. GSFC/Mariner Micrometeoroid Gage

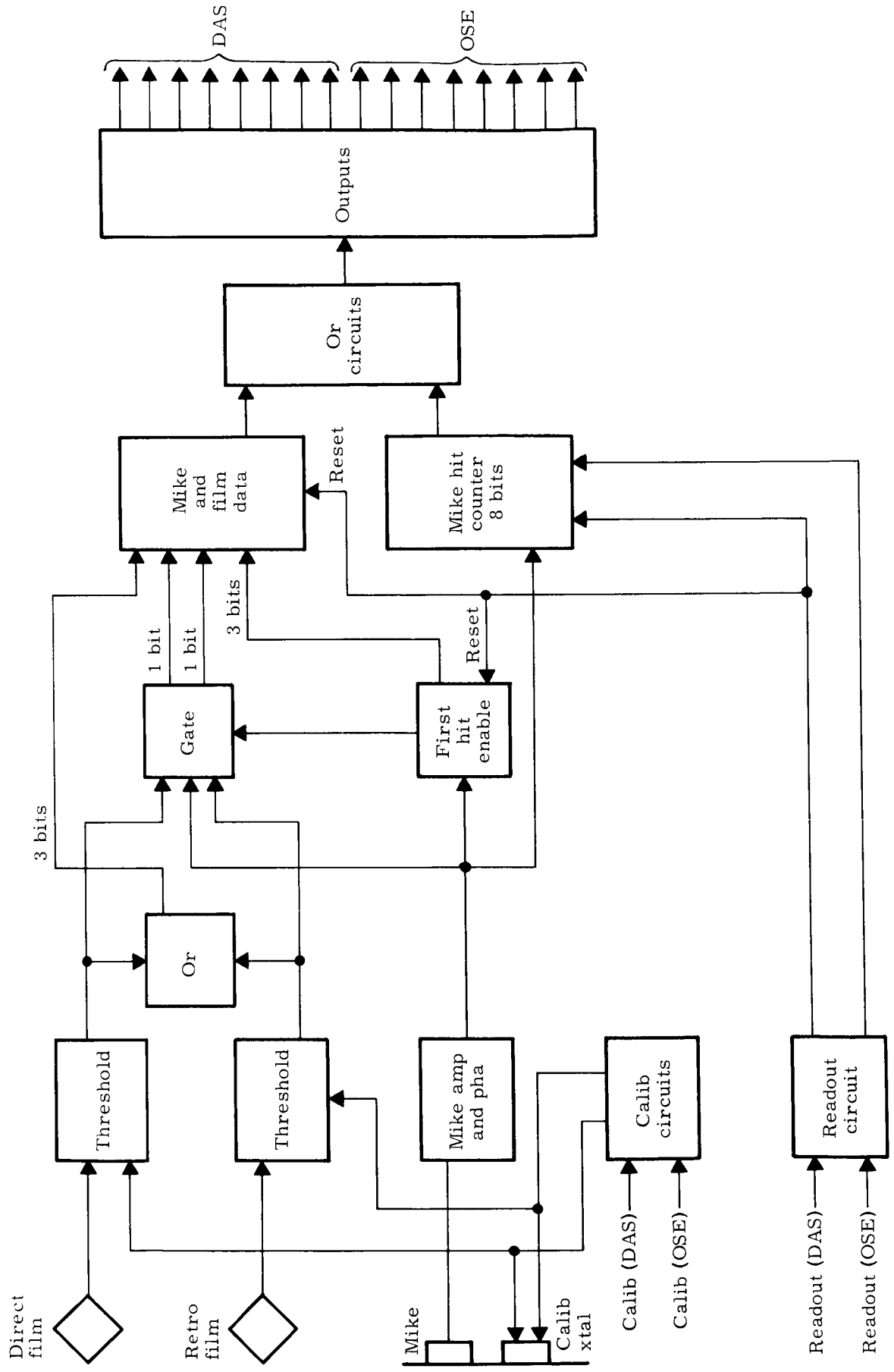


Fig. I-17. Functional Block Diagram GSFC Mariner Gage

Two sensors measure dust particle impact by direct penetration and by microphonic techniques. The microphone is the only analytical sensor. The capacitors are over an order of magnitude more sensitive than the microphone. Because of the experiment's weight, power, and schedule requirements, they are only flown to:

(1) Indicate the side of the sensor that the microphone pulse height analysis (PHA) is taken.

(2) Count the number of impacts that occurred, some of which will be below the microphone threshold.

The sensor is an aluminum impact plate, 0.030 in. thick, with an acoustical transducer bonded to one side. Both sides are coated with 5000 Å of nonconducting material (dielectric of capacitor), and finally covered with an evaporated layer of aluminum, forming penetration capacitor sensors with the microphone plate as a common side of both capacitors. A static potential of 12 volts is applied across the capacitors through a current limiting resistance of 100,000 ohms. An impacting particle produces a current pulse from the capacitor.

The signal from the microphone is amplified by a tuned amplifier having a center frequency of 100 kc. The amplifier output is converted from pulse amplitude to pulse width and is gated with a 5 kc clock for storing 3 bits (7 levels) of momentum analysis of the first microphone data in each data frame.

Two 8-bit data storage units are alternately read out as 3 bits per frame. One storage unit stores: 3 bits, first microphone impact PHA; 2 bits, first microphone impact direction identification; 3 bits, capacitor count. The second storage unit is an 8-bit microphone "hit" accumulative counter. At the time of the readout command the data is parallel dumped.

Upon receipt of a calibration command pulse from the Data Automation System (DAS), a separate acoustical transducer that is mechanically bonded to the microphone impact plate is electrically driven, initiating shock waves on the sensor. Two amplitudes alternately simulate different momentum level particle impacts. At the same time, the direct and retrograde capacitor electronics are alternately checked with a pulse similar to the capacitor shorting pulse.

The power converter converts the basic 2400 cps square wave spacecraft power to +12 volts for capacitor sensors and +3 volts and -7 volts for the remaining electronics.

(a) Electrical inputs

The electrical inputs are: 50 volts, rms, 2400 cps square wave from the power system; calibrate signal from Data Automation System (Unit 20) (approximately once per day); and readout command from DAS (a 10-μ sec pulse occurring at the leading edge of a 100-μsec readout time).

(b) Outputs

Outputs are:data out to DAS, 8 bits AC-coupled and parallel-dumped upon receipt of readout command. Output impedance, Z, is 200 ohms. The output binary state "one" is a pulse of >6 v, 10 μsec wide into a 1.8 K load.

(c) Operating temperature limits

For the sensors operating temperature limits are -100° to +200° C, and -40° C to +100° C for the electronics. Temperature should be known within 20° C for microphone PHA accuracy.

(d) Nonoperating temperature limits

Nonoperating temperature limits are -150° C to +250° C for the sensors and are -70° C to +125° C for the electronics.

Measurements at GSFC have indicated that the mounted thin film capacitor may give a response proportional to the kinetic energy of the penetrating particle. Subsequent versions of this detector may therefore be instrumented for a pulse-height analysis of the capacitor as well as the microphone.

Sensitivity of the capacitor is:

(1) Particles with mass greater than 10^{-13} gm at a minimum velocity of less than 2 km/sec.

(2) Particles with momentum greater than 10^{-5} dyne-sec.

The detector will weigh $\leq$ 2.5 lb (total) of which sensor weight is 0.5 lb and electronics weight is 2.0 lb.

The cosmic dust detector will consume 200 mw of raw 2400 cps power.

(6) Other sensors and combinations

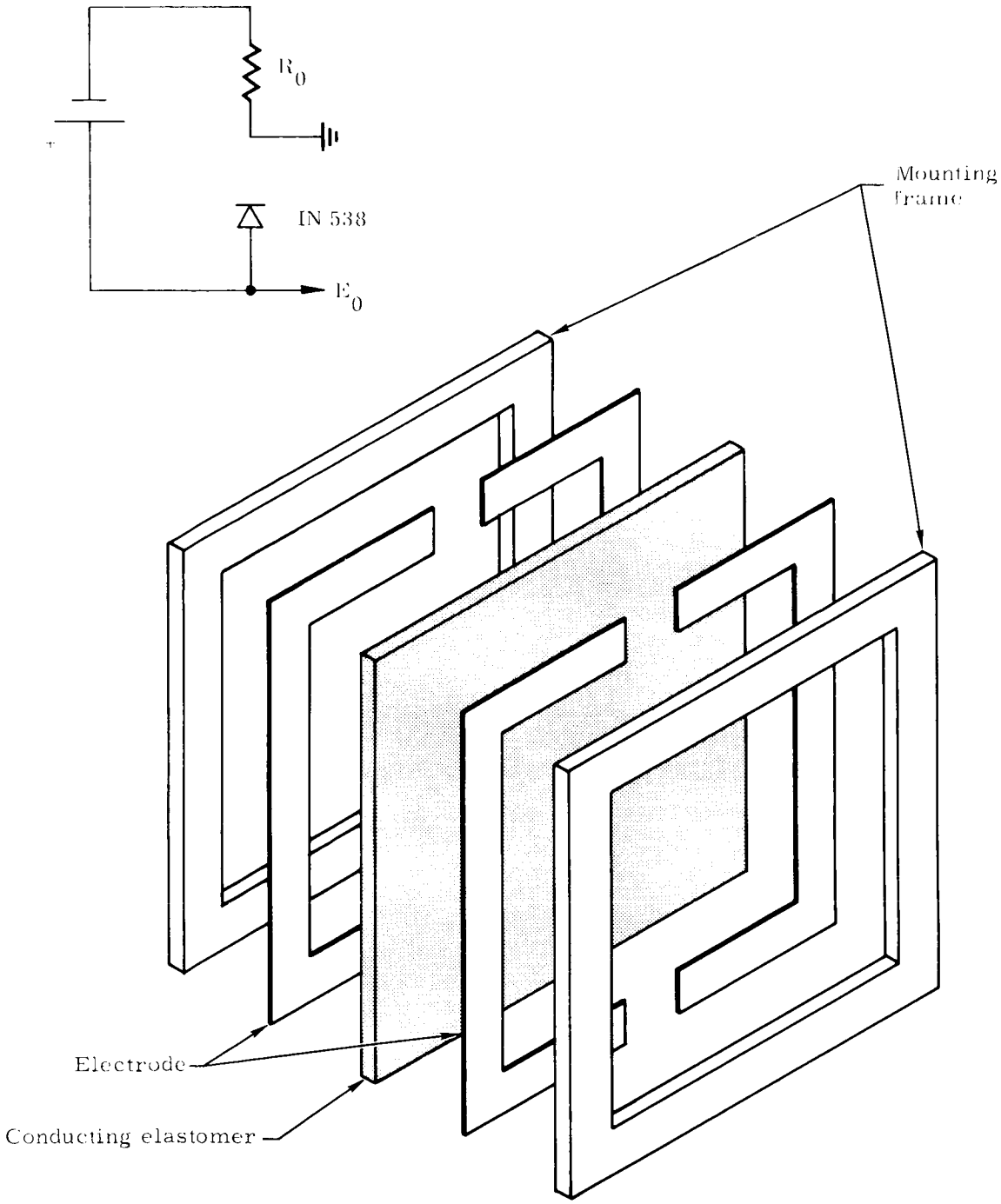
Republic Aviation--conducting elastomer penetration detector. The response mechanism of the sensor is to detect change in current flow in an elastic conductor due to the effect of impact (penetration) on transient resistance of material (Fig. I-18) (Ref. I-26). Peak transient resistance change in an 0.060-in. thick sheet of graphite leaded-silicon to ten particles in the velocity range of 4.75 to 7.87 km/sec indicated linear relationship to incident energy. (Lexan particles 65 mg 5080 μ dia x 2540 μ long, $KE_{min} = 7.4 \times 10^{9}$ g-cm^2/sec^2.) Other materials, thicknesses and conductivity loadings have been investigated only slightly.

No detailed theory or analysis of response mechanism has been formulated as yet. A detector configuration proposed for space vehicle application is shown on Fig. I-19.

Cadmium sulfide plus ceramic beam sensor. This sensor is being developed at Ames Research Center with the CdS cell to be developed and furnished by Goddard Space Flight Center. Information regarding this sensor has been provided by Dr. James Vedder of NASA-Ames. The instrument measures the momentum and size of hole produced by the impacting particle, thus giving a measurement somewhat more meaningful than momentum alone. Since the aperture of the instrument is limited to about π steradians, an evaluation of particle directionality is also obtained. This cannot be done with the CdS cell alone because the time of impact is not known.

The ARC sensor portion developed by Mr. Vernon L. Rogallo is essentially a ballistic pendulum of high sensitivity. The detector utilizes the piezoelectric effect from the bending of electrically polarized ceramic beams to measure the normal component of momentum imparted to a target plate by an impact. As shown schematically in Fig. I-20, a cylinder normal to the plate and rigidly attached by a supporting structure is suspended from the base by two matched piezoelectric beams. The motion of the plate and cylinder is restrained to and limited in axial motion by mechanical stops. For common-mode rejection of mechanical disturbances of the base, another set of ceramic beams support a dummy load having the same center of mass and axis as the target structure and cylinder. The two units are electrically and mechanically balanced to give cancellation of signals originating from vibrations in the base.

Prototypes of the momentum detector have been built and tested in the laboratory. A momentum calibration was done by the bead dropping technique down to 10^{-3} dyne-sec, and was extended to lower levels by



Conducting elastomer penetration detector

Republic Aviation Corp RAC 1378 Feb 64

Fig. I-18. Republic Sensor

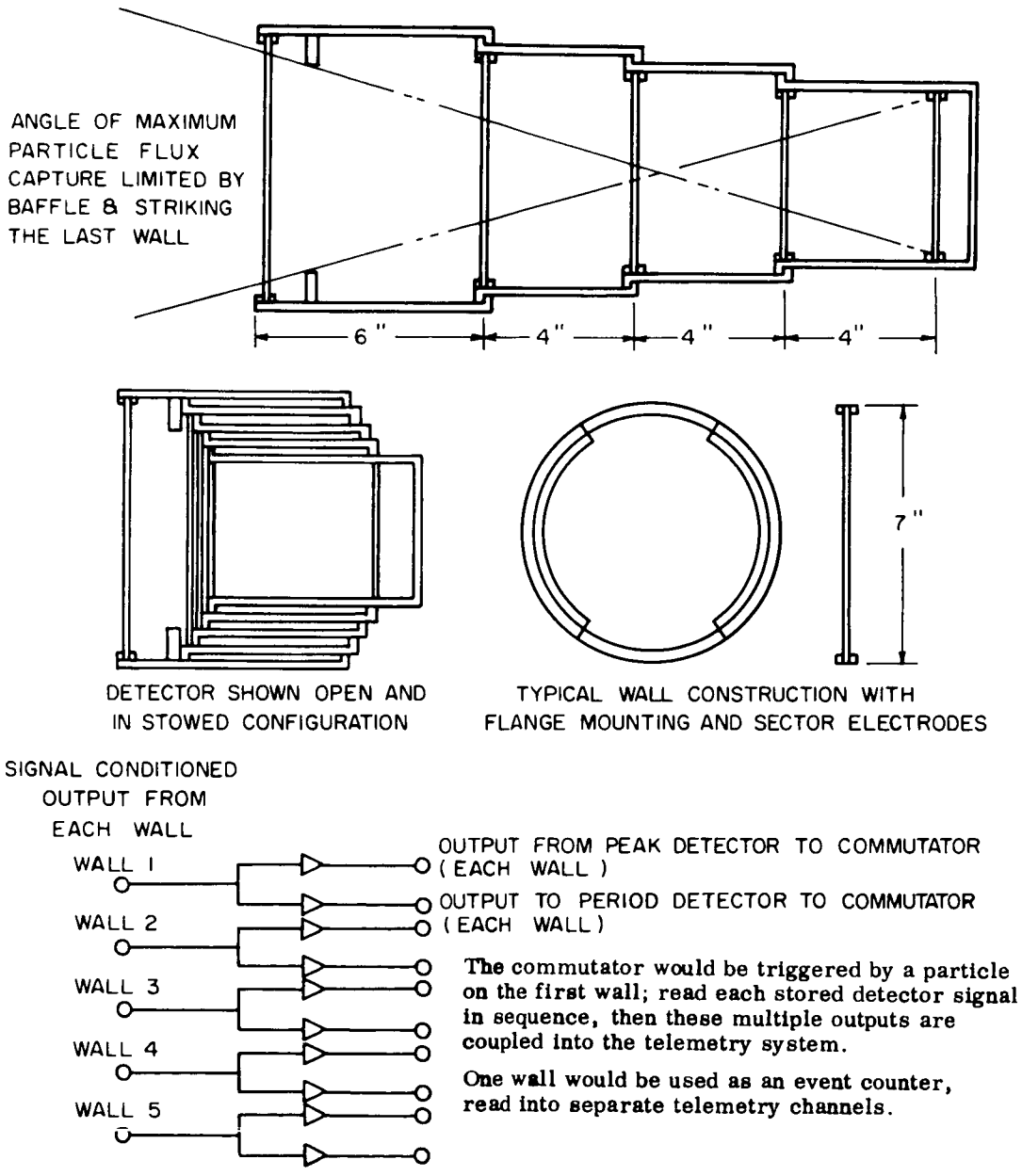


Fig. I-19. Conducting Elastomer Detector Configuration for Space Vehicle Application

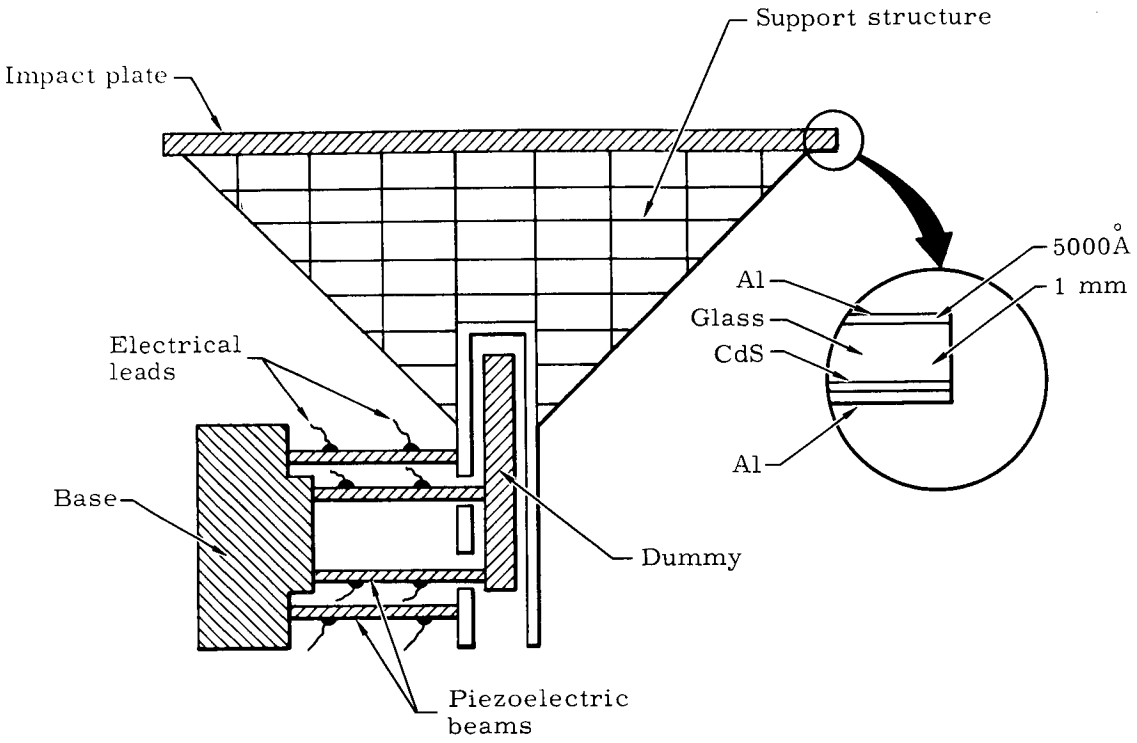


Fig. I-20. Pioneer Detector Schematic

driving one beam with voltage pulses to simulate impacts. This is a convenient technique for in-flight calibration of the instrument and associated electronics. In a rather noisy laboratory, a sensitivity of 10^{-5} dyne-sec, limited by the mechanical noise level, has been attained. The electrical noise is less by a factor of ten. The output is linear for moments up to at least 1 dyne-sec, where the deflection is a few thousandths of an inch. The momentum sensitivity across the plate is insensitive to distance from the axis, and the response as a function of impact angle for low velocity impacts closely follows the expected cosine dependence. Further calibration tests are being carried out at Space Technology Laboratories with hypervelocity microparticle impacts.

It was planned to use a GSFC CdS sensor as the impact plate. With it a measure of the particle size can be obtained. From the size and momentum and an assumed velocity, one can derive a particle density. The ARC/GSFC detector was approved for Pioneer I and II in 1965.

Three pie-slice shaped cadmium sulfide cells were to be used to increase the dynamic range of the instrument. A pinhole calibration segment is planned at the center of the exposed surface. The instrument weight was to be under 1.5 lb and not more than 125 cu in. volume. Power draw averaged 500 mw. The setback of the instrument from the spacecraft surface would limit the acceptance angle to about π steradians. The ceramic beam is a Clevite PZT Multimorph (similar to a stereophonograph pickup). This type of transducer has also been used by Rogallo in a new type of ballistocardiograph (Ref. I-27). The preamplifier uses field effect transistors. A preliminary block diagram of the sensor system is shown on Fig. I-21.

Some difficulties were experienced in providing a suitable mounting to isolate the flight instrument from the spacecraft so that the potential sensitivity of the detector could be realized. Because of the time spent in finding a solution, the instrument could not meet the Pioneer I and II schedules but it may be included in one or more of the later Pioneers.

Velocity tube. This sensor which was flown recently on OGO is a joint development of GSFC and Temple University. Information on the existing sensor was obtained from W. M. Alexander at Goddard. The sensor is shown schematically in Fig. I-22. Heating elements to keep the tube temperatures constant are not shown. At the entrance to each tube is a thin foil supported on a grid. Penetration of the foil produces ions and electrons. Depending on the polarity of the downstream collecting the ions or electrons are detected on a collection grid which provides the initialing signal for a time of flight measurement. Because of the grid surfaces the effective area for penetrating particles is 70% of the tube area. Penetration of the thin foil capacitance gage provides the

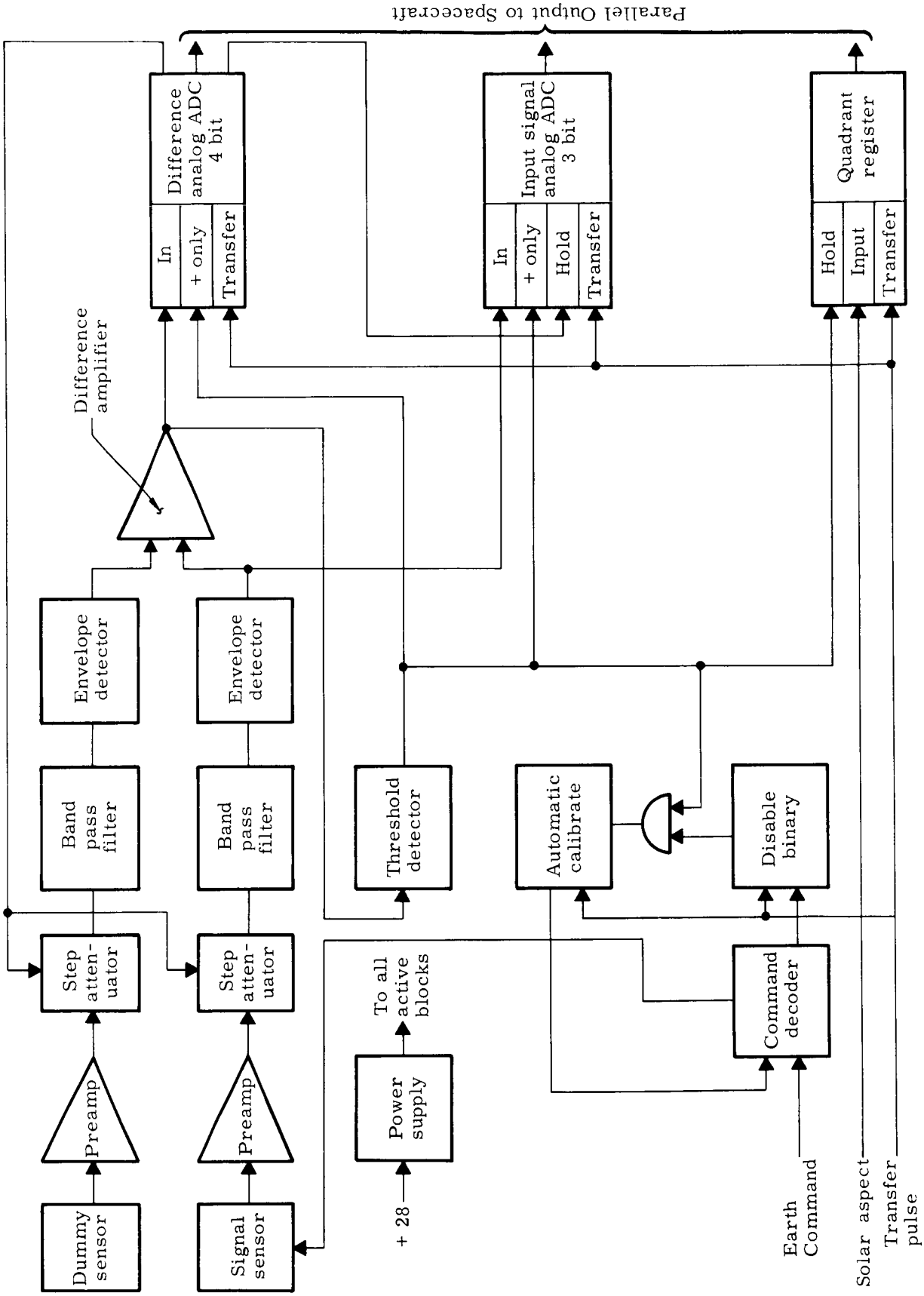
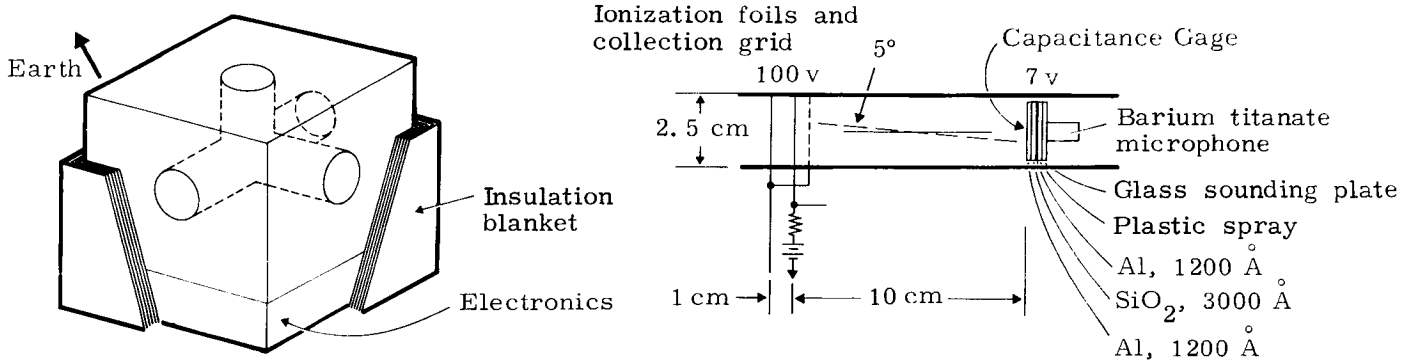
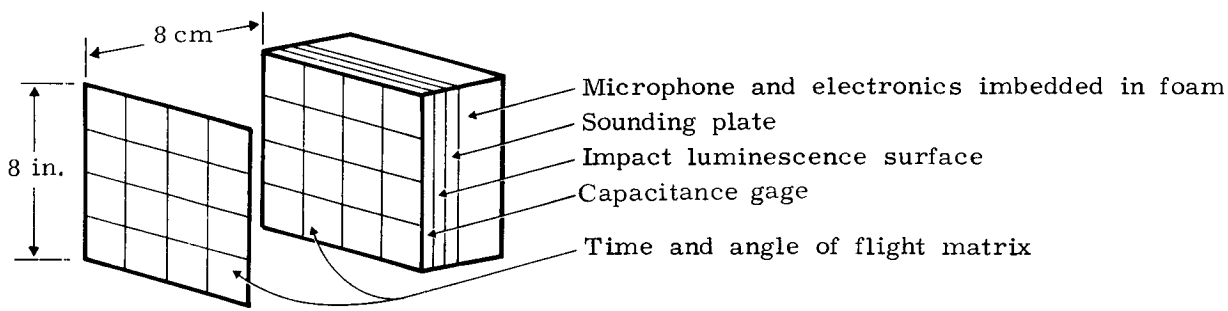


Fig. I-21. Micrometeoroid Detector Block Diagram, Preliminary Ceramic Beam and CdS Cell



1. GSFC Velocity Gage (EGO, POGO)



2. GSFC New Velocity Gage (Pioneer, IMP D&E)

Fig. I-22.

signal to stop the time of flight measurement. Time of flight is determined from the counts of a 2-mc oscillator (see Chapter V of Vol. III for discussion of velocity measurement and effects of attitude uncertainty upon determination of velocity vector).

The amplitude of the capacitance gage signal is approximately proportional to the kinetic energy of the particle. The microphone response is approximately proportional to the particle momentum. The combined outputs provide an indication of velocity, kinetic energy and momentum and enable the particle mass to be determined. The triple coincidence provides for reliable basis for spurious output rejection. Laboratory measurements using iron carbonyl spherules (~1μ dia) have shown that the particle experiences a 10% loss in velocity when penetrating the ionization foil. The microphone threshold is equivalent to a 10^{-12} gm particle. The capacitance gage is an order of magnitude more sensitive. The sensor to be flown on POGO will be instrumented to utilize the maximum sensitivity of the first two transducers. The instrument has a high potential angular resolution capability at the expense of a very small geometric factor (~0.04 steradians and 5.0 cm^2 for each tube).

Figure I-22 also shows a sketch of a modified version of the sensor. The acceptance area of this sensor would be approximately 400 cm^2 and 4.4 steradians. Angular resolution would be 4.4/16 x 16 or about 0.017 steradians (note however that the solid angle subtended by each combination of the matrix elements is not constant) and the sensor would collect data at a rate about 3000 times greater than the existing version. This sensor is intended for deep space use where the flux is anticipated to be lower than near earth. Development of the sensor is hinged upon its acceptance for IMP D& E (lunar orbit) and/or Pioneer (0.8 to 1.2 AU). An additional feature being considered for this sensor is a layer sensitive to the luminescence created by the penetrating meteoroid.

It should be noted that the sensor would require a 16 x 16 matrix storage unit with capacity to handle a very large data word resulting from the time of flight, and the analog outputs from the microphone, capacitor and flash detectors plus real time and/or attitude. Another complication may arise from the observed tendency for penetrating particles to be "refracted" normal to the penetrated surface.

Combined light flash sensor. A combined sensor based principally upon a photomultiplier to detect penetrating flash luminescence is under development by Otto Berg at GSFC and is shown schematically in Fig. I-23. The opaque surface over the lucite is a thin film capacitor. A small microphone is also imbedded in the lucite. The potential triple coincidence response should assure a high rejection of noise and spurious

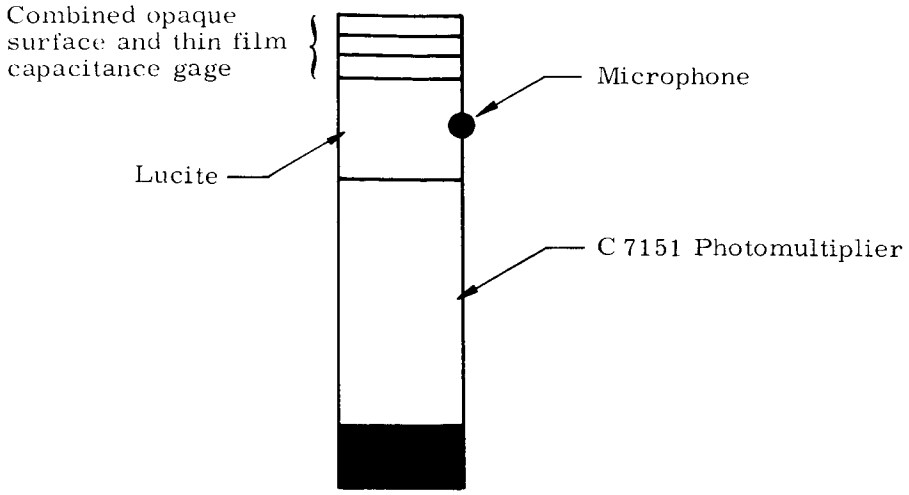


Fig. I-23. GSFC/Photomultiplier Sensor

Electro-Optical Systems, Inc.
Report No. 5150-IR-1

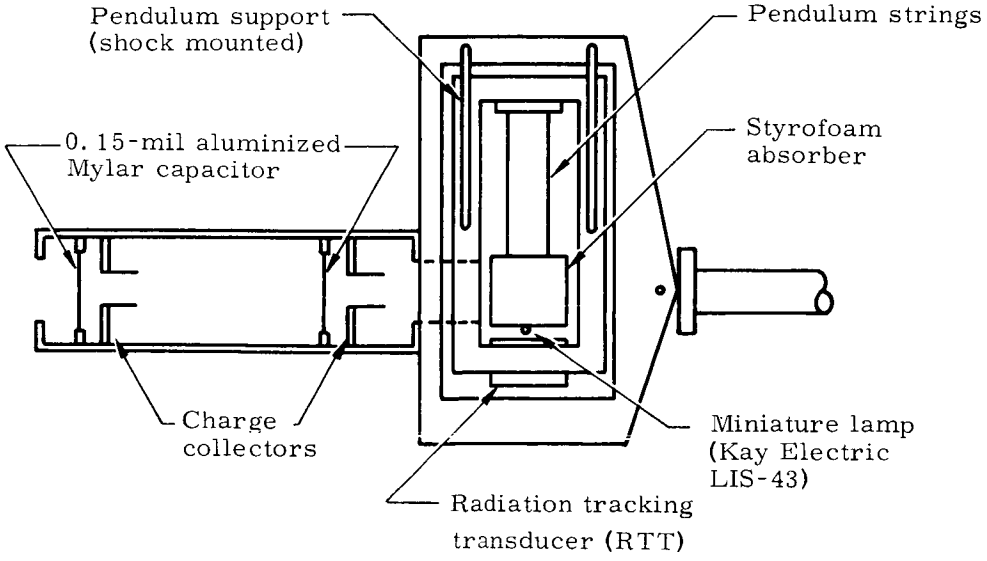


Fig. I-24. EOS/MSC Ballistic Pendulum

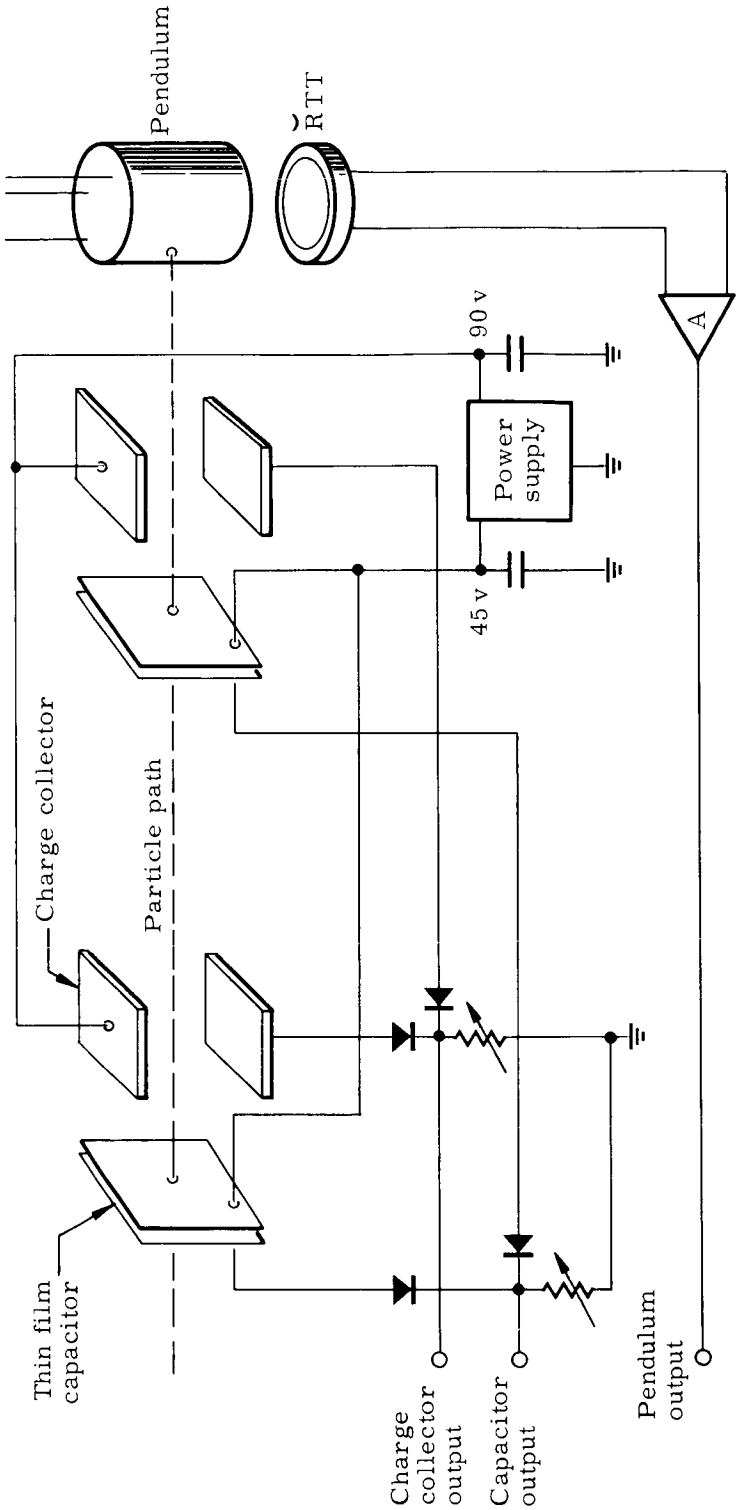


Fig. I-25. Circuit Diagram of EOS/MSC Sensor for Hypervelocity Particle Experimental Program

radiation pulses (however the microphone threshold is somewhat lower than the 10^{-13} gm equivalent of the other two transducers). The three responses should provide a much better basis for deriving particle mass and velocity than the photomultiplier above since one of the basic criterias of the original photomultiplier technique was the uncertainty of the luminous efficiency of the impact both in amplitude and spectrum. A sensor of this type will be flown shortly onboard a rocket probe and possibly a satellite.

Combined ballistic pendulum and velocity detector. A flight version of a ballisitc pendulum sensor has been designed for particles of mass 10^{-6} to 10^{-9} gm and assigned a possible berth on OSO-F. The sensor would be mounted on the aft face of the sail (sun-pointed section) and would therefore always point away from the sun. Data on the flight model were obtained from Mr. Paige Burbank at MSC. Data on the laboratory model were obtained also from Mr. Burbank and Mr. J. W. Keller at Hq NASA-OART. The laboratory model developed by Electro-Optical Systems, Inc. is shown in Fig. I-24 and demonstrates the principles of operation. A particle entering the tube and passing through the collimators will impact and come to rest in the styrofoam absorber. The resulting displacement of the styrofoam is obtained by tracking the motion of light source attached to the styrofoam. In laboratory tests, the response to a one microgram glass bead impacting at 8.4 km/sec was determined to be 0.52 dyne-sec compared to an actual of 0.84 dyne-sec. Saturation of the amplifier was cited as a major factor in the discrepancy (Ref. I-28). Modifications were subsequently made to prevent saturation. The velocity measuring portion of the laboratory model consisted of two independent sets of detectors for particle time of flight. One set consisted of aluminized Mylar capacitors (1/4 mil) at a potential of 45 volts. The secondary system used a thin lacquer film (1.5μ = 0.06 mil). Ionization produced by the penetrating particle would be collected at the 90-v charge collector plates. In both systems, the velocity would be determined from the interval between the first and second capacitor discharge pulse or collector pulse. The waveform characteristics of the charge collector signal was unsatisfactory and was abandoned in favor of the capacitor which gave a very distinct pulse. A circuit diagram for the experimental instrument is shown in Fig. I-25. Other changes include the use of quartz fibres for the pendulum mount instead of nylon or copper. It was also planned to replace the 0.15-mil mylar capacitor with a thin film Al, Al_2O_3, Al-type developed at GSFC. This capacitor would be overall 2000 Å or 0.008 mil. The proposed flight model is shown in Fig. I-26. Radial incidence is imposed by the fins. The second capacitor is mounted directly on the pendulum and the sampling area of the instrument is increased greatly over the laboratory model.

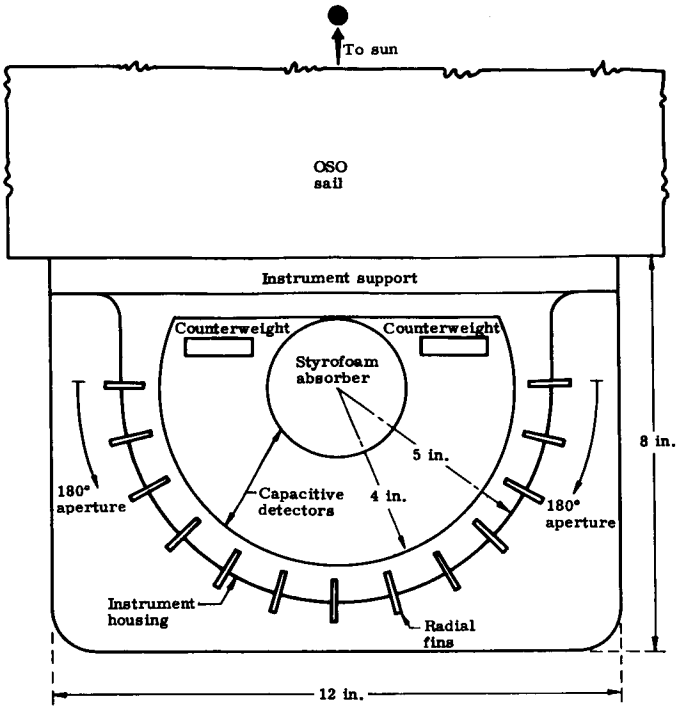


Fig. I-26a. Proposed Configuration of EOS/MSC Sensor for OSO-F, Plan View. (Spacecraft pitch-roll plane)

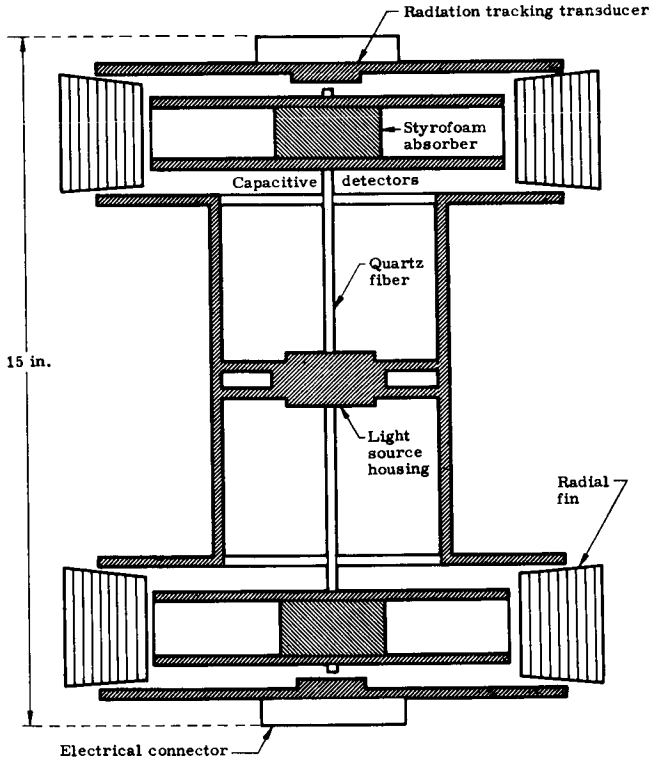


Fig. I-26b. Cross-Section of Elevation View

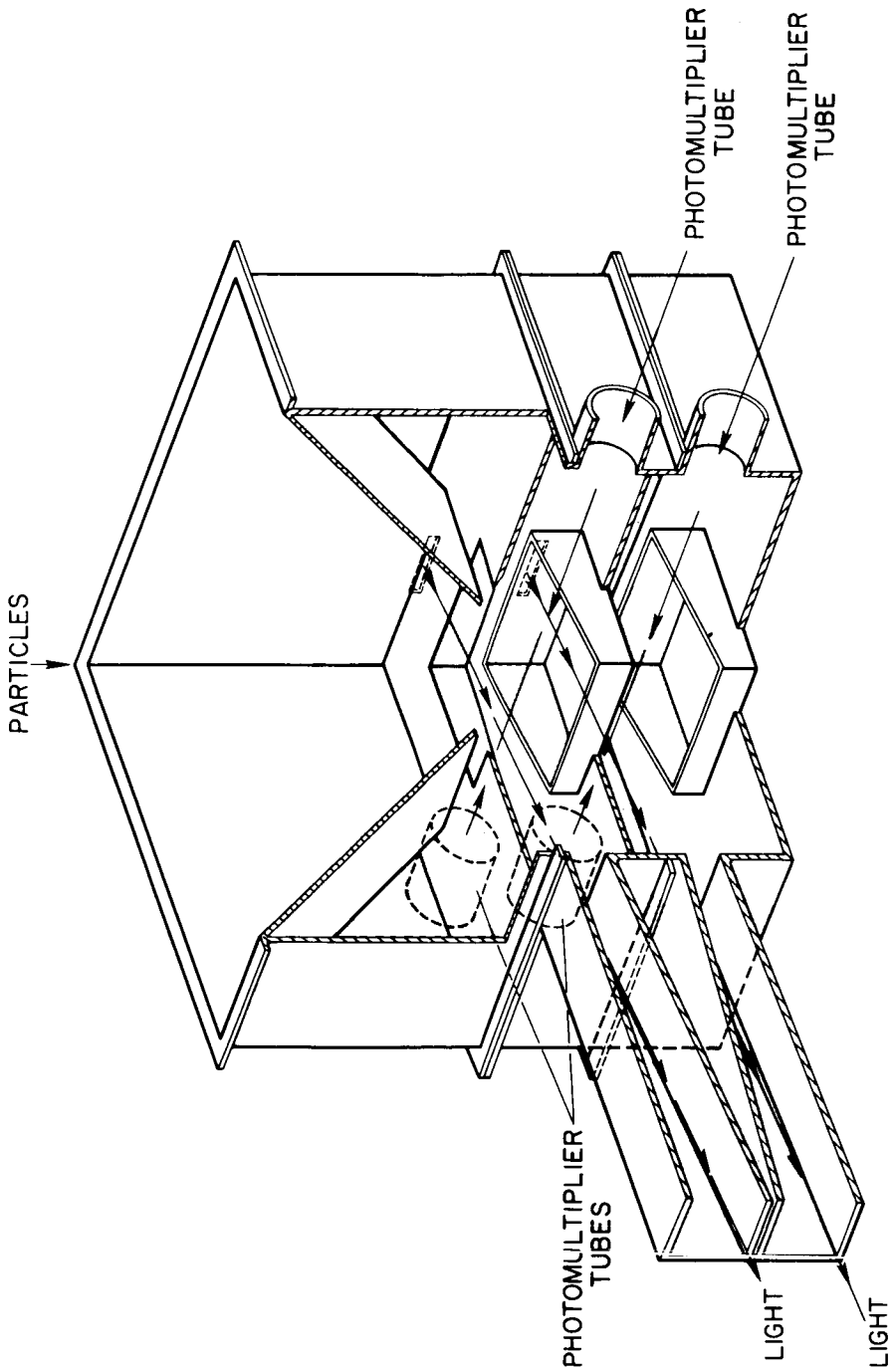


Fig. I-27. Physical Construction of the Micrometeoroid Velocity Detector

Scattered light velocity detector. A feasibility study was conducted by F. Neuman at ARC-NASA (and reported in TN D-1977 (Ref. I-29) on a sensor to measure particle velocity using light scattered by the particle, and initiate and terminate a time of flight measurement. The sensor concept is shown schematically on Fig. I-27. Light scattered by the particle to the upper two PM tubes gives a coincident signal which initiates the timer. Similarly, light scattered by the particle to the lower tubes stops the timer. A block diagram for a sensor version incorporating a momentum detector and a particle area estimate logic is shown on Fig. I-28. Aside from the photomultiplier coincidence, further spurious signal rejection is achieved using a bias setting of 1/3 average pulse height for one electron at the photocathode and requiring at least three pulses within 1.0 μsec in order for the signal to be further processed.

Because of the high speed of the particle through the light beam, the total number of scattered photos is relatively low and the intensity of the light source must be 100 times that of sunlight in order to provide a reasonable sampling rate. It is not shown how this intensity will be obtained and maintained over each of the two light screens. However, it would undoubtedly increase greatly the size, weight, and attitude control (assuming a sunlight focusing technique) requirement of the sensor. The photo tube suggested has a photoelectron multiplication factor of 2.75×10^{8} and a quantum efficiency of 0.1 photoelectrons per photon. With such a large gain a pulse from a single photoelectron would be $\frac{2.75 \times 10^{8}}{0.624 \times 10^{19}} = 4.4 \times 10^{-4}$ coulomb which, with a tube load capacity of 11.5×10^{-12} pf, would give a pulse of 0.293 volts. It is not clear that such a high gain tube is necessary as pulse detection techniques can work with considerably smaller signals. In any event, amplification is not the limiting factor although Neuman proposes detection of cascades from one photoelectron (i.e., a few photos). Noise from starlight is the limiting factor and is rejected on the basis of having an average frequency of one pulse every 5×10^{-4} sec. Real particle pulses are required to give at least three pulses per 2×10^{-6} sec. With this criteria, particles as small as 0.73μ diameter should be detected reliably. Neuman calculates 182 particles/day of 2.5μ diameter based upon the McCracken flux. The limitation can be seen by going up an order of magnitude in size to a particle of 25μ. The incidence rate would be reduced $(10^{3})^{1.7}$ or 1.25×10^{5} to about 1.45×10^{-3}/day. Therefore at least 700 times the area would be required to obtain 1 impact/day. Starlight pulse frequency would go up accordingly (to 1.4×10^{6}/sec) and the error frequency would increase by the sixth power

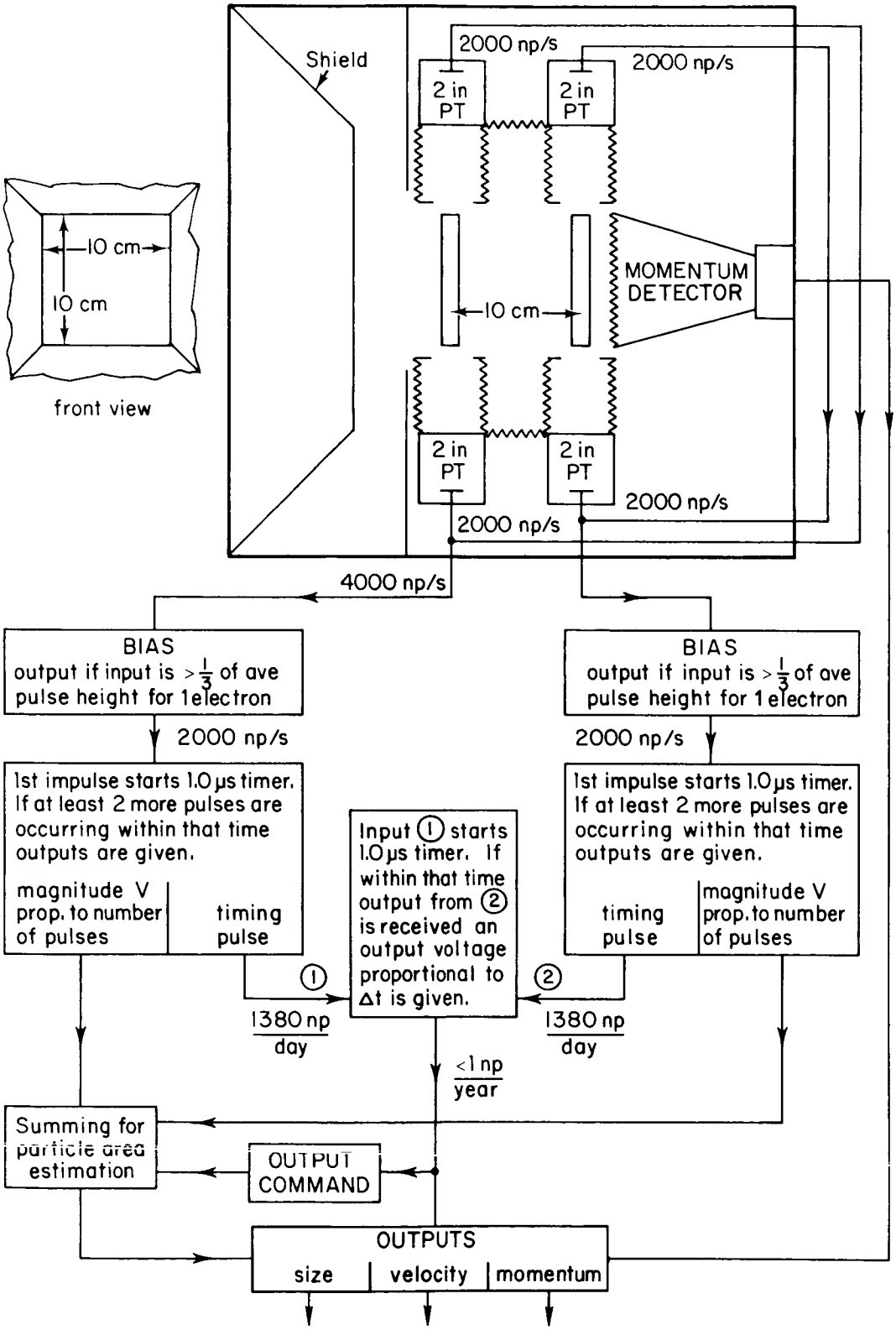


Fig. I-28. Block Diagram of the Velocity Detector

of the noise (starlight) pulse frequency. On the other hand the scattered photon intensity would go up only as the square of the diameter or by 100. This would significantly improve the probability of detecting the particle and/or allow a higher bias setting for starlight pulse rejection. It would not appear that both of these could quantitatively offset the precipitous increase in error frequency. It may therefore only be over a unique range of sensor geometry and particle size that this technique is feasible even if the light intensity requirements could be met.

Electrostatic charge detector. Jennison and McDonnell at Jodrell Bank (Ref. I-30) have proposed and semiquantitatively evaluated a detector based upon the pulse when a charged meteoroid moves between two conducting surfaces, capacitively connected. The particle is not collected or changed. (It appears that this principle is similar to that used by STL to measure velocity of iron carbonyl particles projected from an electrostatic accelerator.) Assuming a 5-volt potential on the meteoroid (under the influence of natural charging mechanisms such as the Van Allen belts, ionosphere and the photoelectric effect of sunlight) particles in excess of 3 μ dia should be detected. The suggested configuration consists of an ion trap and collimating stage, two spaced charge detection stages to give time of flight and a coincidence basis for noise rejection, and a microphone to give momentum. From the independent measurement of velocity and momentum, the mass can be determined. Threshold sensitivity equal to a 3 μ particle would be about 4×10^{-12} gm, so that the microphone and the charge collector should be well matched, as regards to the thresholds. The microphone response varies with mv but the charge collector response varies with r or $(m)^{1/3}$ so that response characteristics of the two transducers do not continue to be well matched above the threshold level.

It does not appear that work on such a detector has proceeded past the conceptual phase.

b. Sensor survey summary

The state-of-the-art of sensors for the objectives of interest is not impressive. Considering first the incident properties of meteoroids--mass, size, density and composition--the only existing sensor is one which can measure velocity. Size may be inferred from the hole size made by the penetrating particle, but the hole size to particle size relationship is really not known. Furthermore, the accuracy in reading hole size is no better than a factor of 2 or 3. Individual sensors giving a response to an incident property parameter such as momentum are in existence and under development. When coupled to velocity sensors they are used to determine particle mass. However, in all of the momentum sensors, the initial properties of this particle are destroyed as the momentum is measured by doing work on the particle. The same

shortcoming is true for kinetic energy sensors. Therefore, measurements of any other incident properties of the particle must be made before momentum or kinetic energy is measured.

The state-of-the-art of penetration sensors is likewise not impressive. By definition, a penetration sensor must destroy the incident properties of the particle as do the momentum or kinetic energy sensors. However, those sensors give a proportional response to the particle's initial properties whereas the existing penetration sensors are threshold detectors only. They do not give either proportional data about the particle's incident properties or proportional data about the residual penetration capability of the particle. One qualified exception is the multilayer Mylar capacitance gage. The concept is an obvious one; however, there is no basis for relating the number of layers penetrated to the depth of aluminum that would be penetrated. Without such a calibration, the proportional measurement must be considered strictly peculiar to that material alone. If this is the case, then it would be more desirable to use honeycomb (or something similar) in a sensor.

Although there exist both velocity sensors and penetration sensors, they are incompatible from the point of view of scale. Penetration thicknesses of interest imply the use of large area sensors. The largest area of an existing velocity sensor is about one square inch. The largest sensor under development is about 64 sq in. This scale incompatibility exists also for momentum and kinetic energy sensors.

In summary, the sensor state-of-the-art is limited by:

(1) The lack of sensors for measuring more than one incident property of the particle.

(2) Very different scales along which penetration and other sensors have developed.

(3) The absence of a proportionally responding penetration sensor.

c. Sensor complements considered

A concept of mounting penetration gages with a spaced foam core or without the use of the foam core was considered early in the study as a means of saving weight and also as a means of reducing the possibility of spurious signals from the discharge of electrons accumulated (from space radiation) in the foam. For a one mil aluminum target plate sensor, approximately half the weight is in the foam.

During our discussion with Dr. Cooley on the experimental results of the infrared impact and penetration detector, it became apparent that the free volume between two capacitors (or between each capacitor and

the detached baffle, if used) could be utilized as the viewing volume of an infrared detector. The infrared detector could be used to analyze the kinetic energy of the penetrating particle or could be used simply to corroborate the capacitor output. Two opposing sensors per bay would be required to "triangulate" the signal because of the $1/r^2$ decrease in signal from the source. Since the proportional (to kinetic energy) response of the infrared sensor was not definitive below 2 to 3 times the minimum penetrating energy, the number of particles capable of analysis would be $2^{-1.34}$ to $3^{-1.34}$ or approximately 2.5 to 4.5 times fewer than the number penetrating the capacitor. If the capacitor (or any other primary penetration gage) were sized for 16 penetrations in each of 5 zones then only 20 to 30 analyzable infrared pulses should be expected. Therefore, complex pulse height analysis circuitry would not appear to be justified. We also considered the following:

(1) Reduce thickness of primary penetration detector so that sample with analyzable infrared signal is increased.

(2) Accept small analyzable sample. However, if primary sensor receives much more data than anticipated, then increase in analyzable infrared sample is effectively analogous to having a thicker primary penetration detector.

(3) Same as 2, except set threshold level of infrared instrument to be equivalent to the signal from a particle capable of penetrating twice the thickness of the primary penetration detector and do no further pulse height analysis.

Number 1 was unattractive because it compromised the primary penetration gage. Number 2 gave a good reserve capacity for penetration but there was a very good possibility that the elaborate PHA would get little use. Number 3 simplified the PHA to a one level threshold but required the signals from the two infrared detectors per bay to be "triangulated" automatically to resolve the flash source strength before going into a level discriminator. Therefore it did not represent a clear cut simplification over No. 3.

A combined sensor to obtain penetration and velocity was also considered. This could be a thin film, grid-mounted capacitor to initiate time of flight ahead of the primary penetration capacitor which would terminate the time of flight measurement. One version considered had a double-face capacitor in the center and two thin film capacitors spaced on either side. The other configuration differed in that two single-faced capacitors spaced by a thin foam layer would be used instead of the double faced capacitor. A basic shortcoming was the loss of total sensor area that would result from increasing the volume of

each group of sensors to give adequate standoff distances for the time of flight measurement. For example, about 600 sq ft could be exposed by an Atlas-Agena launched spacecraft using 1-in. penetration gage frames. For a minimum standoff distance of 1 in. (between thin film and penetration gage), frame thickness would double and the total sensor area would halve. Another shortcoming would be the effective loss of area due to the grid mounting the thin film capacitor. Based upon the GSFC Velocity Tube this loss would be about 30%. Another effective area loss would result from collimation necessary to eliminate shallow angle penetrations. This is necessary because of their large velocity uncertainty and also because of the likelihood of particle or debris "refraction" after passing through the grid. The collimators would take up volume and also reduce the solid angle sampled, both of which cut down the data sample (or reduce the effective sampling area). Practical techniques for velocity measurement coincident with penetration measurement therefore appeared to require considerable compromise in the penetration sample. (Note also that the velocity data sample requirement is four times higher than the penetration data requirement.)

Combining momentum and penetration sensors was suggested. Adding microphones to the penetration gage panels (sizes up to 3 x 4 ft) appeared impractical in terms of interpretation of data, unless a very extensive calibration experiment of microphone response to penetrating particles was made. Another version would have a microphone sounding plate inside the space between the penetration sensors to absorb the remaining momentum (from penetration in either direction). The data sample would be decreased (as for the infrared sensor) and an extensive calibration between penetration and residual momentum would be required.

Another possible arrangement considered arose from the large gap between the thickness of penetration gages that could be used and the thickness of interest to Apollo. We considered using a portion of the available area for thick penetration gages ($\geq$ 0.025 in.) or for bumper penetration gages on the theory that the thin primary gages would give a high confidence sample. If the thick gages received no penetrations, we could also say but with much less confidence that the penetration rate would be less than a certain value, and extrapolating the thin gage data to larger gages could then be made with somewhat increased confidence. In view of the 4.02 power relation of area versus gage thickness such a suggestion appeared worthy of consideration only for the Saturn-launched spacecraft.

Noncoincident measurement combinations were considered because of the difficulty in combining the penetration measurements with other measurements. From the viewpoint of state-of-the-art and reliability, this is a better approach because most of the sensors suitable for the

other objectives (impact momentum, velocity and mass) have been developed for much smaller particles than the existing penetration sensors.

To provide an overlap in particle size between the penetration sample and the others,a number of techniques were considered. One used a thin capacitor (1/4 mil) as the screen for a CdS detector. This would respond to particles as small as 6.6×10^{-10} gm which was within the sample window of the nonpenetration sensors. This would also give a correlation between penetration rate and hole size distribution. A thin capacitor alone (0.1 sq ft) would be a simpler way but would not give the hole size data. A thin film capacitor deposited on a few square inches of the primary penetration gages was also considered for penetration rate data in the 10^{-12} gm region. The Mylar multicapacitor was also considered. A few square feet should give sufficient data at the 5×10^{-9} gm level. Ten to twenty square feet might give sufficient data so that a correlation between the first two or three layers of the multicapacitor and aluminum penetration rates might be obtained.

C. REFERENCES

1. Whipple, F. L., J. Geophys Res., 68, 4929-4939 (1963).

2. Hawkins, G. S. and Upton, E. K. L., The Astrophys. J., 128, 727-735 (1958).

3. Hawkins, G. S., Annual Review of Astronomy and Astrophysics, 2, 149-164 (1964).

4. Brown, H., J. Geophys. Res., 65, 1679-1683 (1960).

5. Brown, H., J. Geophys. Res., 66, 1316-1317 (1961).

6. McCracken, C. W. and Alexander, W. M., "The Distribution of Small Interplanetary Dust Particles in the Vicinity of the Earth," NASA TN D-1349, Washington (1962).

7. Van de Hulst, H. C., Astrophys. J., 105, 471 (1947).

8. Ingham, M. F., Space Science Rev., 1, 576-588 (1962-1963).

9. Kaiser, T. R., Space Science Rev., 1, 554-575 (1962-1963).

10. Whipple, F. L., "Particulate Contents of Space," in Medical and Biological Aspects of the Energies of Space, edited by P. A. Campbell, Columbia University Press, New York (1961).

11. Whipple, F. L., "Meteoroids and Dust," presented at Third International Symposium on Bioastronautics and the Exploration of Space, San Antonio (1964).

12. Dole, S. H., "The Gravitational Concentration of Particles in Space Near the Earth," Planetary Space Science, 9, 541-553 (1962).

13. Volkoff, J. J., "Protection Requirements for the Resistance of Meteoroid Penetration Damage of Interplanetary Spacecraft Systems," JPL, TR No. 32-410, (1964).

14. Southworth, R. B., on S. H. Pole's paper "The Gravitational Concentration of Particles in Space Near the Earth," Planetary Space Science, 11, 499-503 (1963).

15. Singer, S. F., Nature, 192, 321-323 (1961).

16. Beard, D. B., Astrophys. J., 128, 496-506 (1959).

17. Öpik, E. J., Private Communication, Jan 8, 1963.

18. Bradford, D. C. and Dycus, R. D., "A Review of the Meteoroid Environment in Cis-Lunar Space and on the Lunar Surface," preprint No. 64-63, AIAA New York (1964).

19. Shelton, R. D., Stern, H. E. and Hale, D. P., "Some Aspects of the Distribution of Meteroric Flux about an Attractive Center," in Space Research IV, edited by P. Muller, North Holland Publishing Company, Amsterdam (1964).

20. Hale, D. P., and Wright, J. J., J. Geophys. Res., 69, 3709-3717, 3719-3726 (1964).

21. Pollack, F. G., Winslow, Jr., P. C. and Davison, E. H., "Preliminary Experimental Investigation of a Double Capacitor Coincidence Discharge Type Micrometeoroid Penetration Sensor," NASA TM E-2255 (1964).

22. Monteith, L. K. and Smith, A. M., "Theoretical Analysis of Operational Characteristics of Micrometeoroid Capacitor Detector," Research Triangle Institute, Report under Contract NAS1-3343 (1964).

23. Farmer, B. J. and Johnson, J. H., "Final Report on Investigation of Electron Energy and Intensity Effects on Capacitor Type Micrometeoroid Detectors," Ling Temco Vought Report No. 0-71000/4R-15 Contract NAS8-9032, (1964).

24. "Investigation of Feasibility of Infrared Detection of Meteoroid Punctures in Atlas Tanks," Exotech Inc. Report TR-003, Contract NAS9-1268 (1963).

25. "Functional Specification Mariner C Flight Equipment Cosmic Dust Detector," JPL Spec No. MC-4-224B (1963).

26. Webster, R., "Preliminary Report on a New Micrometeoroid Detector," Republic Aviation Corporation, RAC 1878 (1964).

27. Rogallo, V. L., "Measurement of the Heart Beat of Bird Embryos with a Micrometeorite Transducer," NASA SP-5007, Washington (1964).

28. Snyder, L. M., "Advanced Micrometeoroid Detector Analyzer," Electo Optical Systems, Inc. Report 5150, Contract NAS9-2787 (1964).

29. Neuman F., "A Micrometeoroid Velocity Detector," NASA TND-1977, Washington (1963).

30. Jennison, R. C. and McDonnell, J. A. M., Planetary Space Sciences, 12, 627-635 (1964).

31. Hastings, E. C., "The Explorer XVI Micrometeoroid Satellite Supplement III," NASA TMX-949, National Aeronautics and Space Administration, Washington (1963).

32. "Meteoroid Environment in Near-Earth, Cis Lunar and Near-Lunar Space," Engineering Criteria Bulletin, EC-1, NASA/MSC, Houston, November 8, 1963.

33. Frost, V. C., "Aerospace Meteoroid Environment and Penetration Criterion," Aerospace Corp. Rep. No. 70R-269 (4560-40)-2, Los Angeles, August 17, 1964.

APPENDIX I-1

PRESSURIZED SENSOR ANALYSIS

(I) Pressure Loss Versus Hole Size

Pressure-time relationship

$$\frac{A\,t}{V_c} = 0.00891 \left[\left(\frac{P_{co}}{P_c}\right)^{1/7} - 1\right] \quad \text{(for air)}$$

V_c = pressure vessel vol (ft^3)

A = hole area (ft^2)

t = time for pressure to reduce to "P_c" (sec)

P_{co} = initial pressure (lb/ft^2 absolute)

P_c = pressure at time "t" (lb/ft^2 absolute)

Orifice coefficient = 0.60 = θ

	Air	Helium
	ρ = 0.0753 lb/ft^3	ρ = 0.01039
Speed of sound	C = 1126 fps	C = 1480
Ratio of specific heat	$n = \frac{C_p}{C_v} = 1.40$	n = 1.66

General eq:

$$P_c = P_{co} \left\{ \frac{1}{\left[\frac{\theta A C}{V_c} \cdot \left(\frac{2}{n+1}\right)^{\frac{n+1}{2(n-1)}} \cdot \left(\frac{n-1}{n}\right) t\right] + 1} \right\}^{\frac{2n}{n-1}}$$

For helium: n = 1.66

$$\frac{2}{n+1} = \frac{2}{2.66} = 0.7519 \qquad \frac{2n}{n-1} = \frac{3.32}{0.66} = 5.0303$$

$$\frac{n+1}{2(n-1)} = \frac{2.66}{1.32} = 2.0152 \quad \left(\frac{2}{n+1}\right)^{\frac{n+1}{2(n-1)}} = (0.7519)^{2.0152}$$

$$= 0.5639$$

$$\frac{n-1}{n} = \frac{0.66}{1.66} = 0.3976$$

For helium:

$$P_c = P_{co} \left\{ \frac{1}{\left[\frac{\theta A C}{V_c} \times 0.5639 \times 0.3976 \times t \right] + 1} \right\}^{5.0303}$$

$$\left(\frac{P_c}{P_{co}}\right)^{\frac{1}{5.0303}} = \frac{1}{0.22421 \frac{\theta A C}{V_c} t + 1}$$

Using $\theta = 0.60$ and $C = 1480$ fps

$$\left(\frac{P_c}{P_{co}}\right)^{\frac{1}{5.0303}} = \frac{1}{\underbrace{0.22421 \times 0.60 \times 1480}_{= 199.1} \times \frac{A t}{V_c} + 1}$$

Therefore,

$$\frac{A \times t}{V_c} = 0.0050226 \left[\left(\frac{P_{co}}{P_c}\right)^{\frac{1}{5.0303}} - 1 \right] \text{ for helium.}$$

P_c (psi)	$\frac{P_{co}}{P_c}$	$\text{Log}\left(\frac{P_{co}}{P_c}\right)$	$\frac{1}{5.0303} \log \left(\frac{P_{co}}{P_c}\right)$	$\left(\frac{P_{co}}{P_c}\right)^{\frac{1}{5.0303}}$	$\frac{A \times t}{V_c}$
14.7	1	0	0	1	0
14.4	1.021	--	--	--	1.9×10^{5}
13.0	1.13	0.053078	0.010552	1.0245	1.2305×10^{-4}

P_c (psi)	$\frac{P_{co}}{P_c}$	$\text{Log}\left(\frac{P_{co}}{P_c}\right)$	$\frac{1}{5.0303}\log\left(\frac{P_{co}}{P_c}\right)$	$\left(\frac{P_{co}}{P_c}\right)^{\frac{1}{5.0303}}$	$\frac{A\,t}{V_c}$
12.0	1.225	0.088136	0.017521	1.0411	2.0643×10^{-4}
11.0	1.338	0.126456	0.025139	1.0600	3.0136×10^{-4}
10.0	1.47	0.167317	0.033262	1.0795	3.9930×10^{-4}
9	1.632	0.212720	0.042287	1.1025	5.1481×10^{-4}
8	1.839	0.264582	0.052600	1.1290	6.480×10^{-4}
7	2.100	0.322219	0.064056	1.1588	7.9759×10^{-4}
6	2.450	0.389166	0.077364	1.195	9.790×10^{-4}
5	2.94	0.468347	0.093105	1.2395	1.2029×10^{-3}
4	3.67	0.564666	0.112253	1.2950	1.4817×10^{-3}
3	4.90	0.690196	0.137208	1.3718	1.8674×10^{-3}
2	7.35	0.866287	0.172214	1.4868	2.445×10^{-3}
1.5	9.80	0.991226	0.197051	1.5735	2.8805×10^{-3}
1.0	14.7	1.167317	0.232057	1.7062	3.547×10^{-3}
0.5	29.4	1.468347	0.29190	1.9688	4.8657×10^{-3}

(II) Size of Meteoroid Required to Puncture Thin Metallic Targets

(a) For aluminum targets

$P = K\,(mV)^{1/3}$

$\therefore P = 0.102\,(22\,m)^{1/3}$

$m = 42.8328\,P^3$

$m = \frac{\pi}{6}\,d^3 \times \rho_m$

$d = \left(\frac{6}{\pi} \times \frac{m}{\rho_m}\right)^{1/3}$

P = penetrated thickness (in.)

K = 0.102 for aluminum

m = meteoroid mass (gm)

V = meteoroid velocity (km/sec)

(taken as 22 (km/sec))

ρ_m = meteoroid density (gm/cm^3)

d = meteoroid diameter (cm)

Target Thickness P (in.)	P^3	Meteoroid Mass m	Meteoroid Diameter d (cm)		
			ρ_m = 0.50 gm/cm^3	Stony ρ_m = 2.7 gm/cm	Iron ρ_m = 7.9 gm/cm^3
0.0005	0.125×10^{-9}	5.355×10^{-9}	0.00273	0.00156	0.00109
0.001	1×10^{-9}	4.2833×10^{-8}	0.00546	0.00312	0.00218
0.002	8×10^{-9}	3.4270×10^{-7}	0.01092	0.00624	0.00436
0.003	27×10^{-9}	1.1566×10^{-6}	0.01638	0.00936	0.00654
0.004	64×10^{-9}	2.7416×10^{-6}	0.02184	0.01248	0.00872
0.005	125×10^{-9}	5.3548×10^{-6}	0.02730	0.01560	0.01090

(b) For BeCu and stainless steel thin targets

$P = K (mV)^{1/3}$

$P = 0.051 (22\ m)^{1/3}$

$m = 342.6624\ P^3$

See (a), above, for symbols and units

$$d = \left(\frac{6}{\pi} \times \frac{m}{\rho m}\right)^{1/3}$$

Target Thickness P (in.)	P^3	Meteoroid Mass m	Meteoroid Diameter d (cm)		
			ρ_m = 0.50 gm/cm^3	Stony ρ_m = 2.7 gm/cm^3	Iron ρ_m = 7.9 gm/cm^2
0.0005	0.125×10^{-9}	4.2833×10^{-8}	0.00546	0.00312	0.00218
0.001	1×10^{-9}	3.4266×10^{-7}	0.01092	0.00624	0.00436
0.002	8×10^{-9}	2.7413×10^{-6}	0.02184	0.01248	0.00872
0.003	27×10^{-9}	9.2519×10^{-6}	0.03276	0.01872	0.01308
0.004	64×10^{-9}	2.1930×10^{-5}	0.04368	0.02496	0.01744
0.005	125×10^{-9}	4.2833×10^{-5}	0.05460	0.03120	0.02180

(III) Size of Meteoroid Required to Puncture Thin Metallic Targets and Resulting Hole Size

From NASA TN D-1431, tests of penetration of small pyrex-glass spheres, representative of stony meteoroids, into aluminum targets indicated that

$$D/d = 0.0168\ V^{1/2}$$

D = hole diameter (in.)

d = projectile diameter (in.)

V = projectile velocity (fps)

For

V = 22 km/sec (72,180 fps)

$$P/d = 0.0168\ (72,180)^{1/2}$$

$$D/d = 4.51$$

For BeCu and stainless steel thin targets

Target Thickness P (in.)	Meteoroid Mass m	Meteoroid Diameter d ($\rho_m = 2.7$) (in.)	Hole Diameter D (D/d = 4.51) (in.)	Hole Area A (ft^2)
0.0005	4.2833×10^{-8}	0.00123	0.00554	1.67×10^{-7}
0.001	3.4266×10^{-7}	0.00246	0.01109	6.71×10^{-7}
0.002	2.7413×10^{-6}	0.00490	0.02205	2.65×10^{-6}
0.003	9.2519×10^{-6}	0.00738	0.03320	6.01×10^{-6}
0.004	2.193×10^{-5}	0.00983	0.04425	1.069×10^{-5}
0.005	4.2833×10^{-5}	0.01230	0.0554	1.671×10^{-5}

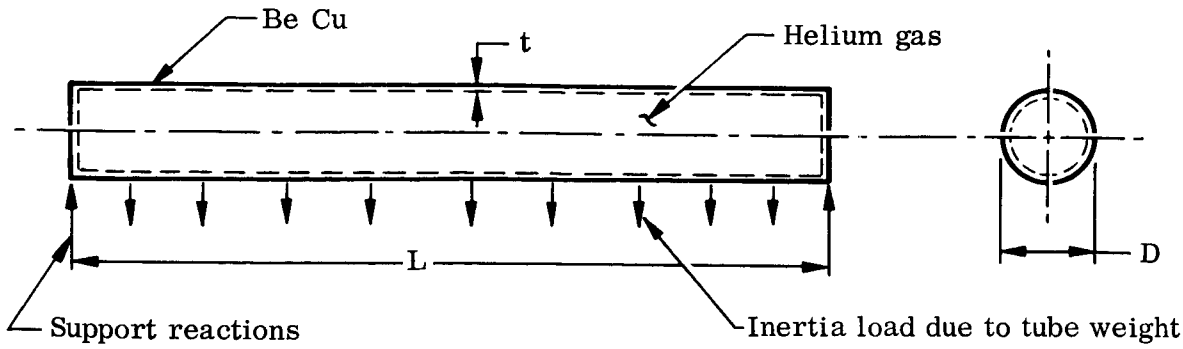
(IV) Pressure Loss Versus Time for Meteoroid Penetration

For BeCu and stainless steel thin targets

Pressure P (psi, absolute)	$\frac{AxT}{V_c}$ (for helium)	Target Thick. (in.)	0.0005	0.001	0.002	0.003	Value of "T" (sec)*
		Hole Dia (in.)	0.00554	0.01109	0.02205	0.00332	
		Hole Area (ft^2)	1.67×10^{-7}	6.71×10^{-7}	2.65×10^{-6}	6.01×10^{-6}	
14.7	0		0	0	0	0	
14.4	1.9×10^{-5}		114	28.35	7.16	3.16	
13	1.2305×10^{-4}		738	183.9	46.50	20.52	
12	2.063×10^{-4}		1,239	308.0	78.0	34.4	
11	3.0136×10^{4}		1,800	448	113.5	50.1	
10	3.993×10^{-4}		2,395	595	150.9	66.5	
9	5.1481×10^{-4}		3,080	766	194.0	85.5	
8	6.480×10^{-4}						
7	7.976×10^{-4}						
6	9.790×10^{-4}		5,860	1460	369	162.9	
5	1.2029×10^{-3}						
4	1.4817×10^{-3}		8,880	2210	559	247.0	
3	1.8674×10^{-3}						
2	2.445×10^{-3}		14,680	3650	925	407.0	
1.5	2.8805×10^{-3}						
1.0	3.547×10^{-3}		21,220	5290	1340	590.0	
0.5	4.866×10^{-3}						
0.0	∞		∞	∞	∞	∞	

*For pressure volume of 1 ft^3 and helium gas at initial pressure of 14.7 psi

(V) Bending Strength of Tubes



Material: Beryllium-copper strip

Spec QQ-C-533 Condition A

Ft_U = 65,000 (psi) $\quad E = 18 \times 10^6$ psi

Ft_y = 42,000 (psi, est) $\quad G = 7.3 \times 10^6$ psi

Fc_y = 42,000 (psi, est) $\quad \rho = 0.297$ lb/in.^{3}

% elong = 35 (in.^{2})

R_B = 45 - 78

Dia D (in.)	Thickness t (in.)	D/t	R/t	$\frac{\sigma_c}{E}$	σ_c (psi)	I (in.^{4})	Allowable Moment (lb-in.)
2	0.0005	4000	2000	0.00002	360	0.00134	0.565
2	0.001	2000	1000	0.00017	3,060	0.003142	9.620
2	0.002	1000	500	0.00047	8,480	0.006270	53.200
2	0.003	667	334	0.00080	14,400	0.009390	135.10
2	0.004	500	250	0.00150	27,000	0.012506	338.00

D (in.)	t (in.)	Area (in.^{2})	Weight per in. (lb)
2	0.0005	0.00314	0.000934
2	0.001	0.00627	0.001861
2	0.002	0.01252	0.003720
2	0.003	0.01880	0.005590
2	0.004	0.02502	0.00744

(VI) Bending Moments due to 15 g Load Factor Normal to Axis of Tube

D (in.)	t (in.)	Weight per In. (lb)	Bending Moment(lb-in.)					
			L = 1 ft	L = 2 ft	L = 3 ft	L = 4 ft	L = 6 ft	L = 8 ft
2	0.0005	0.000933	0.302	1.210	2.62	4.85	10.88	19.39
2	0.001	0.001861	0.502	2.010	4.36	8.02	18.10	32.22
2	0.002	0.00372	1.002	4.020	8.70	16.10	36.20	64.40
2	0.003	0.00559	1.510	6.020	13.05	24.10	54.30	96.80
2	0.004	0.00744	2.015	8.060	17.40	32.20	72.80	128.80

(VII) Equivalent Relation of Internal Pressure Axial Stress to External Moment Axial Stress

For pressure "p"

$$\sigma_p = \frac{p \times \pi R^2}{2\pi R \times t} = \frac{pR}{t}$$

For moment "M"

$$\sigma_M = \frac{MC}{I} = \frac{M \times R}{\pi R^3 t} = \frac{M}{\pi R^2 t}$$

Equating $\sigma_p = \sigma_M$ (pressure stress equal to bending stress)

$$\frac{pR}{t} = \frac{M}{\pi R^2 t}$$

$$M = \pi R^3 p$$

(VIII) Vibration Data--2 in. Diameter BeCu Tubes

For a simply supported beam, the vibration frequency in first mode is

$$n = \frac{\pi}{2} \sqrt{\frac{g E I}{w}} \times \frac{1}{\ell^2}$$

n = frequency (cps)

g = 32.2 (ft/sec^2)

E = elastic modulus (lb/ft^2)

I = moment of inertia (ft^4)

w = unit weight (lb/ft)

ℓ = length (ft)

For BeCu, E = 18×10^6 psi = 2.59×10^9 lb/ft^2

Dia D (in.)	Thickness t (in.)	Weight w (lb/ft)	Moment of Inertia I (ft^4)	$\frac{g E I}{w}$	$n \ell^2 = \frac{\pi}{2}\sqrt{\frac{g E I}{w}}$	For "ℓ" = 3 ft n
2	0.0005	0.0112	6.51×10^{-8}	48.5×10^4	1092	121.6
2	0.001	0.02236	1.528×10^{-7}	57.1×10^4	1185	131.8
2	0.002	0.0446	3.05×10^{-7}	57.1×10^4	1185	131.8
2	0.003	0.0671	4.56×10^{-7}	57.0×10^4	1185	131.8
2	0.004	0.0894	6.08×10^{-7}	56.9×10^4	1181	131.5

II. TELECOMMUNICATIONS

Jack D. Pettus
Sidney Roedel
Charles P. Scheiner
John Donaldson

II. TELECOMMUNICATION SYSTEM

The basic requirement of this micrometeoroid deep space satellite (MDSS) conceptual study is to select techniques for measuring micrometeoroid impacts, associated data handling equipment to register the penetration and/or impact information and communication equipment to transmit these data to the ground. In addition, techniques were considered for measuring, recording and transmitting other information at the event time of micrometeoroid impact, to obtain a complete "hit history". Simple, as well as sophisticated, methods were investigated to obtain significant micrometeoroid data during the satellite mission lifetime.

A large number of tradeoff investigations were conducted. These tradeoffs considered reliability versus: technique simplicity, number of parts required, method of operation, ancillary equipment, storage requirements, power requirements, weight and volume constraints, communication considerations and many other factors. Tradeoff studies also considered the present and anticipated state of the art of equipment.

1. Requirements and Constraints

To evaluate data requirements for the sensors, a priority of possible different scientific and engineering measurements was established. These requirements were modified during the study, by considering:

(1) Simplicity of operation and the related reliability for each component and subsystem.

(2) Feasibility of the recommended technique, as constrained by availability of space-proven hardware.

(3) Limitations imposed by other spacecraft systems.

(4) Convenient formatting of the various measurement data outputs, to reduce onboard storage requirements, power demand during transmission periods and switching operations.

(5) Elimination of insignificant data by onboard data management and, therefore, reduction of ground station monitor time.

(6) Minimum storage requirements, to keep memory units as small as possible to achieve higher reliability (fewer parts).

(7) Adaptability of the data handling system to the outputs of the different sensors to allow flexibility in processing methods.

(8) Sensor measurement and data processing capability during stored data readout and transmission.

(9) Standard length of data frames (number of words), as well as length of data words (number of bits).

(10) Elimination of power on/off switching wherever possible.

(11) Minimum number of commands, to avoid system complexity.

(12) Redundancy for measurements which represent primary objectives.

A general requirement was that, at no time throughout the mission should measurement of any significant micrometeoroid data be jeopardized by either the occurrence of a momentary switching or command function or any other event in the data processing system. At the beginning of this study, emphasis was placed on developing a data processing system which could automatically control any data flow condition which might come up in the course of the mission due to the coincidence of a number of measurement events.

2. Summary

A design concept for MDSS instrumentation and onboard data processing has been established. A number of measurement systems pertinent to particle impact, energy and velocity detection have been investigated. Principal attention has been given to systems for detection of meteoroid penetration, the primary objective. Secondary parameters, for which sensors and associated data processing techniques were investigated include determination of particle influx rate, density, velocity and direction. Sensing and data processing methods for determining satellite orientation at impacts were examined to correlate spacecraft attitude information and particle influx direction.

Each of the measurement systems was evaluated from the point of view of long-term reliability, sensing technique accuracy and compatibility with the requirements of other spacecraft systems. Effects of the individual sensor data outputs on storage and telemetry requirements were considered. Reliability in the design concept was emphasized, specifically for the micrometeoroid penetration measurement system, which was considered most important.

A design concept for the MDSS communication, command and tracking subsystems has been established. A number of communication techniques, associated with existing ground station networks, have been investigated. Each of these techniques was evaluated from the standpoint of compatibility with the primary and secondary measurement requirements, power requirements and especially long-term reliability requirements.

Numerous tradeoff studies were conducted (see Section B). Some of the results are presented in tabulated form in the Appendixes. Detailed reliability analyses are presented in Volume IV.

Preliminary considerations for hardware selection and packaging techniques for components are also discussed in this report (Vol. III, Chapts II and III).

3. System Description

The telecommunication system is shown in a simplified block diagram in Fig. II-1. The telecommunication system consists of a primary and a secondary data processing subsystem and of communication, command and tracking subsystems. The function of the primary subsystem is to continuously monitor and telemeter a count of micrometeoroid penetrations of the capacitance sensor panels. The function of the secondary subsystem is to supplement micrometeoroid penetration information by monitoring and processing data from different types of micrometeoroid impact sensors, as well as spacecraft attitude data and spacecraft housekeeping information. No physical interface exists between the primary and secondary subsystems. Separate power sources supply the two subsystems.

The primary subsystem consists of two identical, continuous operating measurement networks for capacitance sensor panel penetration data. Four counters, two in each network, register cumulative penetrations on the 120, one-mil and the 144, two-mil capacitance sensors. Each counter has a capacity in excess of 30 times the anticipated number of micrometeoroid penetrations. Data collected by the first measurement network is telemetered continuously while that collected by the second network is interrupted only by a command to telemeter secondary data.

The secondary subsystem is composed of:

(1) Data processing and storage units for micrometeoroid hit histories for penetrations sensed by the capacitance sensors and by 36 pairs of IR flash detectors, and for impacts sensed by three Mariner gauges and two velocity gauges.

(2) Data processing and storage units for attitude and diagnostic data.

(3) Real-time telemetry for spacecraft deployment, housekeeping data, delayed command verification measurements, memory overflow data and readout of sensor totalizer counters.

The latter capability is especially interesting, since it allows a higher probability of mission success by providing backup for the memory units.

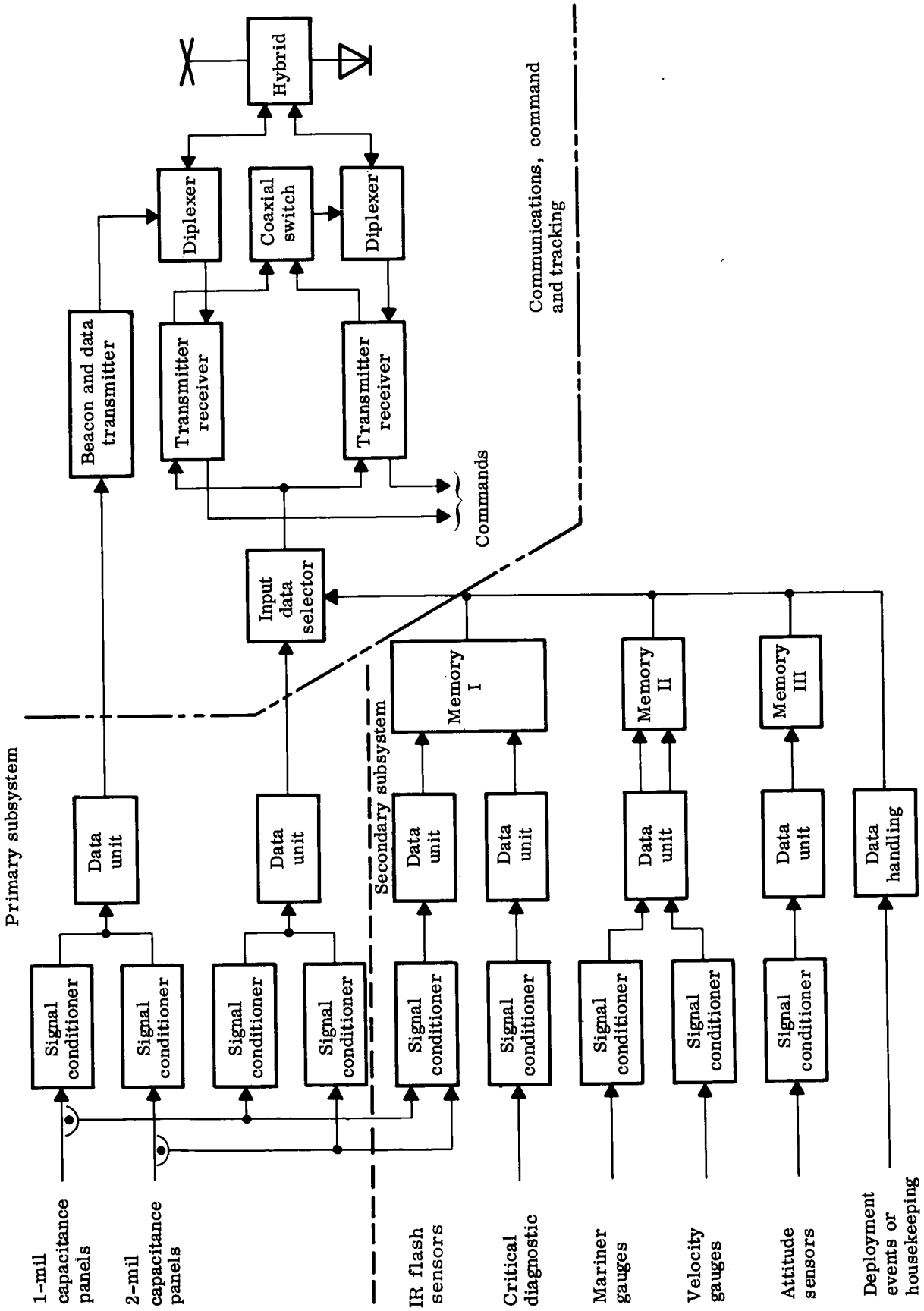


Fig. II-1. Telecommunications System Simplified Block Diagram

The communication, tracking and command subsystem consists of a beacon and data transmitter which continuously telemeters micrometeoroid penetration counts from the primary subsystem, two VHF range and range rate transponders and command decoders, and an omnidirectional antenna. One of the VHF transmitters continuously telemeters redundant primary data or telemeters secondary data by command. The third VHF transmitter is a passive back-up unit, which may be switched on by command. Both receiver sections of the VHF transponders and both command decoders operate continuously.

A. CONCLUSIONS AND RECOMMENDATIONS

1. General

Design goals for the MDSS were achieved using the concept of two separate and mutually independent measurement systems (Fig. II-1). The telecommunication system consists of primary and secondary data processing subsystems, and a communication subsystem (telemetry, tracking and command).

a. Data processing subsystems

The recommended data processing subsystems are a direct result of extensive reliability studies and failure mode analyses (see Volume IV) which were conducted to obtain maximum probability of primary data recovery.

Maximum reliability is achieved throughout the system by development of a basic data module; thus, unit isolation is easily provided and data recovery is not jeopardized. Furthermore, areas of primary importance are further protected by redundancy in either circuit or element.

Handling of primary data is accomplished by two identical data units. The flexibility of this basic data unit is evidenced by the fact that an extended version is utilized throughout the secondary subsystem, with only input and control variations for the different sensors. One primary data unit provides continuous data formats of total capacitance sensor penetrations to a transmitter which operates continuously. The other primary data unit is redundant and provides identical data formats to another transmitter through an electronic data switch.

The secondary data system is composed of data units for each of the sensor groups and three core memories for data storage until data readout and transmission is commanded. Each memory is associated with two particular data units, greatly enchancing the probability of data recovery by reducing the logic required for utilization of a single large memory unit. Also, failure of one memory unit will not prevent recovery of data from the other memories. Data not entered into memory, such as deployment data, housekeeping information and memory

overflow are presented on the secondary data bus in real time for transmission. Real time data units are basically identical to the units entering data into memory, and require no interface to connect to a common data bus with the memory outputs.

Secondary data readout is commanded from the ground. Each memory is read out as a result of a unique command, which is decoded and enters the read data unit in the secondary data system. The function of this unit is to generate sync frames, command the prescribed memory unit to read out twice, and sequence any real-time data prescribed by the received command. The probability of transmission error occurrence is drastically reduced by two readouts per command, in conjunction with parity.

b. Data processing techniques

Parity bit. There is no parity bit associated with the primary or redundant primary data processing subsystems. Since the primary data is continuously transmitted, there is little need for a parity bit. A transmission error can be detected and, hence, corrected simply by noting the correlation between successive data frames.

However, a parity bit has been included in each data word transmitted by the secondary subsystem, due to the latter subsystem's complexity and the fact that data are stored. Inclusion of the parity bit together with the repeated transmission of all information contained in the secondary subsystem, will greatly augment the error detection and correction of the transmitted data. Appendix II-4 shows, mathematically, the gain realized by inclusion of the parity bit.

A parity generator is associated with each memory and with the organization of each real-time format. These parity generators (Fig. II-2) are installed across the data lines, not in series with them; thus, the failure of a parity generator will not have an adverse effect on data recovery.

Format identification. Since the data processing philosophy dictates a fixed format, it is necessary to identify each format in the secondary subsystem. To decode the information, it is necessary to distinguish between any one of 15 different formats. It is recommended that the first four bits of the first data word be reserved for the format identification as shown in Table II-1. It will be noted that the deployment format does not contain a format identification. However, this is not

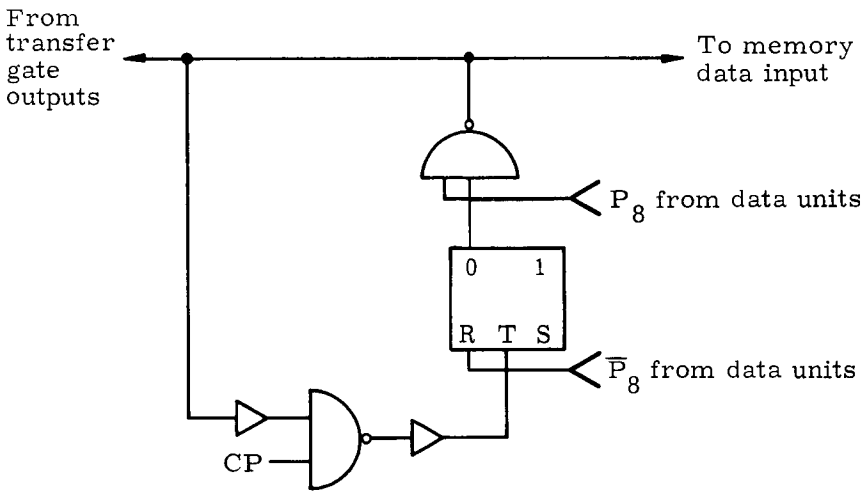


Fig. II-2. Parity Generator

required, since the transmission is continuous and the transmission of the other formats does not take place until the transmission of the deployment format has been terminated by either of the two deployment timers.

Memory overflow data unit. To fully satisfy MDSS system requirements, some means of registering micrometeoroid impacts in excess of anticipated values must be provided. The recommended technique employs a memory overflow data unit which consists of a memory overflow counter for each sensor group. In the event that the particle density encountered is greater than the predicted maximum for which the memory units have been designed, the excess will be recorded on the respective counters in the memory overflow data unit. Simplicity of the recommended technique, and the additional flexibility which it presents to the system are in line with established design philosophies.

Data switch. Secondary data is transmitted upon receipt of a command, which causes the second transmission channel transmitter to be connected to the secondary data bus. It is recommended that the switching be achieved by means of a data switch. This switch normally connects the primary data bus to the transmitter but, upon receipt of a read-out command, the switch is toggled to the secondary data bus. Failure mode protection is accomplished by quad redundant techniques and also by a time function reset to the normal operating mode. As dictated by the requirements for the recovery of primary data, the data switch possesses a high degree of reliability.

Clock synchronization. Since the second transmission channel is common to both redundant primary data and secondary data, it is necessary that sync be established between the two data lines to prevent loss of bit sync at the ground station. Data sync can be accomplished by using a common oscillator or by syncing one master oscillator to another. Reliability analyses have indicated that the former technique is more reliable (See Volume IV) and it is therefore recommended for the MDSS.

Critical diagnostic data. Only spacecraft measurements of prime importance will be stored, to comply with design philosophy and maintain system simplicity; thus, a smaller memory unit may be used. The critical diagnostic format, (Table II-1) contains only measurement data mandatory for accurate data retrieval. Moreover, the critical diagnostic format is entered into storage only once per day, further reducing the size of the memory unit required and increasing system simplicity.

Attitude data. Attitude sensing and determination studies (Volume III, Chapter V) have resulted in a requirement for gathering a large quantity of attitude data near perigee, and considerably fewer data during the remainder of the orbit. The recommended system collects data at two different rates: in the "full attitude" mode of operation, data is

TAB

System

A) SECONDARY SYS

I. Capacitor Panel and IR-Flash Sensor Hit History Fr

W_1	W_2	W_3	W_4	W_5	W_6
Frame ident (4 bits) Cap. hit direc- (3 bits) tion	S/C time (7 bits)	S/C time (4 bits) Days in (3 bits) orbit	1-mil capacitance (7 bits) panel area	2-mil capacitance (7 bits) panel area	Bay number Thickness ident

II. Mariner Gauge Hit History Frame (10 words

W_1	W_2	W_3	W_4	W_5	W_6
Frame ident (4 bits) Spacecraft time (3 bits)	S/C time (7 bits)	S/C time (1 bit) Days in (3 bits) orbit Cap.level B (3 bits) accum hits	Capacitor Level B (5 bits) accumulative hits Mike Level I (2 bits)	Mike Level I (2 bits) Mike Level II (2 bits) Mike Level III (2 bits) Mike Level IV (1 bit)	Mike Level IV Cap. Level I Cap. Level II

III. Velocity Gauge Hit History Frame (10 words)

W_1	W_2	W_3	W_4	W_5
Frame ident (4 bits) Spare (3 bits)	S/C time (7 bits)	S/C time (4 bits) Day in (3 bits) orbit	Microphone level and/or (7 bits) capacitor level ident (1 bit for each of 4 cap. levels and for each of 3 mike levels)	Capacitor and/or microphone (2 bits) initiation Velocity (5 bits)

IV. Full Attitude Frame (10 words) (E

W_1	W_2	W_3	W_4	W_5	W
Frame (4 bits) ident S/C time (3 bits)	S/C time (2 bits) Solar aspect sensor (3 bits) ident Spare (2 bits)	Solar aspect angle 1 (7 bits)	Solar aspect angle 2 (7 bits)	Magnetometer X-axis (7 bits) magnetic field intensity vector	Magnetomet magnetic fiel

V. Hourly Attitude Frame (10 words) (

W_1	W_2	W_3	W_4	W_5
Frame ident (4 bits) Earth sensor ident (3 bits)	Time (7 bits)	Time (1 bit) Solar sensor ident (3 bits) Spare (3 bits)	Solar angle 1 (7 bits)	Solar angle 2 (7 bits)

VI. Memory Overf

W_1 & W_6	W_2 & W_7	W_3 & W
Frame ident (4 bits) Spare (3 bits)	Overflow counter (7 bits) capacitor panels	Overflow counter IR-flash sensor

LE II-1

Formats

TEM FORMATS

ame (10 words) (Entered into Storage on Hit-Demand)

	W_7	W_8	W_9	W_{10}
(6 bits) (1 bit)	1-mil capacitance (7 bits) accumulative hit count	2-mil capacitance (7 bits) accumulative hit count	1-mil Bay IR-flash (7 bits) sensor accumulative hit count	2-mil Bay IR-flash (7 bits) sensor accumulative hit count

) (Entered into Storage on Scaled Hit-Demand)

	W_7	W_8	W_9	W_{10}
(1 bit) (4 bits) (2 bits)	Capacitor Level (4 bits) III, IV Instrument 1 Level (3 bits) A hit count	Instrument 1 Level (7 bits) A hit count	Instrument 1 Level A (2 bits) hit count Instrument 2 Level (5 bits) A hit count	Instrument 2 Level A (7 bits) hit count

(Entered into Storage on Scaled Hit-Demand)

W_6	W_7	W_8	W_9	W_{10}
elocity (7 bits)	Total accumulative (7 bits) capacitor hits	Total accumulative (4 bits) capacitor hits Tube ident (3 bits)	Tube ident (1 bit) Total accumulative (6 bits) capacitor hits, Instrument 2	Total accumulative (5 bits) capacitor hits, Instrument 2 Spare (2 bits)

ntered into Storage on Command)*

6	W_7	W_8	W_9	W_{10}
r Y-axis (7 bits) l intensity vector	Magnetometer Z-axis (7 bits) magnetic field intensity vector	Earth Sensor 1 sighting (4 bits) time Earth Sensor 2 sighting (3 bits) time	Earth Sensor 2 sighting (1 bit) time Earth Sensor 3 sighting (4 bits) time Earth Sensor 4 sighting (2 bits) time	Earth Sensor 4 sighting time (2 bits) Earth Sensor 5 sighting time (4 bits) High or low range flux gate magnetometer identification (1 bit)

Entered into Storage on Command)**

W_6	W_7	W_8	W_9	W_{10}
arth sensor ident (3 bits) pare (4 bits)	Time (7 bits)	Time (1 bit) Solar sensor ident (3 bits) Spare (3 bits)	Solar angle 1 (7 bits)	Solar angle 2 (7 bits)

low Frame***

	W_4 & W_9	W_5 & W_{10}
(7 bits) s	Overflow counter (7 bits) Mariner gauges	Overflow counter (7 bits) velocity gauges

2#

TABLE II-1 (

VII. Critical Diagnostic Data Frame (

W_1	W_2	W_3	W_4	W_5	
Frame ident (4 bits) Capacitor panel diagnostic (3 bits) (charge generator outputs)	Capacitance panel diagnostic (2 bits) (charge generator outputs) Main bus voltage (5 bits)	Battery current magnitude (6 bits) Charge or discharge (1 bit)	Battery temperature (5 bits) Velocity gauge system check (2 bits)	Electronic compartment temperature (5 bits) Master clock temperature (2 bits)	Mast IR-fl ch

VIII. Deployment Verification Data Frame (Realtim

$W_{1,4\&7}$	$W_{2,5\&8}$	
Z wing A 1st fold stowed (1 bit) Z wing A 1st fold erected (1 bit) Z wing A 2nd fold stowed (1 bit) Z wing A 2nd fold erected (1 bit) B 1st fold stowed (1 bit) B 1st fold erected (1 bit) B 2nd fold stowed (1 bit)	B 2nd fold erected (1 bit) C 1st fold stowed (1 bit) C 1st fold erected (1 bit) C 2nd fold stowed (1 bit) C 2nd fold erected (1 bit) D 1st fold stowed (1 bit) D 1st fold erected (1 bit)	D D A T Sp

IX. Full Housekeeping Forma

W_1 (7 bits)	W_2 (7 bits)	W_3 (7 bits)	W_4 (7 bits)	W_5 (7 bits)	W_6 (7

Words 1 to 10	Critical diagnostic frame repeated
Words 11 to 14	4 voltage precision measurements
Words 15 to 18	4 temperature measurements
Words 19 to 20	Spacecraft time and days in orbit
Words 21 to 26	10-1/2 voltage measurements (4 bits each)
Word 27	1-1/2 voltage measurements plus 1 spare bit
Words 28 to 42	24 temperature measurements
Words 43 to 44	IR flash sensor amplifier voltage measurement
Word 45	IR flash sensor amplifier voltage measurement--2 bits; 1 temperature
Word 46	Bias voltage calibration
Words 47 to 51	5 voltage calibration measurements (7 bits each)
Words X to Y:	Cumulative hits capacitance panels: 1-mil panels
	Cumulative hits capacitance panels: 2-mil panels
	Cumulative hits IR flash sensors: 1-mil bays
	Cumulative hits IR flash sensors: 2-mil bays
	Effective capacitance panel area: 1-mil panels
	Effective capacitance panel area: 2-mil panels
	Cumulative hits 3 Mariner gauges Capacitance Level A

B) PRIMARY SY

Capacitance Panel Penetration Count Frame (4

$W_A + W_B$	$W_$
Frame synch (14 bits)	Penetration c (7 bits) panel

* Frame is repeated every 2 minutes for 5 hours near perigee.
** Data repeated to formulate a format as close to 10 words as possible.
*** Format transmitted in readout of Sequences I and II.

:ontinued)

ntered into Storage Once per Day)

W_6	W_7	W_8	W_9	W_{10}
r clock temperature (3 bits) sh sensor system (4 bits) ck	Attitude logic check (5 bits) Mariner gauge system (2 bits) check	Mariner gauge system (1 bit) check Magnetometer system (3 bits) bias Solar aspect logic (3 bits) Temperature 1	Solar aspect logic (2 bits) Temperature 1 Solar aspect logic (5 bits) Temperature 2	Solar aspect logic (5 bits) Temperature 3 Spare (2 bits)

Data Transmitted During Deployment Phase)

$W_{3,6\&9}$	W_{10}
nd fold stowed (1 bit) nd fold erected (1 bit) ennas deployed (2 bits) ner start (1 bit) re (2 bits)	Spare (7 bits)

(Realtime Data on Command)

its)	W_7 (7 bits)	W_8 (7 bits)	W_9 (7 bits)	W_{10} (7 bits)	8 frames 10 words each

Words Y to Z: Cumulative hits 3 Mariner gauges Capacitance Level B
Cumulative hits 3 Mariner gauges Capacitance Level 1
Cumulative hits 3 Mariner gauges Capacitance Level 2
Cumulative hits 3 Mariner gauges Capacitance Level 3
Cumulative hits 3 Mariner gauges Capacitance Level 4
Cumulative hits 3 Mariner gauges Microphone Level 1
Cumulative hits 3 Mariner gauges Microphone Level 2
Cumulative hits 3 Mariner gauges Microphone Level 3
Cumulative hits 3 Mariner gauges Microphone Level 4
Cumulative hits No. 1 Mariner gauge Capacitance Level A
Cumulative hits No. 2 Mariner gauge Capacitance Level A
Cumulative hits velocity gauges Tube No. 1
Cumulative hits velocity gauges Tube No. 2
Cumulative hits velocity gauges Tube No. 3
Cumulative hits velocity gauges Tube No. 4
Cumulative hits velocity gauges Tube No. 5
Cumulative hits velocity gauges Tube No. 6
Cumulative hits velocity gauges Tube No. 7
Cumulative hits velocity gauges Tube No. 8
Command verifications

neasurement--3 bits;
2 spare bits

TEM FORMAT

ords) (Realtime Data Continuous Transmission)

W_2	
nt: 1-mil	Penetration count: 2-mil (7 bits) panels

2A II-10

collected every 2 min during 5 hr in the vicinity of the perigee, and in the "hourly attitude mode" for the remainder of the orbit, when data is collected once every hour. This dual mode of operation simplifies the secondary data processing subsystem, allowing the use of a much smaller memory unit which can be time-shared by the two modes. Also, individual data processing units can be employed for each attitude data mode, adding to system flexibility.

Primary-secondary subsystem isolation. To guarantee the highest probability of mission success, and in keeping with the design philosophy, it is required to isolate the primary, redundant primary and secondary data processing subsystems from one another. Of techniques investigated to date, Hall detector devices have the most desired isolation properties. Since these devices are based on magnetic detection, no physical contact need be made with the primary signal source. Hence, a failure in one of these devices will in no way affect the operation of the primary data processing.

The Hall devices are field-proven items, of high packaging density, with high resistance to radiation and wide temperature tolerance. However, it is recommended that further investigations be conducted to determine the practical application of the device for the intended use on the MDSS, since flux concentrators or other complementary techniques are needed. (This is discussed in Section IIB.)

Memory units. Serial sequential single aperture ferrite core memories have been selected for the purpose of recording data. This type of memory device represents the most reliable storage method available, consistent with the present state of the art.

Velocity gauge and Mariner gauge data processing. The data processing for the velocity gauges includes identification of the individual sensor tube, thus defining the direction of the particle vector in respect to the spacecraft. However, the present data system only identifies the Mariner gauge which has been impacted. It is recommended that further consideration be given to the particle direction data derived from this sensor. The capability exists to identify the side of the sensor which has experienced an impact. Since the storage requirements have been established on the basis of scaled-down total impacts for one orbit, storage capacity need not be altered.

c. Communications

It has been concluded that the STADAN network should be used to support the MDSS program, rather than other NASA controlled networks. Use of an integrated VHF tracking, command and telemetry system is preferred to use of other STADAN frequencies. The recommended MDSS system uses the 136- to 137-mc band for telemetry and 148 mc for command. Use of both bands is required in the range and range rate mode

of operation, the higher frequency being required for the up-link and the lower frequency for the coherent down-link.

The recommended communication subsystem and the conclusions and recommendations given in this chapter are based on an extended study of many configurations for which reliability considerations were heavily weighted. Tradeoff studies accomplished are fully documented in the sections dealing with communications in the reliability volume of this report (Volume IV). A dual-channel communication subsystem is used. Data from the primary data processing subsystem are continuously transmitted over one channel at a fairly low bit rate. Redundant primary or secondary subsystem data is being simultaneously transmitted over the second channel.

An omnidirectional antenna is required for a tumbling spacecraft, but design of a suitable system which will completely satisfy all link requirements appears extremely difficult. The recommended communication system is based on a very low rate of tumble for the spacecraft. Should further studies show tumble rates to be a problem, range and range rate system performance estimates and other possible effects would have to be reviewed.

2. Primary Subsystem Concept

The objective for the primary measurement subsystem is to obtain micrometeoroid penetration data with a reliability better than 90% for a period of one year. Therefore, the conceptual design of the subsystem has been simplified to a level of functional efficiency where this goal is ensured.

The primary subsystem is automatically energized during the deployment mode as soon as solar energy activates the solar cell arrays on the spacecraft "wings". No power switching is used once the primary subsystem is energized. This "no-switching" design philosophy also resolved the problem whether or not to provide command capability for the primary subsystem. The telecommunication system will continue to transmit cumulative micrometeoroid penetration data until a killer timer silences the spacecraft.

A major design requirement was that there should be no physical interface between the primary, redundant primary and secondary data processing subsystems. Several techniques were considered to determine the best way to transfer penetration signals from the capacitance sensors into the secondary subsystem, without any wiring connections. Of the three techniques investigated to date, it is recommended that magnetically coupled transducers (Hall detectors) be used. This device is a space-proven component of high packaging density with high resistance to radiation and wide temperature tolerance. However, further investigation is required to determine the practical feasibility of the device for the intended application.

a. Measurements in the primary system

The primary measurement system uses the simplest means to acquire and telemeter micrometeoroid penetration data detected by the capacitance sensors. The operational mode consists of monitoring the output (penetration signals) of the capacitance sensors and keeping a count of penetrations for each of the two detector gauges.

b. Primary subsystem data processing

The primary data processing subsystem programs, conditions, samples and encodes capacitance sensor penetration data. No other measurements or housekeeping data are taken by the primary subsystem. The recommended conceptual design satisfies the following design criteria:

(1) Reliability of operation is paramount; no single failure will jeopardize the operational capability of other units in the system.

(2) Simplicity of operation defines component size, volume and complexity.

(3) The primary data processing subsystem is independent from other measurement subsystems. Thus, changes in the other systems (such as addition, deletion or replacement of sensors, data processing, etc.) will not affect the probability of successfully obtaining the required primary data.

(4) Measurement data is in such a format that it can be correlated with the outputs of other sensors in the secondary system.

(5) No bit parity is employed in the data encoding process to keep equipment modules to a minimum. Since the primary data is transmitted continuously, transmission errors can be detected, and corrected simply by noting the correlation between successive data frames.

The primary data processing subsystem consists of two identical units (Fig. II-1). Each data unit is self-sufficient, in keeping with the design philosophy which allows no single failure to jeopardize the operational capability of other units in the system. The recommended system represents the most reliable configuration to accomplish the primary mission. The entire unit will be constructed with space-proven high reliability integrated circuits which will perform the function of data collection and format generation. The detailed block diagram of this

system is shown in Fig. II-4. The data format consists of four 7-bit words. The first two words are sync data and the last two are a binary number representing the total number of penetrations recorded in each capacitor gauge. The telemetry format of the primary system is shown in Table II-1. Time of event (penetration) is not included in the primary data format. During the mission lifetime, only 80 penetrations are expected; less than 3 per orbit. It was concluded that ground station monitoring of the continuous primary data transmission can define the time of event with sufficient accuracy. The primary data is continuously presented to the transmitters and is altered only as a result of another penetration. The redundant primary channel shares the second transmission channel with the secondary data processing system such that when secondary data is being transmitted (on command), the primary data bus has been disconnected from the transmitter by the data switch. To enhance the probability of mission success, system design is such that a failure of the data switch will leave the redundant primary line "normally closed".

The effective capacitor sensor area in each gauge (i.e., the respective numbers of operating sensor panels) is not measured by the primary subsystem. This data is obtained by the secondary subsystem, and is used in combination with the penetration counts--to accurately determine micrometeoroid flux variation with orbit altitude.

To gather data during a shadow period, the recommended subsystem requires continuous power, and is therefore powered from an isolated bus (discussed in detail in Volume III, Chapter II). This technique has been selected as a result of reliability tradeoffs versus accumulative NDRO magnetic counters as shown in Volume IV.

3. Secondary Data Processing Subsystem Concept

a. Measurements

Micrometeoroid measurements are taken by the secondary subsystem in two different modes. In one, penetration and/or impact data, as well as supplementary measurements (i.e., event time, particle velocity, direction, energy level, etc.) are monitored and edited into a hit history data frame by hit demand. These hit-demand frames are then entered into memory and read out on command. In the other, counts of cumulative hit registers for each sensor (and in each sensitivity level) along with housekeeping measurements are read out--in real time--by command.

Data collected by the different sensor groups are parallel to, and an extension of, penetration data measured by the capacitance sensors in the primary subsystem. Hence, data from both subsystems can be easily correlated. This is especially true for penetration data. Measurements by the IR flash detectors serve as backup for capacitance

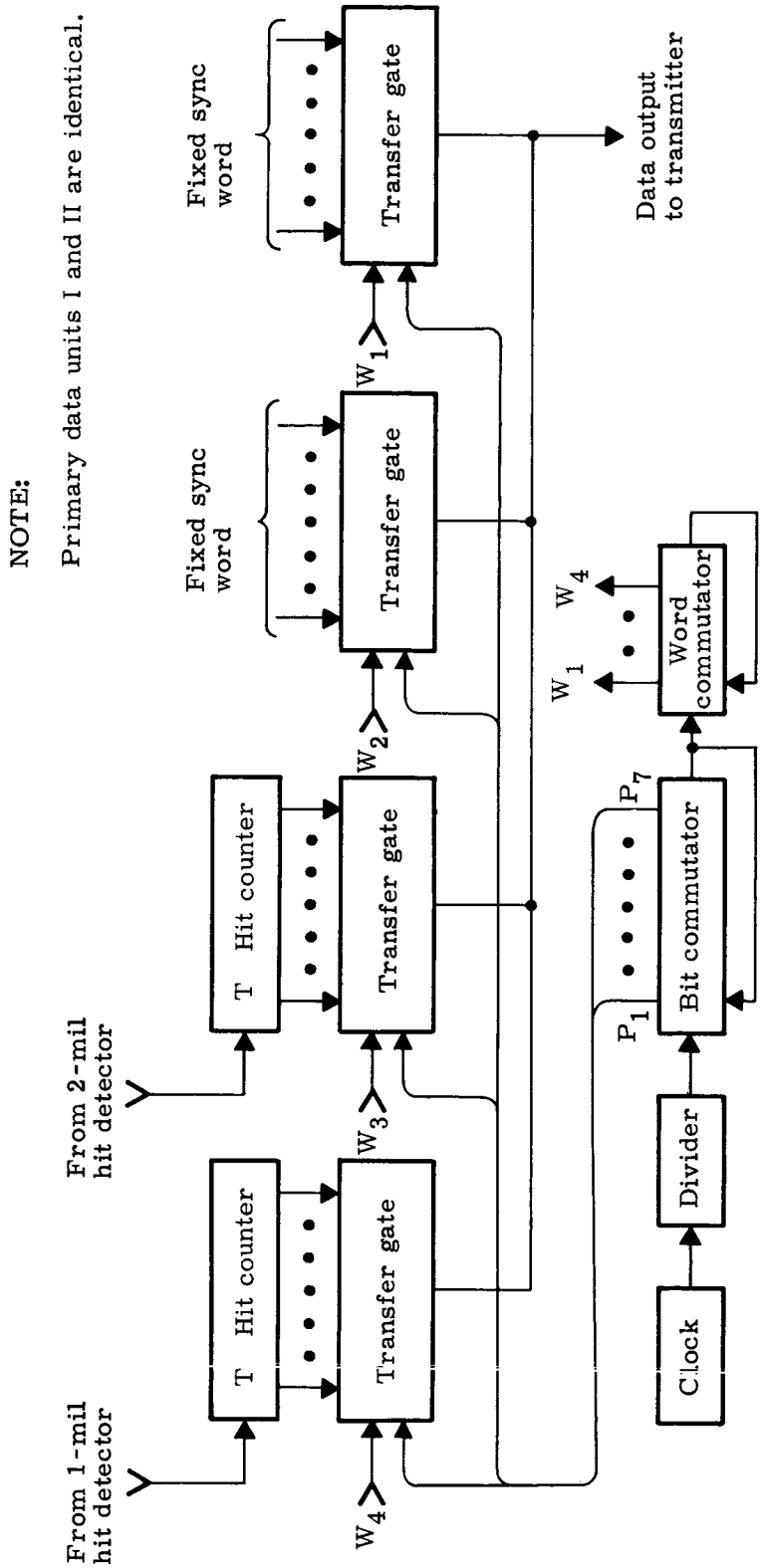
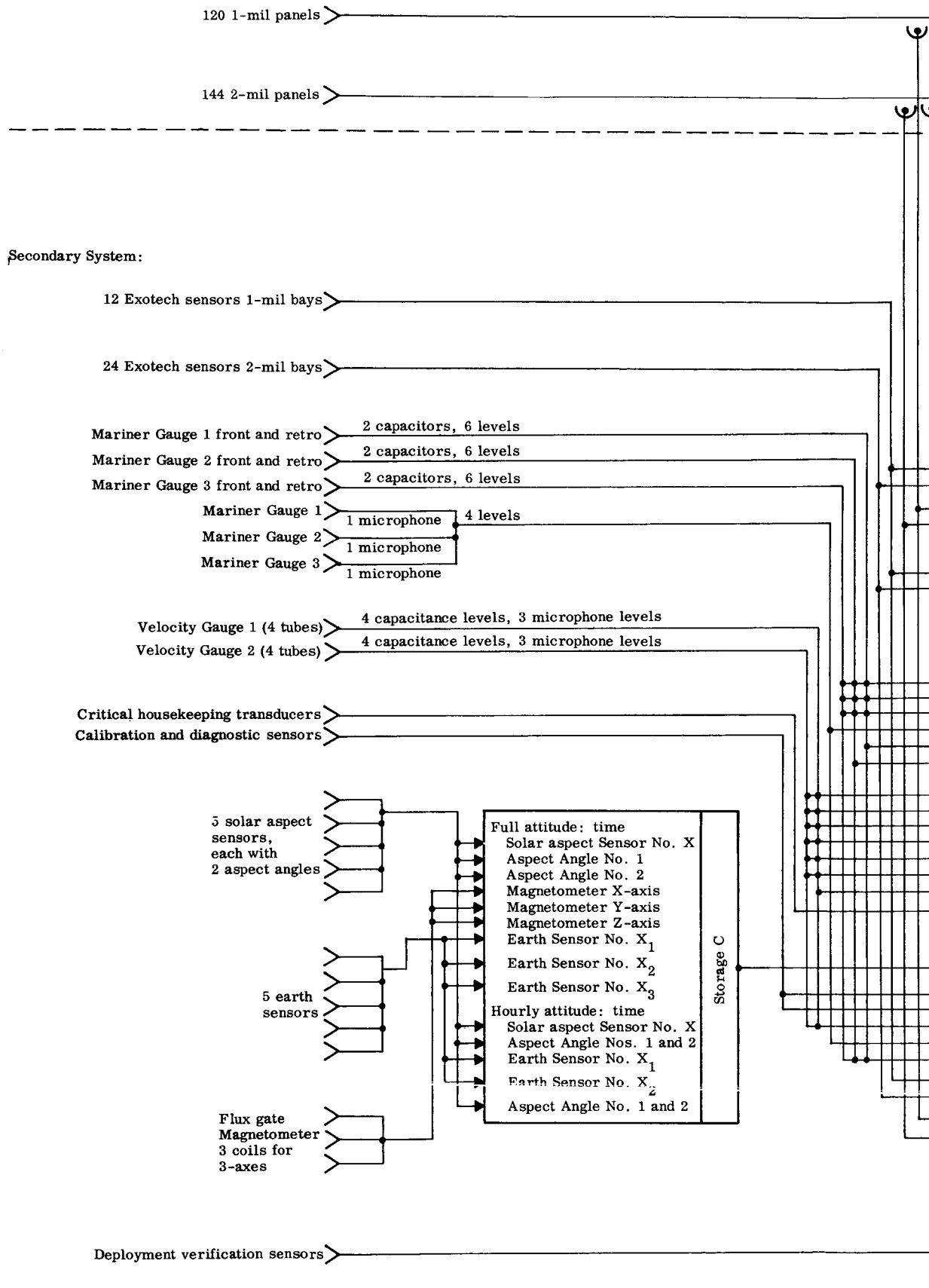


Fig. II-4. Primary Data Unit

Primary System: Capacitance Panel Hit Counts



ER

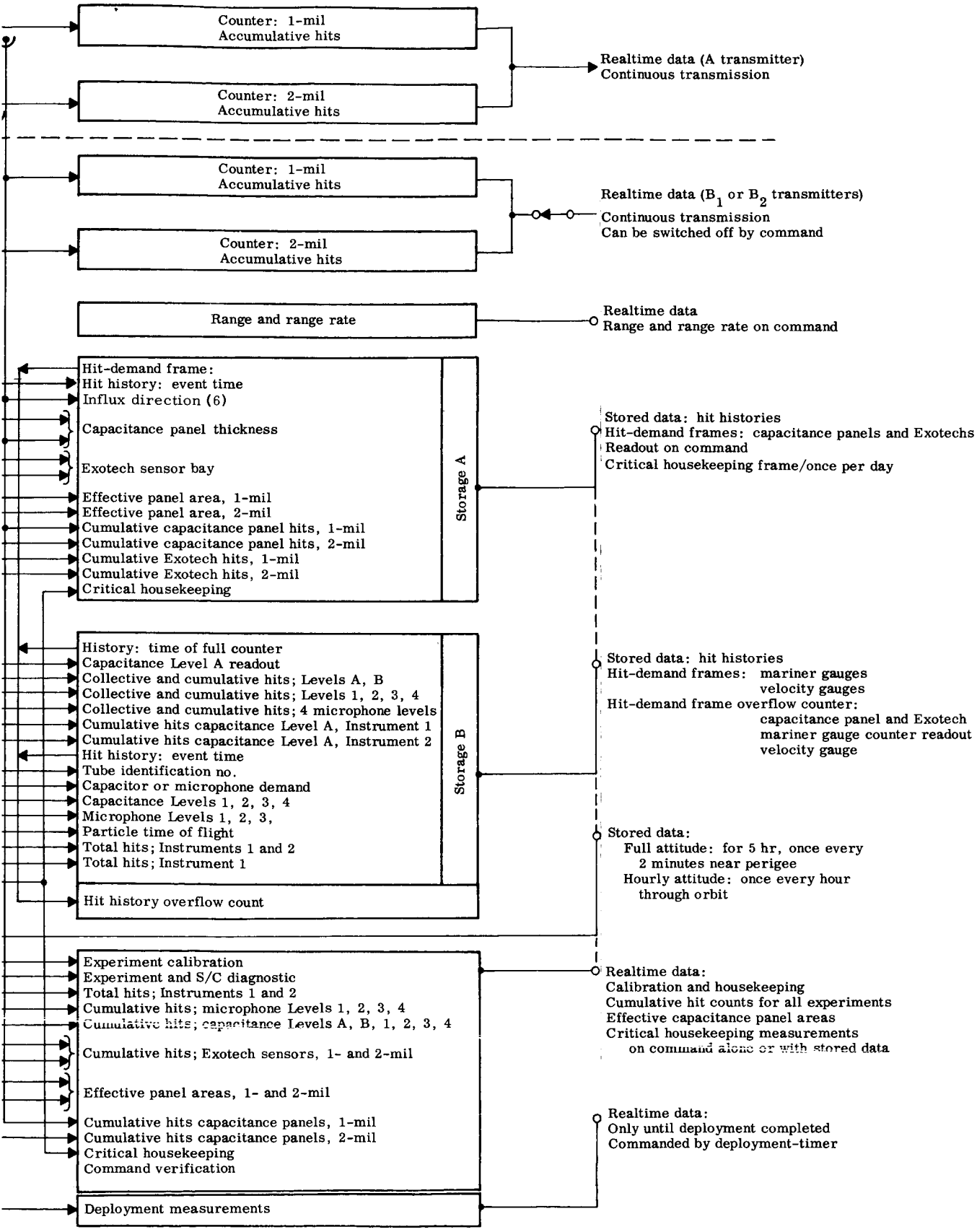


Fig. II-5. Data Signal Flow

sensor data and, in addition, will give information on penetration location. Measurement ranges of the Mariner and Velocity gauges are more sensitive (i.e., can detect smaller particle impacts) than the capacitor sensors.

The secondary subsystem enables the measurement of particle energy level, momentum, velocity, time of event, direction, and effective areas of operating capacitance sensors--in addition to extended measurement ranges for particle impact energy levels.

Attitude data will result in prediction of spacecraft orientation and, consequently, in determination of particle direction. Spacecraft attitude data is recorded in two modes. In one, a "full attitude format" is measured continuously for a 5-hr period around perigee, and stored in memory. In the other, hourly frames of solar and earth aspect data are taken throughout the remainder of the orbital period and stored in memory. Hourly attitude frames are not measured during the full attitude mode.

Deployment measurements, which indicate execution of satellite (sensor panel) deployment functions are taken only during the deployment phase of the mission.

Critical diagnostic measurements are taken once daily and stored in memory. Efforts were made to limit the number of these measurements. These data are intended for status information of sensor group functioning, power supply system performance and critical measurement levels.

The full housekeeping measurement mode comprises miscellaneous measurements of check voltage points, environmental measurements, the critical diagnostic measurements (outlined above), and totalizer count data for all micrometeoroid detectors at all sensitivity levels. Command verification is available on a delayed basis (Sequence I read-out). Further consideration should be given to this area.

Figure II-5 illustrates the flow of data signals from micrometeoroid sensors and all above-mentioned measurements. It can be seen that primary and secondary data flow lines are entirely separated and independent. Real-time data, playback of stored data, satellite attitude information, and range and range rate measurements are indicated. Redundancy of measurement information in the different telemetry data frames is shown by parallel data flow lines.

b. Data gathering function

The secondary subsystem recommended as a result of this study program is shown in Fig. II-6. Each sensor group has an assigned data unit which collects the incoming data and processes it into a fixed format. All data units are basically the same in that each contains an 80-bit commutator, 80-bit transfer gates, and storage in the form of counters or hold registers for 80 bits of data. Differences occur in the storage type and organization; i.e., the number of bits in counters and hold registers, the read gates to enter data into hold registers and basic initiate and control logic.

The three memory concept is a direct result of reliability tradeoff studies. For a single memory, the logic required to sequence data and establish entry priority in the case of attempted simultaneous data entries deteriorates system reliability in that the logic is complex and contains failure modes which could abort the entire secondary data system. The three-memory concept, however, restricts each memory to only two data units, thus simplifying data entry priority logic and increasing reliability by preventing failure modes which jeopardize the remaining data units and their associated memories.

Sufficient storage is provided for a complete orbit so that command functions are not critical in time. Transmission time is simply a function of the data group commanded; each memory is read out only as a result of a unique command.

Where scientific sensor sensitivity results in an excessive amount of data, data is entered into memory on a scaled basis which still records more than the amount statistically required. Therefore, no actual data is lost and, from the hit event time which initiates data entries, the full hit environment may be reconstructed.

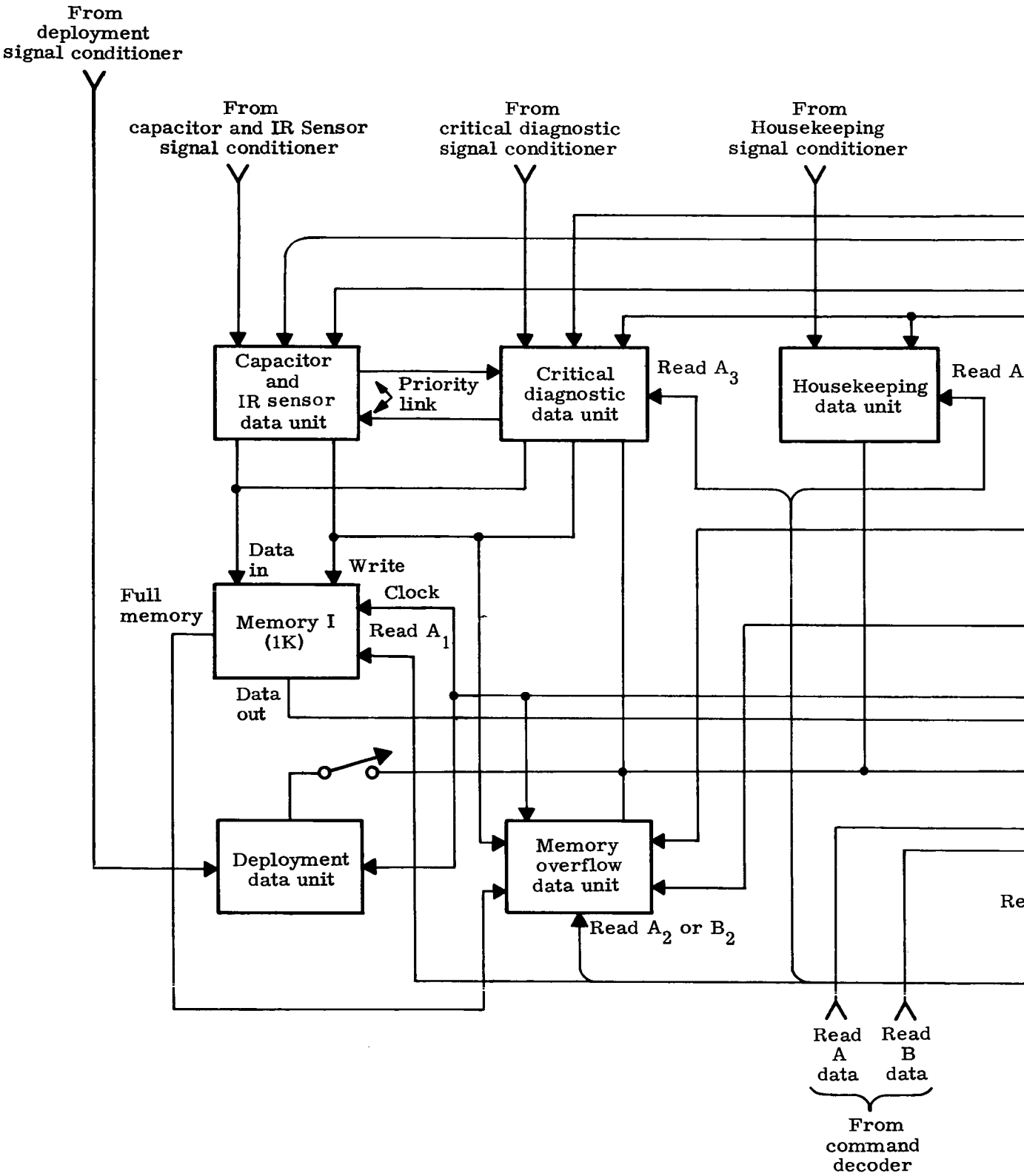
Reliability studies have shown significant gains can be achieved by utilizing integrated circuits plus increased packing density. Although the system shown is not based on a particular integrated logic circuit group, it is readily adaptable. Power requirements and package sizes given are representative of integrated devices (Vol. III, Chapts II and III).

c. Hit history concept

The concept for hit history data frames was developed to obtain additional measurements which will give supplementary information in connection with the micrometeoroid penetration or impact, namely:

(1) Time of event

(2) Sensor identification


From deployment signal conditioner
From capacitor and IR Sensor signal conditioner
From critical diagnostic signal conditioner
From Housekeeping signal conditioner
Capacitor and IR sensor data unit
Priority link
Critical diagnostic data unit
Read A_3
Housekeeping data unit
Read A
Data in
Write
Clock
Full memory
Memory I (1K)
Read A_1
Data out
Deployment data unit
Memory overflow data unit
Read A_2 or B_2
Read A data
Read B data
From command decoder

ER

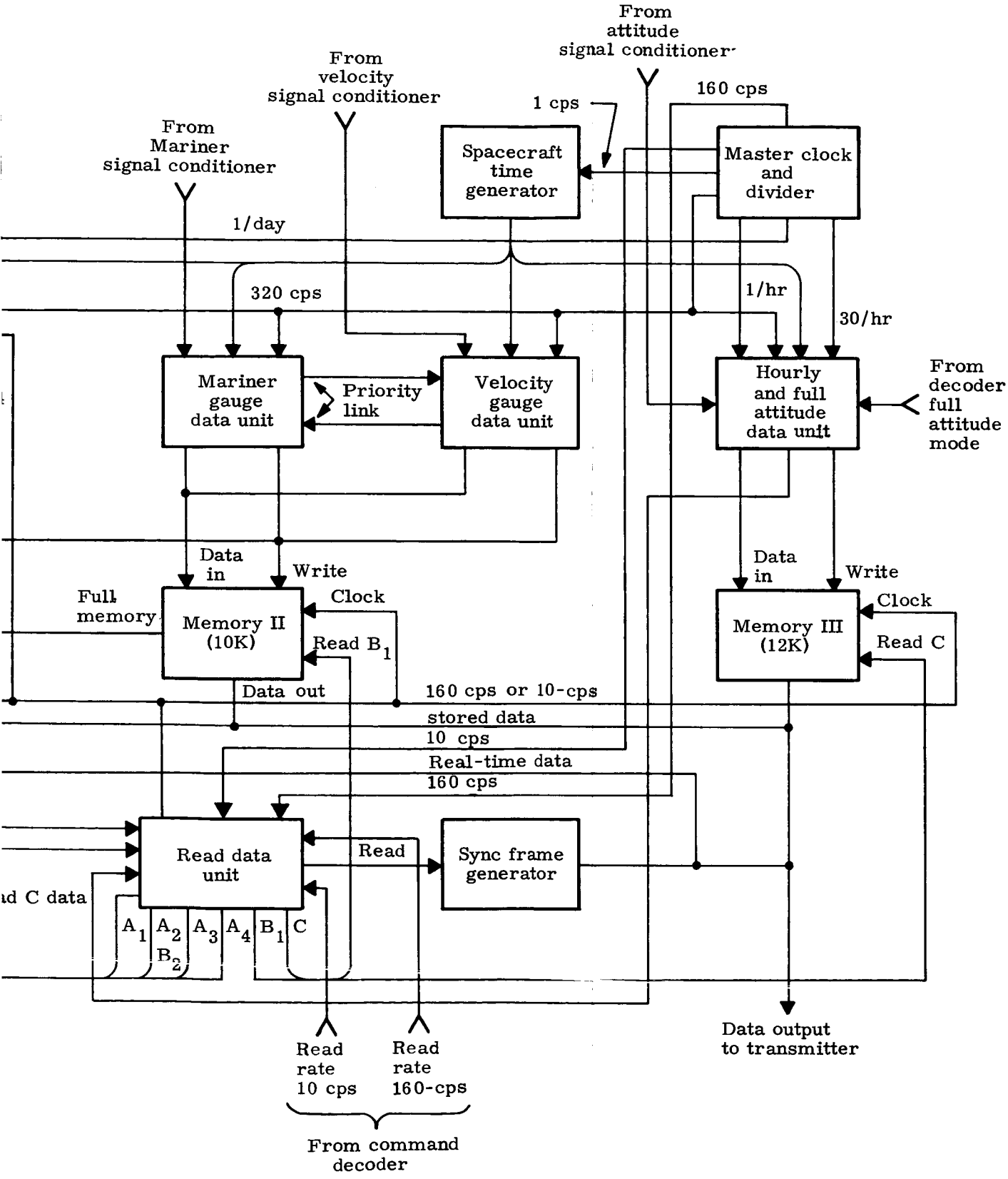


Fig. II-6. Secondary Data Handling Subsystem

(3) Level of impact sensitivity of specific detector

(4) Spacecraft attitude at time of event

(5) Micrometeoroid velocity

(6) Cumulative impacts received by the sensor or group of sensors in a certain sensitivity load.

Since complete hit history data require a certain number of data words, data frames are edited for each measurement. Hit history frames with equal word length were established to facilitate data processing and storage. Thus, data information in a typical hit history frame developed into an arrangement as shown in Fig. II-7.

Hit history frames are initiated on demand when an impact occurs. These frames might then be composed of the following data words.

(1) Event time

(2) Frame identification

(3) Sensor identification

(4) Sensitivity level

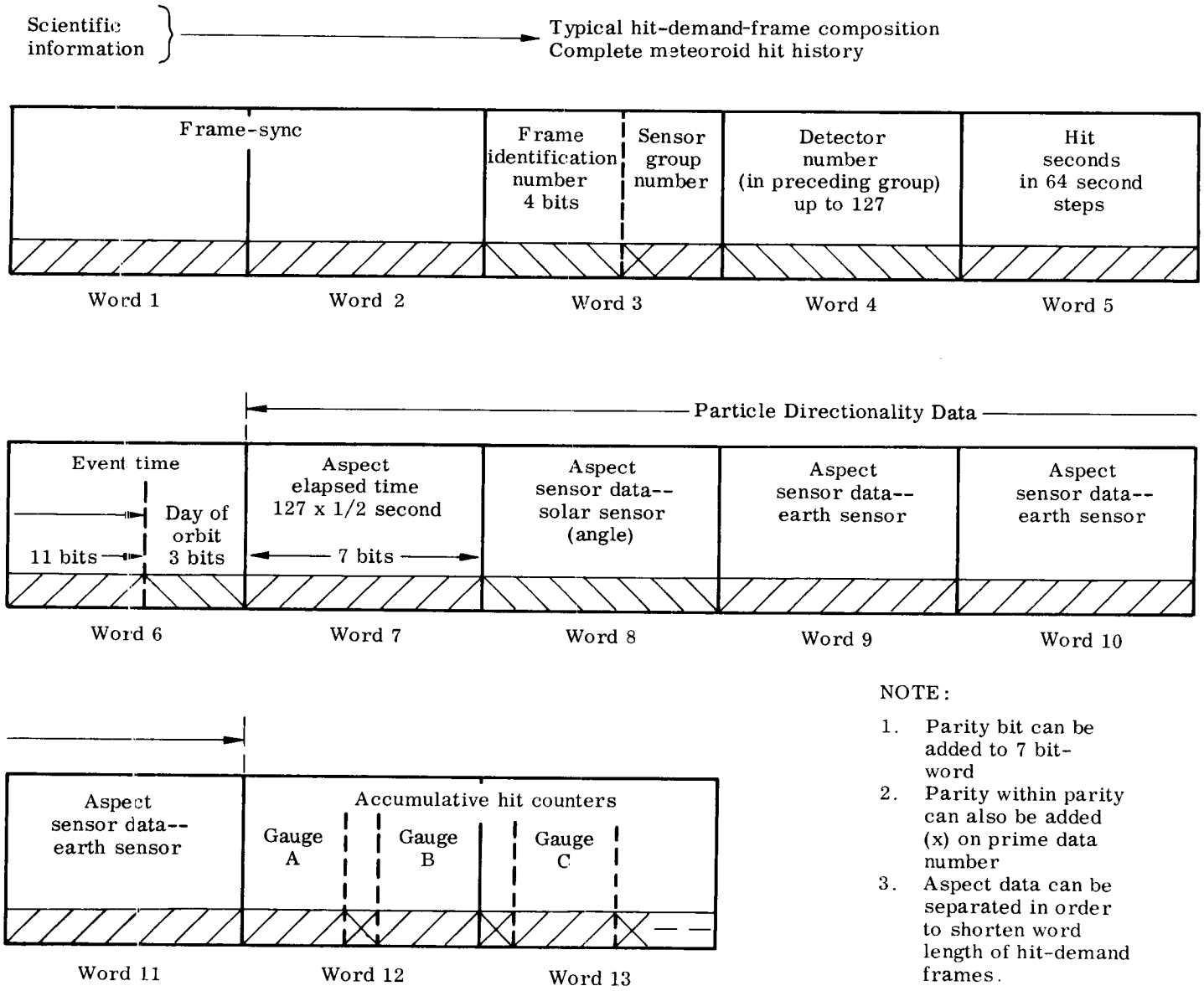
(5) Orientation or location of sensor

(6) Cumulative number of previous hits in one or more sensitivity levels of this particular sensor

A uniform data frame length of 10 words (80 bits) has been established. As a result of tradeoff studies, attitude data was not included in these hit demand frames; spacecraft attitude and, therefore, particle direction will be reconstructed on the ground from stored and transmitted attitude data.

d. Data information

Secondary data is gathered into formats consisting of ten 8-bit words. Scientific data formats are tagged by the first four bits for identification, followed by 14 bits which represent the time of hit or data entry and the day in orbit of occurrence. The remaining bits in the formats contain the scientific data collected and sensor identification. Housekeeping and attitude data are collected in the same basic format but are uniquely identified by complementing the data identity word. Sync



NOTE:

1. Parity bit can be added to 7 bit-word
2. Parity within parity can also be added (x) on prime data number
3. Aspect data can be separated in order to shorten word length of hit-demand frames.

Fig. II-7. Hit History Concept for Hit-Demand Frames

data consists of two 8-bit words which are generated prior to transmission of each 80-bit format. Generation of sync at this time has a two-fold advantage: sync is not stored in memory, thus storage capacity is considerably reduced; only one sync generator is required for the secondary data system.

The eighth bit of each data word is an odd-parity bit which increases the reliability of the data transmission. Also each data group is transmitted twice to ensure the reliability of the data transmission to the highest degree practical.

e. Data handling

All secondary measurement signals are processed by the secondary data handling subsystem into binary formats. The techniques employed are the result of tradeoff studies which considered reliability, performance characteristics, operational simplicity, life expectancy, system flexibility and economy.

Data collected are divided into two groups: scientific data and housekeeping data. Scientific data are stored in memory, and housekeeping data is collected in real time. Secondary data readout is by ground command only.

Stored data. Data to be stored in memory is subdivided into three memories to enhance reliability and system simplicity and flexibility. Each secondary sensor group is associated with a specific memory which has a capacity calculated to contain data collected by those sensors in one full orbit.

Memory I stores data collected by the capacitor and IR flash data unit and the critical diagnostic data unit, each of which performs independently. Capacitor and IR flash data are placed in the same format on impact occurrence. Critical diagnostic data is collected by internal program once per day.

Memory II stores data collected by the Mariner and the velocity gauge data units, each of which performs independently. Since both sensors have a high sensitivity, data is scaled down to a level which permits particle environment reconstruction and also is commensurate with high reliability storage unit capacities. Data entry into memory is on a scaled impact occurrence basis.

Memory III stores only spacecraft attitude data collected by either the full attitude data unit or the hourly attitude data unit. Data requirements are such that these units do not operate simultaneously. Full attitude data is collected only on command during a 5-hr period at perigee. Data is collected every 2 min and entered into memory

during this 5-hr period. Hourly attitude is collected once per hour for the remainder of the orbit. Storage requirements are reduced to a minimum by reading out the memory at the points where the full attitude mode is commanded on and off.

Real time data. Real time data is collected by the deployment data unit, housekeeping data unit, and the memory overflow data unit. Deployment data is collected only during the deployment period and is programmed by the deployment timer. The other two data units collect data for transmission only as the result of a received command.

4. Communication, Command and Tracking Subsystem

a. Telemetry

Two continuous RF telemetry channels in the VHF 136- to 138-mc band are recommended for use in transmitting telemetry data to the STADAN stations.

VHF is preferable to S-band. The preferred modulation for each channel is PCM NRZ biphase modulation of a clock derived subcarrier which, in turn, phase modulates the VHF transmitter. Continuous transmission of "primary PCM data" at a bit rate of 10 bps is provided by a 6-watt VHF "data" transmitter. The second RF channel is provided by the transmitter section of a 6-watt (RF) VHF range and range rate transponder when the transponder is in a data transmission mode (as opposed to a ranging mode).

The transmission on the second channel of real time or stored data and the desired channel bit rate are selectable by command (Table II-2). It should be noted that the transponder serves as a completely redundant transmitter channel for primary hit count data (a reliability requirement). A duplicate VHF transponder is provided to serve as a redundant active command and ranging receiver and as a standby (power off) transmitter for the second channel).

Both the data transmitter and the active transponder transmit continuously; however, as an option to reduce VHF band crowding, the transmitter portion of the active transponder could be commanded off when not being used.

A bit rate of 10 bps has been chosen to provide ground station data acquisition capability from apogee. For stored data readout, a rate of 160 bps has been chosen to provide readout to ranges of 30,000 naut mi on both inbound, toward perigee, and outbound portions of each orbit. Stored data readout at 10 bps may also be accomplished

TABLE II-2

Command List

Number	Name	Priority (Mandatory Desirable)	Function
1	Read rate 160 bps	(M)	Sets PCM transmission rate of secondary data to 160 bps
2	Read rate 10 bps	(M)	Sets PCM transmission rate of secondary data to 10 bps
3	Sequence I	(M)	Playback Memory I contents two times, followed by housekeeping data two times, followed by overflow counter contents two times
4	Sequence II	(M)	Playback Memory II contents two times, followed by memory overflow contents two times
5	5-hr attitude on Read Memory III data	(M)	Playback Memory III contents two times, after which begin 5-hr attitude mode of writing into memory
6	5-hr attitude off Read Memory III data	(M)	Playback Memory III contents two times, after which turn off 5-hr attitude mode of writing into memory
7	Switch to transmitter No. 2	(M)	Turns off transmitter section of active transponder, switch coaxial switch to spare transmitter (transponder), applies power to "spare" transmitter
8	Switch to transmitter No. 3	(M)	Reverse switching of Command 7
9	Turn off transponder (transmitter section only)	(D)	Turn off power to active transponder (transmitter section)

TABLE II-2 (cont'd)

Number	Name	Priority (Mandatory Desirable)	Function
10 & 11	Sensor group off	(D)	Two commands to provide turn off capability for either of two sensor group configurations
12 & 13	Sensor groups off	(D)	Reverse of Commands 10 and 11
14, 15, 16	Spare	(D)	For growth capability or added redundancy switching

for ranges beyond 30,000 naut mi. A third and higher bit rate in the order of 1280 bps and a corresponding shift in subcarrier frequency could be added for data transmission very near perigee if further study shows a significant advantage could be gained thereby (fewer errors, etc.).

Use of odd parity bits (one per word) is recommended for stored data transmission modes to reduce word error rate and limit repeat of data transmissions to one repeat.

b. Command

The tone digital system as described by Goddard Space Flight Center "Aerospace Data Systems Standards" is recommended for this spacecraft. Eight commands are considered mandatory for operation of the spacecraft in the recommended configuration. Eight additional commands are considered desirable from the standpoint of improving operational capabilities or for added redundancy.

Only real time commands are required. No updating of stored command sequences is contemplated. A list of recommended commands is given in Table II-2.

The receiver portions of GSFC-designed VHF range and range rate transponders will serve as both command receivers and range and range rate receivers after suitable modifications to the present design are effected. A redundant receiver and decoder is required to meet the reliability objective.

A reliability VHF command range of 100,000 naut mi is anticipated based on use of 5-kw transmitters and 22-db disc on rod antennas at the major STADAN ground stations. Commanding of spacecraft functions beyond a range of 140,000 naut mi will at times be marginal; however, commanding beyond a range of 100,000 naut mi, though desirable, is not mandatory.

The range and range rate (RRR) mode of operation is commanded from RRR tracking stations using phase modulated tones on the RRR uplink. The decoding for this mode of operation is internal to the VHF transponder.

c. Tracking and acquisition

The STADAN VHF range and range rate (RRR) system is preferable to the S-band system for this application and is recommended for use in tracking the spacecraft following injection into orbit. Minitrack interferometer cosine angles for satellite altitudes below 1000 naut mi (during perigee passes) may be used to supplement the RRR data.

Reliable VHF RRR tracking to ranges of 100,000 naut mi can be accomplished based on use of an omnidirectional spacecraft antenna. This range is more than adequate to obtain the required data for ephemeris determination as discussed in Volume III, Chapter I and Volume III A, Appendix I-4. RRR tracking to ranges of 180,000 naut mi may be accomplished at times depending upon spacecraft orientation and other variable factors.

The active VHF RRR transponder is modulated with PCM telemetry data when it is not used for ranging and also serves as command receiver. Hence, use of the RRR system creates no weight, volume or power problem onboard the spacecraft.

All spacecraft transmitters are phase modulated and provide sufficient unmodulated residual carrier power for beacon acquisition to apogee and Minitrack interferometer tracking on most perigee passes.

Link calculations are shown in Appendix II-2.

d. Antenna

An omnidirectional spacecraft antenna system is recommended because of the impossibility of continuously pointing a higher gain antenna toward earth in a tumbling vehicle.

None of the other spacecraft systems require attitude stabilization. In order to use a directional antenna, 3-axis stabilization would be required. In addition to the antenna pointing problem, there would also be the reliability problems of keeping an attitude control system operating for 6 to 12 months.

The antenna system design presents a real problem because of the size (in wavelengths) and shape of the spacecraft.

Of four systems briefly considered, the system consisting of a turnstile on one side of the spacecraft and an unsymmetrical disc-cone on the other was chosen to be representative of what might be achieved in antenna performance. It is designed to work with the STADAN polarization diversity system (linear) for spacecraft-to-ground telemetry transmission; however, for RRR, where polarization diversity is not employed, it is marginal even at relatively low tumbling rates.

It is recommended that further antenna studies be conducted to provide a better solution to the antenna problem.

5. Ground Net Facilities

Use of the Space Tracking and Data Acquisition Network (STADAN) is recommended for data acquisition tracking and command of the spacecraft following injection into orbit. The STADAN stations recommended for use in orbital support of this program and their functions are shown in Table II-3. These selections are based on a 180° downrange injection from Cape Kennedy and are intended to be representative of support requirements.

TABLE II-3

STADAN Station Selections and Function

Station	Function					
	Data Acquisition		Tracking		Command	
	85-ft Dish	SATAN	RRR	Other	RRR	Other
Ulaska	X		X		X	X
Quito		X		X		X
Santiago		X	X		X	X
Woomera		X		X		X
Johannesburg (Hartebeesthock)		X		X		X
Madagascar			X		X	
Carnarvon			X		X	
Rosman	X		X	X	X	X

Stations shown provide more than adequate support for the program.

Data acquisition. Recording by ground stations (one or more) of the spacecraft telemetered primary hit count date at least five times per data zone is recommended.

Stored data playback is normally expected to be required twice per orbit. This is to be accomplished at spacecraft altitudes below 30,000 naut mi at 160 bps. Use of polarization diversity is recommended for reception of transmissions. Available station coverage time below 30,000 naut mi is expected to exceed 6 hr, with continuously available coverage periods as high as 3.5 hr.

The ground data acquisition facilities are compatible with the recommended spacecraft modulation system except for the requirement to add two biphase subcarrier demodulators. These are minor additions to the network facilities.

Use of 85-ft dish antennas at Rosman or Ulaska is recommended for ranges beyond 100,000 naut mi for 10-bps data rates and between 20,000 and 50,000 naut mi for 160-bps rates.

Command. Use of the 5-kw high power command system with 22 db disc on rod antennas is required at all data acquisition stations for commanding the various data modes. The spacecraft command system and ground systems are compatible.

Tracking. The number and location of range and range rate tracking stations as presently shown provide adequate tracking coverage to support the mission. Use of only the VHF portion of the RRR system is required.

B. TECHNICAL DISCUSSION

1. Basic System Investigations

During the course of the study, three basic systems were investigated. A general discussion of the relative advantages and the disadvantages of each system, including the recommended system, System III, follows:

a. System I

This system (Fig. II-8) employed substorage units for each sensor group which enabled a programmed fixed format to be entered into a main storage unit. The substorage units offered the advantages of having independent sensor group storage and elimination of the possibility of losing data while the main memory was being readout and/or was full. Use of a fixed format resulted in the addition of the frame sync at the time of readout rather than being required to store it.

(1) Data processing

It was proposed that once every hour or once every four hours a format of fixed length be entered into the main storage unit from the various substorage units. The fixed format included scientific data and housekeeping measurements. Thus, every time a format was generated and entered into main storage, housekeeping data would be entered. The housekeeping data amounted to approximately 30% of the total format length. This was not considered to be a very favorable ratio of mandatory-to-desirable data.

Furthermore, if one of the substorage units contained no information upon the generation of the format, this particular subformat would contain blanks. Thus, it would be conceivable to fill a good portion of the main memory with blanks, resulting in the possibility of a relatively inefficient main storage unit.

The commutator required to generate the fixed format was of considerable size and, since the commutator was the sole source for organizing the mandatory data, the success of the mission depended almost entirely on one unit. From a reliability standpoint, it was quite evident that this method of data processing was not the best.

(2) Main memory

This system proposed using a trisectional main storage unit which gave the advantage of being able to read from one section while writing into another. This greatly reduced the possibility of losing pertinent information.

(3) Modes of transmission and command

The basic system consisted of a single transmission channel with the following commands for obtaining data: read out stored data, read out real time attitude data and read out real time housekeeping data.

(4) Conclusion

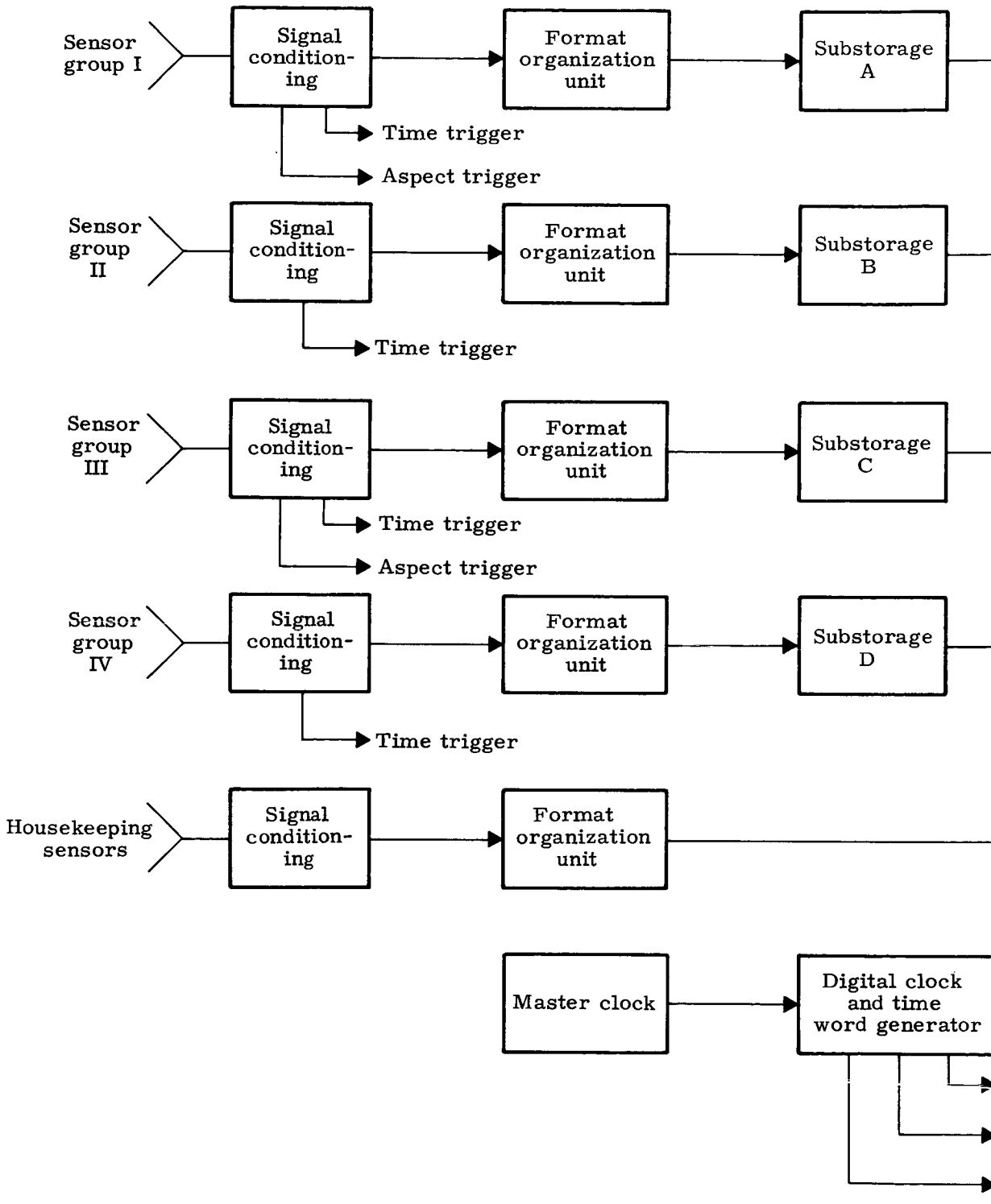
Primarily due to the shortcomings of the data processing technique an approach was sought to eliminate the substorage units and the main commutator, with the hope of being able to reduce the component count and hence increase the probability of mission success.

b. System II

(1) Data processing

This approach required that scientific data be entered into the main storage unit upon hit demand. The block diagram of the system is shown in Figs. II-9 and II-10. Collection of scientific data in this manner eliminated the requirements for substorage units for each sensor group, but necessitated a requirement for a "write priority" unit. Generation of the latter requirement was due to the fact that, if two or more sensor groups were hit simultaneously, the scientific data of the highest priority would be entered into the main memory first, followed by the next, etc. This new requirement did not require nearly as many components as the substorage units and main commutator of the previous system. Moreover, the success of obtaining the scientific information was not dependent upon a single commutator as in the previous system. Thus, if one of the sensor commutators failed, retrieval of the information gathered by the other sensors was not inhibited.

Housekeeping data in this system is not entered into the main storage unit at the same time as the scientific data. Rather, it is stored once per day, increasing the ratio of stored scientific-to-housekeeping data. However, inasmuch as the formats are of a random nature, it is necessary to store a frame sync with each format entered into the memory in order to recognize where one frame terminated and another began. Since the formats of this system are initiated upon hit demand, it does eliminate the possibility of storing blanks. This method of format organization still did not seem optimum, at least from the standpoint of efficiency in the use of the memory capacity, inasmuch as a frame sync had to be stored with each format. However, it showed a considerable improvement over the previous system in both reliability and memory capacity efficiency.


Sensor group I
Signal conditioning
Format organization unit
Substorage A
Time trigger
Aspect trigger
Sensor group II
Signal conditioning
Format organization unit
Substorage B
Time trigger
Sensor group III
Signal conditioning
Format organization unit
Substorage C
Time trigger
Aspect trigger
Sensor group IV
Signal conditioning
Format organization unit
Substorage D
Time trigger
Housekeeping sensors
Signal conditioning
Format organization unit
Master clock
Digital clock and time word generator

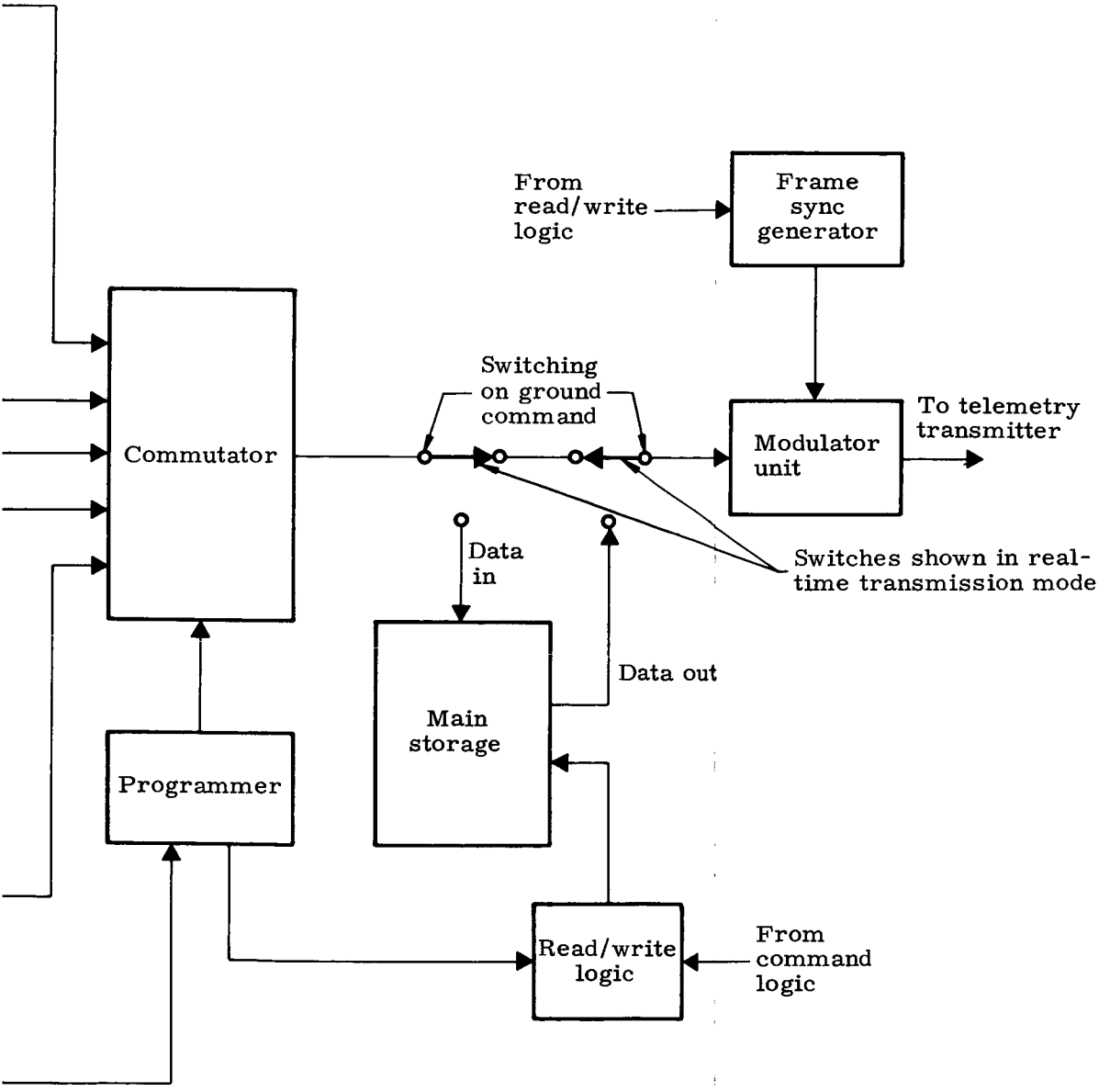


Fig. II-8. System I Block Diagram

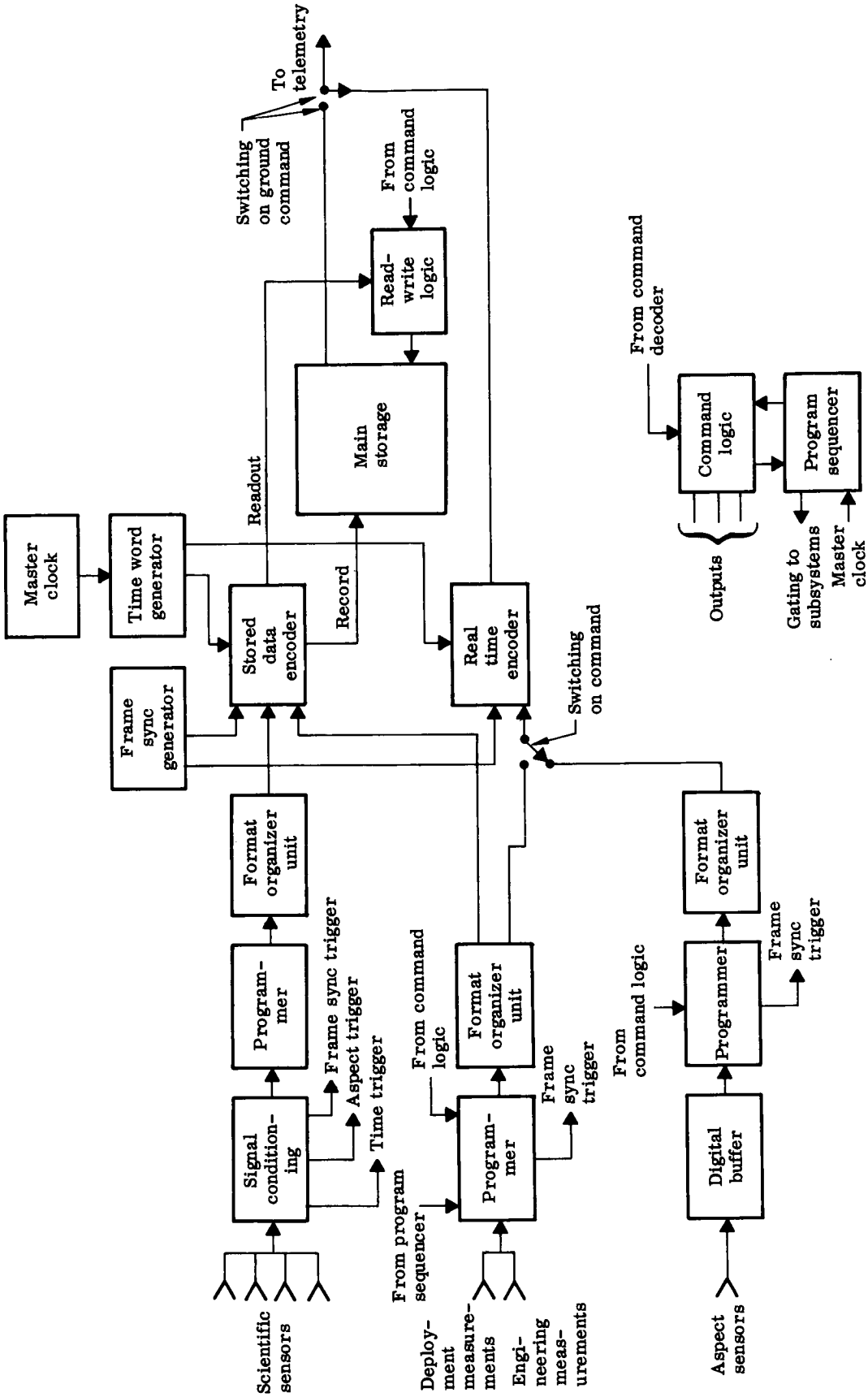


Fig. II-9. System II: Single Channel Transmission System

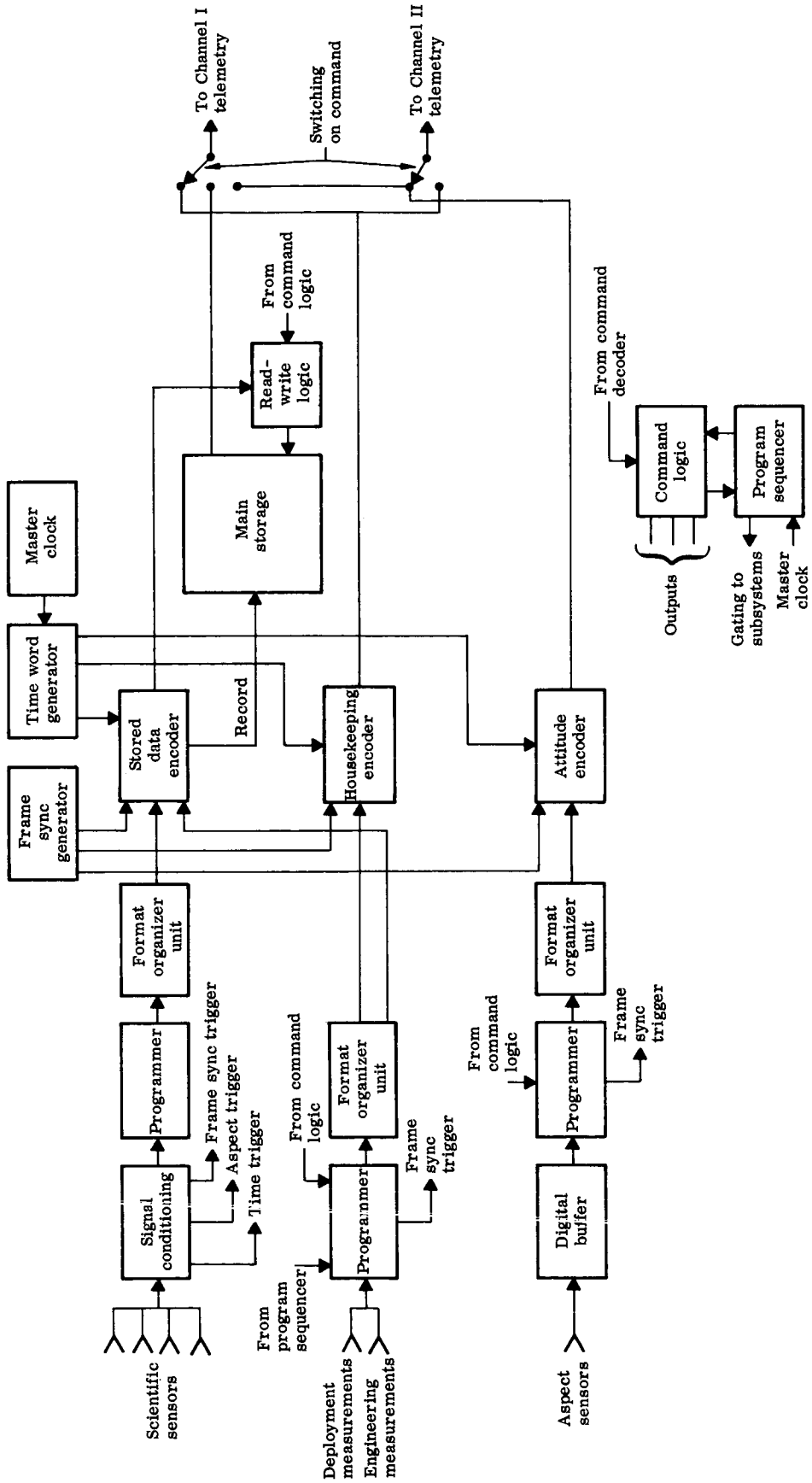


Fig. II-10. System II: Dual Channel Transmission System

(2) Main memory

The main storage unit remained the same as that proposed for System I.

(3) Modes of transmission and commands

Two alternatives to the basic approach of data collection, as described above, evolved. The first was a single-channel transmission system with scientific information and a small amount of housekeeping information being stored and transmitted upon command. Attitude information and housekeeping information were available through individual real time commands. The second alternative was to have a dual-channel transmission system. Stored information, real time attitude and housekeeping data would be obtainable over the one channel, while it would be possible to transmit real time attitude and housekeeping data over the other. This offered the advantage of receiving either real time attitude or housekeeping data simultaneously with stored data, real time housekeeping or attitude data. The latter alternative, however, required a total of five commands--compared with three for the previous system--to increase the probability of obtaining secondary information (primary information being defined as sensor data). The increase in command requirements was not deemed worthy for the particular gain achieved.

(4) Conclusions

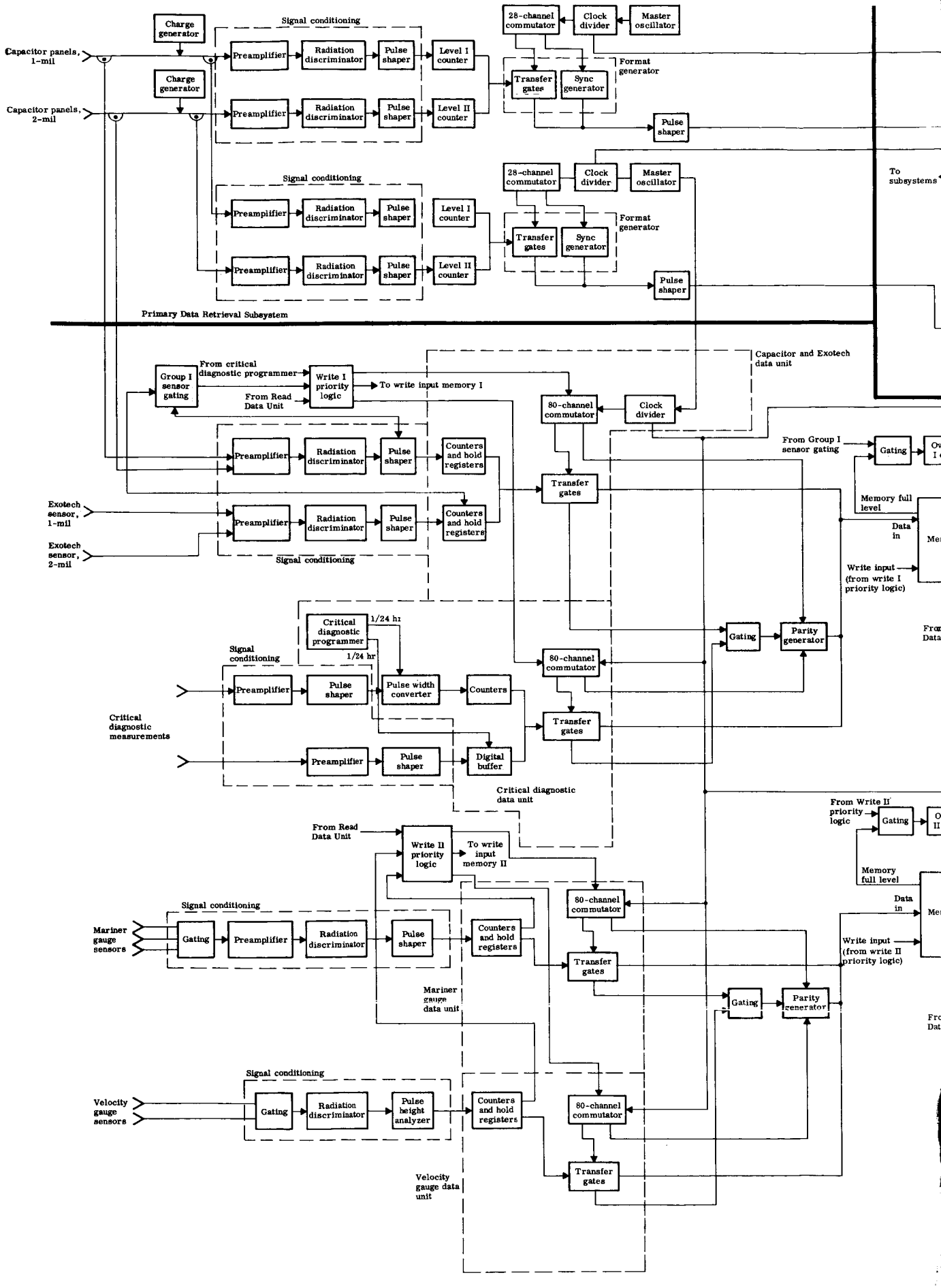
Although this approach was quite an improvement over the data collection process of System I, it still did not seem to offer the optimum approach for the most efficient use of the main memory capacity. Furthermore, the transmission approach did not minimize the probability of failing to obtain the mandatory information. Therefore, it was necessary to investigate other methods for the data processing and the transmission of the data.

(c) System III

(1) Data processing

This system (Fig. II-11) consists of two independent subsystems, one primary and one secondary. A redefinition of primary data is in order at this point, primary data being defined as the accumulated hit counts of the capacitance sensor panels.

The data processing unit of the primary subsystem (containing only accumulated capacitance panel hit counts) consists of its own commutator, sync generator and accumulated hit counters. Furthermore, a redundant data processing unit is added in the primary subsystem to ensure against loss of primary data.


Charge generator
Signal conditioning
Capacitor panels, 1-mil
Preamplifier
Radiation discriminator
Pulse shaper
Level I counter
28-channel commutator
Clock divider
Master oscillator
Transfer gates
Sync generator
Format generator
Capacitor panels, 2-mil
Level II counter
Pulse shaper
To subsystems
Primary Data Retrieval Subsystem
Group I sensor gating
From critical diagnostic programmer
Write I priority logic
To write input memory I
From Read Data Unit
Capacitor and Exotech data unit
80-channel commutator
Clock divider
Counters and hold registers
Exotech sensor, 1-mil
Exotech sensor, 2-mil
From Group I sensor gating
Gating
Memory full level
Data in
Write input (from write I priority logic)
Critical diagnostic programmer
1/24 hr
Parity generator
Critical diagnostic measurements
Pulse width converter
Counters
Digital buffer
Critical diagnostic data unit
From Write II priority logic
From Read Data Unit
Write II priority logic
To write input memory II
Mariner gauge sensors
Mariner gauge data unit
Velocity gauge sensors
Velocity gauge data unit
Pulse height analyzer

ER 1370

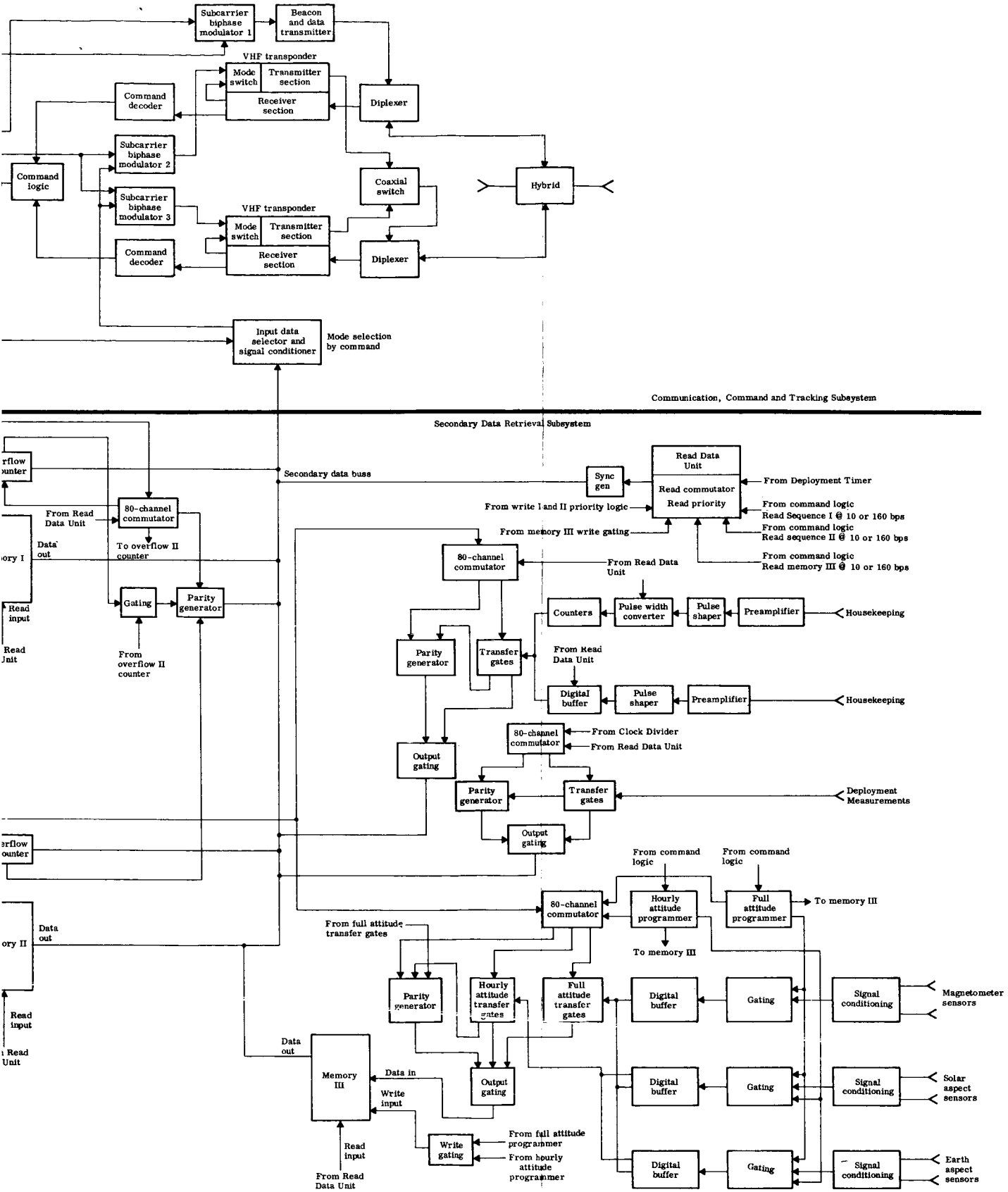


Fig. II-11. Recommended Telecommunications System

The secondary subsystem contains individual data processing units for all the scientific and housekeeping sensors. The format is fixed, with the data being entered into storage either upon hit demand, programming or on a scaled-down hit count. The secondary subsystem is isolated from the primary subsystem and this fact, together with the individual sensor data processing units, greatly enhances the chances of retrieving the desired scientific data. The critical housekeeping format is entered into storage once per day and the format consists of only a 10-word data frame. Furthermore, since the formats are fixed, no sync frame need be stored, and the memory capacity efficiency is optimized.

(2) Main memory

The primary data subsystem does not possess a memory (penetrations are recorded in counters) and data transmission is continuous (i. e., the counters are read out continuously). The secondary subsystem contains three memories, each associated with one or more different sensor groups.

The three separate memories employed in the secondary subsystem still utilize the original concept of System I; i. e., data can be read from one memory while it is being entered into another. Thus, no data from one sensor group is lost when reading the data of another sensor group.

The fact that there is no memory associated with the primary subsystem further enhances the probability of obtaining primary data. Also, since individual memories are employed in the secondary subsystem, the probability of loss of all scientific data is at a minimum.

(3) Modes of transmission and commands

This system employs a dual channel transmission system. Over one channel, data from the primary subsystem is being continuously transmitted at a fairly low bit rate; no switching occurs on this channel. Simultaneously, over the second channel, retrieval of the redundant primary or secondary subsystem data is possible. After the readout of the secondary subsystem data, the second transmission channel automatically reverts to the redundant primary data mode, allowing a minimum number of commands to be employed to read out the data; four commands are required. These will be discussed in detail under data readout.

(4) Conclusions

It is felt that this system represents the optimum combination of techniques and equipment for the purpose of procuring the desired scientific data. Memory capacities are efficiently utilized, each

sensor's data processing unit and associated electronics are separate, and the secondary subsystem is completely isolated from the primary subsystem. These facts, together with the dual channel communication system greatly enhance the probability of success for the MDSS.

2. Instrumentation and Data Handling

Detailed descriptions and discussions of the recommended system are presented in this section. Figure II-1 presents a simplified block diagram of the satellite instrumentation and data processing subsystems. Figure II-11 shows a detailed functional schematic of the overall telecommunication system and Fig. II-5 shows the data flow.

Instrumentation requirements and constraints. In general, requirements for the instrumentation and onboard data processing can be categorized as:

(1) Deployment and injection phase--measurements for verification of satellite deployment functions, status of satellite systems and subsystems in real time telemetry.

(2) Mission phase

(a) Continuous monitoring of micrometeoroid penetrations, all measuring systems operating.

(b) Storage for collected experiment data.

(c) Scheduling of periodic diagnostic and attitude measurements, and storage for these.

(d) Calibration and housekeeping measurements, and real time telemetry for these.

(e) Readout of micrometeoroid counters from all experiments in real time telemetry as backup for stored data.

The most important requirement for the design approach was reliability of operation for all systems. (Volume IV of this report contains the detailed reliability tradeoff analyses.) One of the most serious limitations was large storage requirements for some of the subsystems in the secondary measurements subsystem, since these requirements were deemed detrimental to reliability.

A large portion of the instrumentation equipment will be located inside the satellite housing. However, exposed sensor units will undergo temperature cycling induced by the tumbling vehicle. Therefore, detailed requirements must be established.

The size of the erected satellite configuration necessitates long, parallel lines of wiring. An important requirement, therefore, is to use signal transfer techniques which are immune to cross-talk or any other interference.

Details of the measurement requirements for the various subsystems will be found under their respective headings.

System design approach. The basic system design philosophy of isolated primary data having a high probability of success has essentially established the design approach for the entire data system. The basic primary system data unit has been expanded for the secondary system to contain the 80-bit secondary data format. This basic unit then is adapted to the various data forms and control requirements.

Since the primary concern in the data handling system is to perform the required functions in a manner which prohibits any failure mode within any subunit from jeopardizing the operation of any other subunit, this basic data unit concept is readily adaptable to isolation techniques. Within any memory subgroup, each data unit is isolated and, where failure modes exist, is isolated such that the system will be fail-safe. Data access points to the secondary data bus are also isolated in this manner; thus, only catastrophic failures--such as power failures--can affect the mission as a whole.

Data format concepts and results. As previously mentioned, the recommended system employs fixed formats. The primary subsystem format was dictated by the system design philosophy; simplicity. The format employed is the simplest which can be attained and still contain the desired information. The primary subsystem format is shown in Table II-1.

Secondary subsystem formats were also dictated by the design philosophy, but to a lesser extent. The format for the primary sensors (capacitance panels) and their backup sensors (IR-Flash sensors) dictated, to a large extent, the length of secondary subsystem formats. The capacitance panel and IR-Flash sensor format, being most important, was constructed first and all other formats were required to conform to this one. In some cases, it was necessary to repeat words to satisfy this requirement, but--in the majority of cases--the word allocations were efficiently used. Thus, a secondary subsystem format length of ten words evolved. These formats are shown in detail in Table II-1.

System timing and time generation. System timing is derived from two master oscillators, one in each of the primary data units (Fig. II-11). The basic oscillator frequency of 163.84 kc is divided by a 14-bit counter in each data unit to establish the basic bit rate of 10 bps for the primary data transmission. Also, the modulation frequency of 1.28 kc is taken from the seventh stage of the divider.

The oscillator divider in the secondary data system contains the basic 14-bit counter followed by a four-stage decade to establish 1 cps for the spacecraft time generator. Spacecraft time is provided in octal form for 0 to 60 sec, 0 to 60 min, 0 to 24 hr, and 0 to 8 days, which requires two counts of 60 scalars, one count of 24 scalars and one count of 6 scalars, or a total of 20 stages. Only minutes, hours and days of orbit are required for impact-event-time, time in seconds is utilized to establish earth sensor activation time during the full attitude mode of operation.

The master oscillator divider and spacecraft time generator in the secondary system provide the following timing functions:

(1) 320 cps; data collection and memory write cycle frequency

(2) 160 cps; readout, high bit rate

(3) 10 cps; readout, low bit rate

(4) 1 cycle/day; critical diagnostic write data command

(5) 1 cycle/hr; hourly attitude write data command

(6) 30 cycles/min; full attitude write data command.

a. Primary measurement subsystem description

The function of the primary measurement subsystem is to monitor micrometeoroid penetration of the capacitance sensors. Data are signal conditioned, encoded and registered as cumulative numbers of penetrations. Four counters are employed, two for the total number of penetrations on all 1-mil panels, the other two for all penetrations on the 2-mil units.

For reliability reasons, no switching action for power control is interposed in this continuous telemetry data transmission subsystem. Power is turned on automatically, as soon as the solar arrays are energized after heat shield separation. The satellite will cease operations at the end of its mission by means of a fail-safe killer-timer arrangement.

(1) Requirements and constraints for the primary subsystem

The principal requirement for the primary subsystem is reliability for obtaining the desired objective. For this reason, the design was based on space-proven techniques of satellite instrumentation.

As discussed in Chapter I, the anticipated data rate of the prime experiment will occur at a very slow rate throughout the entire mission. The established flux model with the power law falloff with a 20% margin and a safety factor of 30 results in the following data gathering requirement for the primary system capacitance panel measurement network.

(1) Number of 1-mil thick aluminum capacitance panel sensors = 120.

(2) Number of 2-mil thick aluminum capacitance panel sensors = 144.

(3) Number of penetrations per zone per orbit = 0.526.

(4) Number of micrometeoroid density zones = 5.

(5) Number of anticipated penetrations per gauge per orbit = 5 x 0.526 = 2.63.

(6) 20% margin increase added = 3.16 ≈ 3.

(7) Flux increase factor of 30 = 95 penetrations/thickness/orbit.

(8) Selected counter capacity for 1-mil capacitance panels = 127.

(9) Selected counter capacity for 2-mil capacitance panels = 127.

Thus, chosen penetration counter capacities for each thickness of capacitance panels are capable of registering total number of penetrations per orbit up to a flux increase in excess of 40 times the predicted number of penetrations.

(2) Instrumentation

The original concept for the instrumentation design was centered around the capacitance panel sensing network as the primary experiment for gathering micrometeoroid penetration data. Since the collection of this information has to be accomplished with extremely high long-term reliability, a second primary data channel was provided. This redundant primary data is telemetered over the second transmission channel in the normal transmission mode (Figs. II-1 and II-11). This channel is time shared, however, with secondary data readout by command.

The advantage of this additional backup channel in relation to reliability for long-term operations would be diminished if a direct wire

interface between primary and secondary subsystems were employed. Thus, a decision was made in the design approach to avoid any physical interfaces between these two subsystems. After evaluating a number of techniques for data transfer, a satisfactory method was selected as discussed below.

A subject for further study is the known occurrence of radiation discharges in space-exposed capacitance panel sensors, and preventing their being counted as micrometeoroid penetrations. At this time, a radiation discharge discrimination network has been provided in the primary subsystem signal conditioning units to prevent erroneous penetration counts for just such discharge phenomena.

Penetration detection and signal conditioning. Penetration detection for each thickness of capacitance panels supplied by a charge generator is accomplished by use of the circuit shown in Fig. II-12. Four of these circuits are required for handling penetration detection in the primary and redundant primary subsystems using the penetration detection arrangement shown in Fig. II-13, since penetration detection requires only that the charge generator output current be monitored with the transducer located between points A and B in this figure. The technique employs a Hall effect transducer whose output is sensitive to magnetic field intensity. The transducer, less flux concentrator, is pictured in Fig. II-14. Effective utilization of this device requires that a charge current of sufficient magnitude be present in order that the Hall device produces an output which is compatible with conventional amplifiers. If this requirement is met, then the inherent reliability of this transducer is maintained.

Since this application does not require extreme linearity and very low temperature coefficients, Hall devices composed of indium antimonide rather than indium arsenide are more suitable since they display higher output voltages for a given flux density. This transducer unit is also available with the bulk material sandwiched between ferrite pieces (inset Fig. II-15) to obtain effective air gaps on the order of three mils when used with a flux concentrator. The latter is a toroid which is used to increase the flux coupling with the Hall device. Use of indium arsenide in conjunction with flux concentrators will produce outputs on the order of 6.0 mv for a 10 ma current flowing in the conductor, thus a significant increase in output voltage can be expected by using the indium antimonide type of a Hall effect sensor. The transducer requires a control current on the order of 100 ma, approximately 30 mw/transducer, applied across one face of the bulk material.

The transducer output signal goes through a preamplifier and pulse shaping network to the signal conditioning unit (Fig. II-15). The signal conditioning unit for each thickness group consists of different sections. The front end of the unit serves as a penetration acceptance network, where incoming signals are filtered and either accepted or rejected. Erroneous penetration pulses caused by possible radiation discharge events or other interference sources, signals below an established threshold level, and multiple penetration signals in rapid sequence originated by a panel discharge backsplash are rejected. Accepted penetration signals are conditioned to drive the respective counter for the cumulative number of penetrations. A number of other feasible techniques were developed for penetration detection and determination of effective capacitance panel area. These are discussed further in the secondary measurement subsystem section and in Appendix II-5.

(3) Primary subsystem data information

Primary subsystem data gives the cumulative penetrations for both panel thickness gauges. To analyze influx rates with density zones, the time of penetration has to be established.

Considering the possibility that solely primary system data is obtained, ground station monitor time of the counter readings will be used as time points for determination of influx rates. Cumulative penetration numbers plotted versus station readout times will establish micrometeoroid influx characteristics in the postulated density zones discussed in Chapter I.

(4) Format organization

The master oscillator, operating at 163.84 kc, is divided down to 10 bps by the clock divider network. The 10-bps signal drives the 28-channel commutator which generates four word periods and seven bit periods. During the first two word periods, the sync generator is active and the sync words are generated. Inputs to the transfer gates are connected to the outputs of Levels I and II counters. During the third word period, each stage of the Level I counter is interrogated successively by bit periods one through seven. The same process takes place during the fourth word period to the Level II counter. This completes the generation of one frame of data and the cycle is repeated continuously. Figure II-4 is a block diagram of the primary subsystem format organization.

The format organization for the redundant primary portion of the data processing electronics is accomplished in the same manner as described above.

(5) Data readout

Primary data is continuously transmitted over the first transmission channel and its transmission is never interrupted. Redundant primary

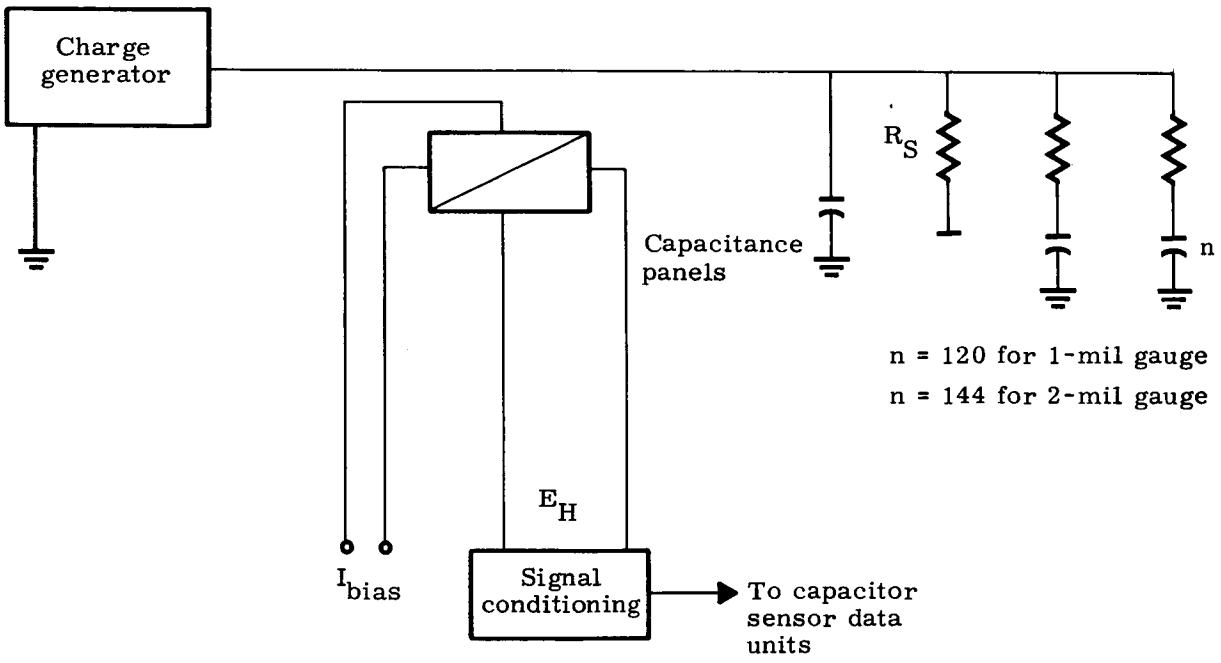


Fig. II-12. Capacitance Panel Penetration Detection Technique

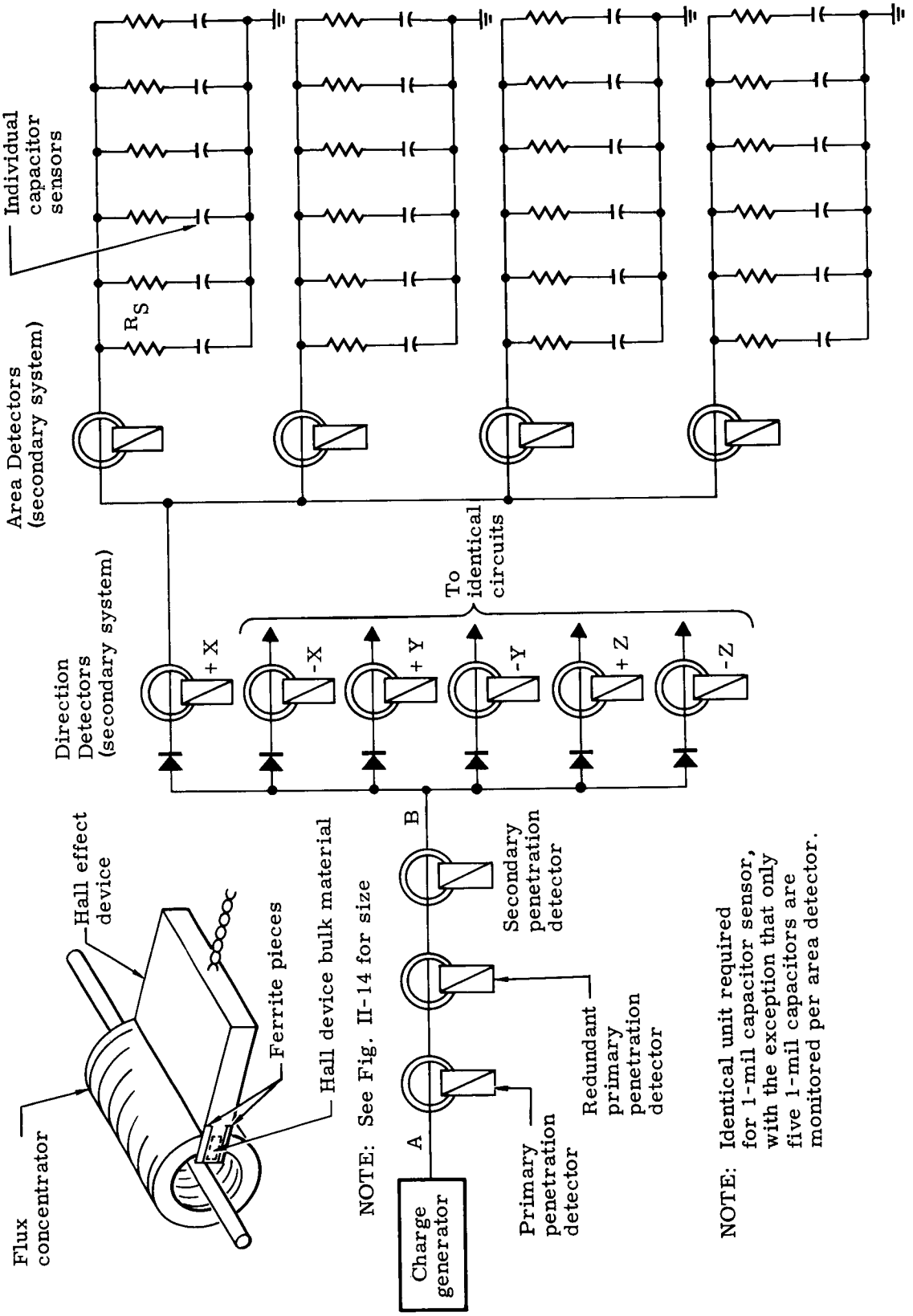


Fig. II-13. Two-mil Capacitor Sensor Hall Detector Arrangement

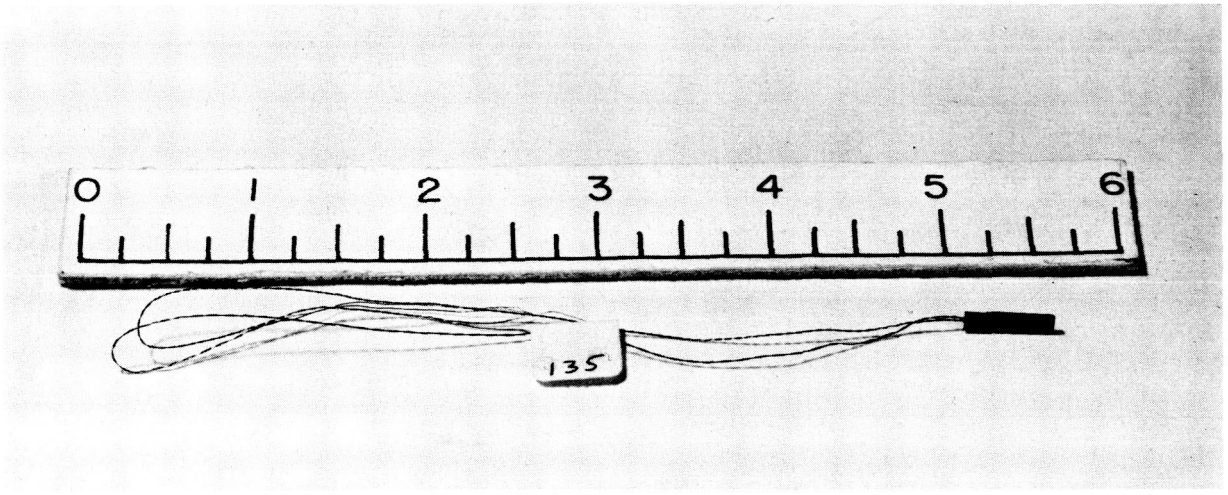


Fig. II-14. Hall-Type Transducer Unit (less flux concentrator)

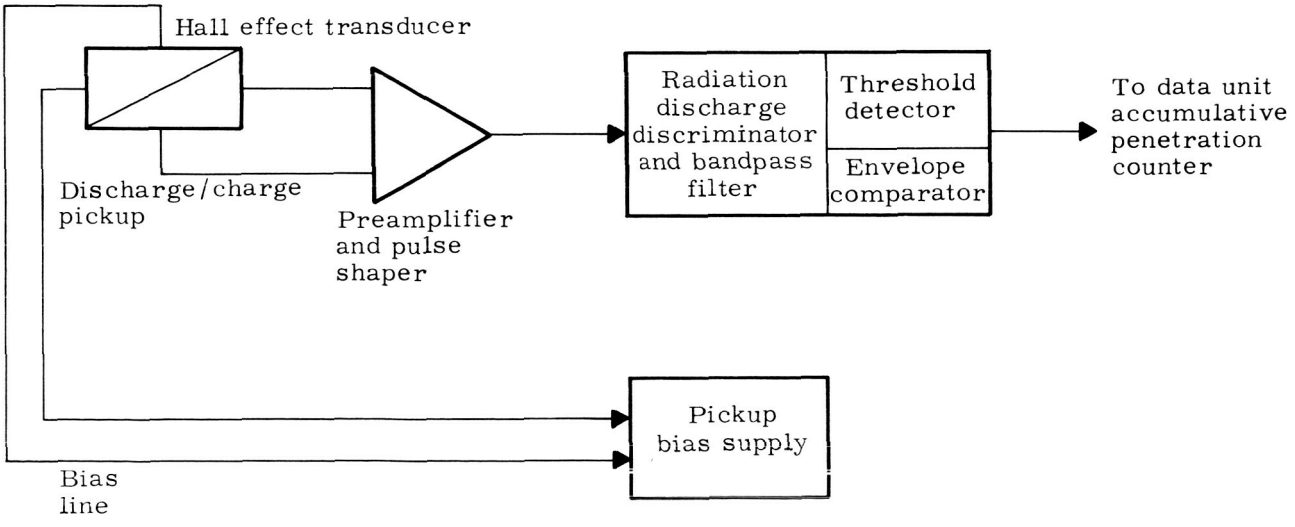


Fig. II-15. Capacitance Panel Sensor Measurement Circuit

data is transmitted over the second transmission channel and its transmission is interrupted only by a ground command to read out the secondary data. The time sharing of the second transmission channel is accomplished by means of the data switch whose operation is discussed in detail later.

c. Secondary measurement subsystem description

(1) Requirements and constraints for the secondary subsystem

In general, data gathering demands for capacitance panel penetrations and IR flash sensor hit detections run parallel with those in the primary system. However, since supplementary data is being added to each of the micrometeoroid measurements, a limitation for storage sizing was imposed to keep memory units within a certain size for reliability. Requirements for Mariner and velocity gauge subsystems necessitate a large amount of data collection with a rapid accumulation rate near perigee. Storage of all these data with detailed supplementary measurement information was considered possible, but not practical with respect to necessary data processing equipment, effects on the length of storage readout transmission times at long ranges and complexity of the overall system. Requirements established for the satellite attitude subsystem were satisfied by obtaining a sufficient number of data points for ground prediction of satellite orientation.

Housekeeping measurements were kept to a minimum to reduce the number of components necessary for this subsystem.

The requirement for no physical interfaces with the primary measurement system was strictly adhered to throughout the design.

At the beginning of the program, a requirement was established to take supplementary measurements upon micrometeoroid penetration for a complete hit history. The developed hit-demand data frame concept fully satisfies this requirement.

(2) Instrumentation

Hit-demand concept. The following section presents a description of the recommended design approach for hit-demand data frames.

Conceptually, hit history data is composed of additional measurements, initiated upon particle impact. These data then will give complementary information about the micrometeoroid particle.

A hit history can contain one or more of the following items:

(1) Event time (spacecraft time).

(2) Identification of the impacted sensor.

(3) Spacecraft attitude at the event time.

(4) Level of impact sensitivity of the specific detector triggered.

(5) Velocity of the impacting particle.

(6) Cumulative hits received by the sensor or sensor group in a certain sensitivity level for correlation.

(7) Direction of the impinging particle.

Items (1), (2) and (3) combined can be utilized to obtain particle direction (7). This requirement is of particular interest for data gathered by the velocity gauge subsystem.

Since hit history information involves a certain number of measurements, data words must be edited for each experiment subsystem. It was a goal in the design approach to establish hit history frames with equal word length to simplify data handling. Words and information arrangement in typical hit history frames are edited as shown in Table II-1.

Hit history frames are initiated upon demand or scaled hit demand. Frames are then composed of some of the following data correlating the event:

(1) Frame identification.

(2) Sensor group or the sensor identification (can be thickness or location).

(3) Sensitivity level of the recorded impact.

(4) Event time; minutes, hours and day of orbit.

(5) Orientation data by sensor location on the satellite. This information might be contained in the sensor identification number.

(6) Cumulative number of hits in one or more sensitivity levels for a particular sensor.

(7) Total number of hits received by a sensor group.

(8) Type of sensor which initiated the hit-demand frame for instruments with more than one type micrometeoroid sensor.

Capacitance panel measurement subsystem. This subsystem serves as a backup measuring system for the primary measurement subsystem. Besides detection of micrometeoroid penetration of the capacitance panels, supplementary data is collected. Passive pickup transducers detect penetration discharge/charge pulses in the capacitance panel lines of the primary subsystem. The output from this pulse detection starts the data processing function of the capacitance panel measurement subsystem.

Requirements and constraints for the capacitance panel measurement subsystem. Basically, requirements for this subsystem are similar to requirements delineated for the capacitance panel sensor network in the primary subsystem. Other requirements for this subsystem are secondary system objectives:

(1) Determine the effective area of operating capacitance panels for each of the 1-mil and 2-mil thickness groups.

(2) Indicate the location of the penetrated panel in terms of three planes of the "Z" configuration (six directions).

(3) Accumulate penetration counts from all the 1-mil and 2-mil capacitance panel sensors.

Table II-1 shows that these requirements were satisfied.

Description of capacitance panel measurement subsystem. The measurement network of the capacitance panel sensors has been outlined previously in the primary subsystem. In this section, a description of the instrumentation is given which is necessary for a complete hit history of a capacitance panel penetration. Supplementary information about the panels and signals from the IR flash sensors (which detect the same event) are edited through a data processing unit as one frame for a hit history. This frame is initiated by hit demand. Combining the two sensor outputs is a logical design approach, since both types detect the same event simultaneously.

The measurement subsystem (Fig. II-16) for the capacitance panel data for a hit history consists of the following major components:

(1) One-mil capacitance panel sensor network.*

*Part of primary subsystem.

(a) Capacitor discharge/charge pickup assembly unit (for 120 units of 1-mil capacitance panel sensors).

(b) Signal conditioning unit for detecting the panel discharge/charge pulse accomplishes the same function for the secondary subsystem as that for the primary subsystem.

(c) Effective area measurement pickup assembly unit.

(2) Two-mil capacitance panel sensor network.**

(a) Capacitor discharge/charge pickup assembly unit (for 144 units of 2-mil capacitance panel sensors).

(b) Signal conditioning unit.

(c) Effective area measurement pickup assembly unit.

Particle Direction Measurement Technique

The Z-wing configuration with the capacitance panel sensor arrangement provides a means of roughly identifying the influx direction of the penetrating particle in relation to spacecraft coordinates.

This is achieved by simply grouping the capacitance panel charge paths such that the output of 6 Hall effect type transducers indicate in which one of the 6 spacecraft coordinates the penetrated panel is facing. The arrangement is shown in Fig. II-13. These data are correlated with spacecraft time and attitude data in the ground analysis to reconstruct particle directionality.

Capacitance panel effective area measurement. Several techniques for determining area have been considered, and the basic concepts will be outlined. Two distinct problem areas exist: detection of a malfunctioning capacitance panel, and determination of effective area. There are two basic ways the capacitance panel sensor may malfunction: either opens or shorts. However, if one considers the overall configuration of the sensor, it becomes obvious that for the sensor to become open circuited involves a mechanical, not an electrical, malfunction. Assume that the mechanical configuration is such as to reduce the probability of an open circuit occurring to a reasonable value. Since detection of an open capacitor is best accomplished by measuring AC impedance and a short by DC methods, it can be seen that the detection of a malfunction has been considerably reduced.

** Part of primary subsystem.

Figure II-17 is a simplified schematic of two short detecting techniques. The simplest involves resistor R connected directly to the capacitor; the output at A is then approximately E_{cg} for an operating capacitor and 0 volt for a shorted capacitor. Although this is the simplest technique, it has two drawbacks: it is connected physically to the capacitor sensor, and requires current from the charge generator.

The other technique involves use of a Hall effect device which generates a voltage across opposite faces of an electrical conductor carrying current when placed in a magnetic field. Simply stated, output B will be 0 volt for a good capacitor and approximately 6.0 millivolts for a shorted capacitor. This technique has the advantage of not being physically connected in any manner to the capacitor or the charge generator. It also has the disadvantage of requiring a reference current source and having a relatively low level output. Since both techniques have obvious advantages and disadvantages, the Hall method has been chosen at this time, principally on its isolation property.

A more detailed diagram of the latter method is shown in Fig. II-13. Each area detector shown monitors a number of panels. This arrangement requires the use of linear amplifiers since the currents measured within one sensor group (thickness) must represent the total area within 5%; otherwise it would be necessary to use one detector per panel. This would not only require 264 detectors, but also present a problem for adding the inputs to the feedback adder shown in Fig. II-18.

Since the detector outputs are proportional to the induced flux and the overall linearity requirement is 5%, the grouping technique appears feasible but further study is recommended.

The circuit shown in Fig. II-13 will require 24 detectors per sensor thickness and 24 linear amplifiers whose outputs are added for effective area determination within 5%.

Determination of area also involves two techniques; however, the choice to be made becomes obvious. The first method is simply to commutate through all the panel detectors and count the number of operating panels. This involves a commutator having 144 contacts for the 2-mil sensors and 120 contacts for the 1-mil sensors and appropriate counters for each. Reliability of such a device makes its util-

ization in this instance questionable. However, if the voltage from the detectors is summed in a feedback adder, the output would be a voltage directly proportional to the number of operating panels. Fig. II-18 is a simplified schematic of a technique for direct conversion of that voltage to a binary form representing the percent of effective area with an accuracy of 5%.

Zener diodes D_1 to D_4 have breakdown voltages in 20% increments of the total feedback adder output. Transistors Q_1, Q_3, Q_5, and Q_7 are analog AND gates which connect the voltage exceeding the zener voltage of D_1 to D_4 to zener diodes D_5, D_6, and D_7, which have breakdown voltages in 5% increments. Transistors Q_2, Q_4, Q_6, and Q_8 provide switching voltages to the analog gates.

Operation is such that, assuming the amplifier output to be maximum, diodes D_1 to D_4 would be active and gates Q_1 to Q_7 would be inactive. Voltage exceeding D_4 (80%) would be connected to the 5% bus through D_8, and diodes D_5 to D_7 would be active. As the amplifier output decreases, diodes D_5 to D_7 would, in turn, become inactive until D_4 ceases to be active. At this time, Q_8 is turned off and Q_7 becomes active, which connects the voltage exceeding D_3 (60%) to the 5% bus. This action continues throughout the output range of the amplifier. A table of binary outputs for 0-100% of the amplifier range is shown in Table II-4. Outputs are taken from Q_2, Q_4, Q_6 and Q_8 for the 20% range and Q_9, Q_{10}, and Q_{11} for the 5% range, and can be transferred directly to storage (Fig. II-19). No delay is required to eliminate hit transients since this is inherent in the placement of this data in the format.

More effective outputs are possibly gained by gating on only the highest active levels. Also, it is advisable that the analog gates be

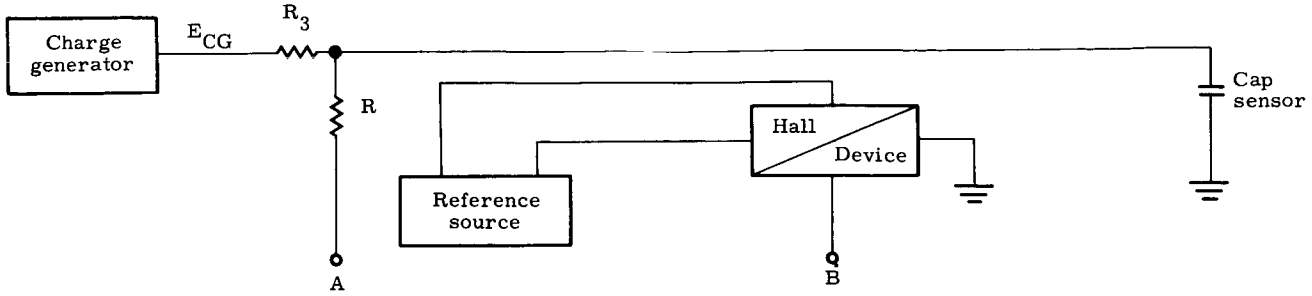


Fig. II-17. Capacitor Sensor Short Detection

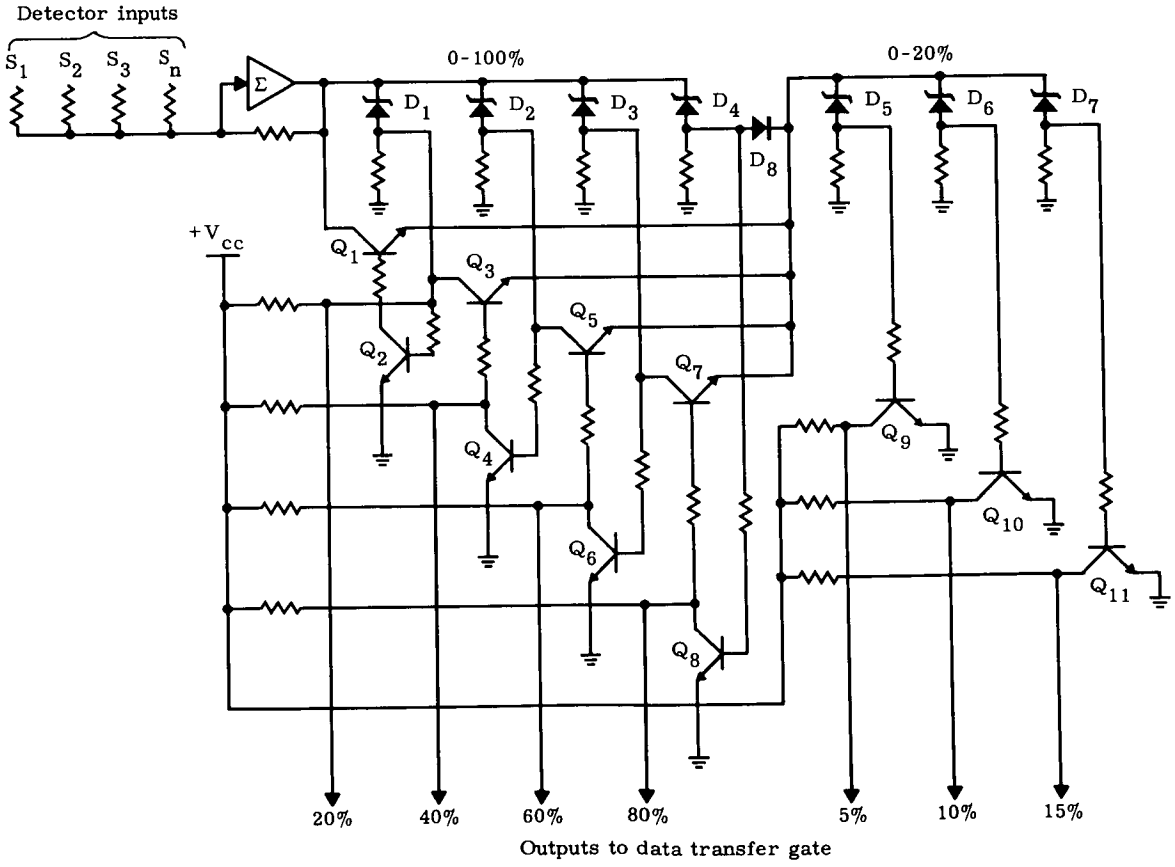
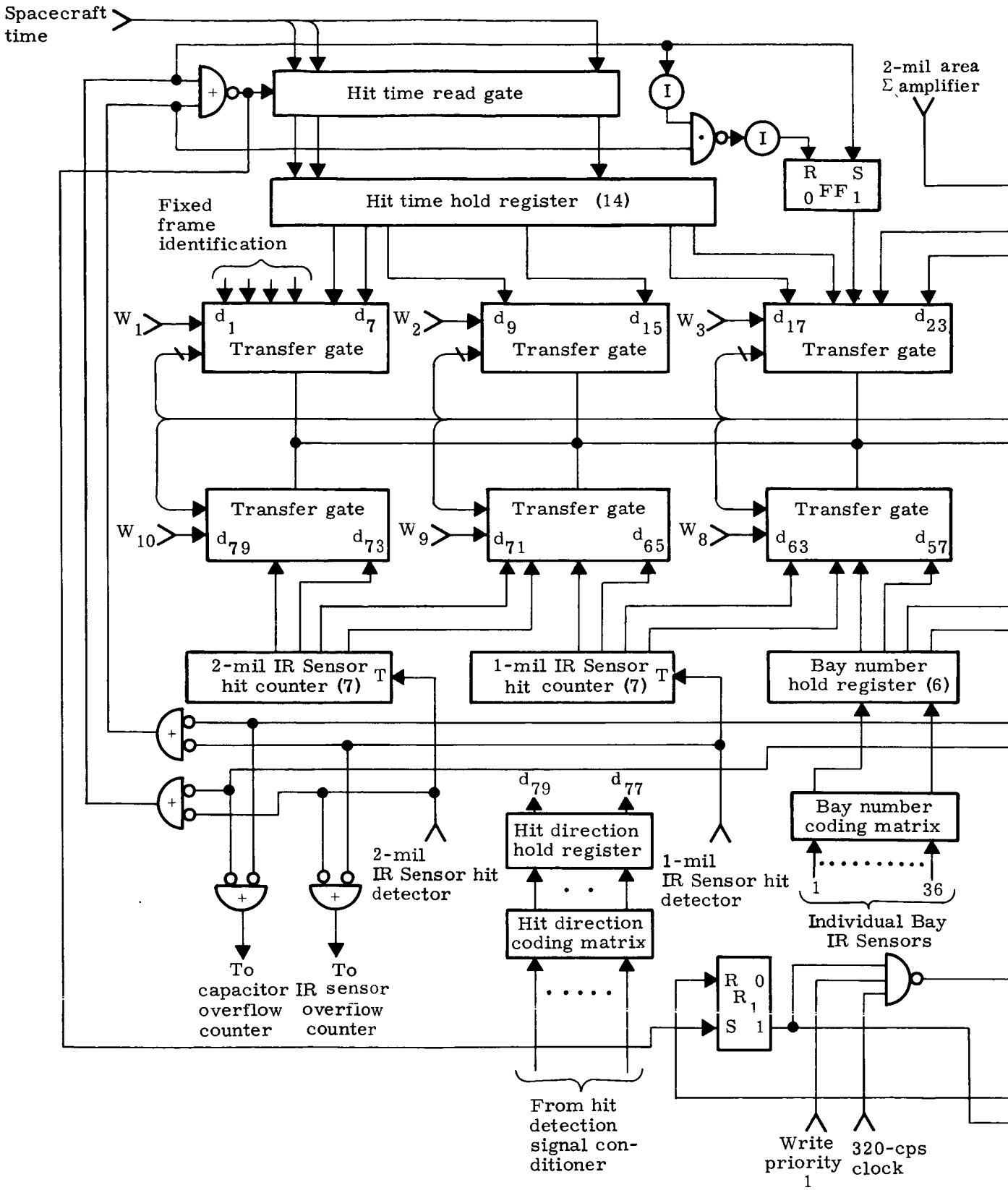


Fig. II-18. Percent of Effective Area Circuit

TABLE II-4

Percent of Effective Area Binary Outputs

Amplifier Output (%)	D_1 20%	D_2 40%	D_3 60%	D_4 80%	D_5 5%	D_6 10%	D_7 15%
95	0	0	0	0	0	0	0
90	0	0	0	0	1	0	0
85	0	0	0	0	1	1	0
80	0	0	0	0	1	1	1
75	0	0	0	1	0	0	0
70	0	0	0	1	1	0	0
65	0	0	0	1	1	1	0
60	0	0	0	1	1	1	1
55	0	0	1	1	0	0	0
50	0	0	1	1	1	0	0
45	0	0	1	1	1	1	0
40	0	0	1	1	1	1	1
35	0	1	1	1	0	0	0
30	0	1	1	1	1	0	0
25	0	1	1	1	1	1	0
20	0	1	1	1	1	1	1
15	1	1	1	1	0	0	0
10	1	1	1	1	1	0	0
5	1	1	1	1	1	1	0
0	1	1	1	1	1	1	1


Spacecraft time
Hit time read gate
2-mil area Σ amplifier
R S
0 FF 1
Hit time hold register (14)
Fixed frame identification
W1
d1 d7
Transfer gate
W2
d9 d15
Transfer gate
W3
d17 d23
Transfer gate
W10
d79 d73
Transfer gate
W9
d71 d65
Transfer gate
W8
d63 d57
Transfer gate
2-mil IR Sensor hit counter (7)
1-mil IR Sensor hit counter (7)
Bay number hold register (6)
d79 d77
Hit direction hold register
Hit direction coding matrix
Bay number coding matrix
1 36
Individual Bay IR Sensors
2-mil IR Sensor hit detector
1-mil IR Sensor hit detector
To capacitor overflow counter
To IR sensor overflow counter
From hit detection signal conditioner
R 0
R1
S 1
Write priority 1
320-cps clock

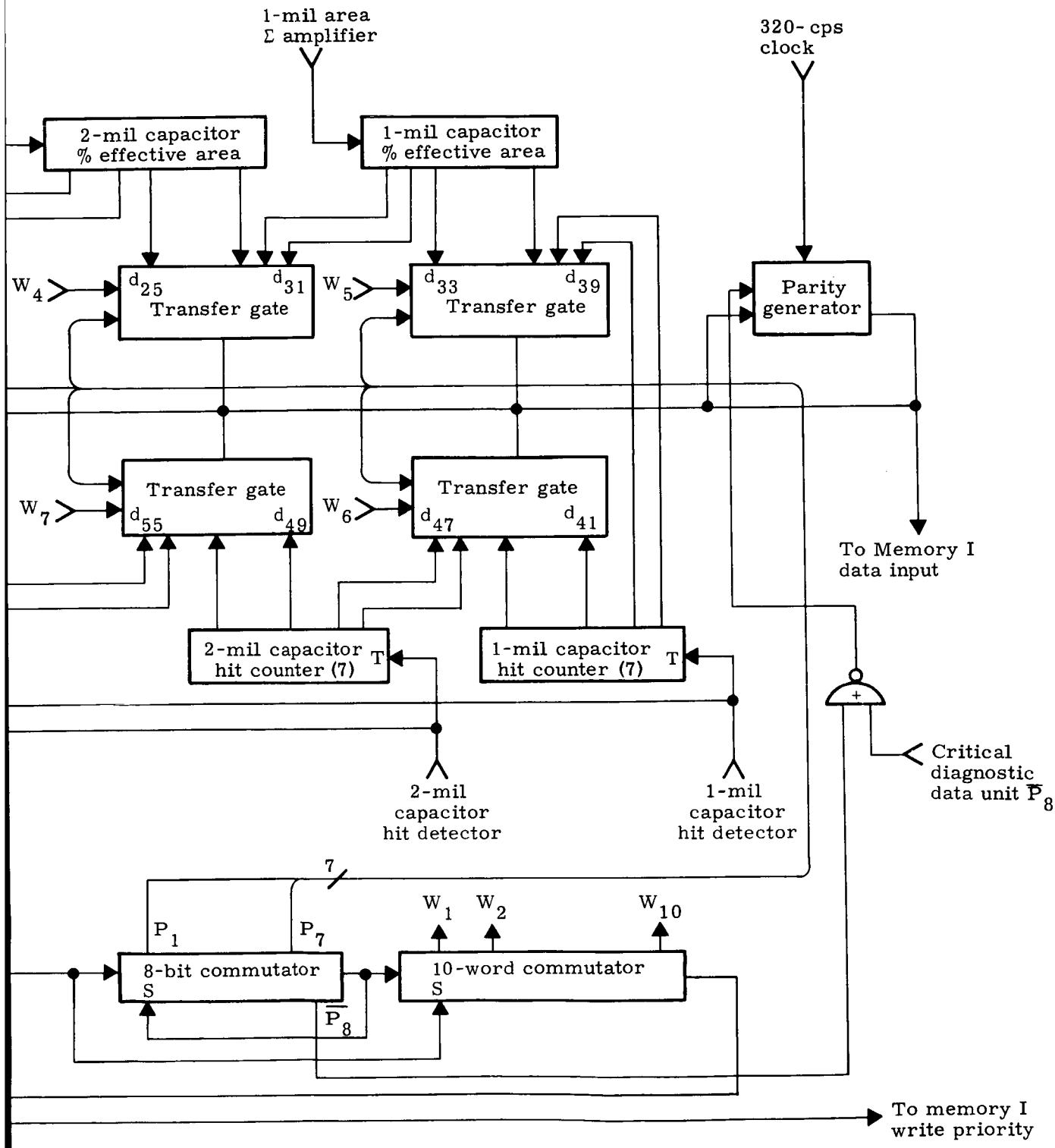


Fig. II-19. Capacitor and IR Flash Data Unit

2H

disabled as the next lower level becomes active. This is accomplished by making Q_4, Q_6, and Q_8 NOR gates, with the other input connected to the preceding transistor's collector; thus, Q_8 has an input connected to Q_6 output, Q_6 input to Q_4 output, and Q_4 input to Q_2 output.

IR flash sensor measurement subsystem

Requirements and constraints for the IR flash sensor measurement subsystem. The subsystem has the same measurement requirements as were established for the capacitance panel subsystem.

Other requirements are secondary system objectives to:

(1) Identify the bay number of the IR flash sensor which detects a penetration. This identification requires a number code from 1 to 36. Bay number identification will relate sensor data to particle influx directions and panel thickness.

(2) Count the cumulative IR flashes for the 1- and 2-mil capacitance panel bays.

(3) Utilize this measurement subsystem as a backup for capacitance panel sensor measurements.

(4) Prevent erroneous hit counting due to other light or flash sources.

Constraints for data storage requirements resulted in six hit-demand frame allocations for storage in this sybsystem. These are the same six frames as for the capacitance panel subsystem, since data from both subsystems are combined in the same format.

A possible problem of panel material backsplash exists, and requires further study and laboratory experimentation. When a penetration on one of the capacitance panels occurs, some of the material might possibly splash on the back of the other panel sensors. This action, in turn, could produce additional discharges and light flashes and, thus, cause false penetration indications.

A buffer plate with absorbing material, inserted between top and bottom capacitance panels inside the bay, might prevent multiple discharges. In this case, twice the number of IR flash sensors would be needed (72 instead of 36).

A hit acceptance time delay circuit in the signal conditioning unit is planned. The purpose of this network is to accept only one event indication for data processing and reject any other signals for a defined time interval. Laboratory experiments with prototype models will be required to prove these theoretical considerations.

Another area for additional study is possible phenomena from radiation discharge in the capacitance panels.

Description of IR flash sensor subsystem. This measurement subsystem is composed of:

(1) 1-mil capacitance panel bay network.

   (a) Two-channel coincidence gate unit--12 units

   (b) Signal conditioning unit.

(2) 2-mil capacitance panel bay network.

   (a) Two-channel coincidence gate unit--24 units

   (b) Signal conditioning unit.

(3) 1- and 2-mil capacitance panel bay networks.

   (a) Bay number coding matrix--1 unit, part of format organization units.

The sensor mounting arrangement should minimize incident sunlight through micrometeoroid penetration pinholes in the capacitance panels of the tumbling satellite. Also, an opaque mylar light block covers the gap between sensors and frame. Low frequency cutoff in the hit-signal input circuit of the signal conditioning unit will also eliminate the solar source for sensor activation.

Sensor bay identification is accomplished with a binary matrix-encoder unit through trigger pulses from respective bay coincidence modules.

Figure II-20 shows a simplified schematic block diagram of the IR flash sensor subsystem with a representative coincidence-pair of flash sensors. When, at the penetration event, a flash occurs inside the bay, the two IR flash sensors, mounted diametrically opposite each other, send detection signals over the dual channel system to a single coincidence gate.

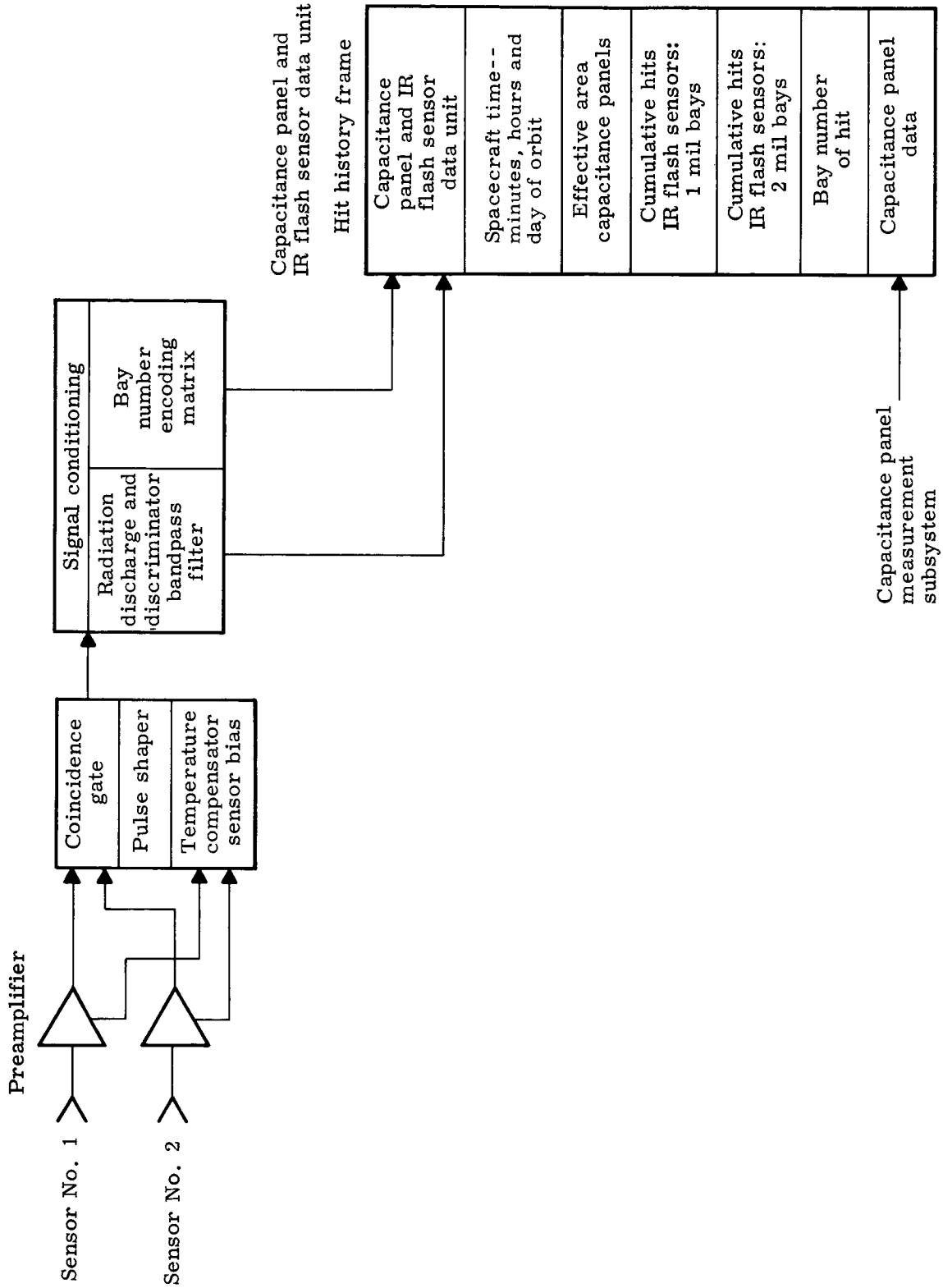


Fig. II-20. IR Flash Sensor Measurement Subsystem (36 pairs of sensors)

After detection of the coincidence count, a time delay network inhibits further acceptance of any coincidence signal for a period of 1 sec. This feature prevents erroneous multiple penetration counts caused by backsplash.

Preamplifiers for the sensors have built-in temperature compensation networks to allow calibration stability over a large operational temperature band.

Hit-demand frame for capacitance panel and IR flash sensors. Hit histories for capacitance panel and IR flash sensors are combined into one data format. This is a logical design approach, since both sensor groups monitor one and the same phenomenon. The data frame contains:

(1) Format identification number--to provide unique and positive format identification in a random sequence of hit-demand frames

4 bits required: count from 1 to 15

Number 1 format

(2) Capacitance panel thickness--to indicate hits on either 1- and/or 2-mil sensors. This information is redundant to primary subsystem data of Transmission Data Channels 1 and 2.

1 bit required: 0 = 1-mil panel

1 = 2-mil panel

(3) Capacitance panel location--to indicate location of impacted panel with respect to the coordinate system of the Z-wing configuration. These data when combined with vehicle attitude data, will coarsely resolve the direction of the impacting particle.

3 bits required: count from 1 to 6

(4) Hit event time--measured as minutes, hours and days of orbit. The information is required for correlation with separately measured spacecraft attitude data to reconstruct spacecraft orientation and particle direction in ground analysis.

(5) Effective capacitance panel areas for the two different thicknesses of panel sensor groups. This measurement is expressed as a code number for the percentage of operating capacitance panels in each thickness. The measurement determination is within ± 5%.

14 bits required

7 bits for 1-mil panel area

7 bits for 2-mil panel area

4 bits in 20% increments

3 bits in 5% increments

(6) IR flash sensor bay number--to indicate in which capacitance panel bay a flash was detected. This information will back up the capacitance panel measurement. The data will also supplement the determination for the impacting particle direction.

6 bits required

Count from 1 to 36 bay numbers

(7) Cumulative hit count for the 1-mil capacitance panel sensors--to totalize the number of penetrations detected. Counter resets to zero when full.

7 bits required

Count from 0 to 127 hits

(8) Cumulative hit count for the 2-mil capacitance panel sensors.

7 bits required

Count from 0 to 127 hits

(9) Cumulative hit count for the IR flash sensors mounted in the bays formed by 1-mil capacitance panel sensors--to totalize number of flashes detected. Counter resets to zero when full.

7 bits required

Count from 0 to 127 hits

(10) Cumulative hit count for the 2-mil bays.

7 bits required

Count from 0 to 127 hits

The described hit demand frame, which is initiated either by hit detection with a capacitance panel sensor or an IR flash sensor--or both, does not require an indication of which sensor type triggered the frame readout. Comparison of the cumulative hit counts with the preceding frame of capacitance panel and IR flash sensor hit history will show how the present frame was initiated.

Mariner gage measurement subsystem. The Mariner gage measurement capability extends the particle detection sensitivity range for the satellite mission.

In contrast to the capacitance panel sensors, a large amount of data at rapid influx rates has to be processed. For this reason, a number of tradeoff studies were conducted to determine the best way of handling data flow. These investigations are discussed in Appendix II-5.

Mariner gages in this subsystem, as well as velocity gages in the following subsystem, are the only experiments with acoustic sensors in the MDSS instrumentation. Chosen mounting locations make the Mariner gage acoustic sensors extremely susceptible to spacecraft structural noise. Tuned preamplifiers and bandpass filters minimized these environmental effects.

Requirements and constraints for the Mariner gage subsystem. To determine measurement requirements for this subsystem, it was necessary to establish impact counter ranges for the various instrument levels. The predicted number of impacts per micrometeoroid density zone per orbit per instrument are: (Refer to Chapter I)

Capacitor Sensor Sensitivity Levels	Microphone Sensor Sensitivity Levels	Impacts/Zone/ Orbit/Unit*
A		39,040
B		1,783
1	1	81.4
2	2	9.4
3	3	3.7
4	4	0.43

*These numbers are based on the most recent predictions of micrometeoroid influx rate. The data system described herein is based on prior predictions which were low by a factor of 1.6. However, a simple modification of the data entry scalars will resolve this problem. Even under present circumstances, the data system described herein is capable of handling the increase in influx. The memory units will fill at a faster rate but the increase in impacts will be recorded in the Mariner and velocity gauge overflow counters.

Since there are five zones per orbit and three instruments, the following number of impacts are encountered:

Capacitor Sensor Sensitivity Levels	Impacts/Orbit/ Instrument*	Impacts/Orbit*
A	195,200	585,600
B	5,355	16,065
1	407	1,221
2	47	141
3	18.5	55.5
4	2	6

To reconstruct the full micrometeoroid environment, it was established that 40 hit histories per orbit were more than sufficient to do so. Thus, a 13-stage binary counter was selected to register the number of impacts on the most sensitive capacitor level. Similarly, the other capacitor and microphone level counters' capacities were established.

Capacitor level A accumulative hit counter was selected to trigger a scaled hit history frame upon full count into memory. This manner of initiating data entry greatly reduces the memory capacity requirement and enhances system simplicity.

Description of Mariner gage subsystems. The two capacitance panel sensors of the Mariner gage detect micrometeoroid particles by penetration. Discharge/recharge pulse amplitude is proportional to particle energy level and can be sorted accordingly. Panel sensor charging circuits are protected with current-limiting series resistors. The applied charging potential is from 7 to 12 volts.

As shown in Fig. II-21, a pulse height analyzer for each capacitor sensor discriminates penetration signals into six sensitivity levels. Hit counters register these level indications.

The microphone sensor analyzes micrometeoroid hits from the mechanical excitation and vibration intensity level caused by particle collison on the impact plate. Sensor signals are amplified by a tuned amplifier with 100-kc center frequency. Output pulses are proportioned in amplitude to particle impact momentum. A four-level pulse height analyzer directs the signals then to their respective hit counters.

Provisions are made for in-flight calibrations of capacitor sensor electronics and the acoustic sensor measuring system. The calibration procedure is initiated and read out during real-time data transmission

*See footnote on page II-60.

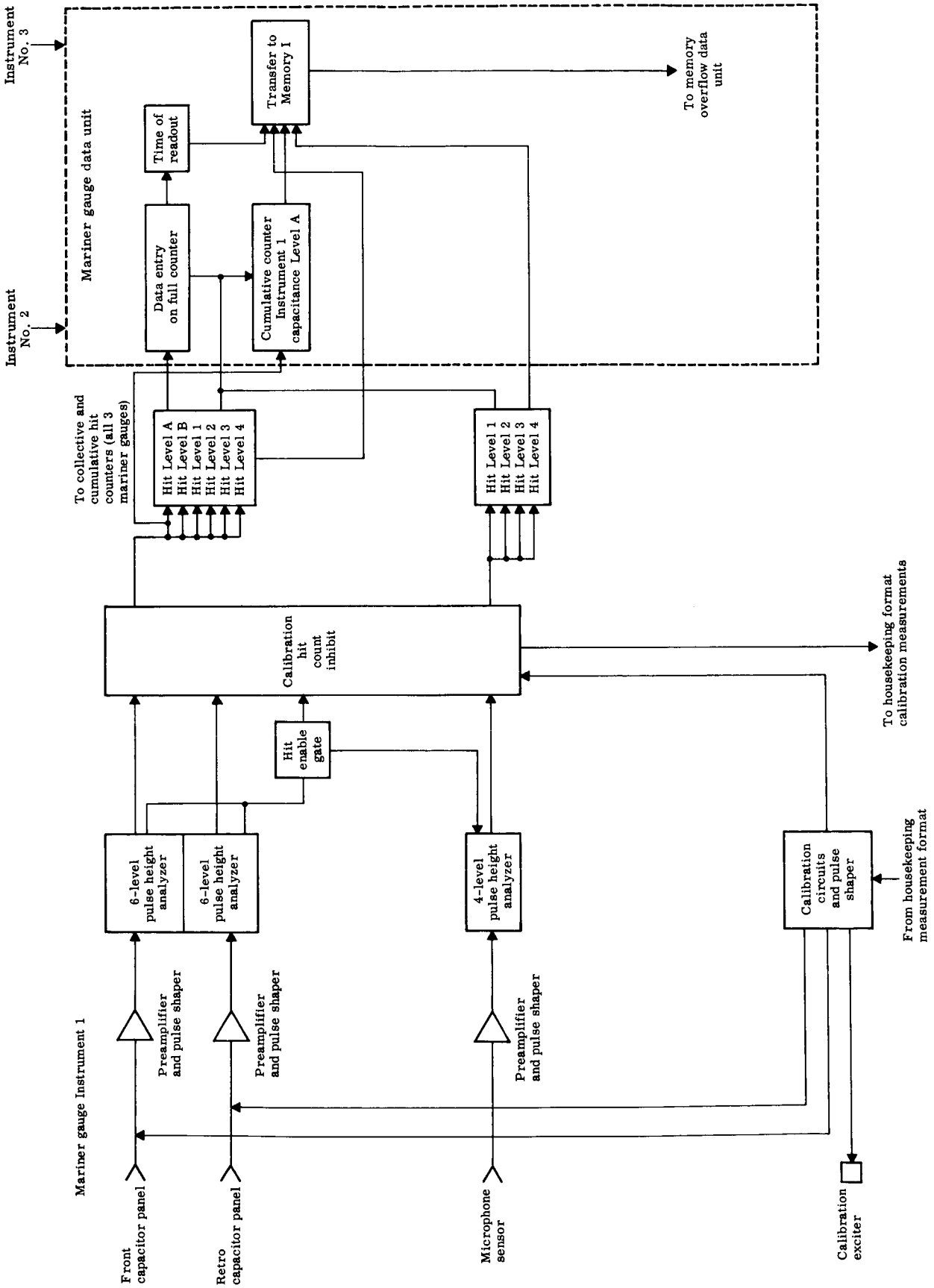


Fig. II-21. Mariner Gauge Measurement Subsystem

of the housekeeping format. A calibration hit-count inhibit circuit prevents erroneous hit registrations.

Hit-demand frame for Mariner gages. The hit history frame for Mariner gages is demanded when the cumulative hit counter for the highest sensitivity level (smallest micrometeoroid particle) is filled. The Mariner gage hit history is composed of cumulative counts of micrometeoroid hits in each sensitivity level for all three gages, cumulative count of hits in Capacitance Level A from Mariner Gage No. 1, cumulative hit count in Capacitance Level A from Mariner Gage No. 2, and the readout time of the hit history frame (when hit counter for Capacitance Level A for all three gages is full).

Hit counts from Instruments 1 and 2 in Capacitor Level A are measured separately. Hit counts on Instrument 3 can be approximated by subtracting the sum of 1 and 2 from the total. This arrangement will verify that all three instruments are operating.

An up-to-date counter readout capability is provided in the real time housekeeping format. Thus, in case micrometeoroid influx rate is lower than anticipated, the cumulative hit counter for Capacitance Level A does not fill to capacity and no frame readout is initiated, all Mariner gage cumulative counters can be interrogated by command.

Velocity gage measurement subsystem. The function of this subsystem is to monitor micrometeoroid particle velocity and to gather particle directional data. Special attention was given in the design approach to provide sufficiently high measurement resolution for particle velocity determination.

Requirements and constraints for the velocity gage measurement subsystem. For determination of the data requirements of the subsystem, the following hit count model is given.

The number of hits per micrometeoroid density zone per orbit per one sensing tube:

Capacitor Sensor Sensitivity Levels	Microphone Sensor Sensitivity Levels	Micrometeoroid Hits *
1		33.2
2	1	2 (1.5)
3	2	1 (0.173)
4	3	1 (0.07)

*See footnote on page II-60.

Zone Count Accumulation for Levels	1 Velocity Gage Hit*	2 Velocity Gage Hits*
1	132.8	265.6
2	6	12
3	0.69	1.38
4	0.4	0.8

Orbit Count Accumulation for each Level per Orbit	2 Unit Subsystem Hits*
1	1328
2	60
3	6.9
4	4

Thus, these numbers establish level criteria requirements.

To reconstruct the micrometeoroid environment and establish memory capacity requirements, a tradeoff between these two requirements was necessary. It was established that approximately 50 hit histories per orbit were sufficient to determine the micrometeoroid environment and, at the same time, maintain the memory capacity at a minimum.

Thus, the following number of hit histories are entered into memory each orbit for the various capacitor and microphone levels based on the preceding number of predicted impacts:

Capacitor Level	Number of Hit Histories Recorded per Orbit
I	8
II	10
III	5
IV	5
Microphone Level	
I	10
II	5
III	5
	48 total entries

These requirements then aid in determining the memory capacity.

*See footnote on page II-60.

Description of velocity gage subsystem. This subsystem has the following major components:

(1) Time of flight sensing unit

(a) 1 unit per tube

(b) 8 units total

(2) Four-level pulse height analyzer

(a) 1 unit per instrument

(b) 2 units total

(3) Three-level pulse height analyzer

(a) 1 unit per instrument

(b) 2 units total

(4) Time of flight signal conversion unit

(a) 1 unit per instrument

(b) 2 units total

(5) Velocity sensing tube number coding matrix

(a) 1 unit (part of data processing)

Each velocity gage unit has four micrometeoroid sensing tubes. Every tube is equipped with a capacitance penetration sensor, acoustic sensor and time of flight measuring network. Figure II-22 shows a schematic diagram of the measurement arrangement for one sensing tube.

Signal outputs from the capacitor sensor are sorted into four levels by means of a pulse height analyzer. Microphone signals are analyzed into three input momentum levels.

Figure II-23 illustrates the scheme for velocity sensing tube identification.

The sensor converts the time of flight of the impacting particle to an analog voltage. This analog data is quantized into a 12-bit data word to obtain sufficiently high incremental resolution. From this measurement, particle velocity can be determined to 1 part in 4096.

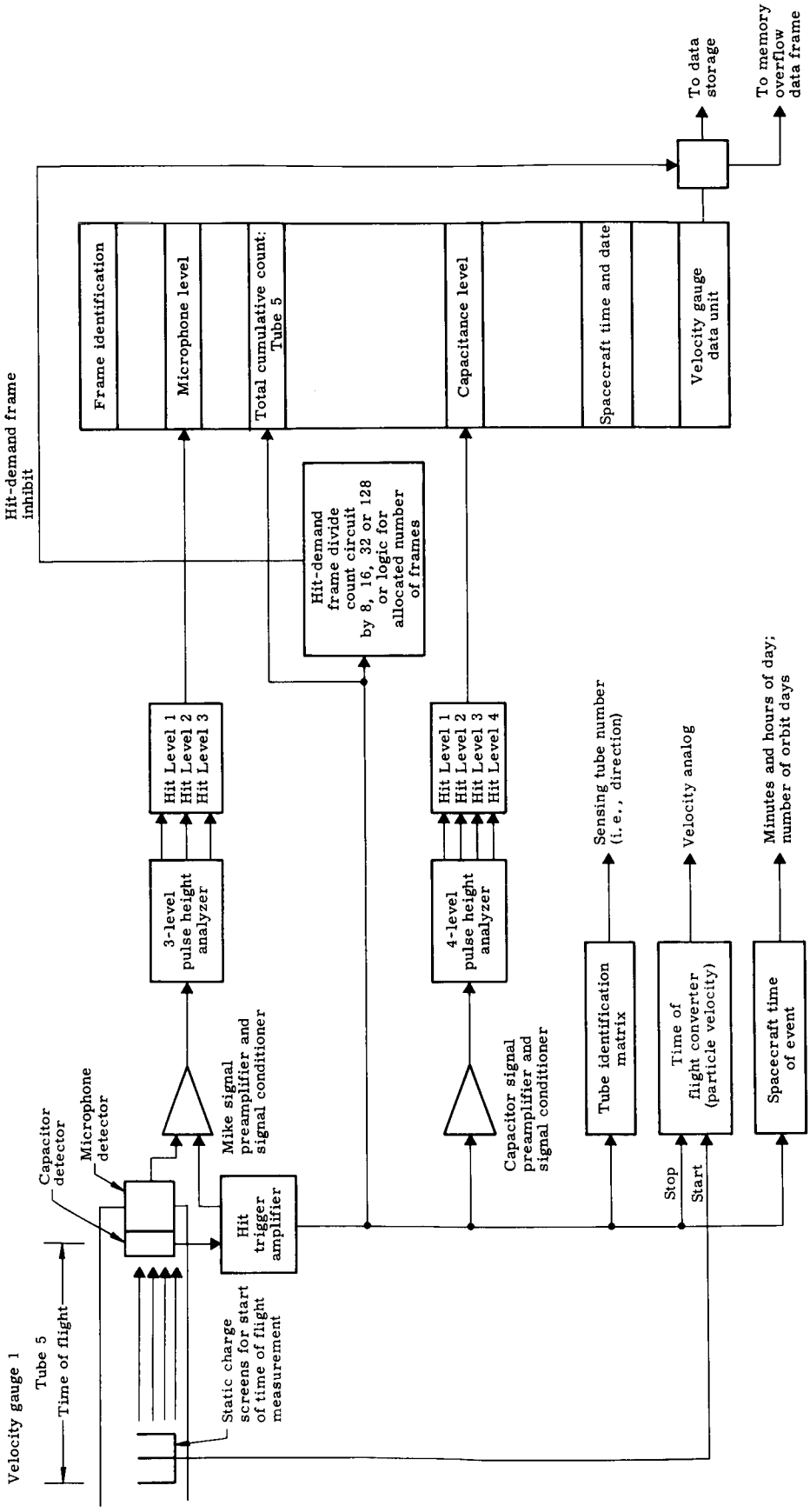


Fig. II-22. Velocity Gauge Measurement Subsystem (8 sensing tubes)

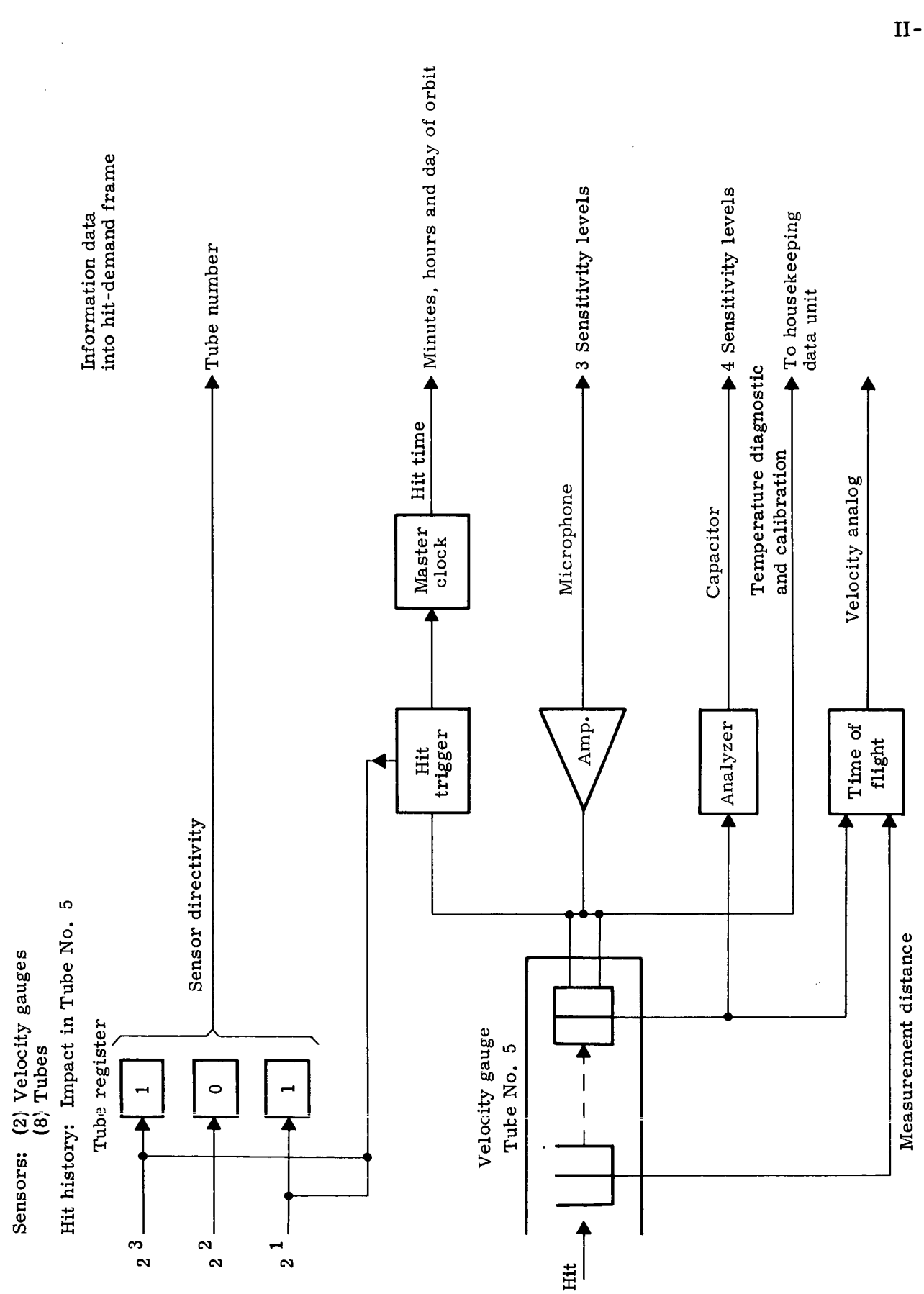


Fig. II-23. Velocity Sensing Tube Identification

The impacted sensing tube is identified into a code number to correlate spacecraft attitude data and event time for determination of influx direction.

Collective counters record the total number of cumulative hits on capacitor and acoustic sensors from all eight sensing tubes. Counters for cumulative hits collected by one instrument only serve as a means to establish data contribution from each of the two velocity gages.

Calibration stability of the velocity gages is protected by built-in heating units in the instrument assembly.

Hit-demand frame for velocity gage. Hit history frames for velocity gages are read out on a scaled hit event basis. However, a large number of impacts is anticipated on this sensor and provisions are made to register every micrometeoroid hit in the cumulative counters for the different sensitivity levels.

The most significant data in this hit history frame are particle velocity and directional measurements.

Hit history words for the velocity gage hit-demand frame are arranged as follows:

(1) Frame identification number--4 bits required, count 1 to 15, No. 3 frame.

(2) Hit event time--in minutes, hours and day of orbit:

14 bits required

11 bits for time of day

3 bits for day of orbit, count from 1 to 8 days

(3) Particle velocity--this measurement is the time of particle flight between two known points. Quantized data resolution will be 1 part in 2^{12} for hit history frame. It is assumed that spacecraft velocity will be determined to about 1 part in 2^{12} to 2^{13}.

(4) Sensor tube identification number--indicates the sensor tube which initiates the hit demand frame. Velocity gage No. 1 has assigned Sensor Tubes 1 through 4; Gage No. 2, Sensor Tubes 5 through 8. The sensor tube number relates location on spacecraft and looking angle of sensor tube in instrument package. These two factors, in combination with attitude and time data enable ground analysis to determine particle directional with an estimated accuracy of $\pm$ 5° angular resolution.

Sensor tube number identification also indirectly verifies operating sensors over the satellite lifetime:

4 bits required

Count from 1 to 8 sensors

(5) Capacitor hit sensitivity level--indicates the capacitor sensor output signal proportional to particle energy. Hit signal is differentiated into one of four predetermined output levels:

4 bits required

Count 1 for sensitivity Level I

Count 2 for sensitivity Level II

Count 3 for sensitivity Level III

Count 4 for sensitivity Level IV

(6) Microphone hit sensitivity level--indicates the microphone sensor output signal proportional to the particle momentum. Hit signal is sorted into one of three predetermined output levels:

3 bits required

Count 1 for sensitivity Level I

Count 2 for sensitivity Level II

Count 3 for sensitivity Level III

(7) Detector identification for hit-history initiation--to afford redundancy in identifying the primary sensor, capacitor or microphone, by which this frame was triggered.

Malfunction of one of these sensors could be deduced from this data:

2 bits required

1 bit for capacitor sensor

1 bit for microphone sensor

(8) Cumulative hit count for all eight capacitor sensors--to totalize the number of hits detected by all eight capacitors of the two velocity gages in all sensitivity levels (4 levels):

11 bits required

Count 0 to 2047 hits

(9) Cumulative hit count for Instrument No. 2 capacitor sensor--this is the cumulative hit count for the four capacitor sensors in all four levels of Velocity Gage No. 2. Purpose of information is twofold: verification for proper functioning of Instrument No. 2 and amount of data contribution to totalizer hit count for both velocity gages. Hit-count contribution from Instrument No. 1 is the difference between word (8) and (9):

11 bits required

Count 0 to 2047 hits

Attitude measurement subsystem. The attitude measurement subsystem is described in detail in Vol. III, Chapter V. The function of this measurement subsystem is to gather satellite orientation data which can be correlated with micrometeoroid hit event times for determination of particle influx direction. The latter information is mandatory for velocity gage data analysis.

Requirements and constraints for the attitude measurement subsystem. Measurement requirements include sensor identification for solar aspect and earth sensors. Orthogonal coil sensors of the flux gate magnetometers are identified by their data word sequence in the measurement format. Accurate voltage calibration measurements are required for magnetometer coil bias voltage.

Since attitude sensor instruments are mounted at extreme ends of the fully deployed satellite, provisions have to be made to minimize signal noise.

Description of attitude measurement subsystem. This subsystem consists of:

(1) Solar aspect sensor logic and coding matrix unit.

(2) Earth aspect sensor logic unit.

(3) Magnetometer logic and calibration unit.

Measurements for two different modes of operation are shown in Table II-1. Logic units for solar aspect, earth aspect and magnetometer coil sensors identify the active sensor with a number and formulate a data format whenever an earth sensor looks at earth.

Housekeeping measurement subsystem. The purpose of this subsystem is to gather information relating to the status of satellite systems. Realtime readout of housekeeping measurements is provided to give spacecraft clock time in real time along with other engineering data. The real time mode is initiated by Sequence I readout command. Once daily, a frame of 10 words of critical diagnostic data is entered in Memory I.

Description of housekeeping measurement subsystem. To avoid interfaces, no housekeeping measurements are taken in the primary subsystem. The housekeeping measurement subsystem is composed of:

(1) A network of status measurements for each major subsystem to monitor proper function. These measurements are combined in a critical diagnostic data frame which can be stored or read out in real time on command.

(2) A network of calibration measurements in a number of subsystems and experiments. The housekeeping mode, when initiated, triggers calibration modes in one experiment. Calibration measurements, taken simultaneously, update information on sensor calibration status.

(3) A number of environmental measurements.

Figures II-24 and II-25 show a conceptual arrangement of the housekeeping format. Table II-1 lists the sequence of measurements in the critical diagnostic and the housekeeping formats.

Delayed command verifications and readouts of all micrometeoroid cumulative counters are formulated in the Sequence I readout telemetry data mode. Provision for real time readout of all hit-counters was made as backup for the stored experiment data.

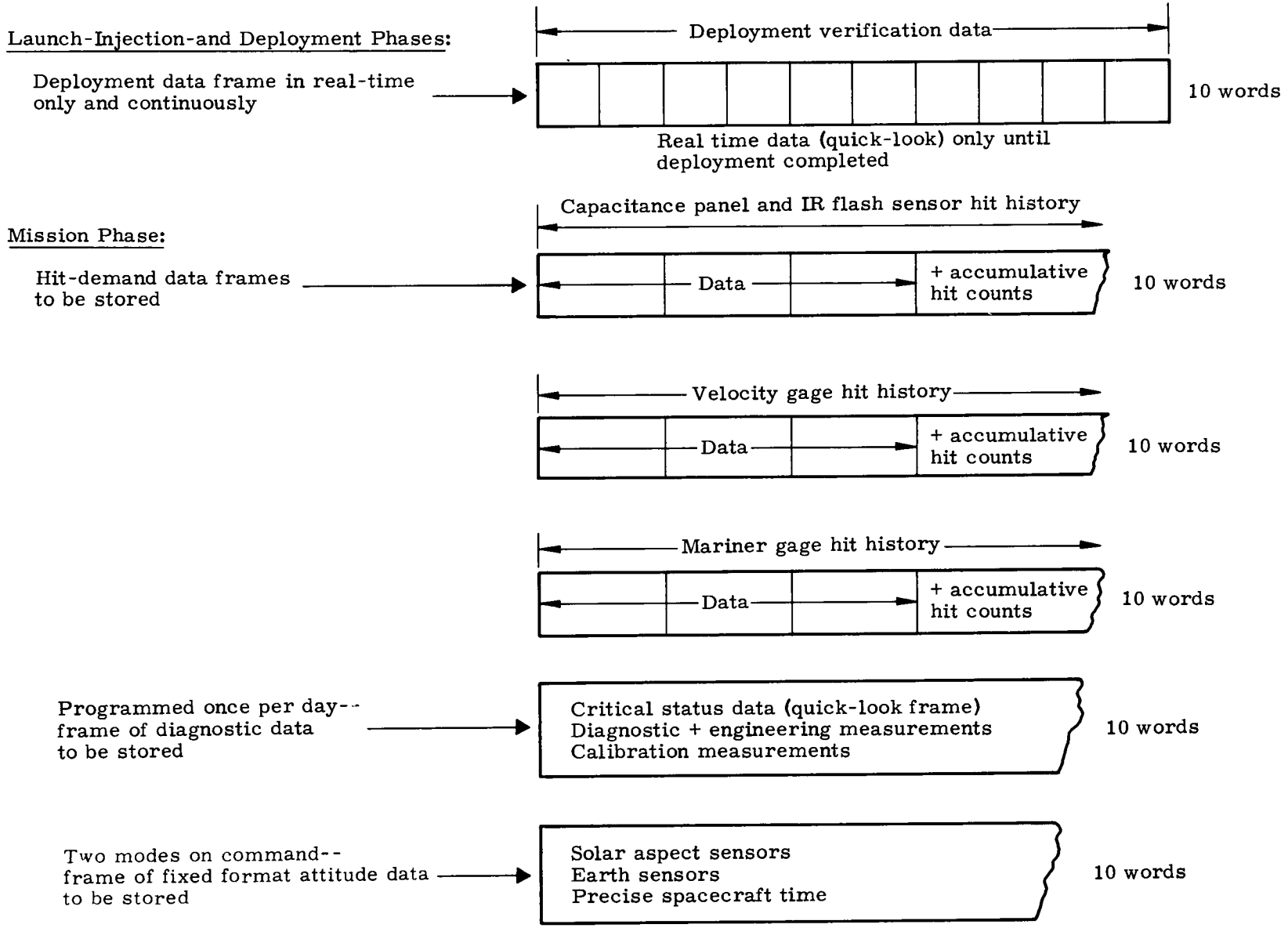


Fig. II-24. Data Frame Arrangement

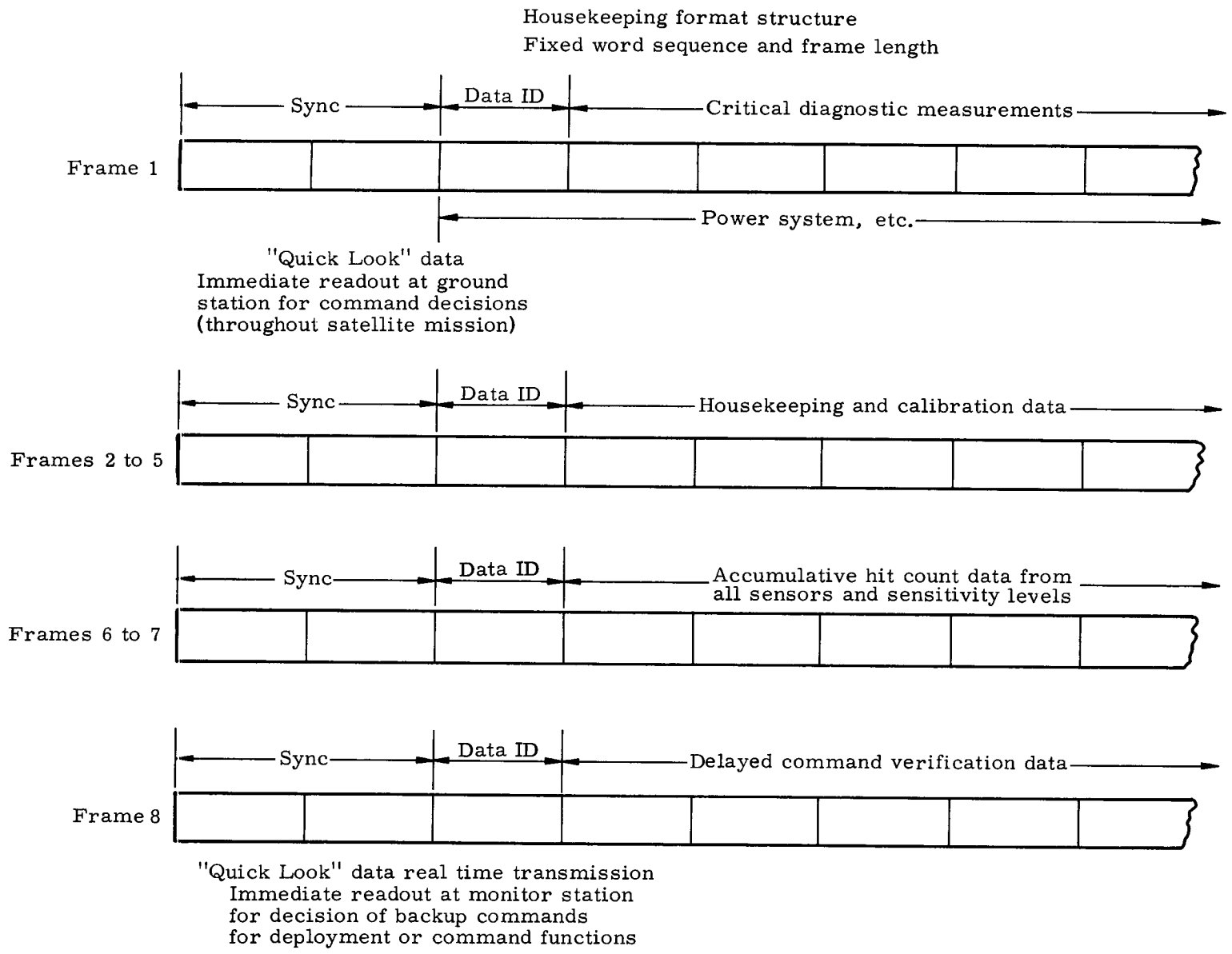


Fig. II-25. Housekeeping Format Arrangement

Deployment data, in real time, are recommended to be used as "quick-look" data in the satellite launch and injection phase, since these data contain mandatory measurements for system status.

Temperature transducers placed on each Z-wing could serve a double function as temperature and as attitude determining devices for the slowly tumbling spacecraft or as backup for the attitude subsystem.

(3) Format organization

Capacitor and IR flash data unit. The capacitor and IR flash data unit shown in Fig. II-17 collects data from two sensor groups, places the data in the format and enters the format into memory. The calculated bit contribution from this data unit for one orbit is 480 bits.

The capacitor and IR flash data are combined in the same format since penetrations will be detected by both sensors simultaneously. Accumulated capacitor sensor penetrations are redundant on the primary data but a penetration detected either on the capacitor or IR flash sensor causes a full hit-history to be entered into the memory. A hit-history is the time of penetration occurrence, the capacitor thickness, accumulated IR flashes for each capacitor thickness, and the accumulated capacitor penetrations for each thickness.

A penetration detected on either sensor causes the time of event to be entered into a hold register and also a bistable to be set which enables the commutator clock gate and interrogates the write priority logic. Provided that the critical diagnostic data unit is not writing into Memory I, or Memory I is not being read out, the write priority logic shown in Fig. II-26 will activate the clock gate. The commutator generates ten word periods and eight bit periods. Coincidence of word and bit periods at each transfer gate allows data to be organized into the capacitor and IR flash sensor format as shown in Table II-1. Data being entered into Memory I also enters the parity generator which is shared with the critical diagnostic unit. A parity bit is generated each eighth bit period of each word. Upon termination of the commutator cycle, the write command to the memory is disabled and the data unit is returned to its initial condition in preparation to generate the next hit-history.

Critical diagnostic data unit. Critical diagnostic data is entered into memory once per day on command from the spacecraft time generator. Data consists of 15 critical measurements concerning the status of the system and contributes 480 bits of data per orbit to Memory I. Upon command, the data unit receives from the signal conditioning equipment, pulses whose widths are proportional to the absolute value of the voltages being measured. An A/PW telemetry

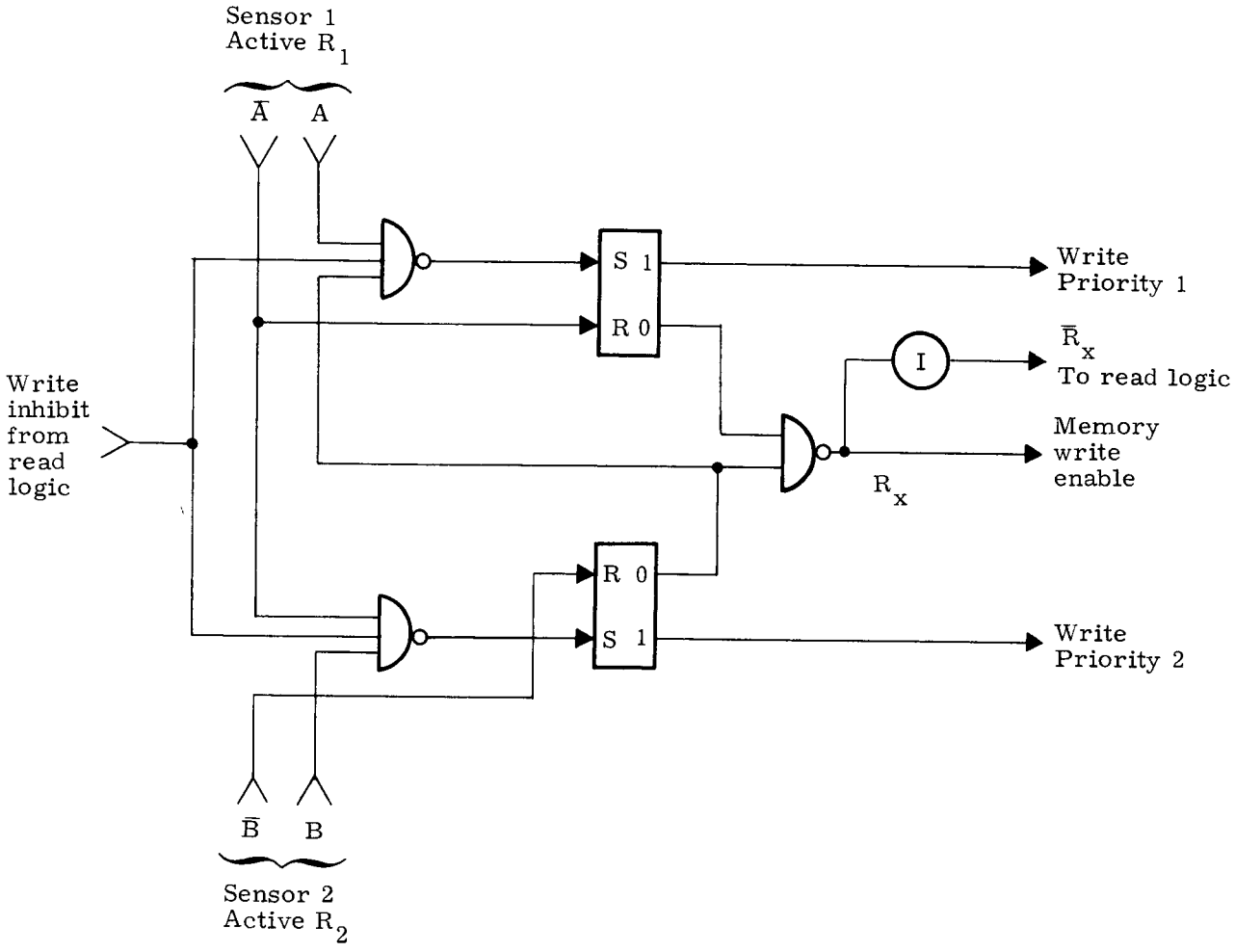


Fig. II-26. Write Priority Logic

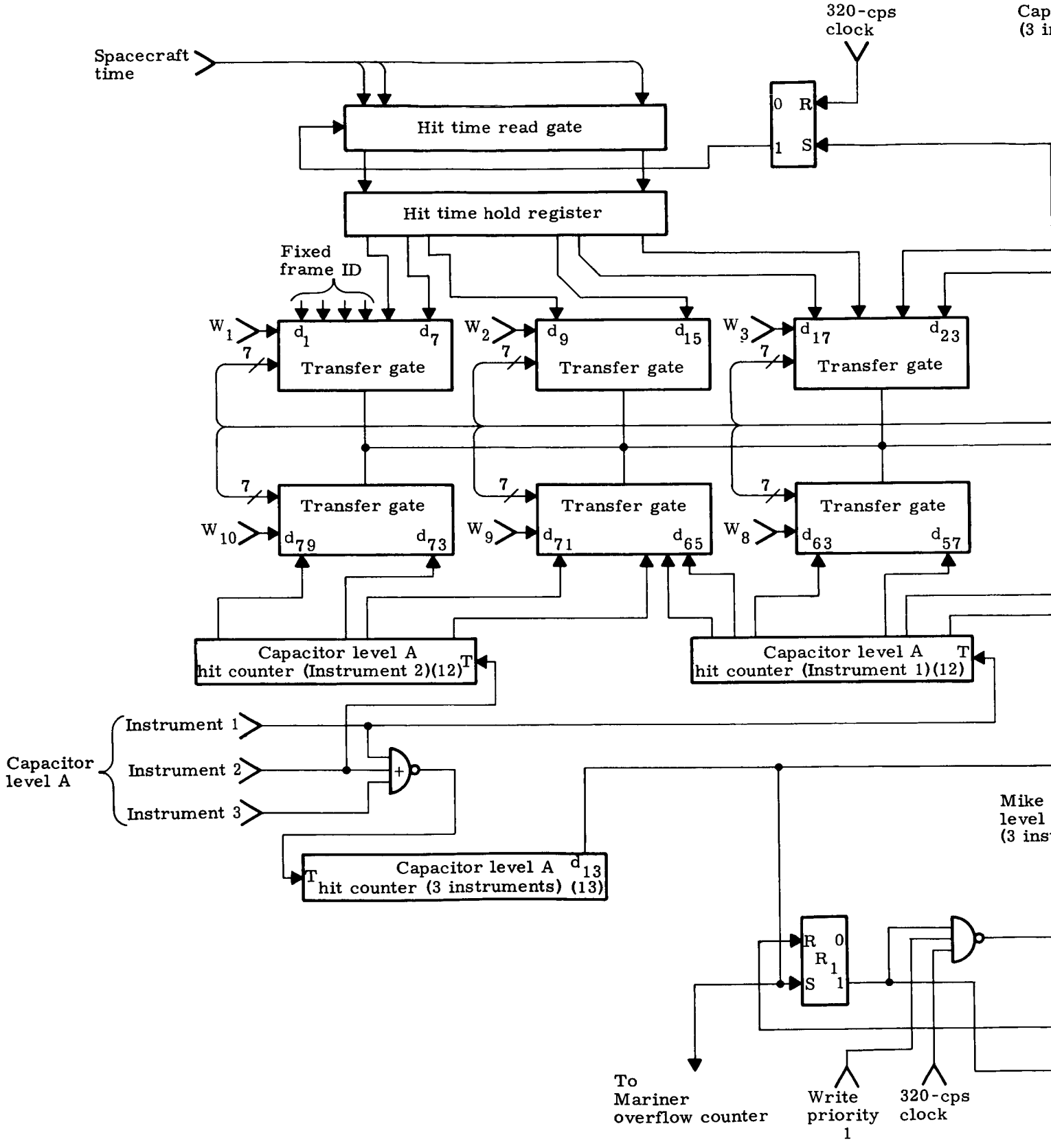
technique is used. Clock pulses are then gated for the duration of the individual pulse widths into the various counters. Upon termination of the pulses, the counters contain a binary number representative of the voltage measured. Fig. II-27 is the block diagram of the critical diagnostic data unit. Upon completion of the conversion period, the commutator is enabled and Memory I write command generated. Since the data input to Memory I is shared with the capacitor and IR flash data unit, access to the memory input is established by the write priority logic. Thus, the aforementioned sequence will be initiated only if no read or write command is in existence.

Should a read or write command exist, the sequence is delayed until the command in progress is terminated. The critical diagnostic format, as shown in Table II-1, is then entered into Memory I in the same manner as that described for the capacitor and IR flash data unit.

Mariner gage data unit. Mariner gage data is entered into memory on a scaled input basis due to the extreme sensitivity of the device. Based on the predicted impact rate, 40 data entries per orbit will provide sufficient data for the reconstruction of the micrometeoroid environment. Since three gages are utilized and the predicted impact rate is approximately 14,000 per zone per orbit per sensor on the most sensitive level, the scaler then required is 13 bits. Data entry then occurs each time the 13th bit changes state.

Figure II-28 is the Mariner gage data unit block diagram. It consists of a spacecraft time read gate and hold register and counters for the various capacitor and microphone levels. Each counter totals the impacts received on all sensors for the particular level being measured. Two additional counters register penetrations on Instruments 1 and 2, respectively, in Capacitor Level A. Thus, there is a counter for the combined hits on Level A from all three instruments and one counter for totalizing Level A impacts of Instruments 1 and 2 individually. Data entry occurs, as previously mentioned, when the combined Capacitor Level A total impact counter's 13th stage changes state. At this time, the clock gate to the commutator is enabled and the write priority logic interrogated. Provided the velocity gage data unit is not writing into Memory II or the memory is not being read out, the Mariner gage format shown in Table II-1 is entered into memory in the same manner as that described for the capacitor and IR flash detector data unit. The calculated bit contribution from this data unit is 3200 bits per orbit.

Velocity gage data unit. Velocity gage data is entered into memory on a scaled basis similar to the Mariner gage data. Scaling of the data is based on predicted impact rates for the instrument such that 48 data entries per orbit are required for micrometeoroid data reconstruction.


320-cps clock
Spacecraft time
Hit time read gate
0 R
1 S
Hit time hold register
Fixed frame ID
W1
d1
d7
Transfer gate
W2
d9
d15
Transfer gate
W3
d17
d23
Transfer gate
7
Transfer gate
W10
d79
d73
Transfer gate
W9
d71
d65
Transfer gate
W8
d63
d57
Capacitor level A hit counter (Instrument 2)(12)
T
Capacitor level A hit counter (Instrument 1)(12)
Capacitor level A
Instrument 1
Instrument 2
Instrument 3
+
Capacitor level A hit counter (3 instruments) (13)
d13
R 0
R1
S 1
To Mariner overflow counter
Write priority 1
320-cps clock

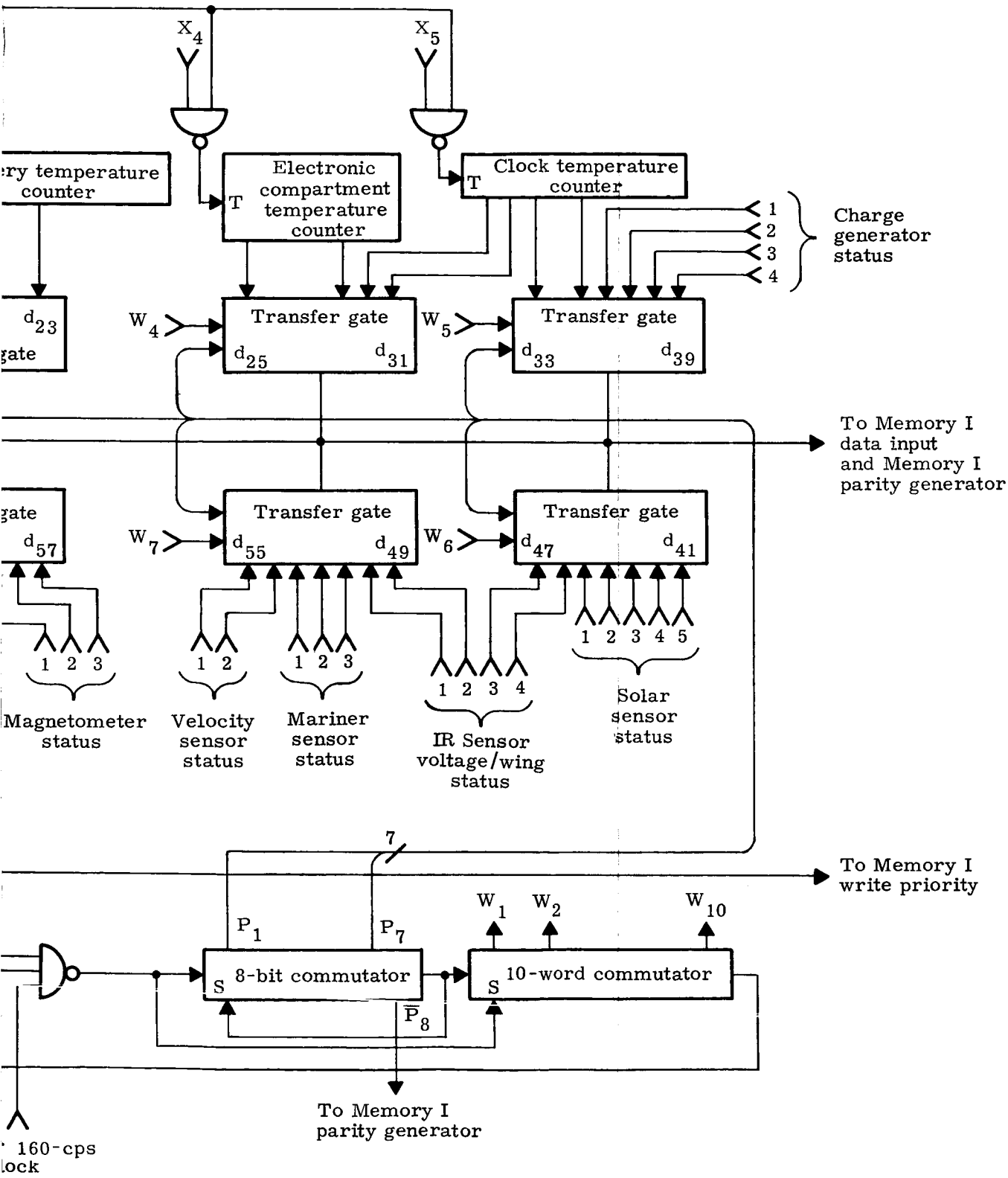
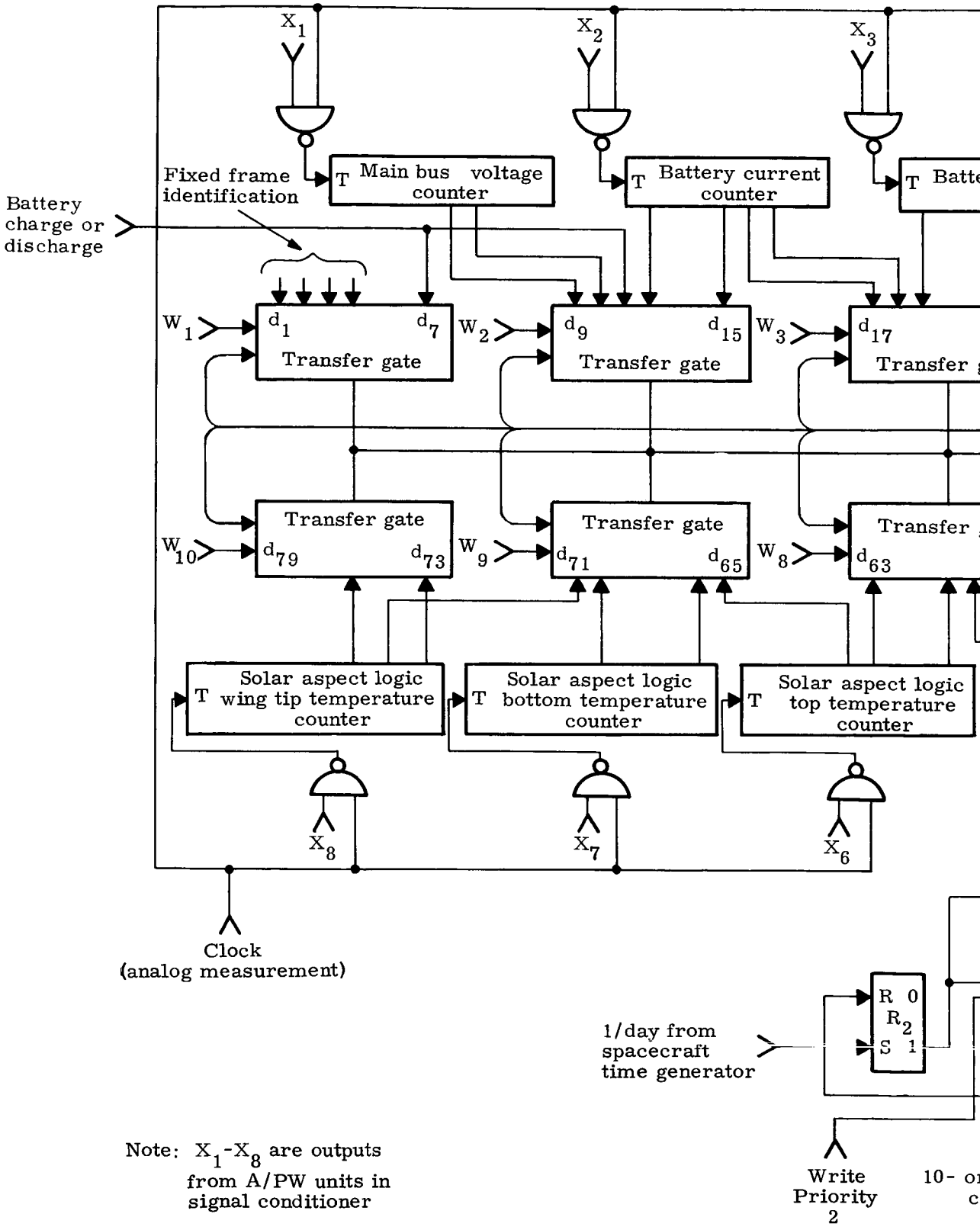


Fig. II-27. Critical Diagnostic Data Unit



Note: X_1-X_8 are outputs from A/PW units in signal conditioner

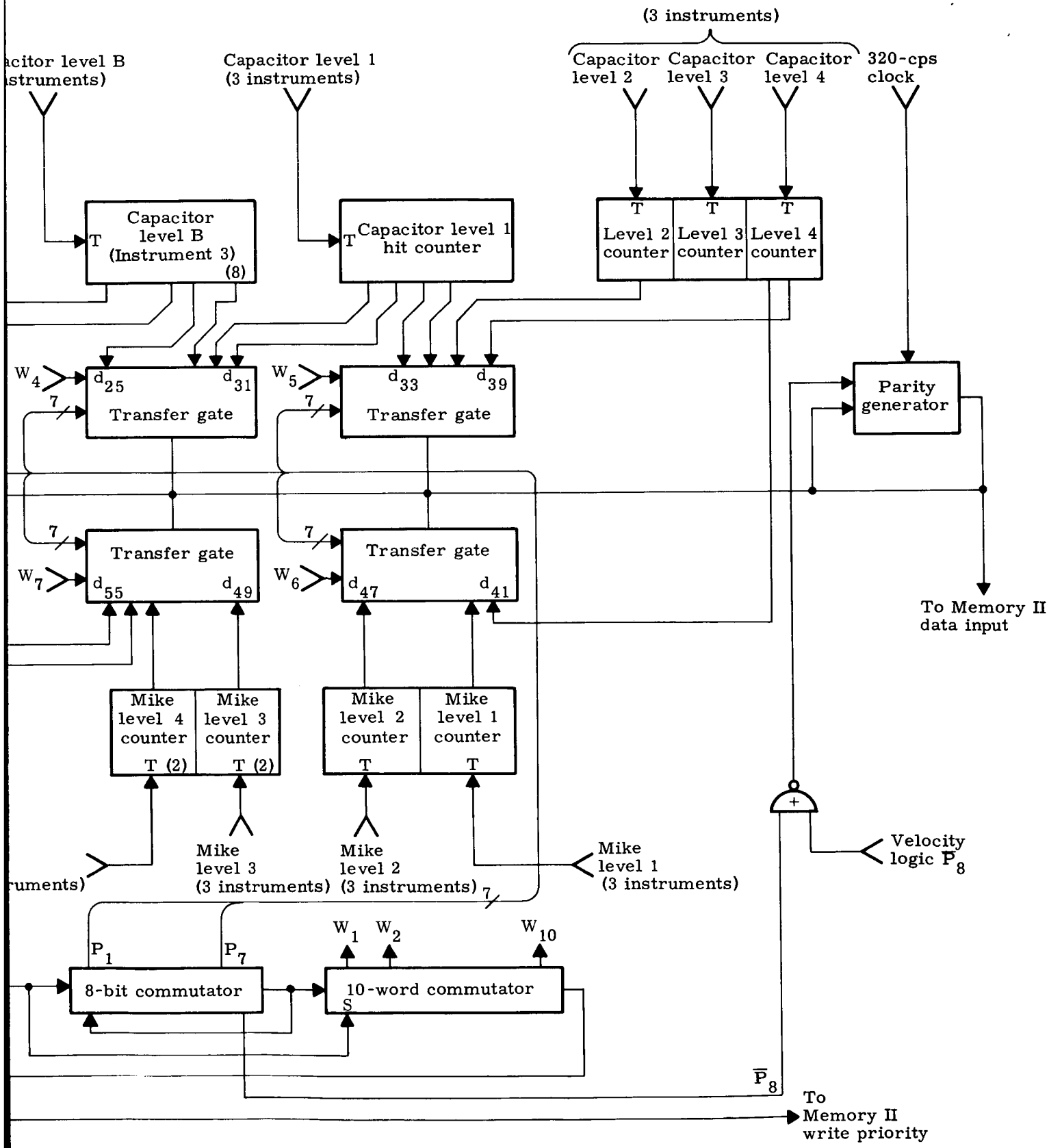


Fig. II-28. Mariner Gauge Data Unit

Impacts detected for all instrument capacitor levels are totaled in a common counter. Upon attainment of the scaled factor, the velocity gage data unit (Fig. II-29) organizes the following information into the velocity gage format: sensing tube identity, capacitor or microphone level initiating the data entry, time of impact, velocity of particle, and number of accumulated impacts on one instrument. The velocity gage data unit is responsible for supplying 3840 bits of data per orbit to Memory II. Data entry is a function of priority logic shared with the Mariner gage data unit which prevents simultaneous data entries into the memory. The manner in which the data format is stored is similar to the description of data recording as discussed previously.

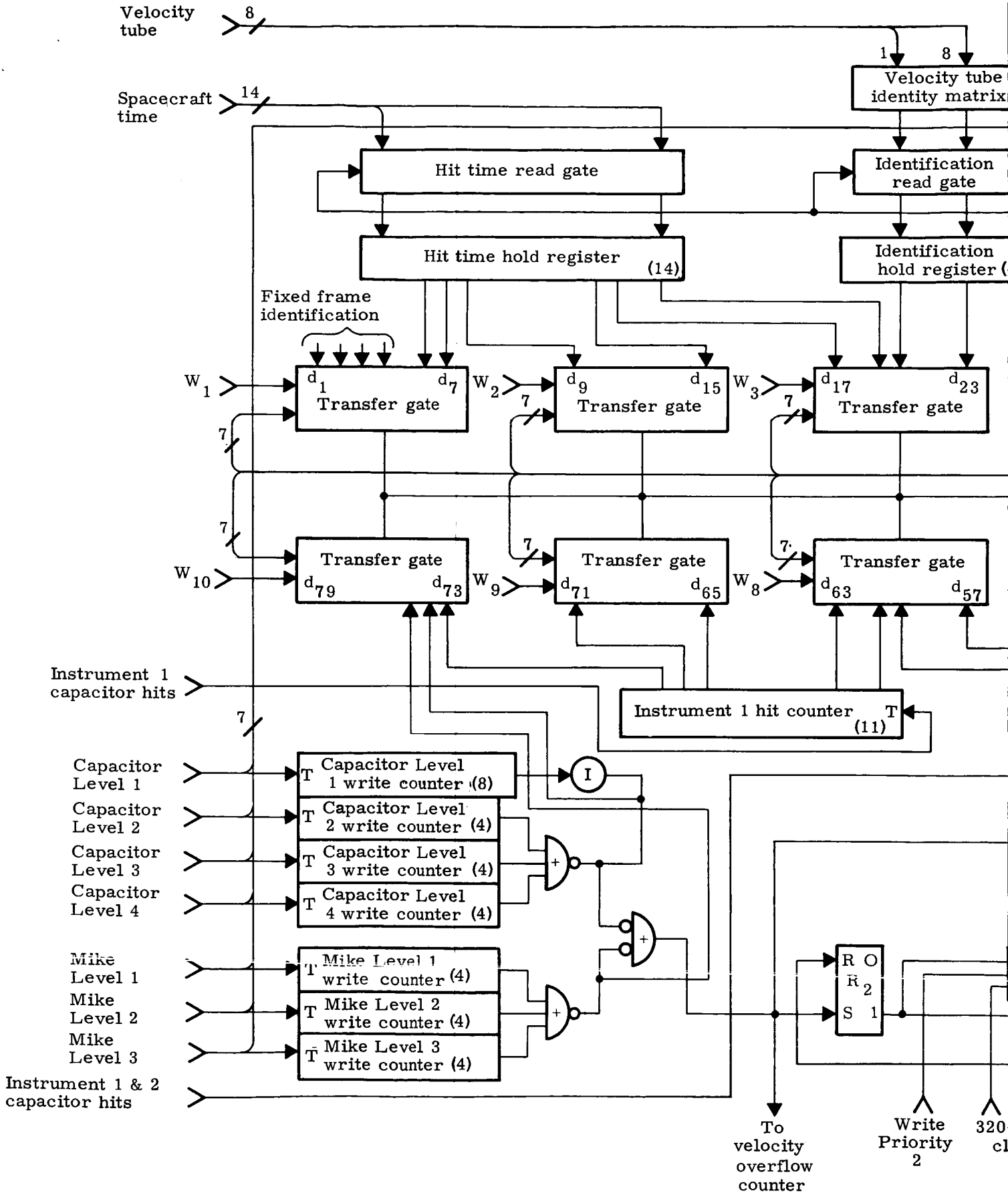
Full attitude data unit. The full attitude mode is initiated by receipt of a ground command when the returning spacecraft is at a point approximately 2. 5 hr from perigee. Magnetometer data and identification, solar aspect angles, earth sensor activation time, and spacecraft time are sampled and entered into memory every 2 min for a 5-hr period approximately centered on the perigee. Upon command, the full attitude mode terminates and, simultaneously, a Read Memory III Cycle is initiated. Completion of data readout enables data entry from the hourly attitude data unit.

Figure II-30 is the full attitude data unit block diagram, composed of the basic data unit adapted to the various data and control requirements.

Hourly attitude data unit. Figure II-31 is a block diagram of the hourly attitude data unit. Upon termination of the full attitude mode of operation, the hourly attitude mode is initiated. However, data is entered into memory every 2-hr, which permits efficient utilization of the 80-bit format since earth sensor identity, attitude time, solar sensor identity and solar angle data require only half a format. The first hour's data is stored in hold registers until the second hour, at which time the hold register data is entered into memory, along with sensor data taken in real time, thus filling out the format.

Data stored in memory is read out upon receipt of the next full attitude "on" command. Write priority is utilized to prevent initiation of a read cycle until completion of a write cycle.

Housekeeping and deployment data units. The housekeeping and deployment formats are real time formats and are not organized until the time at which a read cycle is initiated. Therefore, the manner in which these formats are generated will be discussed under the section on data readout. The block diagram of the deployment data unit is shown in Fig. II-32.


Velocity tube
8
Spacecraft time
14
1
8
Velocity tube identity matrix
Hit time read gate
Identification read gate
Hit time hold register (14)
Identification hold register
Fixed frame identification
W1
d1 d7 Transfer gate
W2
d9 d15 Transfer gate
W3
d17 d23 Transfer gate
7
Transfer gate
W10
d79 d73
W9
d71 d65
W8
d63 d57
Instrument 1 capacitor hits
Instrument 1 hit counter T (11)
Capacitor Level 1
Capacitor Level 2
Capacitor Level 3
Capacitor Level 4
T Capacitor Level 1 write counter (8)
T Capacitor Level 2 write counter (4)
T Capacitor Level 3 write counter (4)
T Capacitor Level 4 write counter (4)
I
+
Mike Level 1
Mike Level 2
Mike Level 3
T Mike Level 1 write counter (4)
T Mike Level 2 write counter (4)
T Mike Level 3 write counter (4)
Instrument 1 & 2 capacitor hits
R O
R 2
S 1
To velocity overflow counter
Write Priority 2
320

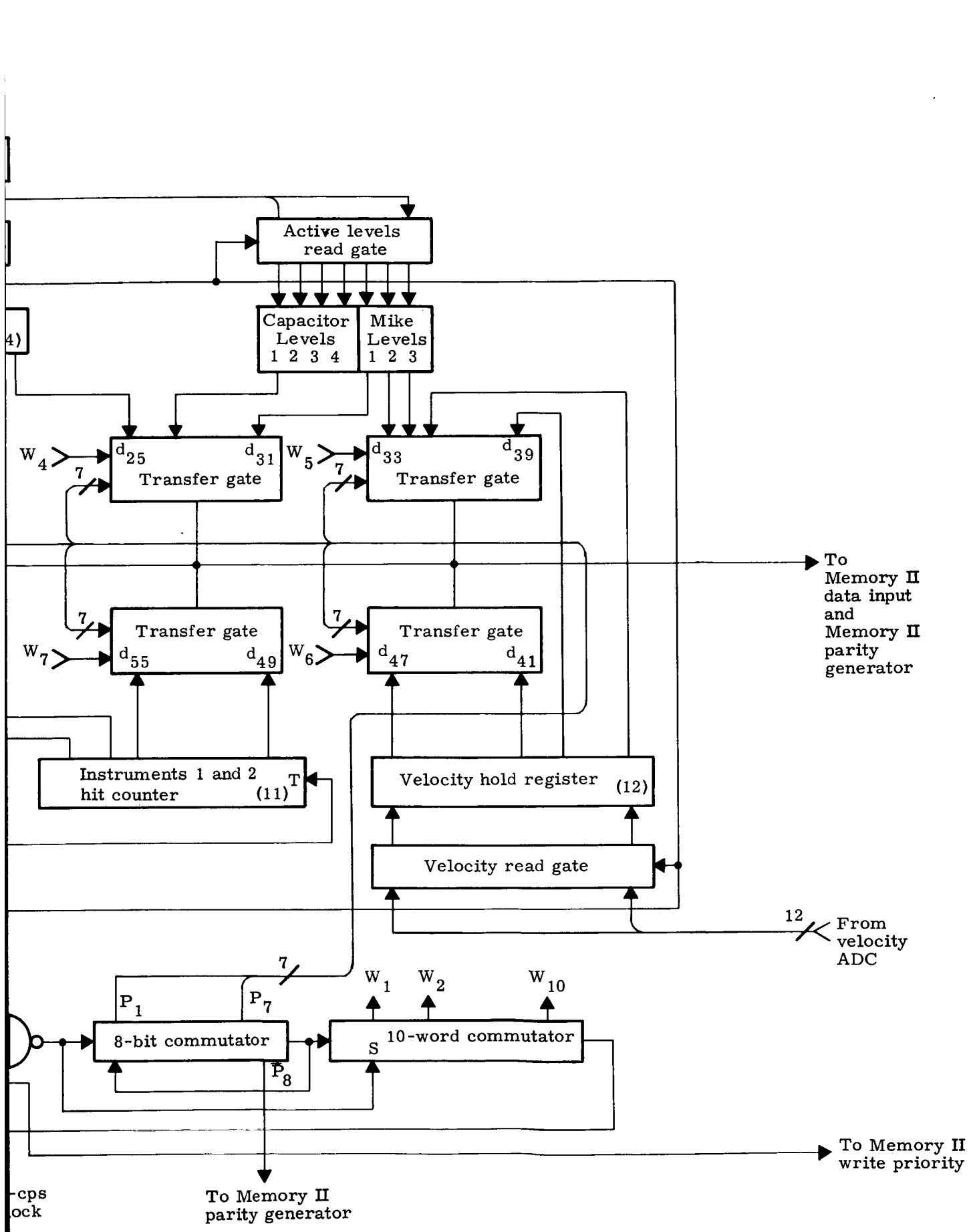
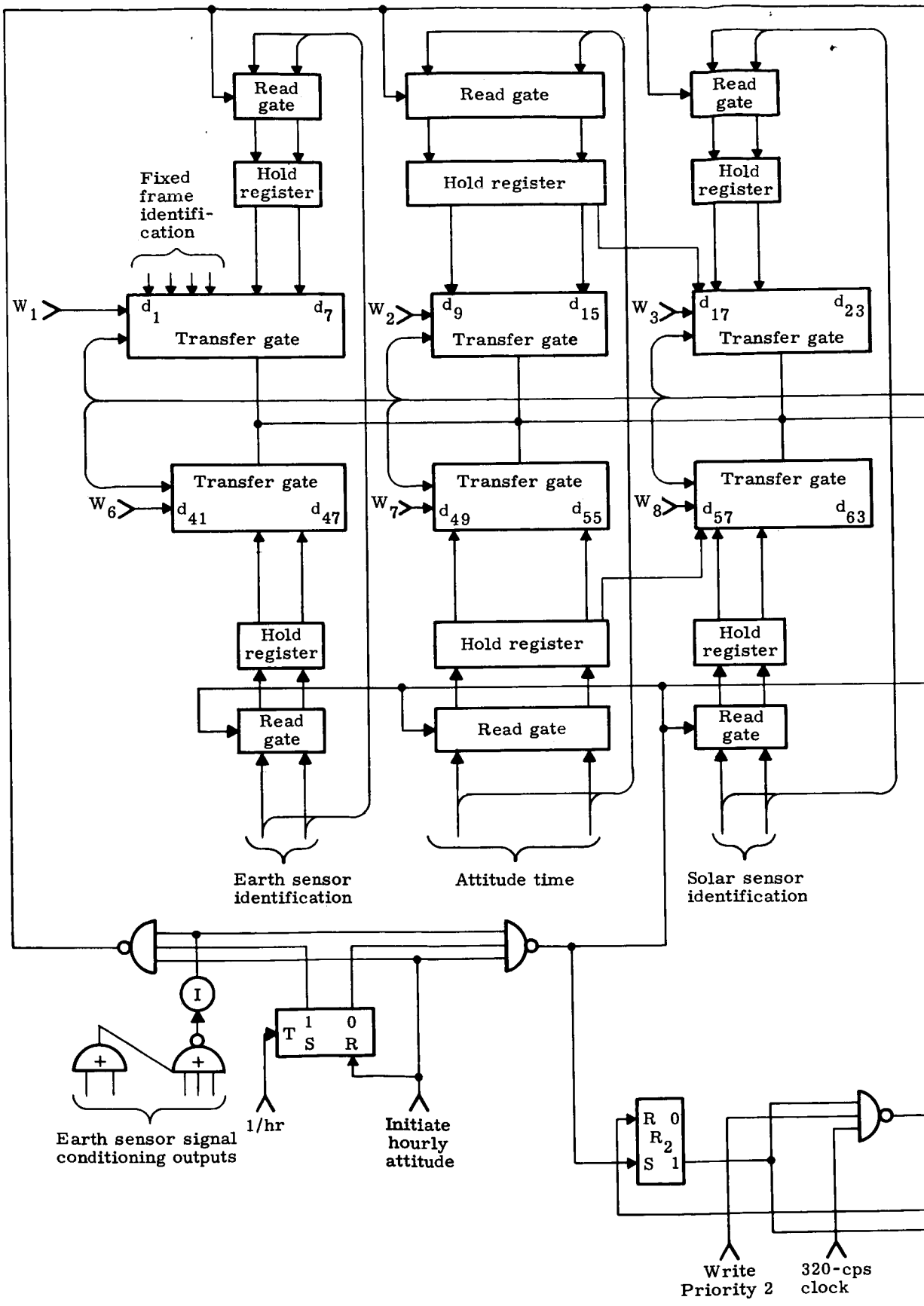


Fig. II-29. Velocity Gauge Data Unit

24


Read gate
Hold register
Fixed frame identification
W1
d1
d7
Transfer gate
W2
d9
d15
W3
d17
d23
W6
d41
d47
W7
d49
d55
W8
d57
d63
Earth sensor identification
Attitude time
Solar sensor identification
I
T
S
R
Earth sensor signal conditioning outputs
1/hr
Initiate hourly attitude
R2
Write Priority 2
320-cps clock

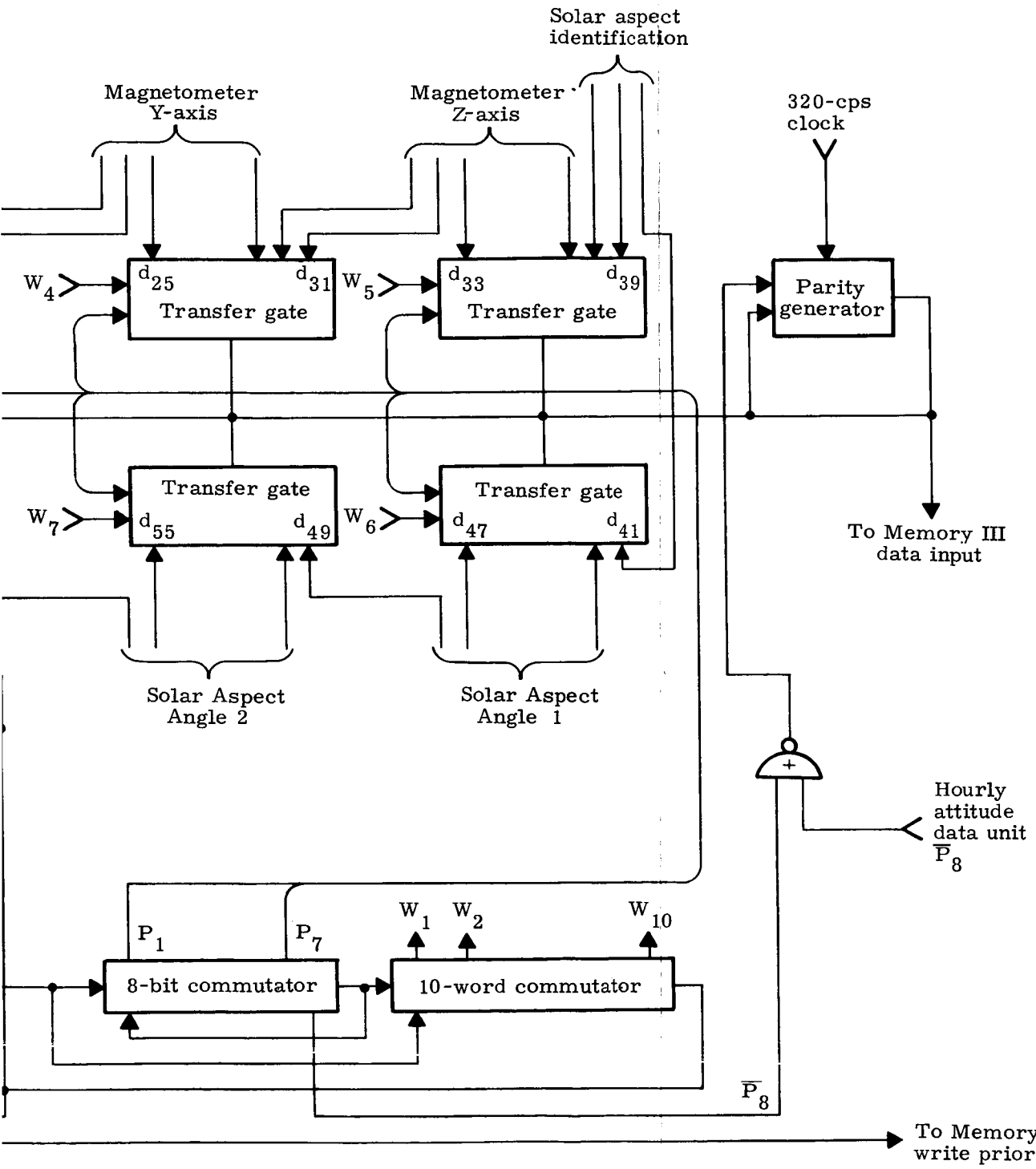
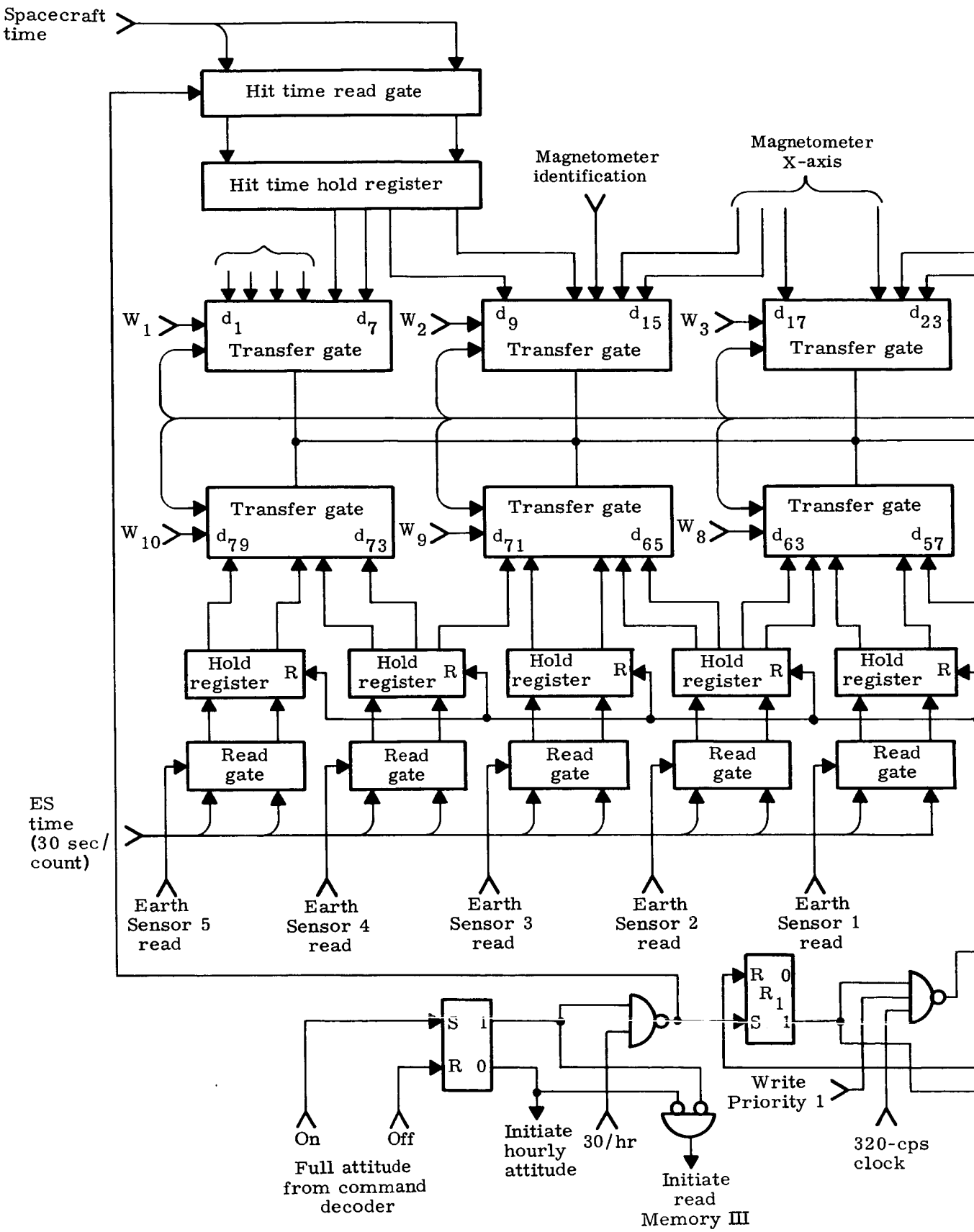


Fig. II-30. Full Attitude Data Unit


Spacecraft time
Hit time read gate
Hit time hold register
Magnetometer identification
Magnetometer X-axis
W1
d1
d7
Transfer gate
W2
d9
d15
Transfer gate
W3
d17
d23
Transfer gate
Transfer gate
W10
d79
d73
Transfer gate
W9
d71
d65
Transfer gate
W8
d63
d57
Hold register
R
Read gate
ES time (30 sec/ count)
Earth Sensor 5 read
Earth Sensor 4 read
Earth Sensor 3 read
Earth Sensor 2 read
Earth Sensor 1 read
S 1
R 0
R 0
R 1
S 1
Write Priority 1
On
Off
Full attitude from command decoder
Initiate hourly attitude
30/hr
Initiate read Memory III
320-cps clock

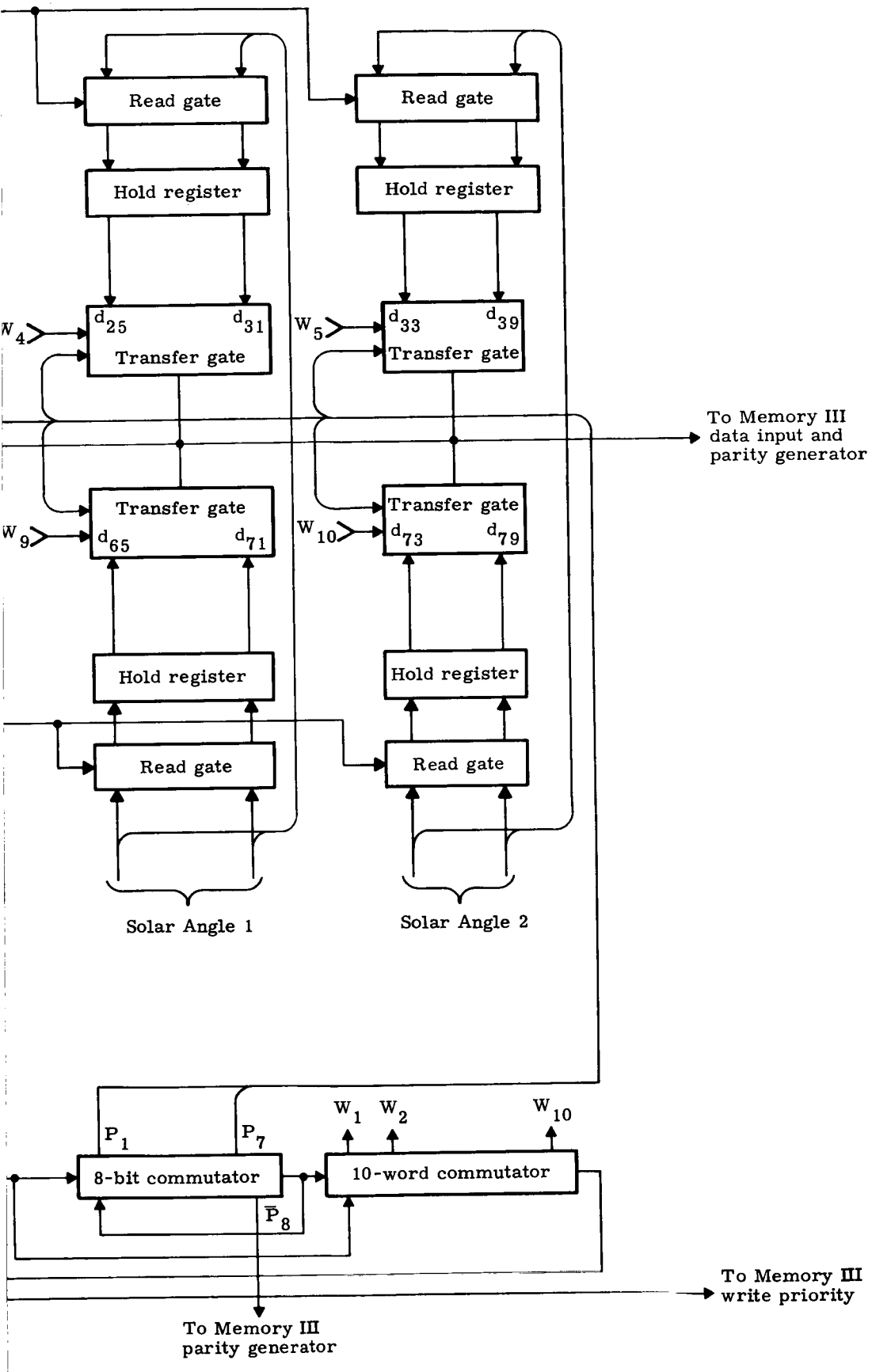
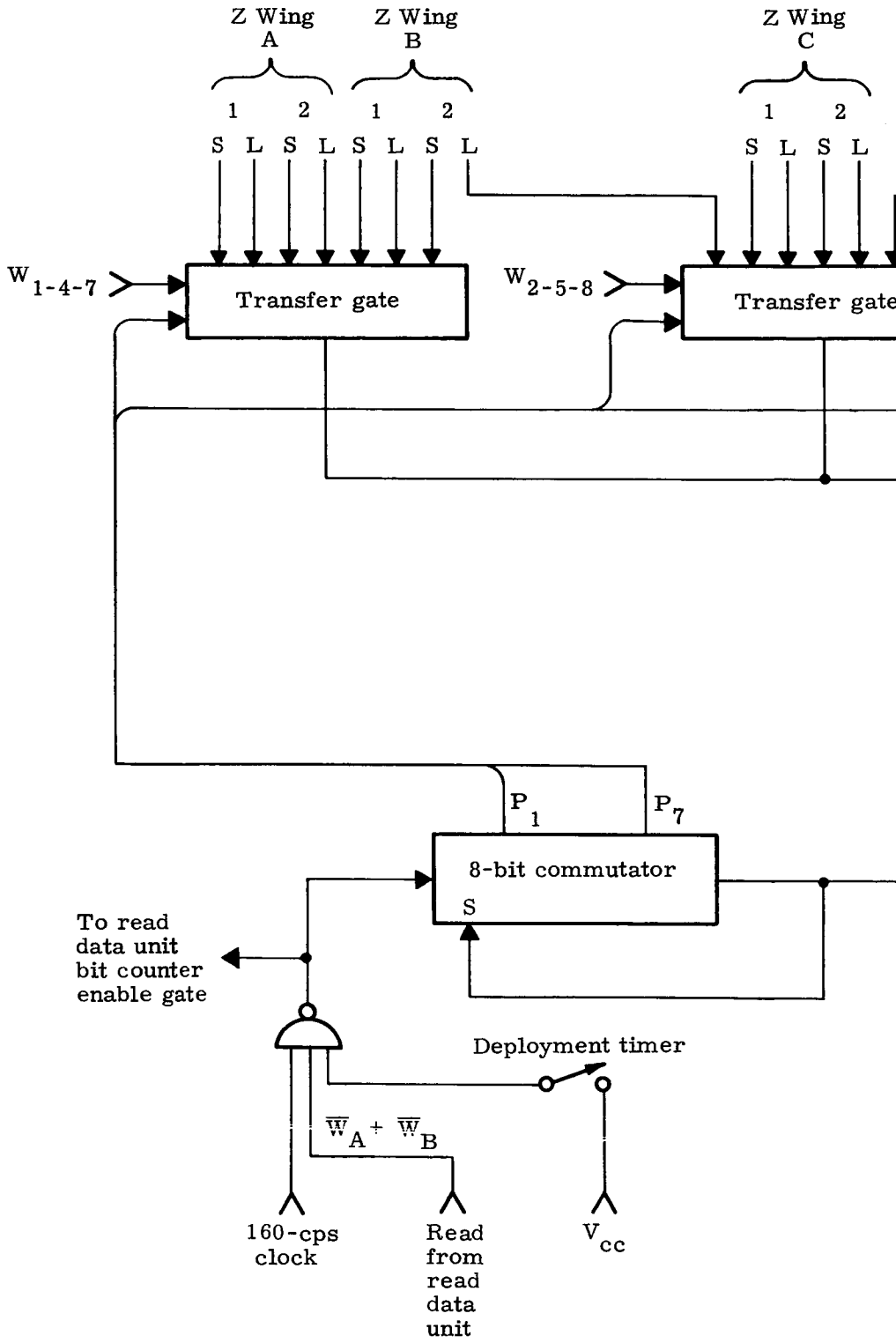


Fig. II-31. Hourly Attitude Data Unit


Z Wing A
Z Wing B
Z Wing C
1
2
S L S L S L S L
S L S L
W 1-4-7
W 2-5-8
Transfer gate
Transfer gate
P 1
P 7
8-bit commutator
S
To read data unit bit counter enable gate
Deployment timer
$\overline{W}_A + \overline{W}_B$
160-cps clock
Read from read data unit
V_{cc}

II-83

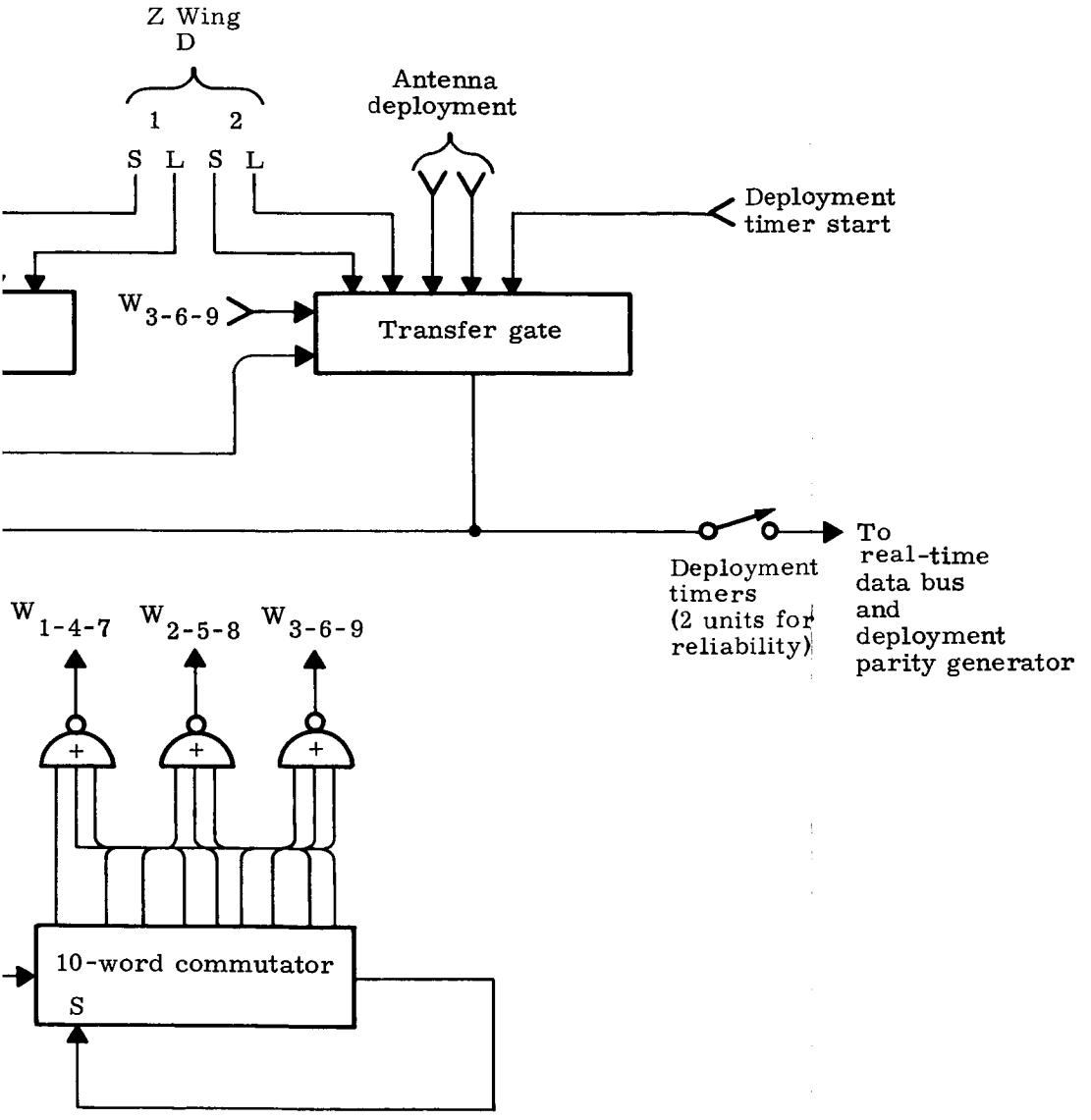


Fig. II-32. Deployment Data Unit

Memory overflow data unit. The memory overflow data unit (Fig. II-33) consists of two counters each for Memories I and II. When Memory I is full, a signal is generated indicating this condition. The inputs to the two counters for Memory I are then enabled and register the total accumulated capacitance panel and IR sensor impacts respectively above that registered in Memory I. Counters for Memory II are activated by Memory II in the same manner and register the total accumulated scaled hit counts for the velocity and Mariner gage sensors, respectively. The overflow counter format is not generated until a read cycle is initiated and will be discussed under the section on data readout.

(4) Data readout

Read data unit and sync frame generator. The function of the read data unit and sync frame generator (Fig. II-34) is to accept decoded read commands and, as a result, generate sync frames for each 80 bits of data, command the specified memory or data unit to readout in the proper sequence, and provide the commanded bit rate to the units being read out.

Operation of this unit is such that the received read command is stored and interrogates the specified memory to determine the write mode status. Should no write cycle exist or, upon completion of an existing write cycle, a sync frame (16 bits) is generated. Completion of the sync frame initiates the read cycle to the specified memory and enables a bit counter. The bit counter counts 80 bits, terminates the read cycle and initiates the sync frame. This cycle continues until the last address counter indicates two readout cycles have been completed, which terminates further read commands to that memory. As shown in Table II-5, each read command selects different data groups. Thus, the read data unit must select the proper units in the required sequence as the result of a specific command. This is accomplished by the last address counter which is preset to the required sequence upon command receipt and features feedback addition for decoding simplification. Upon termination of the last readout sequence, the unit is returned to its static condition.

Data switch. The input data selector shown in Fig. II-35 has the function of switching the Channel 2 transmitter input from the primary data bus to the secondary data bus on command, and may be simply defined as being a momentary, single-pole, double-throw switch. However, due to its system function, considerable effort must be expended to ensure maximum reliability and unwanted failure mode prevention.

The switching function described can be performed digitally by use of two quad NOR circuits having common outputs as shown in Fig. II-36. The basic quad configuration ensures maximum reliability, and control is accomplished by using a quad bistable element having automatic

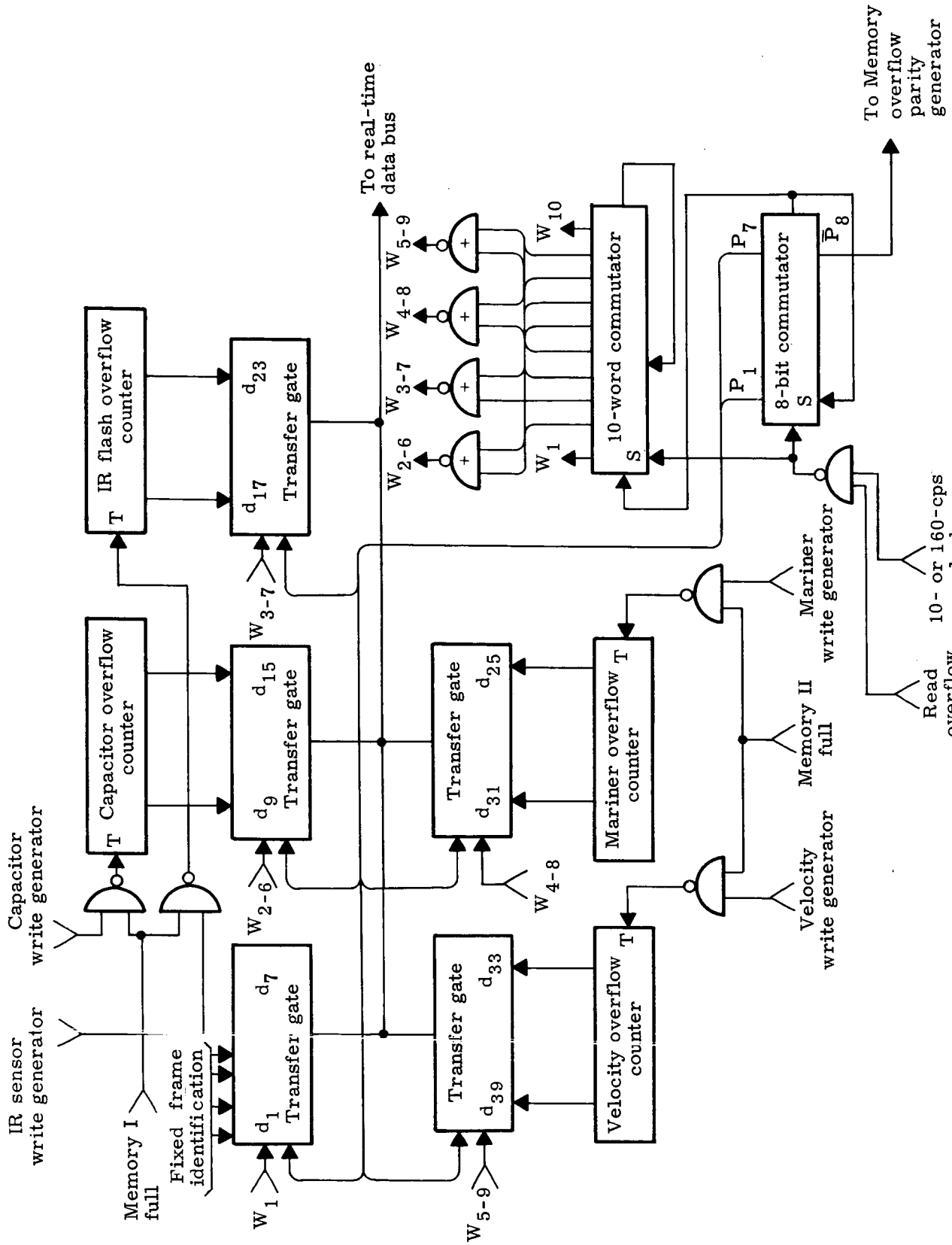
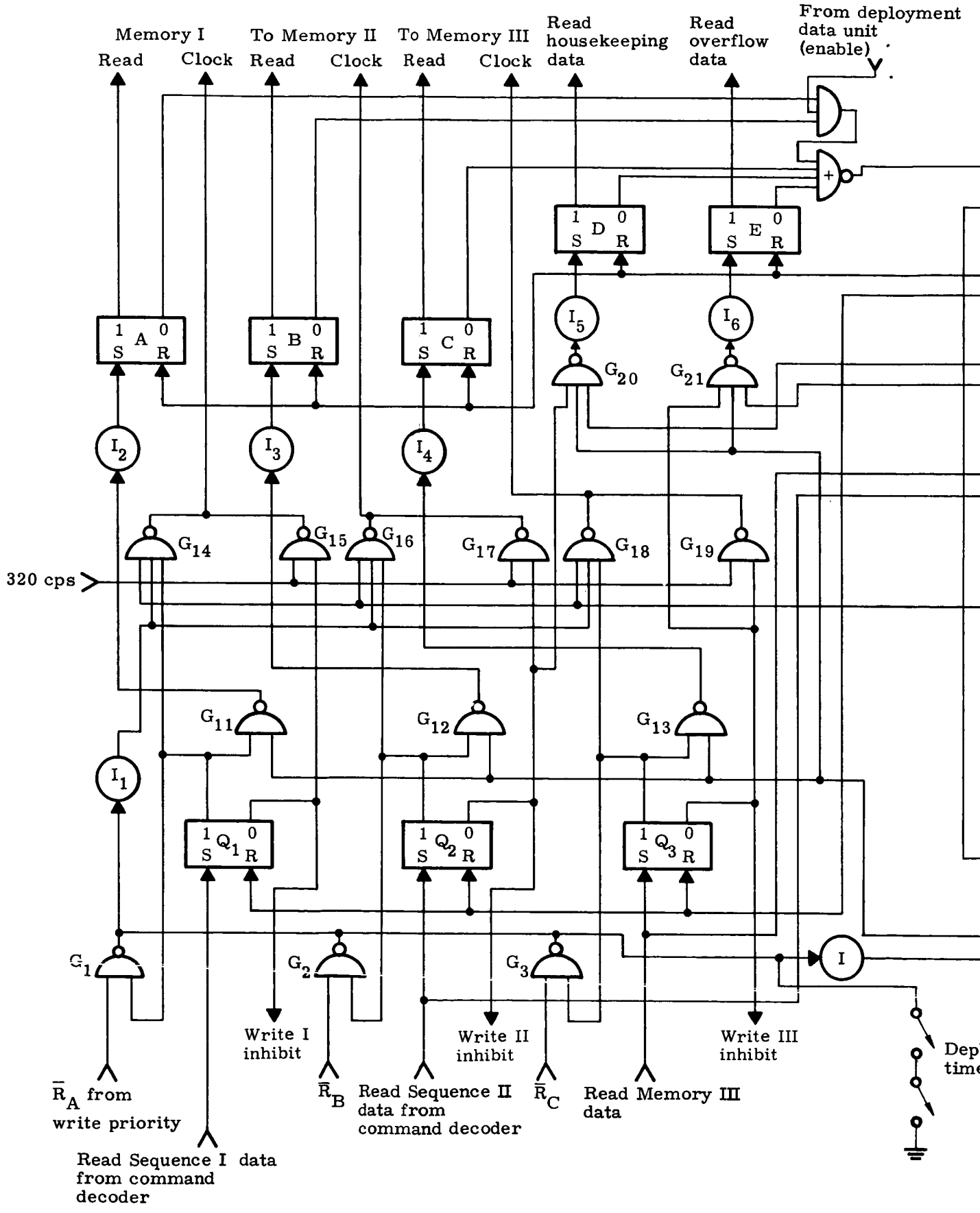
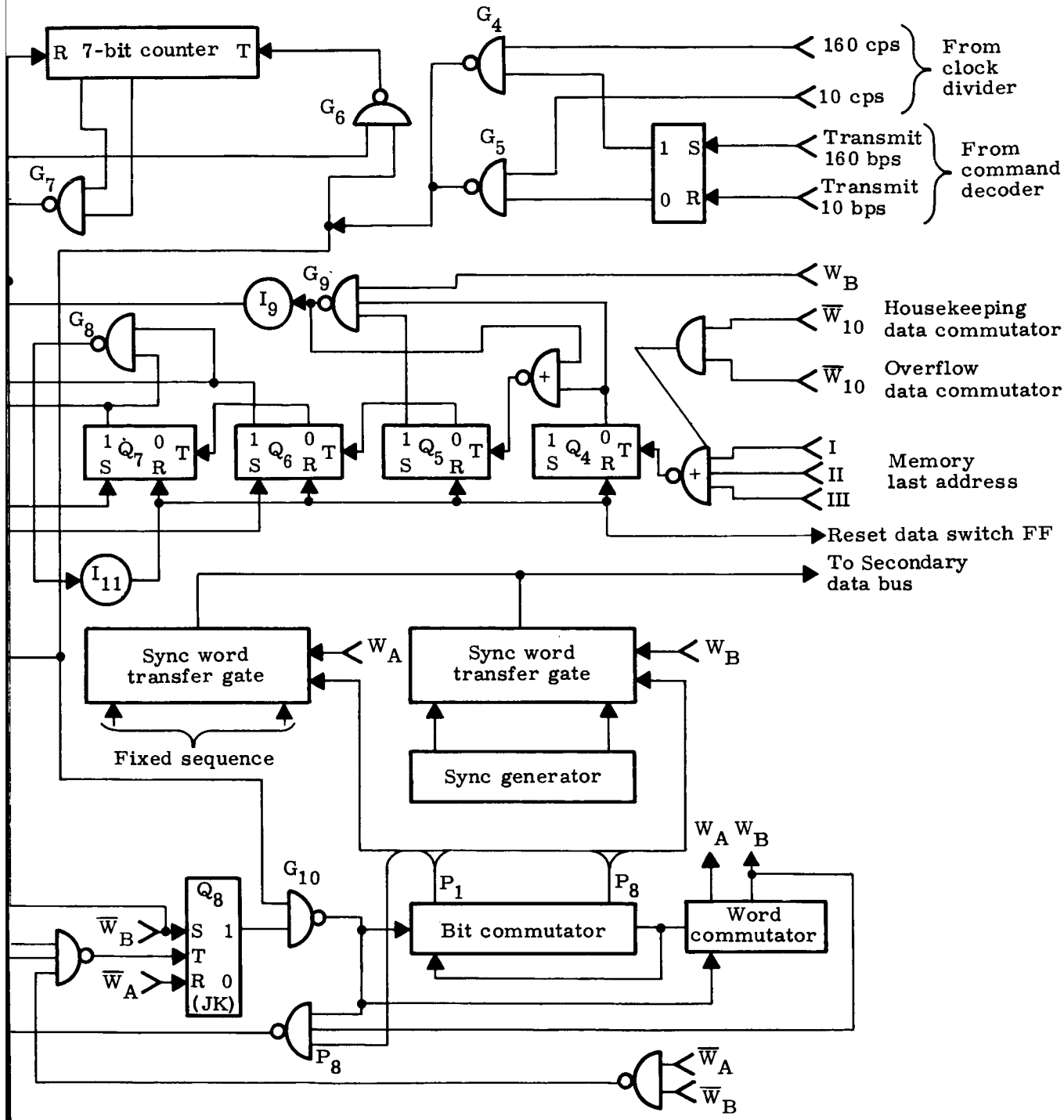


Fig. II-33. Memory Overflow Data Unit


Memory I
Read
Clock
To Memory II
Read
Clock
To Memory III
Read
Clock
Read housekeeping data
Read overflow data
From deployment data unit (enable)
1 S A 0 R
1 S B 0 R
1 S C 0 R
1 S D 0 R
1 S E 0 R
I1
I2
I3
I4
I5
I6
G1
G2
G3
G11
G12
G13
G14
G15
G16
G17
G18
G19
G20
G21
320 cps
1 S Q1 0 R
1 S Q2 0 R
1 S Q3 0 R
I
Write I inhibit
Write II inhibit
Write III inhibit
R̄A from write priority
Read Sequence I data from command decoder
R̄B
Read Sequence II data from command decoder
R̄C
Read Memory III data



oyment
r

Fig. II-34. Read Data Unit and Sync Frame Generator

0-II

II-86 2#

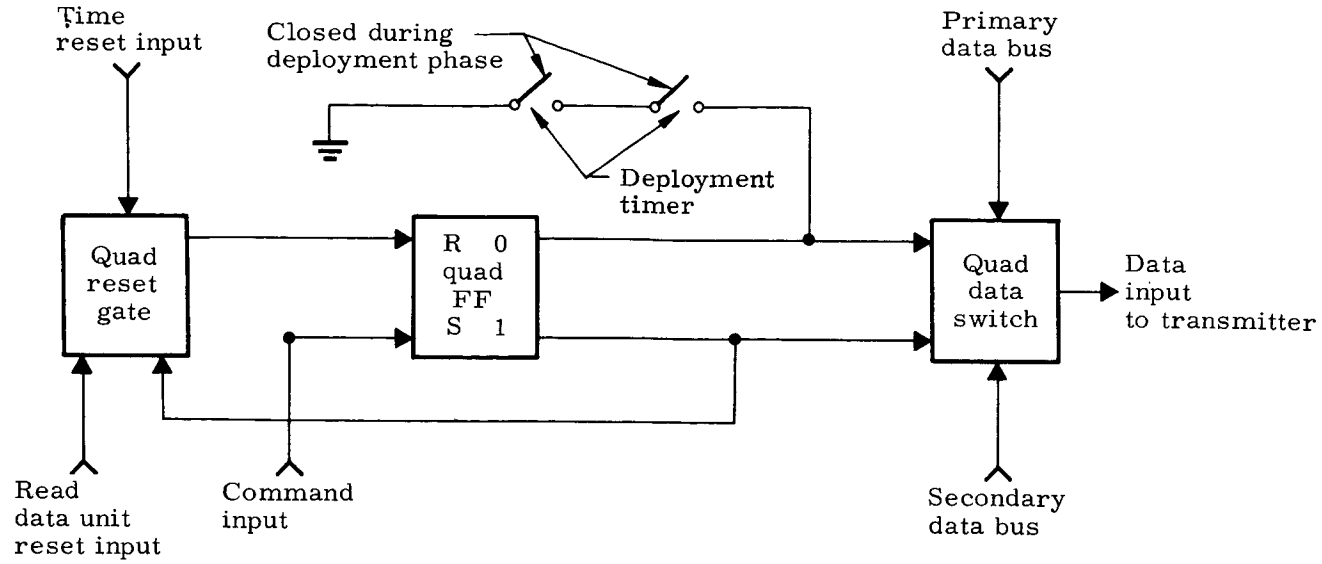


Fig. II-35. Input Data Selector

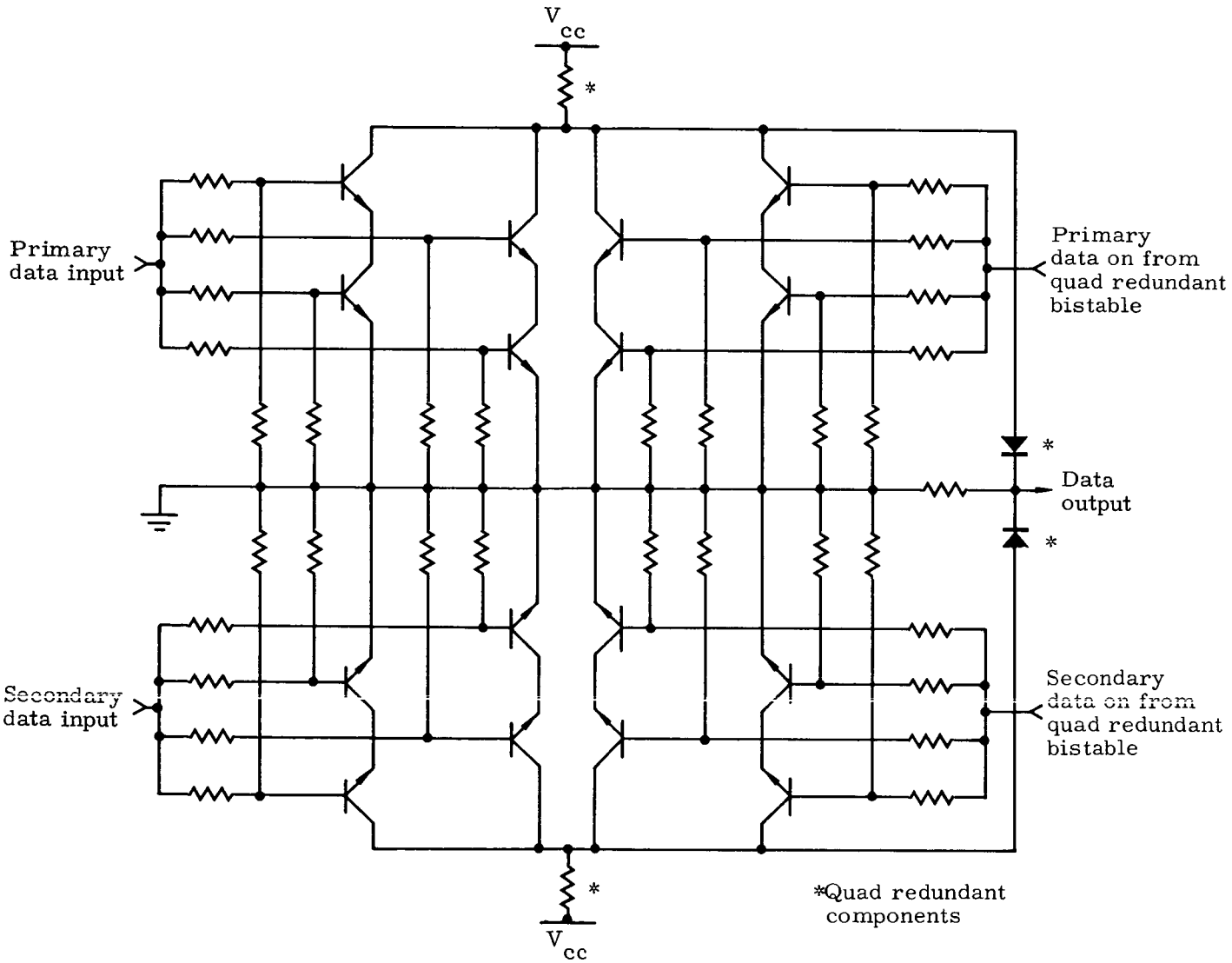


Fig. II-36. Data Switch

TABLE II-5

Time Required for Data Readout

	(bits)
Read Sequence I data	
Memory I data	960
Housekeeping data	640
Memory overflow data	80
Sync	336
Total	2,016
Data is read twice for each command	
Readout time at 10 bps = 6.72 min	
Readout time at 160 bps = 0.41 min	
Read Sequence II data	
Memory II data	7,040
Memory overflow data	80
Sync	1,424
Total	8,544
Data is read twice for each command	
Readout time at 10 bps = 28.5 min	
Readout time at 160 bps = 1.78 min	
Read Memory III data (generated on full attitude on or off command)	
Memory III data	12,000
Sync	2,400
Total	14,400
Readout twice at 10 bps = 48.0 min	
Readout twice at 160 bps = 3.00 min	

time function reset capability. Thus unwanted failure mode prevention is accomplished. Quad redundant circuits are an example of a technique which prevents a single failure from affecting the operation of the system. Although more components are required over conventional switching redundancy, no complicated failure detectors and sensing delays exist.

Storage capacity requirements. Table II-6 lists the bit contributions from each data unit for subsequent storage and the total bit requirement for each memory. Bit contributions are derived from the predicted particle influx for one complete orbit. Where predicted particle influx for a given equivalent mass exceeds practical storage

capacity, data scaling, as previously described is utilized which yields sufficient data to reconstruct the total particle density and be commensurate with practical storage capacities. Memory III capacity, however, is not established by the total bit contributions from the respective data units. To reduce the total storage requirement and, thus, increase reliability, Memory III is read out as a result of the full attitude mode being commanded on or off. This reduces the capacity to the maximum contribution from one unit or, as shown, the full attitude data unit.

Deployment data readout. Prior to launch, one deployment timer is turned on,* the data switch is switched to the secondary data bus, the Channel II transmitter is turned on, and the deployment timers activate the read data unit which generates a signal to start the sync generator. Upon termination of the sync frame, the 80-channel deployment commutator is activated and the deployment format as shown in Table II-1 along with a parity bit for each data word is generated. The sync-data cycle is then repeated for a predetermined time. When the deployment timers turn off, the deployment data unit is effectively disconnected from the system.

Sequence I data readout. The following sequential readouts comprise Sequence I: Memory I read two times, real time housekeeping data read two times, and memory overflow data read two times. When it is desired to transmit data, a ground command for transmitting at either 10 or 160 bps is initiated. The command is decoded by the onboard command decoder and the command logic generates a signal which is sent to the read data unit. At this time either 10 or 160 bps is placed on the clock bus in the read data unit, if it is not already there, and the data switch is switched to the secondary data bus.

If Sequence I is to be read out, it is necessary to initiate a ground command. Like the bit rate signal, a signal to read Sequence I arrives at the read data unit after the Sequence I command is decoded. Providing Memory I is not in the process of entering a capacitor and IR sensor format, or a critical diagnostic format into memory, the read data unit generates a signal which starts the sync generator. If Memory I is writing a format, the sync enable is delayed until the format has been written into memory. Once the Sequence I read cycle commences, Memory I is inhibited from recording information until after the Memory I read cycle terminates. At the same time, the sync enable pulse is generated, the clock bus of the read data unit is connected to Memory I clock input. The sync generator conveys a signal to the read data unit once the sync frame has been generated. This signal then enables the read input of Memory I. When 80 bits of data have been read from Memory I, the read input is disabled and another sync frame is generated. The cycle continues until Memory I

*A second deployment timer is activated at heat shield separation.

has been read out two times. At this time, a read enable for the real time housekeeping data is initiated. Memory I read input is disabled, the clock input of Memory I reverts to the write bit rate of 320 bps, and the write inhibit Memory I is disabled. It is now possible to write into Memory I while reading the remainder of Sequence I.

After the generation of a sync frame, the read enable for the real time housekeeping data is gated to the 80-channel real time housekeeping commutator. The real time housekeeping format shown in Table II-1 is now generated in the same manner as that described for the critical diagnostic format in the section on the description of the data processing. Eighty bits of real time housekeeping data are transmitted, interlaced with the sync frame until the real time housekeeping frames have been read out twice. Upon termination of the real time housekeeping cycle, the read signal for real time housekeeping data is disabled and a read enable for the overflow counters is initiated.

TABLE II-6

Storage Capacity Requirements

	(bits)
Memory I	
1-mil capacitor data	240
2-mil capacitor data	240
Critical diagnostic data	480
Total	960
Memory II	
Mariner gauge data	3200
Velocity gauge data	3840
Total	7040
Memory III	
either	
Full attitude data	12,000
or	or
Hourly attitude data	5,560

Once the sync frame has been generated, the read enable for the overflow counter is gated to the 80-channel overflow counter commutator and the overflow format, as shown in Table II-1, is generated. The overflow data, along with a parity bit for each data word, is transmitted, interlaced with a sync frame until it has been repeated twice. Upon termination of the overflow readout, all units are reset and the data switch reverts to the redundant primary subsystem data bus. Thus,

Sequence I readout is completed. The manner in which the overflow format is generated, and generation of the parity bit, are the same as those described for the capacitor and IR flash detector data unit.

Sequence II data readout. The following sequential readouts comprise Sequence II: read out Memory II twice and read out overflow data twice. Following the readout bit rate command, a command to read Sequence II is initiated. Once the command is decoded and arrives at the read data unit, the manner in which Sequence II readout is accomplished is similar to the description for Sequence I readout.

Memory III data readout. Following the readout bit rate command, Memory III can be read out by either of two commands, one command being "read out Memory III, turn off full attitude mode," while the second is "read out Memory III, turn on full attitude mode." One hour after liftoff, the hourly attitude programmer is turned on, and attitude data is collected every hour and entered into Memory III once every two hours as described under secondary data processing subsystem format organization.

If it is desired to read Memory III, it is imperative that the command to "read out Memory III, turn on full attitude mode" be initiated after the bit rate command has been sent. After decoding, the command signal arrives at the read data unit and the full attitude programmer, where an initiate read Memory III signal and an initiate full attitude write signal is generated respectively. If Memory III is not in the process of storing an hourly attitude format, the hourly attitude commutator is inhibited, the 10 or 160 bps bit rate is placed on Memory III clock input and the sync generator is activated. However, if an hourly attitude format is being written into Memory III when the initiate read Memory III signal arrives at the read data unit, the preceding sequence of events does not occur until after the format is entered in the memory. In either case, upon termination of the sync frame, the read input to Memory III is enabled and a frame of data is transmitted. The read input to Memory III is then disabled and the sync data cycle is repeated until the memory has been read out twice, at which time the full attitude commutator is enabled.

To read the full attitude data, it is imperative that the command to "read Memory III, turn off full attitude mode" be initiated following the bit rate command. Subsequently, Memory III is read out as described above and the hourly attitude commutator is then enabled.

Table II-5 is a tabulation of the number of bits contained in each data readout sequence and the time required for transmission at each bit rate.

d. Secondary measurement subsystem summary

The principal feature of the recommended secondary measurement system is its ability to gather a wealth of data in support of primary system mission objectives. A design plan has been established for a secondary satellite PCM telemeter in which six major subsystems are coordinated into one system in which the mission functions of each subsystem are independent of those from other subsystems.

Instrumentation is provided onboard the spacecraft to monitor experiments and spacecraft equipment status. Data collected by experiment and critical diagnostic measurements are stored in memory. A redundant real time readout capability is provided for all significant experiment and critical diagnostic data.

3. Communications

a. Telemetry

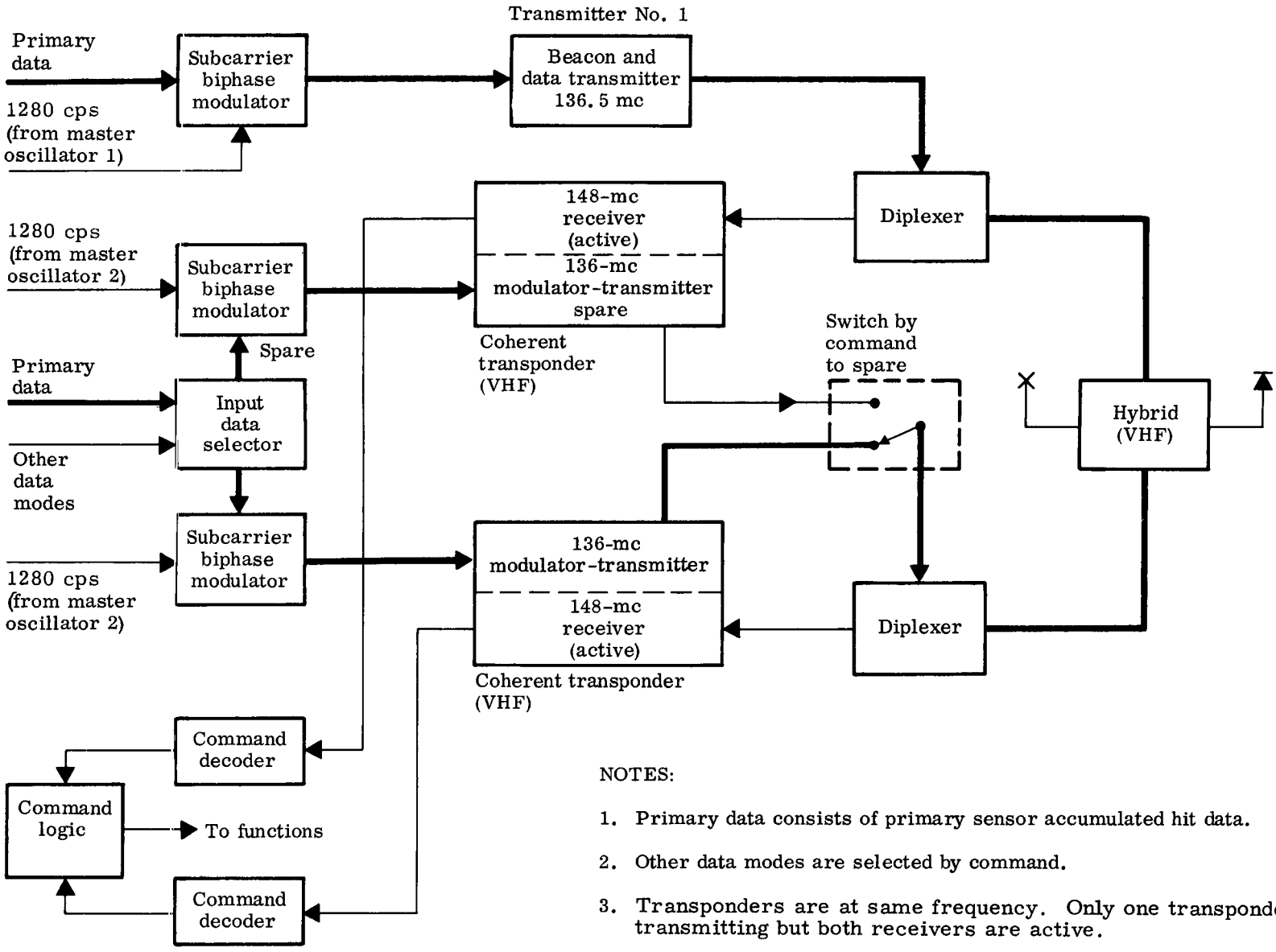
(1) Description of recommended systems

The recommended telemetry communications system (a VHF system for the 136-137-mc frequency band) consists of a pair of antennas, a hybrid, two diplexers, three 6-watt (RF) transmitters and three subcarrier modulators. Two of the transmitters (one is a spare for the other and they are tuned to the same frequency) are, in reality, the transmitter sections of the GSFC-developed VHF range and range rate transponders and are operated in either a telemetry or a range and range rate mode, depending upon command.

The other transmitter (Transmitter No. 1) is an independent unit for continuous transmission of primary hit count data (previously defined). A block diagram of the system is shown in Fig. II-37.

The active transmitters are isolated from each other by 20 db because of the hybrid arrangement. The diplexers provide 100 db of attenuation between transmitter and receiver inputs. For clarity in further describing the system, Transmitter No. 1 will be identified with communication Channel No. 1 and the other active transmitter (No. 2) will be identified with communications Channel No. 2.

Each of the active transmitters is phase modulated by a single biphase-modulated, 1280-cps, clock-derived subcarrier. Modulation of each transmitter by the associated subcarrier is at a modulation index of 1.6 rad (peak). The subcarriers are independently derived (two clocks) in keeping with the philosophy of maintaining isolation between Channels 1 and 2 equipment where possible.



NOTES:

1. Primary data consists of primary sensor accumulated hit data.
2. Other data modes are selected by command.
3. Transponders are at same frequency. Only one transponder is transmitting but both receivers are active.

Fig. II-37. Telemetry Transmission System: Spacecraft-to-Ground Data Flow

The Channel 1 bit rate is maintained at 10 bps, while the Channel 2 bit rate is selectable by command at either 10 or 160 bps for all telemetry data transmission modes execpt Pri II. It is to be noted that both 10 and 160 bps are submultiples of the 1280-cps subcarrier frequency and, further, that only one subcarrier per transmitter is used for the proposed coherent PSK system. A discussion of how to reconstruct a subcarrier phase reference for use in demonstration of the subcarrier data and the advantages of this system for this application are given in the following section.

Input data to the Channel 1 subcarrier modulator are PCM NRZC 7 bits per word without parity. Input data to the Channel 2 subcarrier modulator are PCM NRZC 7 bits, plus 1 parity bit per word. Parity is used for Channel 2, along with a single repeat of stored data playback transmissions, to improve the word error rate (Fig. II-37a), whereas a Channel 1 data frame is only four 7-bit words long and is repeated at such a rate (one frame every 2.8 sec) that parity is not needed on that channel. Use of parity on Channel 1 would actually decrease the reliability of the primary data system in this case. Biphase modulation of the 1280-cps subcarriers can be accomplished simply by providing a phase inverter and flip-flop to select either the initial clock derived subcarrier phase or the inverted phase, depending upon whether a "1" or "0" is to be transmitted.

Both channel transmitters operate continuously when the spacecraft is in sunlight. The Channel 1 transmitter is powered solely by solar energy and is silent when the spacecraft is in darkness. The Channel 2 transmitter power, as an option, may be designed to be commanded off when operation of the transmitter is not required.

Priority of frequency assignment for the transmitters must go to the transponders because of the wide bandwidth required and the fixed receive-transmit frequency ratio. The Channel 1 data transmitter frequency and modulation sidebands should then be assigned to fall between the Channel 2 upper telemetry subcarrier sideband modulation and the upper RRR 807-5KC side band modulation. Both transponders should operate at the same transmitter frequency, but not simultaneously. Interchange of active and spare transmitters by command sequence entails turning off power to the active transmitter section (the local oscillator for the receiver section remains active), switching transmitter output connections to the diplexer by means of a sealed coaxial switch, and applying power to the transmitter section of the other transponder.

Characteristics of the transponder are shown in Table II-9 and are further discussed under tracking.

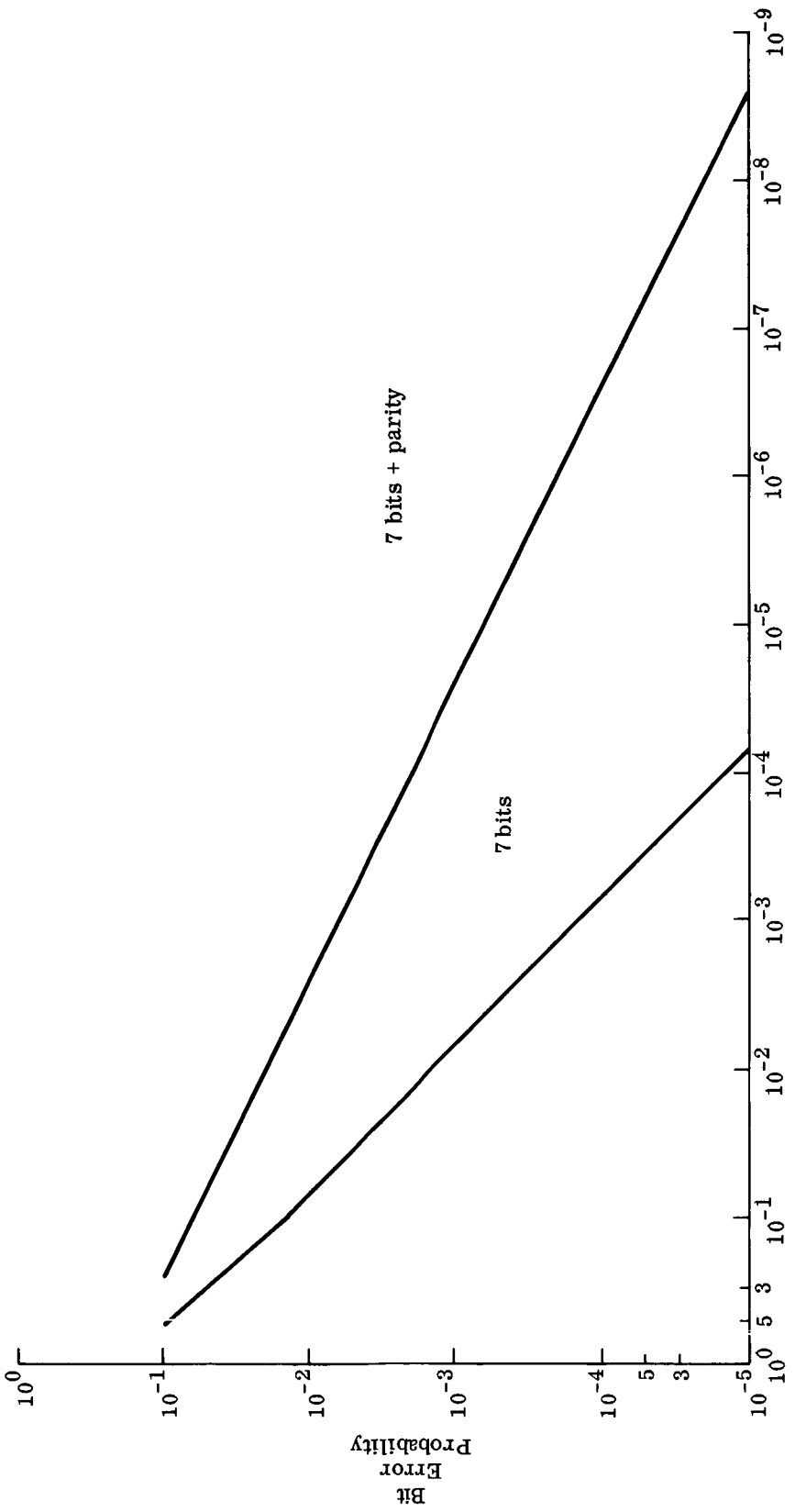


Fig. II-37a. Word Error Probability Versus Bit Error Probability

The transmitter for Channel 1 can be of the same design as the transmitter section of the transponder.

A discussion of transmitter power output, bit rates, transmission ranges, word error rates and tradeoffs follows.

(2) Telemetry tradeoffs

Communications aspects of the telemetry system discussed in this section are related to the number of communications channels required, the type of modulation and encoding to employ, data transmission rates, the radio frequency band to be used, and integration of telemetry with other communications functions.

It was apparent that advantages in size, weight, power and overall complexity of the communications system could be gained by integrating the communication system functions, where possible (common antennas, components serving dual functions, etc.). The integrated system concept, with its apparent inherent advantages, was adopted as a baseline concept which one could expand or from which one could depart and make tradeoff comparisons.

Number of RF channels. Initial thoughts on the subject suggested a single RF telemetry channel that would be silent during most of the orbit and would be commanded near earth to play back the stored data. It soon became apparent, however, that to meet the specified reliability performance of the communication system, a dual RF channel telemetry system was required as well as transmission of data from near apogee. To go beyond two RF channels, one begins to run into size, weight and antenna problems in the spacecraft and add complexity to ground station receiving and recording systems. As a result, more than two RF telemetry channels were never seriously considered.

Various combinations of continuous transmissions of data on Channel 1 and commanded transmission of data on Channel 1 were considered as shown in Volume IV and Table II-7. The second RF channel, in all combinations of data transmission modes considered, was controlled by command from ground stations.

Initially, transmission of data from apogee was not considered necessary, since it appeared that data could be stored and played back at shorter ranges. Reliability studies, however, showed the more

reliable system to be one in which selected data (cumulative hit count) is continuously transmitted on a high reliability channel and monitored on an intermittent schedule by the ground stations; hence, the requirement for transmission ranges to apogee.

Data modulation and coding. Selection of a modulation and coding approach for the cislunar micrometeoroid mission is based mainly on modulation efficiency (minimum power), data accuracy (resolution), and compatibility with the NASA ground networks. These criteria, in combination with the discrete nature of a large bulk of the scientific data, lead logically to techniques compatible with digital coding.

In this connection, it is well known that coherent 180°, biphase modulation (PSK) is superior to all other binary coded modulation schemes from an efficiency point of view; i. e., coherent PSK provides the lowest bit error rate for a given energy per bit to noise power spectral density ratio, E/N_0. This is illustrated in Fig. 3-1 (Appendix II-3) for a number of binary coded modulation techniques.

Not shown are comparisons between binary, M'ary, and error corrective coding systems. These are discussed in Appendix II-3 in some detail, and are reviewed briefly as follows: Coherent M'ary (biorthogonal or orthogonal) systems for the proposed data resolution (7 bits) and word error rates (10^{-4}) can provide a potential advantage over coherent PSK of between 3 and 4 db. The amount of additional onboard equipment required to convert binary coded to orthogonal or biorthogonal coded data is not particularly significant, but a large degree of complexity is required at the ground stations to provide real time demodulation. This must, for example, provide the equivalent of 128 cross correlations of stored reference words with each received data word, the greatest outcome of these processes being the decision criteria used to select the most probable data word (maximum likelihood detection).

Similarly, a noncoherent M'ary system such as multilevel FSK, offers a comparable improvement over binary FSK; it is therefore competitive with coherent binary PSK from a modulation efficiency viewpoint. Again, 7-bit resolution requires the generation of 128 orthogonal signals (in this case, frequencies, one for each possible data word), as well as a set of 128 matched filters followed by a maximum likelihood decision process just as in coherent orthogonal processing.

TABLE II-7

Study Configurations

PRIMARY DATA T/M SYSTEM

Configuration	RF Channels	Command	Range and Range Rate	Transmitter Range	Main Storage	Scientific Data	Bits of Storage	Housekeeping Data	Data Transmission Programmed	RF Carrier As Beacon and Angles + Minitrack
A_0	1	--	--	Apogee	--	Primary hit count	--		Cont	X
A_1	Completely redundant system for A_0									
B_0	1	--	X*	Apogee	--	Hit count and area*	--		Cont	Backup *
C_0	1	Backup only*	X	Apogee	--	Hit count and area*	--	For command backup*	Cont	Backup
D_0	(2 SCO) 1*	Backup only*	X	Apogee	--	Hit count and area*	--	For command backup*	Cont	Backup
E_0	1	--*	--*	100,000 naut mi*	X*	Hit count and area*	7000*	--*	Timer*	X*
E_1	1	--	--	Apogee*	X	Hit count and area*	7000*	--	Timer	X
E_2	1	--	X*	100,000 naut mi*	X	Hit count and area*	7000*	--	Timer	Backup*
E_3	1	--	X	Apogee*	X	Hit count and area*	7000*	--	Timer	Backup
E_4	1	Backup only*	X	100,000 naut mi*	X	Hit count and area*	7000*	For command backup*	Timer or command	Backup
E_5	1	Backup only*	--	100,000 naut mi*	X	Hit count and area*	7000*	For command backup*	Timer or command	X

*Change from one above.

Error correction coding is discussed briefly in Appendix II-3, and is concluded to offer no significant reduction in RF power unless the information rate is reduced. In addition, this approach represents a very significant increase in terminal equipment complexity over PSK.

Additional ground demodulation equipment complexity is considered a sufficient basis for rejection of error correction and orthogonal coding techniques. On the other hand, since coherent binary PSK is easily implemented and is largely compatible with ground station demodulation equipment, it is selected for this application for both communications channels, along with use of one odd parity bit per word on Channel 2. Appendix II-4 discusses parity and word error rates.

Since a coherent reference carrier is required at the receiving terminal for data demodulation, and since direct carrier PSK leaves no carrier component for receiver tracking, use of a 180° biphase modulated subcarrier is recommended. It is, of course, possible to use less than 180° biphase modulation to provide the necessary carrier component, but the difficulty here is that the data sidebands extending to zero frequency can be expected to degrade tracking loop performance This problem can, in certain instances, be resolved by adding the NRZ data bit stream to the bit rate clock signal prior to modulation. This essentially results in the use of the clock frequency as a subcarrier. In the present application, however, the low bit rate does not provide sufficient separation of the carrier and the subcarrier and, consequently, the separate subcarrier is recommended. The data is biphase modulated on the subcarrier and the subcarrier, in turn, phase modulates the carrier with a modulation index selected to provide sufficient carrier component for recovery in the ground receiver phase-locked loop.

Necessity for a coherent reference to demodulate the data still exists, but the problem now resides at the subcarrier instead of the carrier frequency. Fortunately, adequate solutions to this problem are available. One used in DSIF compatible lunar and planetary communications uses a second subcarrier, harmonically related to the data subcarrier. This is recovered in a narrow band ground subcarrier tracking loop and is converted to the data subcarrier frequency for the coherent demodulation references. While this requires a relatively low power level, the additional subcarrier does result in a reduction in data modulation efficiency due to the generation of unusable cross products. While this approach is an acceptable one, our recommendations avoid this second subcarrier and the attendant modu·

lation loss by deriving the reference subcarrier directly from the received 180° biphase modulated subcarrier. This is being investigated, both analytically and experimentally, at the Martin Company and is described briefly in terms of the functions illustrated in Fig. II-38 as follows (also see Refs. II-7 and II-8). The 180° biphase modulated subcarrier at the output of the receiver coherent carrier demodulator and subcarrier filter is applied to a nonlinear diode pair which functions essentially as a square-law full wave rectifier. The double frequency component is extracted in the bandpass limiter and supplies the input signal to the double frequency subcarrier tracking loop. Subsequent frequency division by a factor of two provides a coherent subcarrier for demodulation of the original biphase modulated subcarrier. A complete loop, including data modulation simulation, has been designed and fabricated, and is currently undergoing noise performance tests (a Martin-funded investigation). Final quantitative performance data (experimental) are not yet available, but initial tests show, as expected, that at the E/N_0 ratios required to give acceptable bit error probabilities, the residual phase error on the recovered subcarrier is not significant. Circuit functions required for the implementation of Fig. II-38 are quite straightforward and can be realized in a number of essentially equivalent ways.

Waveforms at selected points in the test breadboards are shown in Fig. II-39.

Bit synchronization can be derived directly from the demodulated data stream appearing at the output of the subcarrier phase demodulator of Fig. II-38 by standard techniques. It is notable, however, that since the data subcarrier and the data rate are related by fixed ratios, a synchronous bit rate can be derived directly from the recovered subcarrier signal by using the same countdown ratio as in the spacecraft. When properly phased, this provides essentially a jitter free rate for matched filter detection of the demodulated data bit stream and for other synchronization functions. The bit rate signal so derived, however, will not have its phase transitions aligned with those of the data since, with as much as 160 subcarrier cycles per bit, there are 160 possible phase relationships between the actual and derived bit transitions.

As previously noted, there are any number of ways for accomplishing this alignment. Our recommended approach utilizes a voltage-controlled oscillator at the same nominal frequency as that of the subcarrier. This is divided to the bit rate frequency and generates an early-late gate to stroke the filtered and processed data stream. The error signal output of the early-late gate tracker is used in a second-order loop to control the VCO for bit transition acquisition and lock-on. When the error signal falls below a preset threshold, the counter is

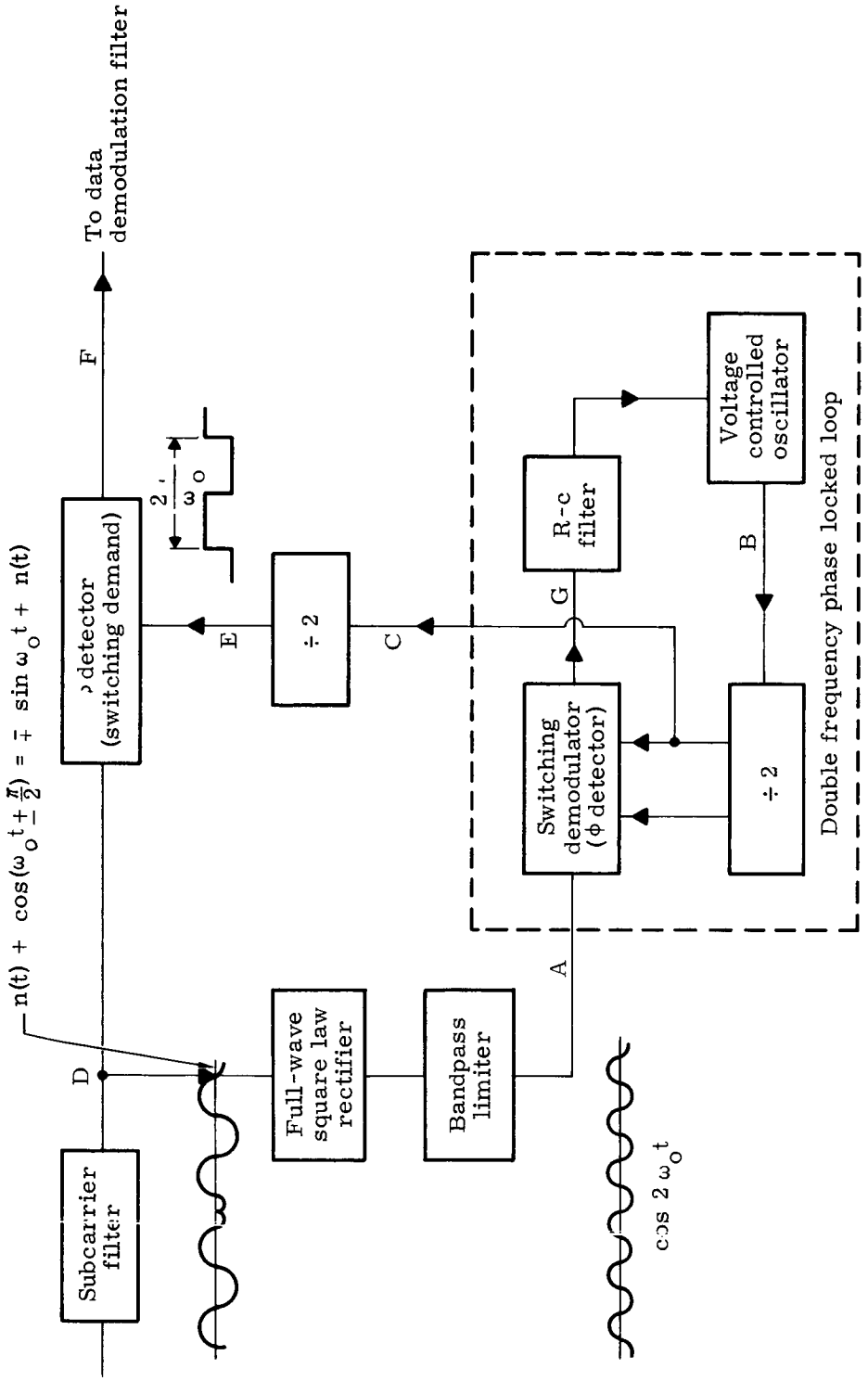
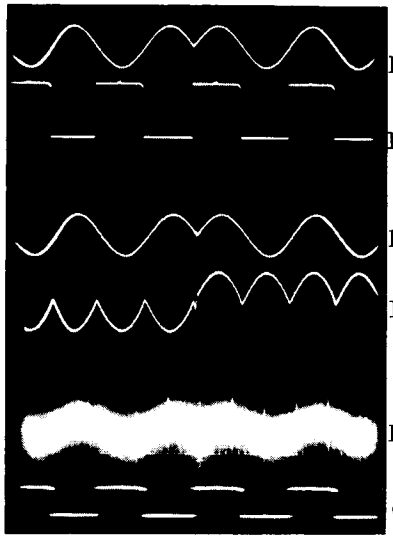


Fig. II-38. Reference Subcarrier Recovery Process

See
Fig. II-36
Reference
Point



D Noise-free biphase modulated signal

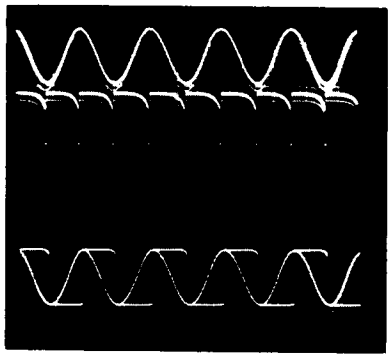
E Extracted square wave reference subcarrier (ω_0)

D Noise-free biphase modulated signal

F Demodulated signal

D Noisy biphase modulation

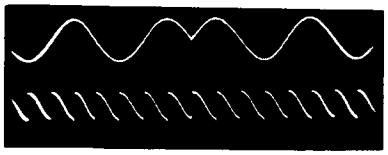
C Extracted square wave subcarrier (2 ω_0) (time exposure)



A Output of bandpass limiter

B VCO pulse output (4 ω_0)

Superimposed bandpass limiter output and VCO output (2 ω_0)



D Noise-free biphase modulated signal

G Phase tracking filter demodulator output at loop lock

Fig. II-39. Reference Subcarrier Recovery Wave Forms

switched to the derived subcarrier and continues to function from this source as long as the tracking loop error signal is below threshold value.

Frequency band selection, transmitter power and bit transmission rates. The final selection of the frequency band transmitter power and bit rates was based on many factors. First, the STADAN was given priority as the tracking network to be used, if possible, in accordance with study ground rules established by the contract statement of work. The telemetry frequency bands available or compatible with STADAN are the 136 to 137-mc, 400-mc and 1700 to 1705-mc bands.

It was concluded early in the study program that stabilization of the spacecraft for a period of six months to a year in an attitude favorable for use of a high gain spacecraft antenna was not practical from a reliability standpoint. This factor, plus a requirement for transmission to apogee, led to transmitter power on the order of 6 watts for the 136-mc band using the modulation technique described above, and 5.75 watts for the 1700-mc region, based on a minimum data rate of 10 bps, assuming polarization diversity at the ground stations. The high power requirement for S-band; the extent of VHF ground instrumentation presently installed on STADAN; the requirement for use of VHF for command and beacon; the opportunity to combine functions in an integrated VHF system command, telemetry and RRR system; plus the uncertainty of the availability of S-band spacecraft and ground instrumentation (many stations are on a planned basis for S-band) led to selection of the 136 to 137-mc VHF band. Bit rates of 10 and 160 bps were chosen on the following basis. Ten bits per second is the lowest bit rate compatible with minitrack PCM signal conditioner consoles. Fortunately, it is not so high as to be impractical from a transmitter power standpoint for transmission from apogee. The higher bit rate (160 bps) allows stored data readout at a reasonable margin and bit error rate to ranges of 30,000 naut mi for stations equipped with SATAN antennas and 50,000 naut mi for 85-ft dish stations using the same transmitter power as for transmission from apogee. These ranges allow stored data dump at the higher rate at least twice per orbit and, as shown later, provide flexibility in station schedules and ease acquisition by reducing antenna slewing rates as compared to acquiring and performing storage dump at or very near perigee at much higher data rates. Further, with the recommended attitude determination system, readout of Storage Unit III is required approximately 2.5 hr prior to perigee time and 2.5 hr following perigee time. For the 180° downrange injection orbits shown later, the spacecraft altitude is approximately 17,000 naut mi.

Table II-5 shows the storage capacity of the spacecraft data storage units and the time required to readout the data at either of the two bit rates. Normally, storage readout will be scheduled at the higher bit rate within the 30,000 naut mi range limit but, by use of the 85-ft dish, this range can be extended to 50,000 naut mi.

b. Command

(1) Recommended command system concept

The recommended command system concept described below (with the exception of commanding the VHF Transponder to the ranging mode*)is compatible with the Tone Digital Command Standard, a section of the Aerospace Data Systems Standards, issued by GSFC, 15 January 1963, as applicable to satellites supported by STADAN.

The tone digital command system is suitable for spacecraft requiring simple, real time, ON-OFF commanding and has a maximum capacity for seventy 8-bit, "execute" codes. (Only 24 codes are provided for in the recommended configuration for this spacecraft.)

Each command consists of a series of five words (8 bits to a word) plus one synchronization and one blank period (Fig. II-40). The five word series consists of two identical unique address words followed by three identical execute words. The reception of one address word and one execute word is sufficient to effect a command.

Error detection and interference rejection are accomplished by forming an address code consisting of two ones and six zeroes or six ones and two zeroes plus an execute code always containing an equal number of ones and zeroes (4 and 4).

This coding arrangement provides a means of detecting all odd and 43% of all two-bit errors (Ref. II-1).

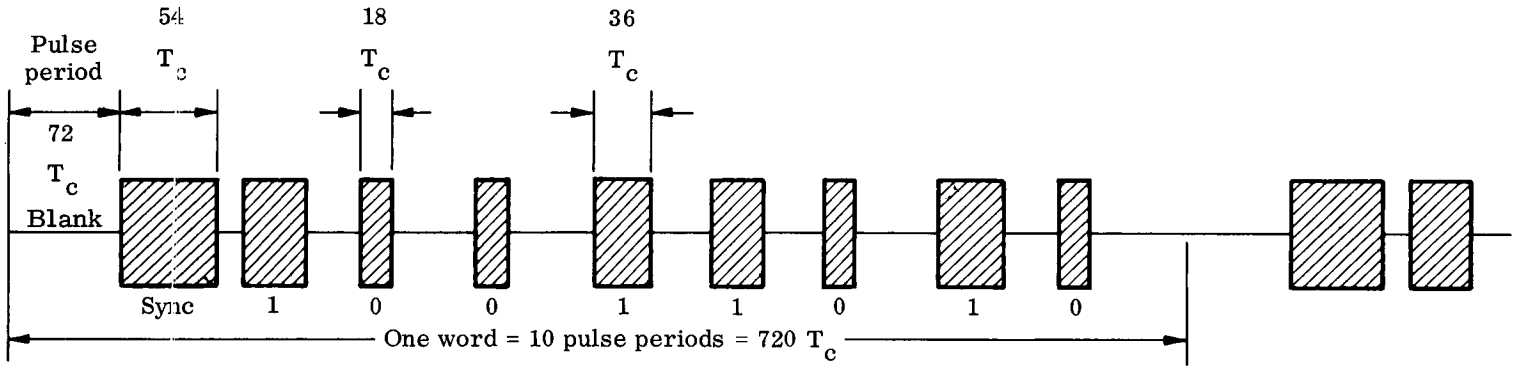
Modulation characteristics of the system are shown in Table II-8.

TABLE II-8

Command System Modulation Characteristics

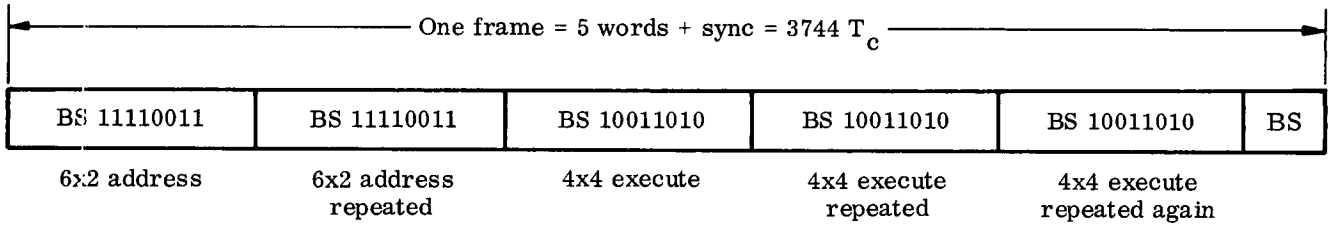
Pulse-duration coded 25, 50, 75 and 100% PPM
Subcarrier (tone) 100% AM
Frequency: Use one of eight standard GSFC tones 7000 to 11,024
RF Carrier: AM, 75%
Frequency: 148 to 150 mc

* To effect transfer of the VHF transponder to the range and range rate tracking mode, phase modulated ranging tones transmitted by ground based range and range rate equipment are employed. This mode of commanding is discussed later in the report.



T_c = period of encoder clock

Command Word Structure



Command Frame Format

Fig. II-40. Command Format and Word Structure

A simplified block diagram of the spacecraft command system showing command data flow is given in Fig. II-41.

The system is completely redundant from receiver input to decoder output. The receivers are all solid state of a double conversion superhet-type with one RF stage (an in-house development of GSFC for use on the Interplanetary Monitoring Platform--IMP--D model). Originally designed as part of the IMP VHF range and range rate transponder, the receivers must be modified by adding an AM detector and amplified audio output to be compatible with the GSFC tone digital command systems (Fig. II-42). The modified transponder will continue to serve as a range and range rate transponder.

In commanding a transfer to the range and range rate mode, a phase modulated audio address tone is sent along with a continuous 4-kc execute ranging tone. These signals are decoded internally in the VHF transponder, causing a transfer of input data to the transmitter portion of the transponder. As long as the ground station continues to transmit the 4-kc ranging tone, the transponder remains in the RRR mode. At the end of the measurement period, (5 min) the ground station transmission ceases and the transponder reverts to transmitting telemetry data.

Tone digital commands are decoded by two digital decoders external to the VHF transponders. An output from either decoder will execute a command. Typical decoder specifications for tone digital systems are given in Ref. II-1, "Aerospace Data System Standards." Consolidated Systems Corporation's command decoder models P-106 and P-105-70-19 are representative of what is presently available on the market.

Performance specifications and operating descriptions for the two decoder models may be found in Refs. II-2 and II-3, respectively. Decoders required for this configuration need only 18 command outputs to provide completely redundant commands for each of the 9 functions and need not be equipped for the full 70 command codes available. The command list for the spacecraft is shown in Table II-2. Command link calculations and discussion of parameters are given in Appendix II-1. A reliable command range of 100,000 naut mi is attainable for the tone digital system with less reliable command to well over 250,000 naut mi depending on spacecraft orientation. A reliable range of 100,000 naut mi for commanding the RRR mode is attainable.

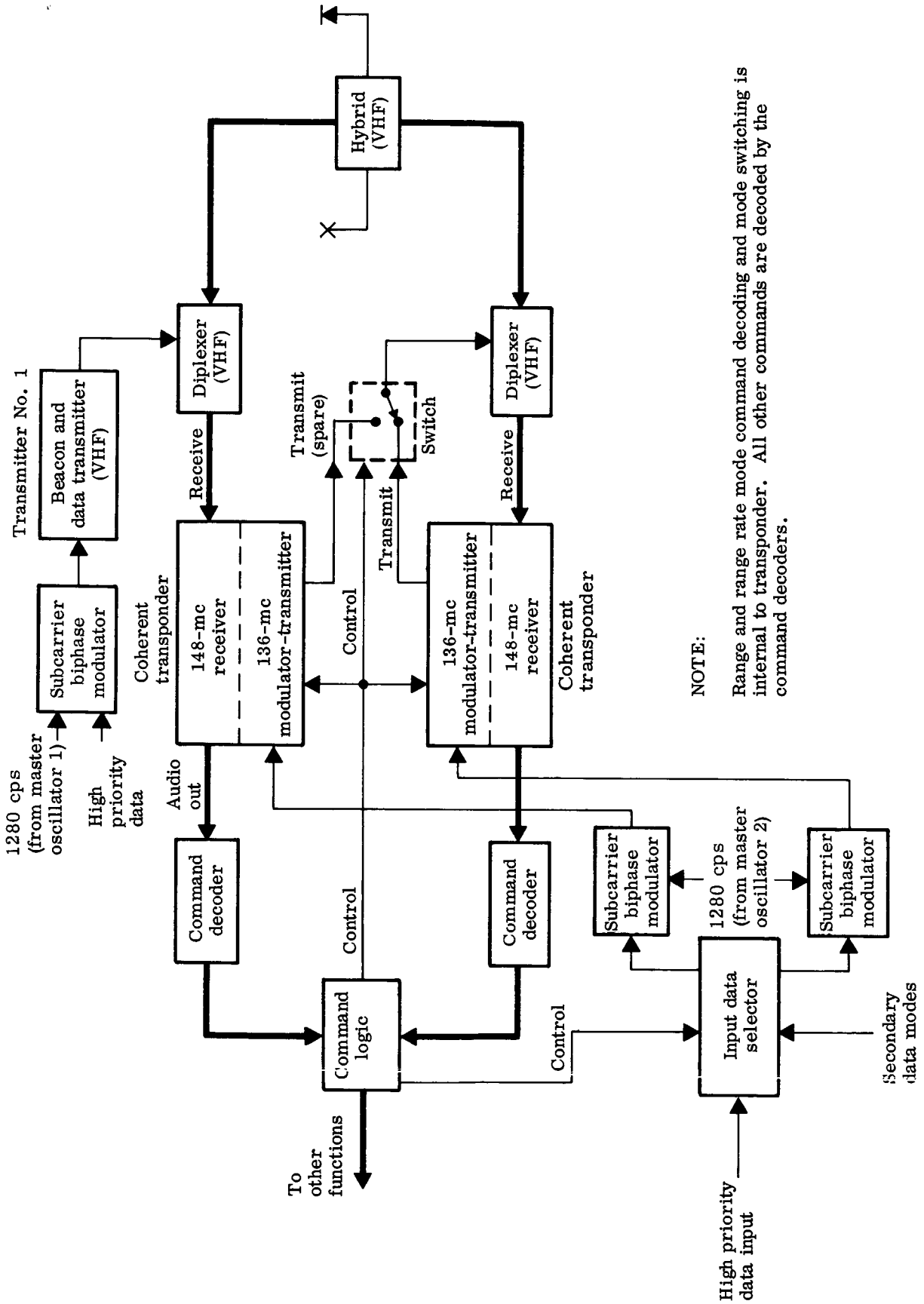


Fig. II-41. Spacecraft Command System Data Flow

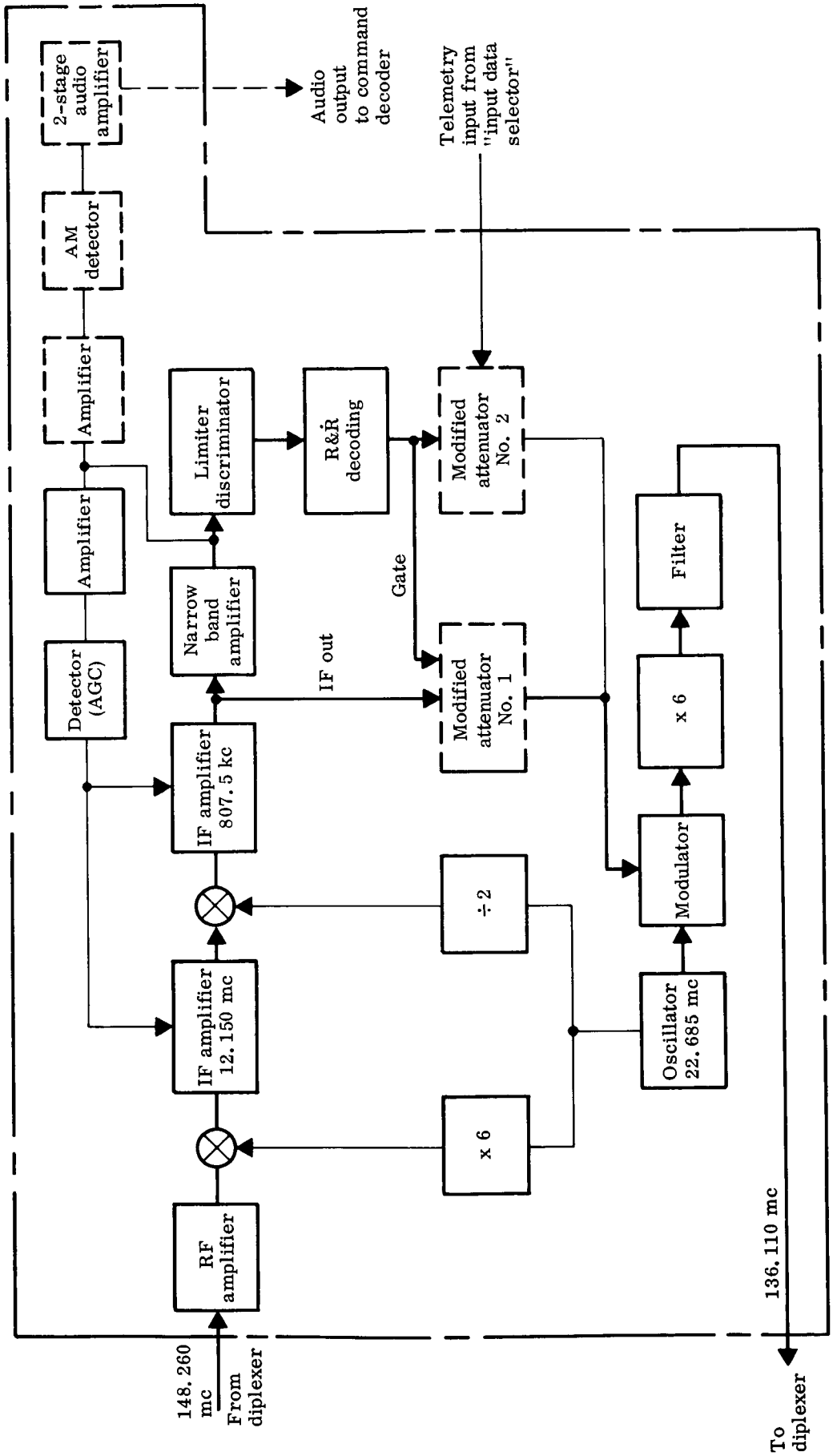


Fig. II-42. VHF Transponder: Range and Range Rate Mode Data Flow

(2) Command tradeoffs

Several command concepts were considered prior to selection of the recommended concept described above. The tone command standard system as described in "Aerospace Data Systems Standards" (GSFC) was considered along with the FSK-type system presently used on OGO.

The tone command standard (address tone followed by three execute tones in sequence), although simpler than the tone digital command system, is less secure and is limited in the number of commands available. The FSK system standard, similar to that used on OGO (the system standards have not been released by GSFC as of this writing), calls for 24-bit words and is intended for spacecraft requiring updating of stored command sequences. The latter system is considered too sophisticated for this application.

The tone digital system is relatively secure and has the capacity for backup channels and spares. No other command systems were considered for use on the STADAN.

Several spacecraft command configurations were considered and are recommended as optional arrangements. Should unforeseen difficulties arise in modifying the GSFC VHF transponders to provide a tone digital output from the receiver IF, a separate IF strip for the command function could be provided. Another optional arrangement is to replace one of the range and range rate transponders (the one in the difference arm of the hybrid) with a standard tone digital command receiver such as AVCO Model 184003 and a phase modulated VHF (136 mc) transmitter. Although one would lose the ranging redundancy, the reliability of the command system might be slightly improved. The recommended configuration is based on the apparent feasibility of modifying the transponder to provide the command receiver functions plus the desirability of not having to provide spares and perform checkout and tests for an additional type of receiver and transmitter.

The STADAN command stations and associated ground equipment are discussed later.

c. Tracking and acquisition

(1) Description of recommended tracking system

The STADAN VHF Range and Range Rate System (RRR) developed by GSFC is recommended for use as the primary tracking system for this spacecraft following orbit injection. It is supplemented by ground telemetry antenna angle data and Minitrack interferometer tracking.

The RRR system makes use of a simple proven technique for obtaining tracking data. Range measurements are accomplished using basic side tone ranging techniques and range rate is determined by use of the established principles of coherent doppler. The VHF system was chosen over the S-band system for reasons related in later paragraphs.

To perform the RRR measurements, a VHF transponder is required in the spacecraft. Range tones are phase modulated on an up-link carrier frequency. This spectrum (Fig. II-43) is heterodyned in the transponder (Fig. II-42) with a local oscillator which is coherent with the transponder output frequency to provide a double frequency conversion. The output of the second IF (the frequency translated up-link signal) is phase modulated on the down-link carrier figure.

By essentially reversing the transponder signal processing in ground receiving equipment and comparing the output with the up-link signal, range rate and side tone phase delays may be determined.

The transponder recommended for this spacecraft is a repackaged version of the VHF transponder presently undergoing design and evaluation by GSFC for use in the lunar-anchored IMP-D satellite. It will have an RF output of 6 watts (min), and use all solid-state circuitry. RCA-2N-3375 transistors are currently being used in the final stages of the transmitter. Some of the performance characteristics for this transponder are shown in Table II-10. The basic transponder was initially developed and used for tracking the IMP (Explorer XXI). It had a power output of 4 watts.

A range of 100,000 naut mi can be anticipated for measurement of range and range rate. Ranges to 180,000 naut mi may be experienced for optimum spacecraft orientation and low tumbling rates. For tumbling rates greater than one revolution per 10 min, spacecraft orientation may, at times, cause the tracking loops to break lock before the normal 5-min tracking interval. Link calculations for both up- and down-links are given in Appendix II-2. The RRR maximum range could be extended by implementing the 85-ft dish antenna for the RRR function; however, the 85-ft dish antennas were not designed for transmission. A 5-db improvement in the down-link could be effected. Unfortunately, it appears that the up-link may be the limiting factor. A comprehensive design evaluation report and a test report on the RRR system are given in Refs. II-3 and II-4, respectively. Both referenced reports include detailed descriptions of the ground system, including performance analyses or measured results.

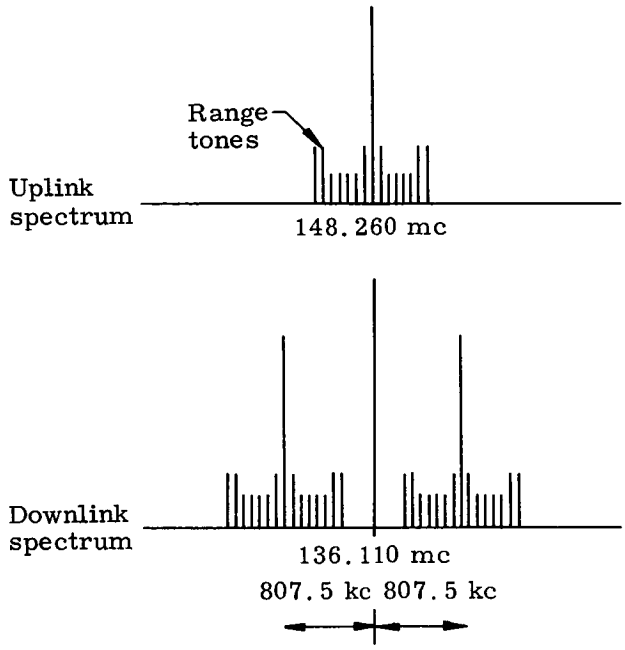


Fig. II-43. Spectrum of VHF Transponder

TABLE II-9

IMP-D VHF Transponder Characteristics

Input frequency	148.260 mc*
Input signal power	-40 to -110 dbm*
Receiver noise figure	9 db
IF frequencies (2)	12.150 mc, 807.5 kc
Second IF bandwidth 6 db	80 kc*
Predetection bandwidth (command)	30 kc
Transmitter power output	6 watts
Modulation	Phase
Power input	15 watts
Volume (estimated repackaging)	160 cu. in.*
Weight (estimated)	7 lb*
Type circuitry	Solid state

* Estimated values, data obtained verbally.

Both spacecraft transmitters (the data transmitter and the active transponder) are phase modulated at a modulation index of approximately 1.6 rad (peak). This results in approximately 1.2 watts of unmodulated residual carrier from each transmitter for use in beacon acquisition of the spacecraft by ground station tracking antennas or for performing Minitrack interferometer measurements. Link calculations (Appendix II-2) show beacon acquiring to beyond 180,000 naut mi using the 85-ft dish antenna and polarization diversity. Acquiring with the SATAN antenna (using polarization diversity) to ranges of over 100,000 naut mi can be anticipated. At ranges well beyond this, spacecraft orientation can, at times, cause the link to be broken. Minitrack tracking to ranges of 3000 naut mi can be anticipated for the most favorable spacecraft orientations; for less favorable orientations, ranges of only about 500 naut mi can be expected.

The STADAN ground stations to be used for tracking and data acquisition are identified in Table II-3.

Prior to separation of the spacecraft from the Agena D, tracking is to be accomplished by C-band radar. Tracking of the Agena at the injection point to provide data for determining initial orbital parameters for the satellite is required.

(2) Tracking tradeoff

The tracking system described above is one of several considered. The systems are VHF range and range rate, S-band range and range rate, Minitrack interferometer, angles only from SATAN and 85-ft dish acquisition antennas, and combinations of the above.

Of these systems, minitrack and common types of radar are too range limited to be considered as primary trackers. Angles-only data is good for updating orbital parameters once the orbit is established, but range and range rate is more valuable in initially establishing an orbit based on a minimum of tracking data. If one combines the range and range rate function with command and telemetry into an integrated system, the RRR function is provided with little penalty in spacecraft volume weight and power.

For these reasons, the RRR system was chosen as the primary tracking system to be investigated. The present STADAN RRR system has both a VHF and an S-band capability. The VHF system is at a disadvantage in measurement accuracy compared to the S-band system, but the VHF system accuracy is more than adequate (see Appendix I-4, Vol. III A), and VHF has many other advantages. For example, a VHF radio beacon and antenna are required for all satellites supported by STADAN. The standard command frequency is VHF. Further, with the present RRR ground system and an omni or near omni spacecraft antenna, the VHF system has a 12-db advantage on the down-link over S-band for a comparable tracking range. This means an S-band transmitter output of 22 watts is comparable with the recommended 6-watt VHF transponder (link calculations are shown in Appendix II-2). Nominal output power for S-band transponders such as that designed for POGO and EGO do not exceed 250 to 500 mw; hence, power amplifiers and added primary power would be required to boost the output to 22 watts.

A further complication to use of S-band for RRR entails a reversal of the up- and down-link frequency bands for all spacecraft launched after January 1967 and supported by STADAN. This means a change-over in transponder frequencies, going from an output frequency of 1705 mc to a frequency of approximately 2253 mc, the input receiver frequency reverting to approximately 1800 mc. This adds a factor of uncertainty to the availability and performance of newly developed S-band transponders. One transponder reportedly under development has a performance target of:

Output frequency	2253 mc
Power output	1 watt
Power input	30 watts
Weight	5-1/2 lb

The output power of 1-watt, even with the planned conversion of ground RRR S-band dish antennas from 14-ft to 30-ft diameter, does not provide a down-link advantage over VHF when an omni spacecraft antenna is required, as is the case for a tumbling spacecraft.

A further deterrent to use of S-band is that there appears to be a conflict in using a combined S-band RRR and telemetry system, since it is understood that telemetry data acquisition antennas, feeds, receivers, etc., are, apparently, to remain at 1700 mc.

Study results on comparison of RRR tracking plus Minitrack versus angles only from data acquisition antennas are shown in Volume III Chapter I and Volume IIIA Appendix I-4.

d. Antenna system

Random tumbling of the micrometeoroid satellite and the necessity to communicate at all times established the requirement for omnidirectional coverage. The size (in terms of wave length) and the "Z" configuration represent very serious obstacles. Several schemes were explored, four of which will be discussed in detail, with emphasis on the two most promising systems. The four approaches to be covered are:

(1) Four stubs--one located on the extreme end of each horizontal sensor support frame (Fig. II-44).

(2) A pair of turnstiles mounted on masts as indicated in Fig. II-43 with unequal power and in phase.

(3) A combination of a turnstile and a discone with a slotted disc fed equal power in phase (Fig. II-44).

(4) A discone with an unsymmetrical disc and a turnstile fed equal power in phase.

The system composed of four stubs and a phasing network produced interference patterns in both θ and ϕ cuts which contained many deep nulls. The interference patterns result from the large spacing (in terms of wavelength) between elements. The number and depth of nulls eliminated this approach as a possible means of achieving omnidirectional coverage.

The two turnstiles, when properly mounted above the satellite surfaces to minimize shadowing, resulted in extremely good coverage between $\theta = 0^{o}$ and $\theta \simeq 65^{o}$, and between $\theta \approx 115^{o}$ and $\theta = 180^{o}$. Coverage in the region of $\theta = 65^{o}$ and $\theta \approx 115^{o}$ was not acceptable. In this region, both elements are simultaneously visible, and the separation

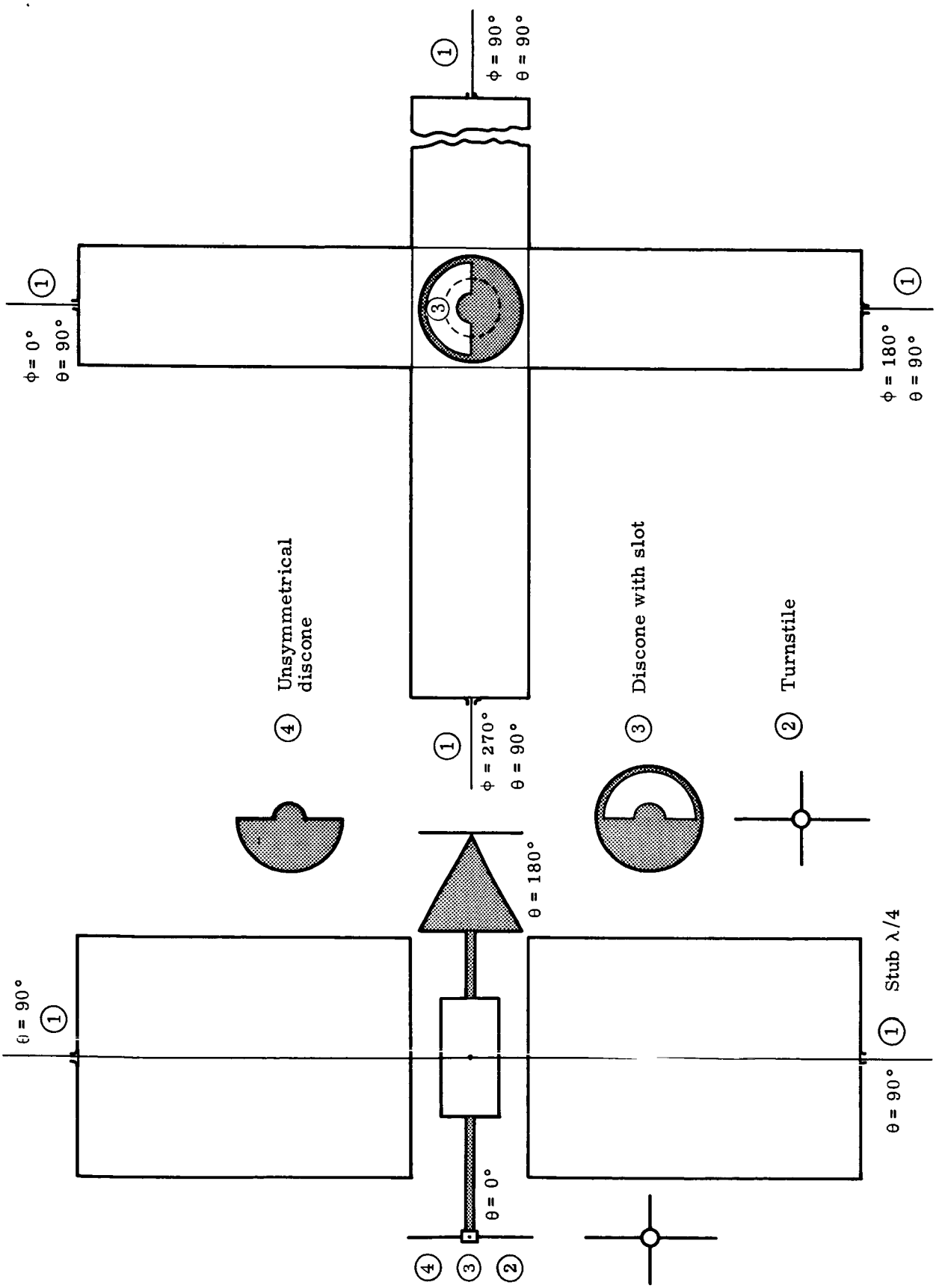


Fig. II-44. Micrometeoroid Antenna Systems

resulting from shadowing considerations is sufficient to produce interference nulls. The power division and phasing between elements was varied without significant improvement in performance.

Results of the tests on the systems discussed above pointed out the low probability of achieving omnidirectional coverage on the proposed satellite configuration unless polarization diversity is employed. The remaining discussion is primarily concerned with systems to work with polarization diversity.

Employing diversity eliminates the interference nulls in the vicinity of $\theta = 90^{o}$, if the elements selected are orthogonally polarized at $\theta = 90^{o}$. Achieving pure orthogonal response from elements mounted on a complex structure such as the one proposed is difficult, but, with careful selection of radiating elements, it can be approached with a minimum amount of pattern inferference.

The turnstile had been proven in earlier tests (Figs. II-45 through II-49) as an acceptable radiator above the satellite structure and was, therefore, selected as one element for the diversity system. The logical selection for the second element was a stub or discone mounted as shown in Fig. II-44. This combination met the requirements of the diversity combination, but not the omnidirectional requirement. The discone and stub have a characteristic null at $\theta = 180^{o}$ which could not be filled by the turnstile because of vehicle shadowing in that area.

Two methods of modifying a discone to reduce the null depth or eliminate the characteristic null and maintain adequate polarization separation at $\theta = 90^{o}$ were tested.

The first modification was inclusion of a slot in the disc (Fig. II-44) which could be excited by currents flowing radially from the center of the disc. The radiation from the slot in phase with the radiation from the discone produced the pattern of Fig. II-50. The pattern of Fig. II-51 was recorded with the model rotated 90°, which placed the slot in a field which was cross polarized. The characteristic null of the discone is evident in Fig. II-51. The discone with slot as mounted is a predominantly horizontally-polarized radiator (Fig. II-52) and the turnstile is a vertically polarized element (Fig. II-46) at $\theta = 90^{o}$. With the discone oriented as shown on Fig. II-53, a pattern was recorded with the source polarization vertical rather than horizontal. Without the slot there would be a very low response under the above conditions. Performance of the slot is evident in the pattern of Fig. II-53, and it was obvious that some difficulties would be experienced due to the strong response indicated at $\theta = 90^{o}$ for the orthogonal polarization.

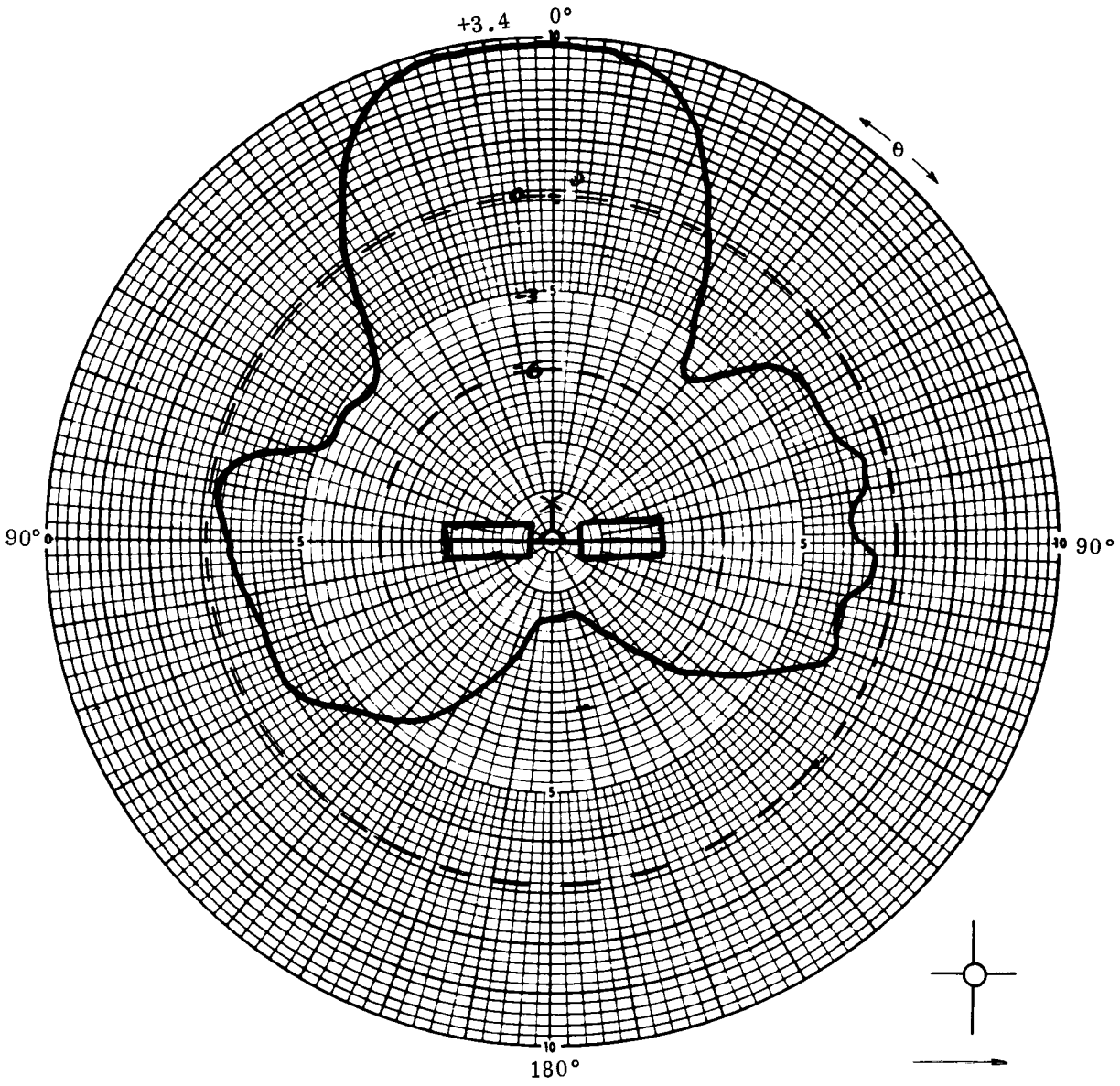


Fig. II-45. Single Turnstile Antenna, 142-mc Frequency, 1420-mc Scale Frequency, Vertical Source

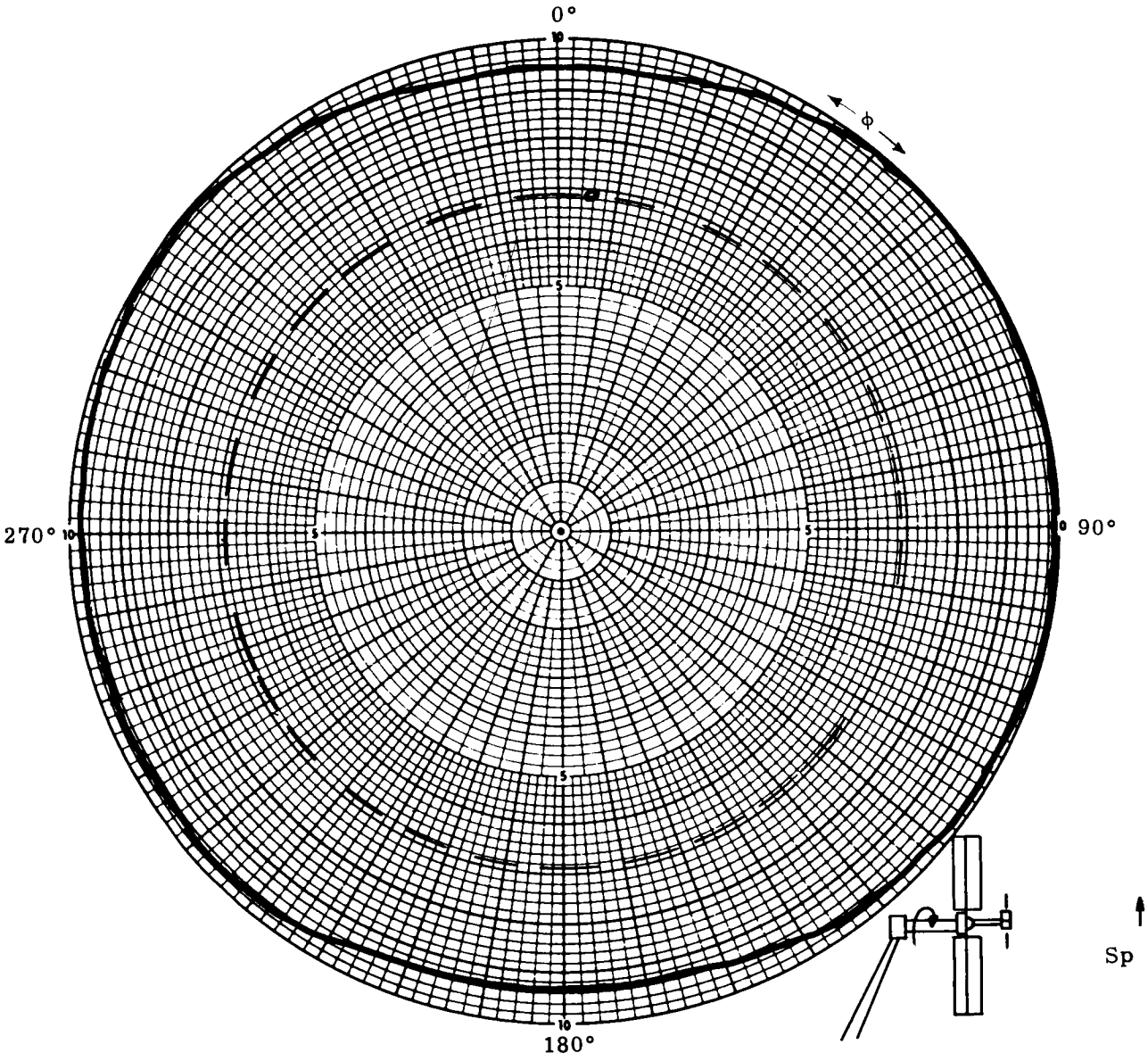


Fig. II-46. Single Turnstile Antenna, 142-mc Frequency, 1420-mc Scale Frequency, Vertical Source, $\theta = 0^{\circ}$

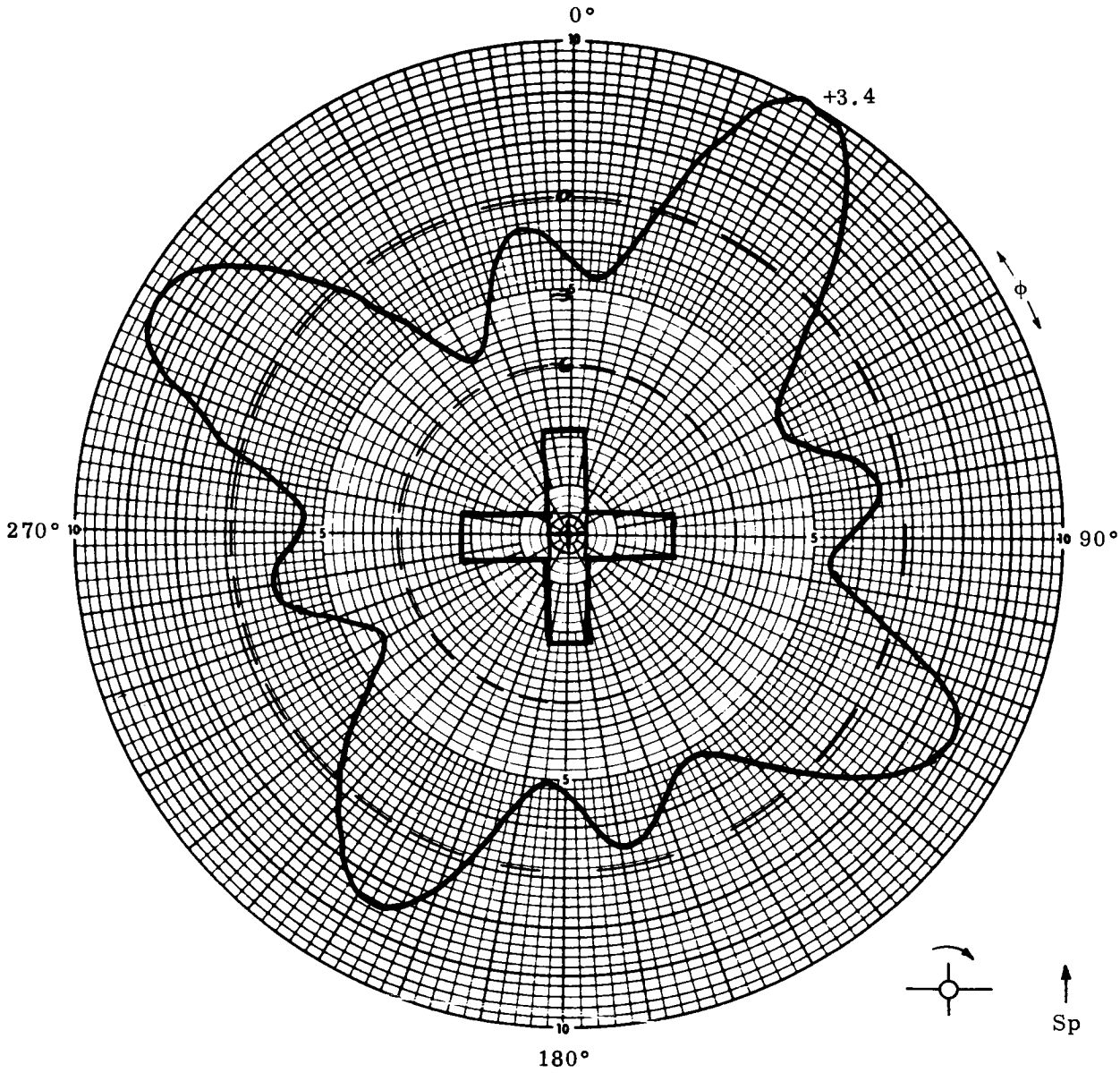


Fig. II-47. Single Turnstile Antenna, 142-mc Frequency, 1420-mc Scale Frequency, Vertical Source, $\theta = 90^{\circ}$

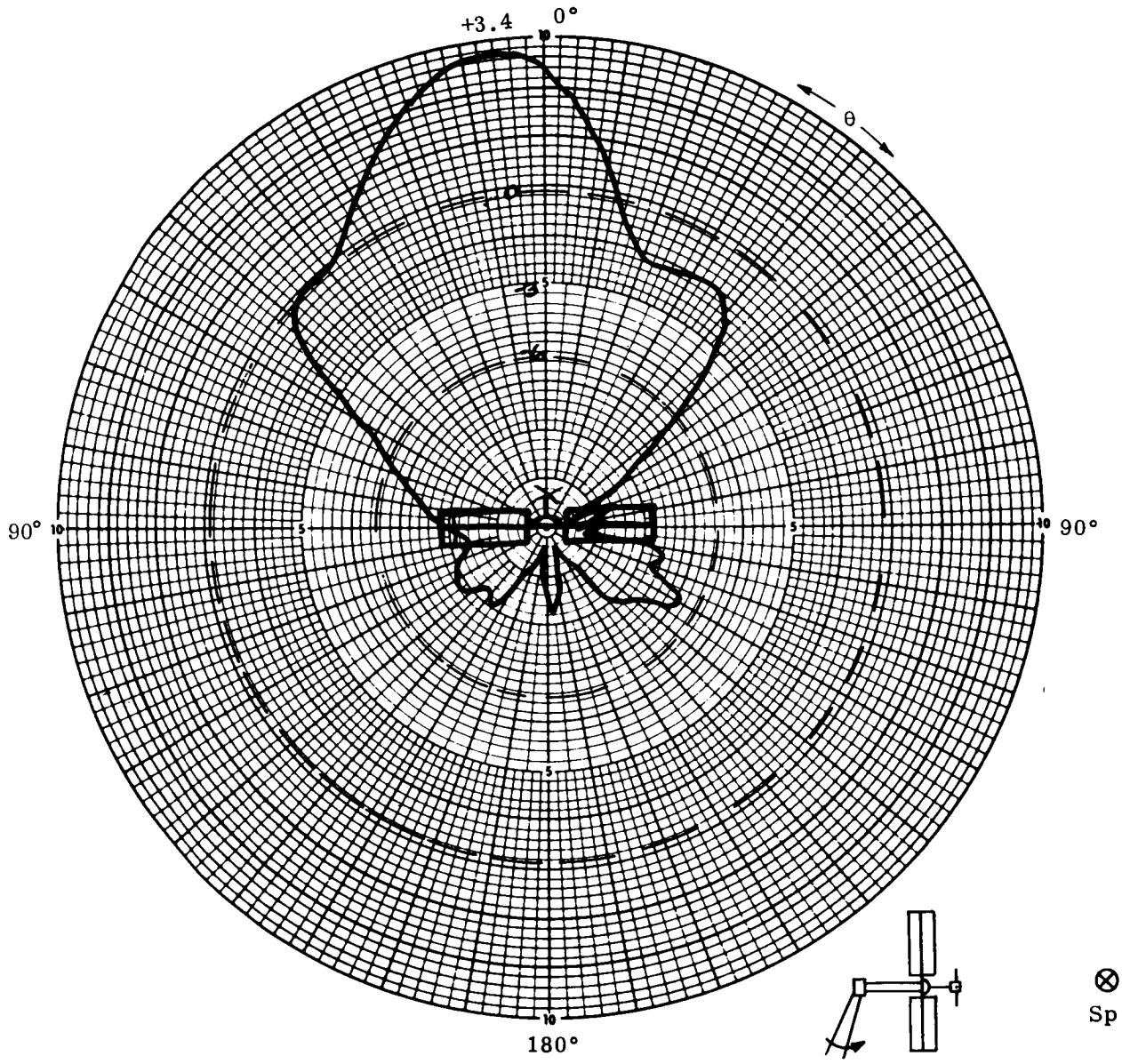


Fig. II-48. Single Turnstile Antenna, 142-mc Frequency, 1420-mc Scale Frequency, Horizontal Source

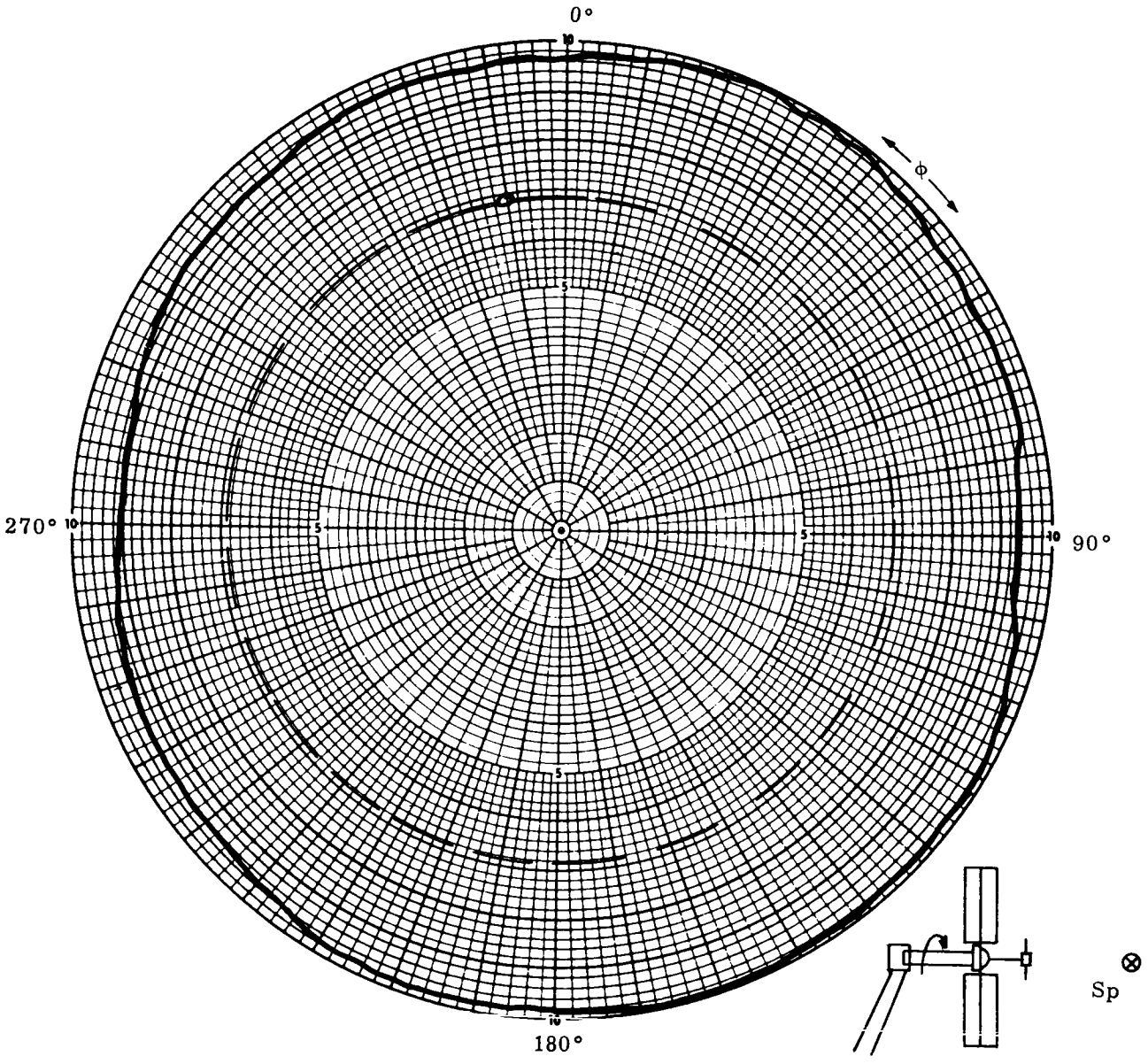


Fig. II-49. Single Turnstile Antenna, 142-mc Frequency, 1420-mc Scale Frequency, Horizontal Source, $\theta = 0^{\circ}$

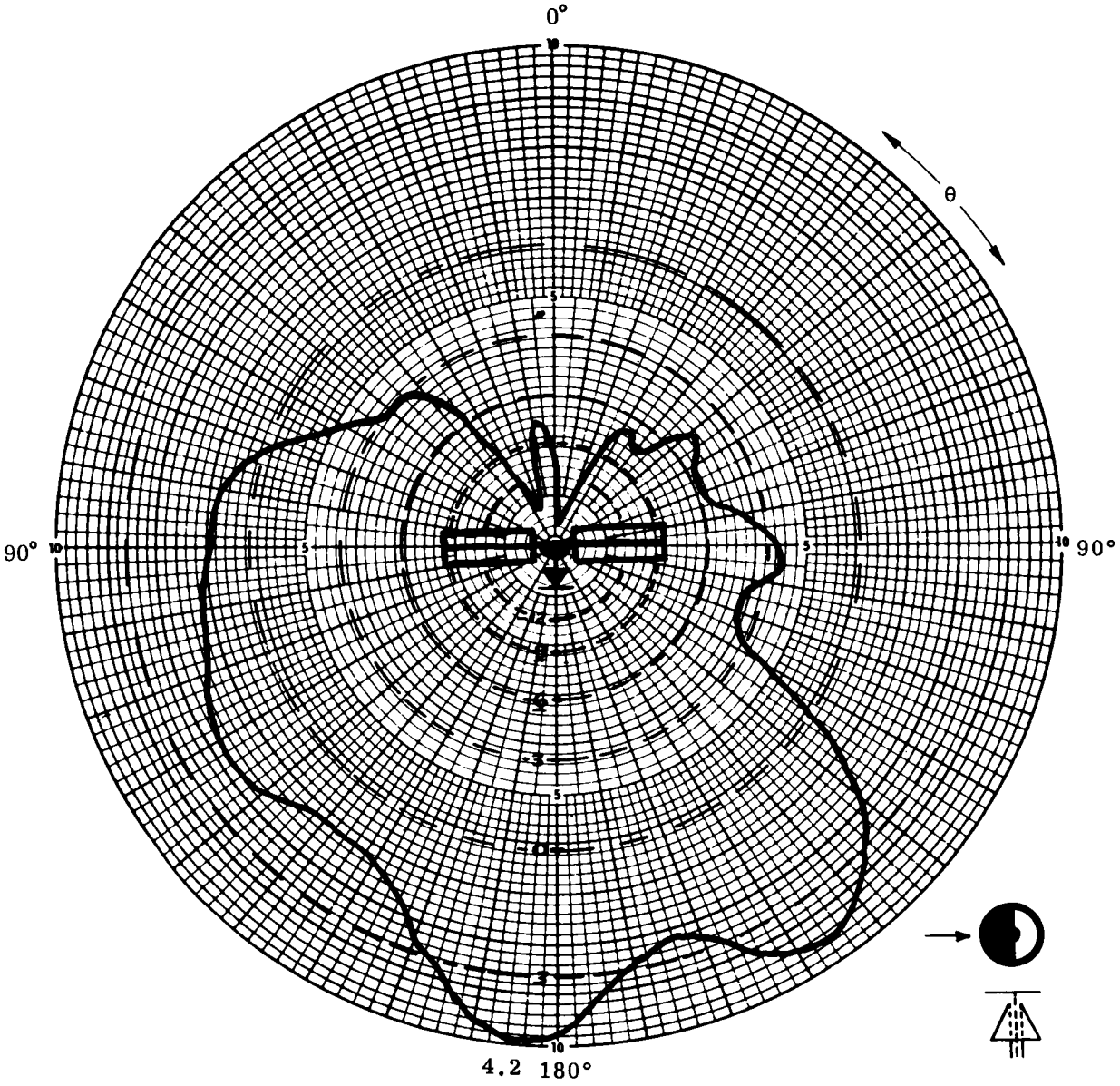


Fig. II-50. Single Discone and Slot Antenna, 142-mc Frequency, 1420-mc Scale Frequency, Horizontal Source

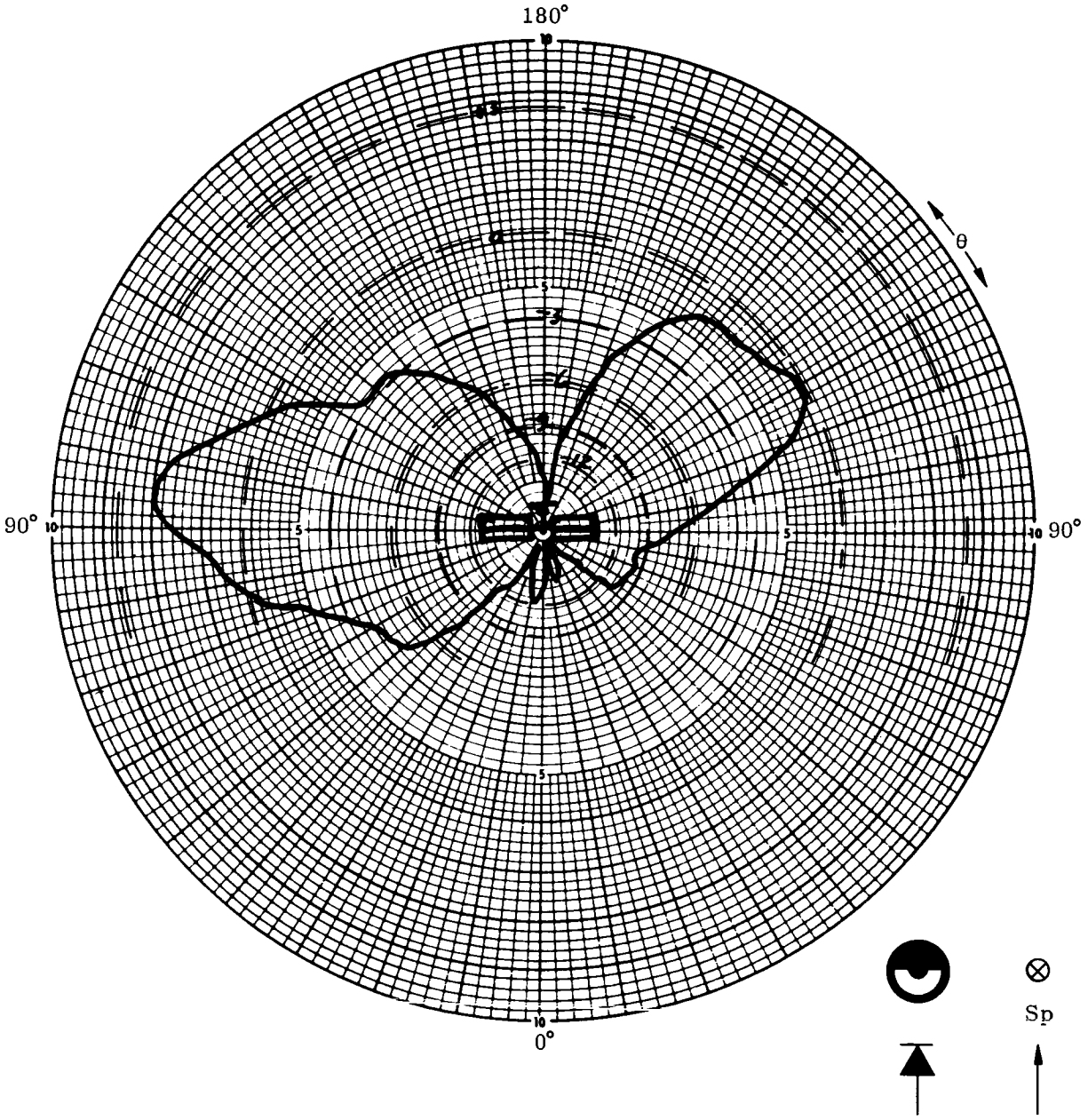


Fig. II-51. Single Discone and Slot Antenna, 142-mc Frequency, 1420-mc Scale Frequency, Horizontal Source

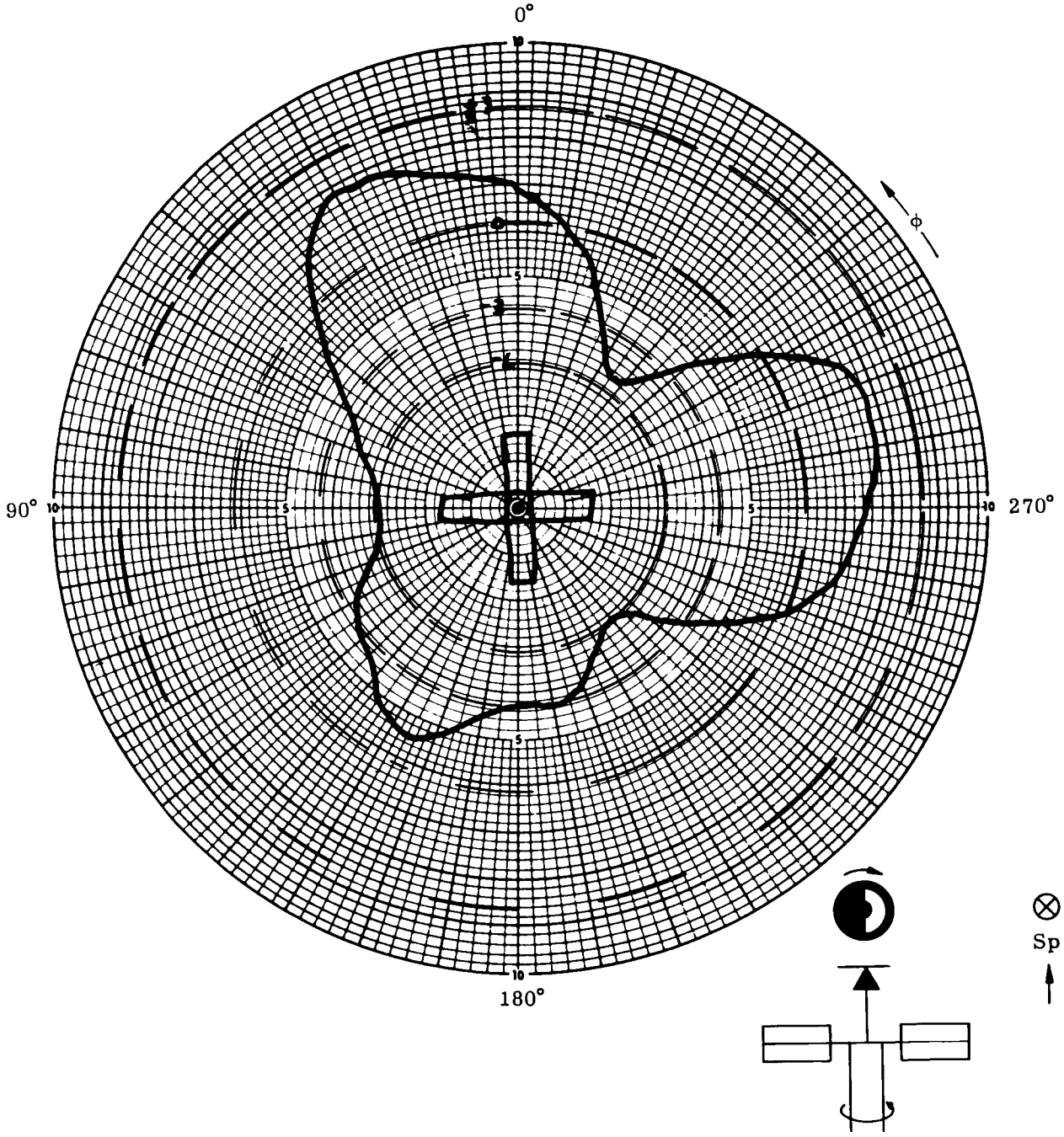


Fig. II-52. Single Discone and Slot Antenna, 142-mc Frequency, 1420-mc Scale Frequency, Horizontal Source

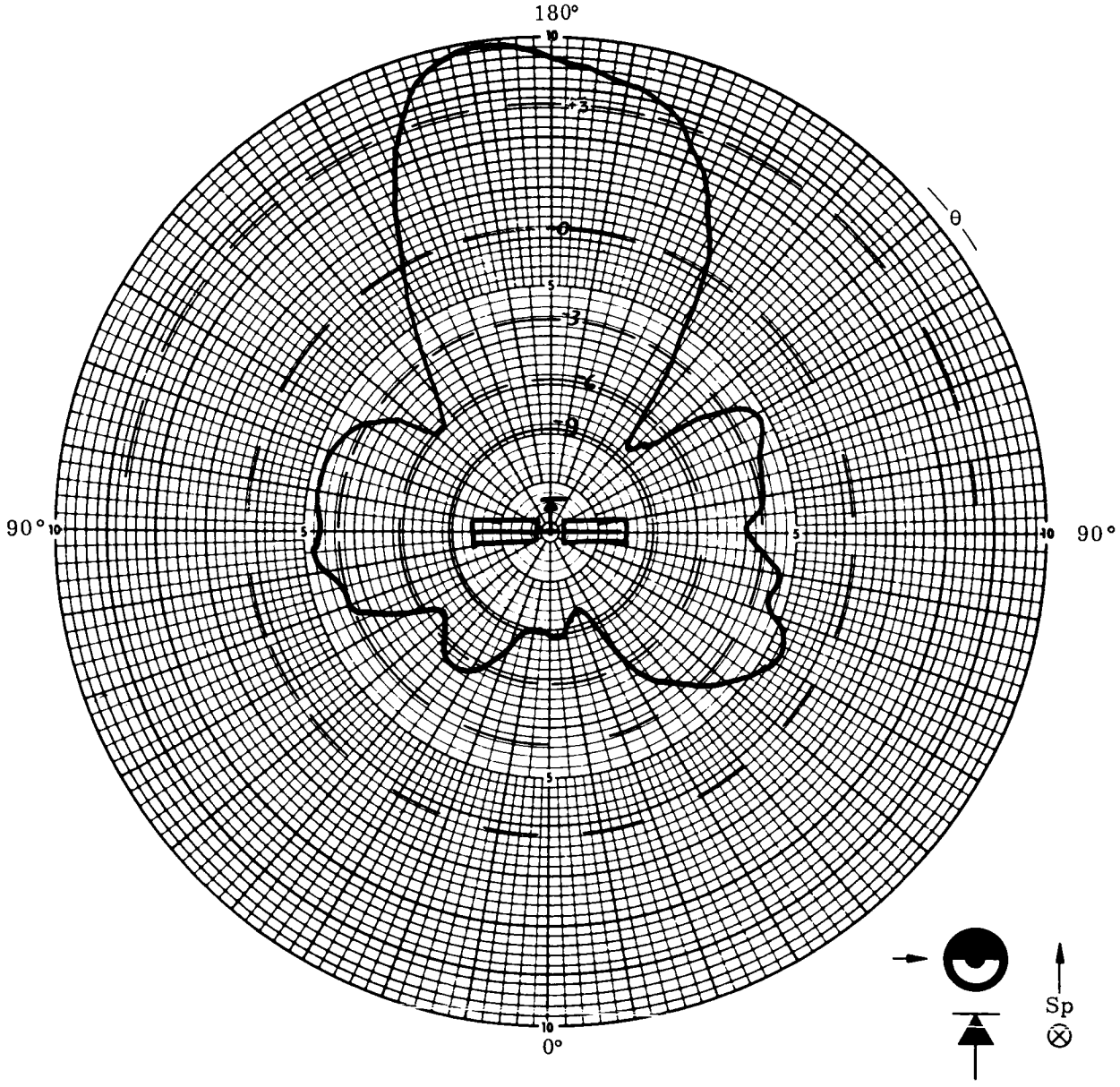


Fig. II-53. Single Discone and Slot Antenna, 142-mc Frequency, 1420-mc Scale Frequency, Vertical Source

The discone with slot will provide high gain in the area normally containing a deep null, and with interference at $\theta = 90^{o}$ which is considerably less than was encountered with two turnstiles. A turnstile and a slotted discone were connected in phase and fed equal power. A complete set of conical patterns was recorded and integrated to obtain a radiation contour, which was plotted for diversity polarization (Fig. II-54). The expected variations along $\theta = 90^{o}$ are evident.

The next approach was to attempt to partially fill the characteristic null without seriously distorting the basic pattern or producing a strong response to the cross polarization. This was accomplished by an unsymmetrical discone (Fig. II-44). The null depth was reduced as indicated in Fig. II-55, and the degree of reduction achieved can be determined by comparing Figs. II-55 and II-56. The discone appears as a symmetrical device for the recording of Fig. II-55.

Improvement in uniformity of coverage is evidenced by comparing Figs. II-52 and II-57, and the reduction in the response to the orthogonal polarization can be seen by comparing Figs. II-53 and II-58.

The contour plot for polarization diversity is Fig. II-59, the simplicity of which is the result of the near symmetry of the system. Most of the conicals (ϕ patterns) approached circular shapes (Fig. II-57). The price paid for the slowly varying coverage was the higher gain at $\theta = 180^{o}$, which was achieved with the previous system.

Combinations of a turnstile and the modified discones on the proposed satellite configuration will approach the desired omnidirectional radiation coverage. The choice of combination will depend on mission requirements of gain and coverage.

There are nulls indicated in the contour plots which are the result of reflections on the test range produced by the metal in the model support. It is difficult to separate the holes produced by the reflections from those produced by element interference and the contours are, therefore, somewhat pessimistic. This configuration and antenna system is unique and would require an antenna range equipped with a special all-plastic mounting and rotating system for final pattern analysis. One of the 1/10th scale antenna test models is shown in Figs. II-50a and 50b.

4. Ground Data Acquisition, Command and Tracking

Three basic network support functions must be provided during the mission lifetime of this spacecraft: recording of telemetered data, commanding operational modes or redundancy switching, and obtaining tracking data for orbital determination and prediction.

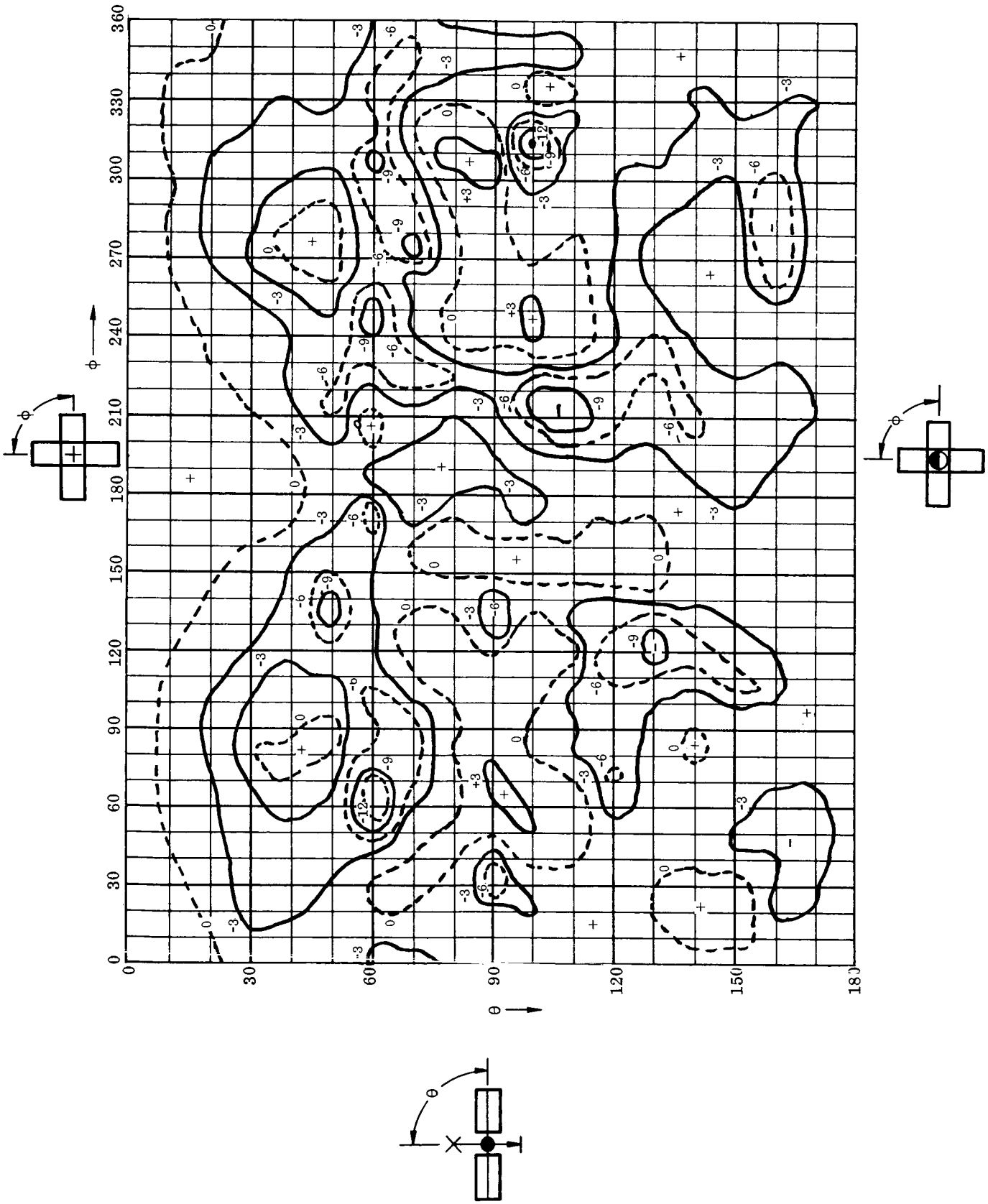


Fig. II-54. Discone and Slot with Turnstile (composite V and H)

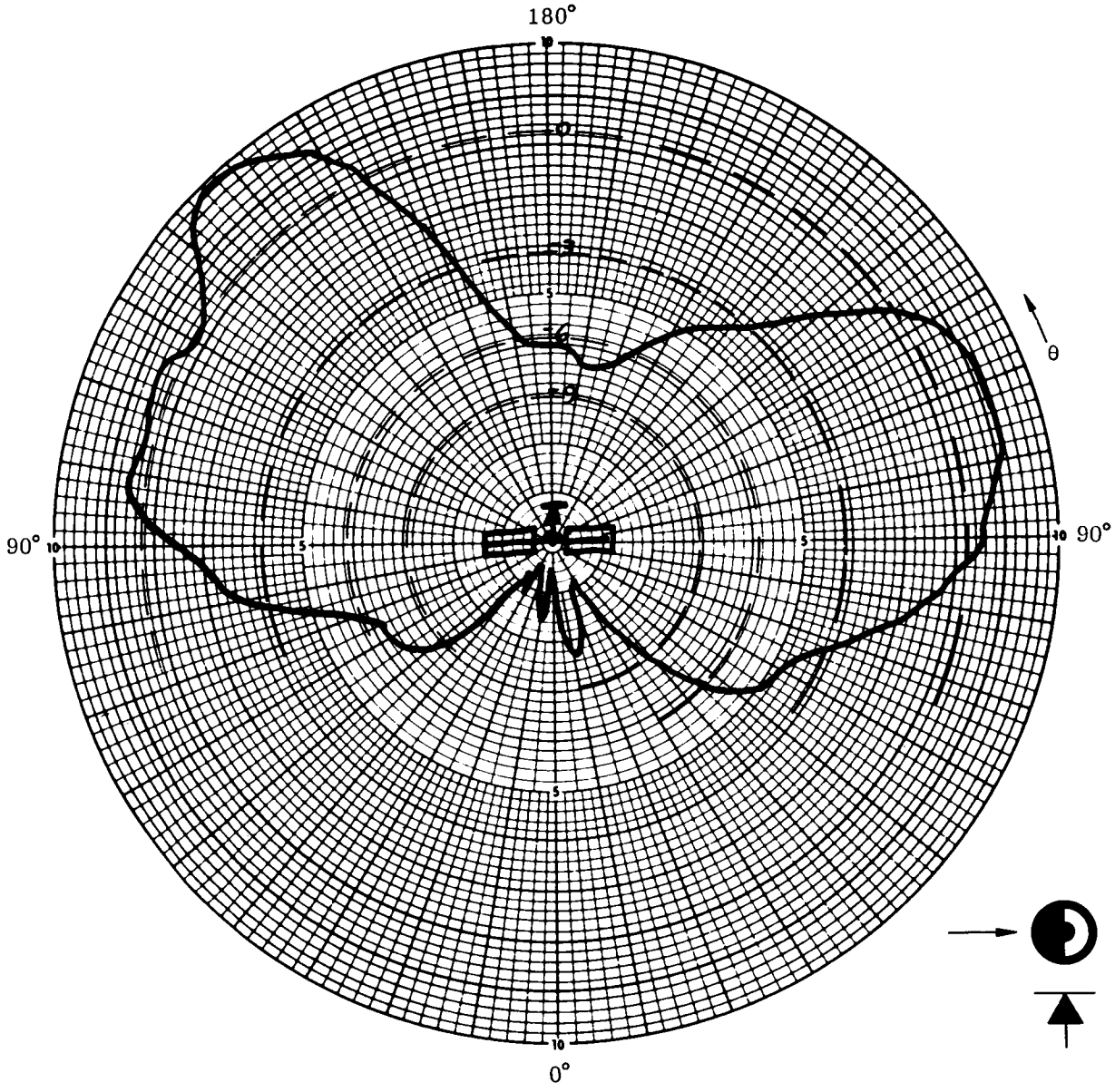


Fig. II-55. Single Unsymmetrical Discone Antenna, 142-mc Frequency, 1420-mc Scale Frequency, Horizontal Source

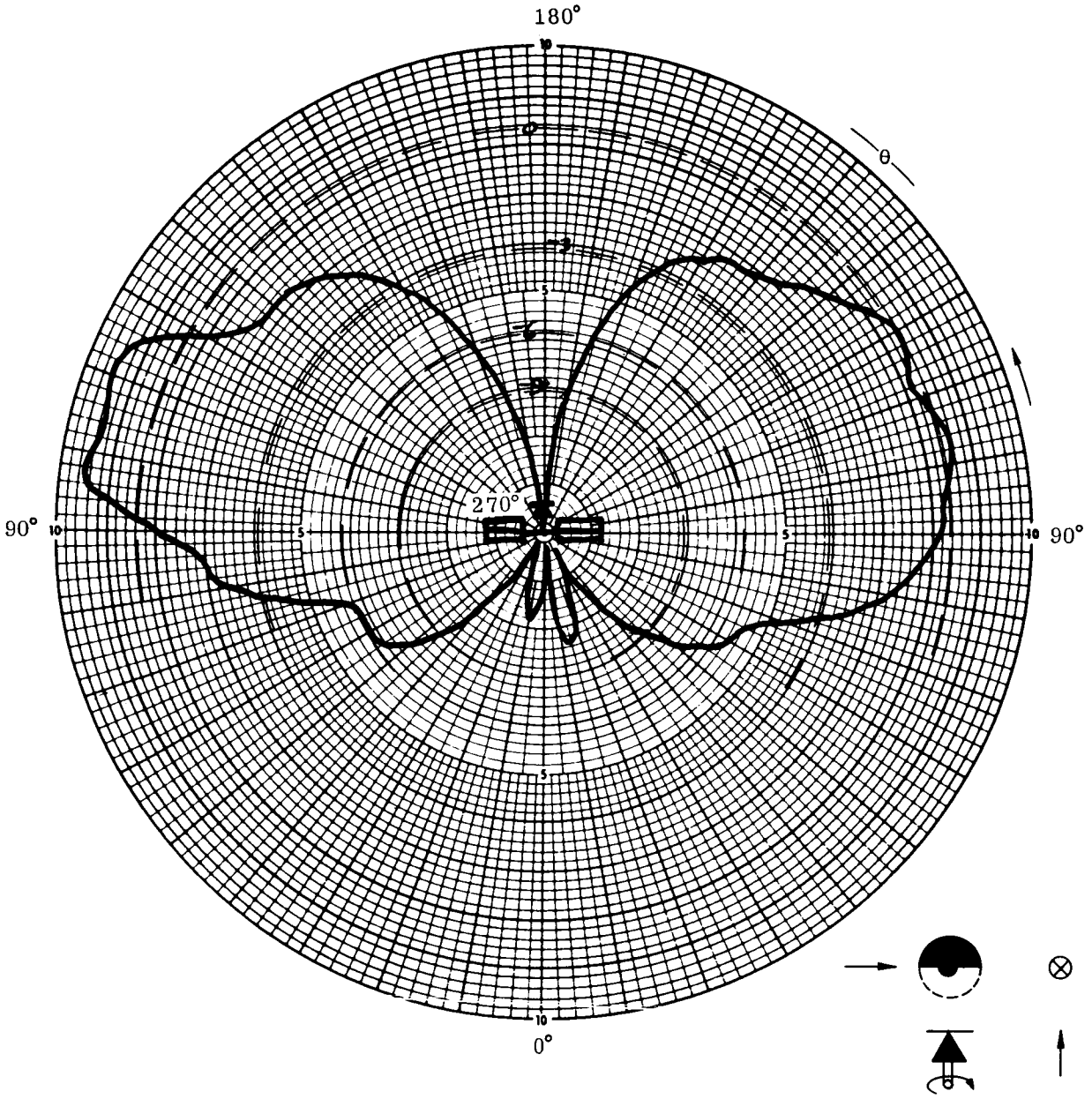


Fig. II-56. Single Unsymmetrical Discone Antenna, 142-mc Frequency, 1420-mc Scale Frequency, Horizontal Source

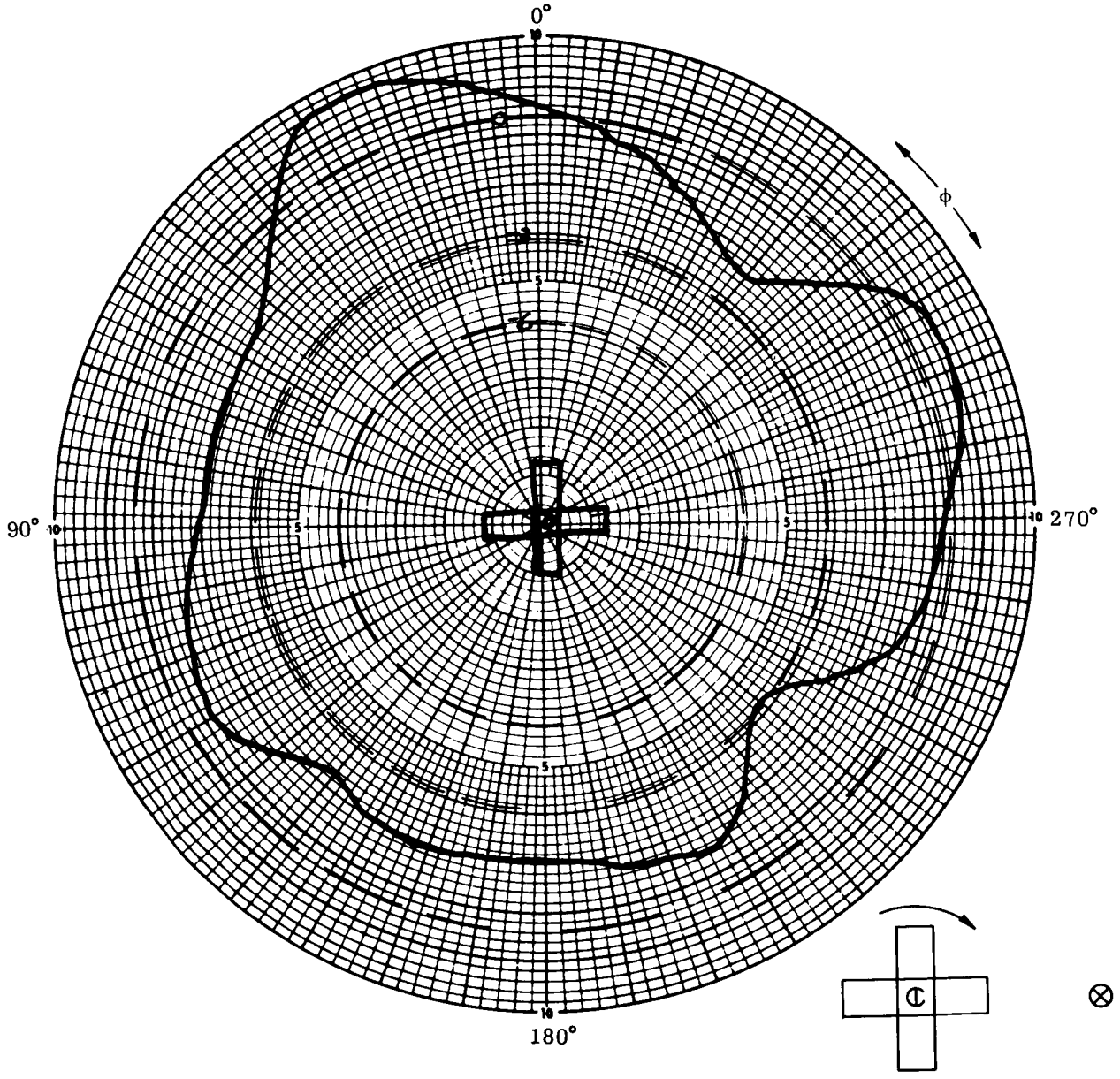


Fig. II-57. Single Unsymmetrical Discone Antenna, 142-mc Frequency, 1420-mc Scale Frequency, Horizontal Source, θ = 90°

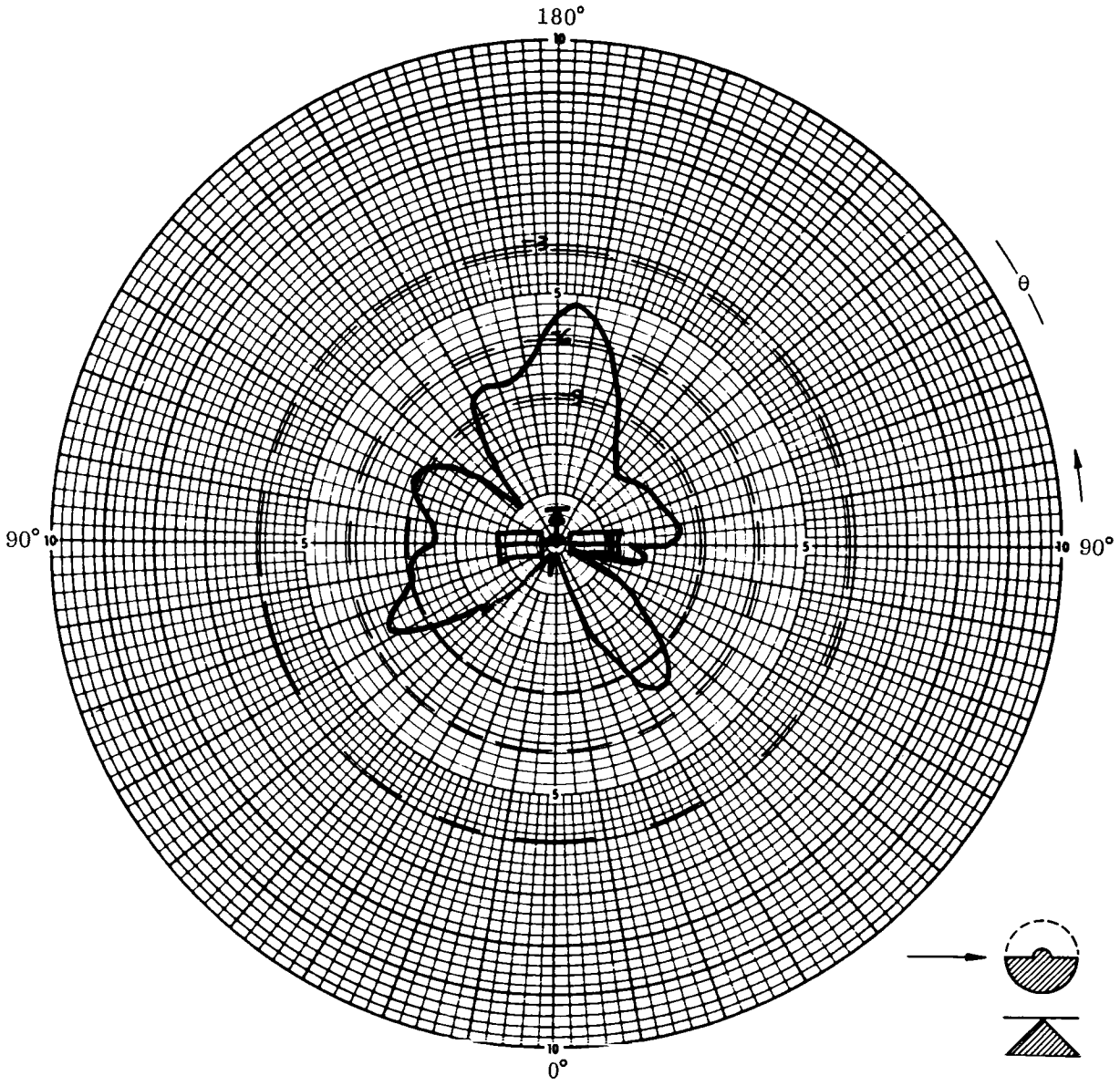


Fig. II-58. Single Unsymmetrical Discone Antenna, 142-mc Frequency, 1420-mc Scale Frequency, Vertical Source

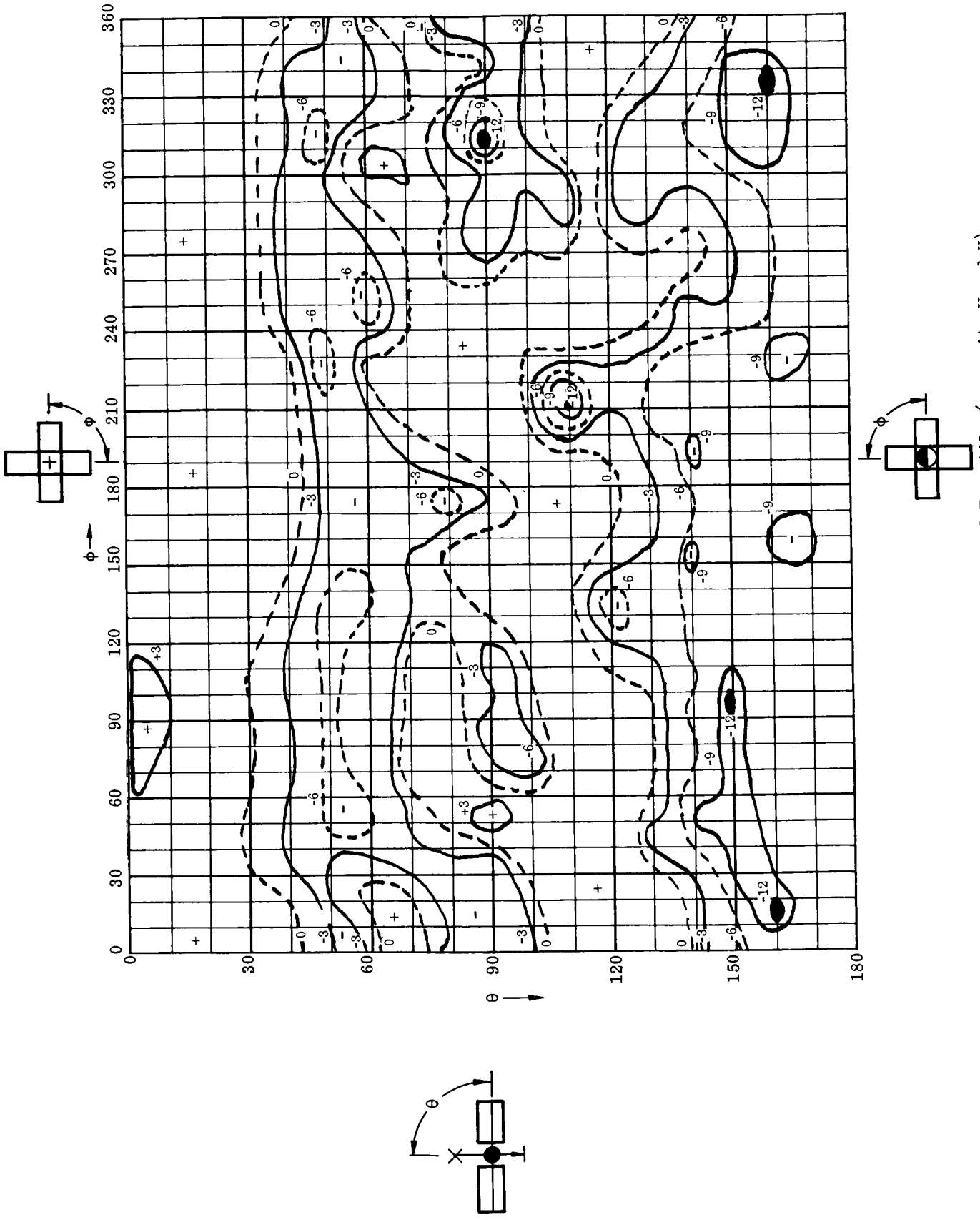


Fig. II-59. Unsymmetrical Discone and Turnstile (composite V and H)

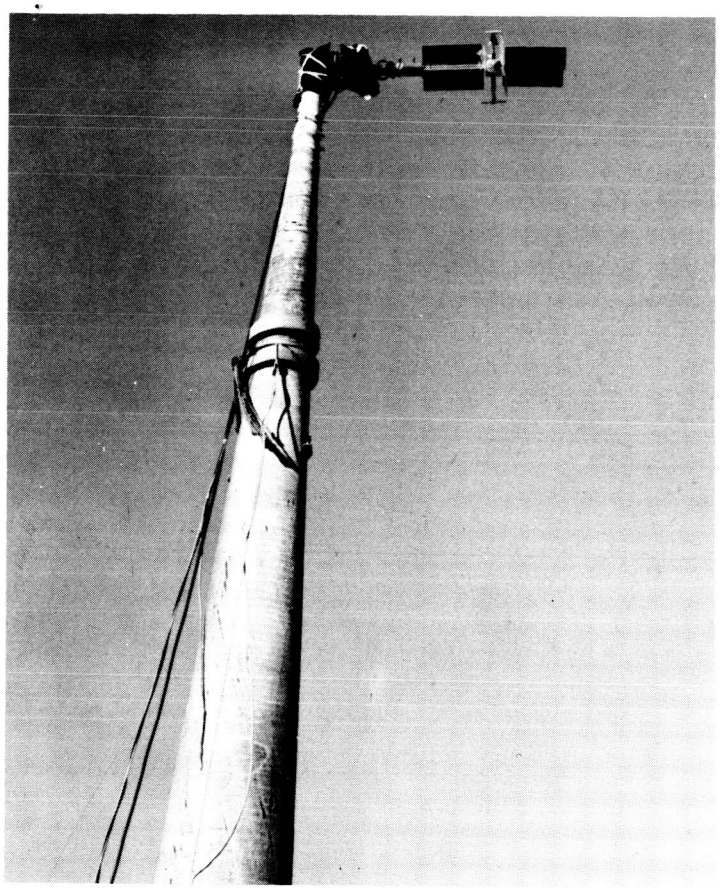


Fig. II-60a. 1/10th Scale Antenna Test Model on Mount

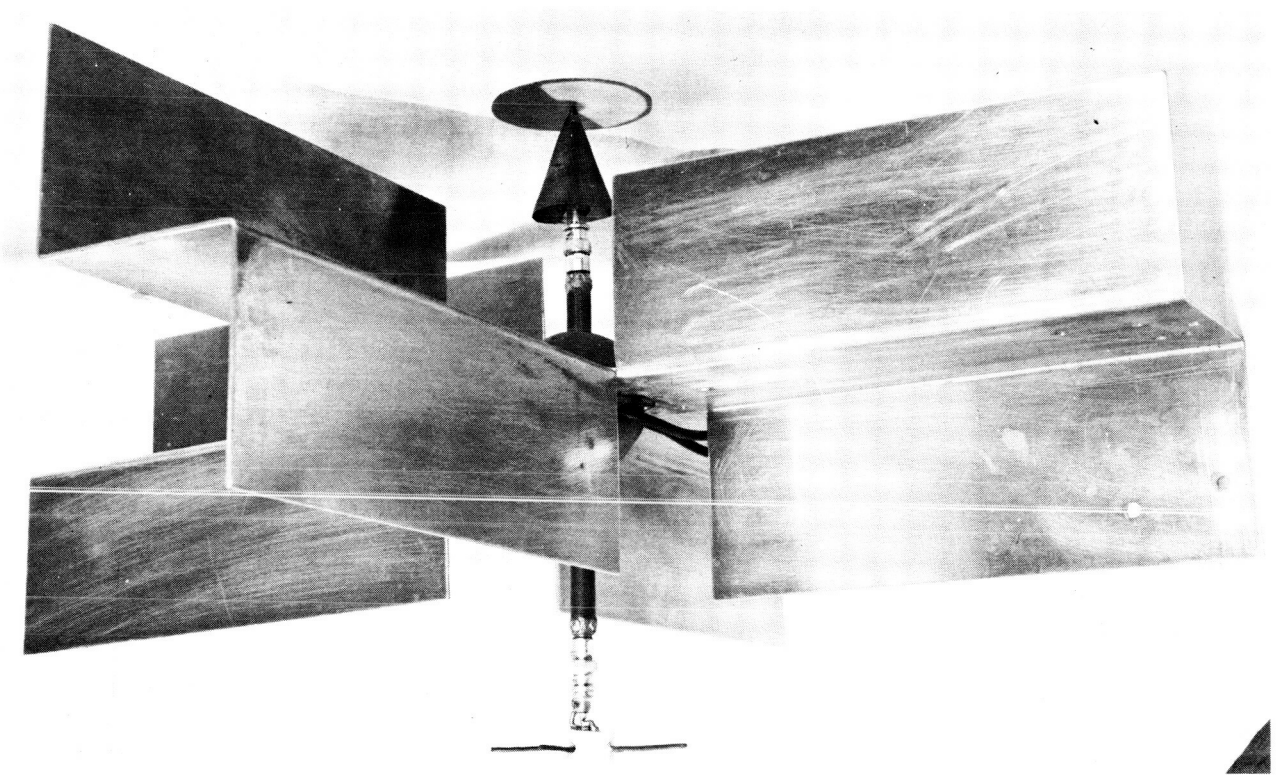
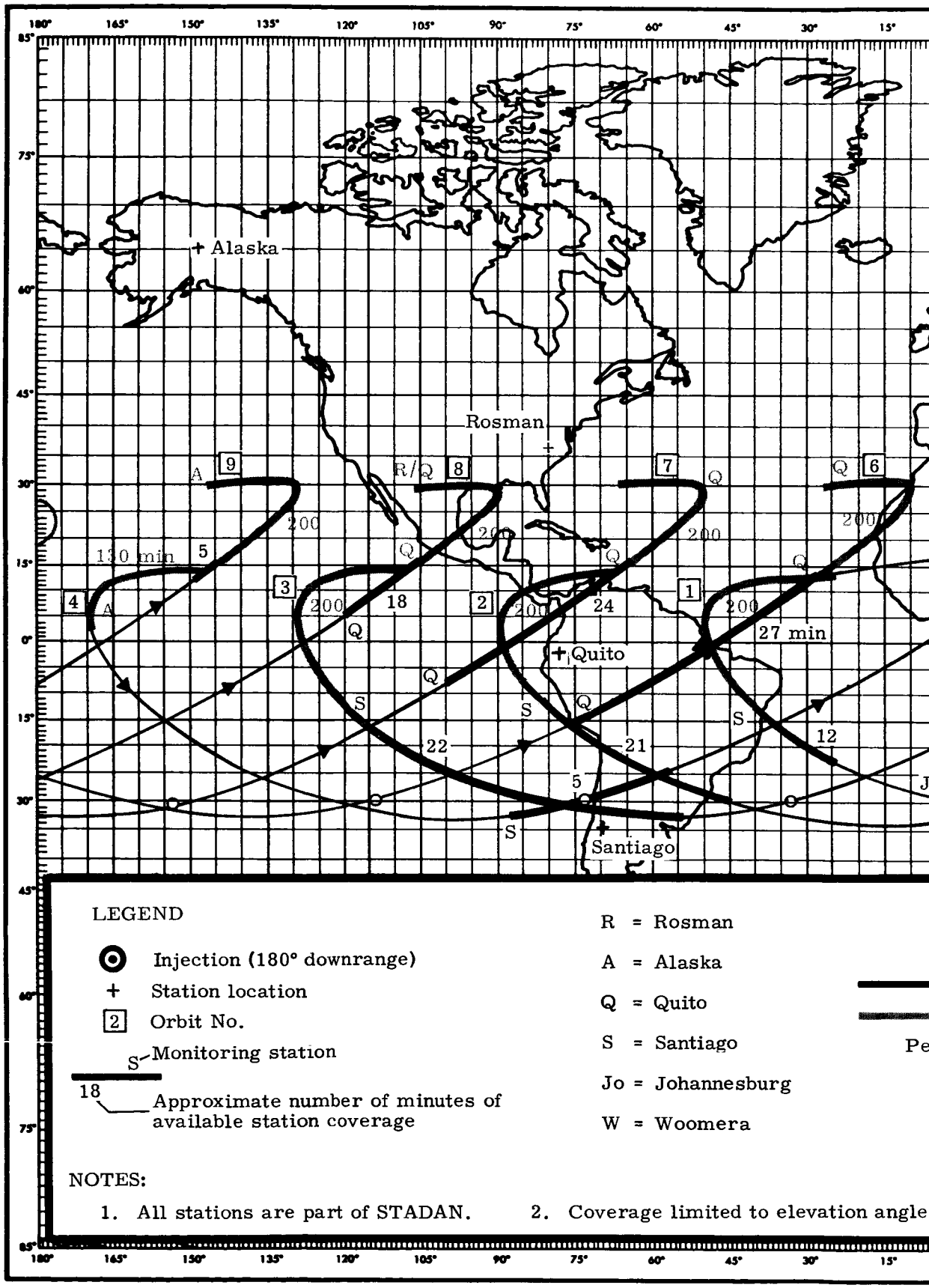


Fig. II-60b. Closeup of Antenna Test Model

The satellite tracking and data acquisition network (STADAN) is recommended to provide this support. Specific stations and their functions are shown in Table II-3. Choice of the stations is based on results shown in Fig. II-61, where the station coverage per orbit below a satellite altitude of 30,000 naut mi is depicted. Minimum antenna elevation angles for this study have been set at + 10°. It should be noted that, in practically every case, at least 3 hr continuous coverage can be provided by a single station as the spacecraft approaches perigee (but not continuous below 5000 naut mi) and again by a different station as the spacecraft begins a new orbit.

A typical perigee pass for spacecraft altitudes below 30,000 naut mi is taken from Fig. II-61, and is described below. It is shown as Orbit No. 3 north-to-south, then changing to Orbit No. 4 south-to-north.

Typical Satellite Altitude (naut mi)	Station Function
20,000	(1) Acquire using Channel 1 carrier
	(2) Begin recording Channels 1 and 2 hit count data
19,000	(3) After 5 min, or as scheduled, continue recording Channel 1 data, command storage readout sequences to be transmitted on Channel 2. Record Channel 2 until all stored data have been recorded (altitude mode goes to high sampling rate)
17,000	(4) If also a RRR station, command Channel 2 into a RRR mode for approximately 5 min.
12,000	(5) Continue recording Channels 1 and 2 data until loss of signal below horizon or perform another RRR measurement if scheduled.
500	(6) Loss of signal
	(12 min no coverage)
	Next Station (Johannesburg)
600	(1) Acquire using Channel 1 carrier or, if in darkness, Channel 2 carrier
800	(2) Record hit count data Channel 1 and Channel 2
1,600	(3) Command RRR measurement (5 min of data)


Alaska
Rosman
Quito
Santiago
130 min
27 min
LEGEND
Injection (180° downrange)
Station location
Orbit No.
Monitoring station
Approximate number of minutes of available station coverage
R = Rosman
A = Alaska
Q = Quito
S = Santiago
Jo = Johannesburg
W = Woomera
NOTES:
1. All stations are part of STADAN.
2. Coverage limited to elevation angle

II-135

1st

ER

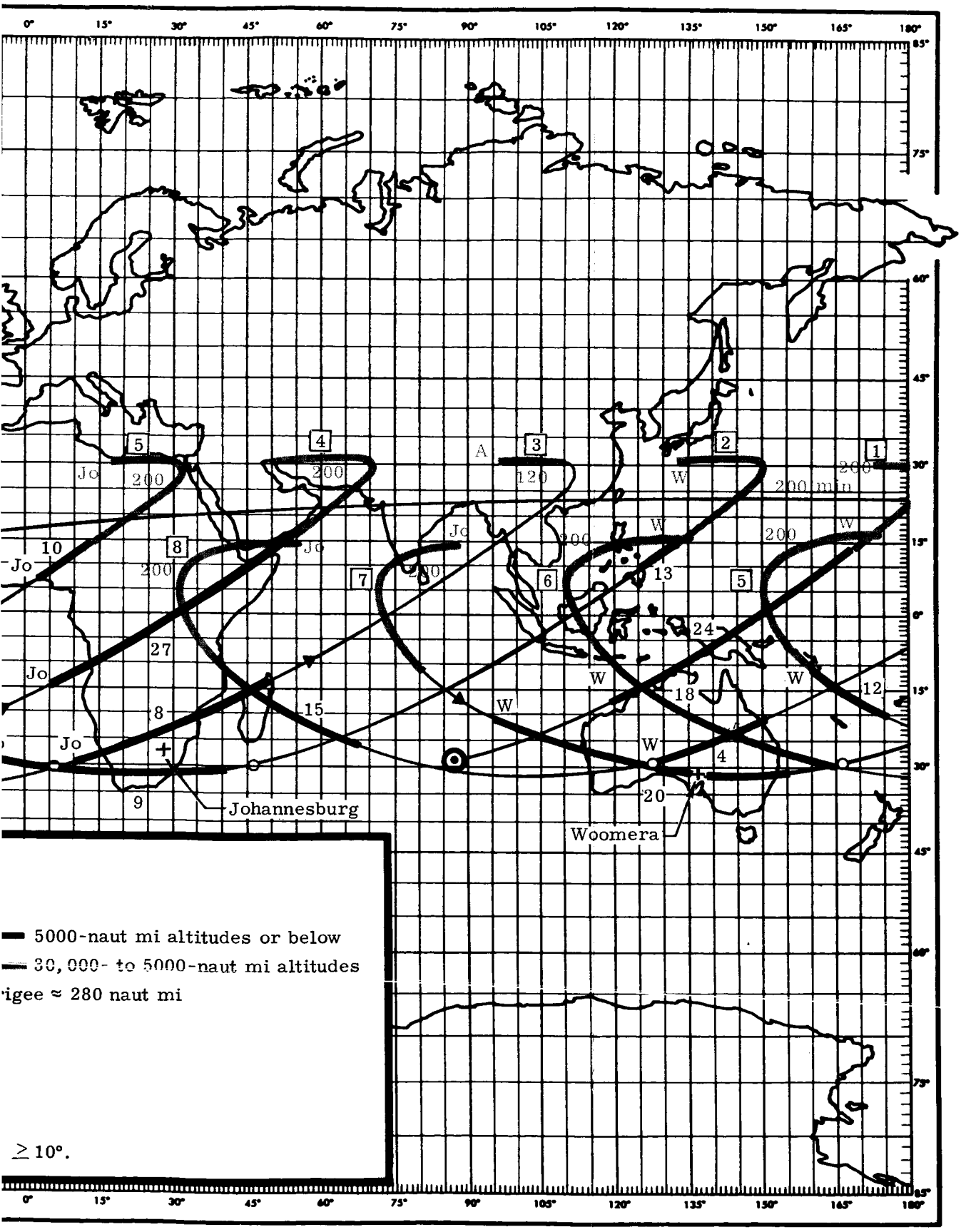


Fig. II-61. Data Acquisition (first nine orbits)

2H

	(4) Continue recording Channels 1 and 2 hit count data
18,000	(5) Command playback of stored data on Channel 2. Continue recording (attitude mode reverted to low rate sampling)
20,000	(6) Continue recording hit count transmitted on Channels 1 and 2
	(7) End pass sequence

It should be noted that continuous recording is not required from 20,000 naut mi, through perigee, and back to 20,000 naut mi. However, since the Zone 1 boundary is estimated to be approximately 12,000 naut mi, it is desirable to continuously record Channel 1 or Channel 2 (primary sensor hit count) below 12,000 naut mi once a station has acquired the signal. This represents approximately 1 hr of recording time per station.

Overhead perigee passes, such as shown on Orbit 1 at Johannesburg, result in about 9 min of recording at that station, with the bulk of the recording being done at Quito and Woomera at spacecraft altitudes above 5000 naut mi.

Major ground station equipment requirements are discussed below.

Data acquisition. The basic data acquisition ground station requirements are: use of a high gain antenna such as the SATAN, with its associated 136 to 137-mc tracking system (see Table II-10 for antenna performance characteristics); use of the Mod I 136 to 137-mc polarization diversity receiving system with predetection diversity combiner, Electrac tracking filters and phase demodulators; biphase demodulators for demodulating the 1280-cps subcarrier must be added.

PCM signal conditioning and display. A capability to display selected words of either Channel 1 or Channel 2 data would be desirable. At least, a means of determining condition of signal such as frame sync, word bit error rate, or equivalent is desired. Capabilities of existing station PCM equipment need further investigation to determine extent of monitoring equipment available.

Recording. Predetection recording is required during stored data playback operations. For recording of VHF Channels 1 and 2 primary sensor hit count data, post-detection recording may be used.

Command. The STADAN tone-digital command console (Consolidated Systems Corporation) system along with the 5-kw high power command system (Ref. II-6) is required. This includes the 22-db disk-on-rod command antenna. Command frequency in the 148-mc region is recommended. Only stations previously scheduled to receive this equipment have been chosen as command stations. See Table II-11 for system performance characteristics.

Tracking. The Goddard VHF range and range rate system equipment, as presently employed on STADAN, plus equipment already planned to bring the present three stations to a total of five is adequate; no additional stations are required for this program. A complete ground system description, analysis and test report is given in Refs. II-4 and II-5, and will not be included here. Standard Minitrack 137 to 138-mc interferometer systems are to be used.

TABLE II-10

SATAN Antenna Characteristics

Antenna velocities	
Autotrack	5 deg/sec
Manual	10 deg/sec
Slew	15 deg/sec
Slave	5 deg/sec
Antenna acceleration	5 deg/sec^2
Antenna angular accuracy (rms)	
Autotrack	0.25^o
Manual	0.5^o
Slave	0.5^o
Antenna beamwidth	16 to 18 deg at 3-db points
Antenna gain	22.5 db
Sky coverage	Hemispheric from 7° above horizon
Receiver sensitivity	-140 db (for 10-cps loop bandwidth)
Receiver loop bandwidth	3 to 300 cps (variable)
Postdetection bandwidth	15 cps $\pm$ 2 cps

TABLE II-11

Command System Performance Characteristics

Power output	5-kw unmodulated into 50-ohm load
VSWR	Not to exceed 1.5:1
Signal inputs	
PCM/AM mode	-0.5 volt across 600 ohms, unbalanced to ground
PCM/AM/AM mode	0 dbm sine wave, 600 ohms, unbalanced to ground
Frequency range	123 mc, 147 to 157 mc; ten oscillator frequencies available, or five frequencies with standby; crystal controlled
Types of emission	PCM/AM Mode--A-1 PCM/AM/AM Mode--A-2
Stability	1.0 part in 10^5/day; rate of change less than 100 cycles per hour
Spurious emission	At least 80 db below carrier
Modulation capability	PCM/AM/AM--100% sinusoidal modulation at 5 kw over operating range 100 to 12,000 cycles
Carrier shift (PCM/AM/AM)	Less than 5% at modulation levels up to 100% at 5 kw (exclusive of carrier shift caused by primary power source regulation)
Audio frequency response	$\pm$ 3 db, 100 to 15,000 cycles, sine wave referred to 1,000 cycles, modulation levels to 95%. In addition, a 100-cycle square wave will have less than 10% tilt or overshoot
Audio frequency distortion (PCM/AM/AM)	Less than 5% between 100 and 12,000 cycles at modulation levels up to 95%
Noise and residual modulation (PCM/AM/AM)	50 db (unweighted) below level corresponding to 100% modulation by sine wave of 1,000 cycles

C. REFERENCES

II-1. "Aerospace Data Systems Standards," National Aeronautics and Space Administration, Goddard Space Flight Center, January 1963.

II-2. "Bulletin 3154 Digital Command Decoder P-106," Consolidated Systems Corporation.

II-3. "Systems Engineering Bulletin number 3225 Detailed Description of Digital Command Decoder Model P 105-70-19," Consolidated Systems Corporation.

II-4. "Goddard Range and Range Rate System Design Evaluation Report" contract number NAS 5-1926, November 1962.

II-5. "Test Evaluation Report for Goddard Range and Range Rate System" contract number NAS 5-1926, August 1964.

II-6. "Satellite Tracking and Data Acquisition Network Facilities Report (STADAN)," National Aeronautics and Space Administration, Goddard Space Flight Center, June 1964.

II-7. Crafts, C. A., "Phase Multilock Communication," MIL Electronics Conference Proceedings, 1958.

II-8. Lawton, J. G., "Comparison of Binary Data Transmission Systems," Mil Electronics Conference Proceedings, 1958.

II-9. Reiger, S., "Error Rates in Data Transmission," IRE Proceedings, May 1958.

II-10. Homic, S., Private Correspondence, Dec 1964.

APPENDIX II-1

Link Calculations for VHF Telemetry and Command Links

VHF telemetry. Table 1-1 shows link calculations for the two VHF telemetry channels. At the 10 bit/sec rate, VHF channel 2 has the same characteristics as VHF channel 1 (except for carrier frequency). At 160 bit/second VHF channel 2 requires 16 times the received data channel signal power. The margins for the two VHF telemetry links are shown in Table 1-2. These margins are based on a spacecraft antenna gain of -6 db assuming a polarization diversity receiving system and no allowance for equipment degradation.

S-Band telemetry. Link calculations for an S-band telemetry system assuming the same modulation as for VHF are shown in Table 1-3 for the purpose of comparing VHF and S-band in a tradeoff of transmitter power requirements and other factors (comparison of VHF and S-band range and range rate is shown in Appendix II-2).

It is to be noted that for equal VHF and S-band margins using the 85-ft dish antenna, a transmitter output power of 5.75 watts at S-band is required as compared to 6 watts for VHF. (With an omnidirectional spacecraft antenna and a dish antenna on the ground, transmitter power is independent of frequency except for equipment loss factors such as line loss, etc.)

For equal performance margins when using the 40-ft dish for S-band and the SATAN antenna for VHF, an S-band transmitter output of 8.3 watts would be required.

Command link calculations. The command link calculations are shown in Table 1-4. A reliable command range of 100,000 naut mi is indicated with a 6-db margin for equipment degradation or additional loss in antenna gain. Command to 200,000 miles and greater should be experienced under favorable spacecraft orientations or with no margin allowance. A bit error rate of 1 in 5000 is assumed for the ranges quoted.

TABLE 1-1

VHF Telemetry Link--Channel 1 (frequency ≈ 136.4 mc)

	85-ft Dish Antenna	SATAN Antenna*
Boltzmann's constant	-198.6 dbm	
Equivalent receiver temperature, 2690°	+34.3 db	
10 bit/sec	+10.0 db	
11-db S/N ($P_E = 10^{-4}$ PSK)	+11.0 db	
Required data channel power	-143.3 dbm	-143.3 dbm
Required carrier power, 10 ~ bw	-144.3 dbm	-140.0 dbm**
Transmitter power (6 w)	+37.8 dbm	+37.8 dbm
Carrier modulation loss, (1.6 rad peak)	-7.0 db	-7.0 db
Spacecraft diplex loss, etc.	-2.0 db	-2.0 db
Ground system loss	-1.5 db	-1.5 db
Spacecraft antenna gain***	-6.0 db	-6.0 db
Ground antenna gain	+27.0 db	+22.0 db
180,000 naut mi space loss	-185.7 db	-185.7 db
Received carrier power	-137.4 dbm	-142.4 dbm
Required carrier power	-144.3 dbm	-140.0 dbm***
Data channel mod loss	-2.0 db	-2.0 db
Received data channel power	-132.4 dbm	-137.4 dbm
Required data channel power	-143.3 dbm	-143.3 dbm
180,000 naut mi signal margin****		
Carrier power margin	+6.9 db	-2.4 db
Data channel margin	+10.9 db	+5.9 db

*SATAN antenna at Quito, Santiago, Johannesburg and Woomera, 85 ft dish at Rosman and Ulaska.

**Per Ref. II-6.

***A polarization diversity receiving system is assumed at ground station.

****No allowance made for equipment degradation.

TABLE 1-2

Margins--VHF Telemetry Link (136 to 137 mc) and Beacon*

Slant Range (naut mi)	Signal Power Margins (db)					
	85-ft Dish Antenna			SATAN Antenna		
	Residual Carrier	Data Channel		Residual Carrier	Data Channel	
		10 bit/sec	160 bit/sec		10 bit/sec	160 bit/sec
	10 cycle carrier tracking loop bandwidth					
180,000	+6.9	+10.9	-1.1	-2.4	+5.9	-6.1
128,000	+9.9	+13.9	+1.9	+0.6	+8.9	-3.1
90,000	+12.9	+16.9	+4.9	+3.6	+11.9	-0.1
63,900	+15.9	+19.9	+7.9	+6.6	+14.9	+2.9
45,200	+18.9	+22.9	+10.9	+9.6	+17.9	+5.9
32,000	+21.9	+25.9	+13.9	+12.6	+20.9	+8.9
22,600	+24.9	+28.9	+16.9	+15.6	+23.9	+11.9
16,000	+27.9	+31.9	+19.9	+18.6	+26.9	+14.9
	Change to 100 cycle carrier tracking loop bandwidth					
11,400	+20.7	+34.9	+22.9	+11.6	+29.9	+17.9
8,050	+23.7	+37.9	+25.9	+14.6	+32.9	+20.9
4,030	+29.7	+43.9	+31.9	+20.6	+38.9	+29.9

*Unmodulated residual carrier.

TABLE 1-3

Link Calculations for S-Band (1705 mc)
(180,000 naut mi)

	Telemetry Link
	85-ft Dish
Required data channel power*	-143.3 dbm
Required carrier power*	-144.3 dbm
Spacecraft antenna gain**	-6.0 db
Carrier modulation loss	-7.0 db
Spacecraft system losses	-3.0 db
Ground system loss	-2.0 db
Ground antenna gain	+50.6 db
Space loss--180,000 naut mi	-207.6 db
	-175.0 db
Received carrier power	-137.4 dbm
Required transmitter power 5.75 watts	+37.6 dbm
Data channel mod loss	-2.0 db
Required data power	-143.3 dbm
Received data power	-132.4 dbm

	Margins (db)	
	85-ft Dish	40-ft Dish***
Carrier power	+6.9 db	-0.3 db
Data power	+10.9 db	+4.3 db

NOTE:

No allowance for equipment degradation.

40-ft dish at Quito, Santiago, Johannesburg and Woomera

*Assumed same as for VHF

**A polarization diversity system is assumed for ground station.

***Gain of 40-ft dish 6.6 db less than 85-ft dish.

TABLE 1-4

148-mc Command Link Calculations Tone Digital System

Equivalent receiver temperature, 3000° K	+34.7 db
3-db bandwidth = 30 kc	+44.8 db
Boltzmann's constant	-198.6 dbm
Receiver noise power	-119.1 dbm
Modulation loss (modulation 75% AM)	+5.5 db
Required receive power* (1 to 1 subcarrier S/N at decoder)	-113.6 dbm
Polarization loss (circular)	-3.0 db
Spacecraft antenna gain	-6.0 db
Spacecraft losses	-5.0 db
Ground system losses	-1.0 db
Ground antenna gain	+22.0 db
Ground transmitter power, 5 kw	+66.9 dbm
Space loss, 180,000 naut mi	-186.6 db
Received signal	-112.7 dbm

Range (naut mi)	Margin (db)
180,000	+0.9
160,000	+1.9
90,000	+6.9
30,000	+16.4
10,000	+25.9

*For a bit error rate of 1 in 5000.

APPENDIX II-2

TRACKING LINK CALCULATIONS

This appendix contains link calculations for Minitrack interferometer and range and range rate tracking systems.

1. Minitrack Interferometer

Link calculations for Minitrack interferometer measurements are shown in Table 2-1. Anticipated range is approximately 1100 naut mi with no margin. Minus 12 db has been used for spacecraft antenna gain in this case. Attitude of the spacecraft will greatly affect the range attainable by possibly as much as plus or minus 12 db due to the fixed linear polarization of the ground antennas and the use of a modified disc cone on the spacecraft.

2. Range and Range Rate

Link calculations for both the recommended VHF system and an S-band system are shown in Tables 2-2 and 2-3 for the up and down links, respectively. The VHF system outperforms the S-band system by about 12 db in both cases. Range and range rate measurements to a slant range of about 100,000 mi are anticipated. With extremely slow tumble rates and favorable spacecraft orientation, ranges to 180,000 naut mi may be experienced.

TABLE 2-1

Link Calculations--Minitrack Interferometer Tracking

Required receive signal strength = 120 dbm*
Frequency = 136.2 mc

Transmitter power	+ 37.8 dbm (6 watts)
Carrier modulation loss	- 7.0 db (1.6 rad peak)
Spacecraft system loss	- 2.0 db
Ground system loss	- 1.5 db
*Spacecraft antenna gain	- 12.0 db
Ambiguity antenna gain	+ 6.4 db
	+ 21.7 dbm
Required carrier signal	- 120.0 dbm
Allowable space loss	- 141.7 db

$$\text{Space loss} = 37 \text{ db} + 20 \log f + 20 \log D$$

$$141.7 \text{ db} = 37 \text{ db} + 42.7 \text{ db} + 20 \log D$$

$$D = \text{antilog } 3.1$$

$$D = 1260 \text{ stat mi}$$

$$D = 1100 \text{ naut mi}$$

where

D = slant range (no margin)

*For fixed, linearly polarized ground antennas it is difficult to choose an appropriate antenna gain for the spacecraft antenna configuration described.

TABLE 2-2

Link Calculations--Range and Range Rate Up-Link

Frequency	148 mc	2271 mc
BW = 80 kc	+ 49.0 db	
NF = 9 db 2010° K		
Antenna temperature = 990° K		
Equivalent receiver temperature = 3000° K	+ 34.8 db	
Boltzmann's constant	- 198.6 dbm	
Receiver noise power (80 kc)	-114.8 dbm	
(in 80 kc BW) allow 6 db S/N ratio	+ 6.0 db	
Required receive power	-108.8 dbm	-105.0 dbm*
(10 kw) ground transmitter	+ 70.0 dbm	+ 70.0 dbm
Ground antenna gain	+ 20.0 db	+ 35.0 db
Spacecraft antenna gain	- 6.0 db	- 6.0 db
Polarization loss	- 3.0 db	- 3.0 db
Spacecraft system loss	- 5.0 db	- 5.0 db
180,000 naut mi space loss	-186.6 db	-210.1 db
Ground system losses	- 1.5 db	- 2.0 db
Total received signal power	-112.1 dbm	-121.1 dbm
Required receive power	-108.8 dbm	-105.0 dbm
	- 3.3 db	- 16.1 db

RRR Up-Link Signal Margin (db)

Range (naut mi)	VHF	S-Band
180,000	-3.3 db	-16.1 db
90,000	+2.7 db	-10.1 db
45,200	+8.7 db	- 4.1 db

*From Ref. II-5 (squelch level)

TABLE 2-3

Link Calculations--Range and Range Rate Down Link

	136.1 mc	1705 mc
Spacecraft antenna gain	- 6.0 db	- 6.0 db
Polarization loss	- 3.0 db	- 3.0 db
Ground antenna gain	+ 19.0 db	+ 33.0 db*
Spacecraft diplex and line loss	- 2.0 db	- 3.0 db
Ground system loss	- 1.0 db	- 2.0 db
Transmitter power	37.8 dbm	(to find) (43.6 dbm)
Modulation loss	- 3.0 db	- 3.0 db
	+ 41.8 dbm	+ 59.6
Required receive carrier power	-144.0 dbm	-148.0 dbm
Received carrier power	-144.0 dbm	-148.0 dbm
Allowable space loss	-185.8 db	-207.6

VHF 6-watt spacecraft transmitter	Range (no margin)	180,000 naut mi	S-band *22.9 watt spacecraft transmitter
	Range 6 db margin	≈ 90,000 naut mi	

*14-ft dish antenna on ground

APPENDIX II-3

MODULATION SYSTEM PERFORMANCE COMPARISONS

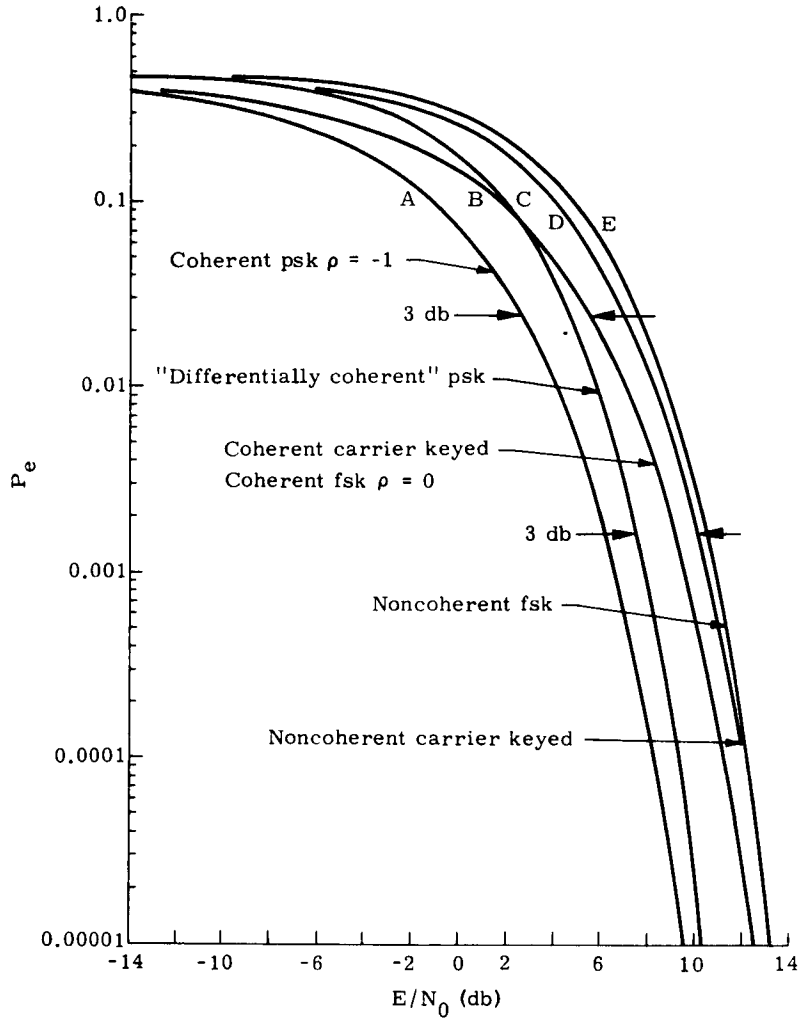
Modulation and coding systems considered potentially applicable to the cislunar micrometeoroid communications system are PCM-FM, PCM-PSK, PFM, coherent and noncoherent orthogonal coding, and error correction methods. These have been considered from the point of view of modulation efficiency, complexity for a given data resolution and compatibility with existing ground networks. Since the data is inherently digital and the resolution requirements essentially rule out analog systems, digital modulation and coding systems have been considered from the outset.

Performance comparisons for binary coded modulation methods are shown in Fig. 3-1. This data shows coherent PSK (180° biphase modulation) to be clearly superior to all other serial binary modulation systems by a factor of at least 2 db. Furthermore, coherent PSK systems are easy to instrument and are compatible with the STADAN networks.

These curves are, of course, theoretical and while they can be approached very closely by practical systems, there are certain practical constraints which must be considered in the use of such data. For example, data shown for coherent PSK assumes carrier and bit synchronization information are available at the demodulation terminal. But since carrier phase information is absent in a 180° biphase modulation system, use of subcarriers is generally required to convey such information.

Similar limitations apply to other modulation techniques and, when these are taken into account, the techniques will, in general, maintain similar performance comparisons.

In the case of coherent PSK, the problem of providing a coherent reference for demodulation is usually solved by phase modulating the carrier by two subcarriers (PCM-PSK-PM). The modulation indices are selected so that sufficient residual carrier remains for carrier acquisition in a narrow band receiver tracking loop. The binary data is biphase modulated on one of the subcarriers and the second subcarrier provides a coherent reference for the data subcarrier demodulation. This process will in general result in a data subcarrier modulation loss (subcarrier power/total power) of between 3 and 5 db, depending upon particular choices of the subcarrier modulation indices. On the other hand, a data subcarrier modulation loss of about 2 db is reasonable with a single subcarrier using full-wave square law



Ref:

"Lawton, J. C., "Comparison of Binary Data Transmission Systems," Cornell Aeronautical Laboratory, Inc., 1958 Conference Proceedings, 2nd National Convention on Military Electronics, pp 54 to 61.

Fig. 3-1. Probability of Error Versus Signal Energy/Noise Power Density

rectification and narrow band filtering with frequency division to extract the reference subcarrier.

Simple relationships for determining carrier and subcarrier modulation loss values as a function of the modulation indices are listed below:

Let $\Delta\theta_n$ = peak modulation index on the nth subcarrier

P_c = carrier power

$P_{sc}(n)$ = nth subcarrier power

P_{tot} = total transmitter power

Then in terms of the 0th and 1st order Bessel functions of the first kind,

$$\frac{P_c}{P_{tot}} = \left[J_0(\Delta\theta_1)\, J_0(\Delta\theta_2)\cdots J_0(\Delta\theta_n)\right]^2 \qquad (3\text{-}1)$$

$$\frac{P_{sc}(n)}{P_{tot}} = 2\left[J_0(\Delta\theta_1)\, J_0(\Delta\theta_2)\cdots J_0(\Delta\theta_n)\, \frac{J_n(\Delta\theta_n)}{J_0(\Delta\theta_n)}\right]^2 \qquad (3\text{-}2)$$

or

$$\frac{P_{sc}(n)}{P_{tot}} = 2\left[J_0(\Delta\theta_1)\, J_0(\Delta\theta_2)\cdots J_0(\Delta\theta_{n-1})\, J_1(\Delta\theta_n)\right]^2 \qquad (3\text{-}3)$$

Thus, for a single subcarrier,

$$\frac{P_c}{P_{tot}} = \left[J_0(\Delta\theta)\right]^2 \qquad (3\text{-}4)$$

and

$$\frac{P_{sc}}{P_{tot}} = 2\left[J_1(\Delta\theta)\right]^2 \qquad (3\text{-}5)$$

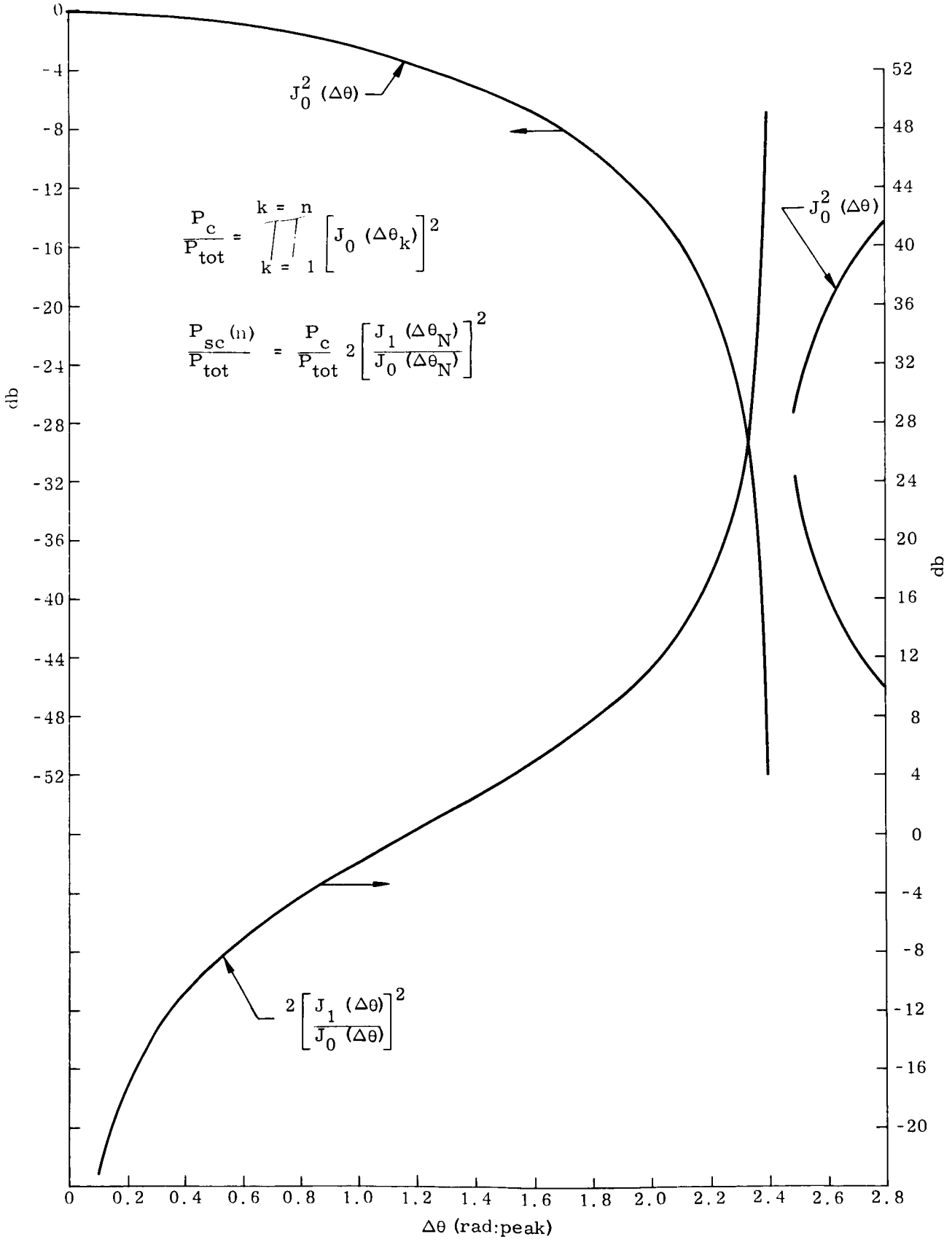


Fig. 3-2. Carrier and Subcarrier Power Nomogram

For two subcarriers,

$$\frac{P_c}{P_{tot}} = \left[J_0(\Delta\theta_1)\, J_0(\Delta\theta_2) \right]^2 \qquad (3\text{-}6)$$

and,

$$\frac{P_{sc(1)}}{P_{tot}} = \left[J_1(\Delta\theta_1)\, J_0(\Delta\theta_2) \right]^2 \qquad (3\text{-}7)$$

$$\frac{P_{sc(2)}}{P_{tot}} = \left[J_1(\Delta\theta_2)\, J_0(\Delta\theta_1) \right]^2 \qquad (3\text{-}8)$$

Pertinent values for use in these relationships are listed in Table 3-1, and these data are plotted in Fig. 3-2.

TABLE 3-1
(Reference II-10)

$\Delta\theta$	$J_0(\Delta\theta)$	$10 \log J_0^2(\Delta\theta)$	$J_1(\Delta\theta)$	$10 \log J_1^2(\Delta\theta)$	$10 \log 2 \left[J_1(\Delta\theta)/J_0(\Delta\theta)\right]^2$
0	+1.0000	-0 db	+ 0		
0.1	+0.9975	-0.02	+ 0.0499	- 26.0 db	- 23.0 db
0.2	+0.9900	-0.09	+ 0.0995	- 20.0	- 16.9
0.3	+0.9776	-0.20	+ 0.1483	- 16.6	- 13.4
0.4	+0.9604	-0.35	+ 0.1960	- 14.2	- 10.8
0.5	+0.9385	-0.55	+ 0.2423	- 12.3	-8.74
0.6	+0.9120	-0.80	+ 0.2867	- 10.9	-7.10
0.7	+0.8812	-1.10	+ 0.3290	-9.66	-5.55
0.8	+0.8463	-1.45	+ 0.3688	-8.66	-4.20
0.9	+0.8075	-1.86	+ 0.4059	-7.83	-2.96
1.0	+0.7652	-2.32	+ 0.4401	-7.13	-1.80
1.1	+0.7196	-2.86	+ 0.4709	-6.54	-0.67
1.2	+0.6711	-3.46	+ 0.4983	-6.05	+0.42
1.3	+0.6201	-4.15	+ 0.5220	-5.65	+1.51
1.4	+0.5669	-4.93	+ 0.5419	-5.32	+2.62
1.5	+0.5118	-5.82	+ 0.5580	-5.07	+3.76
1.6	+0.4554	-6.83	+ 0.5699	-4.88	+4.96
1.7	+0.3980	-8.00	+ 0.5778	-4.76	+6.25
1.8	+0.3400	-9.37	+ 0.5815	-4.71	+7.67
1.9	+0.2818	-11.0	+ 0.5812	-4.71	+9.30
2.0	+0.2239	-13.0	+ 0.5767	-4.78	+11.2
2.1	+0.1660	-15.6	+ 0.5683	-4.91	+13.7

TABLE 3-1 (continued)

$\Delta\theta$	$J_0(\Delta\theta)$	$10 \log J_0^2(\Delta\theta)$	$J_1(\Delta\theta)$	$10 \log J_1^2(\Delta\theta)$	$10 \log 2\ J_1(\Delta\theta)/J_0(\Delta\theta)^2$
2.2	+0.1104	- 19.1	+ 0.5560	- 5.10	+17.0
2.3	+0.0553	- 25.1	+ 0.5399	- 5.35	+22.8
2.4	+0.0025	- 52.0	+ 0.5202	- 5.68	+49.3
2.5	-0.0484	- 26.3	+ 0.4971	- 6.07	+23.2
2.6	-0.0968	- 20.3	+ 0.4708	- 6.54	+16.8
2.7	-0.1424	- 16.9	+ 0.4416	- 7.10	+12.8
2.8	-0.1850	- 14.7	+ 0.4097	- 7.75	+9.96
2.9	-0.2243	- 13.0	+ 0.3754	- 8.51	+7.50
3.0	-0.2601	- 11.7	+ 0.3391	- 9.39	+5.32

While system optimization has not been performed for a two subcarrier combination for this application, it is felt that values of $\Delta\theta_1$ and $\Delta\theta_2$ of 1.6 and 0.8 rad peak are on the favorable side of such an optimization from a modulation loss viewpoint. Using these values, the above relationships, and the data in Table 3-1, it is determined that the carrier modulation loss is -8.2 db, the data subcarrier loss -3.3 db, and the reference subcarrier modulation loss -12.3 db.

In contrast with this is the single subcarrier case. Using the same data subcarrier mod index, the data subcarrier and carrier modulation losses are -1.9 and -7 db, respectively. After square-law rectification of the data subcarrier at the receiver, the recovered double frequency power is reduced from the received data subcarrier power by a maximum of 13 db. This assumes a full-wave linear detector instead of square-law detector. In practice, it is expected that this loss function will be substantially less, a conclusion supported by our laboratory tests which show a value of around 8 db for simple diode detectors operated in the near linear region. Since this now constitutes the reference subcarrier and, in either case (2 subcarriers or one), the reference subcarrier is subjected to the same subsequent processing, it can be reasonably concluded that the single subcarrier system is superior* to the case where the data subcarrier is transmitted directly. Clearly, if a second subcarrier were provided at a comparable level, the modulation loss on the data subcarrier would be substantially in excess of the -3.3 db value quoted in the example. Accordingly, the single subcarrier with reference derivation approach is recommended for this application where spacecraft RF power is at a premium.

* Actually, the noise properties in the two cases are different, and the numerical comparison made here is based on identical noise spectral densities as well as probability densities.

As previously noted, multilevel FSK (PFM) has been considered as a possible competitor to PCM-PSK. While this appears to represent a number of equipment complexities and is rejected largely on this basis, the analyses are included in this report for the sake of completeness as follows:

In the case of binary FSK, the receiver model consists of two filters matched to frequencies F_1 and F_2 (corresponding to ones and zeros), followed by envelope detectors and a "greatest of" decision circuit. In the case of multilevel FSK, there are M such filters, followed by envelope detectors and a "greatest of" decision circuit. Thus, in binary FSK and k bit resolution, 2^k data words are required; each data word consists of n serial bits represented by one of two possible frequencies. In multilevel FSK, there are also 2^k data words but each is represented by one of 2^k frequencies.

For binary FSK, the bit error probability can be shown to be

$$P_e = \frac{1}{2} e^{-E/2N_o} \tag{3-9}$$

where E/N_o represents the energy per bit to noise power density ratio. Since the probability of word error is

$$P_{ew}\,(FSK) = 1 - (1-P_e)^k, \tag{3-10}$$

for small p_e,

$$P_{ew} = k p_e \tag{3-11}$$

also, from (3-9)

$$\frac{E}{N_o} = 2 \ln \frac{1}{P_e} \tag{3-12}$$

thus, from (3-11) and (3-12)

$$\frac{E}{N_o}\,(FSK) = 2 \ln \frac{k}{2 P_{ew}} \tag{3-13}$$

Let the transmission word rate be R bps. Then the bit rate is kR bps so that the received power required for a specified word error rate P_{ew} (FSK) is

$$P_{rec}\ (\text{binary FSK}) = 2\ k R N_o \ln \frac{k}{2 P_{ew}} \qquad (3\text{-}14)$$

Consider now the corresponding power requirement for M'ary FSK.

By straightforward analysis, one can show that the word error rate can be written as

$$P_{ew}\ (\text{M'ary FSK}) \simeq (2^{k} - 1)\ P_e\ (\text{binary FSK}) \qquad (3\text{-}15)$$

for small P_e.

From this and the relationship in (3-12), we can write that the received power required to provide a specified word error rate, P_{ew} (M'ary) is:

$$P_{rec}\ (\text{M'ary}) = 2\ R\ N_o \ln \frac{2^{k-1}}{2 P_{ew}\ (\text{M'ary})} \qquad (3\text{-}16)$$

A comparison of the relative power requirements of binary and M'ary FSK can now be performed by taking the ratio of (3-14) and (3-16): Thus,

$$n = \frac{P_{rec}\ (\text{BFSK})}{P_{rec}\ (\text{MFSK})} = k \frac{\ln k - \ln 2Pw}{\ln 2^{k-1} - \ln 2Pw} \qquad (3\text{-}17)$$

For k = 7 bit resolution, and a word error probability of 10^{-4},

$$n(7) = 5.5 \qquad (3\text{-}18)$$

Thus, for 128 level data, binary FSK requires 7.4 db greater transmitter power than M'ary FSK. Since binary FSK as defined is 3.7 db poorer than PSK, it is concluded that M'ary FSK requires about 3.7 db less power than coherent biphase PSK for 7-bit data resolution and a 10^{-4} word error probability. Thus, noncoherent M'ary FSK and coherent M'ary PSK offer comparable improvements over binary PSK. As previously noted however, 128 orthogonal matched filters are required to achieve this advantage, not to mention the complexities involved in generating these orthogonal signals. For these reasons, M'ary FSK was rejected for this application.

While bi-orthogonal coded PSK is a logical extension of binary PSK and offers improvements comparable to M'ary FSK, this approach was also rejected for complexity reasons, although it is felt that the results obtained for the proposed resolution will more nearly approach the theoretical than will M'ary FSK.

Error correction coding methods have also been considered in this study and are not considered to offer any significant improvement over uncoded data for the same information rate. The form and the results of this analysis are similar to those obtained by Reiger, Ref. II-9, and, for this reason, are not included in this report.

PCM-FM modulation was also considered briefly in this study but was rejected from the outset. The low data rates in combination with available (practical) receiver bandwidths and the thresholding problem appeared to preclude the possibility of approaching an optimum system; for this main reason PCM-FM was not given further consideration.

APPENDIX II-4

DATA PARITY CHECK ERROR PROBABILITIES

Let P_{be} = probability of bit error

The probability of having a sequence of n bits in which there is a single bit error is the joint probability of one error and n-1 successes

$$P_1 = P_{be} (1-P_{be})^{n-1} \tag{4-1}$$

To determine the probability that in given n observations, there would be exactly one bit error, it is necessary to consider all possible sequences of one error in n bits. Since there are n bit positions, there are n ways in which a single error can occur.

Thus,

$$P_1^n = n\ P_{be} (1-P_{be})^{n-1} \tag{4-2}$$

More generally, the probability of r errors in n observations is

$$P_r^n = \underbrace{\frac{n!}{r!\,(n-r)!}}_{\substack{\text{number of arrangements of r errors in n events}}} \underbrace{P_{be}^{\,r}\ (1-P_{be})^{n-r}}_{\substack{\text{probability of a sequence length, n, in which r errors are observed}}} \tag{4-3}$$

Expression (4-3) gives the probability of observing r errors in n observations.

The probability of observing r or more errors in n observations is

$$P_{\geq r}^n = P_{r+1}^n + P_{r+2}^n + \ldots P_n^n$$

$$= \sum_{i=r}^{n} P_i^n = \sum_{i=r}^{n} \frac{n!}{i!\,(n-i)!}\ P_{be}^{\,i}\ (1-P_{be})^{n-1}$$

$$= \sum_{i=r}^{n} \binom{n}{i} P_{be}^{\ i} (1-P_{be})^{n-1} \qquad (4-4)$$

Also, the probability of less than r errors is

$$P_{<r}^{n} = 1 - P_{\geq r}^{n}$$

$$= 1 - \sum_{i=r}^{n} \binom{n}{i} P_{be}^{\ i} (1-P_{be})^{n-1} \qquad (4-5)$$

But this can also be written directly as (6)

$$P_{<r}^{n} = P_0^n + P_1^n + \ldots P_{r-1}^n$$

$$= \sum_{i=0}^{r-1} \binom{n}{i} P_{be}^{\ i} (1-P_{be})^{n-i} \qquad (4-6)$$

An obvious result, since the probability that one of the possible outcomes will be observed must be unity; i.e.,

$$\sum_{i=0}^{r-1} \binom{n}{i} P_{be}^{\ i} (1-P_{be})^{n-1} + \sum_{i=r}^{n} \binom{n}{i} P_{be}^{\ i} (1-P_{be})^{n-i} = 1 \qquad (4-7)$$

Consider the inclusion (or addition) of an odd parity check bit. All even errors are now accepted as being correct and all odd word errors are flagged. Since the sums of the probabilities of all possible events must be unity, we can write

$$\underbrace{P_0^{\,n}}_{\text{probability of correct word } [P_c]} + \underbrace{P_2^{\,n} + P_4^{\,n} + \ldots}_{\text{probability of acceptance of a word in error } [P_c(\text{error})]} + \underbrace{P_1^{\,n} + P_3^{\,n} + P_5^{\,n} + \ldots}_{\text{probability of word rejection due to parity check failure } [P_{\text{rejection}}]} = 1 \qquad (4-8)$$

$$P_c = P_0^n = \binom{n}{0} P_{be}^0 (1-P_{be})^n = \frac{n!}{0!\,n!} (1-P_{be})^n = (1-P_{be})^n \simeq$$

$$1-nP_{be} \qquad (4-9)$$

$$P_c(\text{error}) = 1- P_c - P_{\text{reject}} \qquad (4-10)$$

An upper bound value of this can be established by neglecting all odd parity check failures greater than 1; thus,

$$P_c(\text{error}) < 1-P_c - P_1^n = 1- (1-P_{be})^n - n P_e (1-P_{be})^{n-1} \qquad (4-11)$$

Since $(1-x)^n \simeq 1-nx$ for $x<<1$

$$P_c(\text{error}) < 1-1 + n P_{be} - n P_{be} + n (n-1) P_{be}^2 \cong n(n-1) P_{be}^2$$

for P_{be} small, say less than 10^{-1} (4-12)

Observe that a lower bound for the probability of an incorrect acceptance of a word is just

$$P_c(\text{error}) > P_2^n = \frac{n!}{2\,!\,(n-2)!} P_{be}^2 (1- P_{be})^{n-2}$$

$$= \frac{n(n-1)}{2} P_{be}^2 \left[1-(n-2) P_{be}\right]$$

$$= \frac{n(n-1)}{2} P_{be}^2 - n(n-1)(n-2) P_{be}^3$$

$$\simeq \frac{n(n-1)}{2} P_{be}^2$$

Thus,

$$\frac{n(n-1)}{2} P_{be}^2 < P_c(\text{error}) < n(n-1) P_{be}^2 \qquad (4-13)$$

By similar reasoning, the

$$P_{rejection} < 1 - P_0^n - P_2^n = 1-(1-P_{be})^n - P_2^n$$

$$< n P_{be} - \frac{n(n-1)}{2} P_{be}^2 - n(n-1)(n-2) P_{be}^3 \qquad (4-14)$$

$$< n P_{be} \left[1 - \frac{n-1}{2} P_{be}\right]$$

$$P_{rejection} > P_1^n = nP_{be}(1-P_{be})^{n-1}$$

Thus,

$$nP_{be}(1-n-1P_{be}) < P_{rejection} < n P_{be}(1 - \frac{n-1}{2} P_{be}) \qquad (4-15)$$

The probable fraction of the words in error which will be detected by the parity check is

$$\alpha_{rej} = \frac{P_1^n + P_3^n + P_5^n + \cdots}{P_1^n + P_3^n + P_5^n + \cdots P_2^n + P_4^n + P_6^n + \cdots} \qquad (4-16)$$

$$> \frac{P_1^n}{1-P_0^n} = \frac{\frac{n!}{1!\,(n-1)!} P_{be}(1-P_{be})^{n-1}}{1-(1-P_{be})^n} \cong 1-(n-1)P_{be} \qquad (4-17)$$

Note, this same result would be obtained by the ratio

$$\frac{P_{reject} \text{ expressed in (4-15)}}{P_c \text{ (error) in (4-10)} + P_{reject \text{ in (4-15)}}} = \frac{P_{reject}}{P_{word\ error}}$$

The probable fraction of the words in error which go undetected is

$$\alpha_{acc} = \frac{P_2^n + P_4^n + \cdots}{1-P_c} < \frac{1-P_c - P_1^n}{1-P_c} \text{ from (4-10) and (4-11)} \qquad (4-18)$$

From (4-12) and (4-9)

$$\alpha_{acc}(\text{error}) < \frac{n(n-1)\,P_{be}^{2}}{nP_{be}} = (n-1)P_{be} \qquad (4\text{-}19)$$

If repeated data playbacks are not used, then, for the same bit error probability, the parity coded data requires $\frac{n}{n-1}$ times as much power as does the uncoded transmission.

However, for this small penalty the parity check flags essentially all of the bad data. Specific comparison is made as follows:

The probability of word error in the uncoded case, n-1 bits per word is

$$P_{we_{uncoded}} = 1 - P_0^{n-1} \cong n-1\,P_{be} \quad \text{for } P_{be} << 1 \qquad (4\text{-}20)$$

In the parity coded case,

$$P_{we_{coded}} \cong n\,P_{be} \qquad (4\text{-}21)$$

Clearly from (4-16) and (4-19), the parity coded system detects approximately all errors which go undetected in the uncoded case. The fraction of those in error which go undetected is less than the word error probability of the uncoded system.

If the data are repeated once, however, differences in the uncoded values are unresolvable; thus, twice as many errors result. If the parity check data is repeated once, the probability of the same rejected word being repeated again is the square of the word error rejection probability which will, in general, be low. The probability of not detecting a word in error is still the same in the repeat message, so twice as many words are accepted in error. The probability of the same word acceptance is of course, negligible. Since the error word acceptance probability is already quite low, this is not significant when compared with the uncoded case.

Examples

Let n = 8 bits 7 + parity $P_{be} = 10^{-3}$

From (4-12)

$28 \times 10^{-6} < P_c$ (error) $< 56 \times 10^{-6}$ (acceptance of an incorrect word)

$P_{rejection} \simeq 8 \times 10^{-3}$ (4-15)

Probability of rejection of same word on second playback is $\simeq 64 \times 10^{-6}$

Let n = 5000 words per transmission

The probable number of words accepted in error $\simeq 5 \times 10^3 \times 40 \times 10^{-6}$

$= 0.2$ word

The probable number rejected = 40

If the data were uncoded, there would be, on the average, 40 words in error.

For $P_{b\epsilon} = 10^{-4}$, the numbers become

P_c (error) $\simeq 40 \times 10^{-8}$

$P_{rejection} \simeq 8 \times 10^{-4}$

Number of words accepted in error = $40 \times 10^{-8} \times 5 \times 10^3 = 0.002$

Number of words rejected by parity check = 4

APPENDIX II-5

TRADEOFF STUDIES IN INSTRUMENTATION

General and detailed tradeoff studies were conducted at the start and during the course of this program. Most of these can be classified into two categories: major systems tradeoffs, and minor detailed design tradeoffs for subsystems, techniques, components, etc.

The instrumentation and onboard data processing model which was used as a baseline for comparison at the beginning of the program is presented in some detail in Appendix II-6.

A number of tradeoff investigations are very closely interrelated and, therefore, are discussed as an entity for all the various factors involved in the overall picture, rather than repeat considerations for each item separately. It was also decided to present tradeoff discussions and study results in the different sections of their subject matter to preserve continuity of context.

However, a summary of some tradeoff studies and a brief of derived conclusions is given in the following paragraphs.

A. INSTRUMENTATION AND DATA ARRANGEMENT SYSTEM TRADEOFF SUMMARY

1. Major Systems Tradeoffs

a. Single instrumentation system versus two independent systems

Single measurement and onboard data processing system versus two independent systems (a primary and a secondary section) will guarantee higher reliability for long term operation.

b. Fixed format versus hit-demand frames

This consists of fixed measurement format with one main storage and substorages for each sensor group initiated by onboard programmer or by ground command versus hit-initiated hit history frames without substorage units. A fixed measurement format is used for the primary system. A random format for the secondary system will result in smaller storage requirements. * No substorage units are employed.

---

*Random format, by definition, is a memory read-in of equal and fixed word-length data frames whenever a micrometeoroid hit event occurs. Each hit history frame is tagged for identification.

c. Fixed format versus variable format

Advantages of fixed format (word sequence) versus variable word sequence also fixed word length per measurement channel versus word syllables and editing procedures.

Results. Word syllables per data channel minimize storage requirements.

d. Single format for all data versus separate formats for scientific and housekeeping measurements

Results. Separate formating is more feasible for this satellite application.

e. Single large memory unit versus three small memory units versus complexity versus reliability

Reduced number of ancillary storage circuits for only one memory versus complexity of three separate memories with ancillary circuits versus reliability.

Results. Three separate storage units, each with write-in/read-out modules were used in first study model.

2. Minor Systems Tradeoffs

a. Parity versus no parity

Justification for adding parity bit to data word versus equipment complexity and reliability.

Results. No parity in primary system; parity on all words in secondary system.

b. Measurement resolution versus data word syllable

Requirements for incremental measurement resolution versus length of word syllables and also versus data word length, versus storage requirements.

Result. A seven-bit long data word is used in primary system; the secondary system data word is seven bit plus one bit parity.

c. In-flight sensor calibration and switching functions versus reliability

In-flight calibration of experiment sensor by different techniques, also swtiching versus long-term reliability.

Results. In-flight calibration procedure for some instruments are required. The recommended technique for measurement of effective panel area is not detrimental to reliability.

d. Individual instrumentation subsystem command control versus switching functions and reliability

Command control for each of the different detector groups versus switching equipment complexity and reliability.

Results. No command control for primary measurement system; limited number of commands for secondary system.

e. S/C time accuracy versus attitude accuracy versus storage requirements

Timing resolution and related timing data word length versus attitude measurement accuracy and versus data storing requirements versus related directionality determination.

Results. Event time resolution will be measured in minutes and hours of day and in numbers of day of orbit. Micrometeoroid hit event time for velocity gage sensor tubes has sufficient incremental resolution to derive particle influx directionality.

f. Fixed format frame sequence versus random hit-demand frames with aspect data versus data accumulation

Besides programmed attitude and housekeeping measurements fixed sequence frame format versus random hit-demand frames with aspect data versus orbit data accumulation.

Results. Data storage requirements for hit-demand frames are only 1/3 of that for fixed frames.

g. Data frame accumulation versus data composition versus orbit time

Orbital data accumulation versus different predetermined data accumulation versus data composition.

Results. By regulating by a factor of eight velocity gage hit history frame allocation for storage, data accumulation is reduced by about 60%.

h. Capacitance panel hit history with versus without attitude data versus data accumulation

Results. No attitude data taken. Six directions of influx are measured.

i. Penetrated capacitance panel identification versus no panel number identification

Results. Penetrated panels are not identified by assigned numbers (also location (direction) and calibration identification) to reduce circuit complexity of primary system. Effective areas of operating panels for each thickness is determined by a different technique. Six directions of particle influx (in three planes) are identified in hit history frame.

j. Effective area of capacitance panel determination by different techniques versus reliability

Effective area determination by AC measurements versus by RC network versus by summation amplifier network versus by panel line multiplexer versus by magnetic transducer; all versus switching functions, number of components, reliability of operation.

Results. Magnetic transducers are recommended. No physical circuit connections are required.

k. One Exotech sensor per bay versus two active sensors versus two sensors with coincidence circuit versus one active and one passive reference sensor versus detection efficiency

Results. Two sensors with coincidence gate are used.

l. Separate hit history frames for capacitance panel and Exotech sensors versus combined hit-demand frame versus data accumulation

Separate hit histories require large storage capacity.

Results. Both sensor data are combined in one data frame to reduce storage requirements.

m. Programmed readout of Mariner gage data versus full counter readout-demand

A periodically programmed readout of all sensitivity level hit counters versus highest sensitivity level full counter readout-demand versus data loss and data accumulation

Results. Readout is initiated by full counter of capacitor level A to reduce storage requirements.

n. Separate hit counters for three Mariner gages versus common counters

Separate hit counters give particle direction information, but require large storage capacity.

Results. Common counters are used.

o. Recording of every hit history frame from Mariner and velocity gages versus predetermined number of frames and data storage overflow counter

Recording of every hit history for these.

Results. A predetermined number of frames for each sensor group is allocated for storage in order to reduce storage size.

p. Recording every velocity gage hit history frame versus count-divide circuit with command control versus fixed divide

Results. Fixed divide shown as recommended system. Command control divide is avoided due to possible reliability problems.

B. PRIMARY SYSTEMS TRADEOFFS

1. Primary System Data Content Tradeoffs

Considerations in tradeoffs for primary system format and data content were systems reliability versus format switching functions, value and amount of data information and amount of equipment and parts involved in editing. Figure 5-1 illustrates four different approaches for primary system data information.

- Case 1: Shows the recommended format consisting of only two data words.

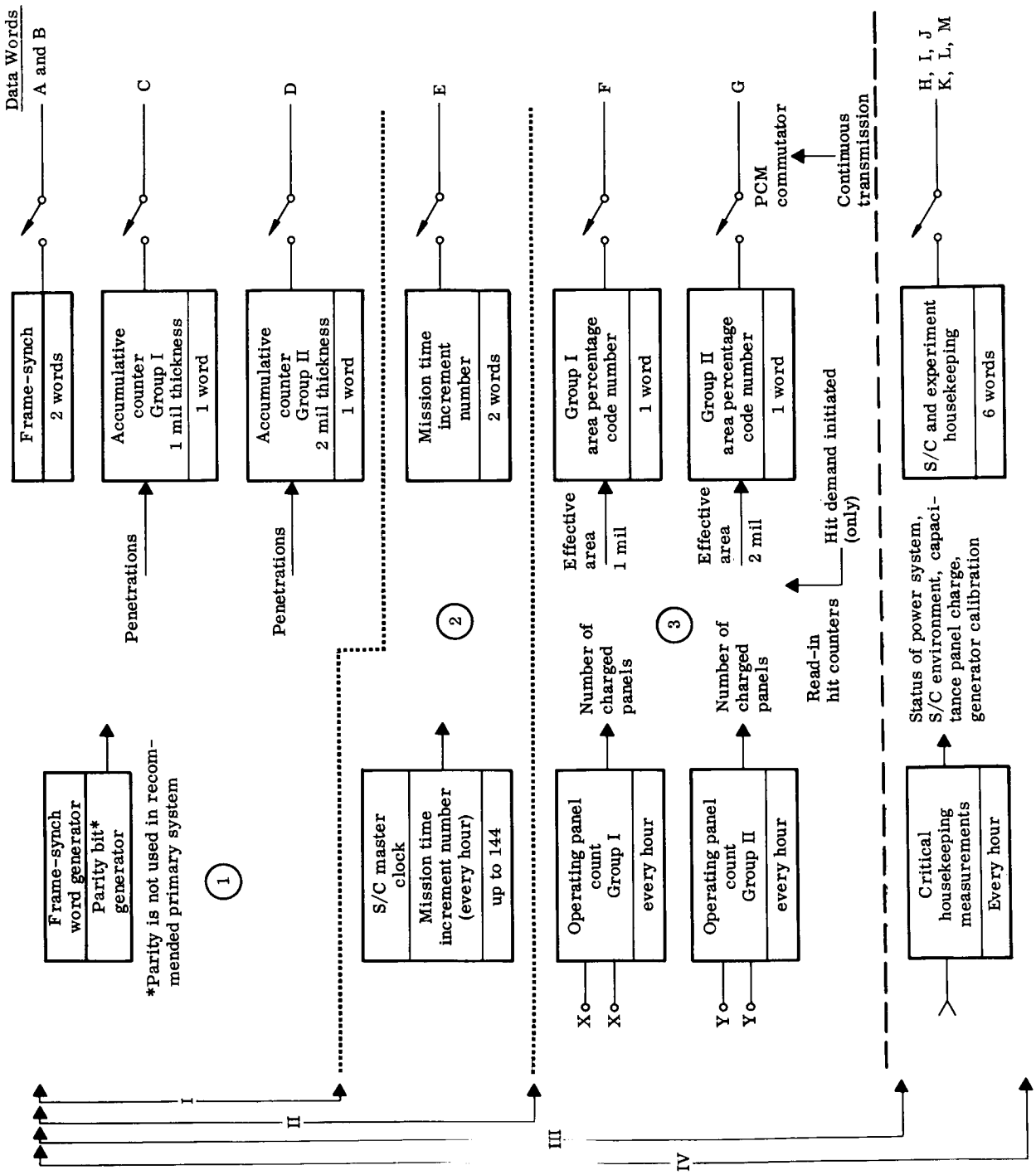


Fig. 5-1. Tradeoff: Format Length of Primary System

● Case 2: Two more data words were added to give code numbers for mission time increments at which a predetermined number of penetrations was reached (in each thickness).

● Case 3: Two more data words give effective area of operating panels as a code number for each thickness. The effective area measurements can be initiated hourly by a programmer and updated.

● Case 4: Six data words were added to give information on status of power system, spacecraft environment, panel charge generators and other critical diagnostic and/or calibration measurements.

The effect on primary systems reliability by these various tradeoff models for format are discussed in section "Reliability."

2. Penetration Detection and Effective Area Determination

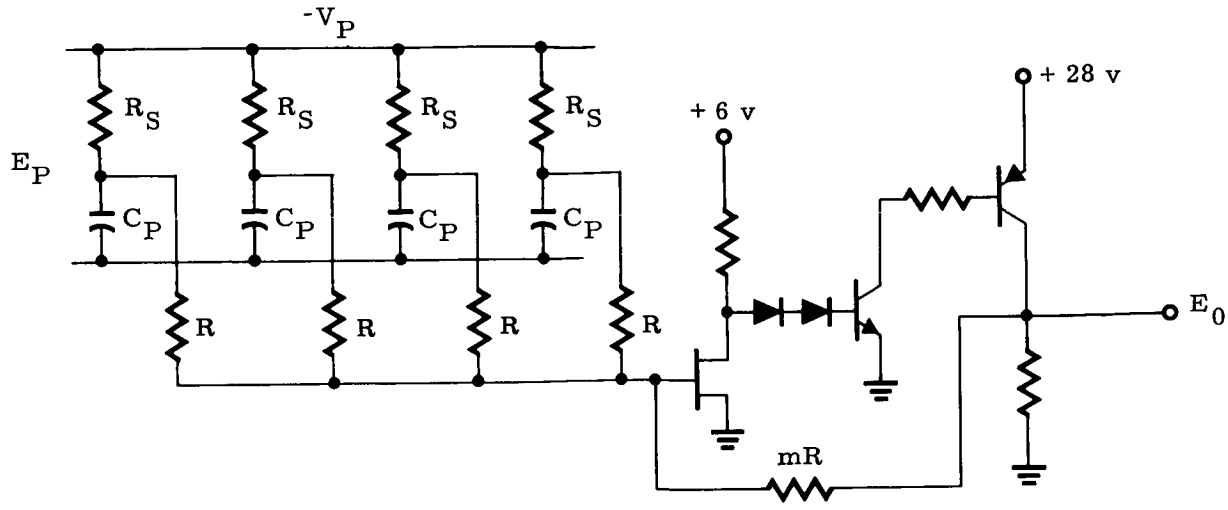
A number of methods for capacitance panel penetration detection and for determination of effective panel area were conducted to derive the best technique for these measurements. Hall effect transducers are used in the recommended system and described in the technical discussion (Chapter II).

In addition, the three methods described below were evaluated. All these methods are workable systems, but require physical circuit connections as interface.

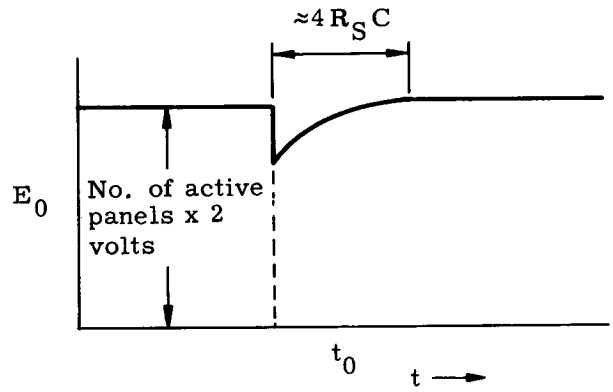
Method I--Voltage Summation. The capacitor sensor panel area can be subdivided into a number of smaller capacitor areas so that the entire area will not be disabled by a single fault. This discussion describes a simple configuration for regrouping the output signals to minimize interaction between sub-segments and at the same time to provide a single terminal for telemetering panel status if desired. The basic configuration is shown in Figs. 5-2a and 5-2c.

Each capacitor panel is fed through the series resistor R_s from a negative 40 to 50 v supply as required. The amplifier circuit shown is a simple feedback adder which produces a "virtual" short circuit at the summing junction of the capacitor sampling resistors R. Thus, the input current from each panel is $\frac{E_{pi}}{R}$ independent of all others.

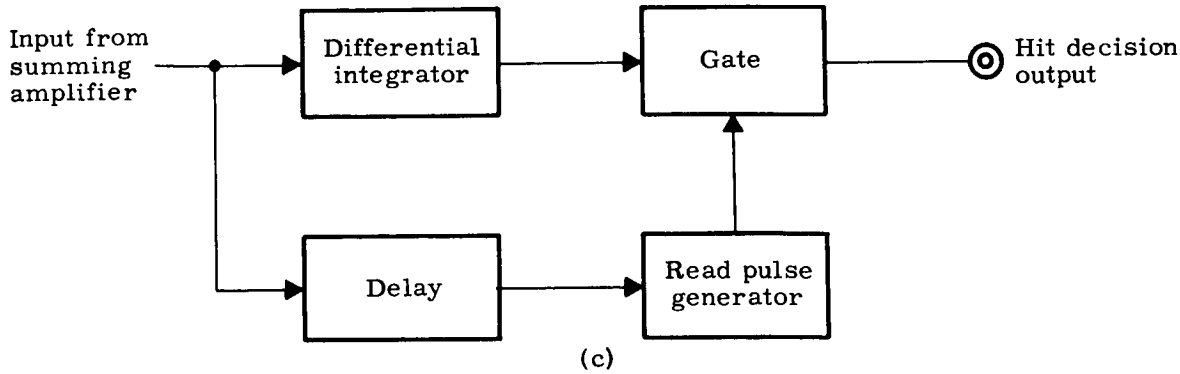
The use of a field effect transistor as the input stage results in negligible input current and thus the output voltage contribution from each panel is the voltage developed in the resistor mR or



(a)



(b)



(c)

Fig. 5-2. Tradeoff: Summation Amplifier Capacitance Panel Penetration Detection Technique

$$E_{oi} = -mR \frac{E_{pi}}{R} = -m E_{pi}$$

The total output is therefore

$$E_o = -m \sum_{i=1}^{i=N} E_{pi}$$

As an example, let V_p* = -50 v, m = 0.04, and N = 10.

When all N = 10 panels are active, the output voltage E_o = 20v. A hit on any one panel thus produces a negative exponential of 2-v peak regardless of the number of inactive (shorted) panels. The steady-state d-c output is a linear measure of the number of active panels. Thus, only one active panel gives a steady-state output of 2 v; two panels, 4 v; three panels, 6 v, etc. The waveform at the output thus appears as in Fig. 5-2b.

In summary, this arrangement provides a highly stable low impedance output signal whose steady-state voltage is a linear measure of the active panel area and whose incremental voltage output in response to a hit is independent of the number of shorted segments.

Since the output impedance is extremely low, i.e., a few ohms or less, further processing to filter radiation excitations and to perform hit decisions can be performed without concern for loading problems. Additionally, all components can be combined at the panel location so that only a single lead is required to carry all information concerning panel status and hit response to the buffer amplifier.

Hit decision processing can be performed by direct triggering a counter circuit with the leading edge (after radiation ringing elimination) or by using a somewhat more elaborate circuit which is almost completely noise immune. This consists of a simple integrator following the buffer amplifier with an output sampler at the termination of the integration period as illustrated in Fig. 5-2c.

Since all hits produce the same output voltage function, the output of the differential integrator at any time, T, following a hit is a constant. Thus, if the leading edge of the hit pulse generated a delayed "read"

*Since feed-back adders are necessarily inverting, the negative supply voltage is used for illustrative purposes. Circuit modifications can be made to eliminate this requirement, however.

pulse to sample the integrator output at some arbitrary time T, and the output is in excess of a preset value, the decision to "hit" and the pulse is passed to the hit counter. If at time T, the output is less than the threshold setting, the decision is noise or extraneous signal and the hit pulse is inhibited.

The large advantage of this type of hit is its inherent immunity to extraneous noise; i.e., an energy threshold must be exceeded for hit acceptance. As noted, there are a large number of ways to implement this function.

The use of a feed-back adder configuration for the direct measurement of the number of active (non-shorted) capacitor panels was discussed above. No consideration was given to the detection of open panels. This is to define a simple addition to the proposed arrangement to accomplish this function.

If an a-c voltage E_{a-c} is superimposed on the d-c panel supply voltage (in series), and all panels are either shorted or are active, the a-c output voltage of the feed-back adder will be for all practical purposes, zero. However, when one or more panels are open, the output voltage

$$E_{o\ a-c} = m \sum_{i=o}^{i=N_o} E_{a-c} = m\, N_o\, E_{a-c}$$

where

m = feed-back factor

N_o = number of open panels

i.e., an a-c voltage exactly proportional to the number of open panels. A simple phase detector at the amplifier output will then provide a d-c voltage proportional to the number of open panels.

Thus, the feed-back adder system provides two d-c outputs for telemetry; one provides a measure of the number of open panels and the other the number of shorted panels. In addition, of course, are the subsequent "bit" detection circuits discussed above.

It should be noted that the use of a phase detector is important since only coherent outputs are obtained. Thus, radiation induced ringing is automatically rejected. The a-c signal is automatically rejected from the bit detection circuits by the low-pace filter included to eliminate radiation induced ringing.

Method II--RC network. Figures 5-3 and 5-4 illustrate a technique for penetration detection and for effective area measurement of the capacitance panel sensors. Diodes are used in all wiring tie-points to achieve isolation.

Results of the investigation were:

(1) The RC network method is a workable system.

(2) The effective area measurements have to be scanned with a commutator and consequently require switching.

(3) Direct circuit interfaces are required.

Method III--AC impedance measurement. Figure 5-5 depicts an a-c measurement method for effective area determination. Capacitance panel penetrations are detected with Hall effect type transducers D_1 for the primary and D_2 for the secondary measurement system. Two signal conditioning units are used in both systems; one unit for each panel thickness.

Effective area is measured with detector D_3. An a-c signal is superimposed on circuit arm XZ. Arms XY and YZ are forming basically an a-c voltage divider. Sensor D_3 then detects the amplitude of a-c current through branch YZ by monitoring its associated a-c field.

If capacitance panel sensor C_1 is charged and therefore operating, the amplitude of the a-c current and field of circuit arm YZ will be at a predetermined level and is detected by sensor D_3.

If capacitance panel C_1 is permanently short-circuited, there will be no voltage drop across panel sensor C_1 and hence a-c current and field increases in branch YZ.

If capacitance panel C_1 is open-circuited, there will be no a-c current flow and detector D_3 sees zero signal.

Capacitors C_2 and C_3 are shunted across current limiting resistor R_s as a-c voltage by-pass. The a-c signal source is isolated from the capacitance panel d-c charging circuit by means of an isolation transformer T_1. The outputs of detector D_3 circuits have to be commutated and encoded by an effective area count logic.

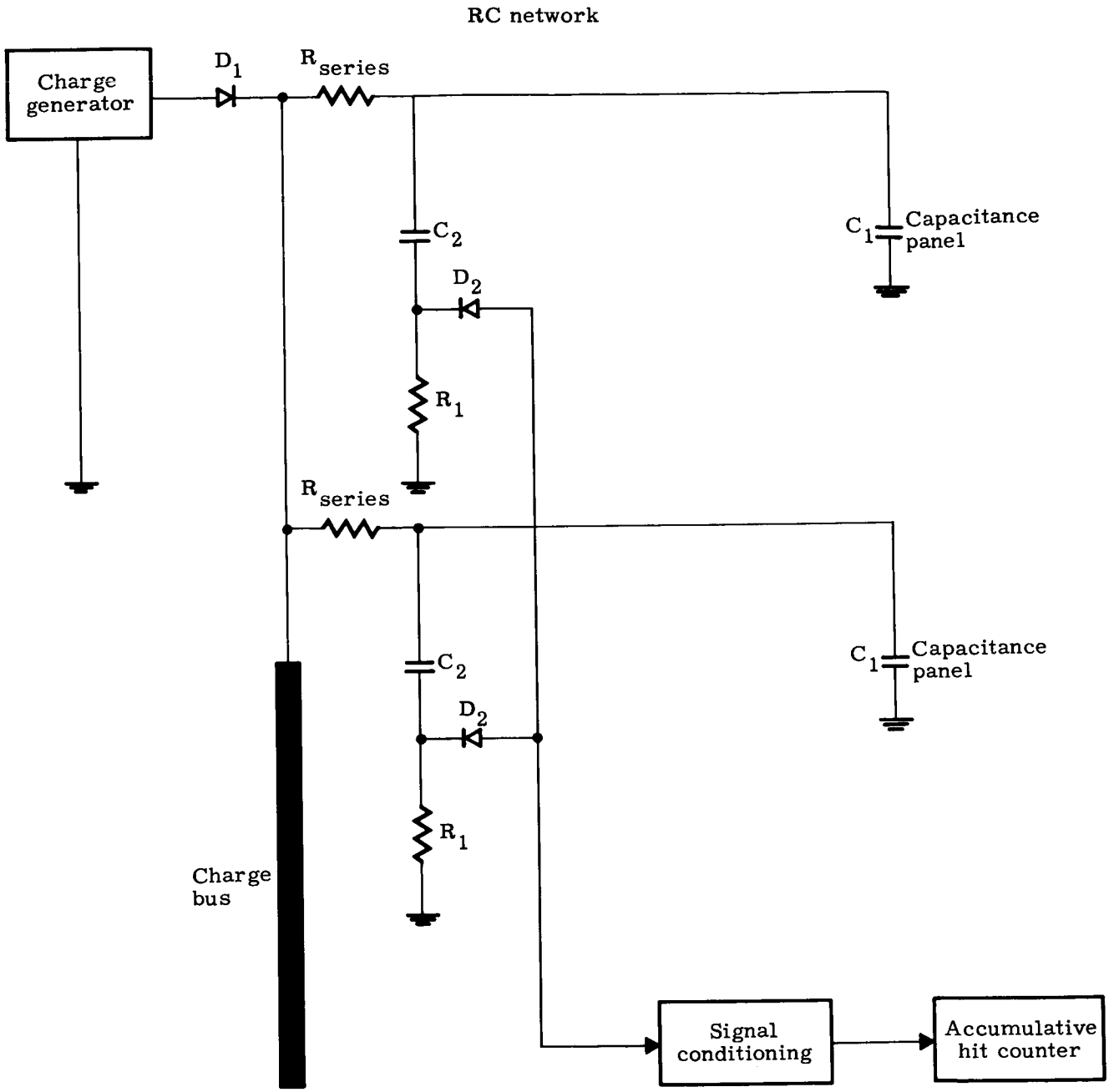
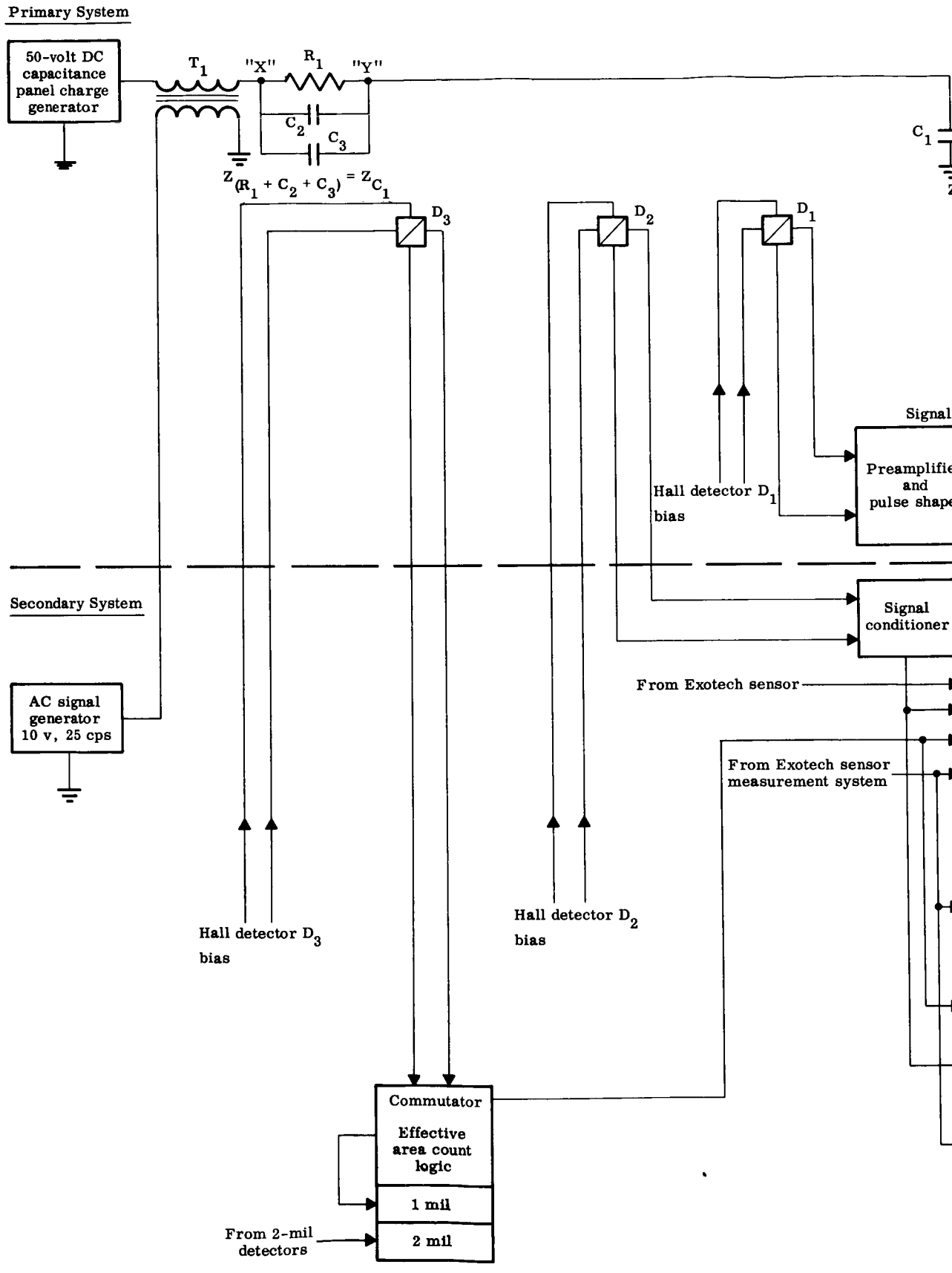
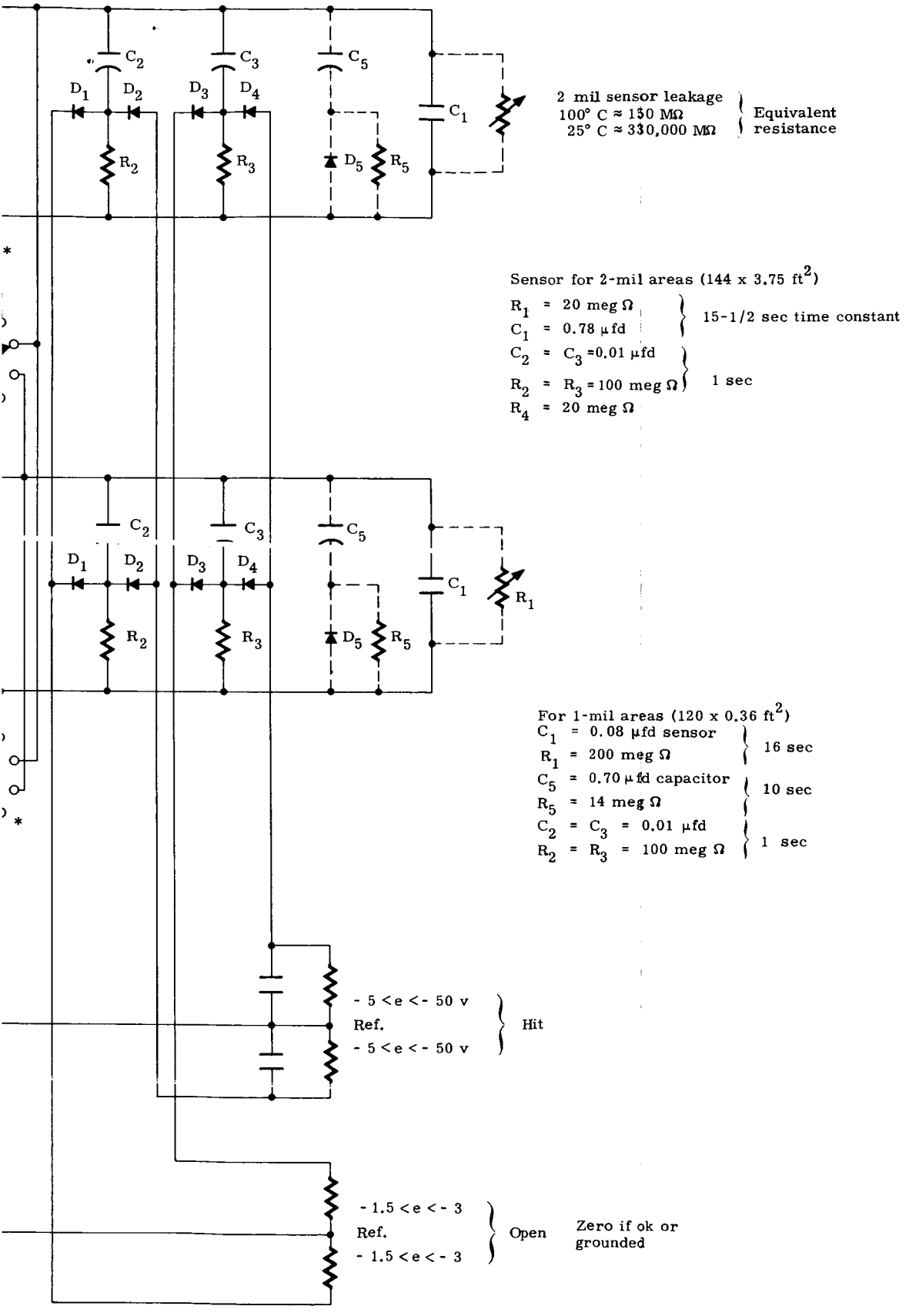


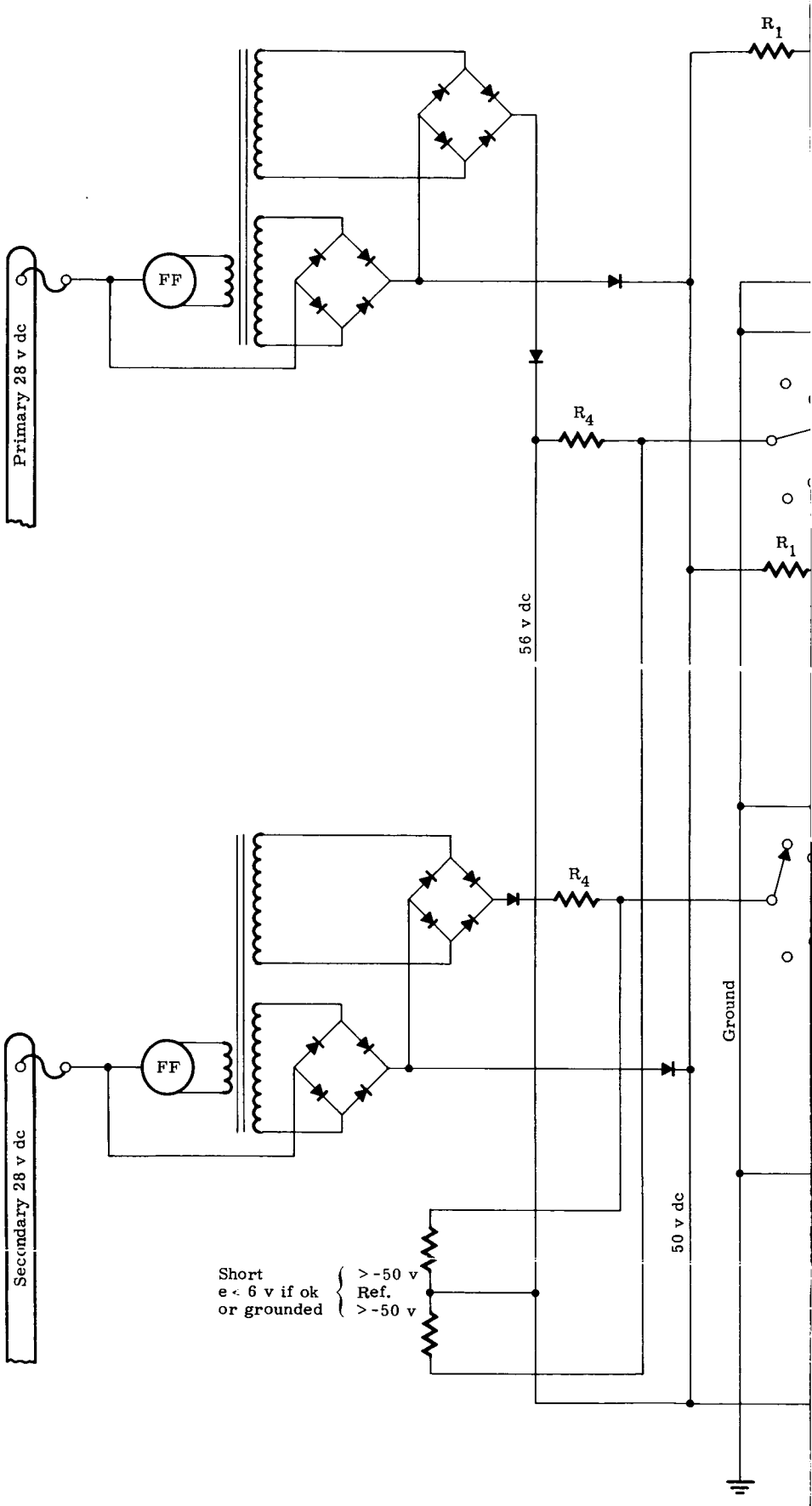
Fig. 5-3. Capacitance Panel Penetration Detection Techniques


Primary System
50-volt DC capacitance panel charge generator
T1
"X"
R1
"Y"
C2
C3
C1
Z(R1 + C2 + C3) = ZC1
D3
D2
D1
Signal
Preamplifie
and
pulse shape
Hall detector D1
bias
Secondary System
Signal conditioner
AC signal generator 10 v, 25 cps
From Exotech sensor
From Exotech sensor measurement system
Hall detector D3
bias
Hall detector D2
bias
Commutator
Effective area count logic
1 mil
2 mil
From 2-mil detectors



*Commutators for 120 and 144 measurement channels

Fig. 5-4. Capacitance Panel Penetration and Effective Area Detection Technique Multiplexing Scheme


R1
FF
Primary 28 v dc
R4
R1
56 v dc
R4
Ground
FF
Secondary 28 v dc
50 v dc
Short
e < 6 v if ok
or grounded
> -50 v
Ref.
> -50 v

I- 5-13

1H

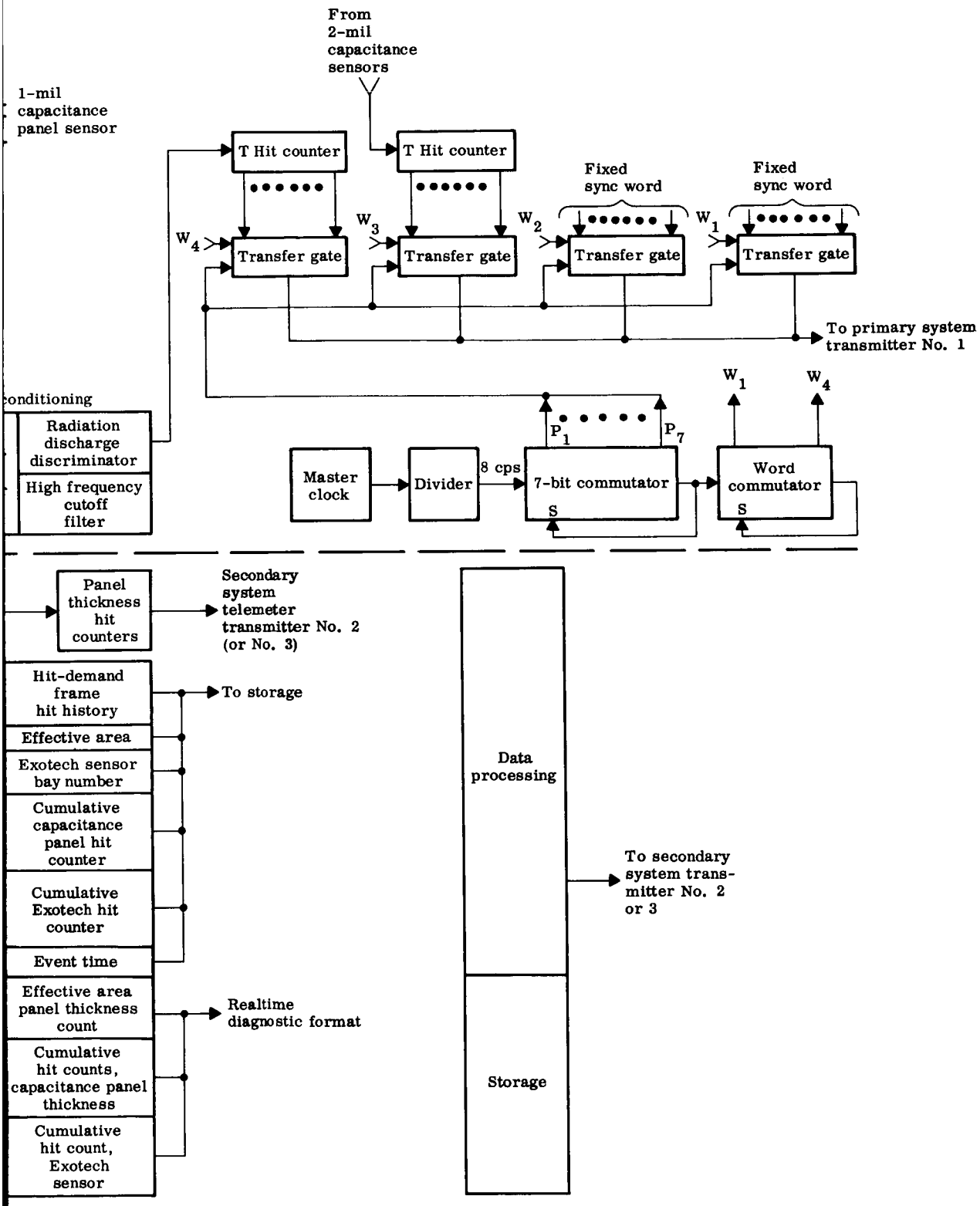


Fig. 5-5. Tradeoff: Capacitance Panel Hit Detection and Effective Panel Area Count

II-5-14

2#

The results of the investigation were:

(1) A-C measuring method for effective area is a workable system.

(2) The insertion of a transformer leg into the d-c panel charging circuit as a series component will reduce reliability of the system.

C. SECONDARY SUBSYSTEM TRADEOFFS

1. Tradeoff Considerations for Hit History Frames for the Secondary System

Tradeoff investigations were undertaken to compare different measurement techniques and functional arrangements in the secondary system versus reliability, data accumulation and other factors.

A large amount of experiment data from the secondary measurement system consists of hit-demand frames for micrometeoroid hit histories. Selected bit allocation for incremental resolution of analog measurements, bit length of data words and word syllables, word length of data frames as well as the functional modes of the data contributing subsystems define capacity requirements for storage units. Such factors also establish the amount of ancillary equipment for storage functions.

Various approaches were investigated to determine the best methods for reduction of storage requirements and for achieving high reliability. Major factors evaluated and quantitative results of different design approaches from which the recommended design was derived are summarized in the following sections.

a. Tradeoff: Fixed format versus hit-demand frames

Conditions:

(1) First model investigation.

(2) Individual and independent substorages for hit history for measurement subsystems.

(3) Substorage write-in initiated by micrometeorid hit.

(4) Readout of substorage units into main storage as fixed-word-sequence-format by programmer, periodically.

(5) Subsystem requirements are established by sensor complement of first conceptual satellite model.

(6) Sensor complement as shown in Table 6-1, Appendix II-6.

Since this concept was the preliminary instrumentation systems model, major key points of this tradeoff evaluation are described in Appendix II-6. Advantage of only one single format with fixed-word-sequence is simplicity of operation; however, requirements for the main data storage are large.

Conclusions from this first model investigation were: to examine further the hit-demand frame system with one or more memory; to reduce data storage requirement; to increase reliability for long-term operation; and to store only significant data.

TABLE 5-1

Sensor Complement for Tradeoff

Quantity	Measurement Groups
256	Capacitance Panel Sensors Three different gage thicknesses
2	Mariner Gages Each two capacitor sensors and one microphone sensor Each capacitor sensor has six impact sensitivity levels Each microphone has four sensitivity levels
2	Velocity Gages Each with four sensing tubes Each tube capacitor sensor has four sensitivity levels Each tube microphone sensor has three sensitivity levels
3	Cadmium Sulfide Cells Each also with a capacitor sensor with one sensitivity level
40	Miscellaneous Housekeeping Transducers
5	Solar Aspect Sensors
10	Earth Sensors
8	Command Verification Sensors

b. Tradeoff: Data accumulation with fixed format versus hit-demand frames with aspect data

Conditions:

(1) Primary and secondary measurement systems.

(2) Sensor complement as shown in Table 5-1.

(3) Secondary system instrumentation and data handling techniques are examined.

(4) Hit history data frames contain satellite attitude data (five words allocated).

(5) Baseline for tradeoff is: both systems gather the same amount of data information.

(6) Simplicity of operation and related reliability are design goals.

(7) Both systems have: housekeeping data and full attitude frame once/day initiated by a programmer.

(8) Both systems: Mariner gauge data to be read out four times in micrometeoroid density Zone I, every four hours in Zones II through V by onboard programmer or at any time when capacitor level A (smallest particle detection) is full.

(9) Reliability tradeoffs for both systems.

The purpose of the tradeoff investigation was to compare two systems with identical sensors, one with fixed word sequence TM format, the other with unequal data word length hit-demand frames. The assumed fixed format system is shown in Fig. 5-6 in simplified form. Both systems would deliver the same type of data information.

The sensor complement shown in Table 5-1 was assumed for comparison of data accumulation.

Evaluation factors were reliability, simplicity of measuring technique, circuit requirements, storage requirements, and equipment availability. Table 5-2 establishes data accumulation up to the 18th orbit hour for data readout convenience at high bit rate transmission mode. Tables 5-3 and 5-4 show the results of orbit profiles for data loading. Both tables are derived from the hit-demand frames tabulated in Tables 5-5 through 5-10. Results for fixed format operations are shown in Table 5-11. This table is also based on the data bit accounting shown in the same six tables as above as well as Fig. 5-7 and 5-8.

TABLE 5-2

Tradeoff: Data Accumulation with Hit-Demand frames After 18 Hours Orbit Time

Satellite Time	Altitude and Zone	256 Units Capacitance Panels				3 Units Capacitor and Cell			2 Units Velocity Gage					2 Units Mariner Gage							Diagnostic Format Words (100)	Full Attitude Format Words (40)	Total Accumulation Words
		Hits			Frame Words (13/hit)	Hits		Frame Words (17/hit)	Hits				Frame Words (16/hit)	Hits						Frame Words (14/hit)			
		Thickness							Capacitor Level Mike Level					Capacitor Levels Mike Levels									
		1	2	3		Capacitor	Cell		1	2	3	4		A	B	1	2	3	4				
										1	2	3				1	2	3	4				
-16 min	I													680	305	59.6	6.9	2.7	0.31				
0	Perigee												400	28	1						100	40	
16 min	1 hr	0.526	0.526	0.526		0.34	0.34		24.3	1.1	0.127	0.05				Readout				14			
32 min																Readout				28			
48 min																Readout				42			
	II																						
1 hr	11,600				13											Readout				56			1009
	4.2	0.526	0.526	0.526	26	0.34	0.34		24.3	1.1	0.127	0.05											
4					39								800			Readout				70			1035
	III																						
5.2	40,000	0.526	0.526	0.526		0.34	0.34		24.3	1.1	0.127	0.05				Readout				84			
8																							
12	13							17					1616			Readout				98			1394
16	IV				39			17					1616			Readout				112	100	40	1924
18.5	88,000				39			17					1616							112	100	40	1924

NOTE: $T_{interrogation}$ = 18 hours is selected to enable high bit rate readout.

Orbit Mission			256 Units Total (now 264 units total)				For Three Units (now 3 units deleted)			For Two
			Capacitance Panels				CdS Cell and Capacitor			Ve
			Hits[1]/Zone				Hits[2]/Zone			
			Thickness							Capacitance Level
Satellite Time (hr)	Altitude (naut mi)	Zone	1 (1.5 mil)	2 (2 mil)	3 (2.4 mil)	Frame Words (13/Hit)	Capacitor	Cell	Frame Words (17/Hit)	1
-16 min										
0	400 Perigee	I	0.526	0.526	0.526	-- -- --	0.34	0.34	-- --	24.3 (24)
1 32 min							Equivalence in particle sensitivity			
48 min										
1 hr	11,600	II	2x(0.526) 1	2x(0.526) 1	2x(0.526)	13 26	2x(0.34)	2x(0.34)	-- --	2x(24.3) (24) 48.6
4.2 4 hr			1.052		1	39	0.68			
5.2	40,000	III								
8 hr			3x(0.526)	3x(0.526)			3x(0.34) (1)	3x(0.34)	17	3x(24.3) 0.9
13 12			1.578	1.578	3x(0.526) 1.578		1.02	(1) 1.02		(24)
16										
18.5	88,000	IV								
20			4x(0.526)			52	4x(0.34)			4x(24.3)
24			2.104	(1) 2.104	4x(0.526) (1)	78	1.36	1.36		(25)
22 28										
32										
36										
40										
40.5	128,000	V								
44										
48										
52										
56										
60			5x(0.526)	5x(0.526)			5x(0.34)	5x(0.34)		5x(24.3) 1.5
64			2.630		5x(0.526) 2.630		1.70	1.70		(25)
68										
63 72	147,000 Apogee									
76										
80										
84										
88										
92										
96										
100										
103.5	128,000	IV								
104			6x(0.526)				6x(0.34)			6x(24.3)
108			(1) 3.156	6x(0.526) (1) 3.156	6x(0.526)	91 104	(1) 2.04	6x(0.34) (1) 2.04	34	1.8 (25)
22 112					(1) 3.156	117				
116										
120										
124										
125.5	88,000	III								
128			7x(0.526)	7x(0.526)			7x(0.34)	7x(0.34)		7x(24.3) 2.1
13 132			3.682	3.682	7x(0.526) 3.682		2.38	2.38		(26)
136										
138.8	40,000	II	8x(0.526)				8x(0.34)			8x(24.3)
140			(1) 4.208	8x(0.526) (1) 4.208	8x(0.526)	130 143	2.72	8x(0.34) 2.72		2.4 (26)
4.2 143	11,600	I			(1) 4.208	156				
+ 16 min			9x(0.526)				9x(0.34)			9x(24.3)
1 + 32 min			4.734	9x(0.526) 4.734	9x(0.526)		(1) 3.06	9x(0.34) (1) 3.06	51	2.7 (28)
+ 48 min					4.734	169 182				
144 or 0		I	(1)	(1)	(1)	195			51	

(1) Allowing 0.5 hit per zone transition and providing data allocation for 15 hit histories/orbit for three different thickness gauges of capacitance panel sensors (now: 2 thickness gauges).

(2) Providing three hit histories/orbit (now: this sensor type deleted).

(3) Considering 241 hit histories/orbit from o sensing tubes from two velocity gauges, hi recorded, but all hits will be counted. Fa hit history number.

(Now: provisions for 48 hit histories and c velocity gauge sensing tubes from 2 instru

* Statistical micrometeoroid impact data used in this tabulation is discussed in Chapter I.

TABLE 5-3

Detailed Micrometeoroid Hit Number Versus Density Zone Accounting and Data Mission Profile

Units (still 2 units)				For Two Units (now increased to 3 units)											
ocity Gauge				Mariner Capacitance and Microphone Gauge											Diagno
its[3]/Zone				Hits[4]/Zone											
	Microphone Level			Capacitance Level						Microphone Level				Frame Words (14/readout)	Program Readout "X"
1	2	3	Frame Words (16/hit)	A	B	1	2	3	4	1	2	3	4		
ice in particle y capacitor/mike			Divide all hits by 8.* (8 tubes)												
				28,680	1305	59.6	6.9	2.7	0.31	59.6	6.9	2.7	0.31	14	1st day
1.1 (1)	0.127 --	0.05 --	25 x 16 400											28	
														42	
2x(1.1) 2.2 (1)	2x(0.127) 0.254	2x(0.05) 0.1	(400) 800											56	
														70	
3x(1.1)	3x(0.127)	3x(0.05)	(400)											84	
(1)	--	--	1200											98	
														112	
4x(1.1) 0.9	4x(0.127)	4x(0.05)	25 x 16 (416)											126	
(1)	--	--	1616											140	2nd day
														154	
														168	
														182	
														196	
														210	
														224	3rd day
														238	
														252	
5x(1.1)	5x(0.127)	5x(0.05)	26 x 16 (416)											266	
(1)	--	--	2032											280	
														294	
														308	4th day
														322	
														336	
														350	
														364	
														378	
														392	5th day
														406	
6x(1.1)	6x(0.127)	6x(0.05)	26 x (416)											420	
(1)	--	--	2448											434	
														448	
														462	
														476	6th day
														490	
7x(1.1)	7x(0.127)	7x(0.05)	27 x 16 (432)											504	
(1)			2880											518	
														532	
8x(1.1)	8x(0.127)	8x(0.05)	28 x 16 (448)											546	
(1)	(1)		3328											560	
9x(1.1)	9x(0.127)	9x(0.05)	33 x 16 (528)											574	
(2)	(2)	(1)	3856											588	
			3856	X	X	X	X	X	X	X	X	X	X	602	Start of next orbit

Equivalence in particle sensitivity capacitor/mike

velocity tube. Since there are eight history for every eighth impact will be or of 2 is included in the allocated

nulative counts of all hits for each of 8 nts.)

(4) Hit counts by Mariner gauges were read out and stored by onboard programmer every four hours in Zones II, III, and V; every 16 minutes during Zone I. (Now: Mariner gauge hit history with hit counts in all levels is read out and stored whenever hit counter for capacitance Level A is full. Time of read-out is recorded.)

(5) Estima and mo (Now: daily.)

(6) Now: and 5 record

tic[5] Frame Words	Full[6] Attitude Frame Words[6]	Storage Totals: Words Scientific	Storage Totals: Words Diagnostic	Storage Totals: Words Total	Interrogation: Diagnostic Real Time	Interrogation: Stored Data	Pressure Cell[7] Hits Thickness 1	Pressure Cell[7] Hits Thickness 2	Pressure Cell[7] Hits Thickness 3	Pressure Cell[7] Frame Words (12/readout)
100	40		100	100			0.5	0.5	0.5	
						1000 words	1	1	1	36
		909			Yes					
		935					1.5	1.5	1.5	
		1394					2	2	2	72
						2000 words				
100	80	1931	200	2131						
		1973					2.5	2.5	2.5	
100	120	2055	300	2355						
		2513								
100	160	2595	400	2995						
		2637								
						3000 words				
100	200	2719	500	3219			3	3	3	108
		3233								
100	240	3315	600	3915						
							3.5	3.5	3.5	
		3789					4	4	4	144
					Yes					
						4000 words	4.5	4.5	4.5	
						5000 words				
600	240	4944	600	5544			5	5	5	180

ed data
le.
nly 10 words stored

0 words stored hourly,
ours of continuous
ng near perigee.

(7) These hit count data words not included in totals. (Now: this sensor type deleted.)

TABLE 5-4

Tradeoff: Fixed Format Versus Hit-Demand Frame System: Summary of Data Accumulation with Hit-Demand Frames in 144 Hours

Orbit Hours	Zone	Capacitance Panels (13 words/hit)	Capacitor and Cells (17 words/hit)	Velocity Gage (16 words/hit)	Mariner Gage (14 words/hit)	Diagnostics Format (100 words)	Full Attitude (40 words)	Accumulation		
								Scientific Words	Diagnostic Words	Totals Words
4	II	39	17	800	56	100	40	935	100	1035
12	III ↓			1200	98			1394		1494
24	IV ↓	78		1616	140	200	80	1931	200	2131
36	↓				182			1973		2173
48	V ↓				224	300	120	2055	300	2355
60	↓			2032	266			2513		2813
72	↓				308	400	160	2595	400	2995
84	↓				350			2637		3037
96	↓				392	500	200	2719	500	3219
108	IV ↓	117	34	2448	434			3233		3733
120	↓				476	600	240	3315	600	3915
132	III ↓			2880	518			3789		4389
	II ↓									
144	I	195	51	3856	602	600	240	4944	600	5544

TABLE 5-5

Tradeoff: Fixed Format Versus Hit-Demand Frame:
Capacitance Panel Sensor Hit History with Aspect Data

Data Function	Hit-Demand Frame			Fixed Format	
	Bits	Count up to	Word No.	Bits	Word No.
Frame synch	7 + 7 = 14		1 + 2	--	--
Frame identification	4	15			
Parity	1				
Panel group number	2	3	3	2	
Panel number (in preceding group)	7	127	4	7	
Hit event time (in 64 sec steps)	11	1350		11	
Orbit day	3	7	5 + 6	--	
Aspect					
Elapsed time	7	127	7	7	
Solar angle	7		8	7	
Earth sensors	21		9 + 10 + 11	21	
Accumulative counters					
Thickness size No. 1	3	7		3	
Parity	1			1	
Thickness size No. 2	3	7	12	3	
Parity	1			1	
Thickness size No. 3	3	7		3	
Parity	1			1	
Spare	2		13	3	
			13 words	70	10 words

Results: 13 words versus 10 words

TABLE 5-6

Tradeoff: Fixed Format Versus Hit-Demand Frame:
Cadmium Sulfide Cell with Capacitor Sensor Hit History with Aspect Data

Data Function	Hit-Demand Frame			Fixed Format	
	Bits	Count up to	Word No.	Bits	Word No.
Frame synch	7 + 7 = 14		1 + 2	--	
Frame identification	4	15			
Parity	1				
Capacitor number	2	3	3	2	
Hit event time (in 64-sec steps)	11	1350		11	
Orbit day	3	7	4 + 5		
Aspect					
Elapsed time	7	127	6	7	
Solar angle	7		7	7	
Earth sensors	21		8 + 9 + 10	21	
Accumulative counter					
Capacitor No. 1	2			2	
Capacitor No. 2	2			2	
Capacitor No. 3	2			2	
Parity	1		11		
			11 words		
Frame synch	7 + 7 = 14		1 + 2	--	
Frame identification	4	15			
Parity	1				
Sensor number	2	3	3	2	
Output change	7	127	4	7	
Temperature	7	127	5	7	
Accumulative counter					
Sensor No. 1	2	3		2	
Sensor No. 2	2	3		2	
Parity	1			1	
Sensor No. 3	2	3	6	2	
			6 words	77	11 words

Results: Total of 17 words versus 11 words

NOTE: See note on Fig. 5-7

TABLE 5-7

Tradeoff: Fixed Format Versus Hit-Demand Frame:
Velocity Gauge Hit History with Aspect Data

Data Function	Hit-Demand Frame			Fixed Format	
	Bits	Count up to	Word No.	Bits	Word No.
Frame synch	7 + 7 = 14		1 + 2	--	
Frame identification	4	15			
Parity	1				
Microphone level number	2	3	3	2	
Tube number	4	8		4	
Capacitor level	3	4	4	3	
Hit event time (in 64-sec steps)	11	1350		11	
Orbit day	3	7	5 + 6	--	
Aspect					
Elapsed time	7	127	7	7	
Solar angle	7		8	7	
Earth sensors	21		9 + 10 + 11	21	
Particle velocity	12			12	
Spare	2		12 + 13		
Accumulative counter					
Capacitor level No. 1					
Instrument No. 1	10	1024		10	
Parity	1				
Capacitor level No. 1					
Instrument No. 2	10	1024	14 + 15 + 16	10	
				4	
			16 words	91	13 words

Results: 16 words versus 13 words

TABLE 5-8

Tradeoff: Fixed Format Versus Hit-Demand Frame:
Mariner Gauge Hit History with Aspect Data

Data Function	Hit-Demand Frame			Fixed Format	
	Bits	Count up to	Word No.	Bits	Word No.
Frame synch	7 + 7 = 14		1 + 2	--	
Frame identification	4	15			
Parity	1				
Capacitor level No. 4	2	3	3	2	
Hit event time (in 64-sec steps)	11	1,350		11	
Orbit day	3	7	4 + 5		
Accumulative counter					
Capacitor level A					
Primary count	5	31		5	
Secondary count	9	511	6 + 7	9	
Capacitor level B	10	1,023		10	
Capacitor level No. 3	2	3	8 + 9	2	
Microphone level No. 3	2	3		3	
Capacitor level No. 2	3	7		3	
Parity	1			1	
Microphone level No. 2	3	7	9 + 10	3	
Capacitor level No. 1	6	63		6	
Microphone level No. 1	6	63		2	
Microphone level No. 4	2	3	11 + 12	2	
Accumulative count instrument 2					
Capacitor level A	14	16,383	13 + 14	14	
				1	
			14 words	77	11 words

Results: 14 words versus 11 words

TABLE 5-9

Tradeoff: Fixed Format Versus Hit-Demand Frame:
Pressure Cell Sensor with Aspect Data

Data Function	Hit-Demand Frame (*)			Fixed Format	
	Bits	Count up to	Word No.	Bits	Word No.
Frame synch	7 + 7 = 14		1 + 2	--	
Frame identification	4	15			
Parity	1				
Thickness group	2	3	3	2	
Cell number (in preceding group)	7	127	4	7	
Hit event time					
(in 64-sec steps)	11	1350		11	
Orbit days	3	7	5 + 6	--	
Aspect					
Elapsed time	7	127	7	7	
Solar aspect	7		8		
Earth sensors	21		9 + 10 + 11	21	
				1	
Accumulative counter					
All pressure cells in all groups	7	127	12		
			12 words	63	9 words

Results: 12 words versus 9 words

*This hit-demand frame is based on possibly 3 different groups (thickness or their location) of sensors with up to 127 pressure cells in each group.

NOTE: This hit-demand frame is not included in the following summary tabulations.

TABLE 5-10

Tradeoff: Hit-Demand Frame Versus Programmed Fixed Word Sequence Format

Hit-History Data	Hit-Demand Frame System Words/Hit	Fixed Format System Words/Hit	Substorage Required* Hit-Histories	Programmed* Format Words
Synch				2
S/C time				2
Capacitance panel	13	10	3	30
Capacitor and cell	17	11	1	11
Velocity gage	16	13	28**	364**
Mariner gage	14	11	5	55
	60	49	37	464**

NOTE: Compared hit histories in each column contain same information.

*Based on a programmed data transfer from substorage to main storage once every 4 hr in Zone I and once every 4 hr in all other zones.

**This amount can be reduced by recording every hit in the accumulative counter but measuring complete hit histories only every 2nd (or 4th, 8th, 16th) or 32nd meteoroid hit.

TABLE 5-11

Tradeoff: Data Accumulation with Fixed Format

Satellite Orbit Time				Data Word Accumulation							
				Column "A"				Column "B"			
				Ascent				Descent			
"A" Ascent	Zone	"B" Descent	Zone	Format No.	Hit History	Diagnostic, Attitude	Total Words	Format No.	Hit History	Diagnostic, Attitude	Total Words
0	I	144 hr	I			140		36	16,704	840	17,544
16 min		16		(*)				(*)			
32		32		(*)				(*)			
48		48 min		(*)				(*)			
1 hr		143	I								
4	II	140		1**	464			35			
8	III	136	II	2	928			34			
12		132		3	1392			33			
16		128	III	4	1854			32			
20	IV	124		5				31			
24		120		6	2784	280	3064	30	13,920	840	14,760
28		116		7				29			
32		112		8				28			
36		108		9				27			
40		104	IV	10				26			
44	V			11							
48		100		12	5568	420	5988	25			
52		96		13				24	11,232	700	11,932
56		92		14				23			
60		88		15				22			
64		84		16				21			
68		80		17				20			
72	V	76	V	18	8424	560	8984	19			

*Denotes readout of Mariner gage accumulative counters into substorage.
**Each format number indicates a readout of 464 words.

NOTE:

Tabulation is based on word length of 7 bits data plus 1 bit parity.

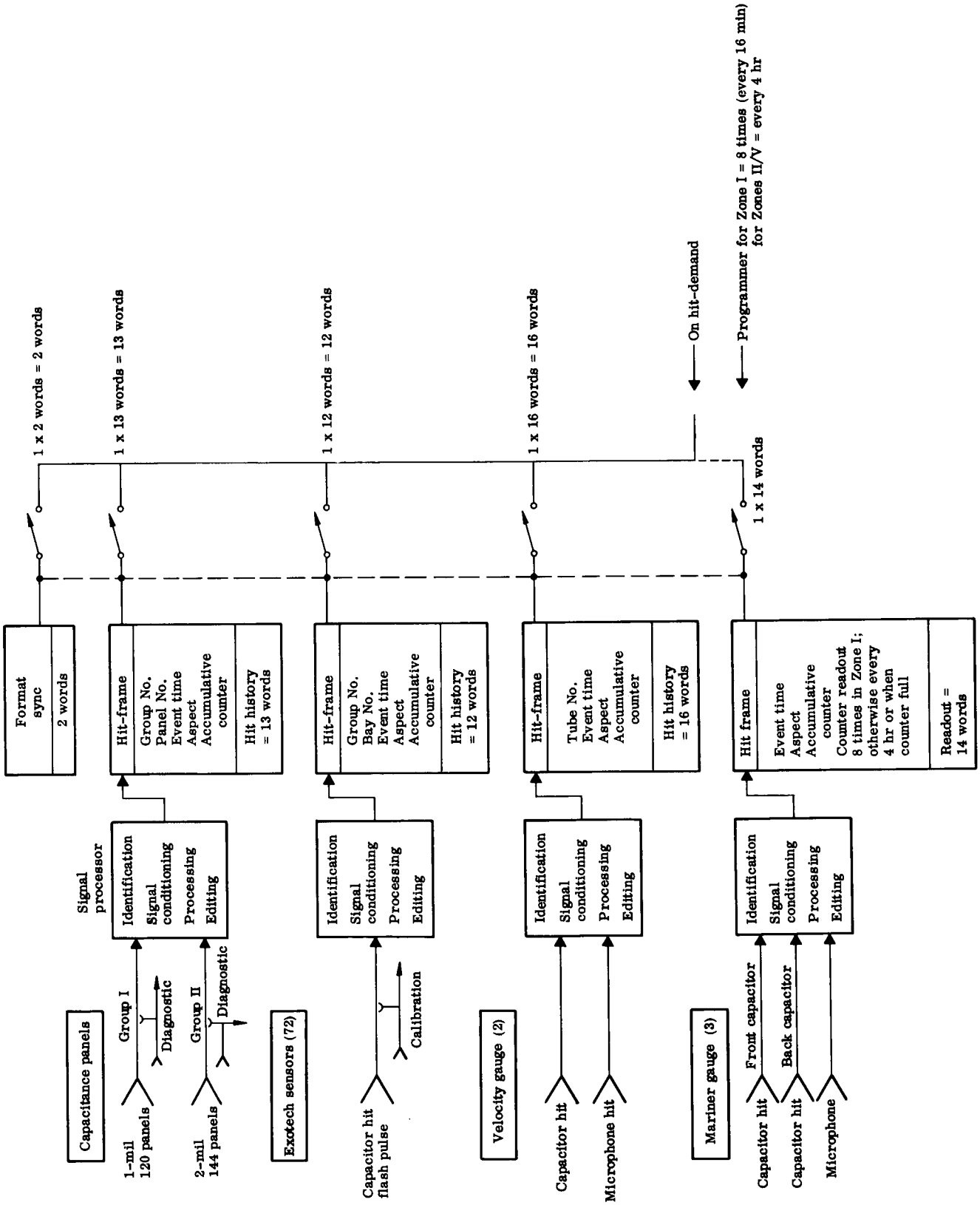
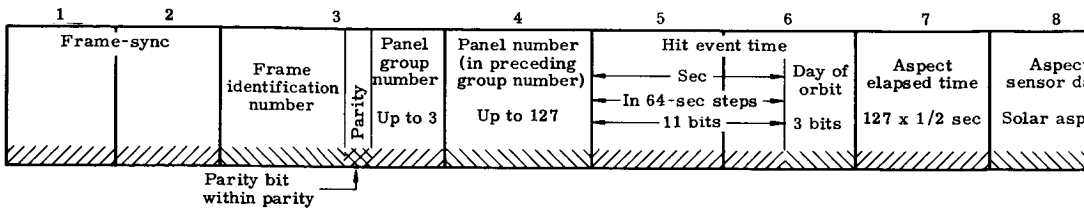
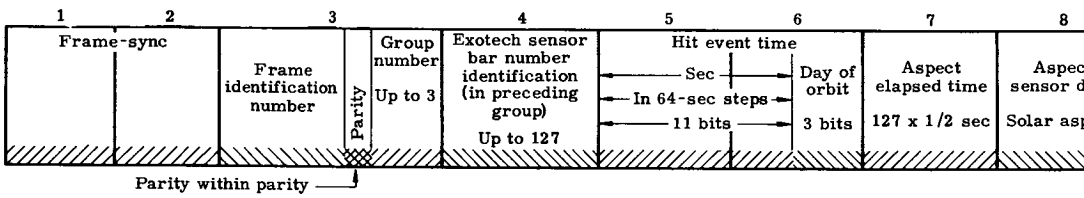


Fig. 5-6. Tradeoff: Fixed Format Versus Hit-Demand Frame--Secondary Measurement System Diagram; Fixed Format for Hit Histories

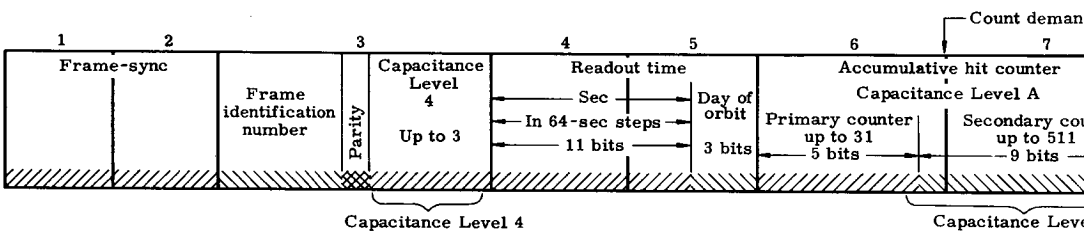
Frame I:
Capacitance panel
hit frame
13 words total



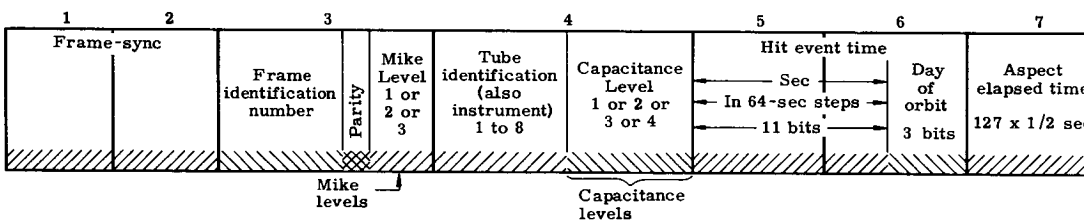
Frame II:
Exotech
sensor
hit frame
12 words



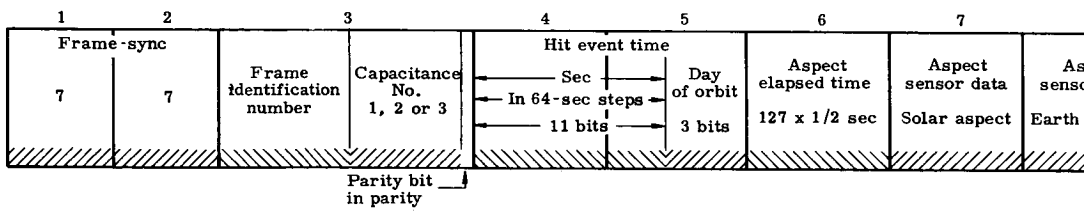
Frame III:
Mariner gauge capacitor
and acoustic sensor
hit frame
14 words



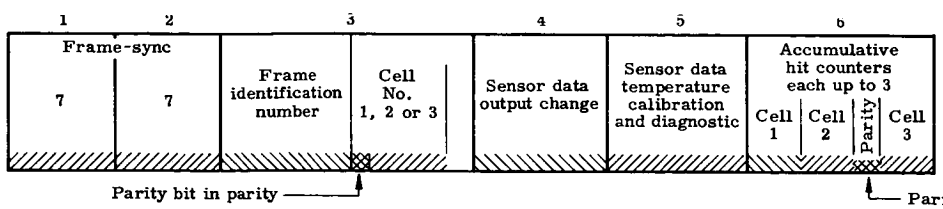
Frame IV:
Velocity gauge
hit frame
16 words



Frame V-a:*
Cadmium sulfide cell/capacitor sensor
Capacitor hit frame
11 words



Frame V-b:*
Cadmium sulfide cell/capacitor sensor
Cell hit frame
6 words



*NOTE: Hit-demand frame has a total of 17 words. Two frames are required since sensor might not be illuminated by sun at hit event time.

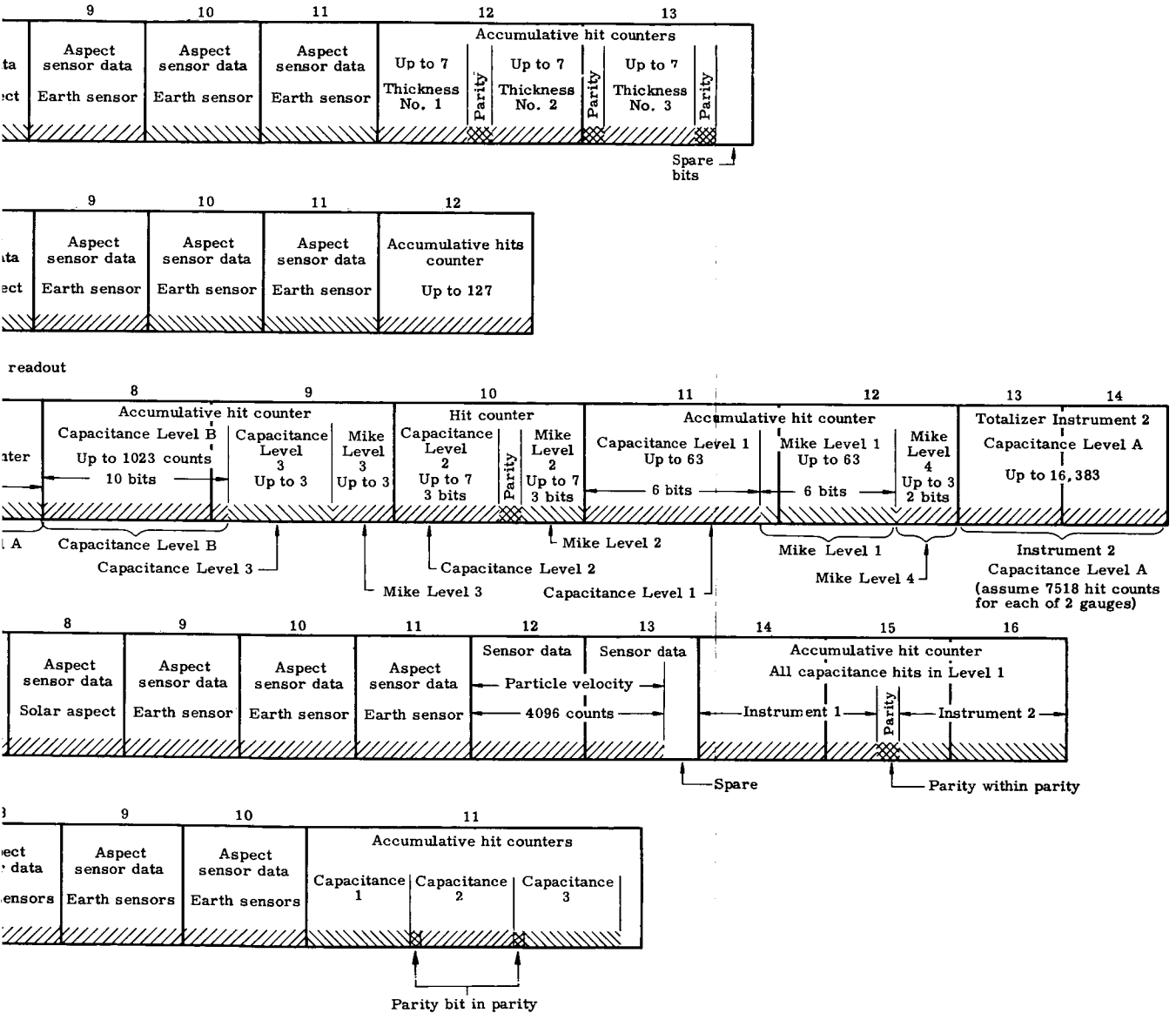


Fig. 5-7. Tradeoff: Fixed Format Versus Hit-Demand Frames: Hit-Demand Frames for Hit History with Aspect Data

Fig. 5-7. Tradeoff: Fixed Format Versus Hit-Demand Frames for Hit History with Aspect Data

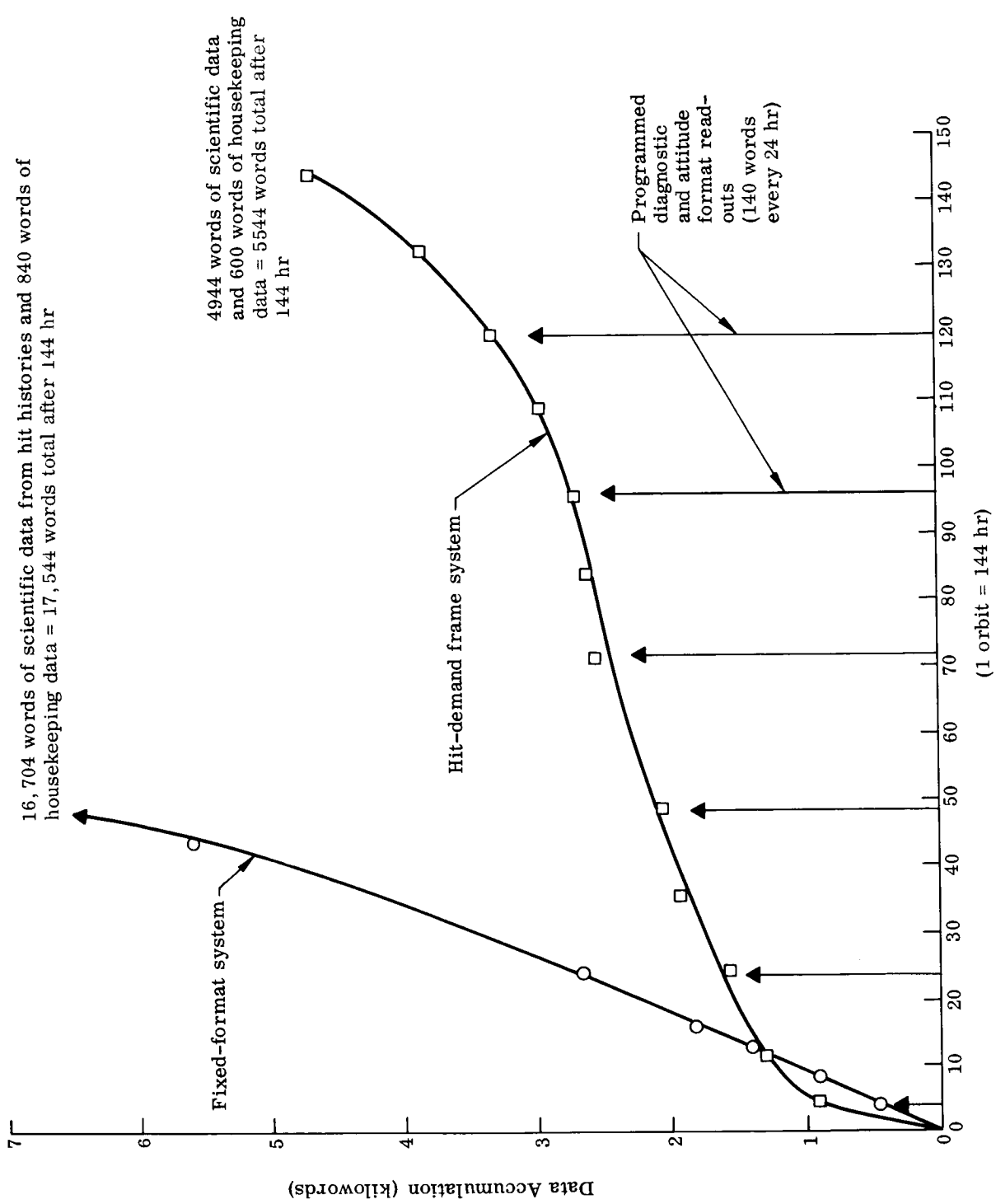


Fig. 5-8. Tradeoff: Fixed Format Versus Hit-Demand Frame, System Data Word Accumulation Versus Orbit Time

Conclusions from this tradeoff were:

(1) Data storage requirements for hit-demand frames are only 1/3 of that for a fixed word-sequence, with single format and programmed periodic measurements readouts.

(2) No complexity by multiple substorages.

(3) Only significant data processed and stored.

(4) Hit-demand frames have fixed word sequence, but require data words for synch and frame identification. Unequal word length of frames posed processing problems.

(5) Random storage read-in requires priority logic in case of simultaneous impacts.

Single format with fixed-word-sequence:

Advantages. This format has simplicity of operation, requires only one format synch, frames have equal word length, only one programmed storage read-in periodically.

Disadvantages. Substorage units required, larger main storage and longer data transmission time, not all transmitted data might be significant.

Further trade-off investigations to achieve equal word length hit-demand frames were undertaken. Hit-demand frames with and without attitude data were examined to minimize storage requirements. The results of these tradeoffs were:

(1) Equal word length hit-demand frames for hit history for all sensor groups, 10 data words.

(2) The attitude data words were removed from the hit-demand frames and consequently aspect data are handled and stored separately.

c. Tradeoff: Data frame accumulation versus data composition and orbit time

Conditions:

(1) Reduction of storage requirements by regulating storage admission for hit history frames; count-divide circuits.

(2) Evaluation of accumulated data composition for one orbit.

(3) Dividing only the number of the most frequently occurring hit-demand frames and repeat data load curve.

(4) Sensor complement as shown in Fig. 5-6.

(5) Hit history with attitude data (five words allocated).

(6) Reduction of storage requirement to increase systems reliability.

(7) Attitude and housekeeping data are programmed once per day.

(8) Mariner gauge data readout on full counter demand or periodic intervals.

The tradeoff study was to reduce storage requirements for orbit accumulation. Preset storage limiters allow only a certain number of hit history frames from each experiment group. Subsystems involved were capacitance panel sensors, cadmium sulfide cells with capacitor, velocity gages and Mariner gages. Housekeeping and attitude data were to be read into storage once daily.

To determine effects of hit-demand frame regulation on overall data loading quantitatively, data composition versus data accumulation versus orbit time was examined. Figure 5-9 illustrates a detailed breakdown of data load composition through a full orbit (6 days). The large contributions by velocity gage hit history frames to the overall data accumulation can be recognized by their respective curves.

In order to reduce this data contribution by the velocity gages (two units, eight sensor tubes) various alternatives were possible:

(1) Reduce the proposed sensitivity of the instrument by simply decreasing number of particle sensitive levels for capacitor and microphone sensors.

The reduction of levels is started with the most sensitive ones, i.e., eliminate microphone sensitivity level I, then eliminate capacitor sensitivity level I.

(2) Reduce the number of sensing tubes.

(3) Accept only a predetermined number of velocity gage hit-demand frames into storage and count the number of unaccepted frames with an overflow counter.

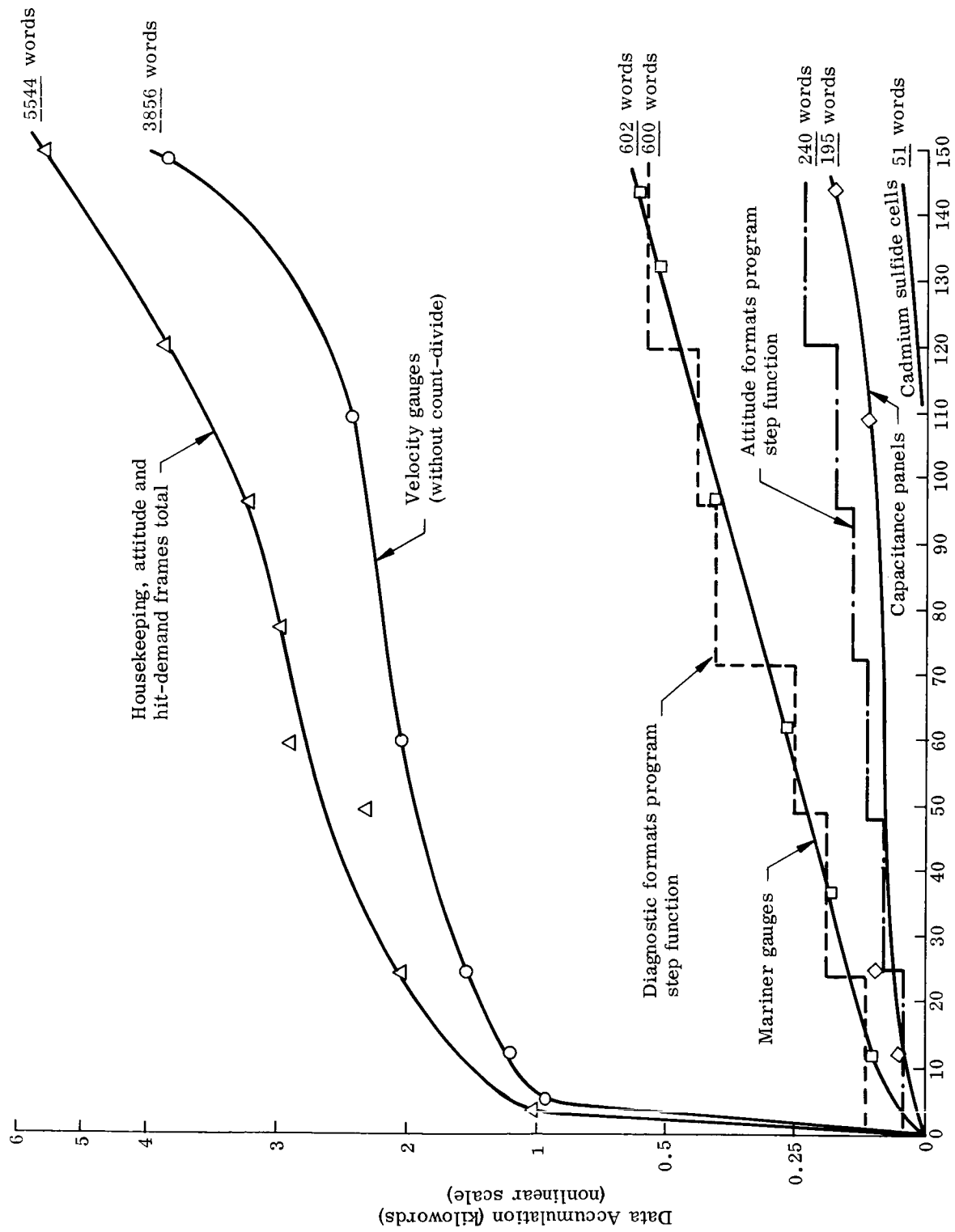


Fig. 5-9. Tradeoff: Hit-Demand Frames Divide Arrangement, Data Word Accumulation Versus Orbit Time

(4) Do not accept every initiated hit-demand frame for storage, but monitor all hits by counting in a counter for respective sensitivity level. Record complete hit history only for every 4th, 8th, 32nd, or 128th impact. A count-divide circuit, switchable by ground command, is feasible.

The latter course was considered the most practical from the point of scientific objectives and telemetry data handling. For example, by providing count-divide switch command capability even with a small storage capacity, all hit histories can be recorded and stored if ground stations can interrogate before data storage overflows. If no ground station is available or if flux density greatly exceeds predictions, count-divide circuits can be command-set to "divide by 8," then every eighth micrometeoroid impact is stored with hit history. This situation is shown in Fig. 5-10 for both cases. The difference in experiment data accumulation using a "divide by 8" regulation for the velocity gage is considerable. An overall data reduction of 61% in bit saving is achieved.

Although the divide down by command concept is desirable from the standpoint of flexibility, it was feared that reliability problems would outweigh the other advantages.

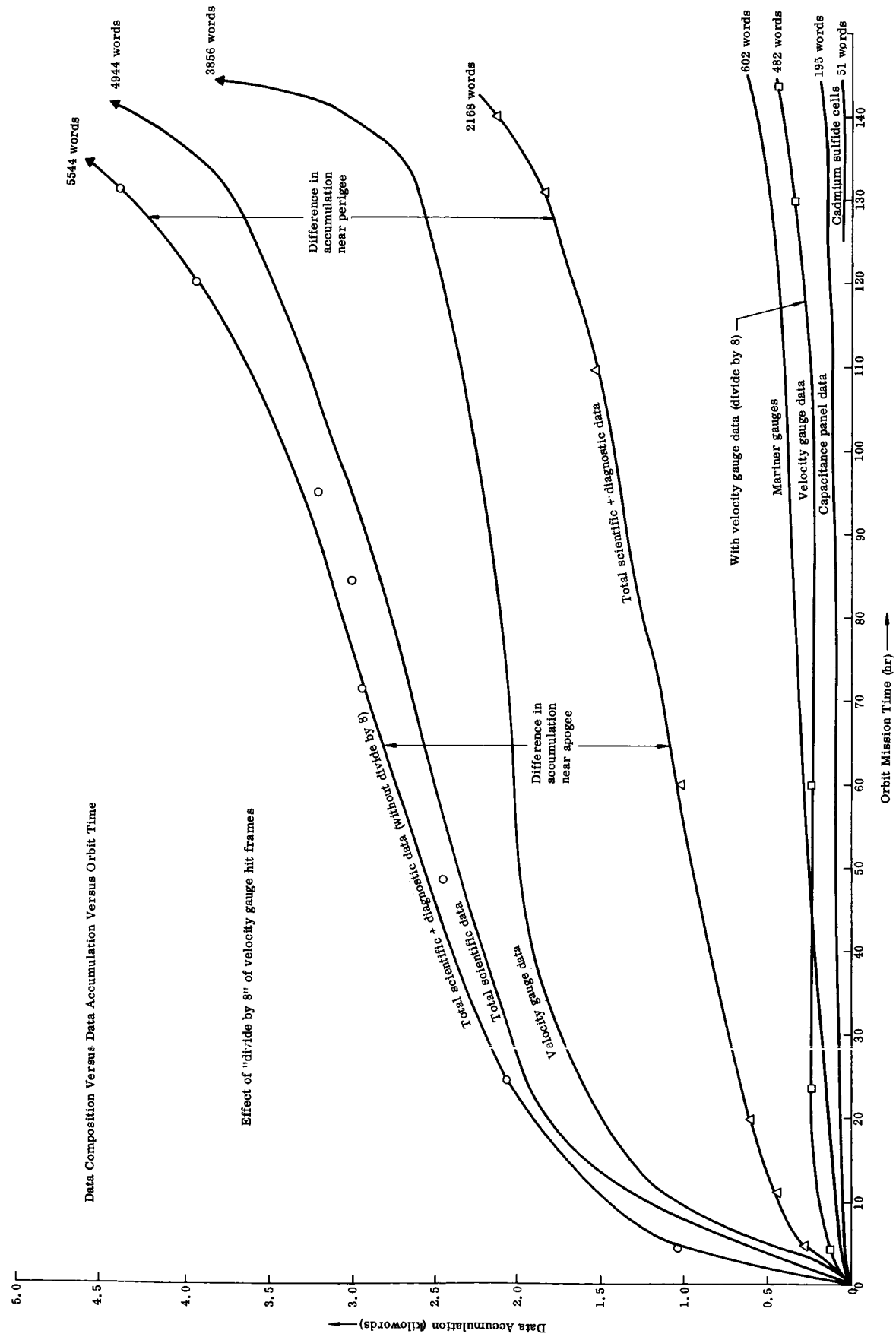


Fig. 5-10. Tradeoff: Hit-Demand Frames Divide Arrangement, Data Composition Versus Data Accumulation Versus Orbit Time

APPENDIX II-6

SATELLITE STUDY MODEL FOR TRADEOFF OF SUBSTORAGE AND FIXED WORD-SEQUENCE FORMAT VERSUS VARIABLE FORMAT

It should be noted that the following is a description of the initially developed model and does not represent the recommended system.

At the beginning, a satellite instrumentation and data processing model was developed based on individual substorages for experiments. Figure 6-1 illustrates the telemetry system, a fixed word-sequence measurement format, programmed at intervals in the micrometeoroid density zones, transferred data frames containing hit histories from substorages to main storage.

1. The Measurement Network

The measurement network consisted of sensors shown in Table 6-1. The network consisted of 181 scientific measurements and 42 sensors; 32 calibration, 34 housekeeping and 16 one-time verification measurements. Measurements comprised micrometeoroid hit data, calibration data, sensor diagnostic data taken instantaneously at hit event time for better calibration compensation, housekeeping data; environmental and performance data, one-time verifications and deployment data, and command verifications.

2. Impact Detection Subsystem

The sensor complement of the tradeoff study model consisted of five groups of hit-detection instrumentation (Table 6-1).

3. Capacitance Panel Sensors

This subsystem consisted of 20 panels of 2-mil and four panels of 1-mil thicknesses. Each penetrated sensor panel was identified by an assigned number to indicate directionality of hit. When two parallel sensors (opposite on top and bottom of frame) would be penetrated by one meteoroid, the hit history data could then, possibly, indicate two hits. A decision logic resolved this event by identical time and aspect data.

Sensor panel identification for impact was provided with five bits in the capacitance sensor data word. If no hits occurred prior to format readout, four different sensor panels were assigned every time

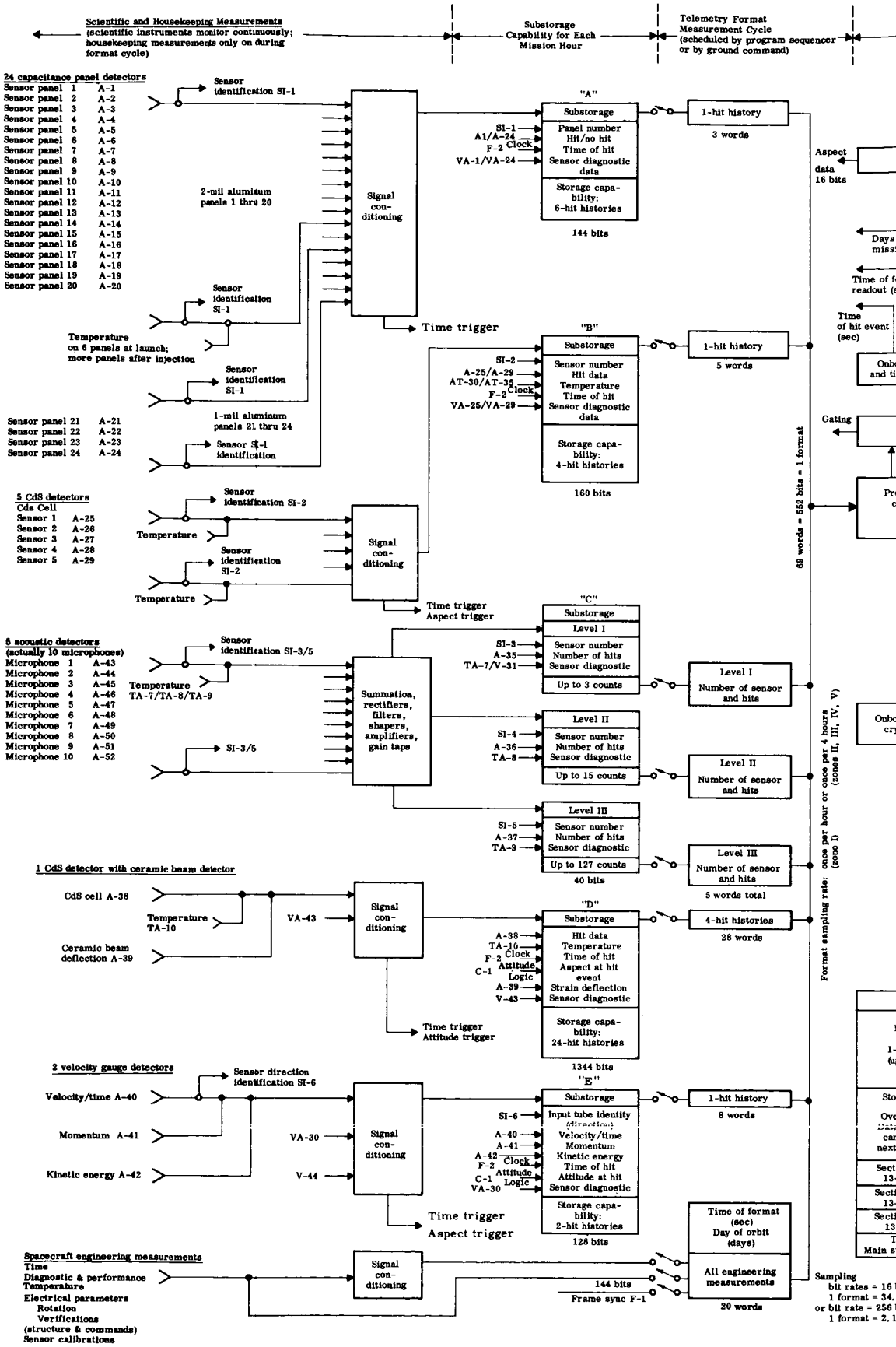
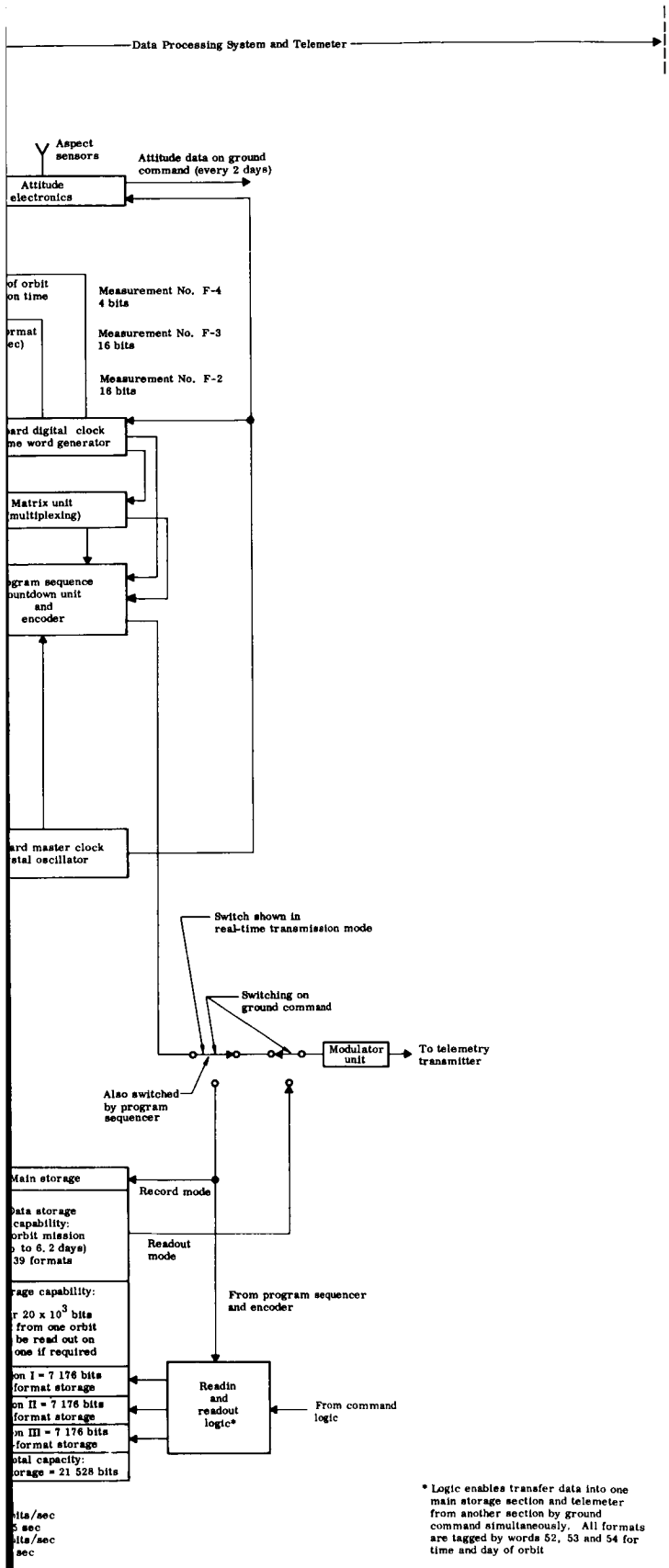


Fig. 6-1. Tradeoff
Instrumer
for Scier



Fixed Versus Variable Format: First Model Satellite
tation and Data Handling System Diagram with Substorage
tific Data (preliminary study model)

00-II

2#

TA

Tradeoff: Fixed Versus Vari
for Fixed F

Quantity of Sensors		Instruments	Micrometeoroid Hit History Inform				
			Bit Account Per Hit	Time of Event	Aspect or Attitude	HR Count	Substorage Capability
Total		Groups of Sensor Systems Type and Description	Bits Per Hit	(sec)	Solar Angle	Number of Hits	Number of Hit Histories
24		Capacitance Panel Sensors		X	--	X	6
	20	2-mil A target	24	X	--	X	
	4	1-mil A target	24	X	--	X	Readout 1 at format once
10		Acoustic Sensors	40 (3 levels)	--	--	X	145
		Microphone level 1	(2)	--	--	X	Read out accumulative hits in each level over 1- or 4-hr period
		Microphone level 2	(4)	--	--	X	
		Microphone level 3	(7)	--	--	X	
5	5	Cds Cell Sensors	40	X**	--	X	4
2	2	Velocity Gage Sensor	64	X	X	X	2
		Particle velocity/tube					
		Microphone output					
		Capacitor output					
		Direction/tube No.					
1	1	Cds Cell with Ceramic Beam	56	X	X	X	24
		Cell output					
		Beam deflection output					
42		All sensors			3 sensors	All	184***

LE 6-1

ble Format: Sensor Complement
ormat System

ation		Data Processing					
Hit Histories Per Format Readout Number of Hit Histories	Identification of Impacted Sensor	Sensor Output Prior to Processing (Fig. 6-1) Analog	 Digital	Assigned Measurement Number (Table 6-2) From/To	Assigned Format Word Number (Table 6-3) From/To	Per Format Number of Words	 Bits
1		X		A-1/A-24	Words Nos. 3 to 5	3	24
	X	X		A-1/A-2			
a time at each hr or once 4/hr	X	X		A-21/A-24			
Up to 145	X		X	A-35/A-37	Words Nos. 11 to 15	5	40
Up to 3			X	A-35	Word No. 11		
Up to 15			X	A-36	Word No. 13		
Up to 127			X	A-37	Word No. 15		
1			X	A-25/A-29	Words Nos. 6 to 10	5	40
1				A-40/A-42	Words Nos. 44 to 51	8	64
	X	X		A-40			
		X		A-41			
		X		A-42			
		X		S1-6			
4	X	X		A-38/A-39	Words Nos. 16 to 43	28	392
	All	32	10				

by a programmer for readout of diagnostic electrical and temperature data instead of hit histories to ensure a representative sampling of the status of all the capacitance panel sensors.

4. CdS Cell Sensors

Measurement would include the assigned number of the impacted sensor to obtain particle directionality and also, indirectly, functional verification of this specific sensor; the hit value, which would be a number proportional to the received light intensity; sensor temperature as reference for calibration compensation; and the hit event time at the instant the sensor would be aligned with the sun. Sensing units were distributed around the perimeter of the satellite.

5. Acoustic Sensor System

Impact signals detected on 10 microphone sensors were sorted into three different sensitivity levels. The collective and cumulative count of each of the three levels was stored in common counter. No hit-event-time was identified, since spacecraft time in the measurement format would identify the period over which these hit numbers were accumulated.

6. CdS Cell with Ceramic Beam Sensor System

Data requirements for this instrument included the hit value of the CdS cell, which would be a number proportional to the sensed light intensity; the quantized signal output proportional to the beam deflection; the event time of the hit; the solar aspect angles at the event time; and temperature/calibration data.

7. Velocity Gauge Subsystem

This subsystem was composed of two velocity gauges, each with four sensing tubes. Measurement data consisted of tube number identification in binary code for interpretation of particle directionality; output signals from microphone, and capacitor impact detectors for momentum and kinetic energy hit information; hit event time; spacecraft attitude data at the time of the hit; and 12-bit resolution data word for the measured particle velocity.

8. Considerations for Measurement Resolution

The required resolution of the various scientific and engineering measurements were examined. A word bit length of 7 was deemed satisfactory for all scientific data; exceptions were hit event time data and time of flight data for the velocity gauges.

9. Considerations for Telemetry Format

The telemetry format was composed of 69 data and 3 spare words. Tradeoffs resulted in a word bit length of 7 plus 1 bit parity. Table 6-2 presents a tabulation of measurements by types and Table 6-3 and Fig. 6-2 illustrate the fixed word-sequence and frame-length format. In Table 6-3, measurements are broken down in word syllables, specifically for housekeeping data.

Considerations were given for allowing a fixed bit word length for each measurement. This method would result in a less complex data handling system, since no logic equipment for word editing would be necessary. However, data storage requirements for this design approach were prohibitive.

10. Format and Storage Requirements versus Orbit Mission Tradeoff: Fixed Format

Considering the above described fixed frame length data format of 69 words (552 bits format length) and requirements of the scientific objectives for the five micrometeoroid density zones, 39 measurement format readouts would be necessary per orbit mission.

Tables 6-4 and 6-5 present the format bit accounting based on an assumed complement of micrometeoroid detectors (Table 6-1), an 8-bit word length, and scientific data substorage. Figure 6-2 illustrates data accumulation for an assumed orbit mission. Data load storage levels for instances when ground station time would be available or not available are indicated by bar graphs.

11. Considerations for Time Measurements

Resolution of incremental time measurements is dictated by requirements from scientific objectives. Other considerations are the effects on the accumulation rate of stored data, if the bit length of timing data words is considerable. This data contribution is specifically noticeable in the hit event time word and the time word for attitude measurements.

12. Resolution for Micrometeoroid Hit Time (fixed format) for First Study Model

An incremental time resolution of 1 sec was originally chosen to establish particle influx directionality from the velocity gauge and attitude data. (This time requirement was later changed to an incremental resolution of only 1 min, since a different attitude system was conceived.)

TABLE 6-2

Tradeoff: Fixed Format Versus Hit-Demand Frames Tabulation of Measurement Channel Allocations (first iteration of all measurements)

Running Number	Channel Designation	Measurand	Parameter	Type of Measurement	Remarks
1	F-1	Synch	Voltage	Formating and time	Frame synch: 16 bits
2	F-2	Time	Voltage	Formating and time	Hit time: 16 bits
3	F-3	Time	Voltage	Formating and time	Format time in seconds
4	F-4	Time	Voltage	Formating and time	Format time in orbit days
5	SI-1	Sensor number	Voltage	Sensor identification	Capacitance panel sensor ID (1-24)
6	SI-2	Sensor number	Voltage	Sensor identification	CdS cell sensors (1-5)
7	SI-3	Sensor number	Voltage	Sensor identification	Acoustic sensors Level I (1-10)
8	SI-4	Sensor number	Voltage	Sensor identification	Acoustic sensors Level II (1-10)
9	SI-5	Sensor number	Voltage	Sensor identification	Acoustic sensors Level III (1-10)
10	SI-6 SI-7	Sensor number Sensor number	Voltage Voltage	Sensor identification Sensor identification	Velocity gauge tubes (No. 1-4) Velocity gauge tubes (No. 5-8)
11 through 34	A-1 through A-24	Hit	Capacitor discharge and charge pulse	Scientific	Capacitance Panels 1 through 24
35 through 39	A-25 through A-29	Current	Hit	Scientific	CdS Cells 1 through 5
40 through 44	AT-30 through A-34	Temperature		Scientific	CdS Cells 1 through 5
45 through 47	A-35 through A-37	Hit counts		Scientific	Microphone Levels I, II and III
48	A-38	Current	Hit	Scientific	CdS cell and ceramic beam
49	A-39	Current	Hit on strain gauge	Scientific	CdS cell and ceramic beam
50	A-40	Velocity/time		Scientific	Velocity gauge: 12 bits
51	A-41	Momentum		Scientific	Velocity gauge: 8 bits
52	A-42	Kinetic energy		Scientific	Velocity gauge: 8 bits
53 through 62	A-43 through A-52	Voltage pulse		Scientific	Microphone outputs 1 through 10
63 through 86	VA-1 through VA-24	Voltage		Voltage	Capacitance panel sensor voltage
87 through 91	VA-25 through VA-29	Voltage		Voltage	CdS Cells 1 through 5
92	VA-30	Voltage		Voltage	Velocity gauge: 2 bits
93	VA-31	Voltage		Voltage	Microphone amplifier
94 through 103	V-32 through V-41	Voltage		Voltage	Microphone voltages 1 through 10
104	V-42	Voltage		Voltage	Microphone amplifier diagnostic
105	V-43	Voltage		Voltage	CdS cell and beam diagnostic
106	V-44	Voltage		Voltage	Velocity gauge diagnostic
107 through 112	T-1 through T-6	Temperature		Temperature	Capacitance panel temperature
113 through 115	TA-7 through TA-9	Temperature		Temperature	Microphone temperature Levels I, II and III
116	TA-10	Temperature		Temperature	CdS cell and beam temperature
117	T-11	Temperature		Temperature	Communication electronics compartment temperature

TABLE 6-2 (continued)

Running Number	Channel Designation	Measurand	Parameter	Type of Measurement	Remarks
118	T-12	Temperature		Temperature	Battery temperature No. 1
119	T-13	Temperature		Temperature	Battery temperature No. 2
120	T-14	Temperature		Temperature	Attitude electronics compartment temperature
121 through 126	TA-15 through TA-20	Temperature		Temperature	Capacitance panel temperatures 1 through 6
127	TA-21	Temperature		Temperature	Velocity gauge temperature
128	C-1	Aspect		Attitude	Aspect data: 16 bits
128	D-1			Electrical power system	Power source voltage No. 1
129	D-2			Electrical power system	Power source voltage No. 2
130	D-3			Electrical power system	Battery current No. 1
131	D-4			Electrical power system	Battery current No. 2
132	E-1	Temperature		Structural systems	Rocket firing verification
133 through 140	E-2 through E-9	Switch action		Structural systems	Capacitance panel erection verification
141 through 143	E-10 through E-12	Switch action		Structural systems	Antenna erection verifications 1, 2 and 3
144 through 147	E-13 through E-16	Switch action		Structural systems	Separation verifications 1 through 4
148	E-17	Switch action		Structural systems	Verifications
(117)	T-11	Temperature		Communication system	Electronics compartment center location
149	G-1	"On" bit	Voltage	Command verification	Turn on all experiments
150	G-2	"On" bit	Voltage	Command verification	Turn off capacitance panel system
151	G-3	"On" bit	Voltage	Command verification	Turn off CdS cell system
152	G-4	"On" bit	Voltage	Command verification	Turn off microphone system
153	G-5	"On" bit	Voltage	Command verification	Turn off velocity gauge system
154	G-6	"On" bit	Voltage	Command verification	Turn off all experiments
155	G-7	"On" bit	Voltage	Command verification	Read out real time data continuously
156	G-8	"On" bit	Voltage	Command verification	Read out real time 3 times and erase
157	G-9	"On" bit	Voltage	Command verification	Read out stored data
158	G-10	"On" bit	Voltage	Command verification	Read out attitude data
159	G-11	"On" bit	Voltage	Command verification	Range and range rate mode
160	G-12	"On" bit	Voltage	Command verification	Turn off telemetry
161	G-13	"On" bit	Voltage	Command verification	Update master clock
162	G-14	"On" bit	Voltage	Command verification	Emergency mode (command receiver and beacon)
164	G-15	"On" bit	Voltage	Command verification	Erection backup command

TABLE 6-3

Tradeoff: Fixed Word Sequence Versus Variable Sequence--Tabulation of Fixed Format Measurements (first iteration of all measurements)

Priority																		
Mandatory	Very Desirable	Desirable	Optional	Running Format (words)	Measurement Number	Designation of Measurement	Type of Data	Measurand	Sampling Rate	Format Time Start (sec)	Range: Actual Units (range or sensitivity)	Range: Count (decimal code)	Range: Bit Accounting (binary)	Accuracy	Measurement Correlation	Remarks
1	2	3	4	5	6	7	8	9	10	11	12	13	14	15	16	17
X				1	F-1	Format synch	Timing	--	1/hr or 1/4 hrs	0.0	Frame code	--	8	--		Unique code for identification for start of format and format synchronization in ground stations.
X				2		Format synch	Timing	--	1/hr or 1/4 hrs	0.5	Frame code	--	8	--		
				3		Capacitance Panel Detector Hit History	Scientific		Continuously	1.0					Correlates with Words 64, 65, 66	
X					SI-1	Sensor identification	Scientific	Number of detector	Continuously		Instrument code	0/24	5	±1/2 bit	Correlates with Word 61	Number and location of capacitance panel detector where micrometeoroid hit occurred.
X					A-1/A-24	Sensor hit data	Scientific	Meteoroid hit data	Continuously		Hit count	0/1	1		With SI-1	Discharge and recharge pulse indicate hit.
	X				V-1/V-24	Sensor diagnostic	Diagnostic	Voltage	Continuously		0/40 volts	0/3	2	±10 volts	With SI-1	Functional monitoring of sensor.
	X			4	F-2	Time of hit event	Timing	Time	Continuously	1.5	0/86 400 sec	0/86 400	8	±0.5 sec	Correlates with Words 52, 53, 54 (meas F-3 and F-4)	Time of micrometeoroid impact in seconds counted from 0^{00} hr spacecraft time; clock is reset every 24 hr to 0. Can be referred to satellite time (F-3) and orbit days (F-4).
	X			5		Time of hit event	Timing	Time	Continuously	2.0						
				6		CdS Cell Detector Hit History	Scientific		Continuously	2.5						
X					SI-2	Sensor identification	Scientific	No. of detector	Continuously		Instrument code	0/5	3	±1/2 bit		Number and location of CdS cell detector where hit occurred.
	X				VA-25/ VA-29	Sensor diagnostic	Diagnostic	Voltage	Continuously		0/volts	0/31	5	±10%	With SI-2	Functional verification of sensor operation.
X				7	A-25/A-29	Sensor hit data	Scientific	Meteoroid hit data	Continuously	3.0	Current	0/127	8	±0.5%	With SI-2	Current variation indicates meteoroid hit.
X				8	AT-30/ AT-35	Sensor data calibration	Calibration	Temperature	Continuously	3.5	$-30^{0}/+30^{0}$ C	0/127	8	$\pm 0.5^{0}$ C	With SI-2	Temperature is monitored for calibration compensation of each sensor data.
	X			9	F-2	Time of hit event	Timing	Time	Continuously	4.0	0/86 400 sec	0/86 400	8	±0.5 sec	With SI-2	Same as Word 4 above for SI-2.
	X			10		Time of hit event	Timing	Time	Continuously	4.5			8			Same as Word 4 above.
				11		Acoustic Sensor Level I Hit History	Scientific		Continuously	5.0						
X					SI-3	Sensor identification	Scientific	Microphone No.	Continuously		Number of detector	0/10	4	--		Number and location of microphone which registered last hit.
X					A-35	Cumulative hit number	Scientific	Meteoroid hit data	Continuously		Hit count	0/3	2	±1/2 bit	All microphones	Cumulative number of hits since last format read-out for Level I.
	X				V-31	Amplifier function	Scientific	Amplifier voltage	Continuously		Voltage	0/25	2	±10%	All microphones	Functional verification of sensor group for all 3 Levels.
X				12	TA-7	Microphone temperature	Scientific	Calibration	Continuously	5.5	Temperature $-20^{0}/+40^{0}$ C	1/16	4	$\pm 4^{0}$ C	With SI-3	Temperature is monitored for calibration compensation of sensor which registered last hit.
						Acoustic Sensor Level II Hit History	Scientific		Continuously							
X					SI-4	Sensor identification	Scientific	Microphone No.	Continuously		Number of detector	0/10	4	±1/2 bit		Number and location of microphone which registered last hit.
X				13	A-36	Cumulative hit number	Scientific	Meteoroid hit data	Continuously	6.0	Hit count	1/16	4	±1/2 bit	All microphones	Cumulative number of hits since last format read-out for Level II.
X					TA-8	Microphone temperature	Scientific	Calibration	Continuously		Temperature $-20^{0}/+40^{0}$ C	1/16	4	$\pm 4^{0}$ C	With SI-4	Temperature is monitored for calibration compensation of sensor which registered last hit.
				14		Acoustic Sensor Level III Hit History	Scientific			6.5						
X					SI-5	Sensor identification	Scientific	Microphone No.	Continuously		Number of detector	0/10	4	±1/2 bit		Number and location of microphone which registered last hit.
X					TA-9	Microphone temperature	Scientific	Calibration	Continuously		Temperature $-20^{0}/+40^{0}$ C	1/16	4	$\pm 4^{0}$ C	With SI-5	Temperature is monitored for calibration compensation of sensor which registered last hit.
X				15	A-37	Cumulative hit Number	Scientific	Meteoroid hit data	Continuously	7.0	Hit count	0/127	8	±1/2 bit	All microphones	Cumulative number of hits since last format read-out for Level III.
X				16	A-38	CdS with Ceramic Beam Sensor	Scientific	Meteoroid hit data	Continuously	7.5	Current	0/127	8	±0.5%		Current variation indicates impact.
X				17	TA-10	Sensor data calibration	Scientific	Temperature	Continuously	8.0	$-20^{0}/+40^{0}$ C	1/128	8	$\pm 10^{0}$ C	With A-38	Temperature is monitored for calibration compensation of sensor.
X				18	A-39	Sensor data strain gauge	Scientific	Deflection	Continuously	8.5	Current	0/127	8	±0.5%	With A-38	Indicates impact momentum.
X				19	C-1	Aspect data	Orientation	Solar angle	Continuously	9.0	$0/180^{0}$	0/127	8		Correlates directionality of impacting particle.	Angle of sun line to spin axis at hit event for A-38.
X				20		Aspect data	Orientation	Rotation time	Continuously	9.5	200 cps signal	0/127	8	±0.005 sec		Time to first sun sighting after hit for A-38.
X				21	F-2	Time of hit event	Timing	Time	Continuously	10.0	0/86 400 sec	0/86 400	8	±0.5 sec	With Word 16	Same as Word 4 above for A-38.
X				22		Time of hit event	Timing	Time	Continuously	10.5			8		With Word 16	Same as Word 4 above for A-38.
X				23	A-38	Repeat word 16	Scientific			11.0			8			2nd storage hit history for CdS beam sensor
X				24	TA-10	Repeat word 17	Scientific			11.5			8			
X				25	A-39	Repeat word 18	Scientific			12.0			8			
X				26	C-1	Repeat word 19	Orientation			12.5			8			
X				27		Repeat word 20	Orientation			13.0			8			
X				28	F-2	Repeat word 21	Timing			13.5			8			
X				29		Repeat word 22	Timing			14.0			8			
X				30	A-38	Repeat word 16	Scientific			14.5			8			3rd storage hit history for CdS beam sensor
X				31	TA-10	Repeat word 17	Scientific			15.0			8			
X				32	A-39	Repeat word 18	Scientific			15.5			8			
X				33	C-1	Repeat word 19	Orientation			16.0			8			
X				34		Repeat word 20	Orientation			16.5			8			
X				35	F-2	Repeat word 21	Timing			17.0			8			
X				36		Repeat word 22	Timing			17.5			8			
X				37	A-38	Repeat word 16	Scientific			18.0			8			4th storage hit history for CdS beam sensor
X				38	TA-10	Repeat word 17	Scientific			18.5			8			
X				39	A-39	Repeat word 18	Scientific			19.0			8			
X				40	C-1	Repeat word 19	Orientation			19.5			8			
X				41		Repeat word 20	Orientation			20.0			8			
X				42	F-2	Repeat word 21	Timing			20.5			8			
X				43		Repeat word 22	Timing			21.0			8			
				44		Velocity gauge sensor	Scientific		Continuously							
X					A-40	Velocity data	Scientific	Time	Continuously	21.5	Time count	0/4 096	8		Correlates with words 46, 47	Particle velocity 8 out of 12 bits.
X				45		Velocity data	Scientific	Time	Continuously	22.0	Time count		4			Particle velocity 4 out of 12 bits.
X					SI-6	Sensor identification	Scientific	Direction	Continuously		Number of tube	0/4	2	$\pm \frac{\pi}{2}$ steradians		Directionality of impacting particle.
		X			VA-30	Sensor function	Diagnostic	Voltage level	Continuously		Voltage		2		With SI-6	Functional verification of sensor operation.
X				46	A-41	Momentum data	Scientific	Momentum	Continuously	22.5			8		With SI-6	Momentum of impacting particle.
X				47	A-42	Kinetic energy	Scientific	Kinetic energy	Continuously	23.0			8		With SI-6	Kinetic energy of impacting particle.
X				48	C-1	Aspect data	Orientation	Solar angle	Continuously	23.5			8		Correlates directionality of impacting particle	Same as Word 19, but for SI-6.
X				49		Aspect data	Orientation	Rotation time	Continuously	24.0			8			Same as Word 20, but for SI-6.
X				50	F-2	Time of hit event	Timing	Time	Continuously	24.5	0/86 400 sec	0/86 400	8		Correlates with words 52, 53, 54	Same as Word 4 above for SI-6.
X				51		Time of hit event	Timing	Time	Continuously	25.0			8			Same as Word 4 above for SI-6.
	X			52	F-3	S/C Housekeeping Format time (sec)	Timing	Time	1/hr or 1/4 hr	25.5	0/86 400 sec	0/86 400	8		Correlates with Words 4, 5, 9, 10, 21, 22, 28, 29, 35, 36, 42, 43, 50, 51	Hit times are referred to satellite time in sec; orbit mission time in days.
	X			53		Format time (sec)	Timing	Time	1/hr or 1/4 hr	26.0			8			
	X			54	F-4	Orbit time (days)	Timing	Count of days	1/hr or 1/4 hr	26.5	0/7 days	0/16	4			
		X			T-11	Compartment temperature	Diagnostic	Temperature	1/hr or 1/4 hr		Temperature $-20^{0}/+50^{0}$ C	1/16	4	$\pm 4.5^{0}$ C		Status measurement of Telecommunications Electronics Compartment temp.
		X		55	D-1	Power source voltage 1	Diagnostic	Voltage level	1/hr or 1/4 hr	27.0	Voltage 24/36 V	1/128	8	±1%	Word 57	Status measurement of power subsystem.

TABLE 6-3 (continued)

Priority*																	
Mandatory	Very Desirable	Desirable	Optional	Running Format (words)	Measurement Number	Designation of Measurement	Type of Data	Measurand	Sampling Rate	Format Time Start (sec)	Range: Actual Units (range or sensitivity)	Range: Count (decimal code)	Range: Bit Accounting (binary)	Accuracy	Measurement Correlation	Remarks
1	2	3	4	5	6	7	8	9	10	11	12	13	14	15	16	17
			X	56	D-2	Power source voltage 2	Diagnostic	Voltage level	1/hr or 1/4 hr	27.5	Voltage 24/36 V	0/15	8	±1%	Word 58	Status measurement of power subsystem.
		X		57	D-3	Battery 1 current	Diagnostic	Charge level	1/hr or 1/4 hr	28.0	Current		8	±1%		Status measurement of power subsystem.
			X	58	D-4	Battery 2 current	Diagnostic	Charge level	1/hr or 1/4 hr	28.5	Current		8	±1%		Status measurement of power subsystem.
		X		59	T-12	Battery 1 temperature	Diagnostic	Status	1/hr or 1/4 hr	29.0	-20°/+50° C	0/15	4	±10%	Word 57	Status measurement of power subsystem.
			X		T-13	Battery 2 temperature	Diagnostic	Status	1/hr or 1/4 hr		-20°/+50° C		4	±10%	Word 58	Status measurement of power subsystem.
		X		60	T-14	Compartment temperature	Diagnostic	Temperature	1/hr or 1/4 hr	29.5	-20°/+50° C		4	±10%	Measurement C-1	Performance measurement of aspect sensor optics and attitude electronics.
		X			E-1	Rocket firing	Verification	Acceleration	One-time		0/30 g	0/15	4	±10%		Verification for rocket operation by measuring spacecraft acceleration.
		X		61	E-2	Capacitance panel erection 1	Verification	Switch action	One-time	30.0	Voltage	On/off	1		Words 3, 4, 5, 64, 65, 66	Status of capacitance detection system.
			X		E-3	2	Verification						1			Note: An additional bit for each panel erection verification measurement must be allocated since 1 bit is necessary for verification or unlock-from-stowed-position and 1 bit for lock-in-deployed position verification.
		X			E-4	3	Verification						1			
			X		E-5	4	Verification						1			
		X			E-6	5	Verification						1			
			X		E-7	6	Verification						1			
		X			E-8	7	Verification						1			
			X		E-9	8	Verification						1			
X				62	E-10	Antenna erection 1	Verification			30.5			1			Status of telecommunication system.
	X				E-11	2	Verification						1			
			X		E-12	3	Verification						1			
	X				E-13	Separation 1	Verification						1			Status of squib firing.
	X				E-14	2	Verification						1			Note: All one-time measurement channels will be replaced with channels for temperature measurements for capacitance panel sensors after injection phase (in addition to 6 below).
	X				E-15	3	Verification						1			
	X				E-16	4	Verification						1			
	X				V-31	Microphone amplifier	Diagnostic	Voltage	1/hr or 1/4 hr		Voltage	0/1	1		With V-31	Gain calibration check of amplifier output
X				63	E-17	Spin rotation	Performance	Rotation	One-time	31.0	0/200 rpm	0/127	8	± 2 rpm		Verification for spin-up and despin procedures.
	X			64	TA-15	Capacitance panel sensor temperature 1	Diagnostic	Temperature	1/hr or 1/4 hr	31.5	-110°/+110° C	1/16	4	±15° C	Correlates with Words 3, 4, 5	Status measurement of capacitance sensors.
		X			TA-16	Capacitance panel sensor temperature 2	Diagnostic	Temperature	1/hr or 1/4 hr		-110°/+110° C	1/16	4	±15° C	Correlates with Words 3, 4, 5	
	X			65	TA-17	Capacitance panel sensor temperature 3	Diagnostic	Temperature	1/hr or 1/4 hr	32.0	-110°/+110° C	1/16	4	±15° C	Correlates with Words 3, 4, 5	
			X		TA-18	Capacitance panel sensor temperature 4	Diagnostic	Temperature	1/hr or 1/4 hr		-110°/+110° C	1/16	4	±15° C	Correlates with Words 3, 4, 5	
			X	66	TA-19	Capacitance panel sensor temperature 5	Diagnostic	Temperature	1/hr or 1/4 hr	32.5	-110°/+110° C	1/16	4	±15° C	Correlates with Words 3, 4, 5	
			X		TA-20	Capacitance panel sensor temperature 6	Diagnostic	Temperature	1/hr or 1/4 hr		-110°/+110°	1/16	4	±15° C	Correlates with Words 3, 4, 5	
		X		67	V-32	Microphone status 1	Diagnostic	Bias voltage	1/hr or 1/4 hr	33.0	Voltage	0/1	1		Correlates with Words 11, 12, 13, 14, 15	Voltage check and status of microphones.
			X		V-33	2			1/hr or 1/4 hr			0/1	1			
		X			V-34	3			1/hr or 1/4 hr			0/1	1			
			X		V-35	4			1/hr or 1/4 hr			0/1	1			
		X			V-36	5			1/hr or 1/4 hr			0/1	1			
			X		V-37	6			1/hr or 1/4 hr			0/1	1			
		X			V-38	7			1/hr or 1/4 hr			0/1	1			
			X		V-39	8			1/hr or 1/4 hr			0/1	1			
		X		68	V-40	9			1/hr or 1/4 hr	33.5		0/1	1			
			X		V-41	10			1/hr or 1/4 hr			0/1	1			
			X		V-42	Microphone ampl electronics	Diagnostic	Voltage	1/hr or 1/4 hr			0/1	1		Words 11, 12, 13, 14, 15	Status of microphone electronics.
		X			V-43	CDS and ceramic beam sensor	Diagnostic	Voltage	1/hr or 1/4 hr			0/3	2		Correlates with Word 16	Instrument status.
		X			V-44	Velocity gauge sensor *	Diagnostic	Voltage	1/hr or 1/4 hr			0/7	3		Words 44, 45, 46, 47	Instrument status.
X				69		Spare channel	——	——	1/hr or 1/4 hr	34.0			8			
56	18	19	17	69		Totals/Format	All	1/hr or 1/4 hrs					552			

*Can be replaced with command verification.

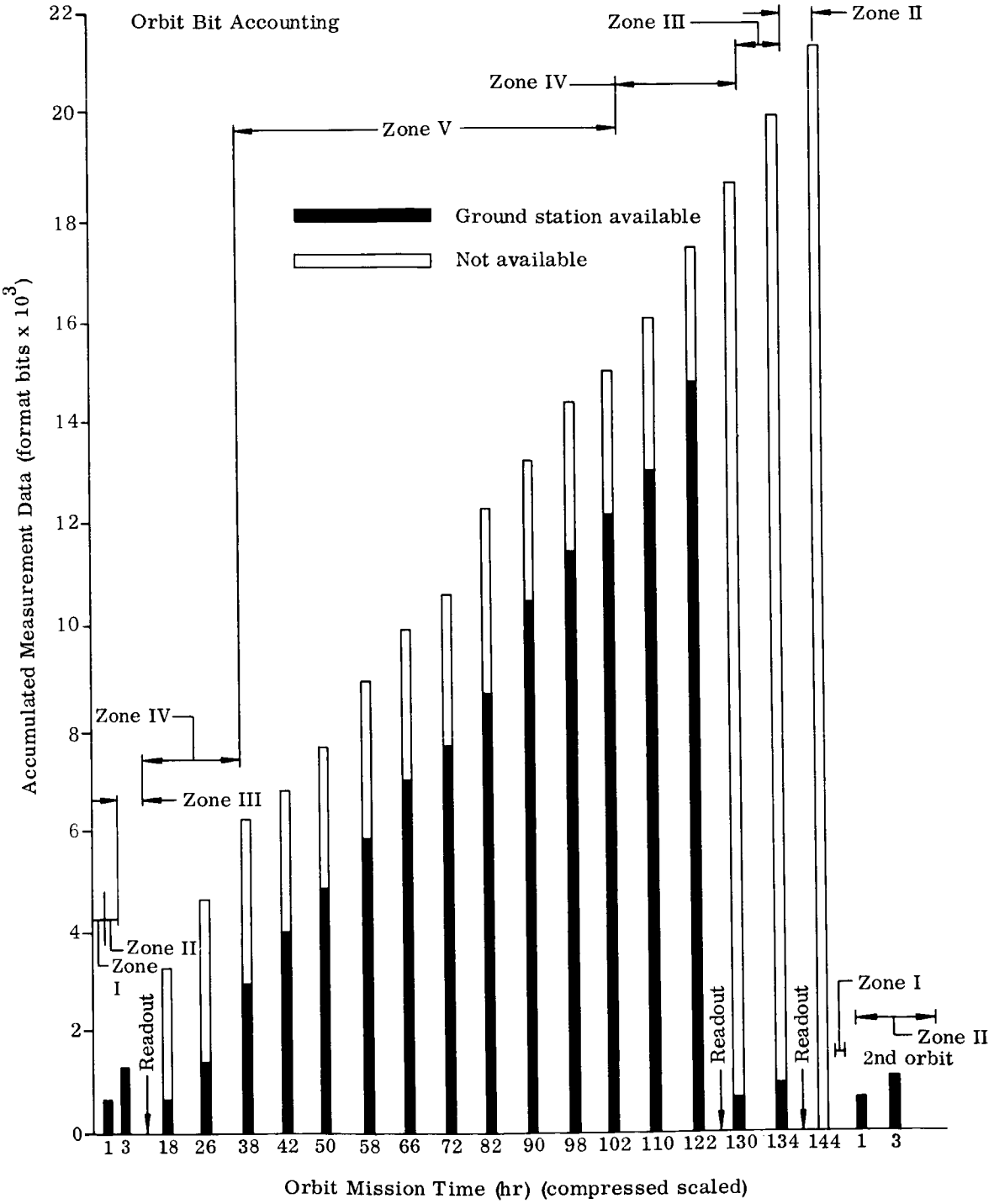


Fig. 6-2. Tradeoff: Fixed Versus Variable Format: Substorage Versus Random Storage Readin (first iteration of data requirements)

TABLE 6-4

Tradeoff: Fixed Versus Variable Format; Substorage Versus Random Storage Read-in
(first iteration of data requirements)

Format Bit Accounting

Data	Per Sensor		Total Format	
	Words	Bits	Words	Bits
Format sync	2	16	2	16
(24) capacitance panels, 1 read-out of 6 stored	3	24	3	24
(5) CdS sensors, 1 read-out of 4 stored	5	40	5	40
(10) acoustic sensors, accumulative counts in 3 levels	5	40	5	40
(1) CdS sensor + beam, 4 read-out of 24 stored	7	56	28	228
(2) velocity sensors, 1 read-out of 2 stored	8	64	8	64
(50) spacecraft housekeeping measurements	18	144	18	144
			69	552

TABL

Fixed Word Sequence Format
Micrometeoroid

Micrometeoroid Density Zone	Altitude (naut mi)		Orbital Time (hr)	Hit History Scientific Data								
				24 Capacitance Panel Sensors			5 CdS Cell Sensors			5 Paired Acoustic Sensors		
	Perigee	Apogee		Total Hit Probability Hits/Yr	Data Bits/1 Hit	Sub-storage Capability (bits x 6)	Total Hit Probability Hits/Yr	Data Bits/1 Hit	Sub-storage Capability (bits x 4)	Total Hit Probability Hits/Yr	Data Bits/1 Hit/1 of 3 Levels	Subst Capa (hi Le I II
Zone I	100	12×10^3	2	60	24	144	34	40	160	6810	12	
Zone II	12×10^3	29.5×10^3	4	32	24	144	18	40	160	3030	12	
Zone III	29.5×10^3	70×10^3	18	48	24	144	27	40	160	4545	12	
Zone IV	70×10^3	123×10^3	48	54	24	144	30	40	160	5105	12	
Zone V	123×10^3	150×10^3	72	50	24	144	28	40	160	4750	12	

12 bits or up to 3 hits in Level I

145 h
total
levels

E 6-5

Data Accumulation Versus Density Zones

	1 CdS Cell with Ceramic Beam Sensor			2 Velocity Gauge Sensors			Data Processing and Telemetry					
									Accumulated Telemetry Data During 1 Orbit Mission, No Ground Station Available			
									Orbit Mission on the Way Out		Orbit Mission Coming In	
rage bility s) vel III	Total Hit Probability Hits/Yr	Data Bits/1 Hit	Sub-storage Capability (bits x 24)	Total Hit Probability Hits/Yr	Data Bits/1 Hit	Sub-storage Capability (bits x 2)	Storage Required S/C House-keeping per 1 Format (bits)	Selected Format Sampling Rate (1/unit time)	Frame Number	Accumulated Bits	Frame Number	Accumulated Bits
16 bits or up to 127 hits in Level III	951	56	1344	120	64	128	160	1/hr	2	1,104	39	21,528*
	507	56	1344	64	64	128	160	1/4 hr	3	1,656	36	19,872
	762	56	1344	96	64	128	160	1/4 hr	5	2,760	35	19,320
	855	56	1344	104	64	128	160	1/4 hr	11	6,072	34	18,768
	792	56	1344	104	64	128	160	1/4 hr	19	10,488	28	15,456

*Can be read out in next orbit if no ground station was available during previous orbit.

ts
or 3

2 #

II-6-12

The time of each meteoroid hit (with the exception of hits sensed by the acoustic detection system) would then be recorded in standard 16-bit binary time code (0- to 86,400-sec range). This count gave hit event time (in sec) of each day and is reset every 24 hr. Reference is made to Table 6-3, where format Words 52, 53 and 54 relate the satellite time (in sec) up to 24 hr and the number of days of each orbit period, respectively. Thus, each hit event time could be referred to the satellite time in the format.

A tradeoff against hit penalty for data storage with this hit timing scheme was made by counting hits (in sec) between measurement format sampling. Since the longest periods of 4 hr between format cycles occur in Density Zones II through V, a second-count of 14,400 sec was satisfactory (2^{14} bits). This would be a bit storage saving of 7 x 2 = 14 bits per format or 39 x 14 = 546 bits saving for orbital data accumulation. Other tradeoff studies in bit accounting versus space-borne and ground station equipment complexity and weight considerations did not justify these counting operations in octal, duodecimal or special code to reduce onboard storage and telemeter requirements.

Timing data for hit event time are obtained in digital code from the master clock by a trigger pulse from a sensor at a hit. Figure 6-1 illustrates this concept. Hit time resolution is within ± 0.5 bit ± 0.5 seconds. Since solar aspect (or earth aspect) is measured at the same time, and sensor location is identified with assigned numbers, particle directionality can be reconstructed by analysis.

13. Timing for Attitude Data

Time measurements for attitude determination for the tumbling spacecraft is required. The attitude logic received a high resolution timing signal from the master clock to determine sun position. When the CdS cell ceramic beam sensor or velocity gauge registered a hit, a trigger pulse initiated transfer of aspect data in digital format into the substorage of the respective sensor. A full complement of attitude data was read out by ground command from the onboard attitude logic periodically.

14. Hit History Data in Substorage

Hit history information to supplement impact measurement was deemed to be of singular importance, although a heavy bit penalty has to be paid. Considerations were given for data sharing of hit history information in cases of simultaneous events by different type sensors.

Originally, the concept of sensor identification for each capacitance panel in the hit history data would serve a dual purpose: crude

recognition of the particle directionality, and verification by this identified sensor of its functional operation. If, for example, the data from a number of unidentified sensors would indicate an incredible low hit number in correlation with the data obtained by other experiments, it would remain unresolved as to whether this would be true data or if the sensors had ceased to operate at some time during the mission. In the recommended model, ambiguity of the number of operating panels was resolved by the effective area measurements.

15. Tradeoff Considerations for Substorage Concept

Separate and independent substorage units for each group of micrometeoroid hit sensors were considered in determining the first model requirements.

A probability analysis of the number of anticipated micrometeoroid impacts for each of the different type sensor groups was conducted to determine the required storage capacity of a substorage unit for this particular sensor group, and to determine the minimum number of required measurement format cycles for transferring micrometeoroid hit data from all substorage units into main storage.

Independent substorage units for each group of micrometeoroid hit detection experiments served a number of purposes in a fixed measurement format system:

(1) In case of simultaneous hits on two sensors from different experiment groups, each hit data is registered in the respective substorage for this particular sensor group--no significant data would be lost. For the same case, without substorage units, a priority logic and hold-shift registers would be required to transfer one group of hit data from one of the detectors and then the other group of hit data into a single storage.

(2) Micrometeoroid hit data which might occur at the time of a commanded stored data readout from the main storage would now be shifted into a substorage until the next programmed measurement cycle for transferring data from substorage to main storage takes place: no data are lost.

(3) The various groups of sensor systems, each with separate substorage remain independent of each other and afford a better isolation between subsystems in case of a malfunction in a particular group.

A probability analysis for the data substorage requirements for each sensor group was conducted. Table 6-5 shows the results for each

micrometeoroid density zone under the worst anticipated condition and their respective substorage requirements. Figure 6-1 illustrates a possible arrangement for the different substorage units, each shown with bit requirements.

The following substorage provisions resulted:

Quantity	Sensor Group Subsystem	Substorage Capacity (Storage time = 1 or 4 hr)
24	Capacitance panel detectors	6 hit histories
5	CdS cell detectors	4 hit histories
10 x 1/2	Acoustic detectors	up to 145 hit counts in 3 levels
1	CdS with ceramic beam	24 hit histories
2	Velocity gauges	2 hit histories
Total 42	All sensors	181 hits recorded

This scheme would enable the system to store in the various substorage units up to 181 micrometeoroid hit data measurements covering a period of 1 hr in Density Zone I and a period of 4 hr in Density Zones II through V. During the measurement format sampling, only one hit history of the capacitance panel sensors, one hit history of the CdS cell sensors, all accumulated hit counts of the acoustic sensors (in 3 levels), four hit histories of the CdS cell with ceramic beam sensor and one hit history of the velocity gauge sensor would be read out. The number of hit histories per format read out from each substorage was based on a probability analysis.

16. Disadvantage of a Substorage

In case of no meteoroid impacts between format sampling cycles, substorage data would include excessive words consisting of all zeros. Only sensor calibration data, like temperature and voltage levels would give significant information.

Another disadvantage of a number of substorage units would be the required number of ancillary circuits such as write-in and readout modules, which would increase systems complexity.

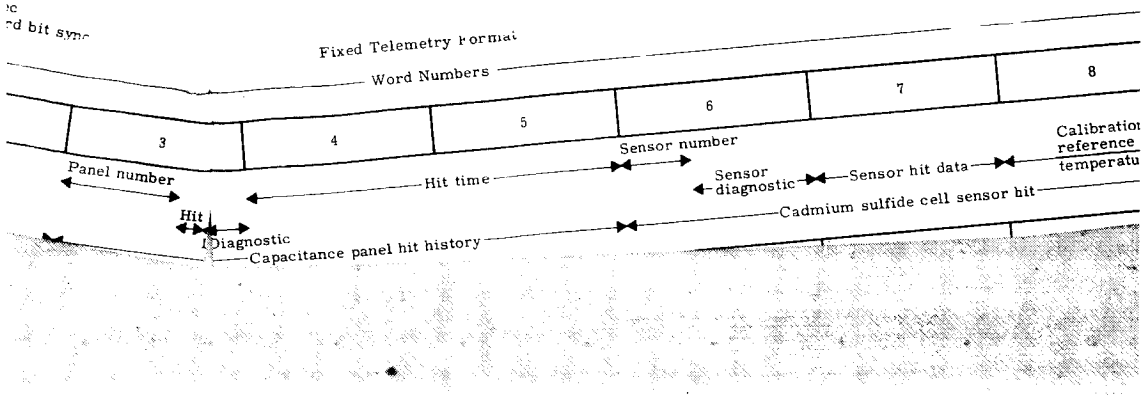
17. Tradeoff Considerations for the Main Storage with Fixed Format and Substorage

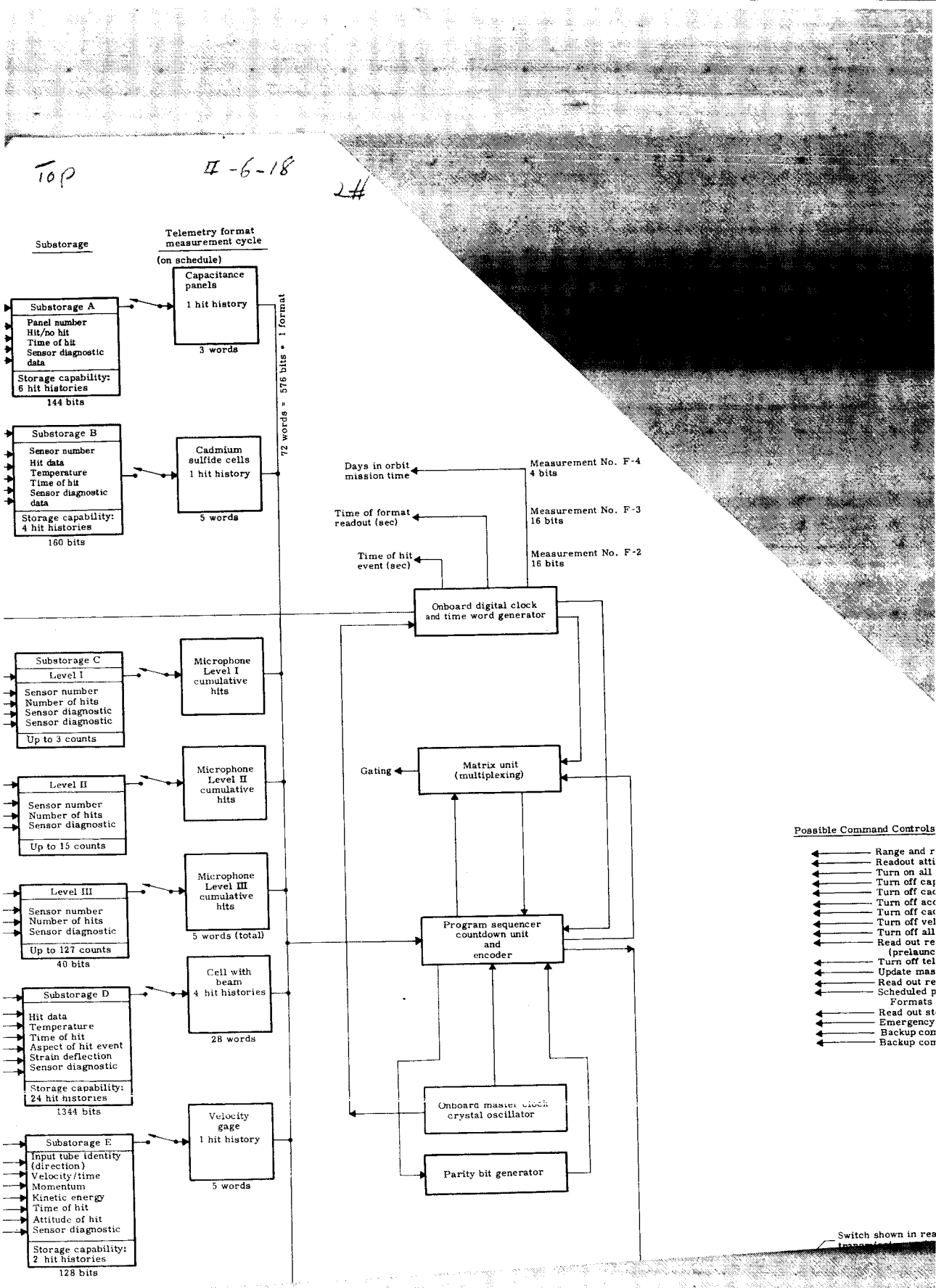
Data frame length, measurement requirements and associated substorage sizes defined the requirements for a main data storage of about 20 kilobits. Typical design values for this storage unit were about 60

cu. in., 2 lb in weight and 300 mw power demand. In addition, ancillary circuit modules were required to control write-in and readout functions. A main core storage unit with 22,000 bits (552 bits /frame x 39 frames/ orbit = 21,428 bits) would have permitted a readout of complete data collection from one orbit (6 days) during the beginning of the successive orbit in case no ground station time was available for six days. Examples of possible regular scheduled readouts from this main storage on ground station command are indicated in Fig. 6-2 for a complete orbit mission.

In case a ground command for stored data readout would have been given just during a measurement format cycle onboard (substorage into main storage), data would have been lost. Therefore, the main storage was visualized as consisting of three sections, each with a capacity of 7,176 bits (13 frames). This would have increased the main storage from 21,428 to 21,528 bits. Its function would have been: the first 13 formats transferred into Main Storage Section I, the next 13 into Section II, etc. When ground command for storage readout is given, data is telemetered from a storage section which is filled, or from any section into which no data is being transferred by format sampling. In case one section was halfway filled and a command was given during format sampling, readout is delayed until this measurement format cycle is completed.

Using this design approach, a scheduled 1/hr format readout, including spacecraft time, for data transfer from substorage to main storage was satisfactory in Meteoroid Density Zone I. Programmed readout cycle in Density Zones II through V (Figs. 6-3 and 6-4) was once every 4 hr.


Fixed Telemetry Format
Word Numbers
3
4
5
6
7
8
Panel number
Hit time
Sensor number
Sensor diagnostic
Sensor hit data
Hit
Diagnostic
Capacitance panel hit history
Cadmium sulfide cell sensor hit


Top
4-6-18
24
Substorage
Telemetry format measurement cycle
(on schedule)
Capacitance panels
1 hit history
3 words
Substorage A
Panel number
Hit/no hit
Time of hit
Sensor diagnostic data
Storage capability: 6 hit histories
144 bits
72 words = 576 bits = 1 format
Substorage B
Sensor number
Hit data
Temperature
Time of hit
Sensor diagnostic data
Storage capability: 4 hit histories
160 bits
Cadmium sulfide cells
1 hit history
5 words
Days in orbit mission time
Measurement No. F-4
4 bits
Time of format readout (sec)
Measurement No. F-3
16 bits
Time of hit event (sec)
Measurement No. F-2
16 bits
Onboard digital clock and time word generator
Substorage C
Level I
Sensor number
Number of hits
Sensor diagnostic
Sensor diagnostic
Up to 3 counts
Microphone Level I cumulative hits
Level II
Sensor number
Number of hits
Sensor diagnostic
Up to 15 counts
Microphone Level II cumulative hits
Gating
Matrix unit (multiplexing)
Level III
Sensor number
Number of hits
Sensor diagnostic
Up to 127 counts
40 bits
Microphone Level III cumulative hits
5 words (total)
Program sequencer countdown unit and encoder
Cell with beam
4 hit histories
28 words
Substorage D
Hit data
Temperature
Time of hit
Aspect of hit event
Strain deflection
Sensor diagnostic
Storage capability: 24 hit histories
1344 bits
Onboard master clock crystal oscillator
Velocity gage
1 hit history
5 words
Substorage E
Input tube identity (direction)
Velocity/time
Momentum
Kinetic energy
Time of hit
Attitude of hit
Sensor diagnostic
Storage capability: 2 hit histories
128 bits
Parity bit generator
Possible Command Controls
Range and r
Readout atti
Turn on all
Turn off cap
Turn off cac
Turn off acc
Turn off cac
Turn off vel
Turn off all
Read out re
(prelaunc
Turn off tel
Update mas
Read out re
Scheduled p
Formats
Read out st
Emergency
Backup con
Backup con
Switch shown in rea

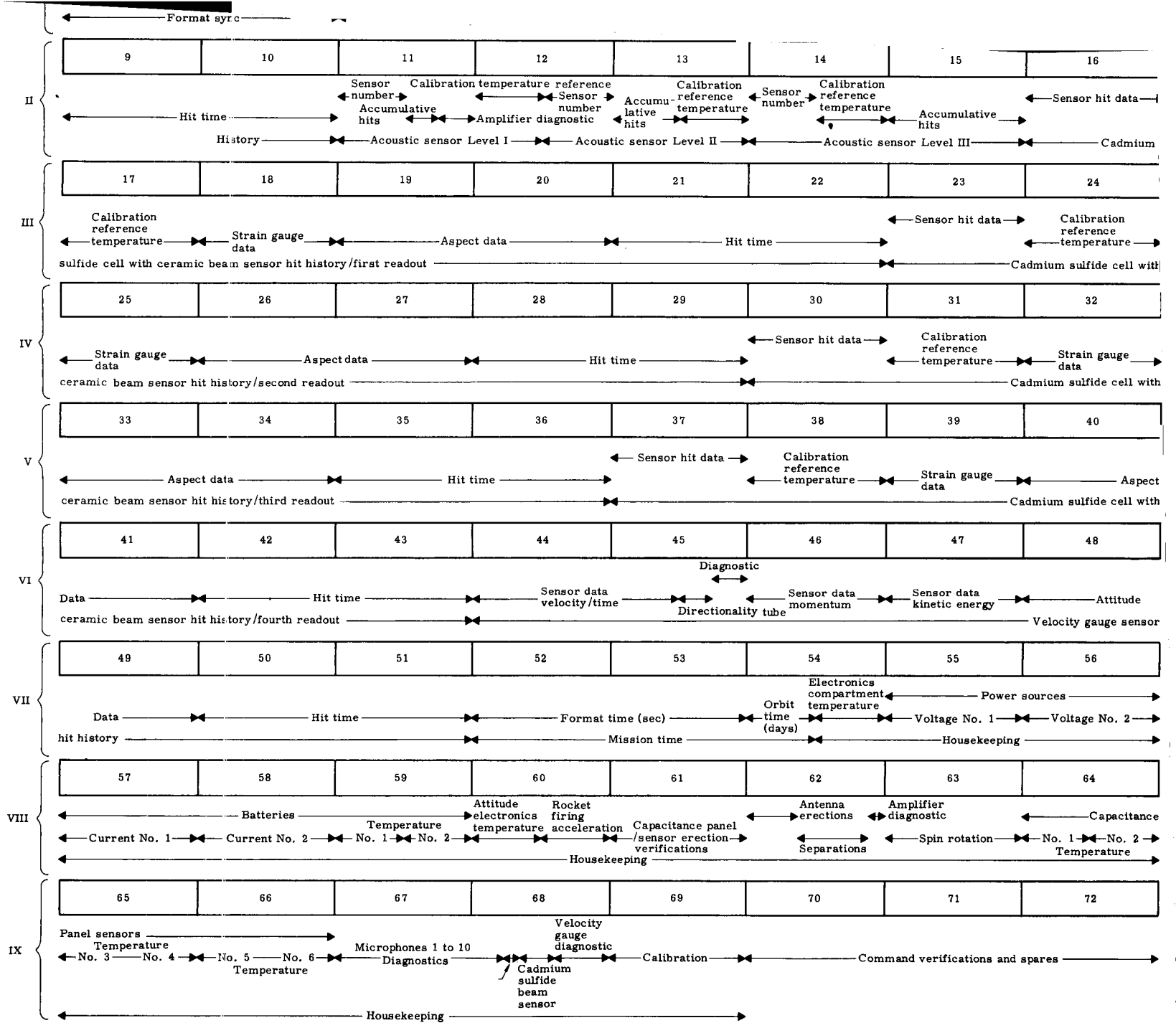
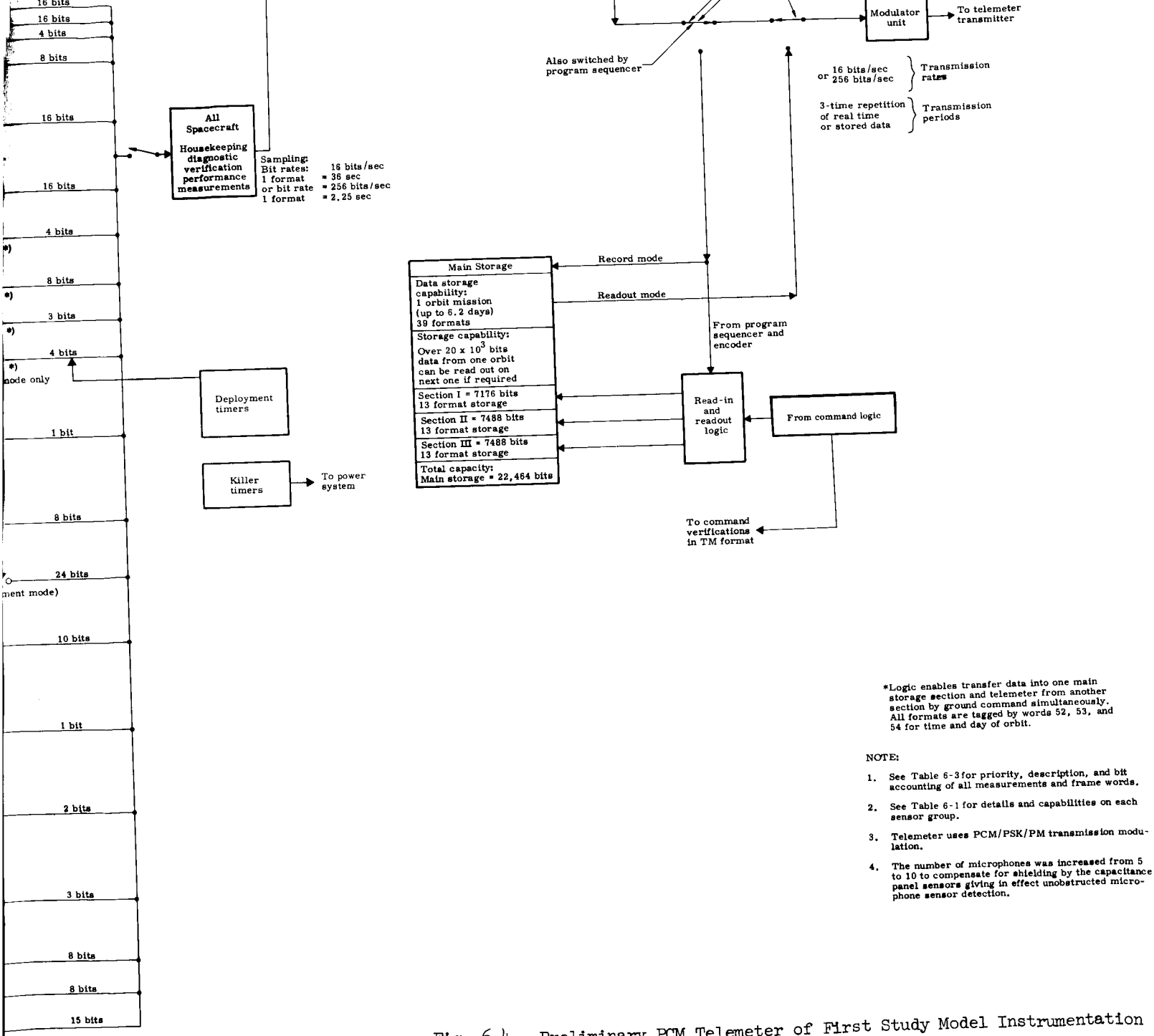


Fig. 6-3. First Model Telemetry Format



*Logic enables transfer data into one main storage section and telemeter from another section by ground command simultaneously. All formats are tagged by words 52, 53, and 54 for time and day of orbit.

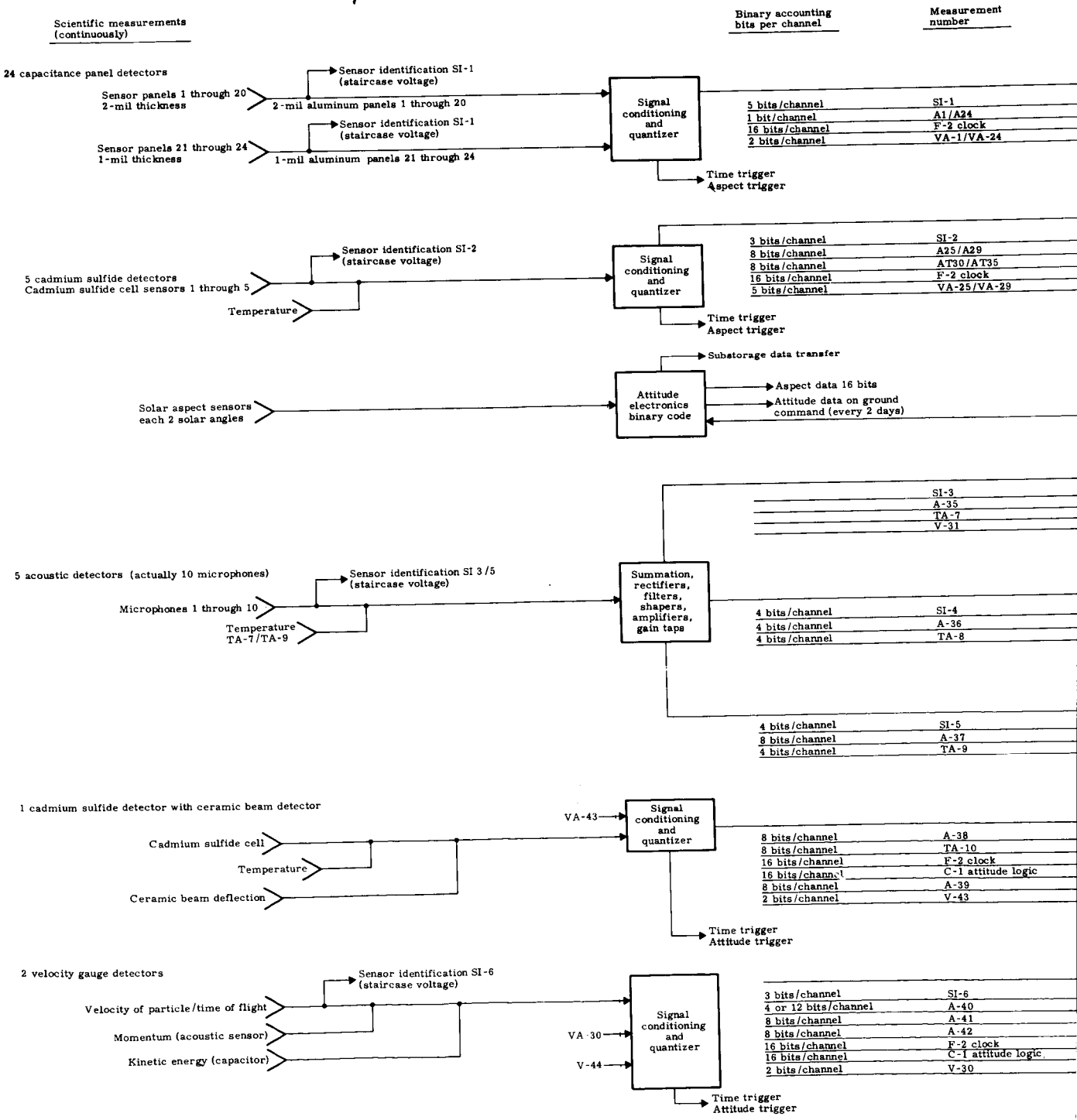
NOTE:

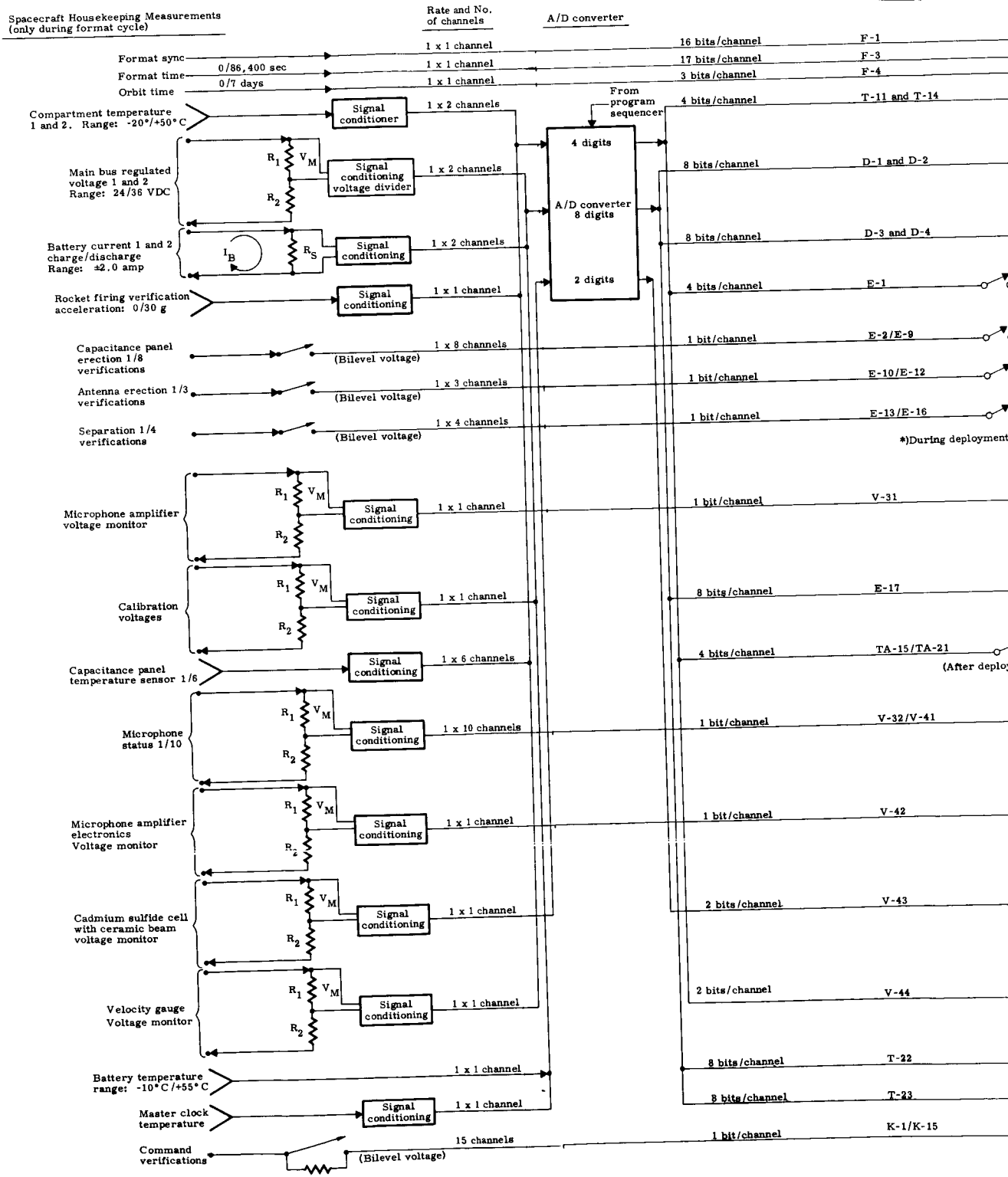
1. See Table 6-3 for priority, description, and bit accounting of all measurements and frame words.
2. See Table 6-1 for details and capabilities on each sensor group.
3. Telemeter uses PCM/PSK/PM transmission modulation.
4. The number of microphones was increased from 5 to 10 to compensate for shielding by the capacitance panel sensors giving in effect unobstructed microphone sensor detection.

Fig. 6-4. Preliminary PCM Telemeter of First Study Model Instrumentation and Data Processing

Bo Hom

Top of Diagram 1 of 4




Spacecraft Housekeeping Measurements (only during format cycle)
Rate and No. of channels
A/D converter
Format sync
Format time
0/86,400 sec
Orbit time
0/7 days
1 x 1 channel
16 bits/channel
F-1
17 bits/channel
F-3
3 bits/channel
F-4
From program sequencer
Compartment temperature 1 and 2. Range: -20°/+50°C
Signal conditioner
1 x 2 channels
4 bits/channel
T-11 and T-14
4 digits
A/D converter 8 digits
2 digits
Main bus regulated voltage 1 and 2 Range: 24/36 VDC
Signal conditioning voltage divider
8 bits/channel
D-1 and D-2
Battery current 1 and 2 charge/discharge Range: ±2.0 amp
Signal conditioning
D-3 and D-4
Rocket firing verification acceleration: 0/30 g
E-1
Capacitance panel erection 1/8 verifications
1 x 8 channels
(Bilevel voltage)
1 bit/channel
E-2/E-9
Antenna erection 1/3 verifications
1 x 3 channels
E-10/E-12
Separation 1/4 verifications
1 x 4 channels
E-13/E-16
*)During deployment
Microphone amplifier voltage monitor
V-31
Calibration voltages
E-17
Capacitance panel temperature sensor 1/6
1 x 6 channels
TA-15/TA-21
(After deploy
Microphone status 1/10
1 x 10 channels
V-32/V-41
Microphone amplifier electronics Voltage monitor
V-42
Cadmium sulfide cell with ceramic beam voltage monitor
2 bits/channel
V-43
Velocity gauge Voltage monitor
V-44
Battery temperature range: -10°C/+55°C
T-22
Master clock temperature
T-23
Command verifications
15 channels
K-1/K-15

a -6-18

APPENDIX II-7

INVESTIGATION OF MEMORY DEVICES

The feasibility of using the following memory devices as the primary means of storing data in aerospace applications was investigated:

(1) Transfluxor

(2) Biax

(3) Ferrite thin film

(4) Single aperture ferrite toroid

(5) Thin film plated wire

(6) Delay line

(7) Magnetic drum

(8) Magnetic disc

(9) Magnetic tape

A discussion of the relative advantages and disadvantages of the devices for aerospace application follows. Table 7-1 is a tabulation of the characteristics of some memory systems.

1. Transfluxor Memory

The main advantages of a transfluxor memory is that it is a nonvolatile device and possesses a NDRO capability. However, for satellite memory applications, the disadvantages of this device heavily outweigh its advantages. The disadvantages of a transfluxor memory device are readily seen when it is compared to a single aperture ferrite core memory. Probably the most undesirable feature, at least where power is at a premium, is the fact that it requires more switching power than a single aperture core. Furthermore, two complete sets of current drivers are required, compared to one for the single aperture core device. Thus, power requirements are further increased along the component count. The increased component count, coupled with a more complex wiring array than that of a single aperture core memory makes the transfluxor memory far less reliable. Because of its complex nature, the transfluxor cannot be reduced to the size of a single aperture core. This places a limiting factor on the packaging density and, hence, the size and weight of a practical memory. Since the size,

TABLE 7-1

Memory Systems

Option	Element	Access	Mode of Organization	Size* (cu in.)	Weight* (lb)	Maximum Operating Power	Standby Power	Speed of Operation	Electronic Component Count	Calibration Reliability	Mean Failure Rate
A	Rectangular transfluxor	Parallel, random	WSM, NDRO, 2000 words, 16 bits/word	550	24	36.6 watts	8.8 watts	--	8926	19,300-hr MTBF**	EMI
B	Shmoo transfluxor	Parallel, random	CCM, NDRO 2000 words 16 bits/word	500	21	27.8 watts	8.8 watts	--	3974	34,500-hr MTBF**	EMI
C	Isodrive core	Parallel, random	CCM, NDRO 2000 words 16 bits/word	256	12	27.9 watts	10.8 watts	--	1731	78,000-hr MTBF**	EMI
D	Core	Serial sequential	CCM, DRO 30,464 bits	120	3.5	250 mw	20 mw	128 bits/sec write 2048 bits/sec read	491	135,900-hr MTBF**	EMI
E	Core	Serial sequential	CCM, DRO 30,096 bits	65	2.75	<2 watts	50 mw	5 kc	--	6,250-hr MTBF**	DI/AN
F	Plated wire, using discrete electronic components	Serial sequential	WSM, NDRO 30,000 bits	95	2.5-2.8	115 mw	85 mw	5 kc	--	--	Univac
G	Plated wire, using integrated circuits	Serial sequential	WSM, NDRO 30,000 bits	63	2.3-2.5	1100 mw	1000 mw	5 kc	--	--	Univac

*Does not include power supply weight

**Entries do not use same failure rates
Operating frequency of entries 1-3 not same as entry 4

weight and power are of prime concern in satellite memory applications, the transfluxor memory device leaves a lot to be desired for this application. One further disadvantage is the fact that the transfluxor memory is not as economical as a single aperture core memory.

2. Biax Memory

Biax memories are organized as a word select memory (WSM) or linear selection memory (LSM). The biax memory is a nonvolatile device and possesses a NDRO capability. When compared to the ferrite core memory, the only advantage, besides the NDRO capability, that the biax device has over the core memory is a faster read cycle time. The read cycle time for a core memory may be four times as long, compared to that of a biax memory.

The biax element, like the transfluxor, is a multiaperture device and, consequently, is more complex than a single aperture ferrite core. For this reason, the biax element cannot be made as small as the single aperture core. Furthermore, since the wiring array of a biax memory is more complicated, it cannot be made as compact or as light as a core memory.

In general, a memory unit organized as a WSM requires more current drivers above a certain word capacity than one organized as a CCM. Therefore, the biax memory may require more components than a core memory, since the latter can be organized as a CCM. This fact, together with the more complex wiring array may tend to make the biax memory less reliable than the core memory. Furthermore, the biax memory is more noise sensitive and is not as economical as a core memory.

One further fact of importance which would tend to disqualify the biax memory as being applicable for a satellite memory at the present time or in the near future is that it is not a space-proven device. Biax memories for commercial use are now available, but an aerospace biax memory will not be developed before March 1966.

For the latter reason, the biax memory cannot be used for aerospace applications at the present time or in the near future. Even if it were developed to the extent that it could be used in aerospace applications, unless a definite requirement for fast read cycle times and NDRO capability was imperative, the biax memory would not seem to be as desirable a memory as the core memory for aerospace use.

3. Thin Film Memory

Thin film memories have NDRO and DRO capabilities. Furthermore, they are nonvolatile devices and have the capability of being operated at

very high bit rates. For fast speed operation, the thin film memories have a very small power requirement. However, they are organized as a WSM and, thus, for a particular bit capacity, may require more current drivers than a memory organized as a CCM. The higher number of current drivers may tend to offset the low switching power requirements at high bit rates. The magnetic thin film memory element has a higher packaging density than the single aperture core element; thus, the memory array is more compact. However, because of the WSM organization of the thin film memory, usually necessitating more components, the thin film memory and the single aperture core memory can be packaged in about the same space.

The magnetic thin film memory is much more expensive, and more sensitive to shock, vibration and radiation effects than core memories. Also, the thin film memory device possesses smaller output signals than a single aperture core. Thus, they are more noise sensitive and require more elaborate sense amplifiers.

Unless a high bit rate and/or NDRO capability is required, the use of a thin film memory for aerospace application does not seem warranted, especially when price is taken into consideration.

4. Single Aperture Ferrite Toroid Memory

Single aperture ferrite toroid memories can be organized as a CCM as well as a WSM. This device is nonvolatile, but the readout is of a destructive nature; if it is required to retain data, a read/restore cycle must be provided. The single aperture ferrite toroid memory can be organized as a serial sequential CCM. Since data is transmitted serially in telemetry systems, a memory thus organized is easily adapted to aerospace applications. Furthermore, relatively few components are required for a serial sequential CCM. This fact further enhances this type of memory for aerospace use, since for a given capacity memory the standby power can be minimized and the reliability is relatively high.

A ferrite core memory organized as described above can be made relatively compact and light due to the number of components involved and the fact that the wiring of the memory array is not too complex. The single aperture ferrite toroid memory device is one of the most economical memory devices on the market and a fairly inexpensive memory can be built when organized as a serial memory. The data transmission rate for deep-space telemetry systems is usually slow and, thus, the relatively slow speeds of ferrite cores are tolerable in such an application. The output, when compared to most other memory devices, is fairly large and the device is more immune to noise effects. All in all, the serial sequential CCM using single aperture/

toroids as memory elements is well suited for aerospace applications. Moreover, this type of memory has been successfully proven in several spaceborne programs.

5. Thin Film Plated Wire Memory

The thin film plated wire memory is organized as a WSM. It can be operated in a NDRO or DRO manner, and is a nonvolatile device. Although this memory is inherently more suitable for parallel operation, it can be operated in a serial fashion without being penalized too much in size, weight and power consumption. When this film-plated wire memory is organized as a serial sequential memory, it is comparable in size, weight and power to the serial sequential single aperture ferrite toroid memory.

However, this type of memory possesses a few outstanding disadvantages when compared to the single aperture core memory. Presently it is much more expensive than a core memory but, at some future date, it has the possibility of becoming relatively inexpensive. This type of memory has never been flown in an aerospace application and is not space proven. Also, compared to the single aperture core devices, the thin film plated wire memory device has a nominal output which is about 1/10 that of the core device: it is far more noise sensitive.

However, in the event the disadvantages of this memory device become tolerable (in some cases they may be trivial), the thin film plated wire memory seems to be potentially well suited for aerospace applications.

6. Delay Lines

Delay lines are cyclic nonvolatile storage devices. Since the information contained in a delay line is continuously circulating, more power can be consumed in this type of memory unit than in a static one (depending upon the organization of the static memory). Furthermore, delay lines tend to be larger, heavier and possess quite a long access time when compared to most static memories.

However, they do possess some qualities which are advantageous for aerospace use. Namely, they are NDRO devices capable of being operated at fairly high speeds. Delay lines are relatively insensitive to shock and vibration, and glass delay lines are independent of radiation. They have been space proven in aerospace applications. However, from the standpoint of size, weight and power--of prime importance in aerospace application--the delay line does not seem optimum for use as a memory unit in this particular application.

7. Drums, Discs and Magnetic Tapes

These three types of memory elements are nonvolatile devices and possess NDRO capability. However, they do not seem as suitable to aerospace applications as other memory devices. They are cyclic memory devices and the access time is greater than that for a static memory (especially sequential access memories). Because the cyclic feature is of a mechanical nature rather than electronic, a drive motor is required which, in turn, requires an ac source. Furthermore, the motors are bulky and heavy which tend to make these memories larger and heavier than static ones. Since they are cyclic and require an ac source, the reliability of the overall data storage unit tends to be less than that of noncyclic storage units. Moreover, cyclic memories require more complex selection circuitry than static memories, since time is a factor in the selection of a stored bit as well as space. Drums and discs have to be mounted in a particular manner, presenting a mounting attitude problem not present with static memories. Magnetic tape deteriorates with time, is temperature sensitive and, thus, is quite unreliable for long periods of use. For these reasons, the magnetic drum, disc and tape does not seem to be as suitable for aerospace applications as some of the other memory devices investigated.

8. Summary

Of the discussed memory devices, the single aperture ferrite core device evolved as the most optimum storage device for aerospace use. When the memory unit is organized as a serial sequential memory, a minimum number of components is required, and memory size, weight and power dissipation are minimized and memory reliability is greatly enhanced. Furthermore, a memory organized in such a manner is most suitable for use in telemetry systems, since data is transmitted serially. Single aperture core memory systems have been successfully proven on previous space missions. The single aperture core memory, organized in a serial sequential manner, most favorably meets the requirements of minimal size, weight and power consumption and maximum reliability, all of which are of prime importance in selection of a memory system for aerospace use.

9. References

1. "Digital Applications of Magnetic Devices," edited by A. J. Meyerhoff, John Wiley & Sons.

2. "Ferrite Memory Systems and Devices," edited by Electro Technology Staff, 1963.

3. "Thin-Film Plated-Wire Low-Power Computer Memory Systems," Univac Publication.

4. "Glass Memories," RPP8/635M, Corning Electronics.

5. "Magnetostructive Delay Lines," BA 2333 FT/5M/1163, Ferranti Electric.

6. "Thin Magnetic Film Memories," MO5462A, Univac Publication.

7. Egger, Alex and Knowles, William, "Data Storage in Spacecrafts," Computer Design, 1962.

8. Lubkin, Y. J., "Cyclic Memories--A Comparative Evaluation," Electronic Design, 1961.

9. Retschauer, R. J. and Leenay, K., "Matrix Memories--A Comparative Evaluation," Electronic Design, 1961.